APPENDIX K

HYDROLOGIC MODEL REPORT

ERDC/CHL Letter Report

Coastal and Hydraulics Laboratory

US Army Corps of Engineers®
Engineer Research and Development Center

Confined Disposal Facility Evaluation

Cleveland Harbor, Ohio Thermal Plume Transport Investigation

David J. Mark, Raymond S. Chapman, and Phu V. Luong

September 2008

Cleveland Harbor, Ohio Thermal Plume Transport Investigation

David J. Mark, Raymond S. Chapman, and Phu V. Luong

Coastal and Hydraulics Laboratory
U.S. Army Engineer Research and Development Center
3909 Halls Ferry Road
Vicksburg, MS 39180-6199

Prepared for U.S. Army Engineer District, Buffalo

Preface

The U.S. Army District, Buffalo (LRB) plans to construct a Confined Disposal Facility (CDF) within Cleveland Harbor. One potential site is located at the eastern entrance to the Harbor. However, this CDF site resides in close proximity to the cooling water intake and outfall structures servicing the First Energy Power Plant; concern exists that the planned CDF will change the circulation pattern in the Harbor area such that water discharge from the power plant will be subsequently drawn into the intake without adequate cooling.

Potential adverse impacts due to the proposed CDF, reported herein, were determined by examining changes in model-generated current circulation and thermal transport patterns. Modeling efforts concentrated on quantifying the change in circulation patterns with and without the CDF in place for storm and quiescent/non-storm conditions. For evaluating changes in the thermal plume transport, a two-month period of July and August 2002 was used as it reflects a period of limited wind-induced mixing.

This study was conducted for the CELRB. Mr. Joshua J. Feldman served as the study program manager and Mr. Michael C. Mohr served as the senior coastal engineer, as well as provided technical support and review for this study. Research and development activities for this study were conducted at the U.S. Army Engineer Research and Development Center (ERDC), Coastal and Hydraulics Laboratory (CHL), Vicksburg, MS. The study was performed by Mr. David J. Mark, Estuarine Engineering Branch (HF-EL), Dr. Raymond S. Chapman, Coastal Processes Branch (HF-C), and Dr. Phu V. Luong, HF-EL.

This investigation was performed under the direct supervision of Dr. Robert McAdory, Chief, HF-E, and Mr. Ty Wamsley, Chief, HF-C. General supervision was provided Mr. Bruce A. Ebersole, Chief, Flood and Storm Protection Division. In addition, Dr. William D. Martin served a Deputy Director, CHL, and Mr. Thomas W. Richardson served as its Director. COL Richard B. Jenkins was Commander and Executive Director of ERDC, and Dr. James R. Houston was Director.

Unit Conversion Factors

Multiply	By	To Obtain
feet	0.3048	meters
knots	0.5144444	meters per second
miles (nautical)	1,852	meters
miles (U.S. statute)	1,609.347	meters
miles per hour	0.44704	meters per second

1 Introduction

The U.S. Army District, Buffalo (LRB) plans to construct a Confined Disposal Facility (CDF) within Cleveland Harbor. One potential site is located at the eastern entrance to the Harbor. However, this site is located in close proximity to the cooling water intake and outfall structures servicing the First Energy Power Plant; concern exists that the planned CDF will change the circulation pattern in the Harbor area such that water discharge from the power plant will be subsequently drawn into the intake without adequate cooling. Figure 1-1 displays the existing harbor configuration and location of the power plant. To assess potential impacts from the planned construction, the LRB requested the U.S. Army Engineer Research and Development Center (ERDC), Coastal and Hydraulics Laboratory (CHL) to develop and apply numerical circulation and thermal transport models for making this determination.

Potential adverse impacts due to the proposed CDF, reported herein, were determined by examining changes in model-generated current circulation and thermal transport patterns. The initial modeling efforts concentrated on quantifying the change in circulation patterns with and without the CDF in place for storm and quiescent/non-storm conditions. For simulating quiescent conditions, a two-month period of July and August 2002 was chosen because summertime conditions reflect the worst-case scenario; less frequent passages of weather fronts and longer periods of relatively weaker winds induce less mixing of the Lake waters and plume than during other season. With the increased temperature of the ambient Lake water and less storm-induced mixing, the power plant's heated discharge may not sufficiently cool, resulting in warmer water being drawn into the power plant.

Circulation of Lake Erie varies on a yearly, seasonal, and daily basis and is primarily driven by wind and atmospheric pressure, together with inflows from the Detroit River and outflows through the Niagara River. Other phenomena influencing circulation in the Lake include baroclinic gradients induced by air-lake temperature differences and river inflow/lake temperature differences. In order to replicate the primary processes that induce circulation, a nested modeling technique was selected and employed in this study. As such, one model was

developed for the entire Lake and used to supply boundary-forcing data to a second model that highly resolves the Harbor proper.

The Lake-wide model includes wind forcing and river discharges at the Detroit, Niagara, Maumee, and Cuyahoga Rivers. As such, this model predicts the overall barotropic circulation within Lake Erie, and replicates the seiche oscillations induced by the passage of weather fronts.

The second model simulated hydrodynamic conditions and thermal transport of the heated water discharged from the power plant within the Harbor proper. The open-water boundary condition specified in this model is the water-surface elevations generated with the Lake-wide model. Furthermore, this model investigates two-dimensional (in plan) barotropic and baroclinic circulation. Future three-dimensional simulations can be conducted to investigate the vertical structure of the thermal plume and marina flushing should these tasks be deemed necessary.

This report contains four chapters, the first being the Introduction. Chapter 2 describes the Lake-wide modeling effort, including model development, calibration and validation, and evaluation of CDF configurations. Chapter 3 describes the thermal plume modeling. Chapter 4 summarizes the study findings. Appendices A and B describe the Lake-wide and Harbor models, whereas Appendix C contains comparisons of model-generated and measured water-surface elevations generated in the calibration and validation exercises of the Lake-wide model.

Figure 1-1. Existing Harbor configuration.

2 Lake-Wide Circulation Modeling

This chapter summarizes the circulation modeling conducted for Lake Erie, including Cleveland Harbor, using the ADCIRC long-wave hydrodynamic model. This component aims to characterize water levels and currents throughout the Harbor as it exists today and to predict any potential impacts that may result from constructing a Confined Disposal Facility (CDF). Comparing model-generated currents and water-surface elevations between pre- and post-construction conditions can provide insight, for example, into whether the CDF will reduce flushing of nearby marinas.

This chapter is composed of three sections, with the first describing the model development, which includes developing the numerical grid was well as in generating the forcing mechanisms used in driving the model. In the second section, the calibration and validation procedure is described, which ensures the model accurately depicts water-surface elevations and currents in the study area. The third section presents how the calibrated model was adapted for testing the three CDF configurations, together with comparing current patterns during storm and quiescent conditions.

Model Development

The ADCIRC numerical model, a large-domain, two-dimensional (2-D) depth-integrated finite-element hydrodynamic circulation model, was applied in this study to provide water level and depth-averaged current (circulation) information for Cleveland Harbor, Ohio. Described in Appendix A, the model solves the shallow-water equations in full nonlinear form and can be forced with time-varying water-surface elevation, wind, wave, and river inflow/outflow boundary conditions.

Figure 2-1 displays the grid developed for this study. As shown, the model domain encompasses the entire Lake, and includes the lower reaches of the Cuyahoga, Maumee, Detroit, and Niagara Rivers. Figure 2-2 displays the grid in the vicinity of Cleveland Harbor. Figure 2-3 displays an aerial photograph of the

eastern Harbor, were the planned CDF will be constructed, and Figure 2-4 displays the grid

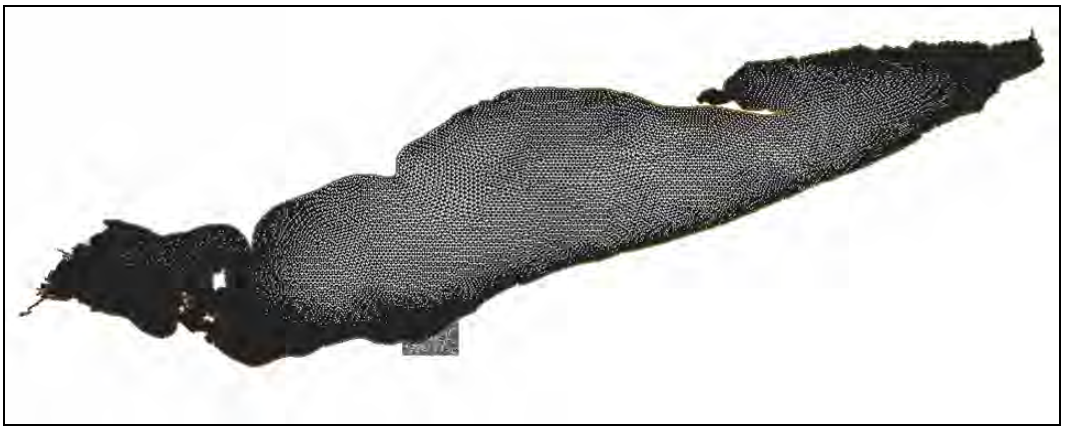

Figure 2-1. Lake Erie ADCIRC grid.

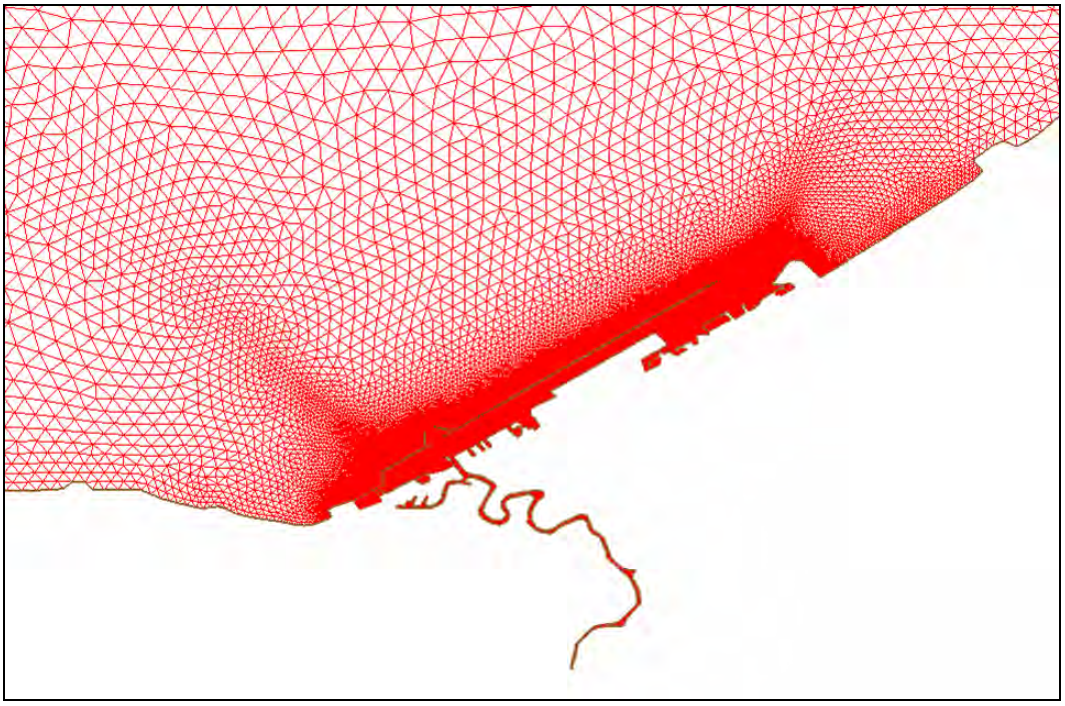

Figure 2-2. Lake Erie ADCIRC grid at Cleveland Harbor, Ohio.

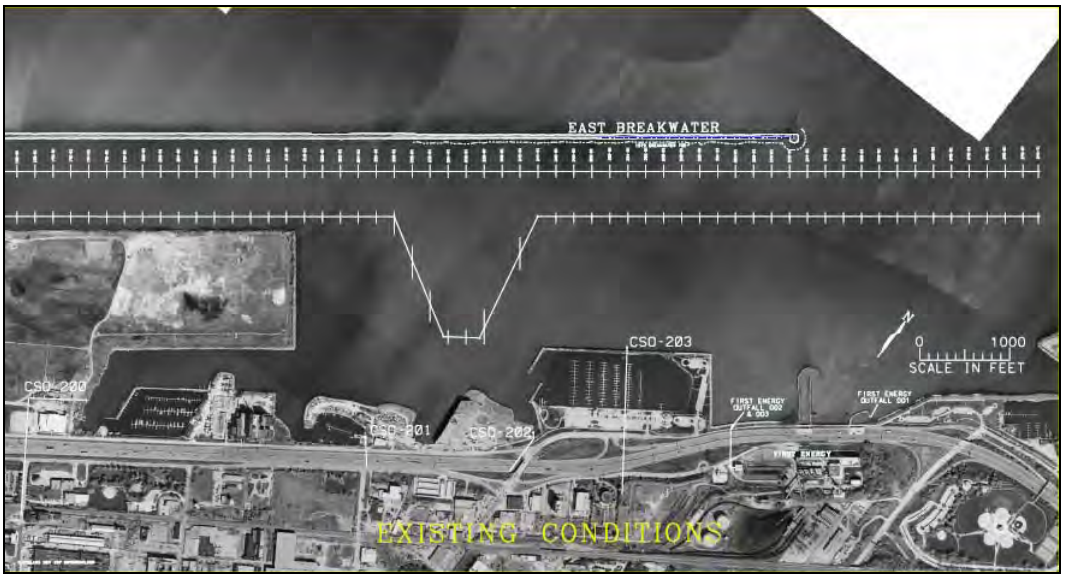

Figure 2-3. Base Harbor configuration.

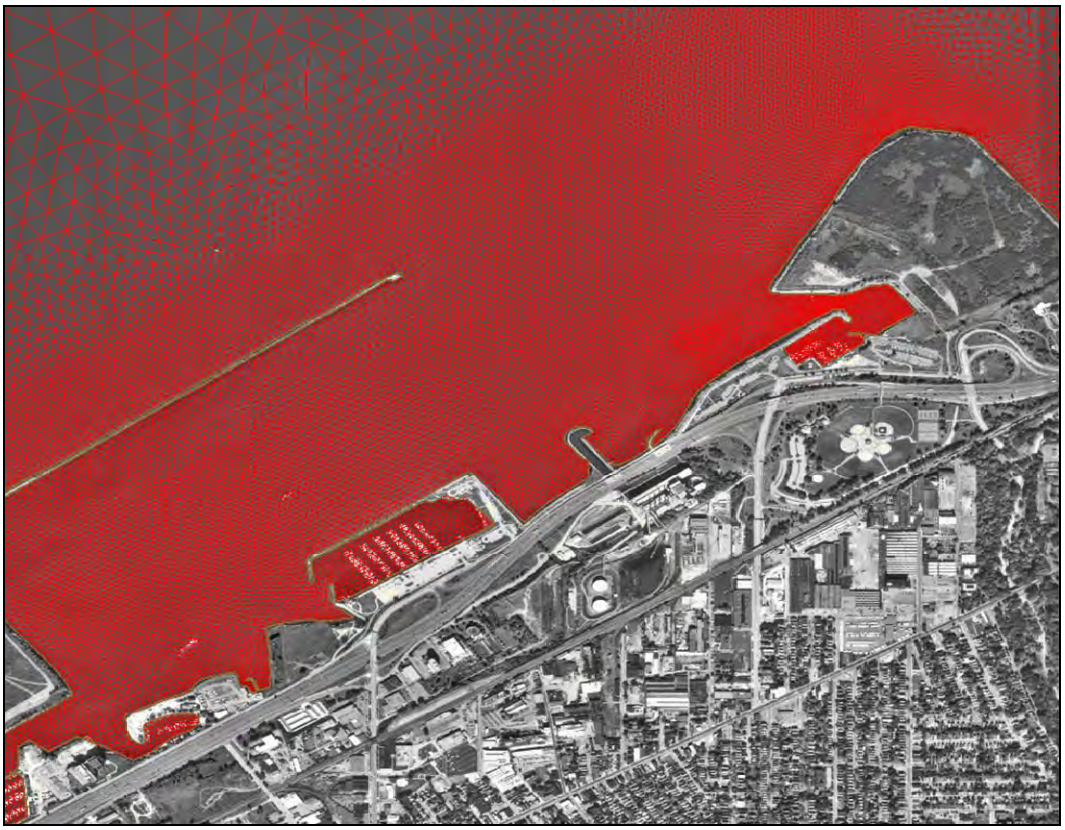

Figure 2-4. Lake Erie ADCIRC grid in project area.

of the same area. As shown in the above figures, the grid highly resolves the entire Harbor and its main, western, and eastern entrances, together with the lower reaches of the Cuyahoga River.

This existing-configuration or base grid consists of 95,255 nodes and 183,034 elements, of which 30,628 nodes and 62,038 elements resolve the Harbor. The largest elements reside in the central Lake basin, having nodal spacing of about 24 km, whereas the smallest elements resolve the western Harbor entrance, where their widths are approximately 15 m. For most of the Harbor, including the area of the proposed CDF, nodal spacings are approximately 20 m. Included in the grid are the power plant's outfall and intake structures.

The grid boundary along the Canadian shoreline was aligned with the shoreline shown on satellite imagery published by NaturalVue, which are digitally enhanced images taken by the Landsat satellite. These images have a 15-m resolution. For areas within the United States, shoreline positions are based on satellite imagery published by the U.S. National Geo-spatial Intelligence Agency (formerly the Defense Mapping Agency), and have a resolution of 5 meters. In the vicinity of Cleveland Harbor, U.S. Geological Survey Digital Orthographic Quarter-Quadrilateral (DOQQ) imagery was used in aligning the grid shoreline and its coastal structures. The DOQQs have a resolution of about 1 m.

Bathymetry specified in the grid were obtained from two sources. For Cleveland Harbor, bathymetry were extracted from contours and soundings residing in the U.S. National Oceanic and Atmospheric-published Electronic Nautical Chart. For the remaining regions outside of the Harbor, bathymetry data were extracted from the National Geophysical Data Center (NGDC) Coastal Relief Model database for Lake Erie as well as Lake St Clair. For both data sources depths are referenced to the International Great Lakes Datum 1985 (IGLD).

Forcing Data

Wind data were obtained from the National Oceanic and Atmospheric Administration's (NOAA) Great Lakes Environmental Research Laboratory (GLERL), and were generated as part of their Great Lakes Coastal Forecasting System (GLCFS). One component of the GLCFS is the generation of wind fields subsequently used in circulation and water level now-cast simulations. Hourly wind speeds and directions were extracted from GLCFS archives. These data are provided at 5-km intervals that encompass the entire Lake. Time periods for the extracted wind data include October and November, 2004, as well as Summer 2002.

Water level data for model calibration and validation consist of 12 gauges and were obtained from the U.S. National Ocean Service (NOS) and the Environment Canada-Canadian Marine Environment Data Service (CMEDS). River inflow data measured in the Detroit River were obtained from the U.S. Army District, Detroit, whereas flow rate data specified for the Cuyahoga, Niagara, and Maumee Rivers were obtained from the USGS stream flow web site.

Model Calibration and Validation

For the initial calibration, the time period of 13-19 October 2004 was selected for comparing model results to measured data. A relatively large seiche that generated a 1.6 m peak displacement in water level measured at the Toledo gauge occurred during this period. ADCIRC was forced with GLERL wind fields for the one-month period, and model-generated water levels were compared with measurements recorded at 12 NOS and the CMEDS gauges located throughout Lake Erie. The twelve gauge locations are shown in Figure 2-5, and include Cleveland and Toledo, Ohio, Erieau, Ontario, and Buffalo, New York, which were selected for comparisons in the text. The complete set of comparisons is contained in Appendix C. Model-generated water levels for this period compare favorably well in range and phase to the measured data in the western and central Lake basins (Figures 2-6 through 2-9). However, accuracy of the model-generated water levels diminished in the eastern basin, with the least favorable comparison being observed at Buffalo, New York. Discrepancies between model-generated and measured water levels are attributed to inaccuracies in the wind fields in the eastern Lake basin and the neglect of barometric pressure variation.

Figure 2-10 compares a time-series of measured and GLERL-generated wind speed and direction for Buoy No. 45005, maintained by the NOAA National Data Buoy Center. This buoy resides approximately 28 nm northwest of

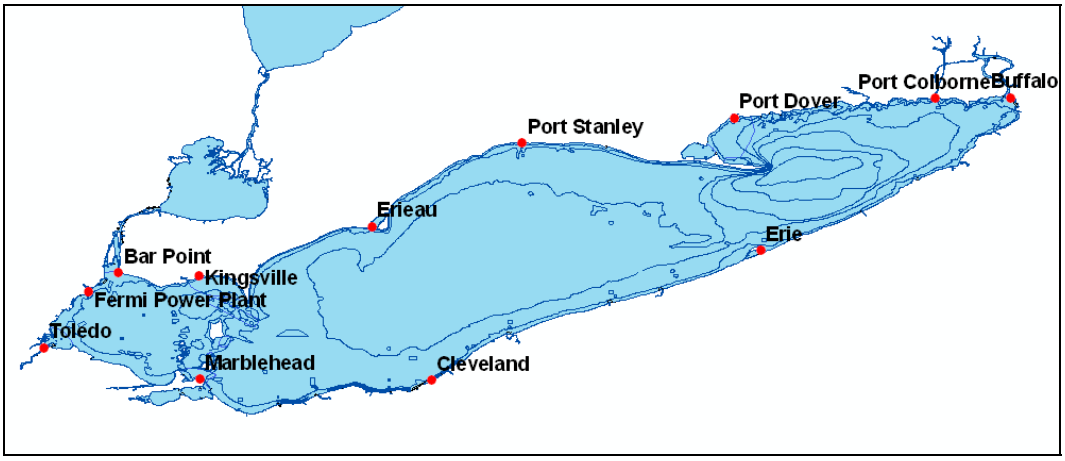

Figure 2-5. Location of Gauges used in Calibration and Validation Exercises.

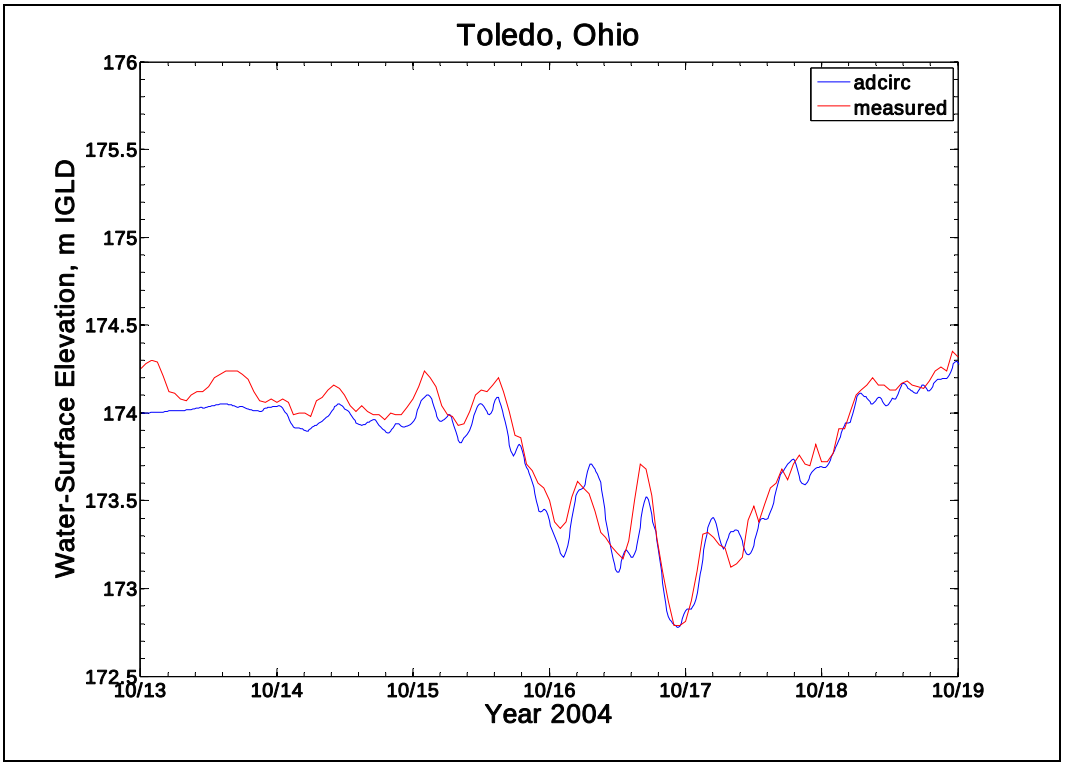

Figure 2-6. Comparison of model-generated and measured water-surface elevations: Toledo, OH, 13-19 Oct 2004.

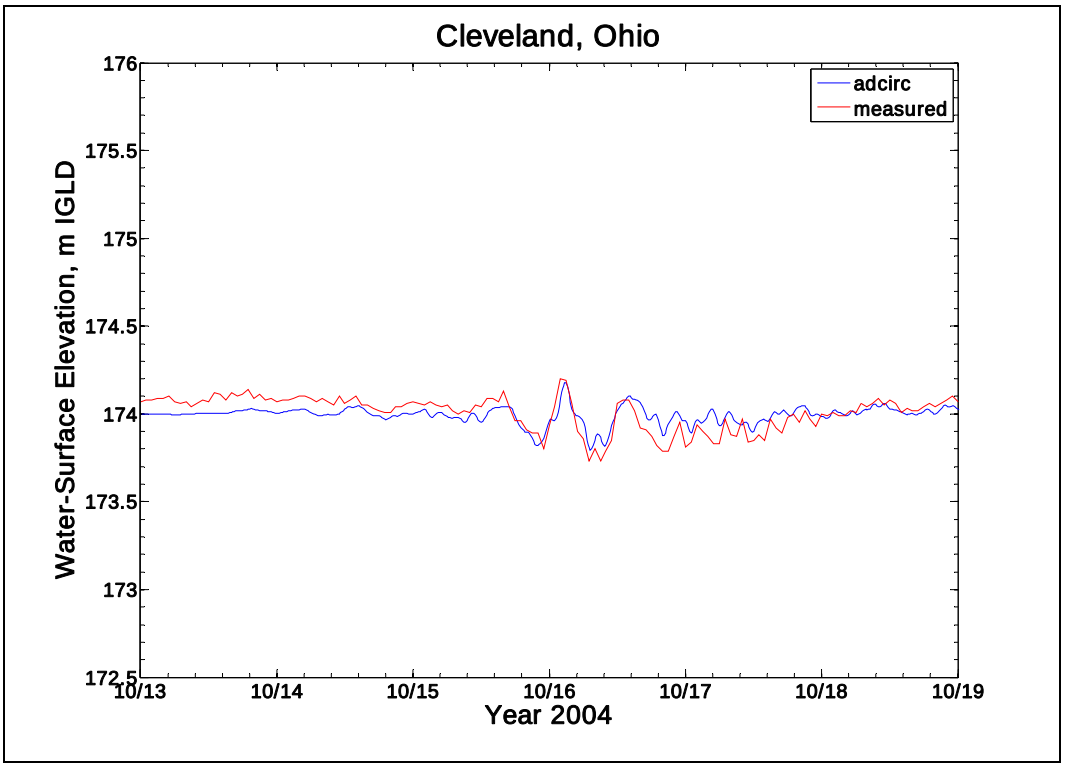

Figure 2-7. Comparison of model-generated and measured water-surface elevations: Cleveland, OH, 13-19 Oct 2004.

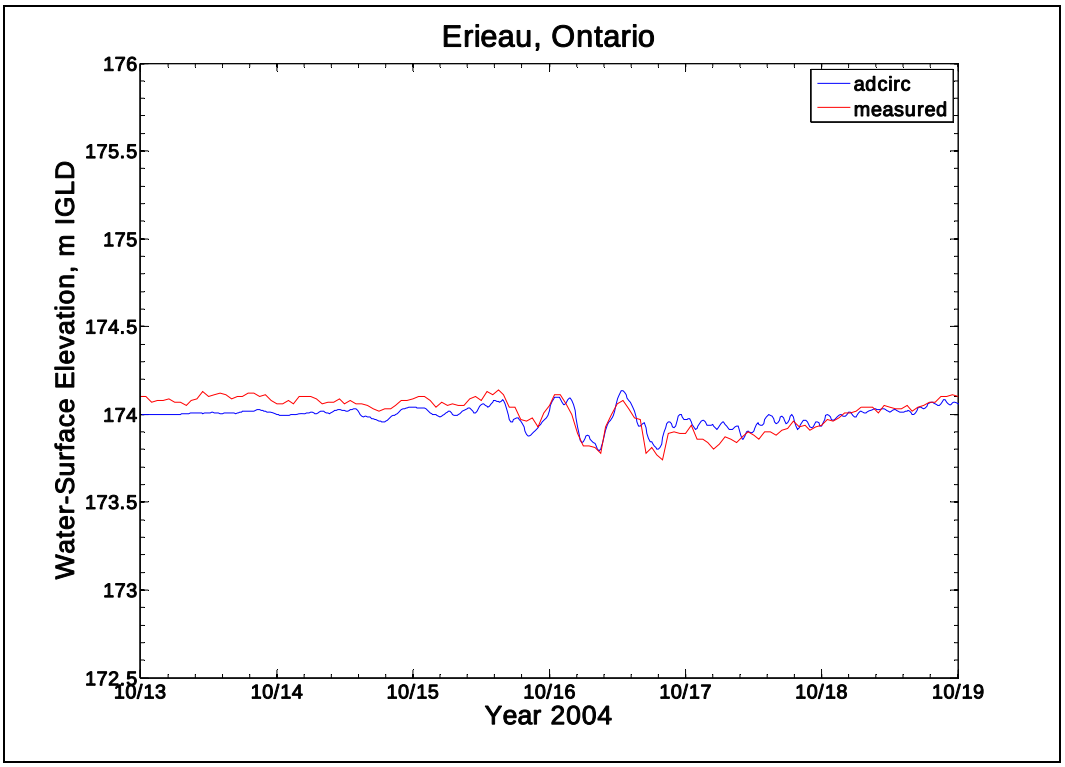

Figure 2-8. Comparison of model-generated and measured water-surface elevations: Erieau, Ontario, 13-19 Oct 2004.

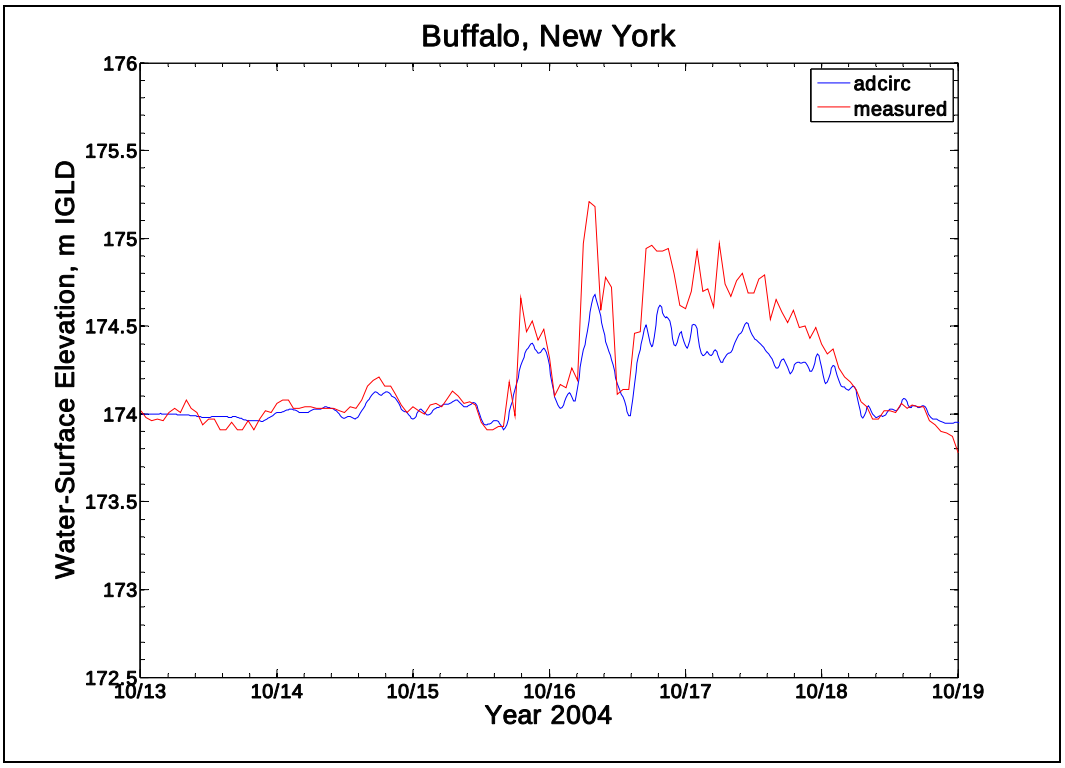

Figure 2-9. Comparison of model-generated and measured water-surface elevations: Buffalo, NY, 13-19 Oct 2004.

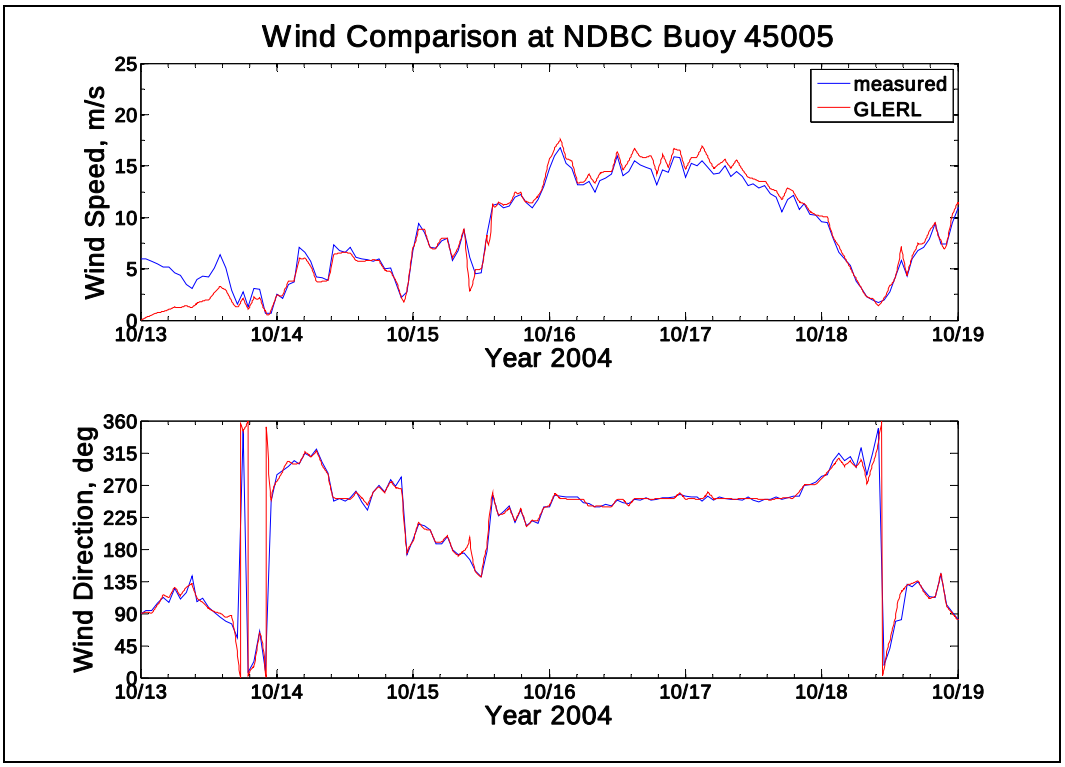

Figure 2-10. Comparison of GLERL-generated and measured wind speeds and directions: NDBC Buoy 45005, 13-19 Oct 2004.

Cleveland Harbor, in the western extent of the central Lake basin. As shown in this figure, the GLERL-generated winds compare very well with the measured winds, in both speed and direction. Differences in wind speeds are less than 1 m/s throughout the calibration period.

Figure 2-11 compares time-series of GLERL-generated winds with those measured at Burke Lakefront Airport, which is located in the Cleveland Harbor complex. For the majority of the calibration period, the GLERL-generated winds over estimated the measured wind speed by approximately 5 m/s, and wind direction differed by about 15 deg.

Figure 2-12 compares a time-series of GLERL-generated winds with those measured at Buffalo International Airport, which is located approximately 8.5 miles east of the lakefront. The GLERL-generated winds tend to be greater than the peak measured winds by about 2 m/s, whereas computed wind directions compare favorably with the measured directions. Discrepancies between the GLERL-generated winds and measured winds recorded at Burke and Buffalo International Airports are attributed to adjustments made to the GLERL-generated winds to account for over-land wind effects inherently included in the measured winds.

Substantial differences are found, however, when comparing measured winds recorded at Buffalo and Port Colborne, which is located 19 miles west of Buffalo. Shown in Figure 2-13, wind speeds measured at Port Colborne can be twice as strong during a storm as those measured at Buffalo. (No wind records were found for the calibration and validation period, necessitating the use of the Fall 2002 period as a proxy.) A similar comparison and findings were made between the GLERL-generated and measured winds for Port Colborne during this period (Figure 2-14), where the GLERL-generated winds were much weaker than the measured winds during storms.

The differences in wind strength are attributed to: a) the Port Colborne anemometer being located on the lakefront, whereas the Buffalo anemometer residing inland; and b) the GLERL-generated being tuned to the Buffalo anemometer. As such, the GLERL-generated winds imposed in the circulation model were too weak in the eastern Lake basin, resulting in reduced storm surge levels at Buffalo.

The November 2004 time period was selected for model validation. As in the calibration exercise, ADCIRC was forced with GLERL-generated wind fields for this second period. ADCIRC water level results were again compared with water levels measured at the 12 NOS and the CMEDS gauges. The model-

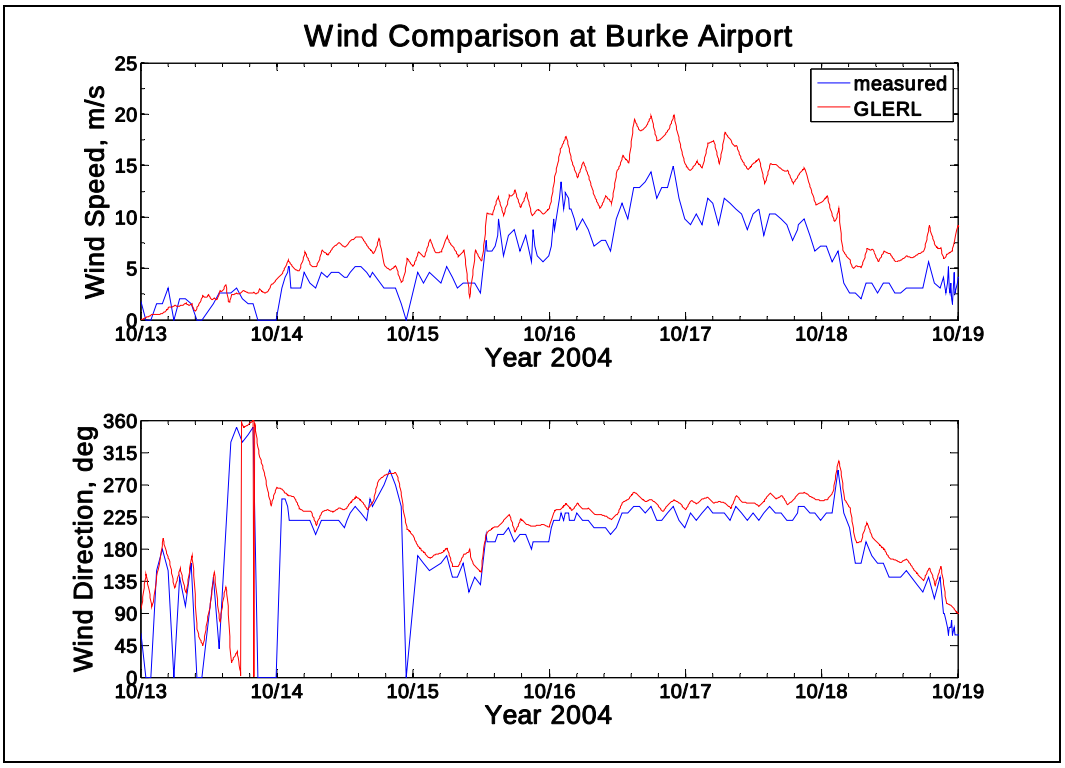

Figure 2-11. Comparison of GLERL-generated and measured wind speeds and directions: Burke Lakefront Airport (Cleveland, OH), 13-19 Oct 2004.

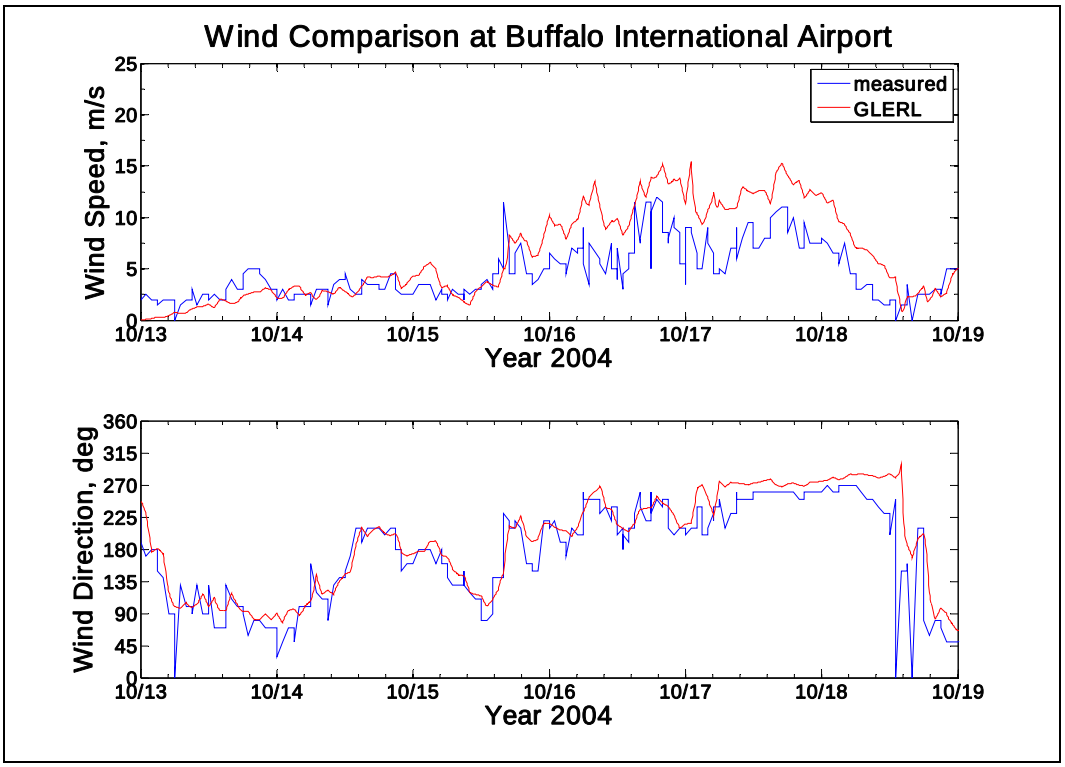

Figure 2-12. Comparison of GLERL-generated and measured wind speeds and directions: Buffalo International Airport, 13-19 Oct 2004.

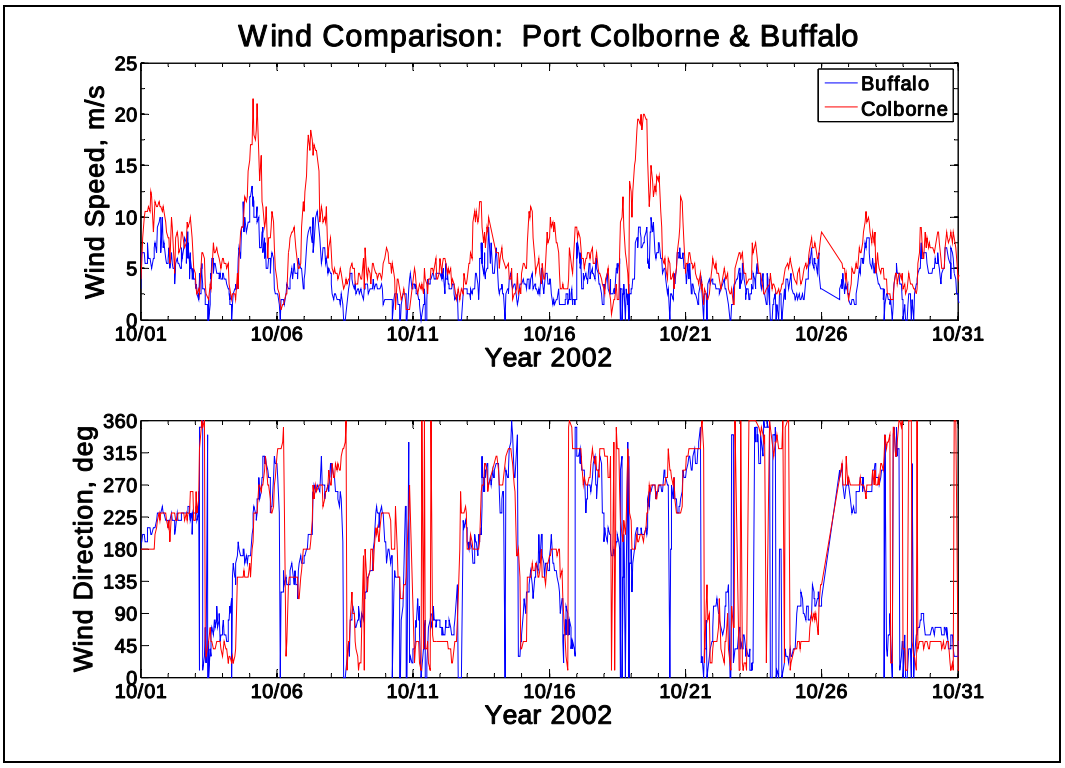

Figure 2-13. Comparison of measured wind speeds and directions at Port Colborne, Ontario and Buffalo International Airport: 1-31 Oct 2002.

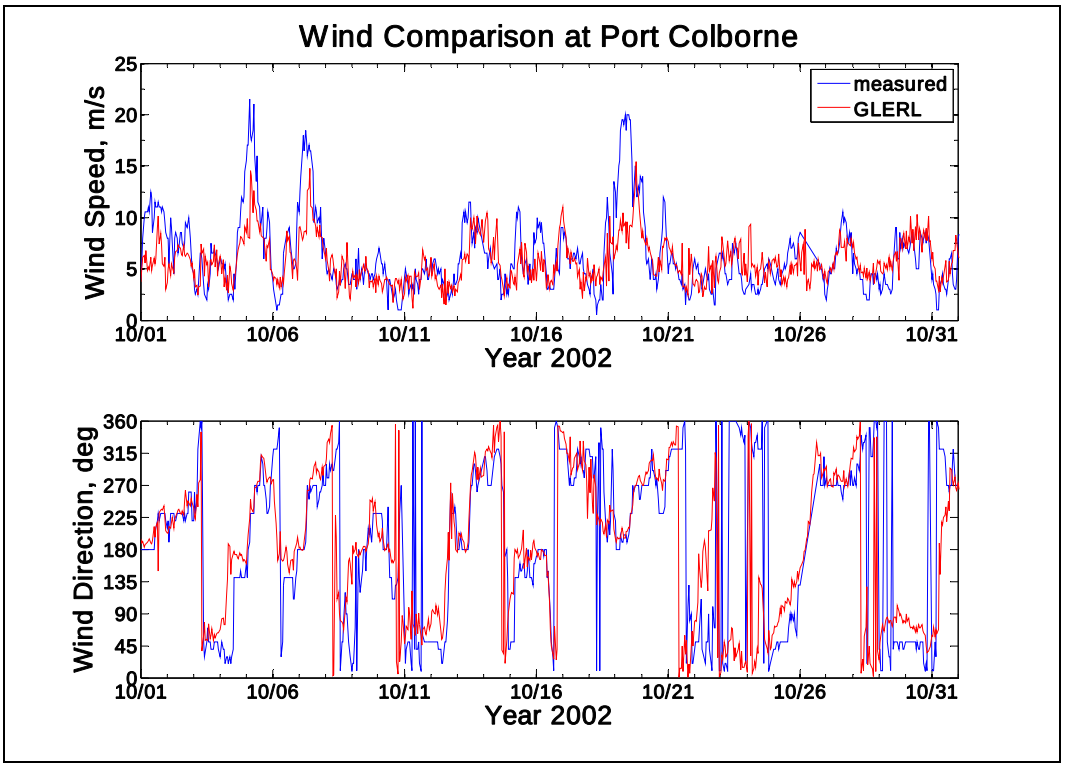

Figure 2-14. Comparison of GLERL-generated and measured wind speeds and directions: Port Colborne, Ontario, 1-31 Oct 2002.

generated water levels again compared favorably in range and phase with the NOAA gauge measurements (Figures 2-15 through 2-18) at Toledo, Cleveland, and Erieau. As with the calibration period, the model did not generated water levels to a high degree of accuracy at Buffalo (Figure 2-19). Again, this discrepancy between model-generated and measured water levels at Buffalo is attributed to the winds being too weak in the eastern Lake basin. Figures 2-19 through 2-21 compare GLERL-generated winds with measured winds for Buoy 45005, Burke Airport, and Buffalo International Airport, respectively.

Harbor Configuration Testing

The grid constructed for the existing Harbor configuration was adapted to represent each of the three proposed CDF configurations. Figures 2-22 and 2-23 display the outline of the CDF and the grid, respectively, for Configuration 1. Figures 2-24 and 2-25 display the outline of the CDF and the grid, respectively for Configuration 2. Figures 2-26 and 2-27 display the outline of the CDF and the grid, respectively, for Configuration 3. Each configuration represents a particular phase in construction, with Configuration 1 representing the earliest phase and Configuration 3 depicting final construction.

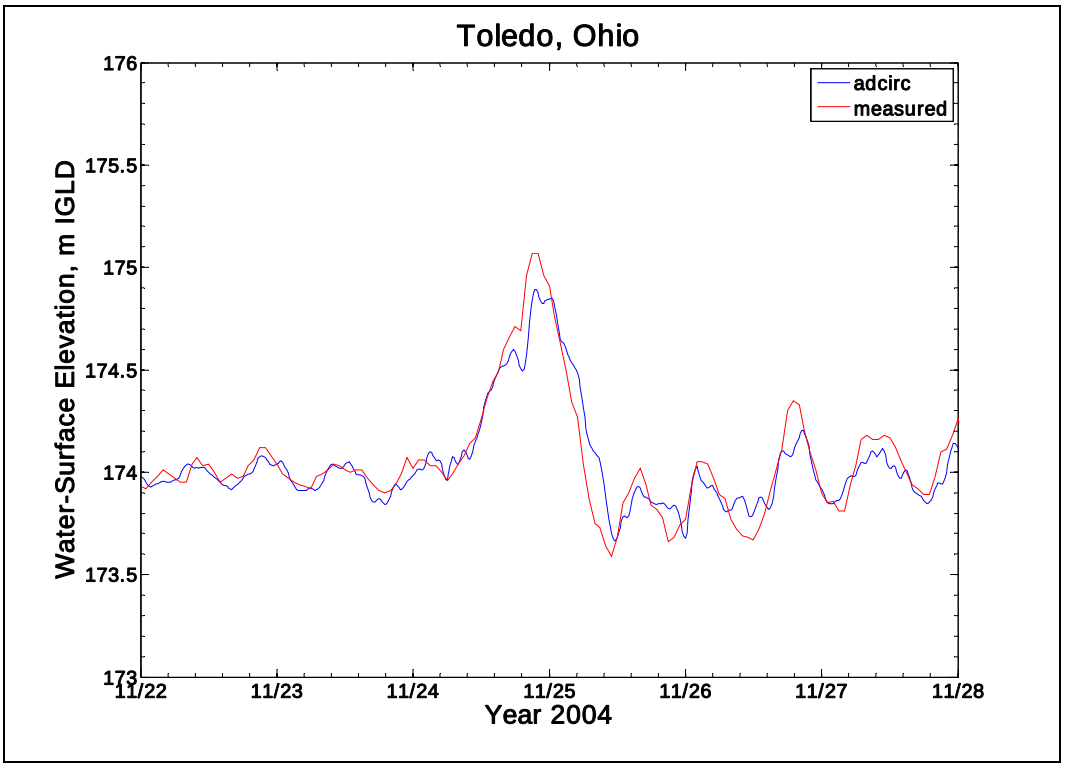

Figure 2-15. Comparison of model-generated and measured water-surface elevations: Toledo, OH, 22-28 Nov 2004.

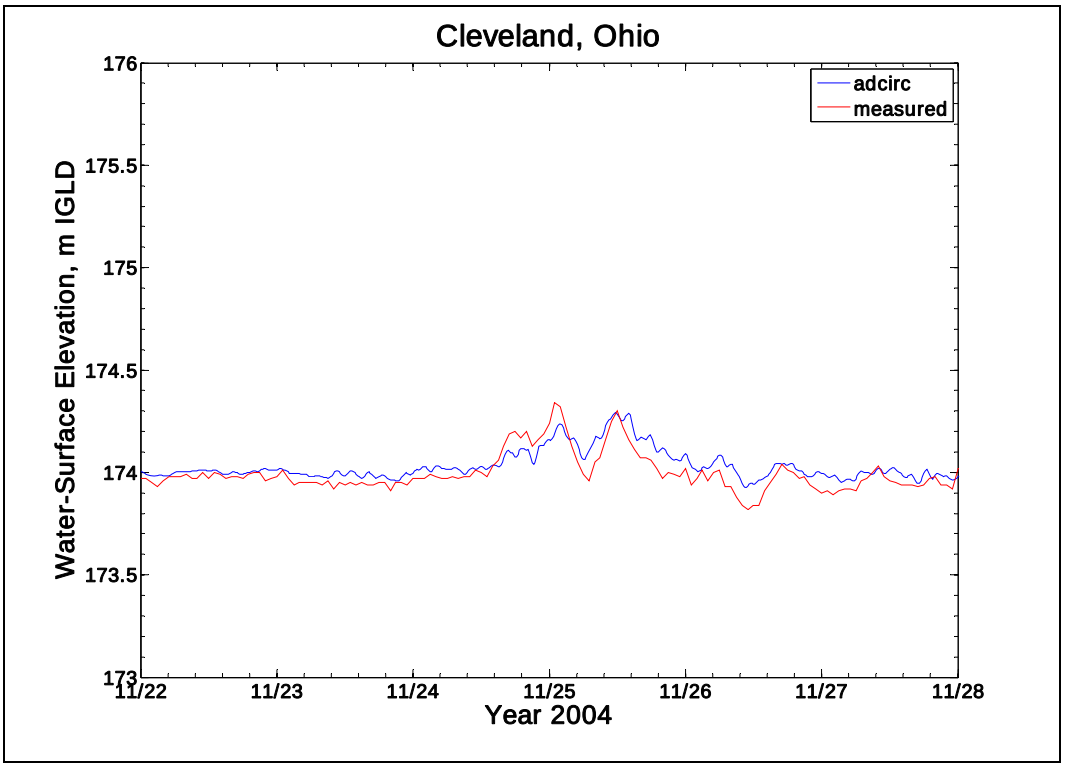

Figure 2-16. Comparison of model-generated and measured water-surface elevations: Cleveland, OH, 22-28 Nov 2004.

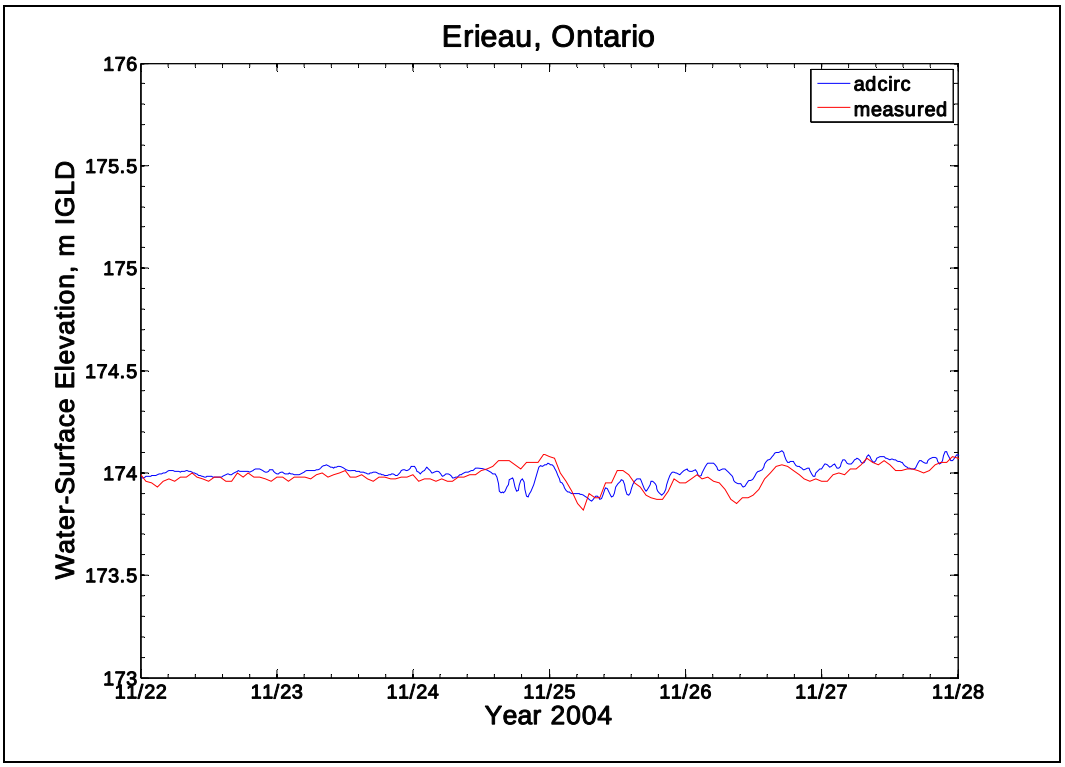

Figure 2-17. Comparison of model-generated and measured water-surface elevations: Erieau, Ontario, 22-28 Nov 2004.

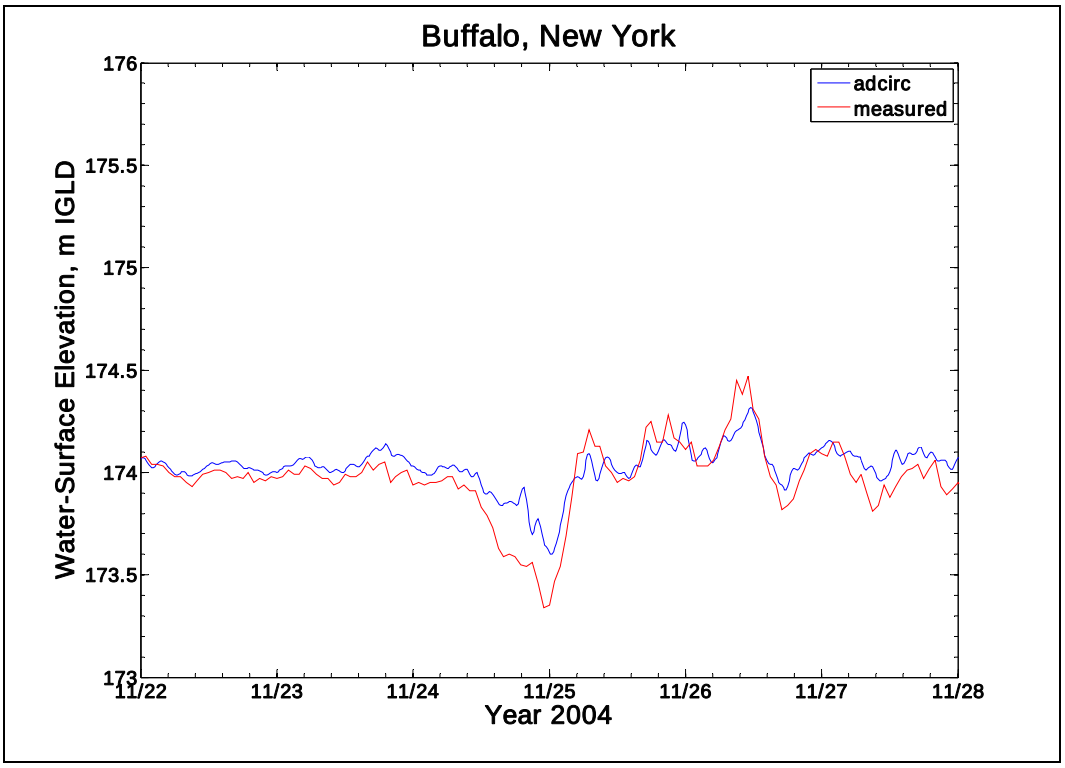

Figure 2-18. Comparison of model-generated and measured water-surface elevations: Buffalo, NY, 11-28 Nov 2004.

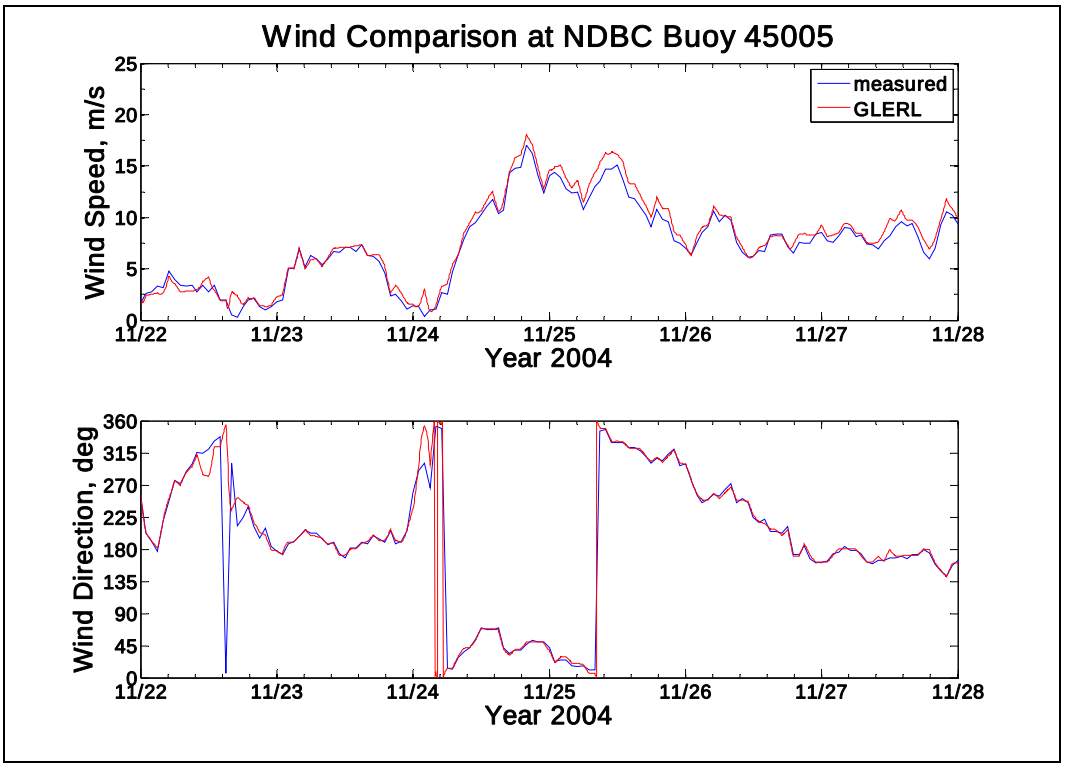

Figure 2-19. Comparison of GLERL-generated and measured wind speeds and directions: NDBC Buoy 45005, 22-28 Nov 2004.

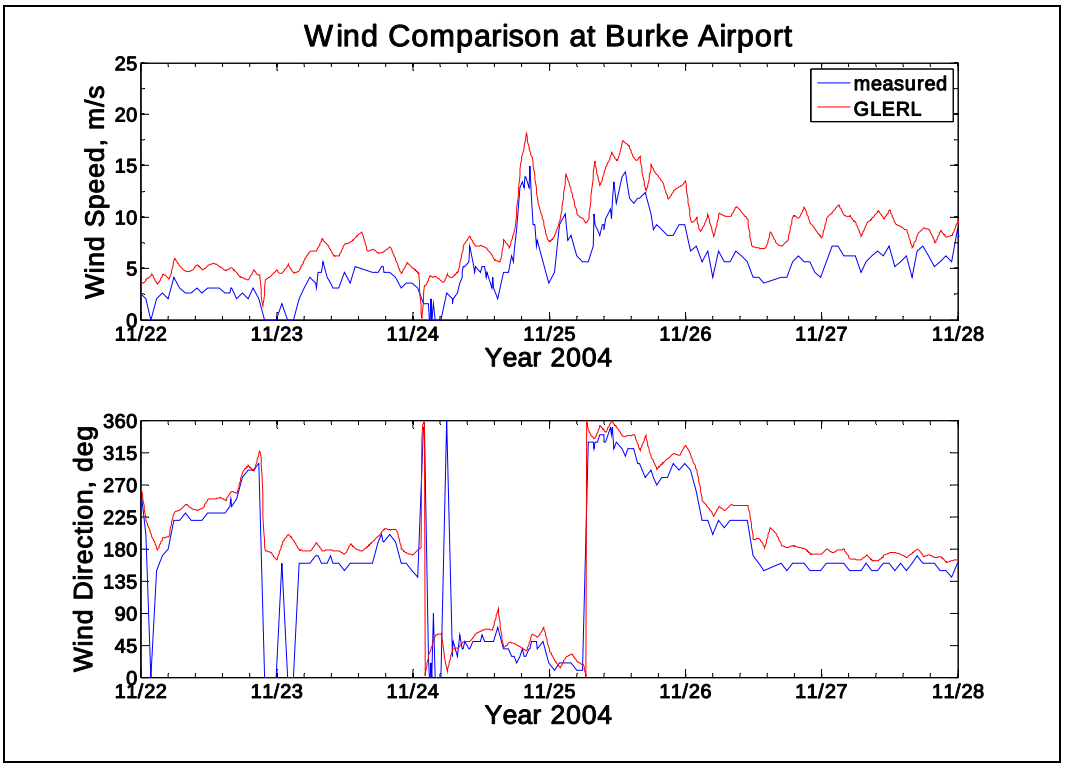

Figure 2-20. Comparison of GLERL-generated and measured wind speeds and directions: Burke Lakefront Airport (Cleveland, OH), 22-28 Nov 2004.

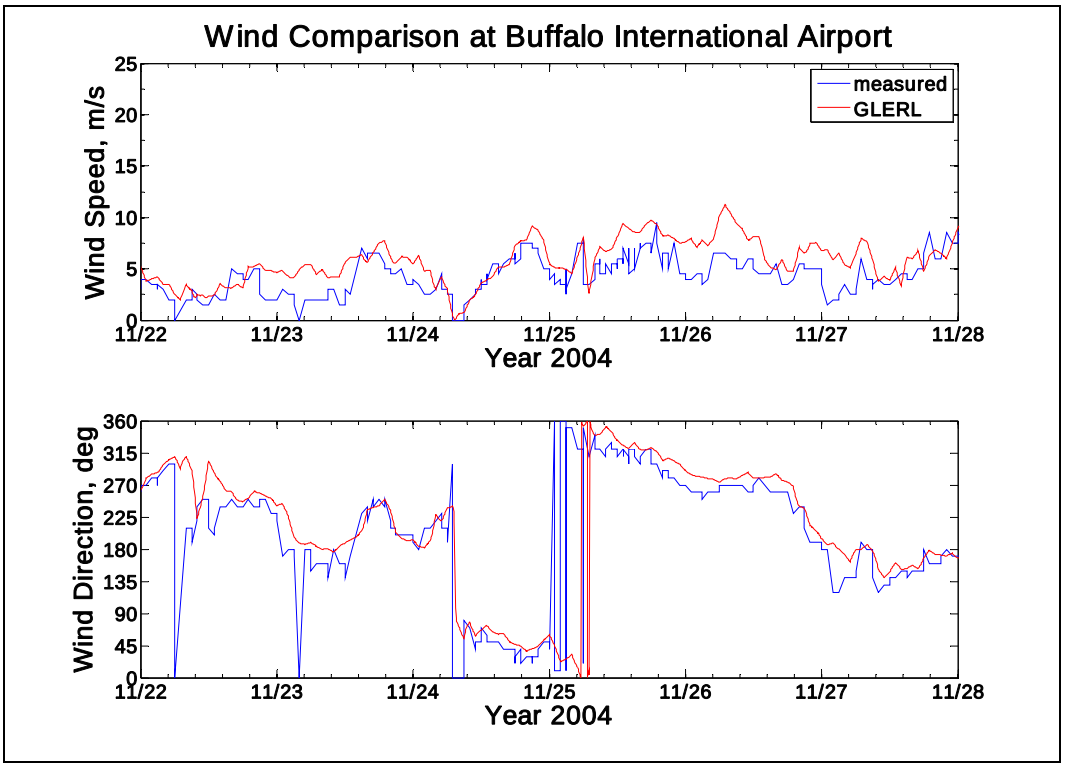

Figure 2-21. Comparison of GLERL-generated and measured wind speeds and directions: Buffalo International Airport, 22-28 Nov 2004.

Figure 2-22. Plan CDF Configuration 1.

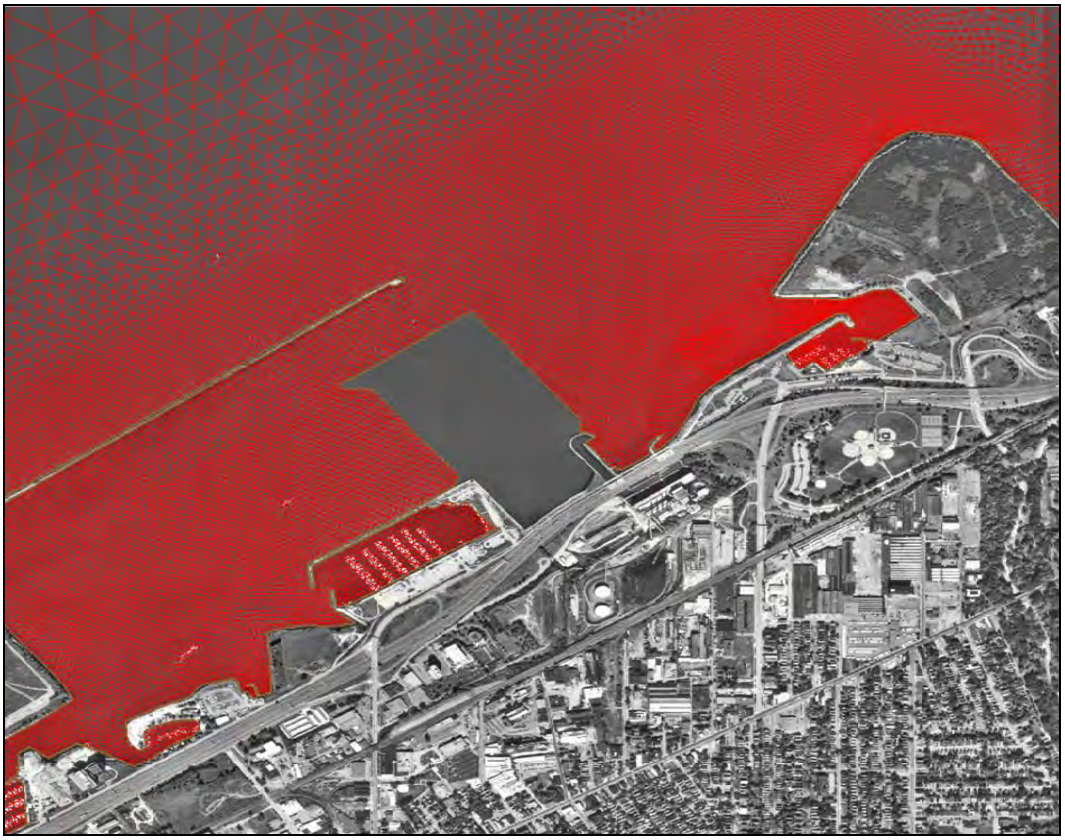

Figure 2-23. Plan Configuration 1.

Figure 2-24. Plan CDF Configuration 2.

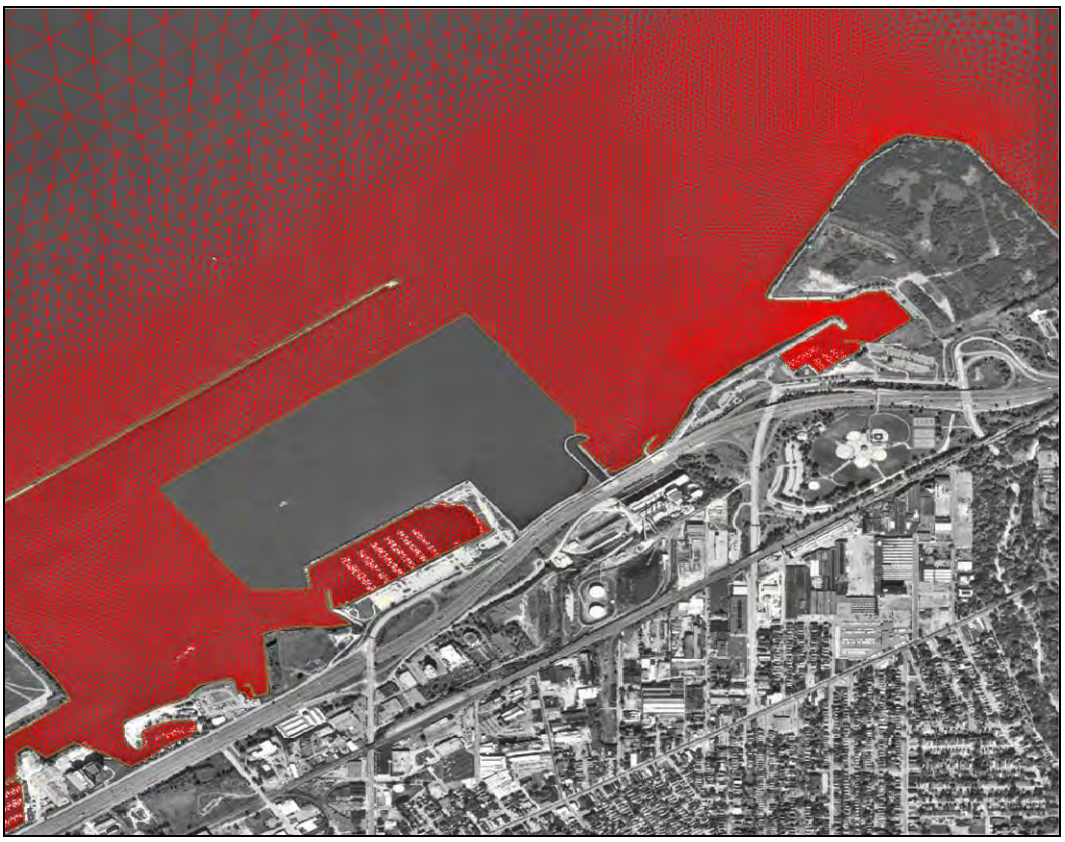

Figure 2-25. Plan Configuration 2.

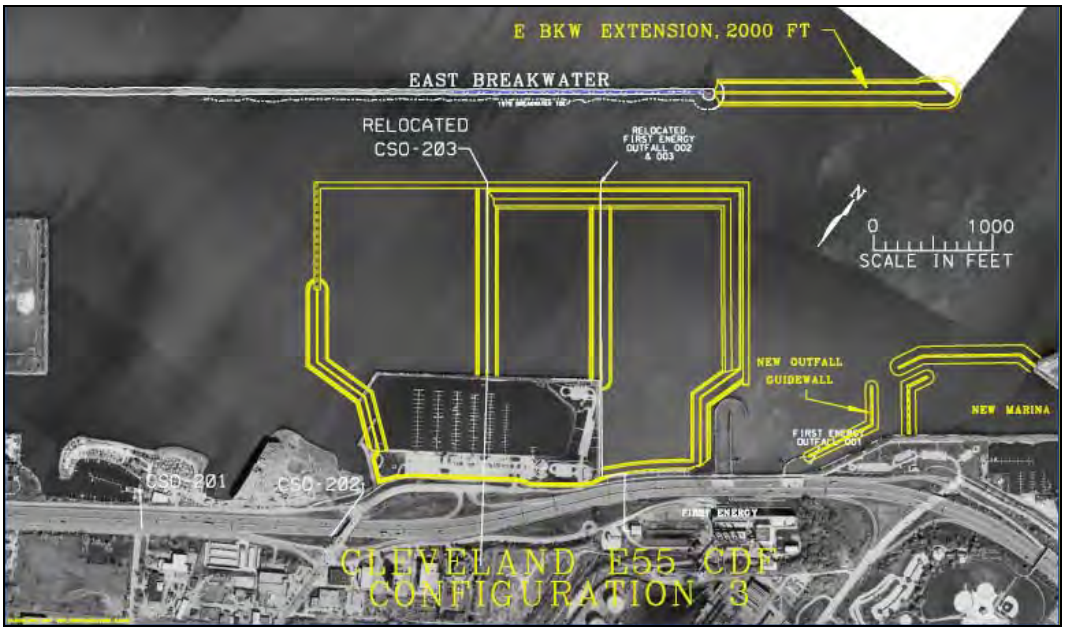

Figure 2-26. Plan CDF Configuration 3.

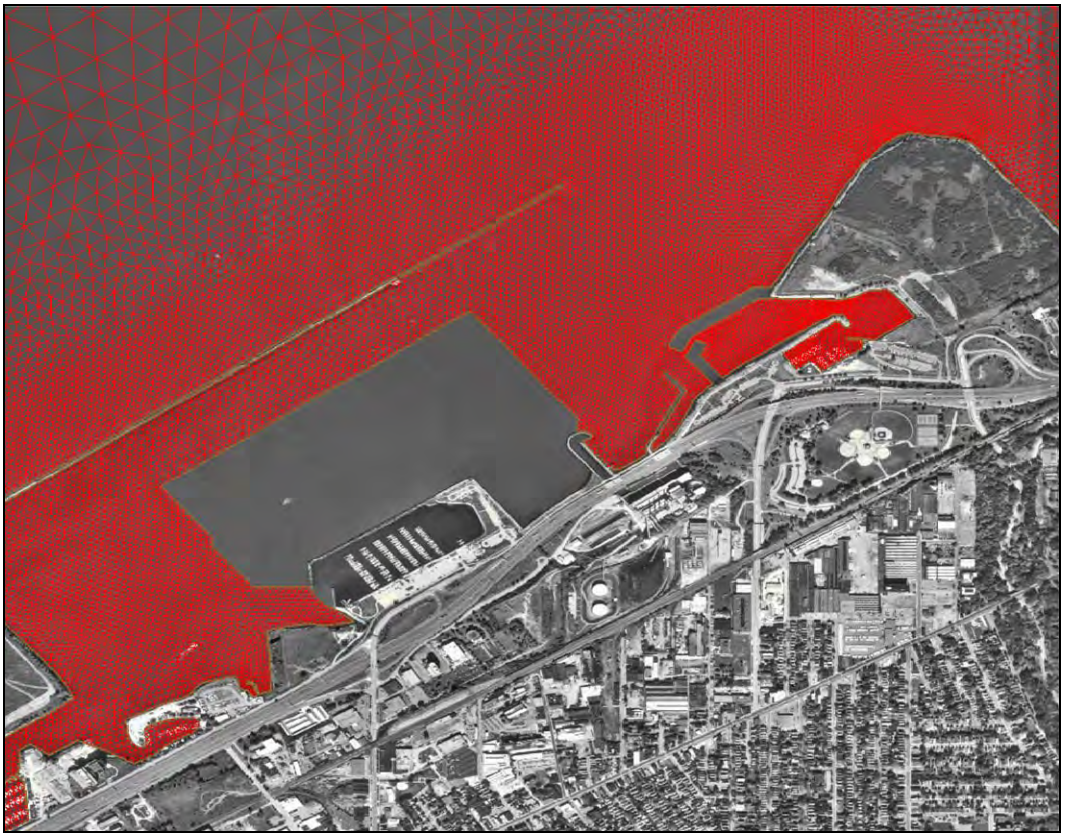

Figure 2-27. Plan Configuration 3.

Aligned with the eastern limit of the breakwater sheltering the East 55th St. Marina, Configuration 1 extends 730 m from the shoreline towards the northwest and measures 470 m in the alongshore direction. As such, the width of the federally-maintained Harbor channel is decreased from 65 m to 50 m.

Relative to Configuration 1, Configuration 2 extends further to the southwest by approximately 638 m, terminating at the entrance to the East 55th St. Marina. Differences between Configuration 2 and 3 are: 1) the East 55th St. Marina is filled, becoming part of the CDF; 2) jetties are placed at the entrance to the Gordon Park marina, which resides east of the power plant outfall; 3) a guide wall separates the outfall discharge from the intake; and, 4) the East Breakwater is extended by 610 m.

The existing-condition or base grid was developed with nodes lying along the outer extents/limits of each CDF configuration. Developing the grid in this manner permits each CDF to be readily incorporated into the base grid by deleting those elements and nodes lying within the lateral extents of each particular CDF. This also permits more accurate comparison between alternatives to be made because the nodal positions and their connectivity (i.e., elements) were not changed.

A series of simulations were conducted for evaluating the hydrodynamic changes induced by constructing the three CDFs. The first series is a hindcast simulation of the November 2004 storm used in validating the ADCIRC model where the base and three configurations were simulated for this period.

Figures 2-28 through 2-31 display the peak westerly current during the November storm, whereas Figures 2-32 through 2-35 display the peak easterly current. Under easterly wind conditions, the westerly currents within the modified channel increased from about 0.05 m/s to approximately 0.4 m/s for Configuration 1 (Figure 2-36). Similar increases were noted for Configurations 2 and 3, where the peak currents increased to 0.4 m/s for both planned conditions. Stronger currents induced by the planned CDFs are attributed to the reduced cross-sectional area within the channel.

Current in Gordon Park Marina can be characterized as weak. Time-series of model-generated current for the base and three planned configurations for the marina is presented in Figure 2-37. As shown, the planned configurations do not appear to have an appreciable impact on current strength in the marina. This observation should not be construed that the CDFs will have no impact on flushing rates in this marina or that the planned construction will not degrade

water quality. To make these determinations, a particle-tracking or water-quality model, which account for transport and flux of material within the Harbor system will need to be used.

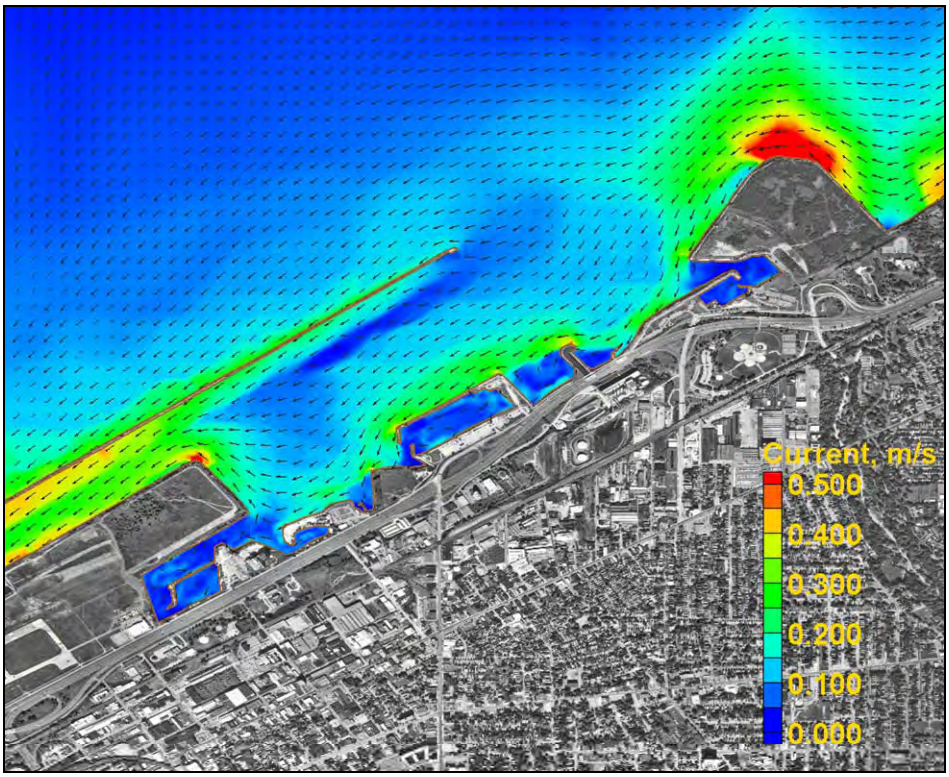

Figure 2-28. Base Configuration: Peak model-generated current during November 2004 storm (16 November 20:00:00 GMT).

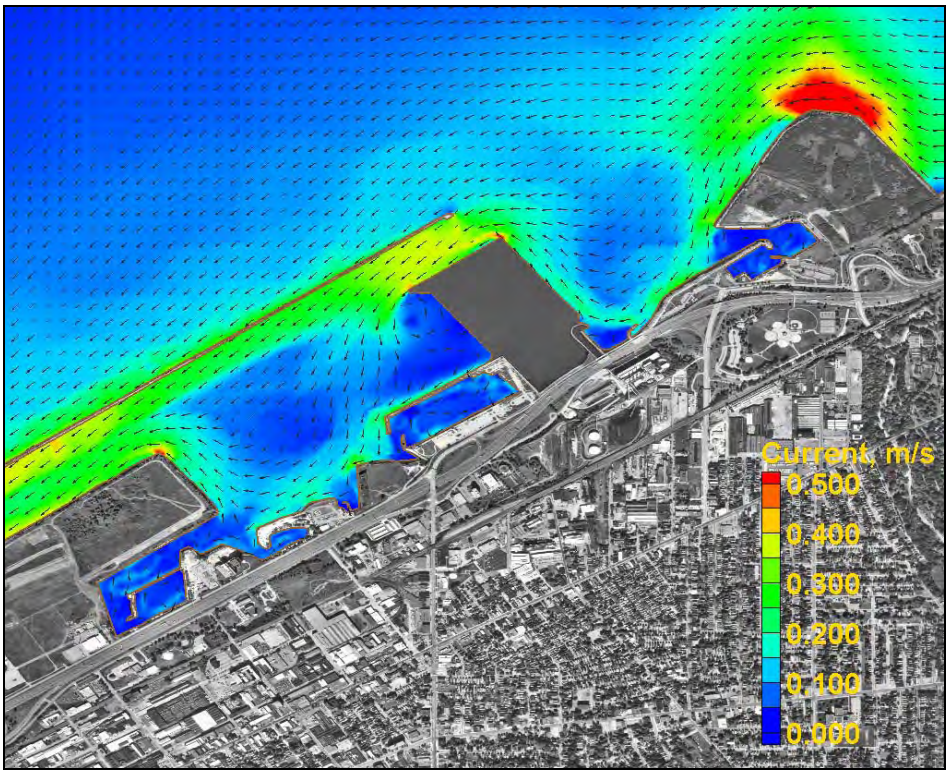

Figure 2-29. Plan Configuration 1: Peak model-generated current during November 2004 storm (16 November 20:00:00 GMT).

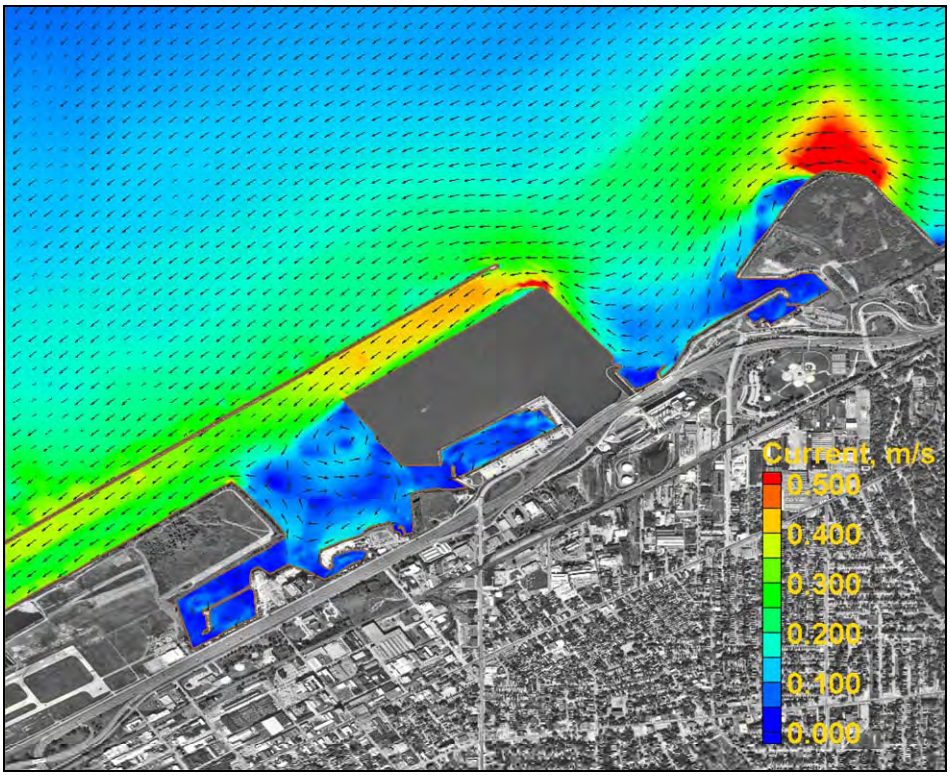

Figure 2-30. Plan Configuration 2: Peak model-generated current during November 2004 storm (16 November 20:00:00 GMT).

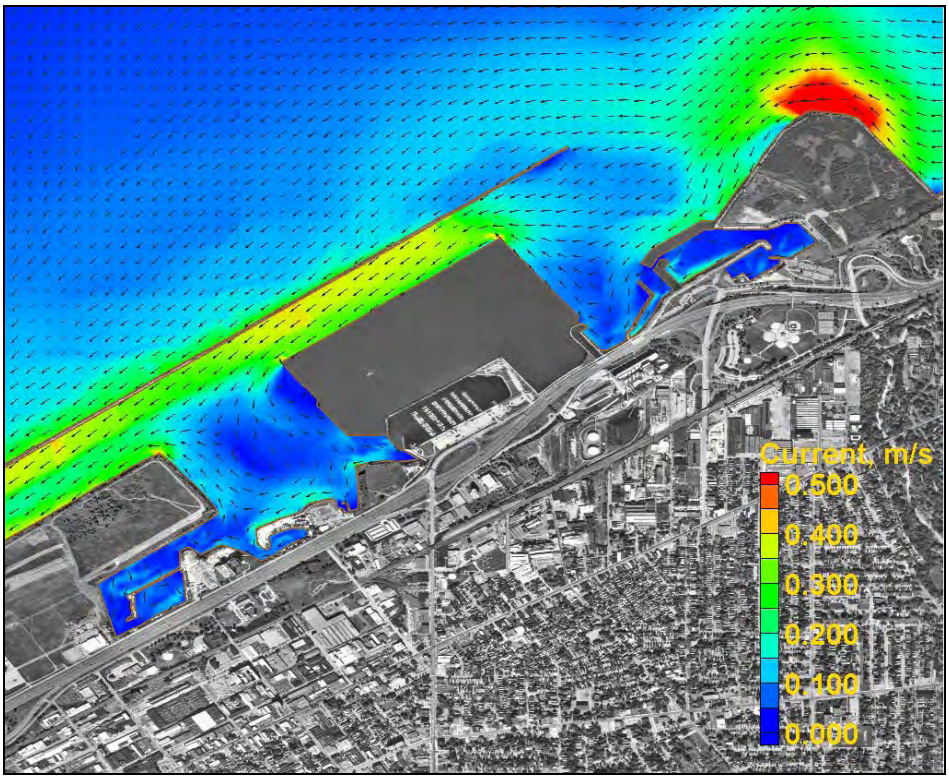

Figure 2-31. Plan Configuration 3: Peak model-generated current during November 2004 storm (16 November 20:00:00 GMT).

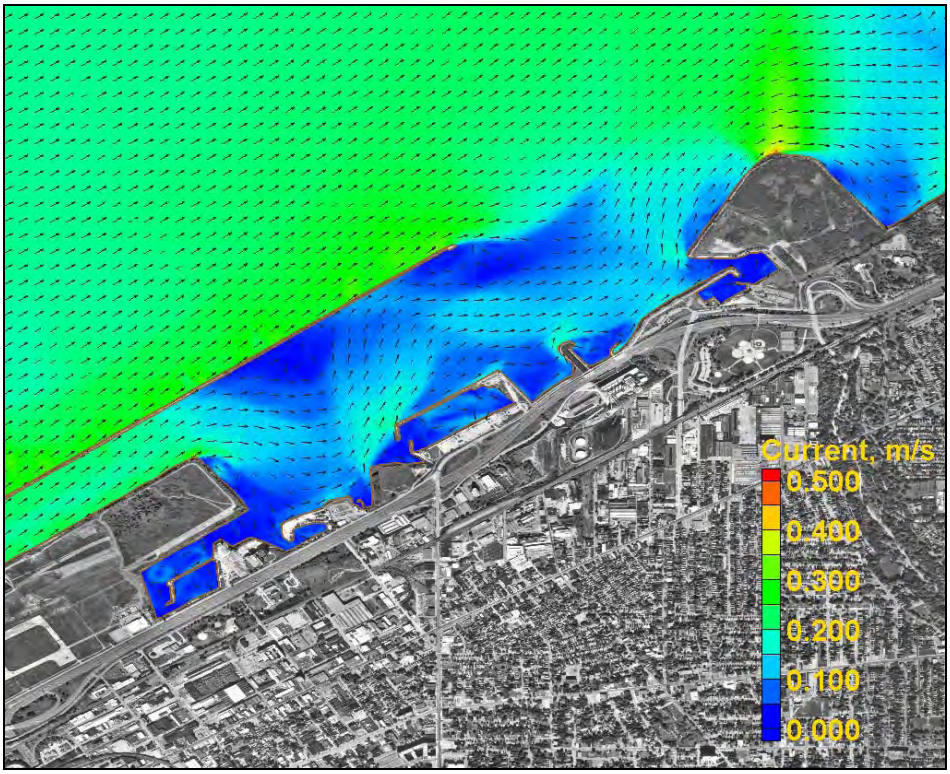

Figure 2-32. Base Configuration: Peak model-generated current during November 2004 storm (17 November 19:00:00 GMT).

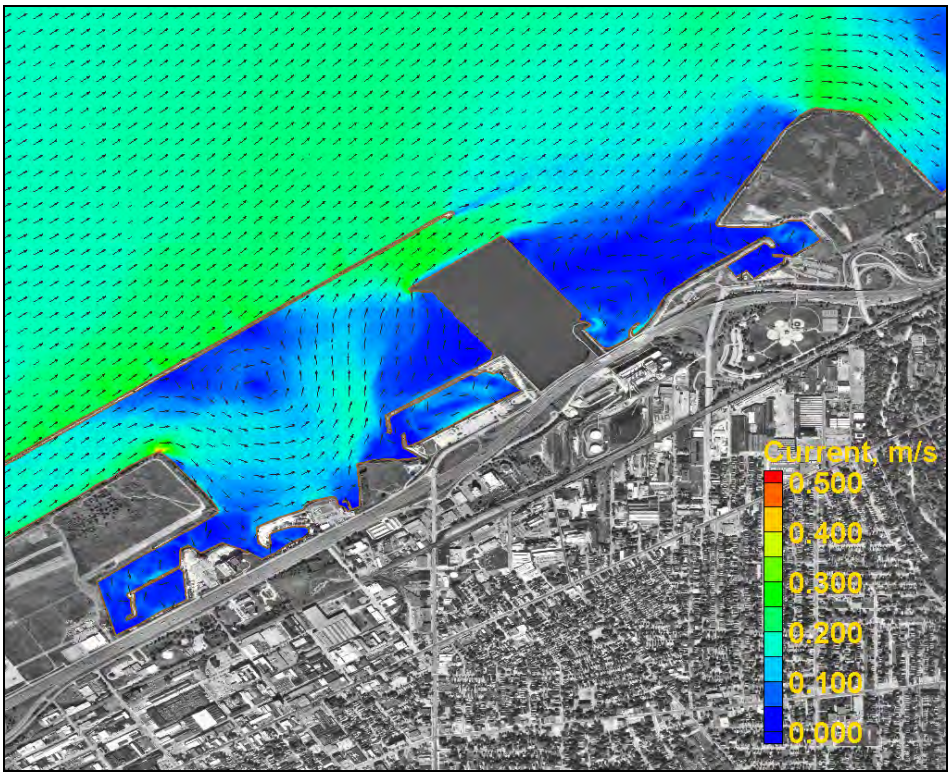

Figure 2-33. Plan Configuration 1: Peak model-generated current during November 2004 storm (17 November 19:00:00 GMT).

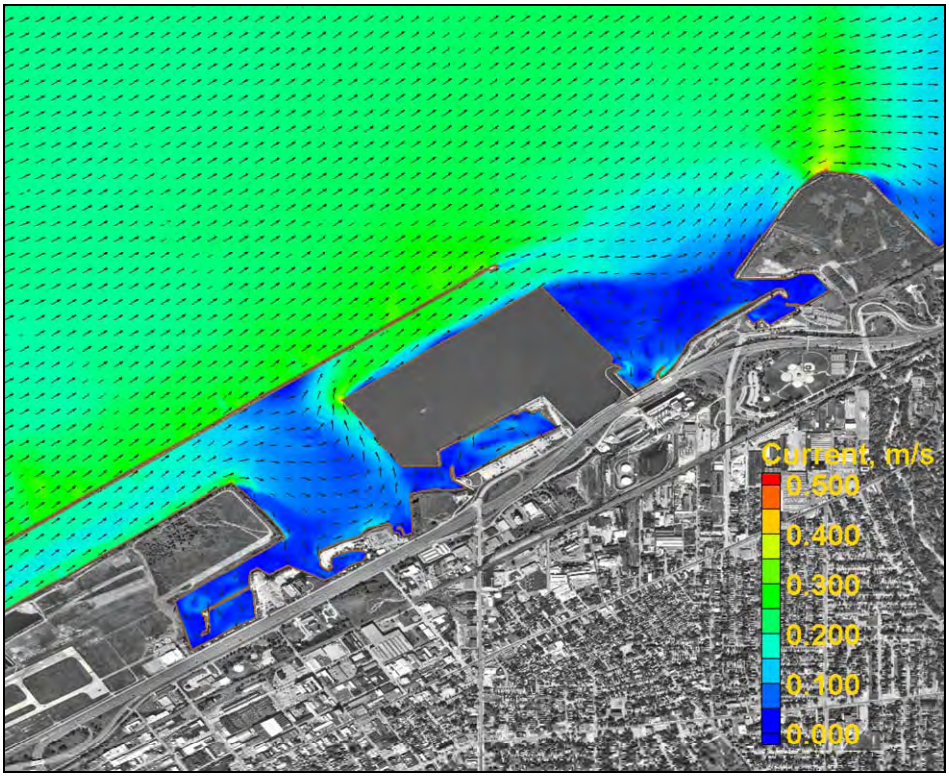

Figure 2-34. Plan Configuration 2: Peak model-generated current during November 2004 storm (17 November 19:00:00 GMT).

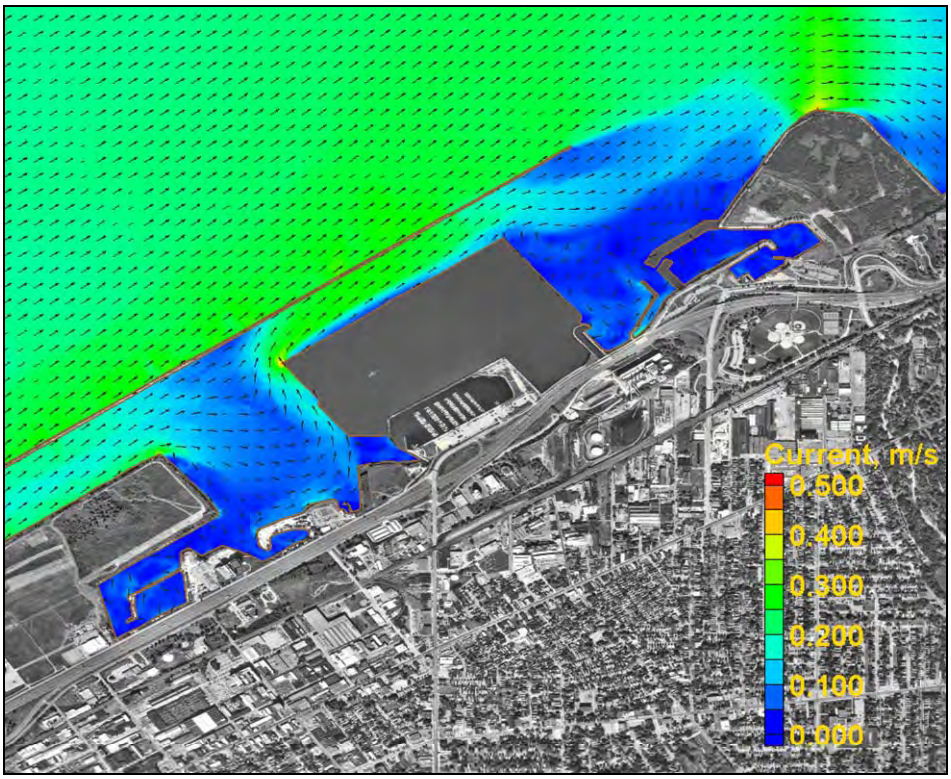

Figure 2-35. Plan Configuration 3: Peak model-generated current during November 2004 storm (17 November 19:00:00 GMT).

Current at the East 55th Street Marina entrance can, also, be characterized as weak. Time-series of model-generated current for the base and three planned configurations for the marina is presented in Figure 2-38. As shown, the planned configurations appear to weaken the current, from about 0.15 m/s to 0.10 m/s during peak westerly current. The change in current strength is attributed to the sheltering caused by the planned configurations. As with the Gordon Park Marina, this observation should not be construed that the CDFs will impact flushing rates in this marina or that the planned construction will not degrade water quality.

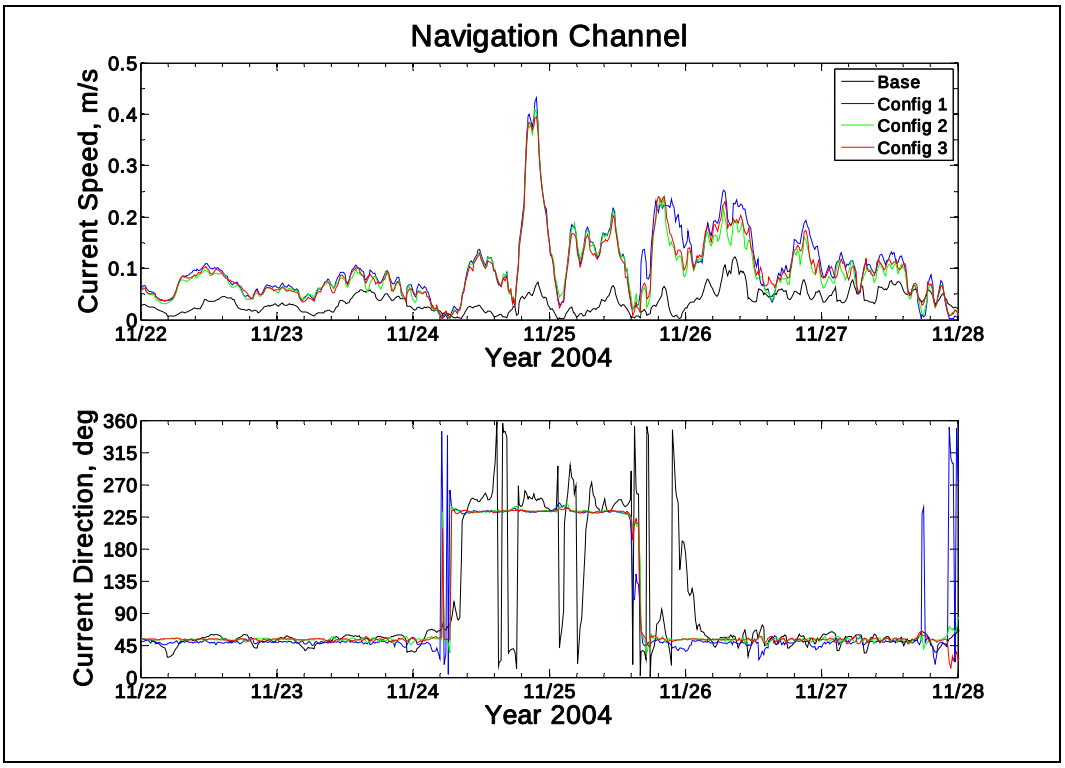

Figure 2-36. Comparison of current within the Navigation Channel.

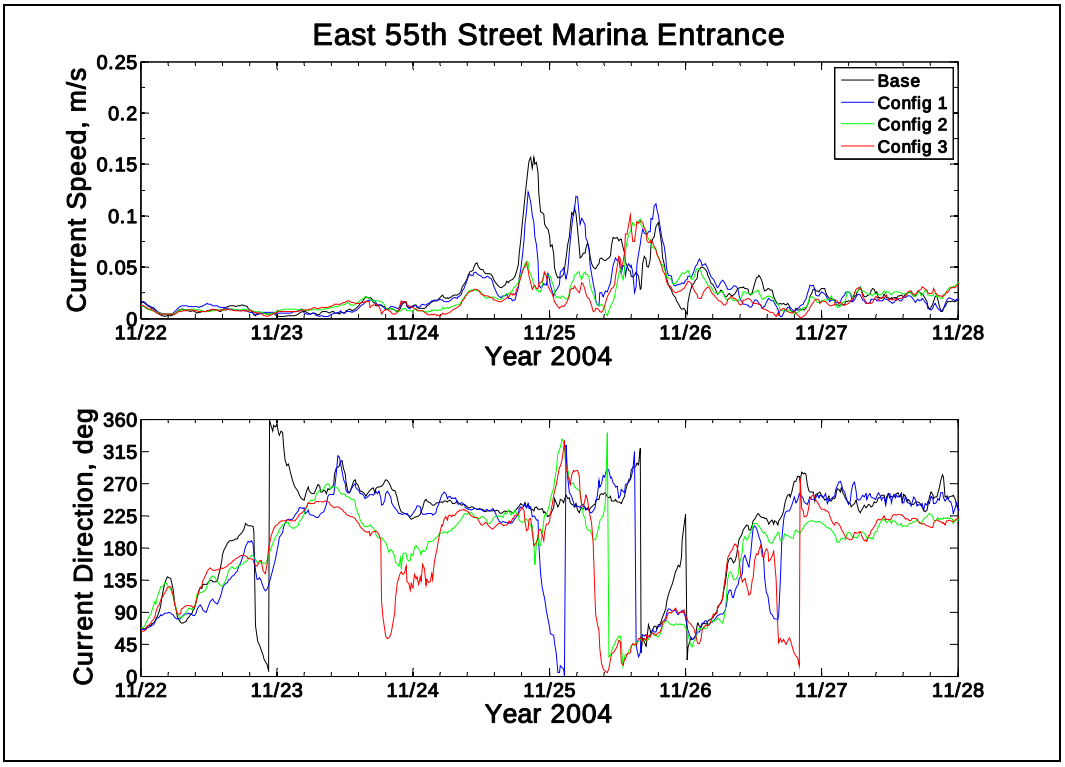

Figure 2-37. Comparison of current at the East 55th Street Marina Entrance.

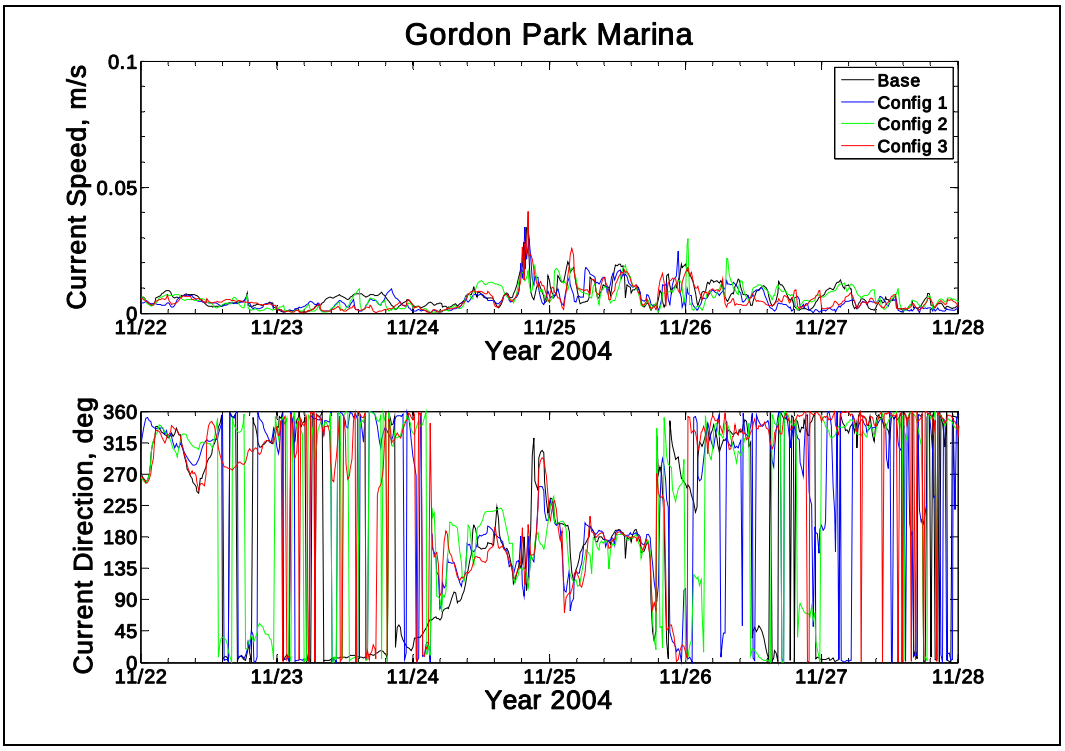

Figure 2-38. Comparison of current within Gordon Park Marina.

3 Thermal Transport Modeling

The three dimensional numerical hydrodynamic model CH3D-WES (Curvilinear Hydrodynamics in Three Dimensions–Waterways Experiment Station) can be applied in two vertical resolution modes, Z-grid and Sigma–grid. The Z-grid version is documented in Johnson, et al. (1991b). The Sigma-grid version, used in this study, is documented in Chapman et al. (1996). The basic Sigma-grid model (CH3D) was developed by Sheng (1986) for WES but has been extensively modified, including the development of the Z-grid version. These modifications have consisted of implementing different basic numerical formulations of the governing equations as well as substantial recoding of the model to provide additional computational efficiency. As its acronym implies, CH3D-WES performs hydrodynamic computations on a curvilinear or boundary-fitted plan-form grid. Physical processes impacting circulation and vertical mixing that are modeled include tides, wind, density effects (salinity and temperature), freshwater inflows, turbulence, and the effect of the earth's rotation.

The boundary-fitted coordinate feature of the model provides grid resolution enhancement necessary to adequately represent deep navigation channels and irregular shoreline configurations of the flow system. The curvilinear grid also permits adoption of accurate and economical grid schematization software. The solution algorithm employs an external mode, consisting of vertically averaged equations, which provides a solution for the free surface displacement for input to the internal mode, which contains the full 3D equations.

CH3D Hydrodynamic and Thermal Transport Simulations

The potential impact of the planned construction of the E 55th Street CDF on the near-field temperature distribution associated with the heated water discharge from the First Energy power plant (Figure 3-1) was investigated utilizing a depth averaged or single vertical layer CH3D hydrodynamic grid (Figure 3-2). The CH3D grid consists of 236 alongshore cells and 85 cross-shore cells, of which 14,944 are active computation cells with a fine-scale resolution of 5 to 10 meters. Details of the near-field region in the vicinity of the intake and outfall structures are shown in Figure 3–3 with overlays of proposed construction options. The modified grid resulting from the implementation of Configuration 2 is shown in

Figure 3-4, where it is seen that formerly active computational cells have been removed to represent the CDF.

Figure 3-1. Google Earth snapshot of the First Energy Power Plant, thermal outfall (right) and cooling water intake (left) structures.

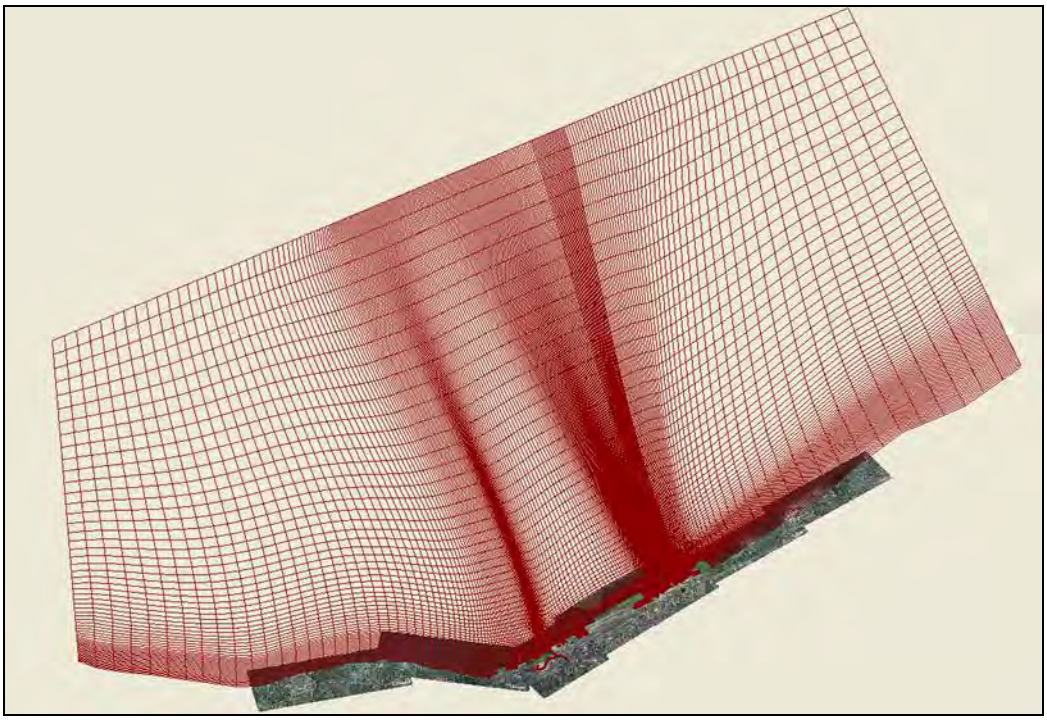

Figure 3-2. Cleveland Harbor CH3D boundary-fitted grid.

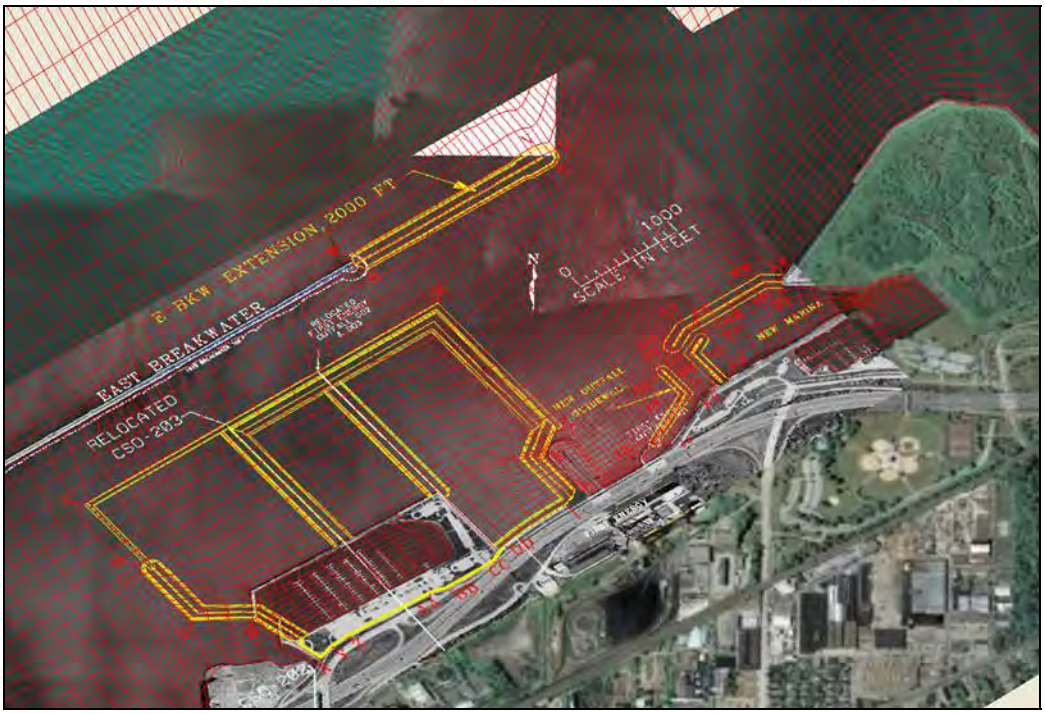

Figure 3-3. Near-field Cleveland Harbor CH3D grid with planned configuration options.

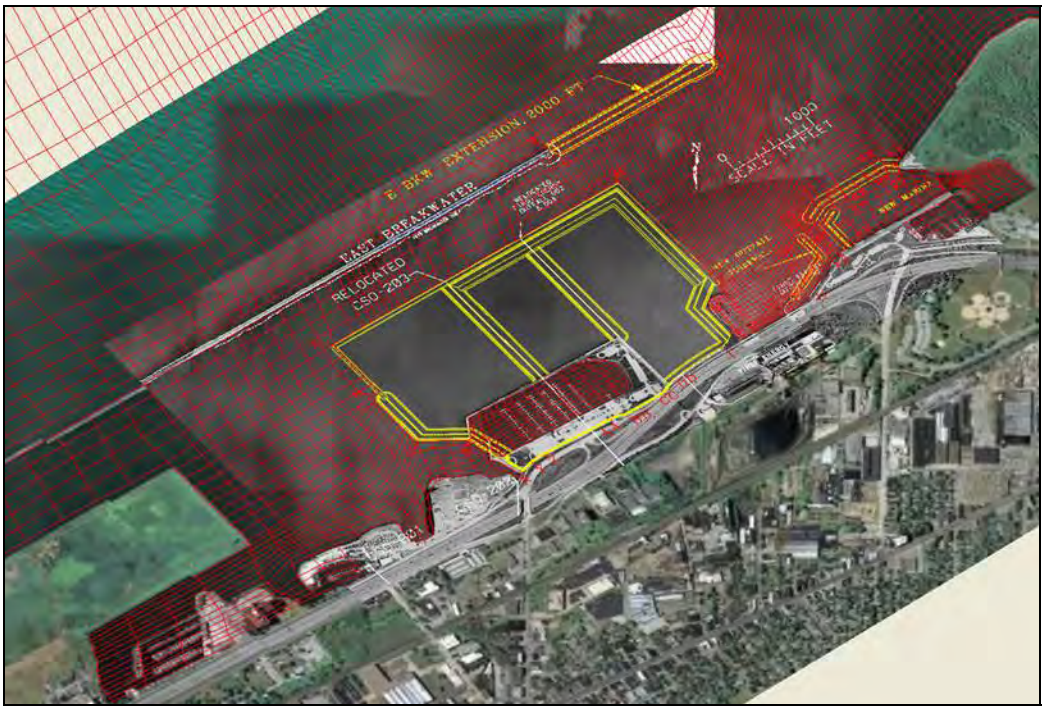

Figure 3-4. Near-field Cleveland Harbor CH3D Configuration 2 grid.

The physical boundaries and bathymetry defined within the CH3D grid were extracted from the ADCIRC grid, as described in the previous chapter. Boundary forcing utilized ADCIRC surface elevations at the open-water boundaries, spatially constant time-varying NDBC and Burke Airport wind components, USGS-measured Cuyahoga River flows, together with outfall and intake flow and temperature data measured at the 1st Energy Plant. In order to investigate variation in temperature distributions within Cleveland Harbor, the temperature of Lake Erie was initialized to 22° C. Hydrodynamic and thermal distribution results were generated for the months of July and August, 2002 subsequent to a 15-day model spin-up period. The results of these simulations have been provided to the District in the form of AVI's and Gulfview animation data along with the required programs to view the results. In addition to viewing temperature and velocity files, particles can be distributed interactively throughout the grid using Gulfview. Examination of the simulation animations illustrates the large variation in the circulation and thermal patterns. For example, Figure 3-5 is a Gulfview snapshot of the existing configuration temperature on 4 August 2002 when the wind was blowing from the east-northeast (Figure 3-6). As shown in Figure 3-5, significant recirculation of the thermal outfall discharge into cooling water intake occurs. The variation of temperature (Celsius) is shown in the bar scale at the bottom of Figure 3-5.

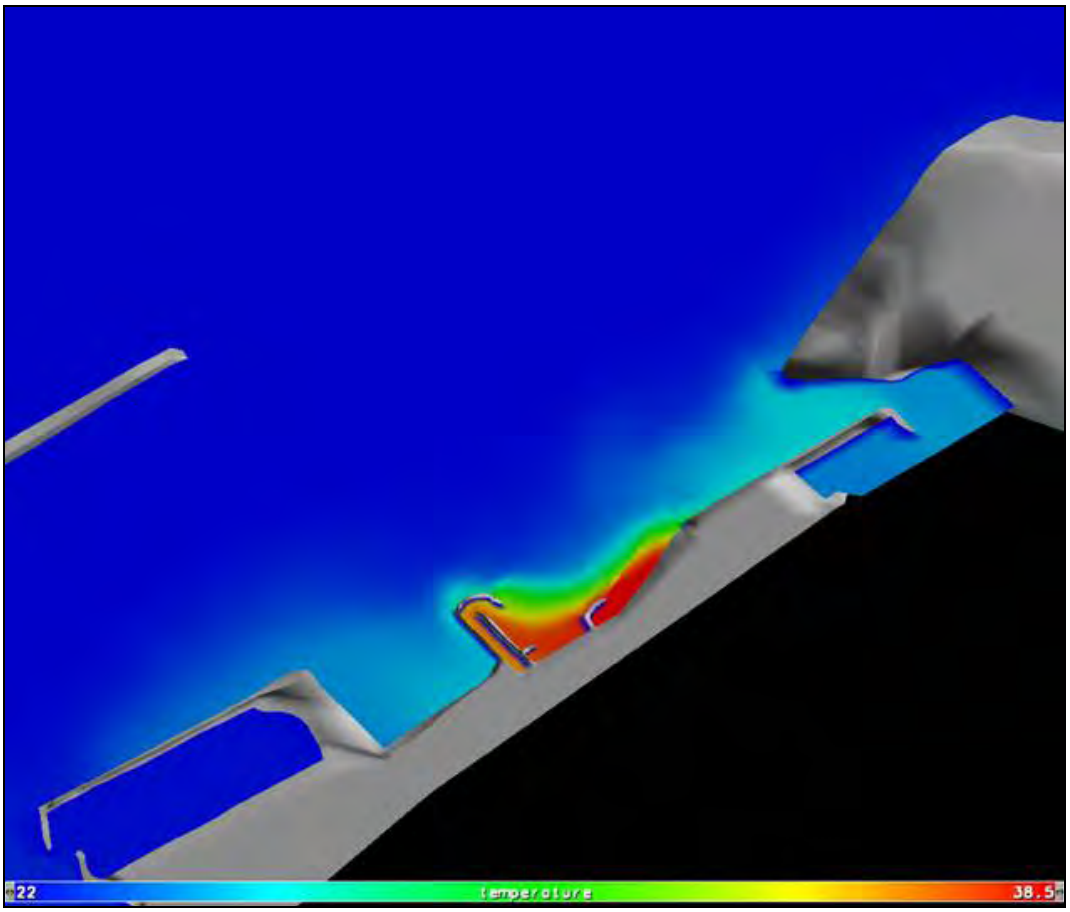

Figure 3-5. Gulfview snapshot of existing configuration temperature distribution during an easterly wind event (4 August 2002); Temperature in deg C.

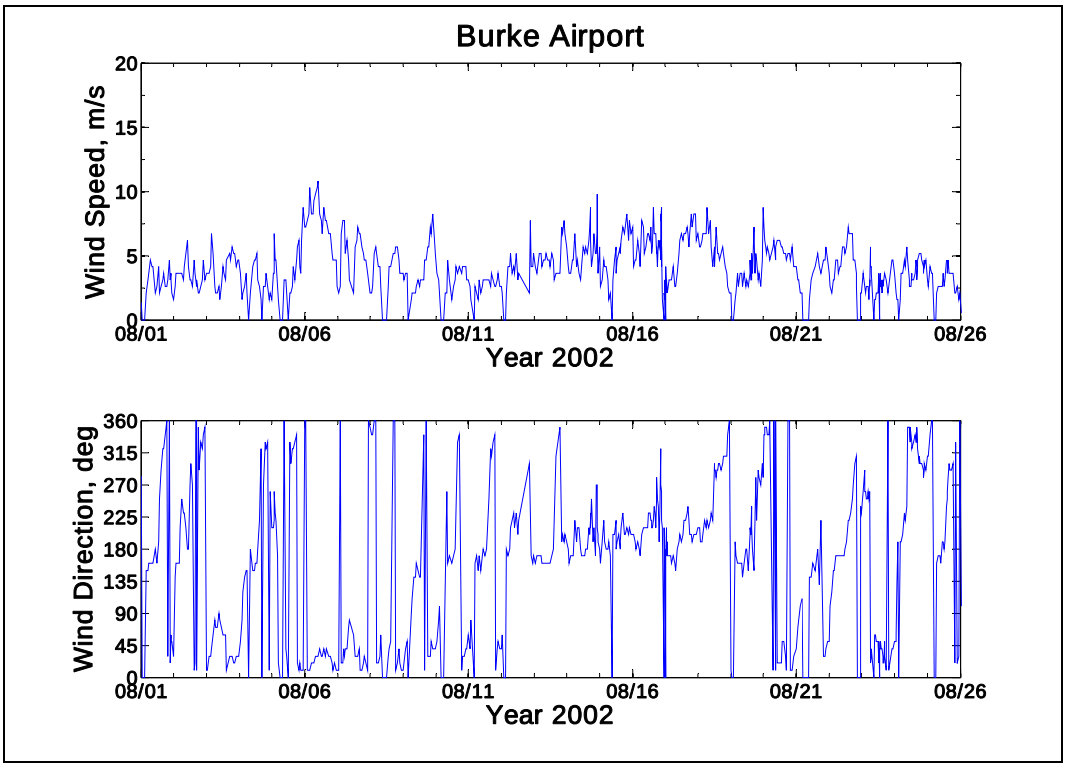

Figure 3-6. Time-series of wind speed and direction measured at Burke Airport.

A Gulfview snapshot corresponding to 25 August 2002, in which the wind had shifted to the northwest, is shown in Figure 3-7. It is seen that as the wind shifts westerly more of the thermal discharge energy is transported away from the intake structure resulting in lower intake temperatures.

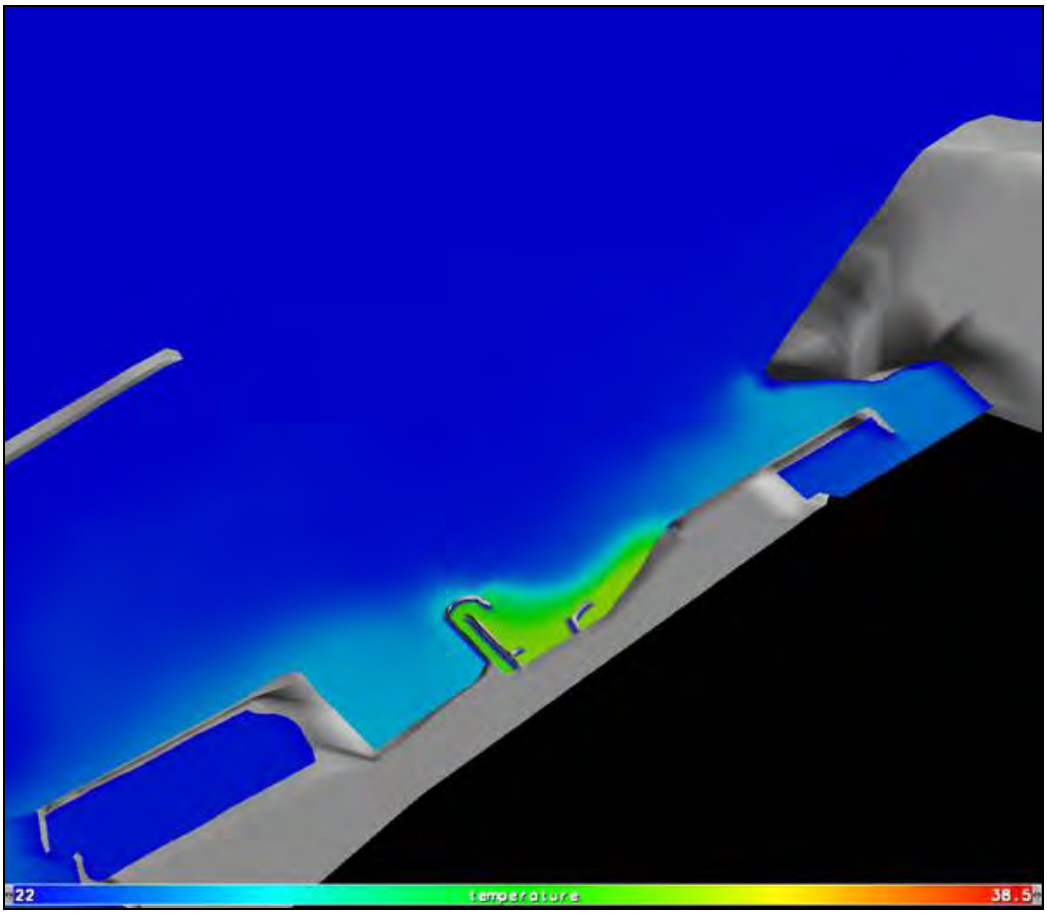

Figure 3-7. Gulfview snapshot of existing configuration temperature distribution during a westerly wind event (25 August 2002); Temperature in deg C.

A similar response is seen in Figures 3-8 and 3-9 where AVI snapshots are presented for the Base configuration and Configuration 2 during the 5 July northeasterly event, respectively. Winds recorded at Burke Airport for this period is presented in Figure 3-10. It is seen that the intake temperature exceeds 33° C with northeasterly wind forcing and is less than 25° C during southwesterly wind forcing. Further analysis of the influence of the CDF configuration on the harbor wide temperature distribution was pursued by developing temperature difference animations. The temperature difference animations were generated by subtracting the predicted base condition temperature throughout the grid from that of the three CDF configurations. Harbor temperatures are displayed in Figures 3-11 and 3-12 for the Base configuration and Configuration 2 during the 28 June southwesterly wind event. Figures 3-12 through 3-14 display the temperature differences between the Base and the 3 planned configurations.. These figures show that the maximum temperature increase associated with Configurations 1 and 2 is less that 4° C, a minimal effect on the intake temperature and an increase of 2° C within the Gordon Park Marina. Configuration 3, with the extended outfall guide wall and additional breakwaters, shows local temperature increases of 5^{0} C and a 1° C increase at the intake and in the Gordon Park Marina.

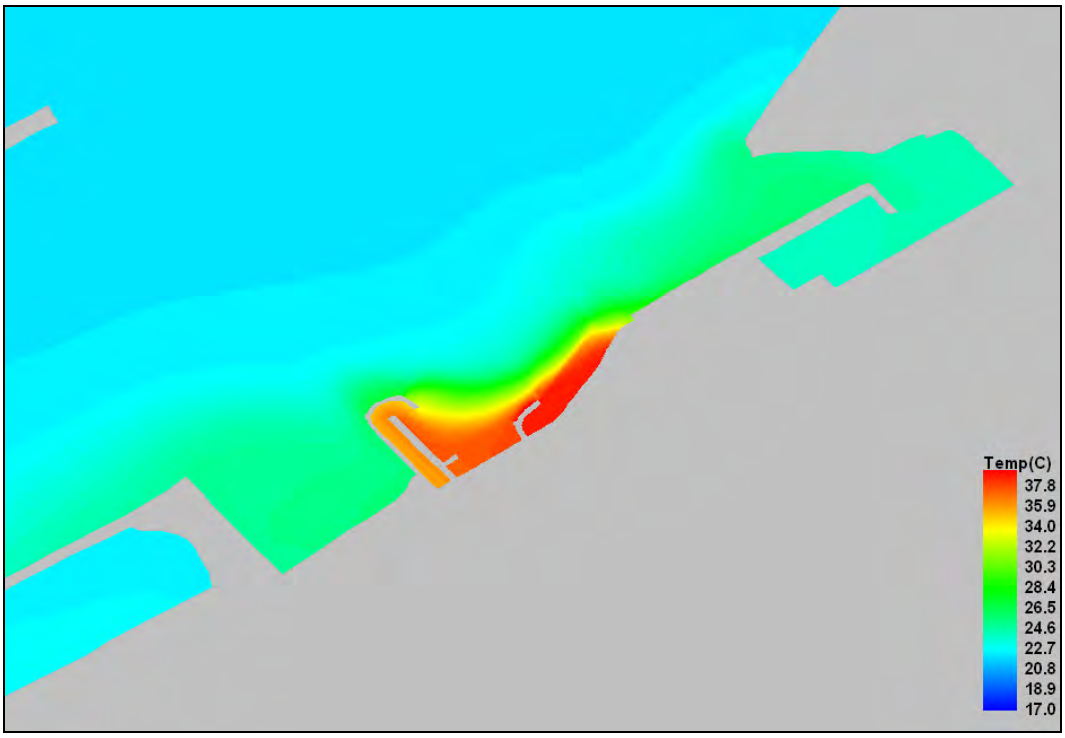

Figure 3-8. AVI snapshot of Base Configuration temperature during a northeasterly wind event (5 July 2002); Temperature in deg C.

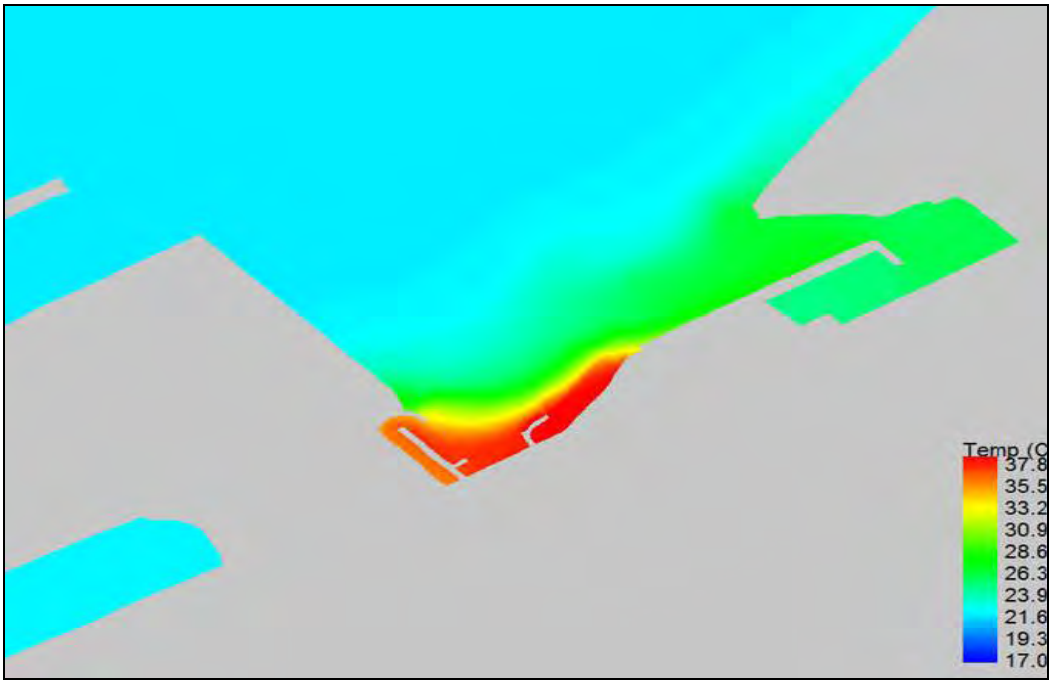

Figure 3-9. AVI snapshot of Configuration 2 temperature during a northeasterly wind event (5 July 2002); Temperature in deg C.

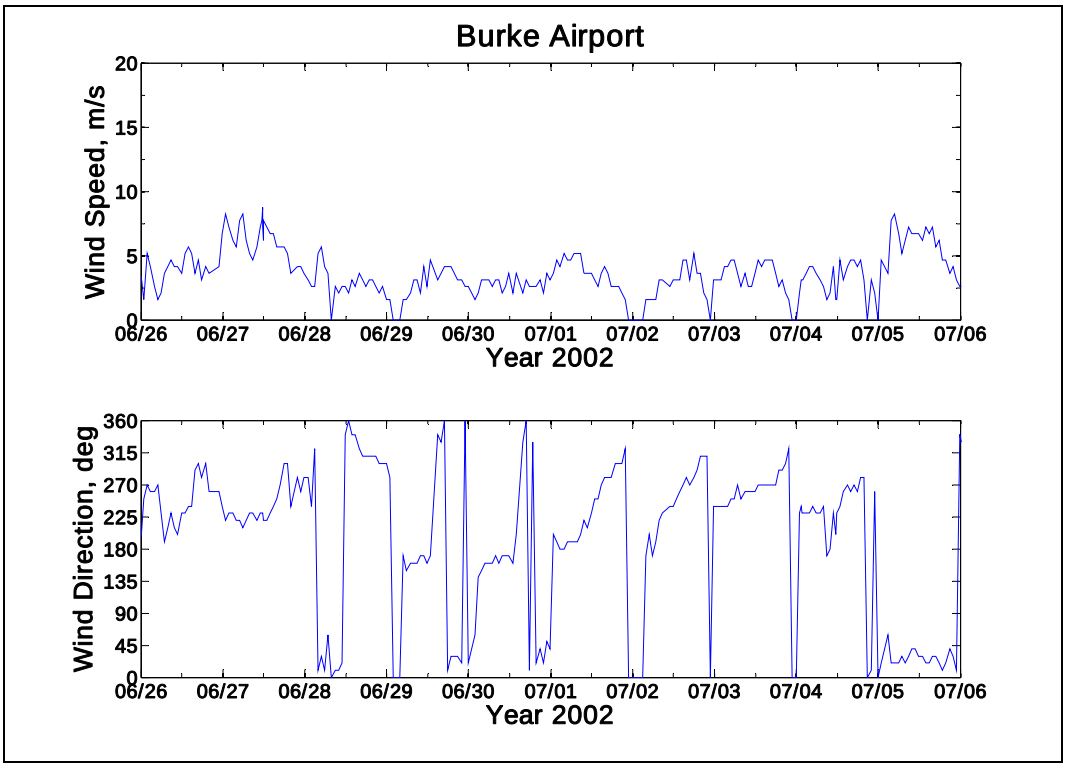

Figure 3-10. Time-series of wind speed and direction measured at Burke Airport.

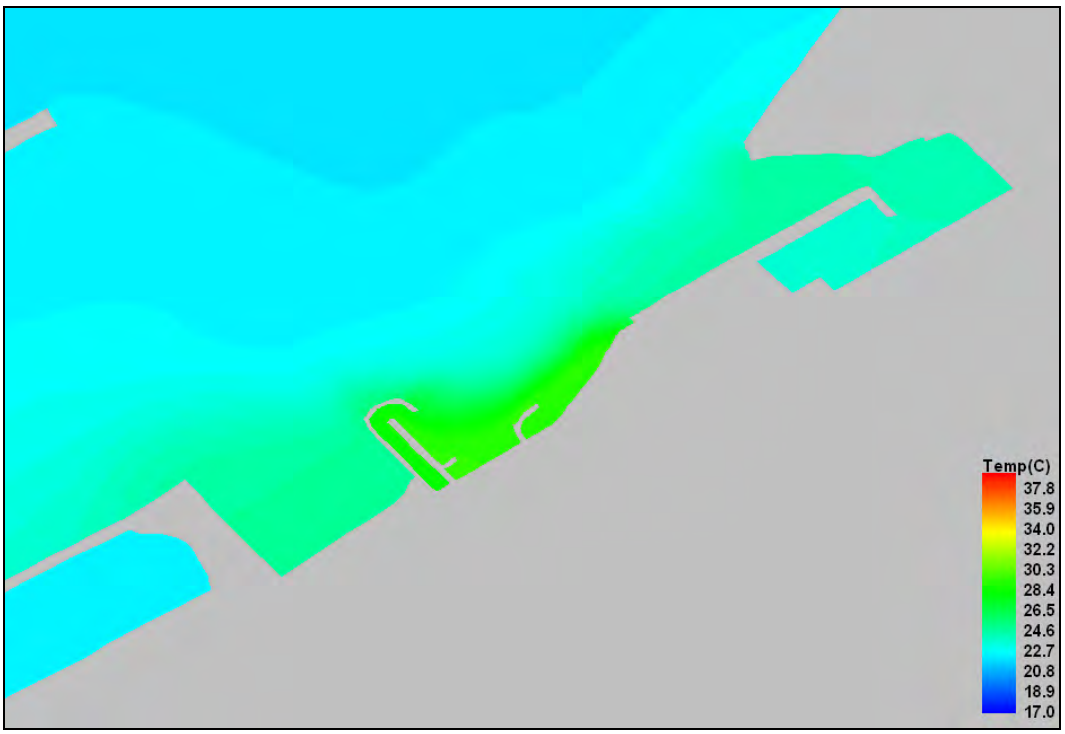

Figure 3-11. AVI snapshot of Base Configuration temperature during a southwesterly wind event (28 June 2002); Temperature in deg C.

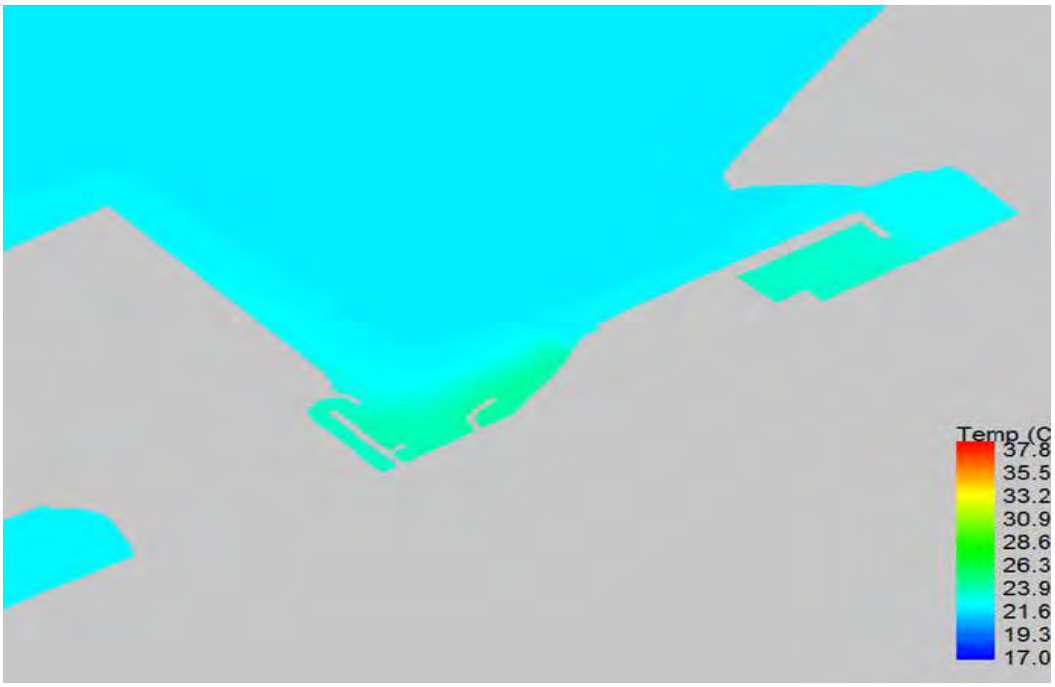

Figure 3-12. AVI snapshot of Configuration 2 temperature distribution during a southwesterly wind event (28 June 2002); Temperature in deg C.

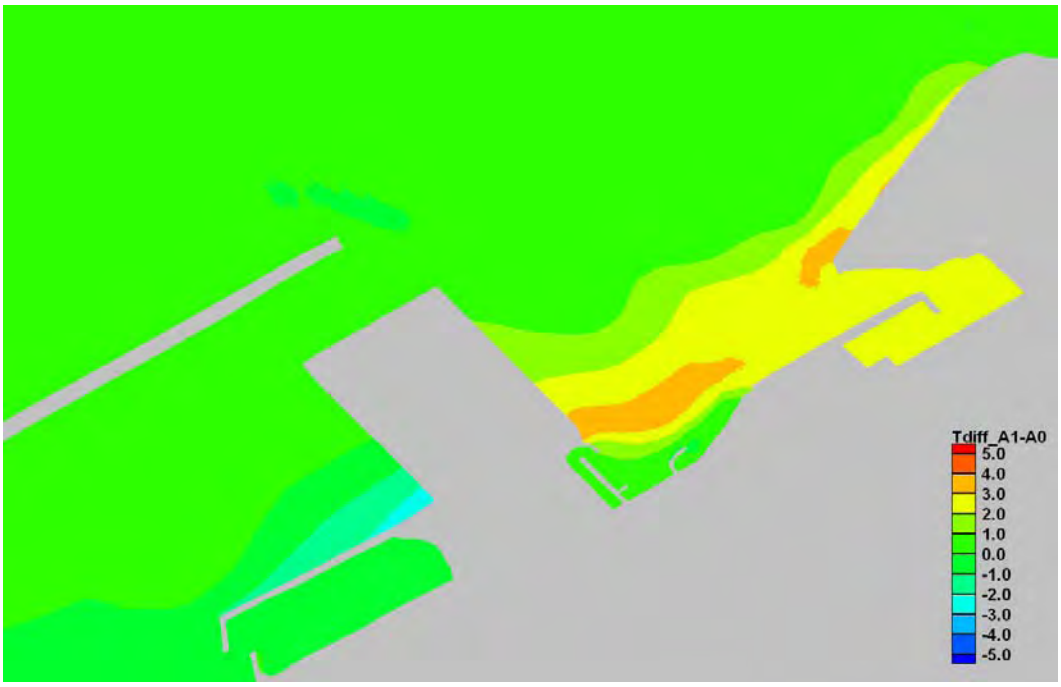

Figure 3-13. AVI snapshot of Configuration 1 temperature differences during a northeasterly wind event (5 July 2002); Temperature in deg C.

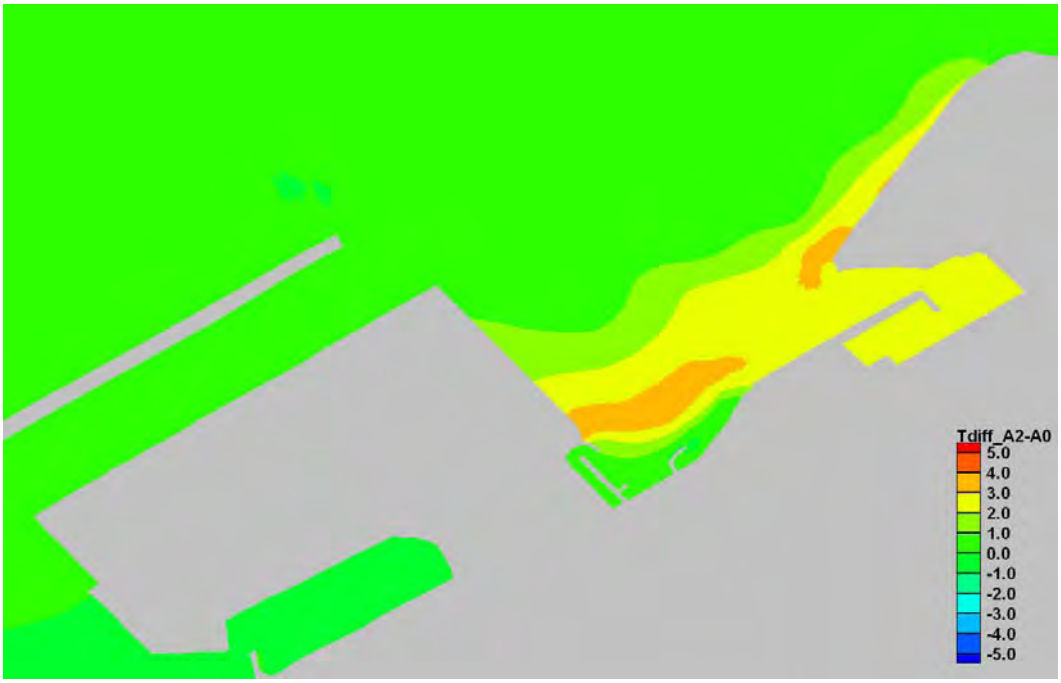

Figure 3-14. AVI snapshot of Configuration 2 temperature differences during a northeasterly wind event (5 July 2002); Temperature in deg C.

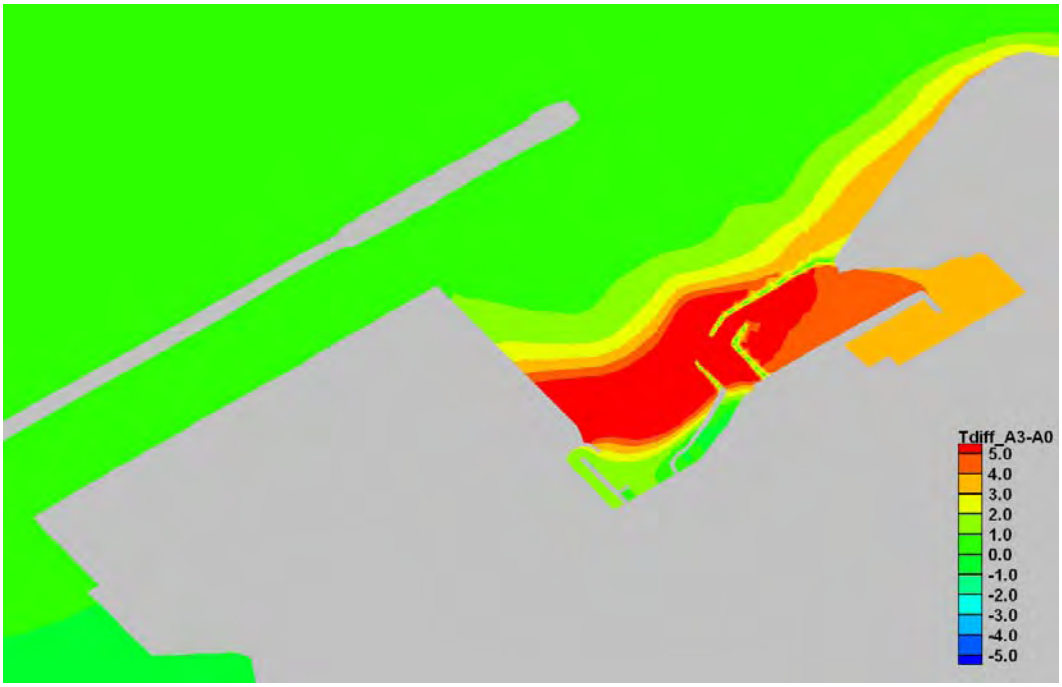

Figure 3-15. AVI snapshot of configuration 3 temperature differences during a northeasterly wind event (5 July 2002); Temperature in deg C.

Figure 3-15 displays the Harbor temperatures on 28 June during a southwesterly wind event for the base condition. Figures 3-16 through 3-18 display temperature differences for Configurations 1 through 3, respectively. These figures show that the maximum temperature increase associated with Configurations 1 and 2 are less that 3° C and a minimal effect on the intake temperature. Configuration 3 results in a local temperature increased of 5^{0} C and about a 1° C increase in temperature at the intake and in the Gordon Park Marina.

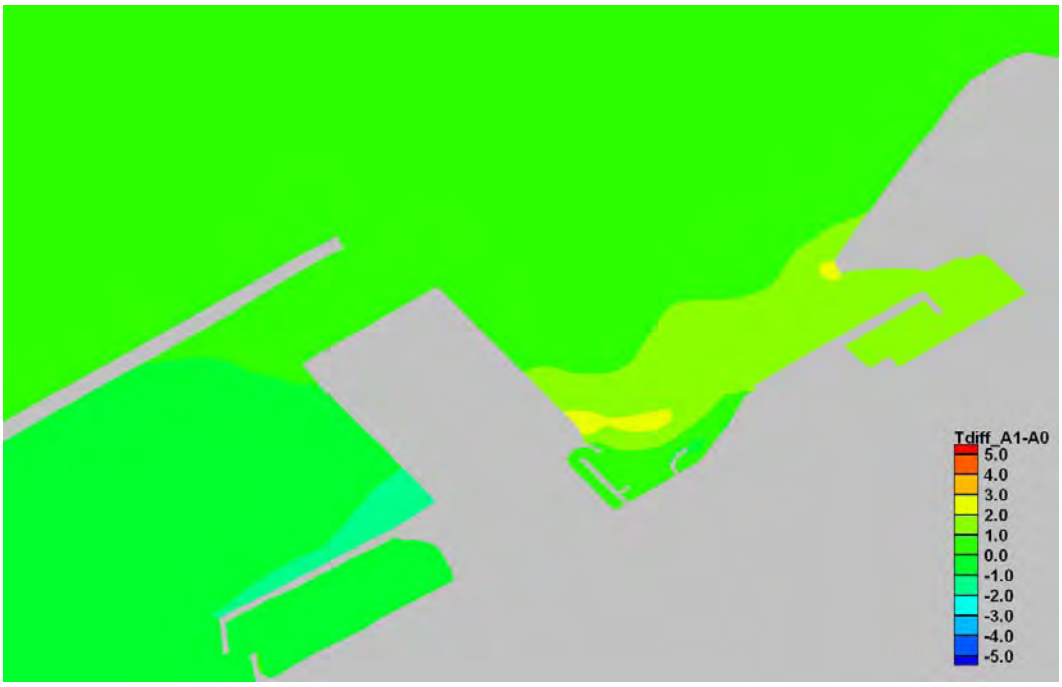

Figure 3-16. AVI snapshot of Configuration 1 temperature differences during a southwesterly wind event (28 June 2002); Temperature in deg C.

Figure 3-17. AVI snapshot of Configuration 2 temperature differences during a southwesterly wind event (28 June 2002); Temperature in deg C.

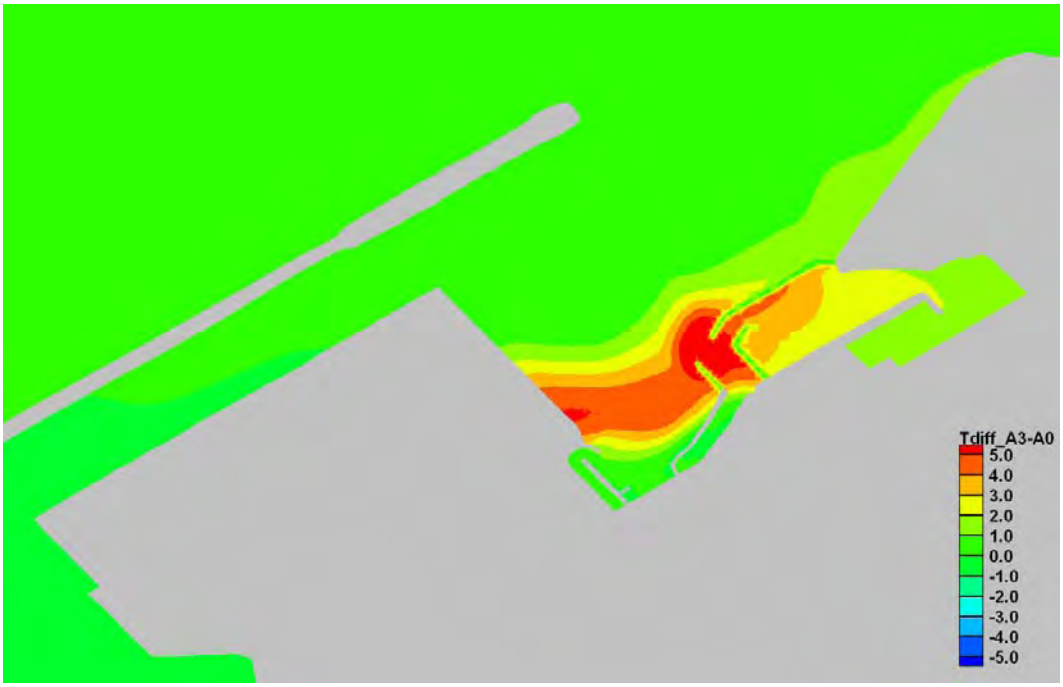

Figure 3-18. AVI snapshot of Configuration 3 temperature differences during a southwesterly wind event (28 June 2002); Temperature in deg C.

4 Summary

The U.S. Army District, Buffalo (LRB) plans to construct a Confined Disposal Facility (CDF) within Cleveland Harbor. One potential site is located at the eastern entrance to the Harbor. However, this site is located in close proximity to the cooling water intake and outfall structures servicing the First Energy Power Plant. Concern exists that the planned CDF will change the circulation pattern in the Harbor area such that water discharge from the power plant will be subsequently drawn into the intake without adequate cooling.

Potential adverse impacts due to the proposed CDF, reported herein, were determined by examining changes in model-generated current circulation and thermal transport patterns. ADCIRC modeling efforts concentrated on quantifying the change in circulation patterns with and without the CDF in place for storm and quiescent/non-storm conditions. For evaluating changes in the thermal plume transport, the two-month CH3D simulation period of July and August 2002 was chosen because the relatively weak winds experienced during summer limit mixing of the plume with Lake waters, the worst-case scenario.

A two-dimensional, depth-averaged, version of the hydrodynamic model ADCIRC was applied in this study. This model required grid development and calibration/validation of the bathymetric grid to wind forcing. For the model calibration and validation, ADCIRC results were compared with 12 NOS and the CMEDS water level gauges throughout Lake Erie. The calculated water levels from the ADCIRC simulation compared well in range and phase with the NOS gauge measurements considering that the locations of the eastern gauges were well outside the area of high resolution in the project area.

Under easterly wind conditions, each CDF will increase peak storm-induced westerly currents within the channel from about 0.05 m/s to approximately 0.4 m/s. The stronger currents induced by the planned CDFs are attributed to the reduced cross-sectional area within the channel.

Current in Gordon Park Marina can be characterized as weak, and the planned configurations do not appear to have an appreciable impact on current strength in the marina. Current at the East 55th Street Marina entrance can, also, be characterized as weak. For this marina, the change in current strength is attributed to the sheltering caused by the planned configurations. These observations should not be construed that the CDFs will have no impact on flushing rates in this marina or that the planned construction will not degrade water quality. To make these determinations, a particle-tracking or water-quality model, which account for transport and flux of material within the Harbor system will need to be used. Furthermore, potential issues relating to possible erosion or to wave-induced resonance induced by constructing the CDF were investigated.

The CH3D hydrodynamic and thermal transport model was applied to investigate the effect of the three alternative CDF configurations on the heated water discharge temperature distribution within Cleveland Harbor. The third configuration included a breakwater extension, relocation of E55th St. Marina and lengthening of the First Energy guide wall. For each of the three alternative CDF configurations, the spatial distribution of the thermal plume is shown to be primarily influenced by wind direction and speed, and temperature at the intake and can vary significantly depending on the prevailing wind conditions. However, there is minimal temperature change between the base configuration and the three plan configurations. (In addition to this report, the District has been provided the data and software to examine animations of the thermal simulation results.)

References

Chapman, R. S., Johnson., B. H., and S. R. Vemulakonda. (1996). "Users Guide for the Sigma Stretched Version of CH3D-WES; A Three-Dimensional Numerical Hydrodynamic, Salinity and Temperature Model," Technical Report HL-96-21, U.S. Army Engineer Waterways Experiment Station, Vicksburg, MS.

Cialone, M. A., Mark, D. J., Tubman, M., and Chapman, R. S. (2005). "Summary Report: Development of Nearshore Circulation Modeling Suite for Toledo Harbor, Ohio", Draft Report, U.S. Army Engineer Waterways Experiment Station, Vicksburg, MS.

Flather, R. A. (1988). "A numerical model investigation of tides and diurnal-period continental shelf waves along Vancouver Island," *Journal of Physical Oceanography* 18, 115-139.

Garratt, J. R. (1977). "Review of drag coefficients over oceans and continents," *Monthly Weather Review 105*, 915-929.

Johnson., B. H., Heath, R. E., Hsieh, B. B., Kim, K. W., and H. L. Butler. (1991b). "Users Guide for a Three-dimensional Numerical Hydrodynamic, Salinity and Temperature Model of Chesapeake Bay," Technical Report HL-91-20, U.S. Army Engineer Waterways Experiment Station, Vicksburg, MS.

Kolar, R. L., Gray, W. G., Westerink, J. J., and Luettich, R. A. (1993). "Shallow water modeling in spherical coordinates: Equation formulation, numerical implementation, and application," *Journal of Hydraulic Research*.

Luettich, R. A., Jr., Westerink, J. J., and Scheffner, N. W. (1992). "ADCIRC: An advanced three-dimensional circulation model for shelves, coasts, and estuaries," Technical Report DRP-92-6, U.S. Army Engineer Waterways Experiment Station, Vicksburg, MS.

Sheng, P. Y. (1986). "A Three-Dimensional Mathematical Model of Coastal, Estuarine and Lake Currents Using Boundary Fitted Grid," Report No. 585, A.R.A.P. Group of Titan Systems, New Jersey, Princeton, NJ, 22.

Westerink, J. J., Luettich, R. A., Jr., Baptista, A. M., Scheffner, N. W., and Farrar, P. (1992). "Tide and storm surge predictions using finite element model," *Journal of Hydraulic Engineering*, American Society of Civil Engineers, 118(10), 1373-1390.

Appendix A
Description of the ADCIRC Model

The ADvanced CIRCulation (ADCIRC) numerical model was chosen for simulating the long-wave hydrodynamic processes in Lake Erie. Imposing wind fields extracted from the National Center for Environmental Prediction database, or wind and atmospheric pressure fields computed with the PBL model, the ADCIRC model can accurately replicate tidally-driven currents and hurricane-induced storm-surge levels. The ADCIRC model was developed in the USACE Dredging Research Program (DRP) as a family of two- and three-dimensional finite element-based models (Luettich, Westerink, and Scheffner 1992; Westerink et al. 1992). Model attributes include the following capabilities:

a. Simulating tidal circulation and storm-surge propagation over very large computational domains while simultaneously providing high resolution in areas of complex shoreline configuration and bathymetry. The targeted areas of interest include continental shelves, nearshore areas, and estuaries.

b. Representing properly all pertinent physics of the three-dimensional equations of motion. These include tidal potential, Coriolis, and all nonlinear terms of the governing equations.

c. Providing accurate and efficient computations over time periods ranging from months to years.

In two dimensions, the model is formulated using the depth-averaged shallow water equations for conservation of mass and momentum. Furthermore, the formulation assumes that the water is incompressible, that hydrostatic pressure conditions exist, and that the Boussinesq approximation is valid. Using the standard quadratic parameterization for bottom stress and neglecting baroclinic terms and lateral diffusion/dispersion effects, the following set of conservation equations in primitive, nonconservative form, and expressed in a spherical coordinate system, are incorporated in the model (Flather 1988; Kolar et al. 1993):

$$\frac{\partial U}{\partial t} + \frac{1}{r\cos\phi} U \frac{\partial U}{\partial \lambda} + \frac{1}{R} V \frac{\partial U}{\partial \phi} - \left[\frac{\tan\phi}{R} U + f \right] V = \tag{A-1}$$

$$-\frac{1}{R\cos\phi}\frac{\partial}{\partial\lambda}\left[\frac{p_s}{\rho_0}+g(\zeta-\eta)\right]+\frac{\tau_{s\lambda}}{\rho_0 H}-\tau_* U$$

$$\frac{\partial V}{\partial t}+\frac{1}{r\cos\phi}U\frac{\partial V}{\partial\lambda}+\frac{1}{R}V\frac{\partial V}{\partial\phi}-\left[\frac{\tan\phi}{R}U+f\right]U = \qquad \text{(A-2)}$$

$$-\frac{1}{R}\frac{\partial}{\partial\phi}\left[\frac{p_s}{\rho_0}+g(\zeta-\eta)\right]+\frac{\tau_{s\lambda}}{\rho_0 H}-\tau_* V$$

$$\frac{\partial\zeta}{\partial t}+\frac{1}{R\cos\phi}\left[\frac{\partial UH}{\partial\lambda}+\frac{\partial(UV\cos\phi}{\partial\phi}\right] \qquad \text{(A-3)}$$

where

t = time

λ and φ = degrees longitude (east of Greenwich is taken positive) and degrees latitude (north of the equator is taken positive)

ζ = free surface elevation relative to the geoid

U and V = depth-averaged horizontal velocities in the longitudinal and latitudinal directions, respectively

R = the radius of the Earth

$H = \zeta + h$ = total water column depth

h = bathymetric depth relative to the geoid

$f = 2\Omega \sin\varphi$ = Coriolis parameter

Ω = angular speed of the Earth

p_s = atmospheric pressure at free surface

g = acceleration due to gravity

η = effective Newtonian equilibrium tide-generating potential parameter

ρ_0 = reference density of water

$\tau_{s\lambda}$ and $\tau_{s\varphi}$ = applied free surface stresses in the longitudinal and latitudinal directions, respectively

τ = bottom shear stress and is given by the expression $C_f(U^2 + V^2)^{1/2} / H$ where
C_f = the bottom friction coefficient

The momentum equations (Equations 1 and 2) are differentiated with respect to λ and τ and substituted into the time differentiated continuity equation (Equation 3) to develop the following Generalized Wave Continuity Equation (GWCE):

$$\frac{\partial^2\zeta}{\partial t^2} + \tau_0\frac{\partial\zeta}{\partial t} - \frac{1}{R\cos\phi}\frac{\partial}{\partial\lambda}\left[\frac{1}{R\cos\phi}\left(\frac{\partial HUU}{\partial\lambda} + \frac{\partial(HUV\cos\phi}{\partial\phi}\right) - UVH\frac{\tan\phi}{R}\right]$$

$$\left[-2\omega\sin\phi\, HV + \frac{H}{R\cos\phi}\frac{\partial}{\partial\lambda}\left(g(\zeta - \alpha\eta) + \frac{p_5}{[}p_0\right) + \tau_* HU - \tau_0 HU - \tau_{s\lambda}\right]$$

$$-\frac{1}{R}\frac{\partial}{\partial\phi}\left[\frac{1}{R\cos\phi}\left(\frac{\partial HVV}{\partial\lambda} + \frac{\partial HVV\cos\phi}{\partial\phi}\right) + UUH\frac{\tan\phi}{R} + 2\,\omega\sin\phi\, HU\right] \quad \text{(A-4)}$$

$$+\frac{H}{R}\frac{\partial}{\partial\phi}\left(g(\zeta - alfa\eta) + \frac{p_s}{\rho_0}\right) + \tau_* - \tau_0 HV - \frac{\tau_{s\lambda}}{\rho_0}]$$

$$-\frac{\partial}{\partial t}[\frac{VH}{R}\tan\phi] - \tau_0[\frac{VH}{R}\tan\phi] = 0$$

The ADCIRC-2DDI model solves the GWCE in conjunction with the primitive momentum equations given in Equations 1 and 2. The GWCE-based solution scheme eliminates several problems associated with finite-element programs that solve the primitive forms of the continuity and momentum equations, including spurious modes of oscillation and artificial damping of the tidal signal. Forcing functions include time-varying water-surface elevations, wind shear stresses, atmospheric pressure gradients, and the Coriolis effect. Also, the study area can be described in ADCIRC using either a Cartesian (i.e., flat earth) or spherical coordinate system.

The ADCIRC model uses a finite-element algorithm in solving the defined governing equations over complicated bathymetry encompassed by irregular sea/ shore boundaries. This algorithm allows for extremely flexible spatial discretizations over the entire computational domain and has demonstrated excellent stability characteristics. The advantage of this flexibility in developing a computational grid is that larger elements can be used in open-ocean regions where less resolution is needed, whereas smaller elements can be applied in the nearshore and estuary areas where finer resolution is required to resolve hydrodynamic details.

Appendix B
Description of the Three-Dimensional Circulation Model (CH3D)

A general overview of the sigma-stretched CH3D model background is provided with emphasis on the pertinent details for application of the model for this study. Much of the model background is extracted from the model user's guide (Chapman et. al. 1996), and the reader is referred to this document for additional details about the model.

CH3D was developed by Sheng (1986), but has been modified to implement different basic numerical formulations of the governing equations and to provide more efficient computing. A description of modifications to the model is provided in Chapman et al. (1996). Physical processes impacting circulation and vertical mixing that are modeled include tides, wind, density effects (salinity and temperature), freshwater inflows, turbulence, and the effect of the earth's rotation.

The boundary-fitted coordinate feature of the model provides grid resolution enhancement necessary to adequately represent deep navigation channels and irregular shoreline configurations of the flow system, important factors for the present study. The curvilinear grid also permits adoption of accurate and economical grid schematization software. The solution algorithm employs an external mode, consisting of vertically averaged equations, which provides a solution for the free surface displacement for input to the internal mode, which contains the full 3D equations.

Governing equations

The governing partial differential equations are based on the following assumptions: a) the hydrostatic pressure distribution adequately describes the vertical distribution of fluid pressure; b) the Boussinesq approximation is appropriate; c) the eddy viscosity approach adequately describes turbulent mixing in the flow.

The basic equations for an incompressible fluid in a right-handed Cartesian coordinate system (x,y,z) are (Johnson et al., 1991b):

$$\frac{\partial u}{\partial x} + \frac{\partial v}{\partial y} + \frac{\partial w}{\partial z} = 0 \tag{B-1}$$

$$\frac{\partial u}{dt} + \frac{\partial u^2}{dx} + \frac{\partial uv}{\partial y} + \frac{\partial uw}{\partial z} = fv - \frac{1}{\rho_o}\frac{\partial p}{\partial x} + \frac{\partial}{\partial x}\left(A_h \frac{\partial u}{\partial x}\right) + \frac{\partial}{\partial y}\left(A_h \frac{\partial u}{\partial y}\right) + \frac{\partial}{\partial z}\left(A_v \frac{\partial u}{\partial z}\right) \tag{B-2}$$

$$\frac{\partial u}{\partial t} + \frac{\partial uv}{\partial x} + \frac{\partial v^2}{\partial y} + \frac{\partial vw}{\partial z} = -fu - \frac{1}{\rho_o}\frac{\partial p}{\partial y} + \frac{\partial}{\partial x}\left(A_h \frac{\partial v}{\partial x}\right) + \frac{\partial}{\partial y}\left(A_h \frac{\partial v}{\partial y}\right) + \frac{\partial}{\partial z}\left(A_v \frac{\partial v}{\partial z}\right) \tag{B-3}$$

$$\frac{\partial p}{\partial z} = -\rho g \tag{B-4}$$

$$\frac{\partial T}{\partial t} + \frac{\partial uT}{\partial x} + \frac{\partial vT}{\partial y} + \frac{\partial wT}{\partial z} = \frac{\partial}{\partial x}\left(K_h \frac{\partial T}{\partial x}\right) + \frac{\partial}{\partial y}\left(K_h \frac{\partial T}{\partial y}\right) + \frac{\partial}{\partial z}\left(K_v \frac{\partial T}{\partial z}\right) \tag{B-5}$$

$$\frac{\partial S}{\partial t} + \frac{\partial uS}{\partial x} + \frac{\partial vS}{\partial y} + \frac{\partial wS}{\partial z} = \frac{\partial}{\partial x}\left(K_h \frac{\partial S}{\partial x}\right) + \frac{\partial}{\partial y}\left(K_h \frac{\partial S}{\partial y}\right) + \frac{\partial}{\partial z}\left(K_v \frac{\partial S}{\partial z}\right) \tag{B-6}$$

$$\rho = \rho\,(T, S) \tag{B-7}$$

where

(u,v,w) = velocities in (x,y,z) directions

t = time

f = Coriolis parameter defined as $2\Omega \sin \varphi$

where

Ω = rotational speed of the earth

φ = latitude

ρ = density

p = pressure

A_h, K_h = horizontal turbulent eddy coefficients

A_v , K_v = vertical turbulent eddy coefficients

g = gravitational acceleration

T = temperature

S = salinity

Equation 4 implies that vertical accelerations are negligible and thus the pressure is hydrostatic. Various forms of the equation of state can be specified for Equation 7. In the present model, the formulation given below is used:

$$\rho = P/(\alpha + 0.698P) \tag{B-8}$$

where

ρ = density in grams per cubic centimeter

$$P = 5890 + 38T - 0.375T^2 + 3S$$

$$\alpha = 1779.5 + 11.25T - 0.0745T^2 - (3.8 + 0.01T)S$$

and T is temperature in degrees Celsius and S is salinity in parts per thousand (ppt).

Within the model, the basic equations presented above are normalized, boundary-fitted, and sigma-stretched as presented in Chapman et al. (1996).

Boundary Conditions

The governing equations presented above are subject to boundary conditions at the surface, bottom and lateral boundaries. These boundary conditions are discussed generally here and the reader is again referenced to Chapman, Johnson, and Vemulakonda (1996) for additional details.

The free-surface boundary condition is affected primarily by wind stresses and heat exchange. Wind stresses enter as source terms into the momentum equations (Equations 5-2 and 5-3) for the top layer in the following form:

$$\mathrm{A_v}\left(\frac{\partial \bar{\mathrm{u}}}{\partial \mathrm{z}}, \frac{\partial \bar{\mathrm{v}}}{\partial \mathrm{z}}\right) = \left(\tau_{s_\xi}, \tau_{s_\eta}\right)/\rho = \left(\mathrm{C\,W}_\xi^2, \mathrm{C\,W}_\eta^2\right) \tag{B-9}$$

where

τ_s = wind shear stress

C = surface drag coefficient

W = wind speed (m/s)

The surface drag coefficient is calculated by the method of Garratt (1977) as follows:

$$C = (0.75 + 0.067\ W) \times 10^{-3} \tag{B-10}$$

Heat exchange at the surface is represented through a surface heat exchange coefficient and the daily equilibrium temperature and enters as a source term in Equation 5-5. The surface heat exchange coefficient and equilibrium temperature are calculated from geographical and meteorological conditions (latitude, wind speed, cloud cover, and wet and dry bulb temperatures). Zero salinity flux is imposed in the surface layer.

The bottom boundary condition is primarily influenced by bottom friction, expressed in the governing equations for the bottom layer as:

$$A_v \left(\frac{\partial \bar{u}}{\partial z}, \frac{\partial \bar{v}}{\partial z} \right) = \left(\tau_{b_\xi}, \tau_{b_\eta} \right) / \rho = \frac{U_r}{A_{vr}} Z_r C_d \left(\bar{u}_1^2 + \bar{v}_1^2 \right)^{1/2} \left(\bar{u}_1, \bar{v}_1 \right) \tag{B-11}$$

where

τ_b = bottom shear stress

U_r = reference velocity

Z_r = reference height

C_d = bottom drag coefficient

u_1, v_1 = near-bottom horizontal velocity

Bottom friction can be specified by a variety of methods. The bottom friction for the present study was specified as a spatially constant bottom friction coefficient, and values applied are discussed with model calibration. Other bottom boundary conditions imposed by the model include zero temperature and salinity fluxes.

Open-water boundaries include specification of water-surface elevation and temperature. River boundaries are prescribed as input flow and temperature.

Appendix C
ADCIRC Calibration and Validation Results

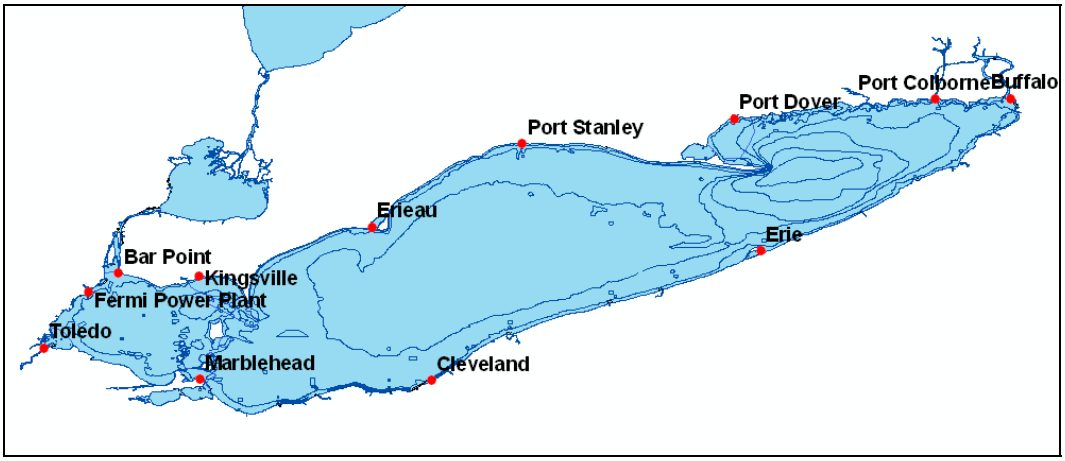

Figure C1. Gauge Locations used in Calibration and Validation Exercises.

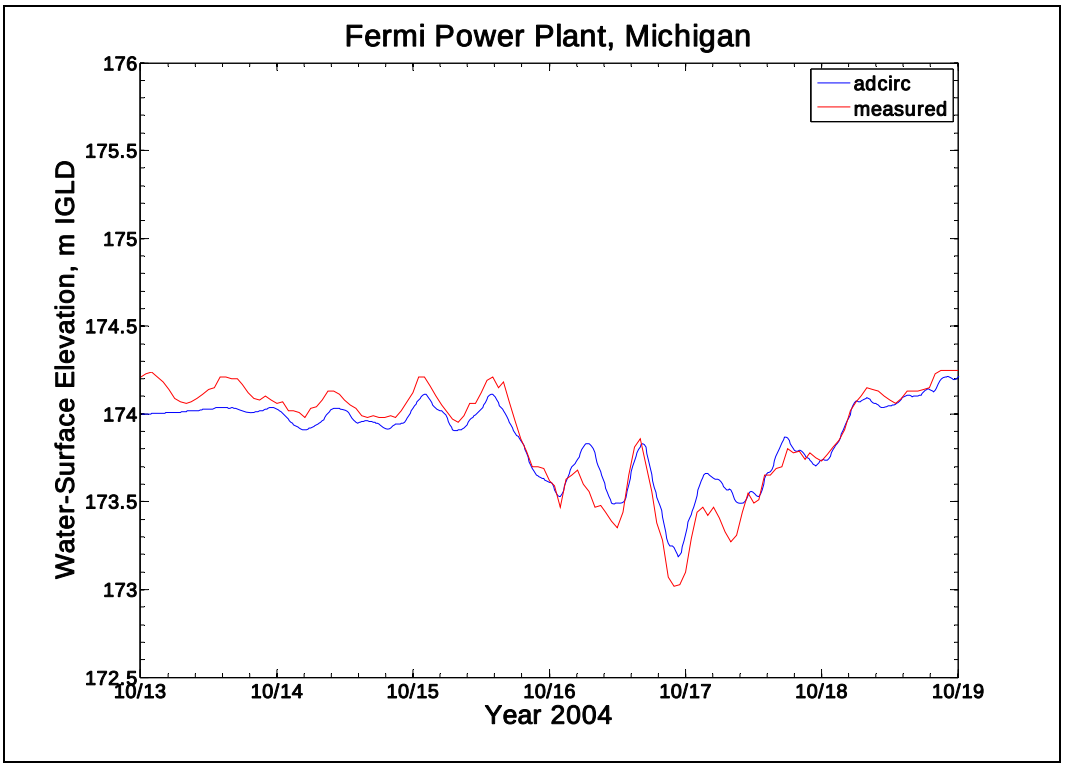

Figure C2. Comparison of model-generated and measured water-surface elevations: Fermi Power Plant, MI, 13-19 Oct 2004.

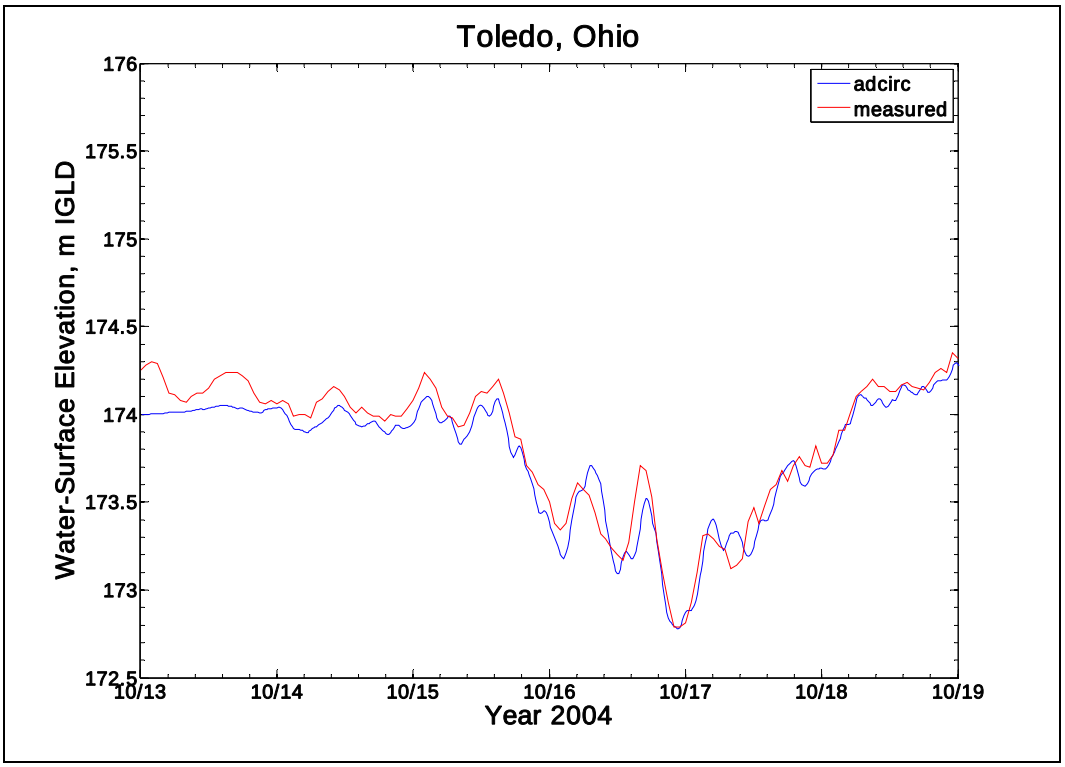

Figure C3. Comparison of model-generated and measured water-surface elevations: Toledo, OH, 13-19 Oct 2004.

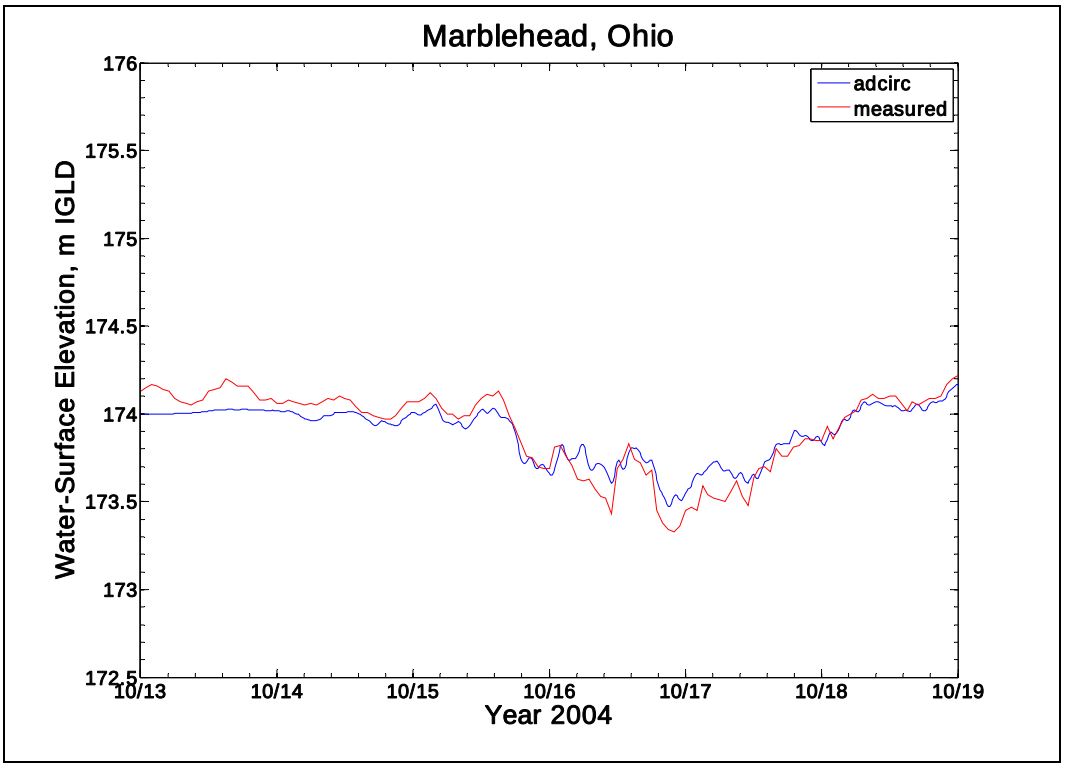

Figure C4. Comparison of model-generated and measured water-surface elevations: Marblehead, OH, 13-19 Oct 2004.

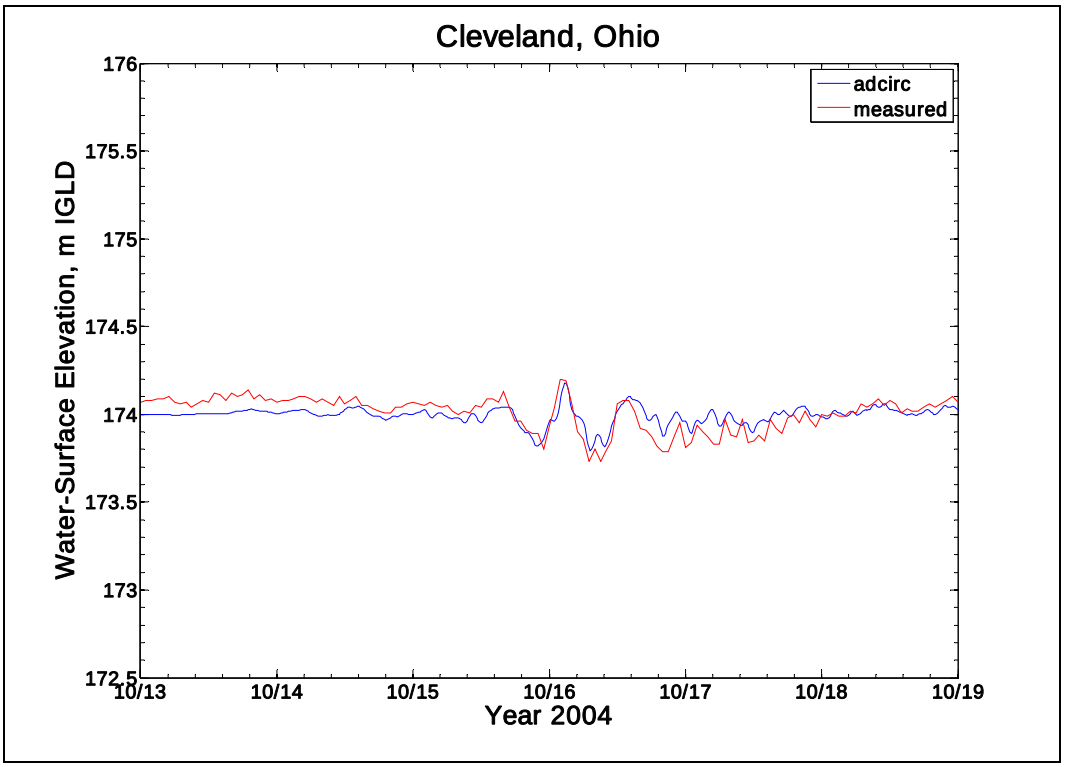

Figure C5. Comparison of model-generated and measured water-surface elevations: Cleveland, OH, 13-19 Oct 2004.

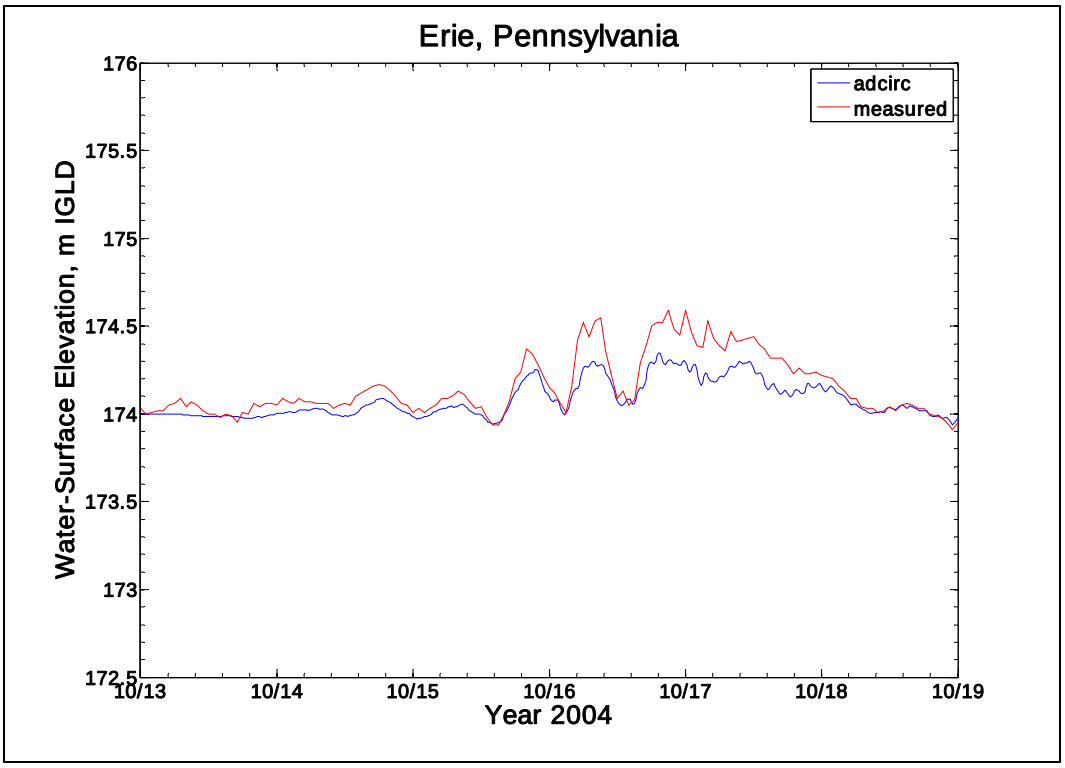

Figure C6. Comparison of model-generated and measured water-surface elevations: Erie, PA, 13-19 Oct 2004.

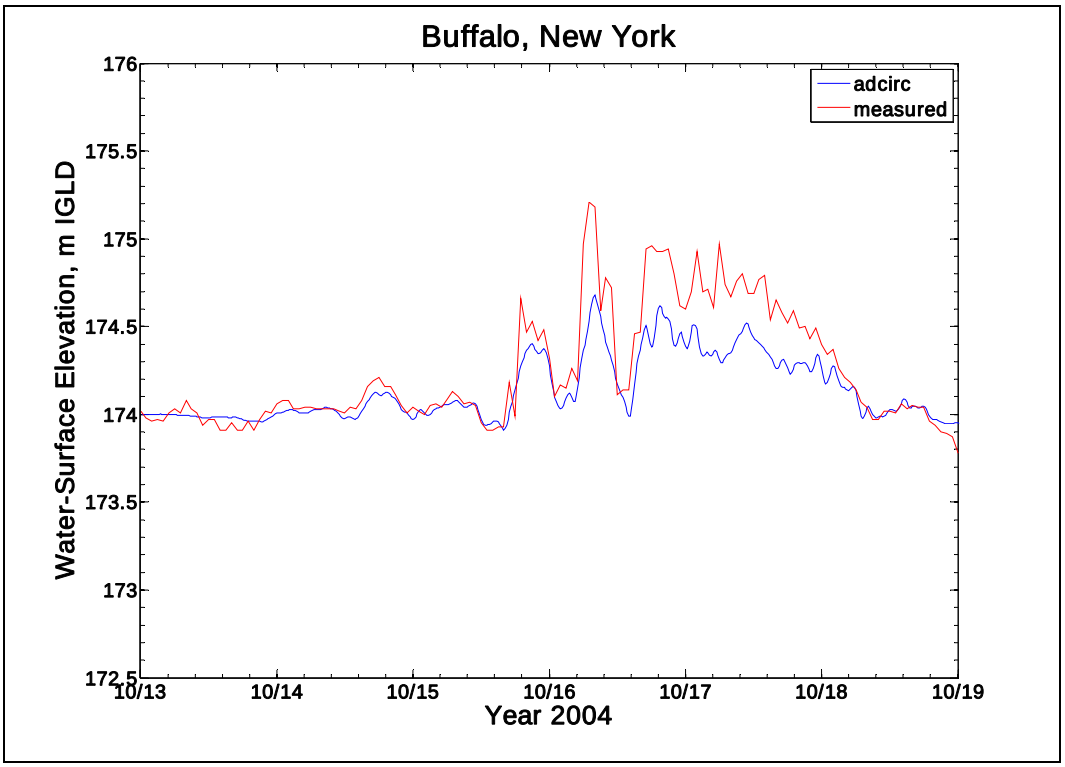

Figure C7. Comparison of model-generated and measured water-surface elevations: Buffalo, NY, 13-19 Oct 2004.

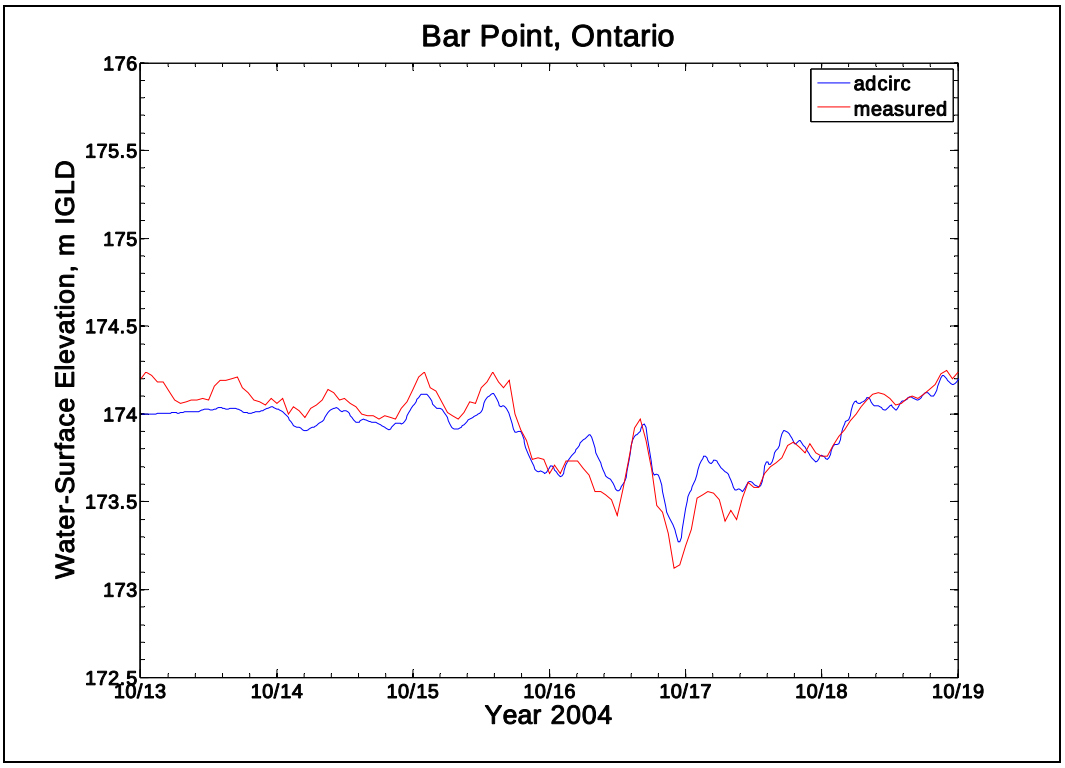

Figure C8. Comparison of model-generated and measured water-surface elevations: Bar Point, Ontario, 13-19 Oct 2004.

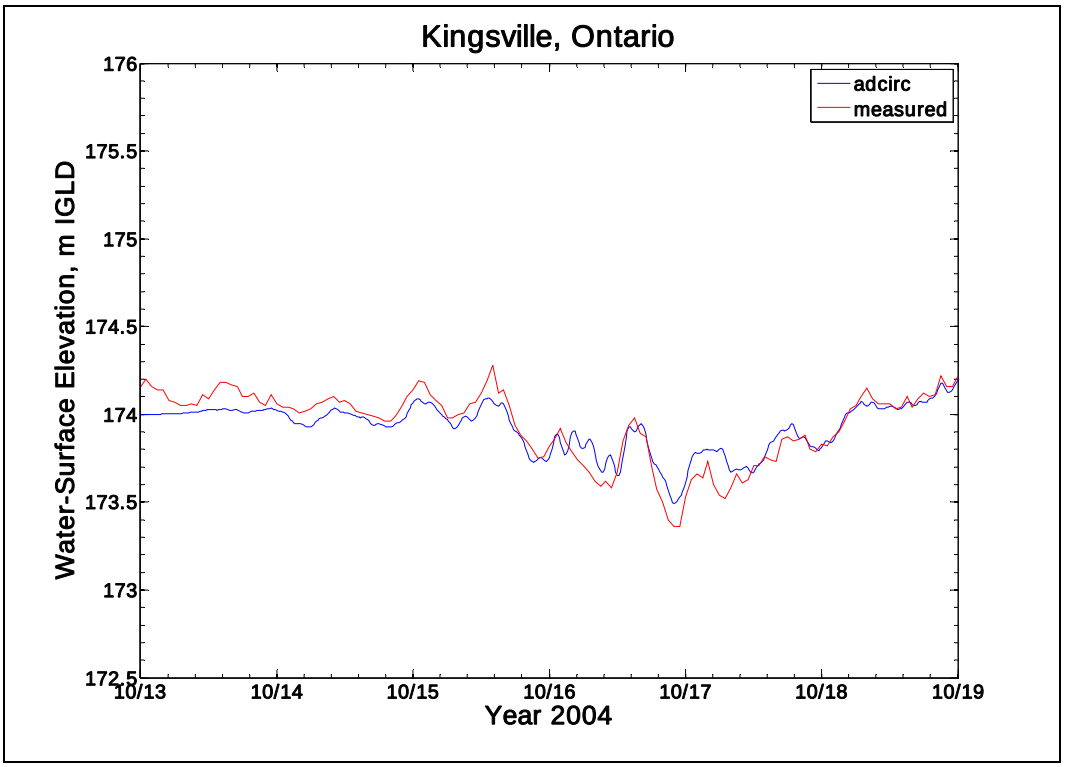

Figure C9. Comparison of model-generated and measured water-surface elevations: Kingsville, Ontario, 13-19 Oct 2004.

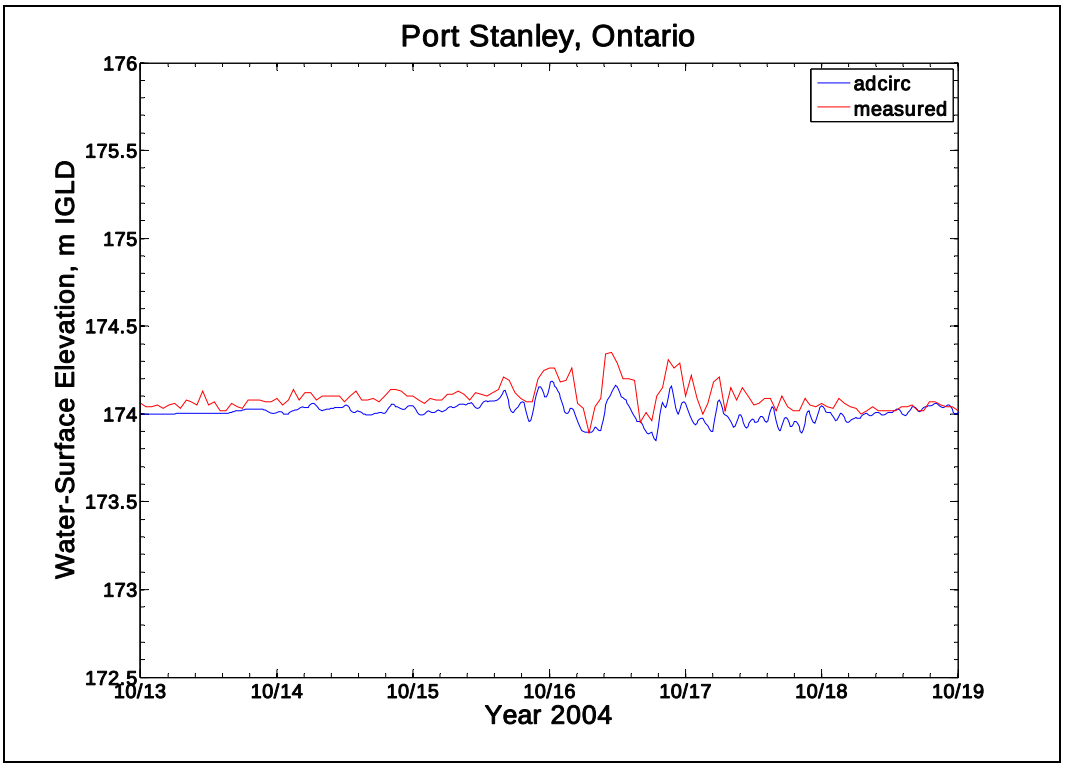

Figure C50. Comparison of model-generated and measured water-surface elevations: Port Stanley, Ontario, 13-19 Oct 2004.

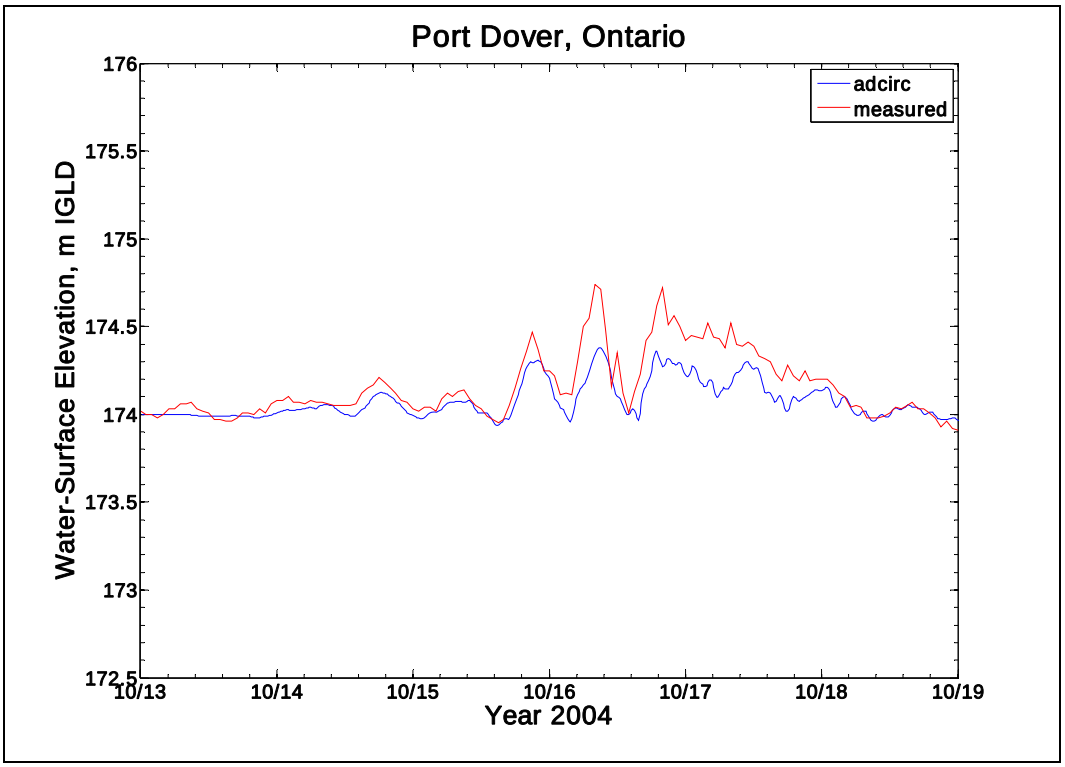

Figure C61. Comparison of model-generated and measured water-surface elevations: Port Dover, Ontario, 13-19 Oct 2004.

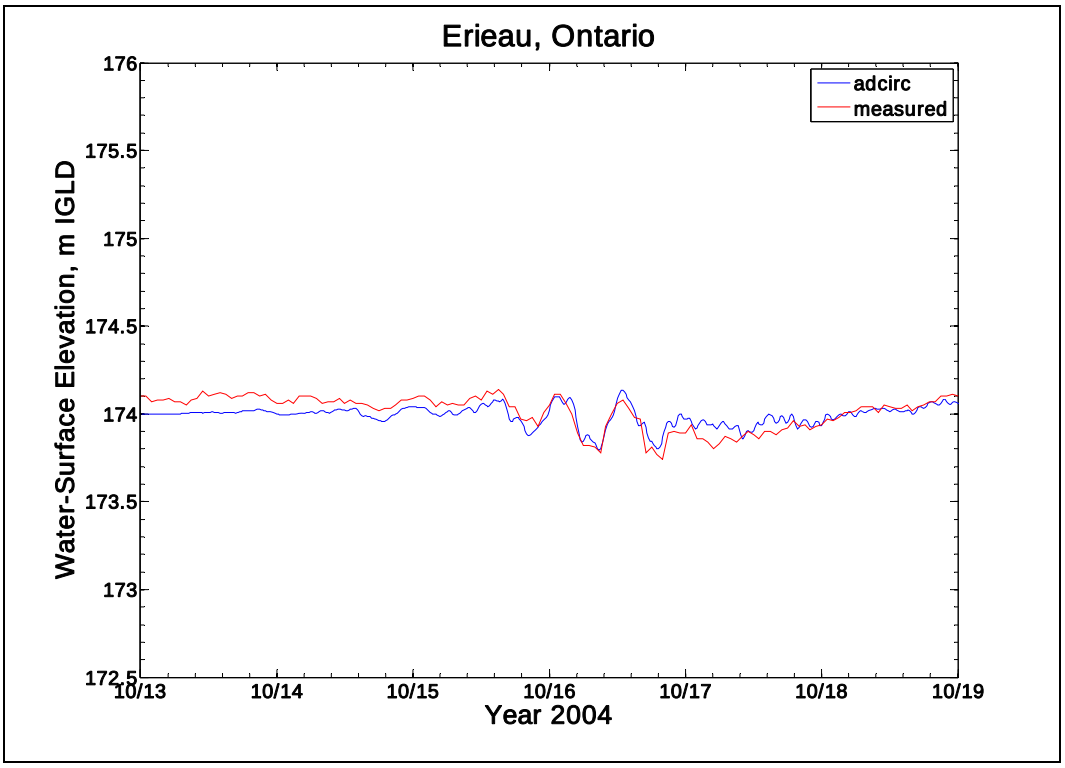

Figure C72. Comparison of model-generated and measured water-surface elevations: Erieau, Ontario, 13-19 Oct 2004.

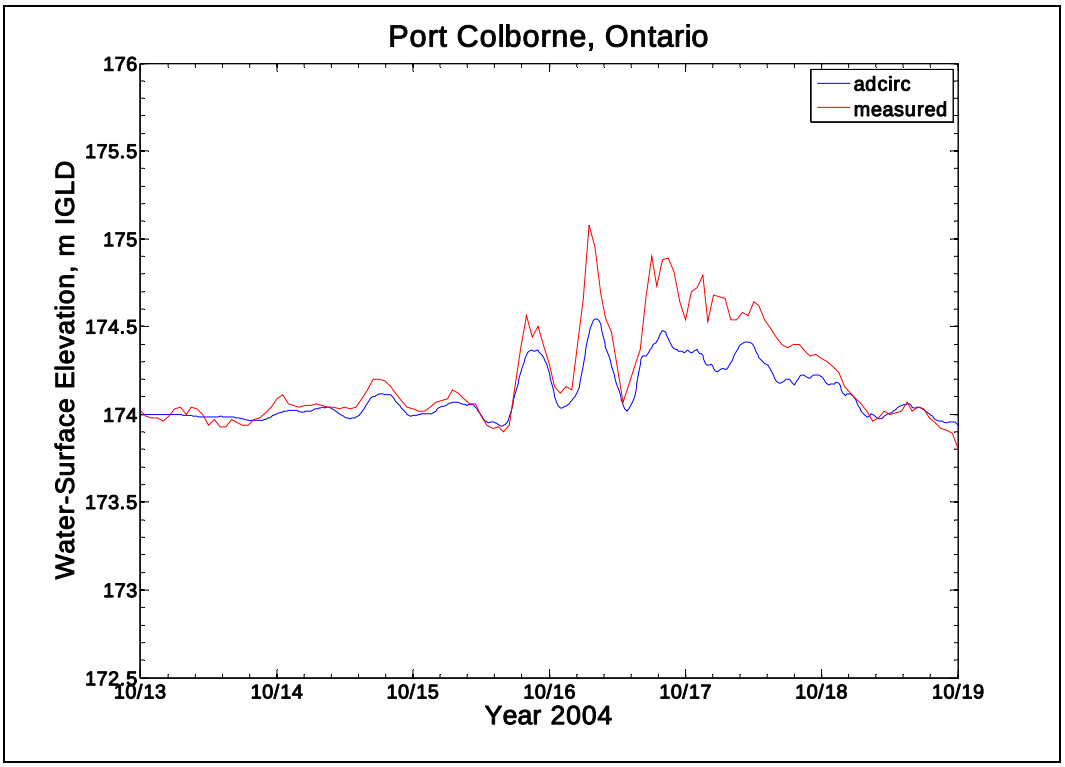

Figure C83. Comparison of model-generated and measured water-surface elevations: Port Colborne, Ontario, 13-19 Oct 2004.

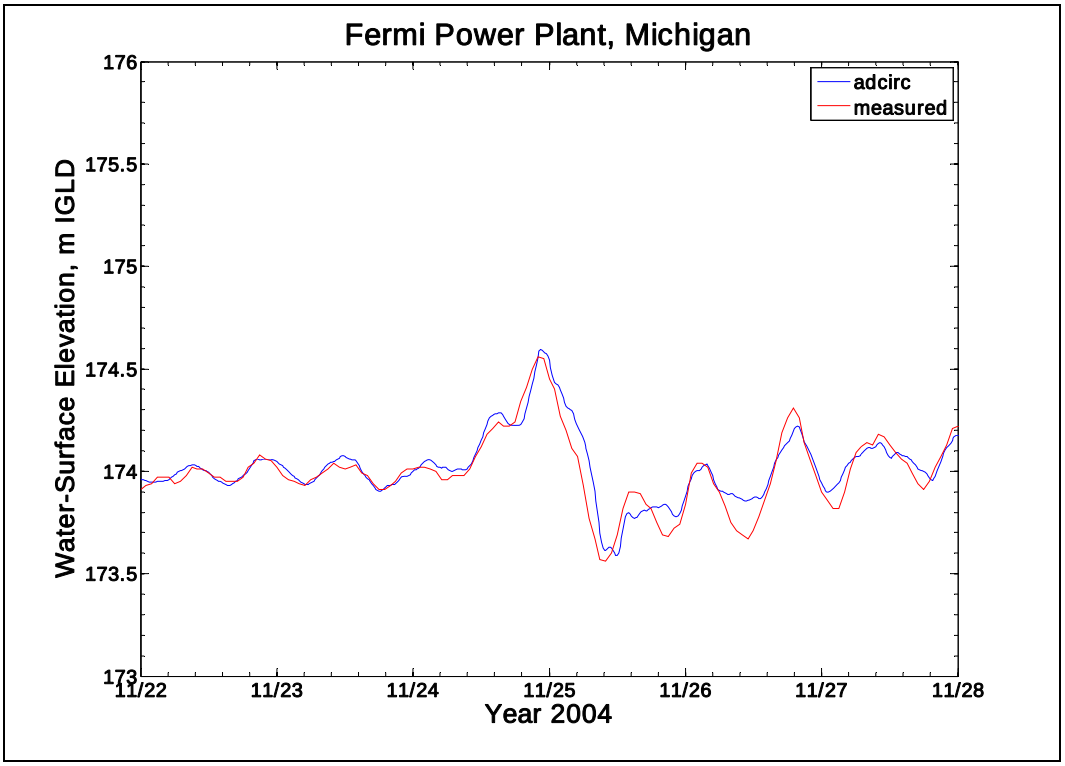

Figure C94. Comparison of model-generated and measured water-surface elevations: Fermi Power Plant, 22-29 Nov 2004.

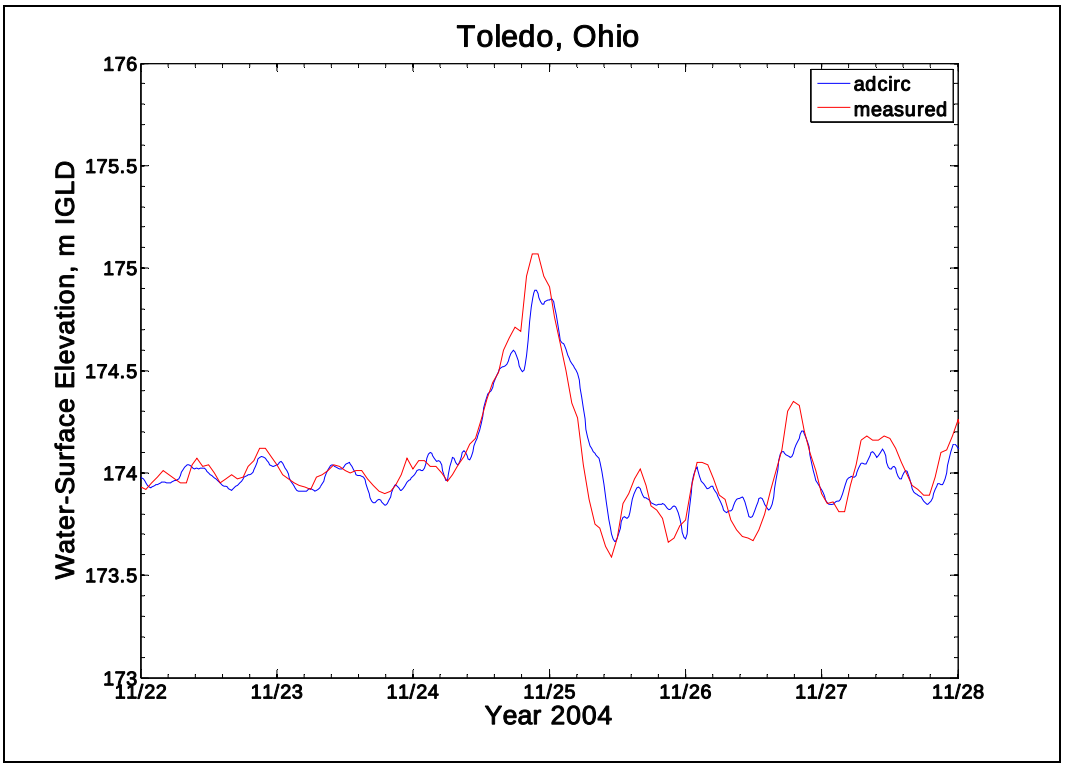

Figure C105. Comparison of model-generated and measured water-surface elevations: Toledo, OH, 22-29 Nov 2004.

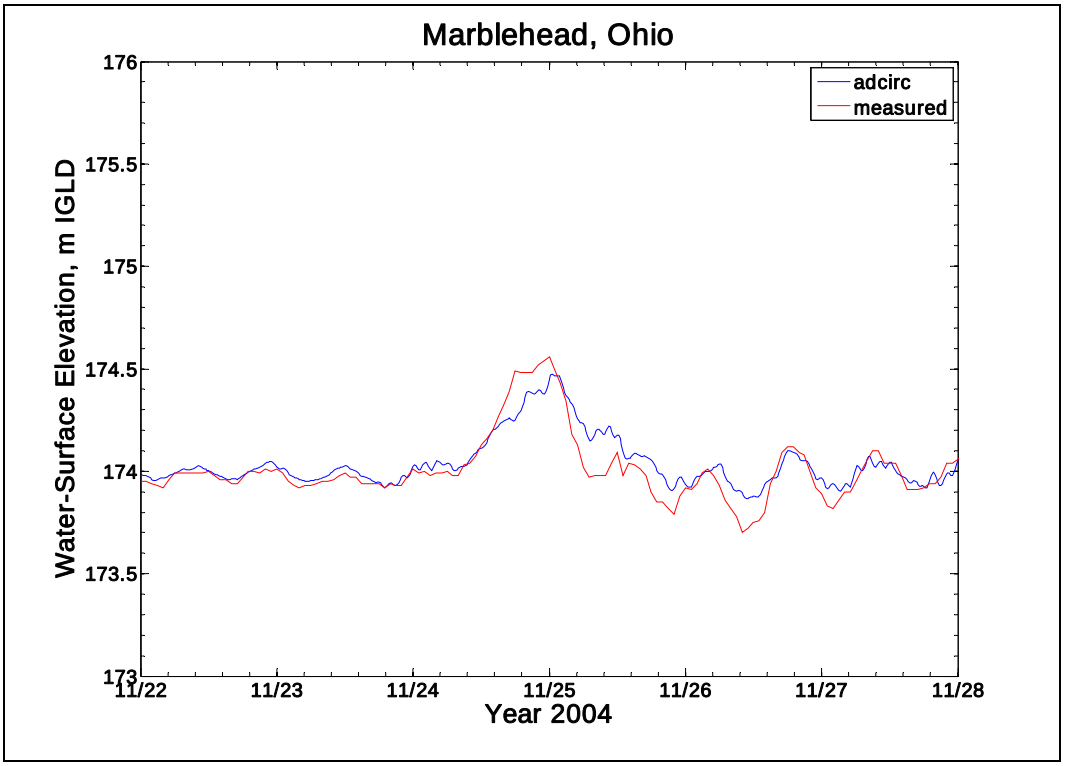

Figure C16. Comparison of model-generated and measured water-surface elevations: Marblehead, OH, 22-29 Nov 2004.

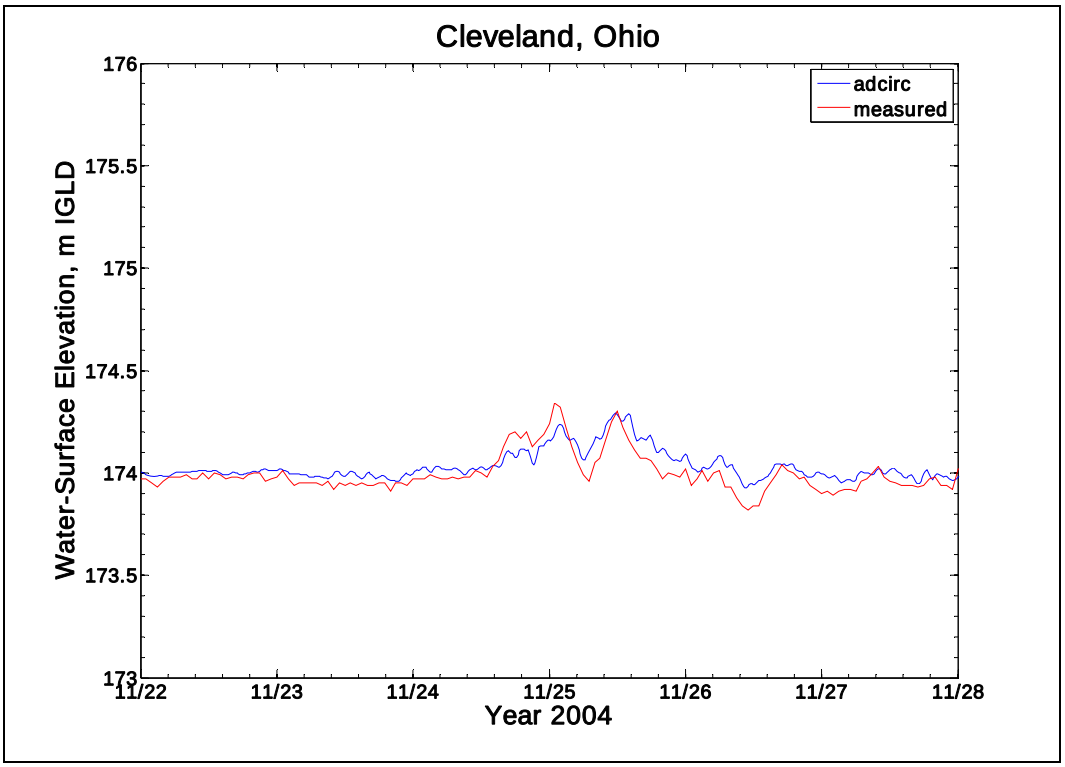

Figure C17. Comparison of model-generated and measured water-surface elevations: Cleveland, OH, 22-29 Nov 2004.

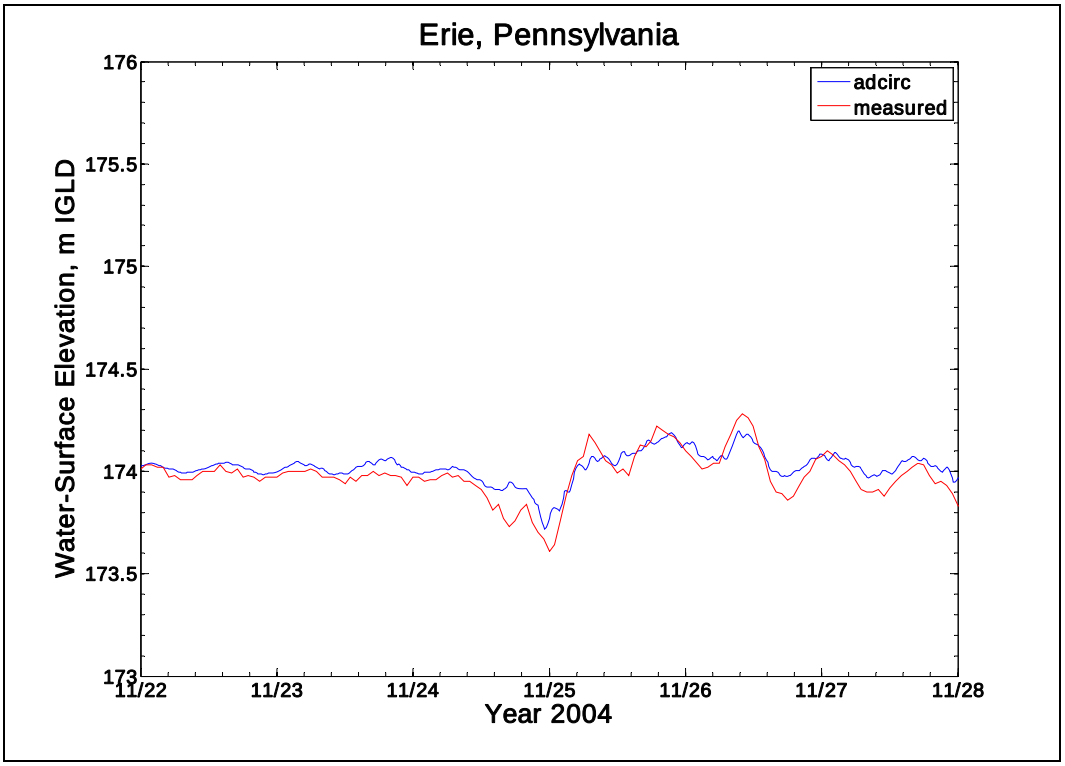

Figure C18. Comparison of model-generated and measured water-surface elevations: Erie, PA, 22-29 Nov 2004.

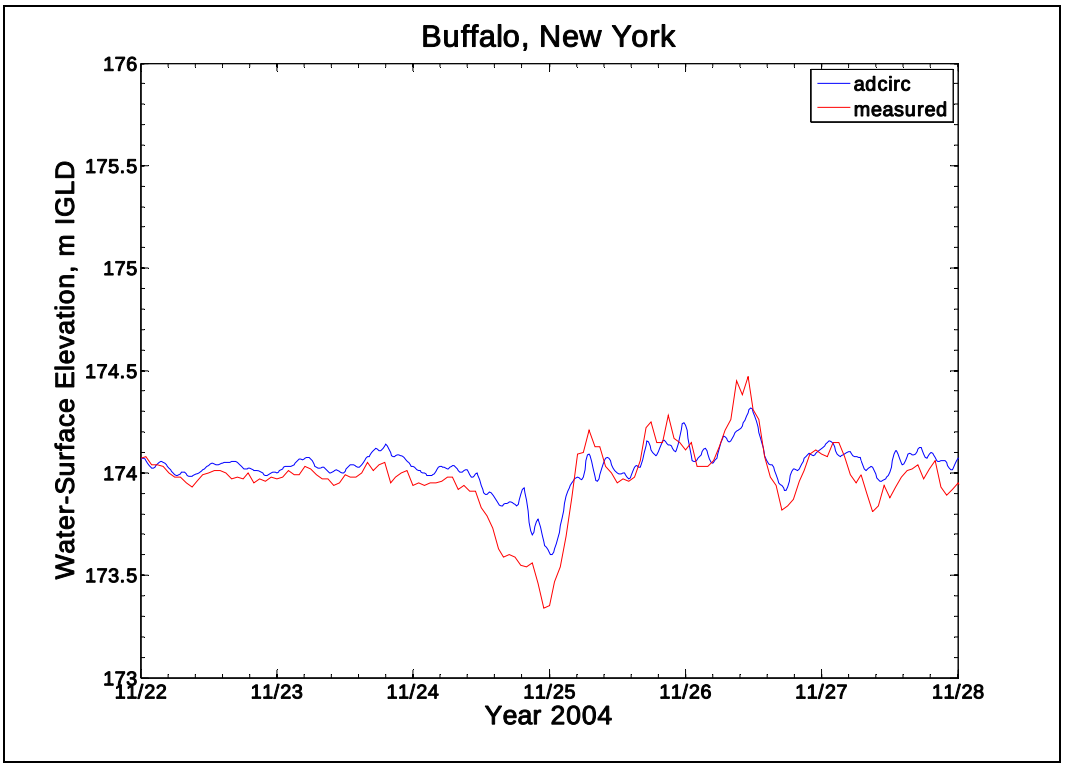

Figure C19. Comparison of model-generated and measured water-surface elevations: Buffalo, NY, 22-29 Nov 2004.

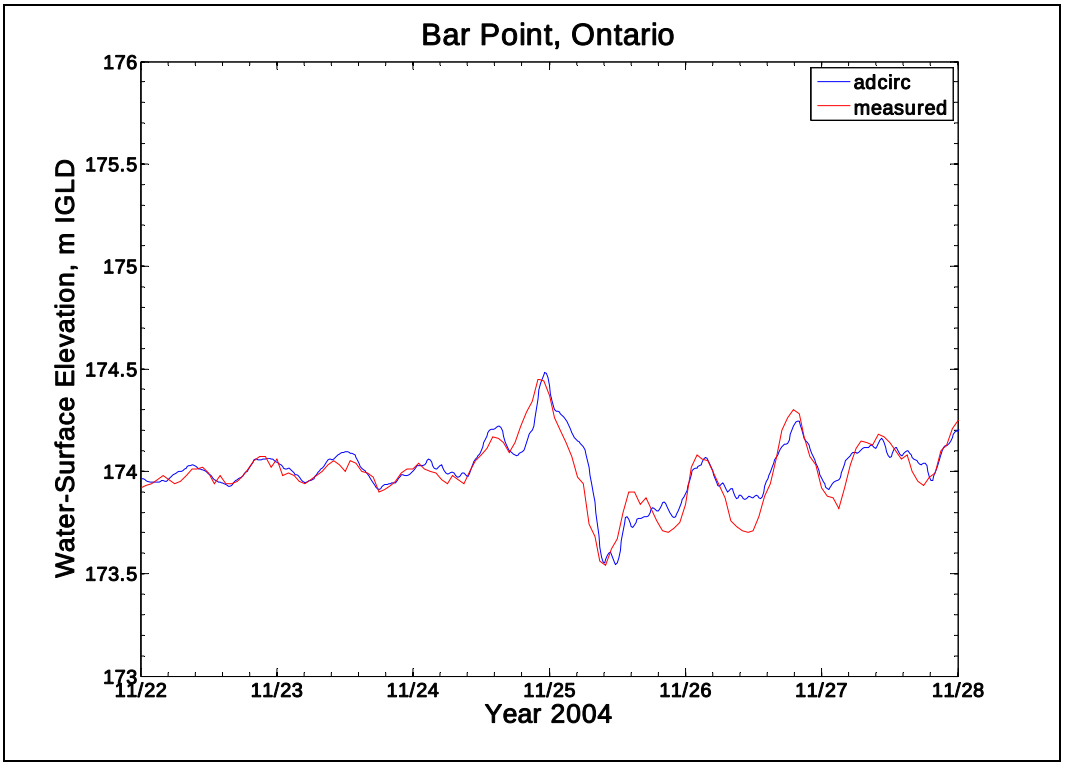

Figure C110. Comparison of model-generated and measured water-surface elevations: Bar Point, Ontario, 22-29 Nov 2004.

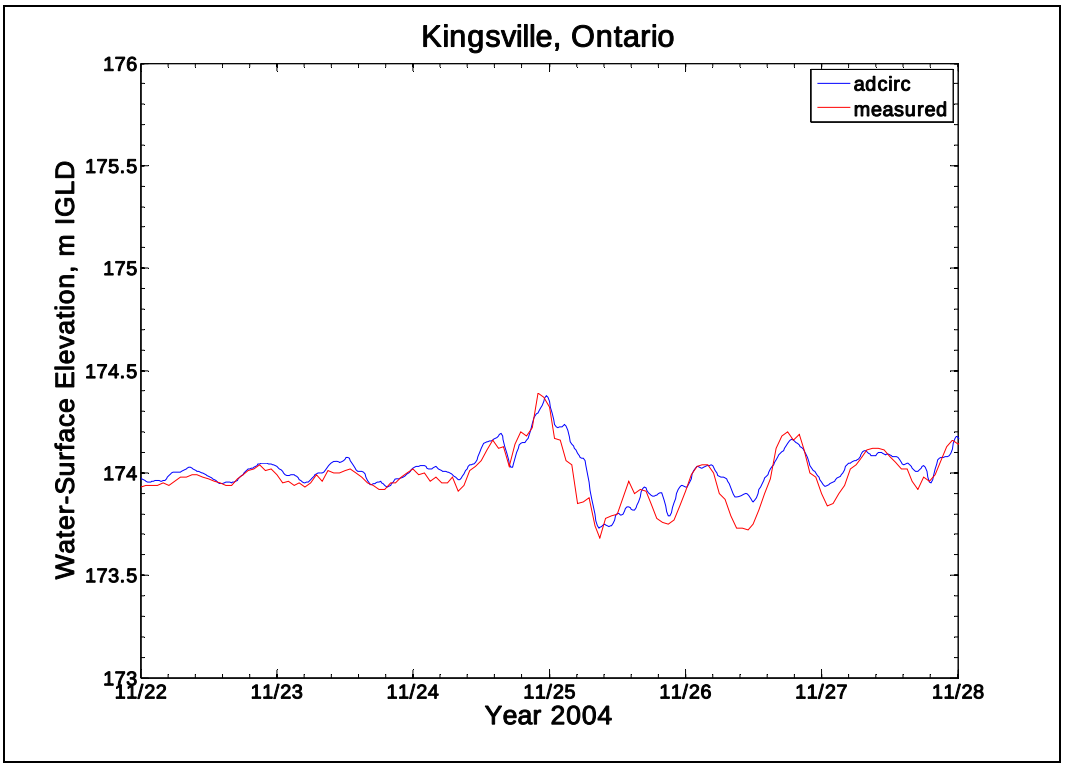

Figure C121. Comparison of model-generated and measured water-surface elevations: Kingsville, Ontario, 22-29 Nov 2004.

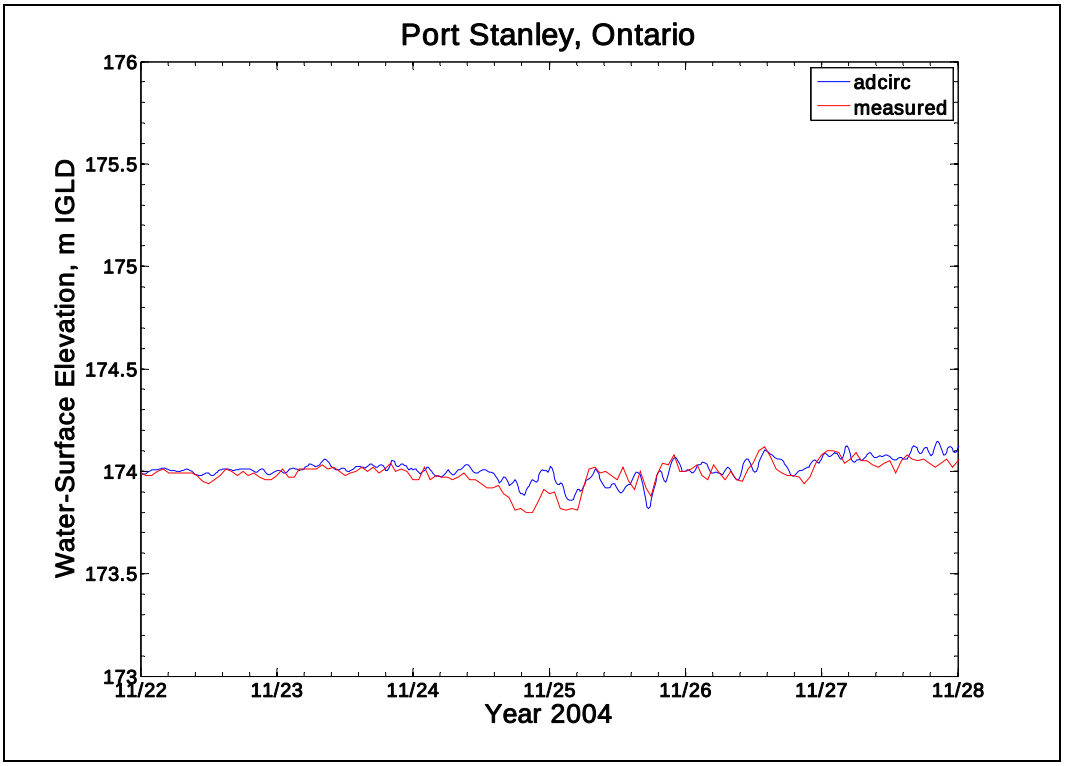

Figure C132. Comparison of model-generated and measured water-surface elevations: Port Stanley, Ontario, 22-29 Nov 2004.

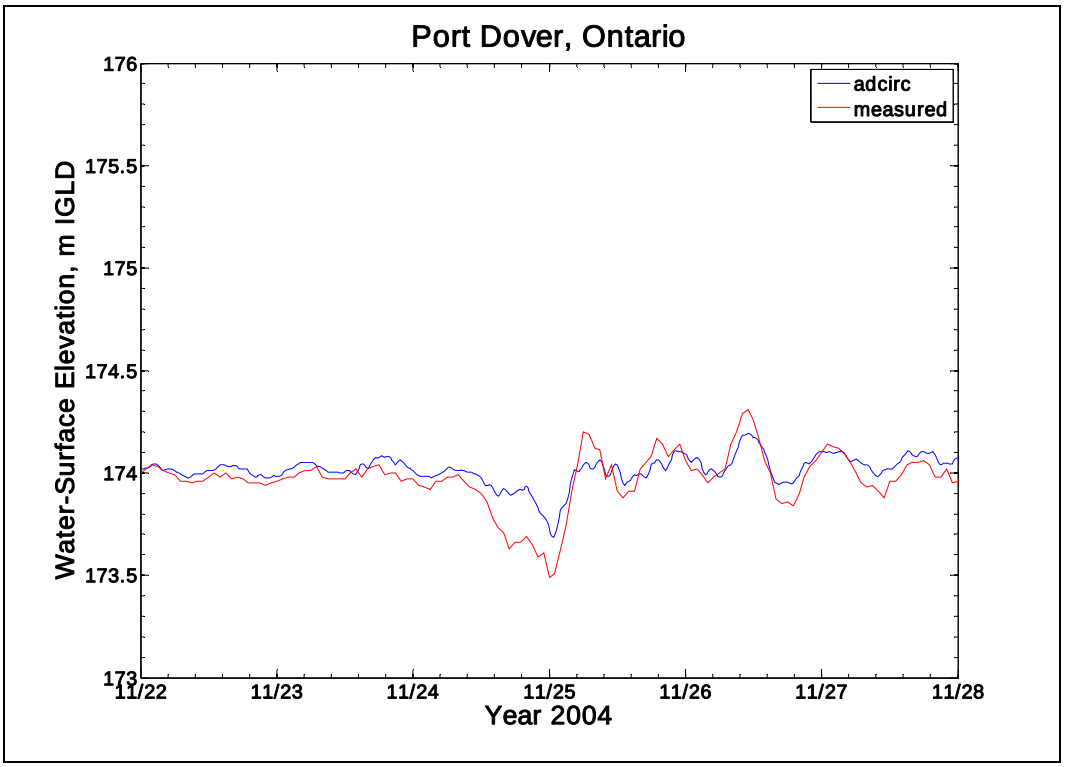

Figure C143. Comparison of model-generated and measured water-surface elevations: Port Dover, Ontario, 22-29 Nov 2004.

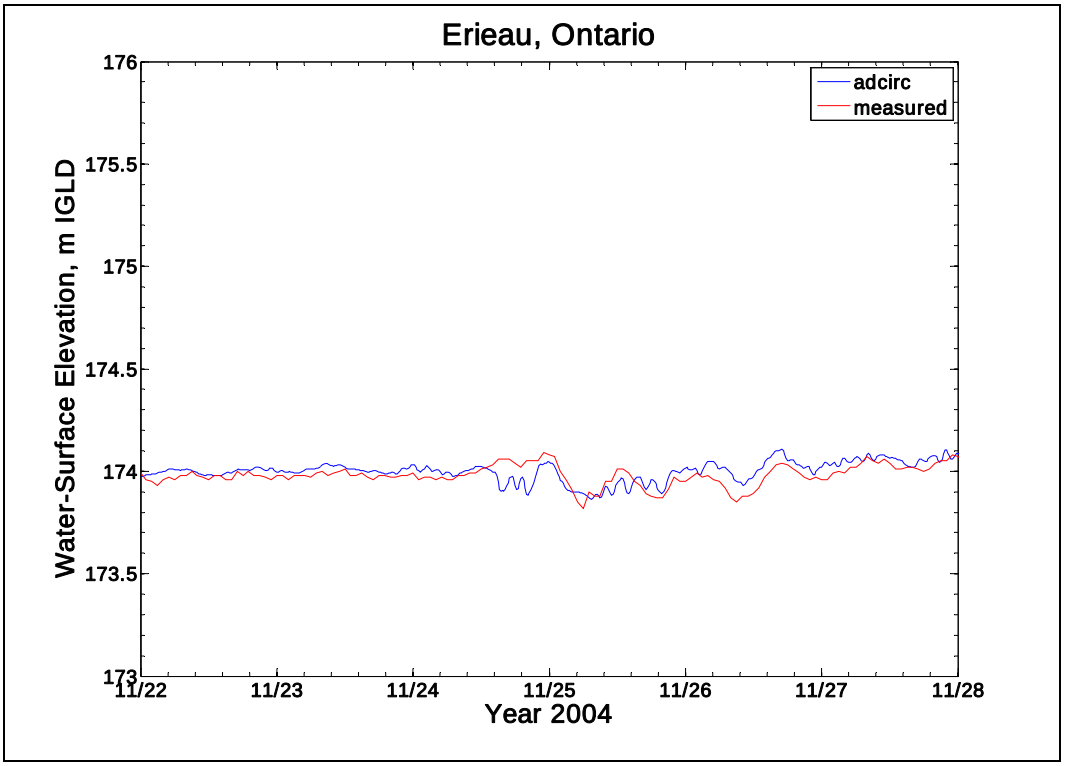

Figure C154. Comparison of model-generated and measured water-surface elevations: Erieau, Ontario, 22-29 Nov 2004.

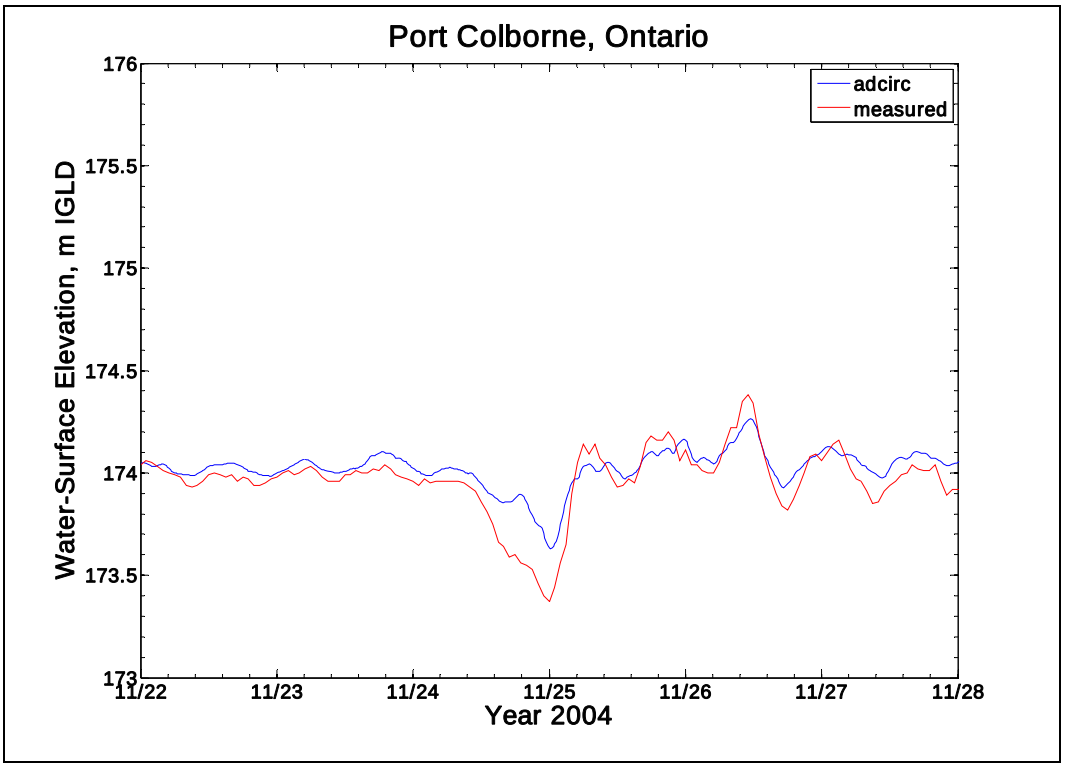

Figure C165. Comparison of model-generated and measured water-surface elevations: Port Colborne, Ontario, 22-29 Nov 2004.

Modeling of Cleveland Harbor CSO Constituent Fate

Introduction and Background

The Buffalo District (LRB) has requested assistance from the Engineering Research and Development Center of the Army Corp of Engineers with developing models to predict the fate of Combined Sewer Outflow (CSO) constituents entering Cleveland Harbor. LRB is currently undergoing plans for building a Confined Disposal Facility (CDF) in this area. One potential site is located at the eastern entrance to the Harbor. However, this site is located in close proximity to the cooling water intake and outfall structures servicing the First Energy Power Plant. This study focuses on comparisons between CSO constituent transport during different design phases of the CDF construction for portions of the harbor, Cuyahoga River, and Lake Erie that may be influenced by CSO material. The modeled phases consist of the existing Harbor configuration as well as three stages of construction (figure 1). Included in this analysis will be three types of sources: 1) neutrally buoyant particles which will represent chemical constituent transport, 2) floatable particles which are representative of debris, and 3) sediment particles. Each particle type is designed to accurately characterize the constituents released from the CSOs utilizing data supplied by LRB. The results of this work will assist LRB with assessing changes to CSO material fate due to these harbor modifications.

To address the issue of the CSO constituent fate, the Particle Tracking Model (PTM) is utilized. One major motivation to use the model is that PTM has been designed to focus on sources expressly indicated by the user. In situations for which the sources of contamination or sediment resuspension are known, PTM works optimally and can simulate multiple scenarios faster than Eulerian constituent transport models. This report presents a concise description of the particle tracking model, an accounting of model input information utilized in the project, and results and analysis of the simulations.

Existing Harbor configuration

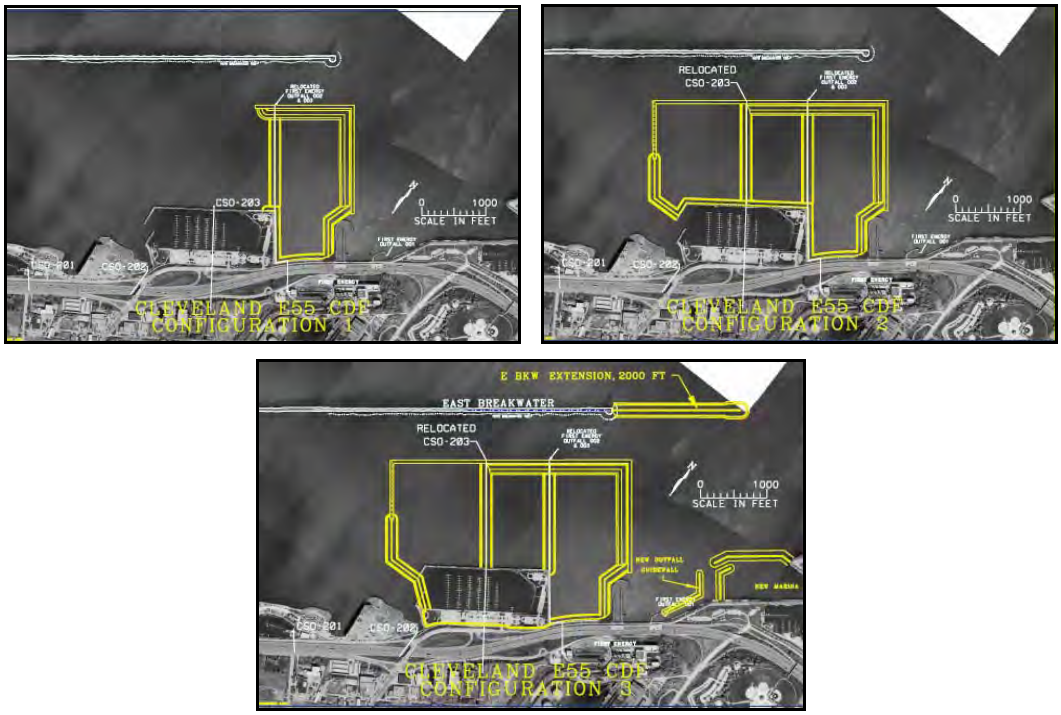

CDF construction configurations

Figure 1. Harbor configurations

PTM Model

PTM is an ERDC-developed model designed specifically to track the fate of point-source constituents (sediment, chemicals, debris, etc) released from local sources (outfalls, dredges, etc) in complex hydrodynamic and wave environments. Each local source is defined independently and may have multiple constituents. Therefore, model results include the fate of each constituent from each local source. PTM simulates transport using pre-calculated periodically saved hydrodynamic (and wave) model output. The hydrodynamic model is not coupled to the sediment transport model and therefore can be run once for multiple PTM simulations. Each particle in PTM represents a specific mass (or number of particulates) of one constituent. Total mass is conserved because particles are conserved. Hydrodynamic output does not need to be conservative, so the user can specify hydrodynamic model output for PTM without concern for conservation of water mass. A random walk method is used, in part, to represent particle diffusion. PTM simulations can be either 3D or 2D. For this application, 3D mode is used.

In addition to the hydrodynamic input (i.e. water surface elevation and velocities) that is used as a forcing for particle dynamics, PTM requires mesh and bathymetry information, and sediment characterization of the native or bed sediment (Figure 2). Although PTM does not model native sediment bed transport, it does model interactions between native bed sediments and deposited particles (hiding, burial, etc); therefore bed sediment characteristics must be described by the user. PTM also needs detailed constituent or source information. The user specifies particle characteristics and processes, including settling, critical stresses, and erosion rates. If processes data is not available, these values may be calculated within the model based on verified theoretical relationships. The specific equations for those processes are discussed in detail by McDonald et al (2006). Particles can be positively, neutrally, or negatively buoyant. Positively buoyant, for example, would represent floating debris while neutrally buoyant may represent chemicals and negatively buoyant may represent sediment.

Model output includes a time dependent parcel positions throughout the domain. Various other attributes such as mass, density, and suspension status are also assigned to each of the output parcels. Elevation in the water column is calculated and stored. PTM setup and execution are done within the ERDC-sponsored Surface Water modeling System (SMS) interface. SMS includes multiple tools for post-processing PTM output to assess distribution of concentration, deposition, and other results at any time during the simulation. These results are processed for each constituent from each source or for combined constituents or sources.

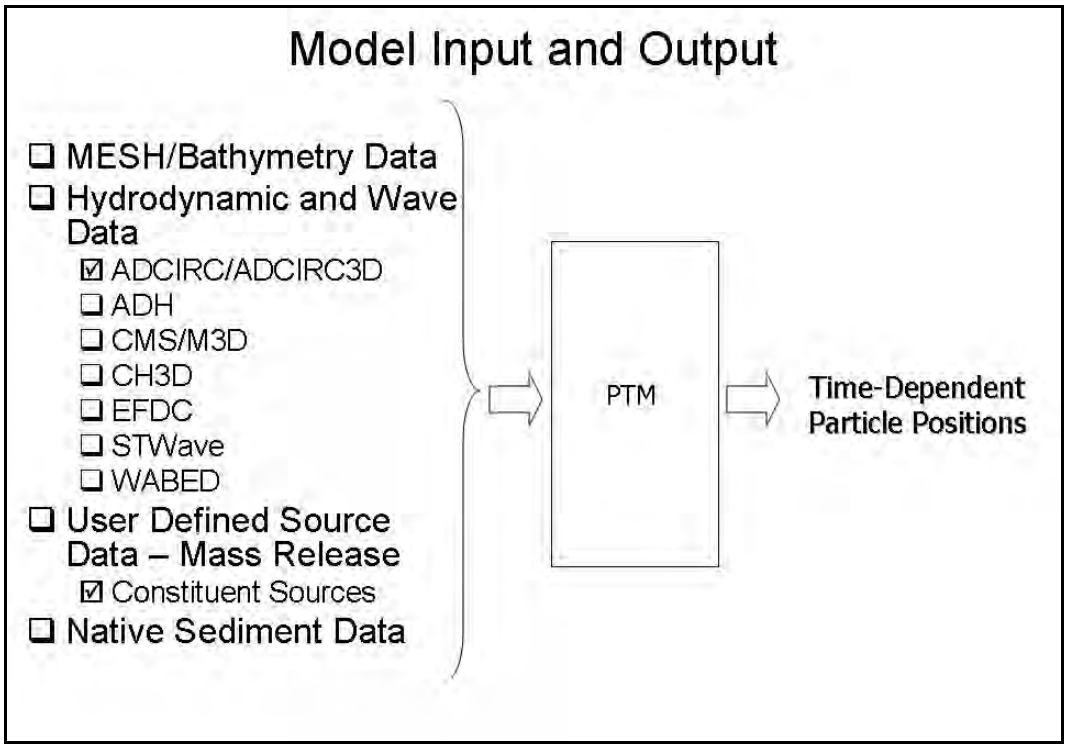

Figure 2

PTM Model Input

Hydrodynamic Modeling

The following sections summarize the PTM input for bathymetry and hydrodynamic forcing. The circulation modeling conducted for Lake Erie, including Cleveland Harbor, was performed using the ADCIRC long-wave hydrodynamic model. The ADCIRC numerical model, a large-domain, two-dimensional (2-D) depth-integrated finite-element hydrodynamic circulation model, was applied in this study to provide water level and depth-averaged current (circulation) information for Cleveland Harbor, Ohio (Mark et al 2008). This component aims to characterize water levels and currents throughout the Harbor presently in existence and to predict any potential impacts that may result from constructing a Confined Disposal Facility (CDF).

Bathymetry and Mesh

Figure 3a displays the grid developed for this study. As shown, the model domain encompasses the entire Lake, and includes the lower reaches of the Cuyahoga, Maumee, Detroit,

and Niagara Rivers. Figure 3b shows the grid in the vicinity of Cleveland Harbor projected onto a map of the area.

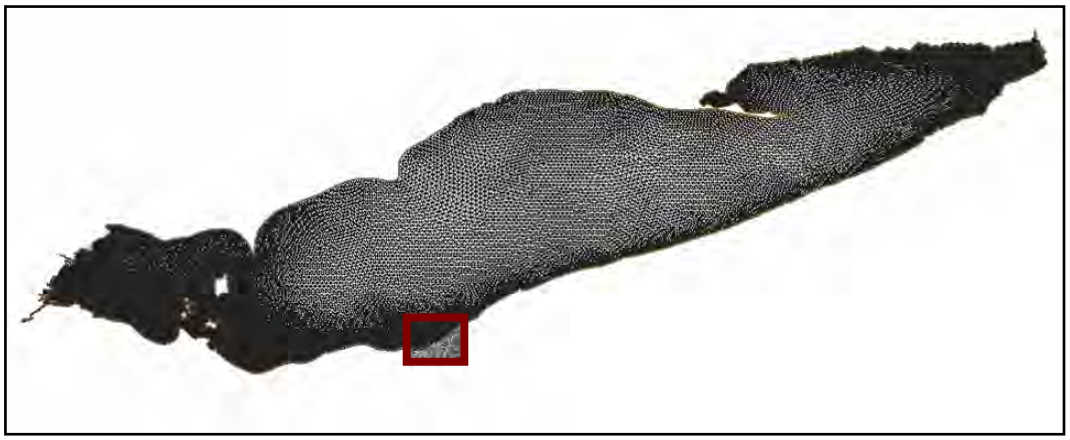

a) Lake Erie ADCIRC grid

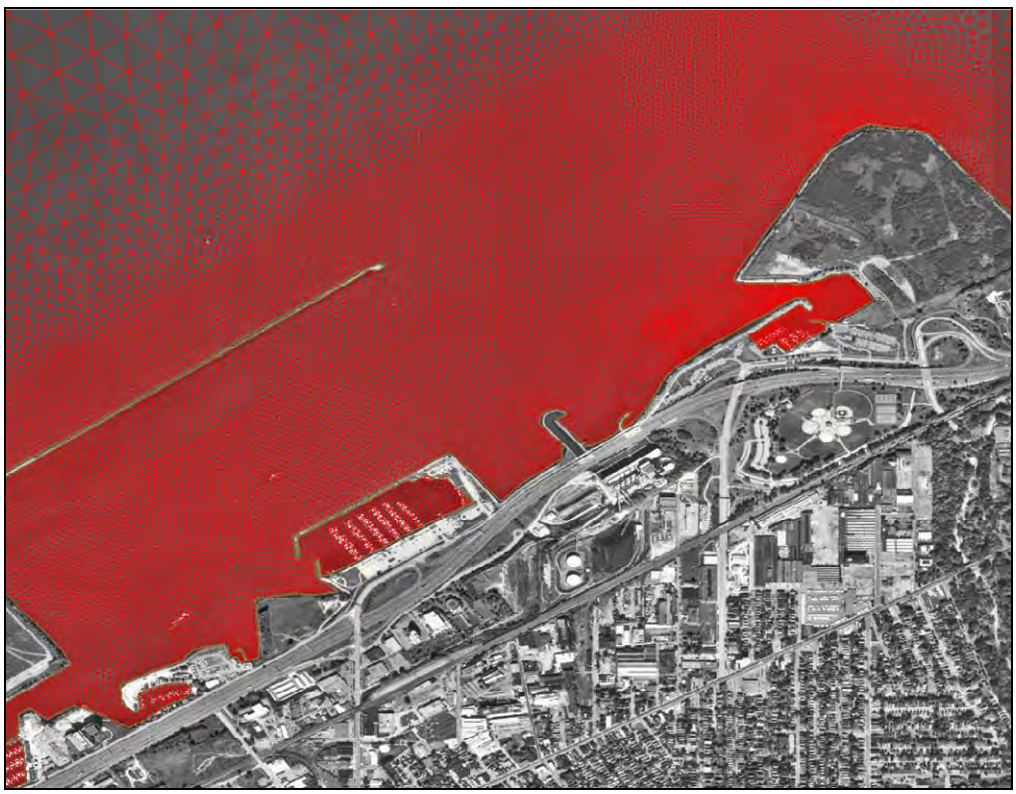

b) Lake Erie ADCIRC grid in project area.

Figure 3

The grid highly resolves the entire Harbor and its main, western, and eastern entrances, together with the lower reaches of the Cuyahoga River. This existing-configuration or base grid consists of 95,255 nodes and 183,034 elements, of which 30,628 nodes and 62,038 elements

resolve the Harbor. The largest elements reside in the central Lake basin, having nodal spacing of about 24 km, whereas the smallest elements resolve the western Harbor entrance, where their widths are approximately 15 m. For most of the Harbor, including the area of the proposed CDF, nodal spacings are approximately 20 m. Included in the grid are the power plant's outfall and intake structures.

The grid boundary along the Canadian shoreline was aligned with the shoreline shown on satellite imagery published by NaturalVue, which are digitally enhanced images taken by the Landsat satellite. These imagery have a 15-m resolution. For areas within the United States, shoreline positions are based on satellite imagery published by the U.S. National Geo-spatial Intelligence Agency (formerly the Defense Mapping Agency), and have a resolution of 5 meters. In the vicinity of Cleveland Harbor, U.S. Geological Survey Digital Orthographic Quarter-Quadrilateral (DOQQ) imagery was used in aligning the grid shoreline and its coastal structures. The DOQQs have a resolution of about 1 m.

Bathymetry specified in the grid was obtained from two sources. For Cleveland Harbor, bathymetry was extracted from contours and soundings residing in the U.S. National Oceanic and Atmospheric-published Electronic Nautical Chart. For the remaining regions outside of the Harbor, bathymetry data was extracted from the National Geophysical Data Center (NGDC) Coastal Relief Model database for Lake Erie as well as Lake St Clair. For both data sources depths are referenced to the International Great Lakes Datum 1985 (IGLD). Figure 4 shows the base and plan configurations with bathymetry contours. The arrows indicate the location of the CSO outfall locations. As seen in the figures, the depth varies between the CSO release points (approximately 3 meter depth) and the East breakwater (> 10 meters). Also noted is the change in the position of CSO 203 between the existing condition and the addition of the CDF.

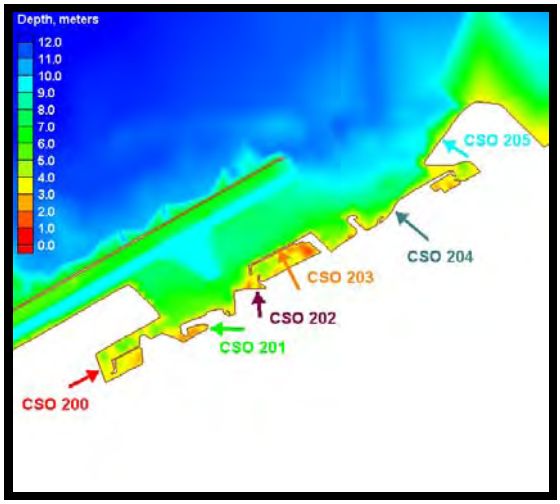

Base Grid (Existing Conditions)

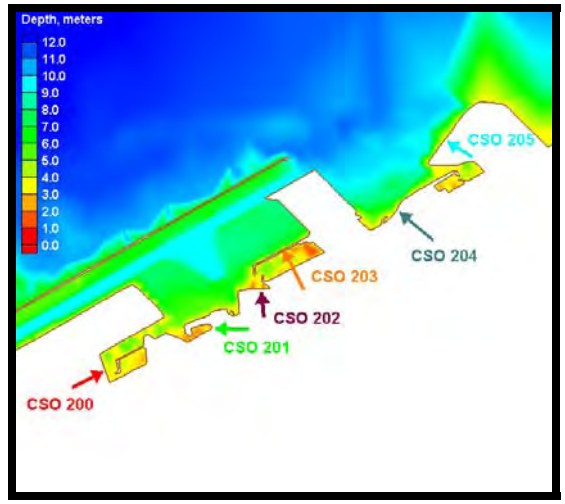

Alternative 1Configuration

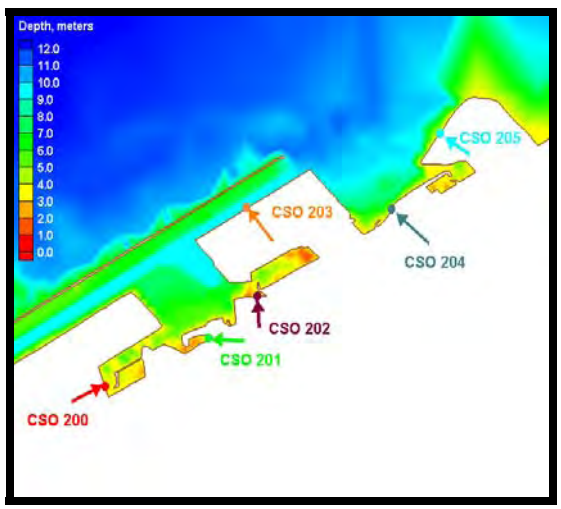

Alternative 2 Configuration

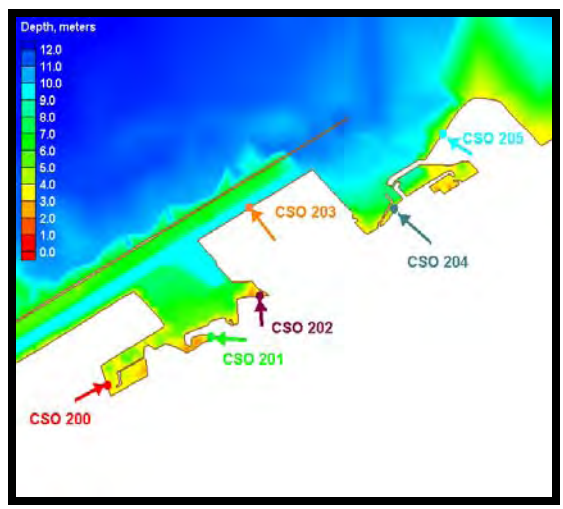

Alternative 3 Configuration

Figure 4

Boundary Conditions and Forcing

Wind data were obtained from the National Oceanic and Atmospheric Administration's (NOAA) Great Lakes Environmental Research Laboratory (GLERL), and were generated as part of their Great Lakes Coastal Forecasting System (GLCFS). One component of the GLCFS is the generation of wind fields subsequently used in circulation and water level now-cast simulations. Hourly wind speeds and directions were extracted from GLCFS archives. These data are provided at 5-km intervals that encompass the entire Lake.

Water level data for model calibration and validation consist of 12 gauges and were obtained from the U.S. National Ocean Service (NOS) and the Environment Canada-Canadian Marine Environment Data Service (CMEDS). River inflow data measured in the Detroit River were obtained from the U.S. Army District, Detroit, whereas flow rate data specified for the Cuyahoga, Niagara, and Maumee Rivers were obtained from the USGS stream flow web site.

The CSO inflows were time-varying flows with the hydrographs being provided by the LRB for the 6-month and 5-year design storms (Appendix A). Further details concerning the CSO input can be found in the Hydrodynamics and PTM Source Development sections.

Figure 5 shows velocity contours and vectors at CSO 204 for the 5-year design storm. The first picture depicts a time (8/14/2002 23:30) during outflow into the harbor and the second shows a period where there is no outflow (8/15/2002 02:00). Because the outflow effect on the surrounding flow was unknown, it was important to add the discharge into the harbor as a boundary condition for the hydrodynamic model as well as modeling the outflow particle sources to determine the overall fate of constituents.

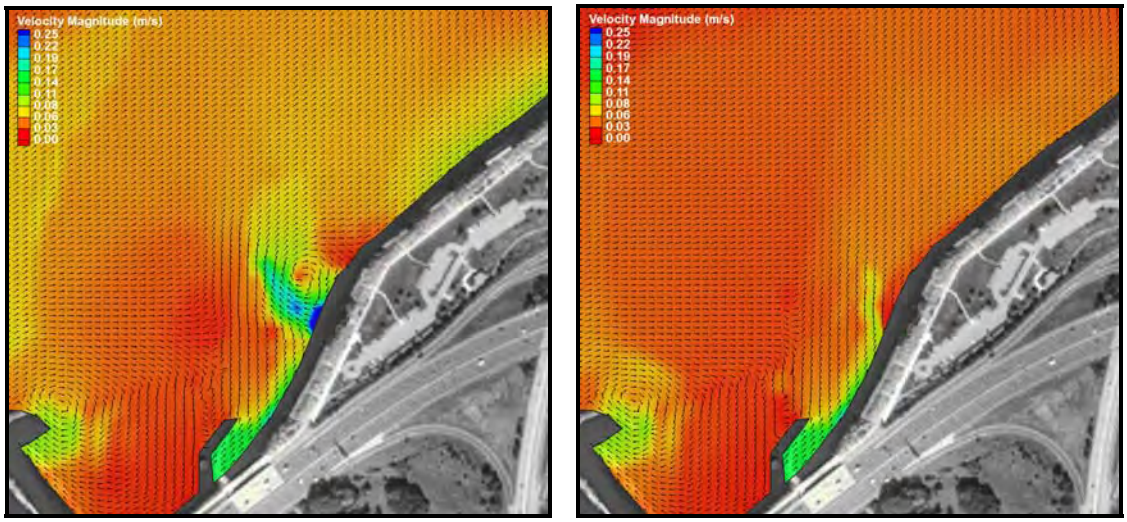

CSO 204 – During outflow into Harbor CSO 204 – After outflow into Harbor

Figure 5. Velocity contours and vectors at CSO 204 for the 5 year design storm

Hydrodynamics

ADCIRC was run from July 30 at 0:00, 2002 to September 24 at 24:00 with the solution being saved every half hour. Hydrodynamic conditions were run for two specific design storms: 6-month and 5-year. Initially, the intent was to obtain actual discharges during the simulation

period (summer 2002). However, due to the unavailability of the data, it was determined that instead two design storms would be utilized to represent normal and extreme conditions. The

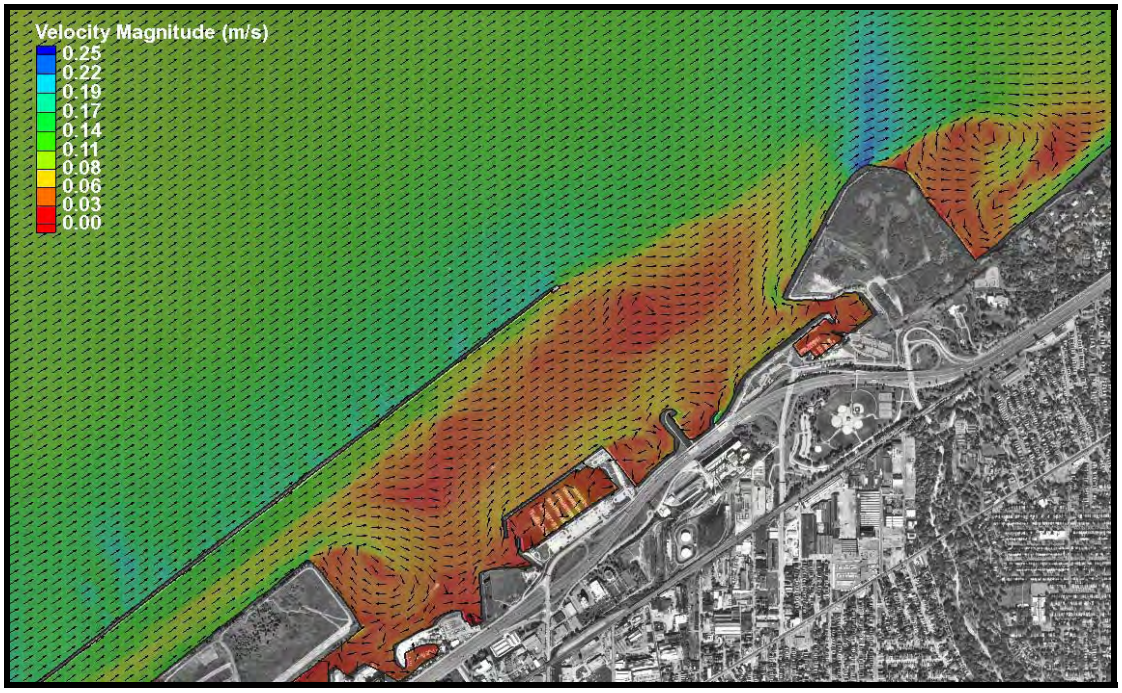

Existing Conditions – 8-16-2002 (00:00)

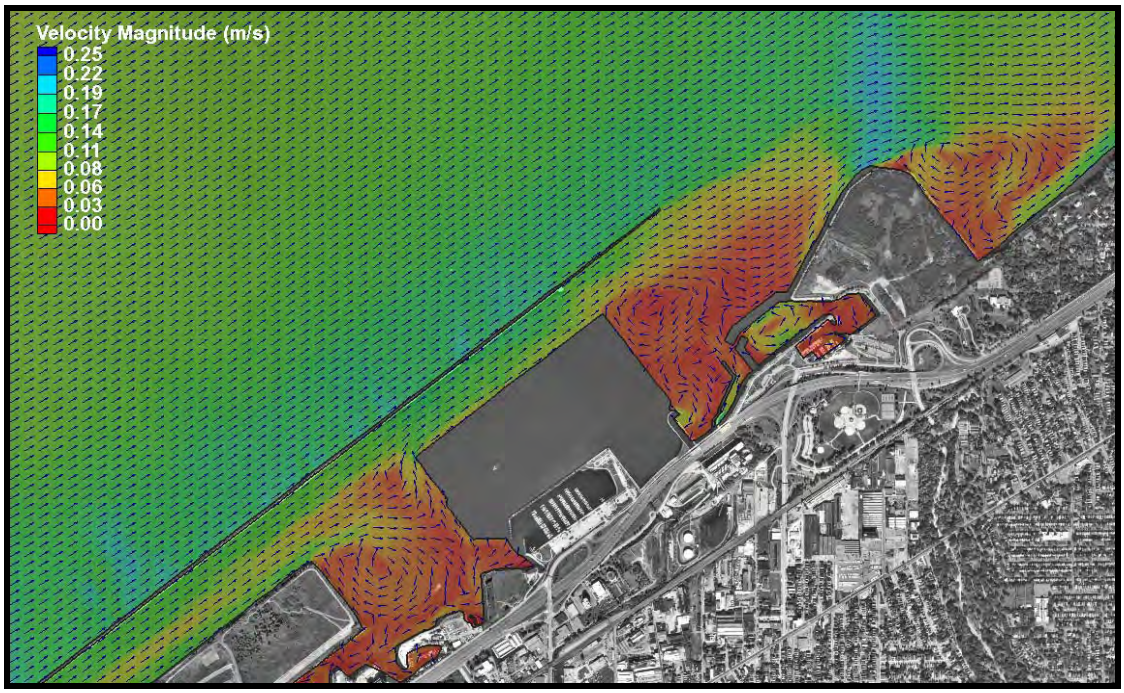

Configure 3 – 8-16-2002 (00:00)

Figure 6 contours of velocity magnitude and vector

actual precipitation recorded at the Cleveland airport during the simulation period was plotted and used as a basis for the CSO inflow by inserting the 6-month and the 5-year flows during the times of significant recorded precipitation. Within the data it was determined that a significant rainfall event occurred on August 14. The timing of the maximum rainfall occurring in the design storms were matched to the maximum measured rainfall during this period. Therefore, the design storms were run during a measured rainfall event to best replicate the behavior of true storm conditions. The PTM simulation, which will be described in another section, starts at 19:00 August 14, 2002 which is directly following the significant storm event and therefore when the CSOs discharge into the harbor and particles exist to be tracked.

Seen in figure 6 are hydrodynamic results (contours of velocity magnitude and vector) at 00:00 August 16, 2002. This is a point at which the storm event has past and all particles have been released into the harbor for transport. It does not appear as if the CDF structure has changed the magnitude of the flow in the area. However it is immediately noticeable that the recirculation patterns on both the westward and eastward side of the CDF are different. This change has the potential to greatly affect the transport of the particles. For neutrally buoyant particles, this means that particles may passively mix in different patterns. That is, the mixing rate may be the same but the coherent structures that are visible during mixing may be altered. For sediment particles, tight areas of recirculation may impede immediate transport which might allow particles a greater opportunity to deposit.

PTM Source Development - CSO flows

In this study, six CSO locations were identified (Figure 4). To simulate these sources, PTM requires the following user specified data:

- Date/Time of CSO release
- Positions (x,y,z) of CSO introduced into the water column
- Rate of constituent introduction
- Size distribution of suspended constituent
- constituent density

The date and time release were determined based on the design storm conditions (figure 7). PTM sources were introduced at each CSO at the top of the water column. CSO flows for two design

storm conditions—6 month and 5 year storms—were used in this study (figure 7). As mentioned in the hydrodynamic section, due to the unavailability of actual discharges during the simulation period, in order to capture the result from larger discharge events, hypothetical CSO discharges were developed. The City of Cleveland computed 1-, 4- and 6-month and 1-, 2-, and 5-year rainfall amounts and discharge hydrographs at the six CSOs. Only the 6-month and 5-year discharge hydrographs were used, with the 5-year hydrograph computed by increasing the 6-month hydrograph by the ratio of the 5-year and 6-month rainfall amounts. Generally it can be seen that rainfall and discharges for the 5 year storm were approximately double of those for the 6 month storm. Each storm-induced CSO event lasts about 7 hours lagging the precipitation.

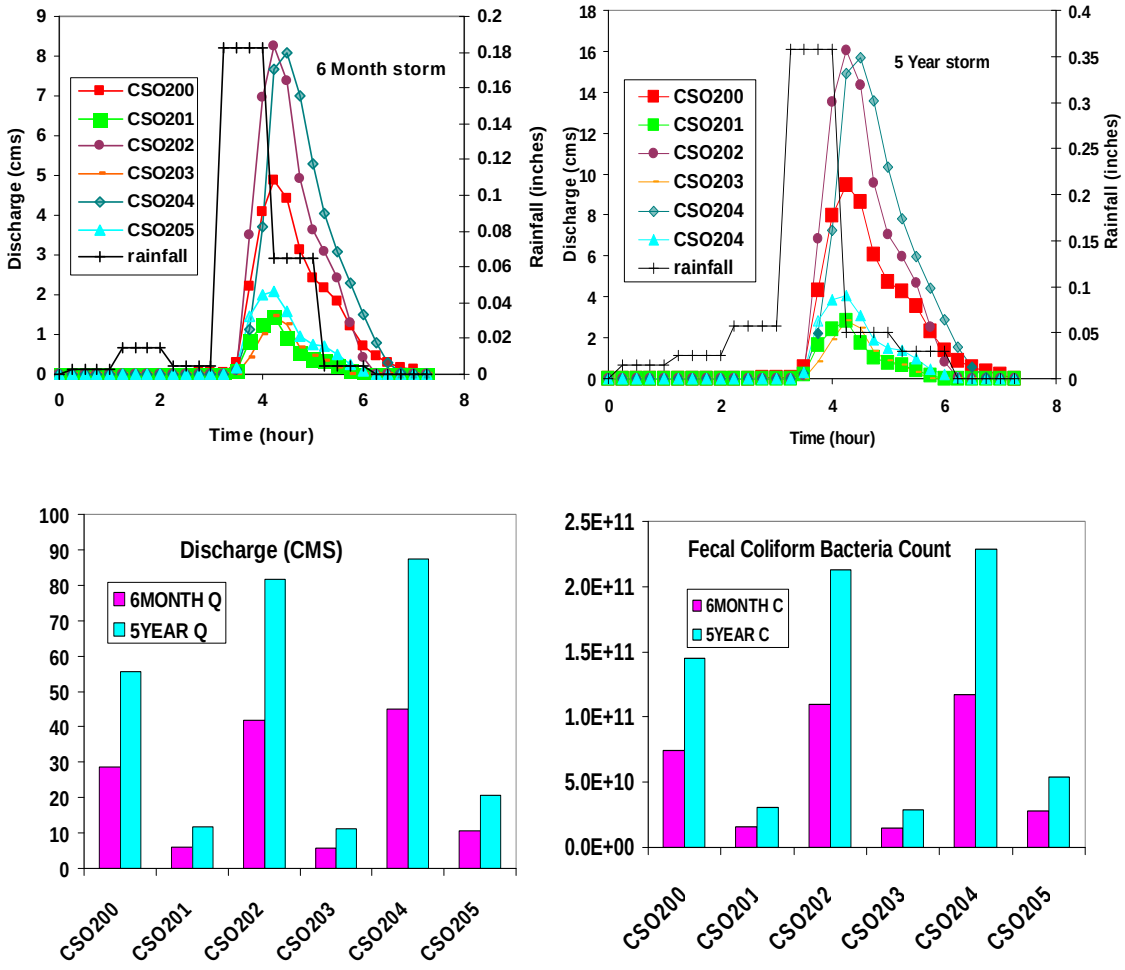

Figure 7. Storm conditions. Upper panels show CSO discharges from 6 month and 5 year storms. Also shown are the rainfalls. Lower panels show total discharges and FCB counts during events.

There are strong correlations between CSO flows and fecal coliform bacteria (FCB) counts. The time 00:00 of events were set at 19:00 of August 14, 2002 which coincides with wind events. The raw data for CSO flows and FCB counts are given in Appendix A, while Figure 7 displays a graphical representation of this data. The FCB counts were developed from a constant concentration value of 261,000/100ml, supplied by the City of Cleveland. The rate of introduction for particles into the Harbor was determined based on the CSO discharge and subsequently the FCB count. The ratio of simulation to FCB counts were set as 1: 107 so that total number of particles released were approximately 1200 and 2400 for 6 month and 5 year storms, respectively.

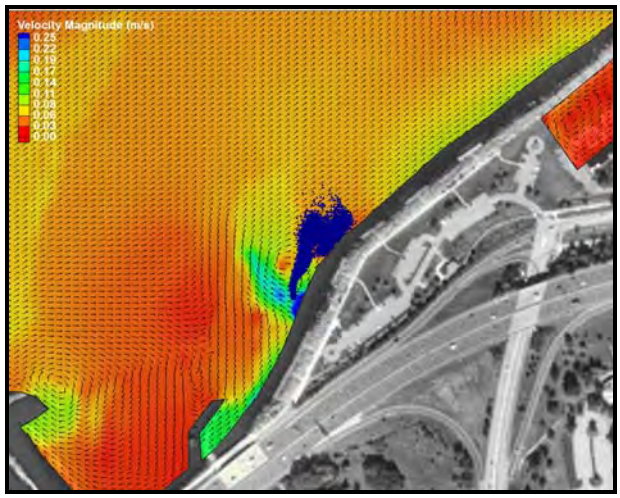

Figure 8 – CSO 204 During outflow into Harbor

Native Sediment

Native sediment grain size distributions did not influence the outcome of particles introduced into the Harbor which were neutrally buoyant or floating. Particle deposition was extremely limited, only occurring due to the vertical fluctuations in the particle position due to the random walk diffusion calculations. However, for sediment particle transport, native sediment characteristics were required to accurately determine particle bed interactions. A fine grain sediment distribution was utilized (D50=100 microns).

PTM Simulation Details and Results

The PTM simulation starts at 19:00 August 14, 2002 and ends 00:00 September 15, 2002. The calculation time step is 30 seconds. Three sets of runs were implemented—(1) neutrally

buoyant particles (particle density = water density), (2) floatables (particle density < water density), and (3) sediment particles (particle density > water density). No-decay of particles was assumed for each of these sets.

Chemical Transport (Neutrally Buoyant Particles)

Advection of the particles released from the six CSOs closely followed the circulation patterns (figures 9 through 12). In these figures, particles are colored based on the CSO from which they originate (figure 4) and snapshots are shown of transport one, six, eleven, seventeen, and thirty days after release. The final figure shows a zoomed in view of day thirty after release. For succinctness, only the base case (figures 9 and 10) and configuration 2 (figures 11 and 12) are shown to depict the transport currently in existence and the predicted worst case scenario. However, general trends will also be discussed and appendix B contains results for all configurations. Figures 9 and 11 show results based on the six month design storm. Figures 10 and 12 depict results based on the five year design storm. In figure 9, a common trend is visible that is generally followed throughout figures 10-12. Initially there is very little mixing of particles for all CSOs. However, particles from CSO205 (turquoise dots) were immediately advected Eastward by currents induced by dominant Southwesterly winds. After six days particles are diffused throughout the harbor region and have escaped past the East Breakwater. At this point it is hard to find particles from CSO205 in and near the Harbor for the base and all three alternative design configurations. After seventeen days particles are dispersed throughout the system though it begins to be very noticeable that particles are trapped in CSO200 (red dots) for all designs. For the base configuration some particles also remain trapped near the CSO 203 location. This characteristic is even more evident in configuration 2. It should be mentioned, that due to the completion of the CDF, these particles are no longer trapped in configuration 3. Finally after the thirty day period, most of the particles have been advected away except those previously mentioned, confined particles. Investigation of the hydrodynamics shows that not many particles from CSO200 (red dots) escape from the Harbor because of poor circulations in the adjacent water in the base and all three alternative design conditions.

The particles from CSO202 (purple dots) and CSO204 (teal dots) dispersed rapidly in all configurations. Most particles from CSO201 (green dots) and CSO203 (orange dots) exited from system eventually but this is probably due to the small number of particles associated with low discharges. The hot spot near CSO200 was associated mostly with particles originated from

CSO200 (red dots). Another hot spot, for Configuration 3 is linked to the particles released from CSO204 (teal dots). Particles in this configuration become trapped in that area.

Figures 13 and 14 show the particles on 00:00 of August 16th—approximately 1 day after 6-month and 5-year storm events, respectively for all four configurations. The distribution patterns for the two storm events are similar. However, 5-year storm events are associated with more densely packed particles. The majority of particles from CSO200, CSO201, CSO202, and CSO204 are trapped in the system because of the structural confinements. Particles from CSO205 were swept eastward soon after release. Particles from CSO203 moved east for the base configurations but remained between two protruding structures for all the other configurations. Even after 1-month, some particles are trapped near CSO200 and CSO201 for base and alternative configurations (figures15 and 16).

The distribution patterns of neutrally buoyant particles from 6-month and 5-year storm conditions were similar. The only visible distinction was the number of particles in the system—the number of particles from the 5-year storm was roughly double the one from the 6-month storm. After 1 month from release, a hot spot is visible in the Harbor near CSO200 for the base and all three alternative design configurations. For configurations 1 and 2, East 55th State Marina appears to be a hotspot though to a lesser degree than the water adjacent to CSO200. For configuration 3, Gordon Park Marina would be a possible secondary hot spot.

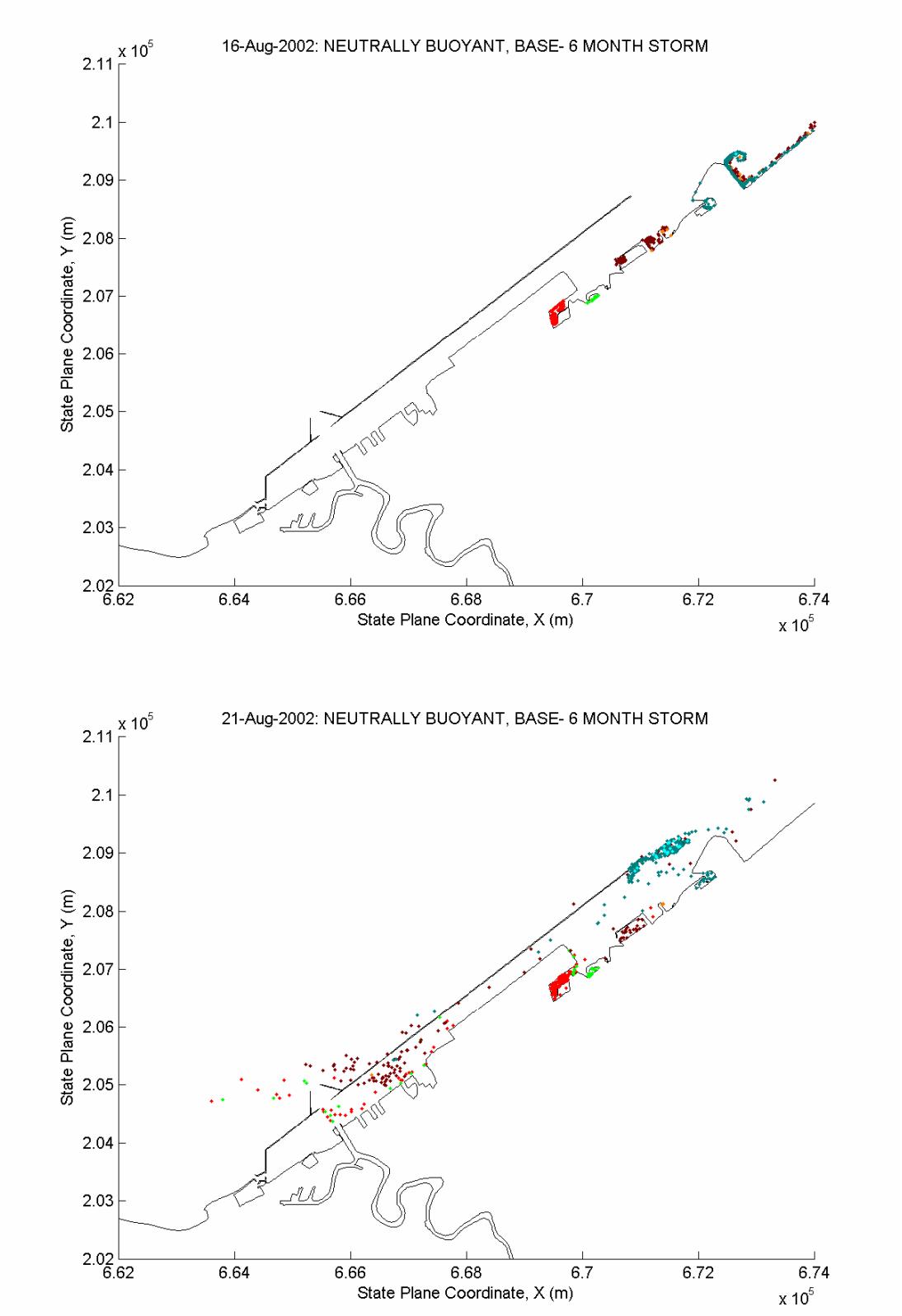

Figure 9. Particle position with time from 6-month storm (particles colored to differentiate CSO) – Base configuration (a and b)

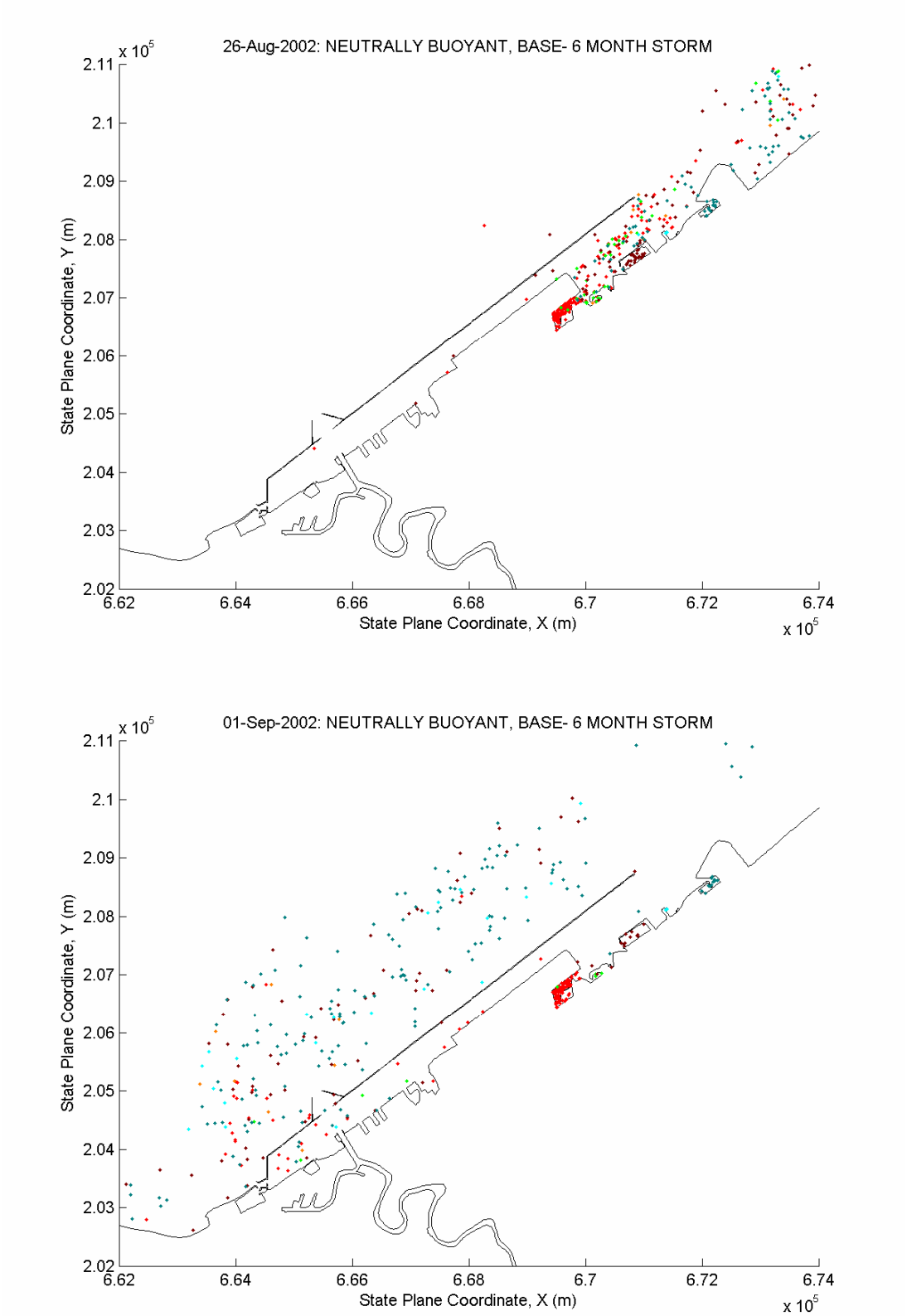

Figure 9. cont (c and d)

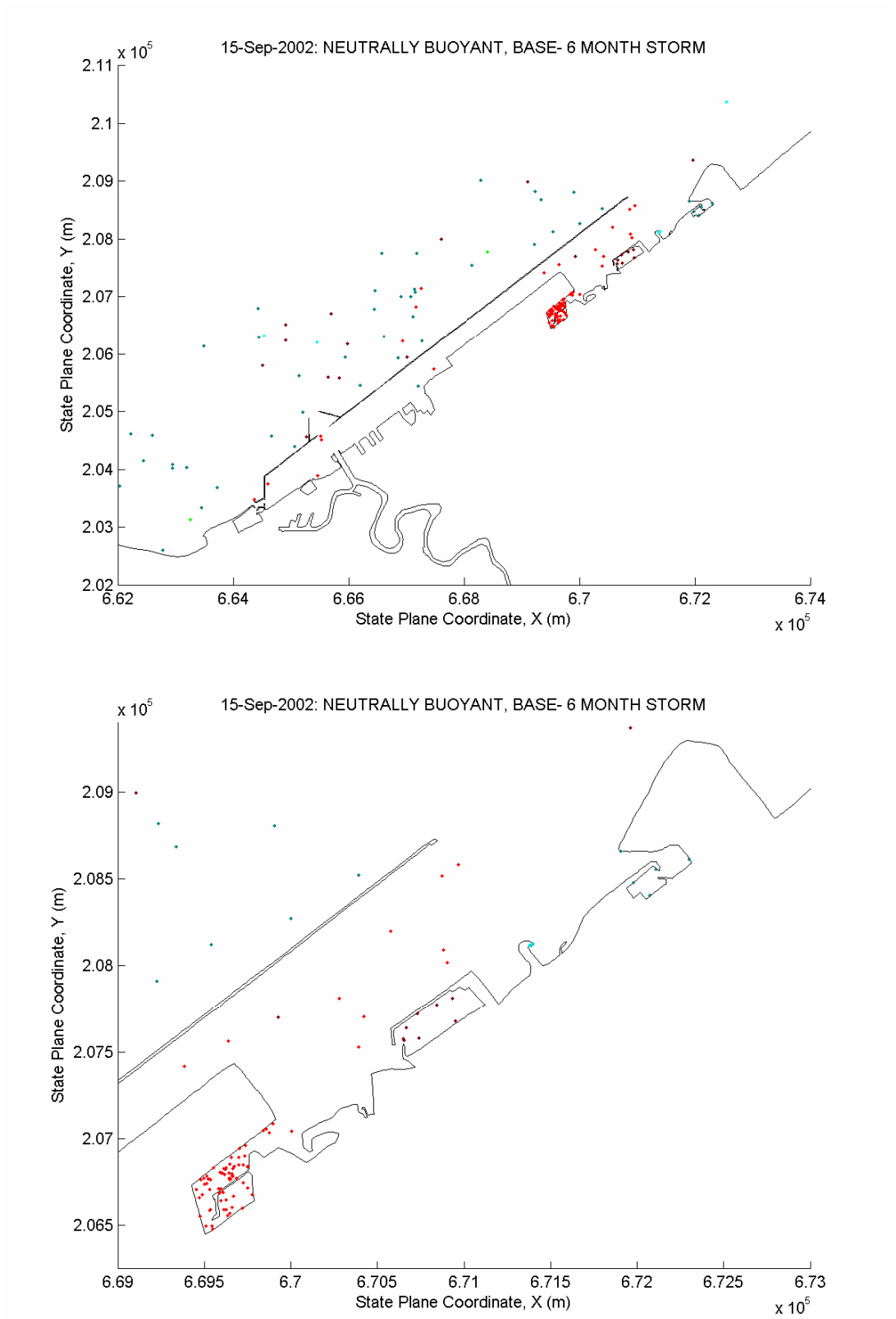

Figure 9. cont (e and f)

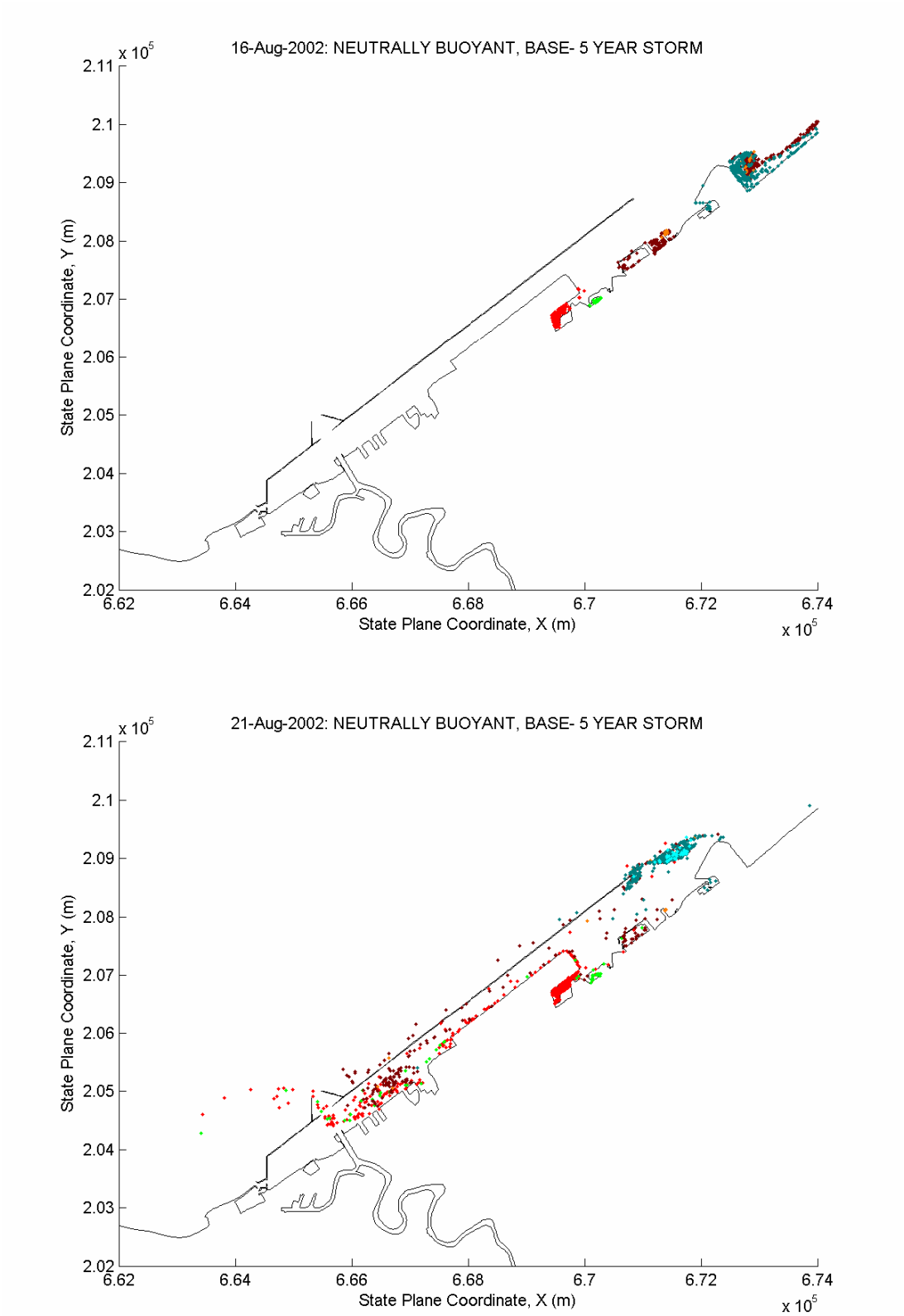

Figure 10. Particle position with time from 5-year storm (particles colored to differentiate CSO) – Base configuration (a and b)

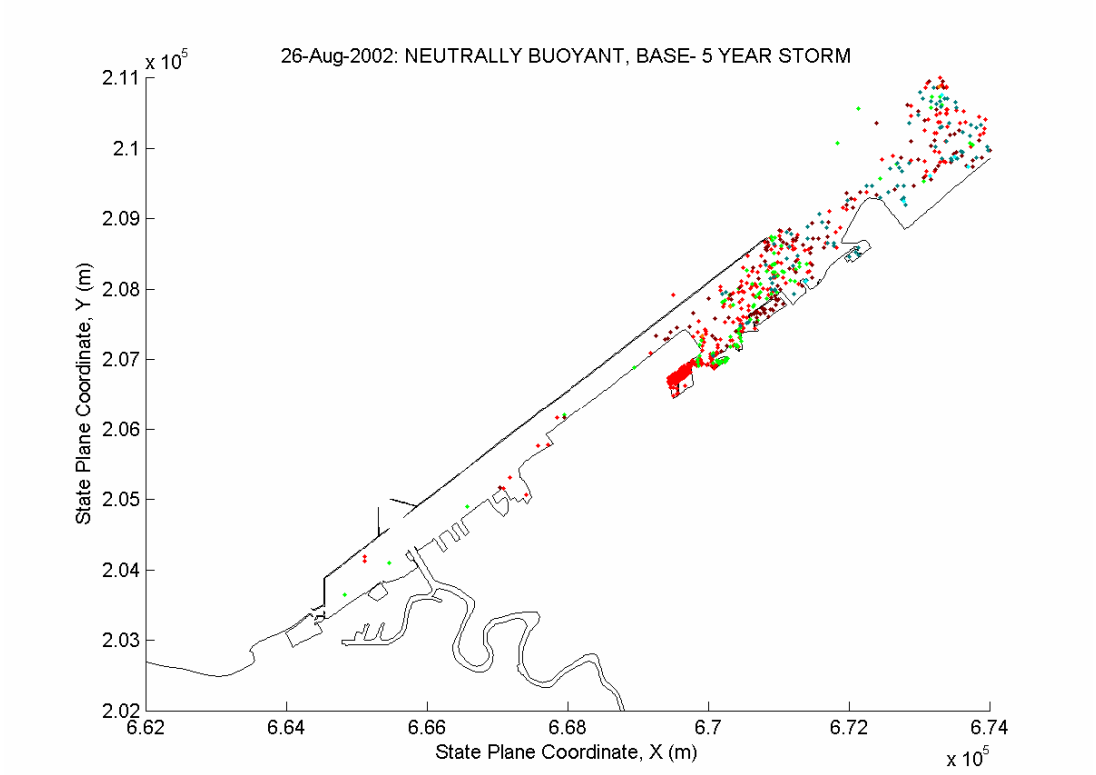

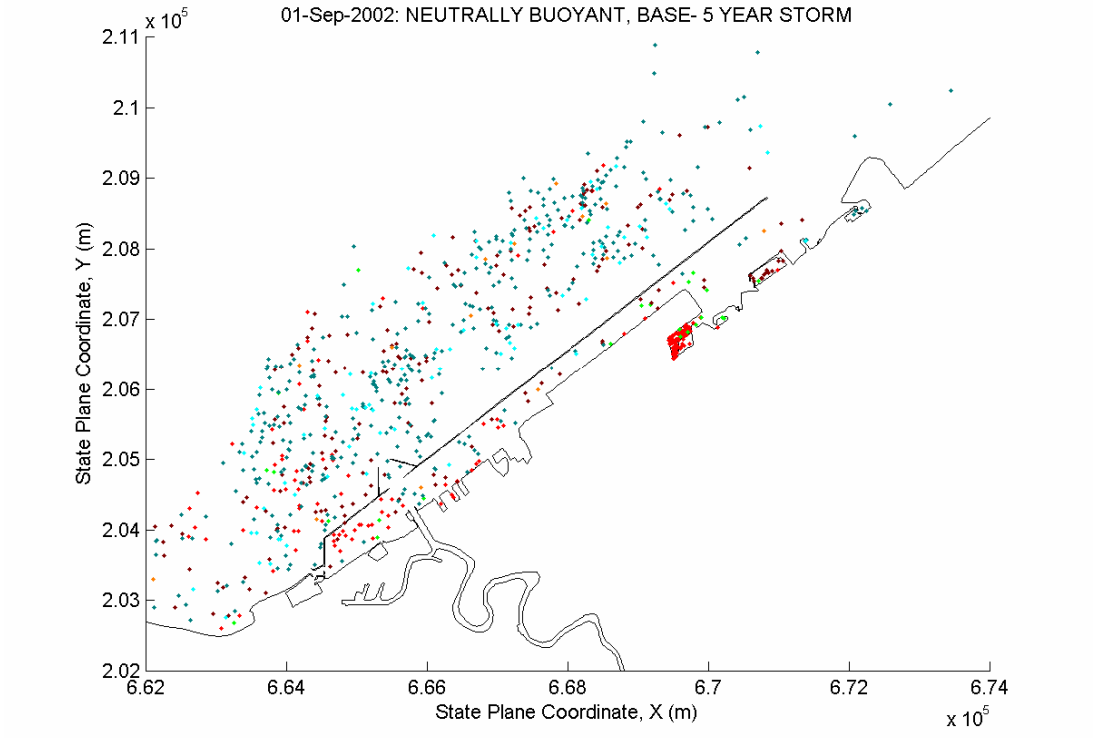

Figure 10. cont. (b and c)

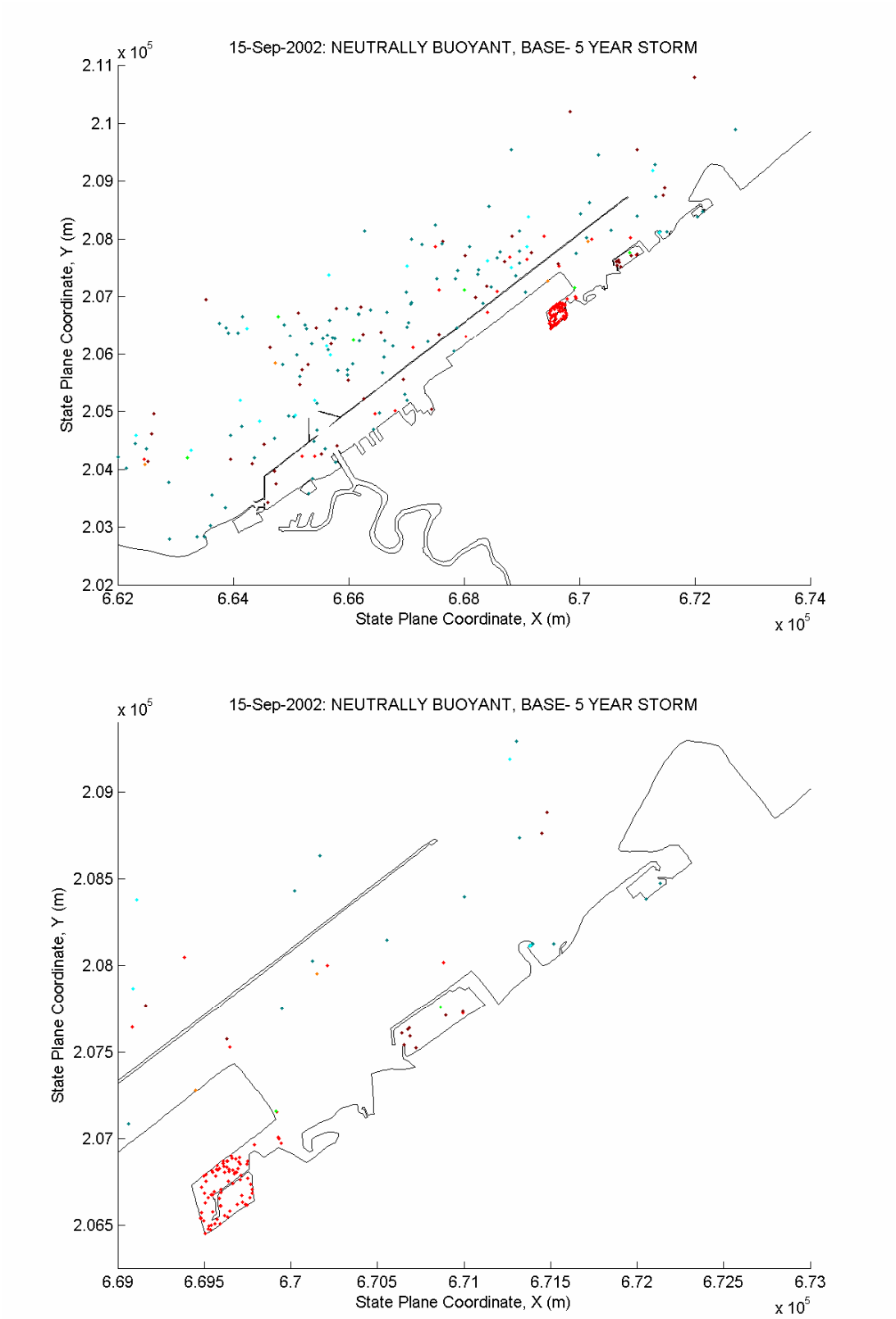

Figure 10. cont. (b and c)

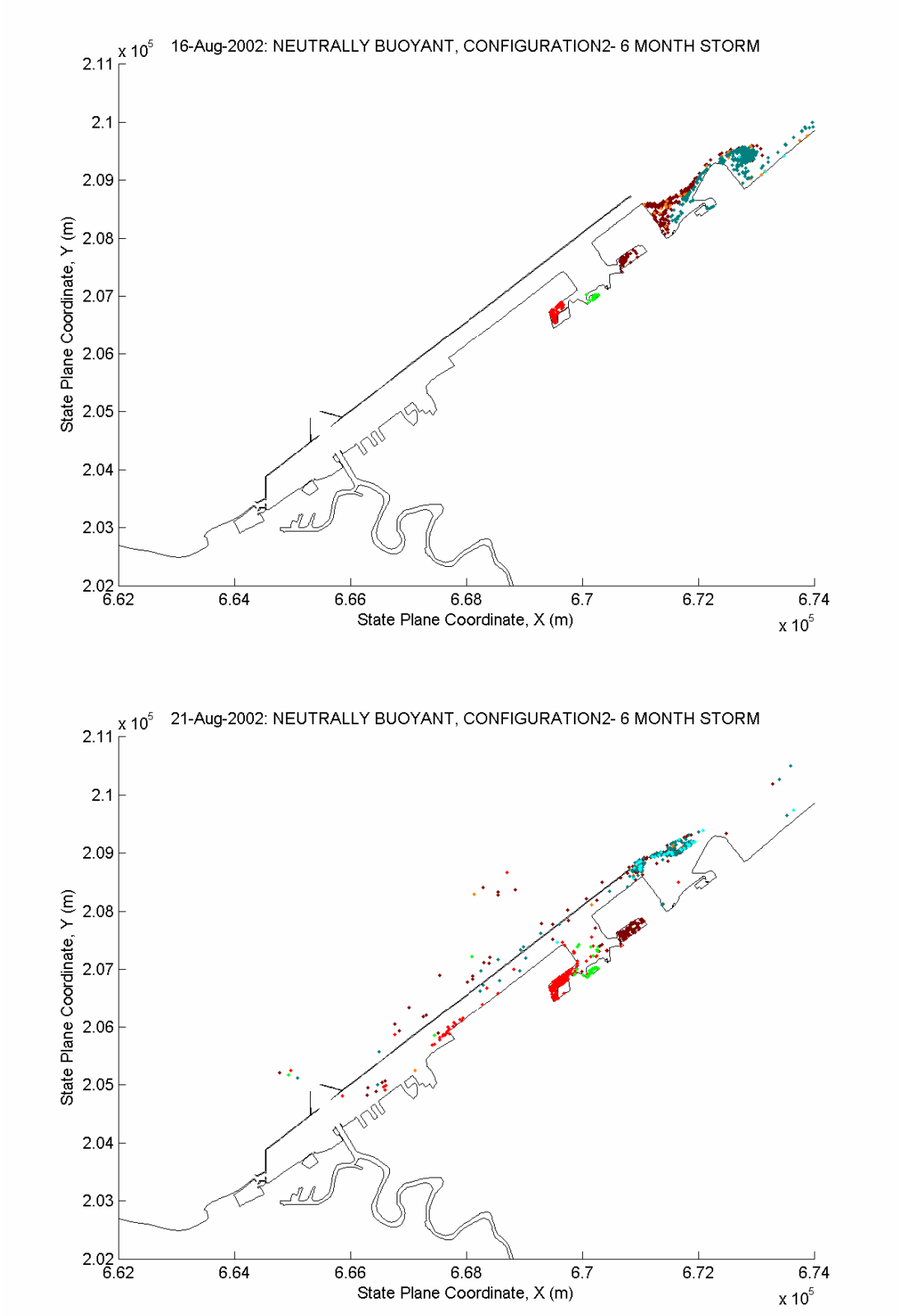

Figure 11. Particle position with time from 6-month storm (particles colored to differentiate CSO) – Configuration 2 (a and b).

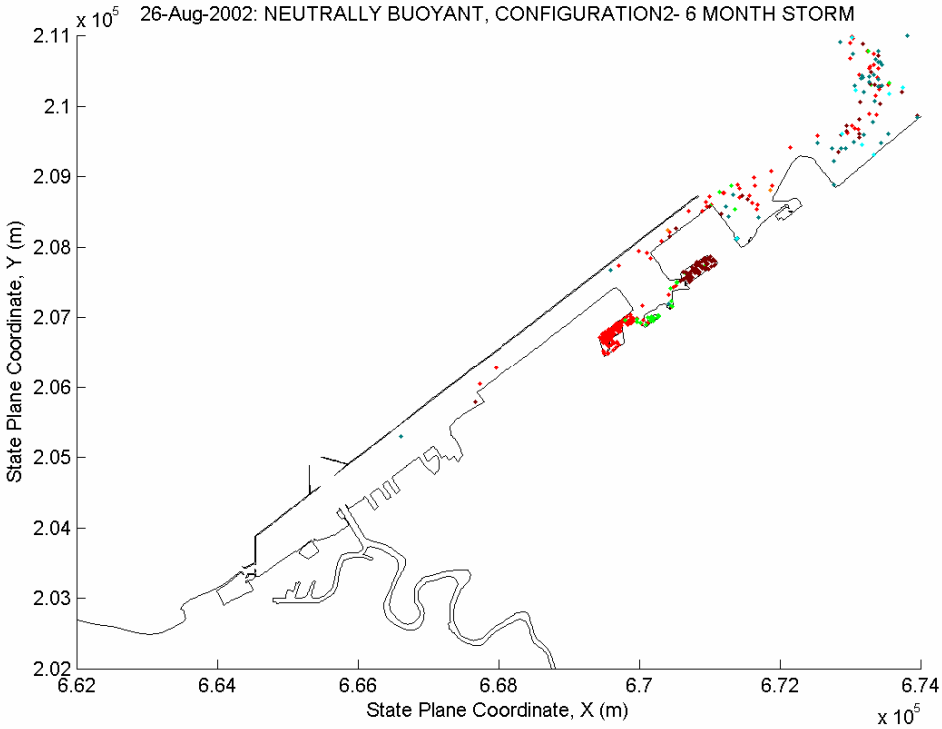

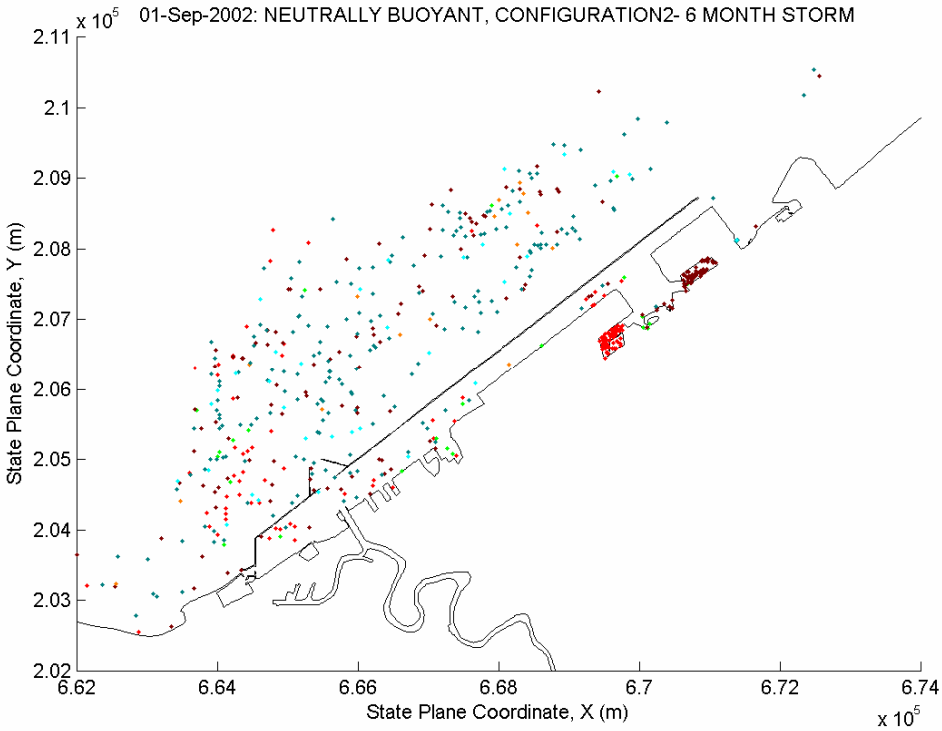

Figure 11 cont. (c and d).

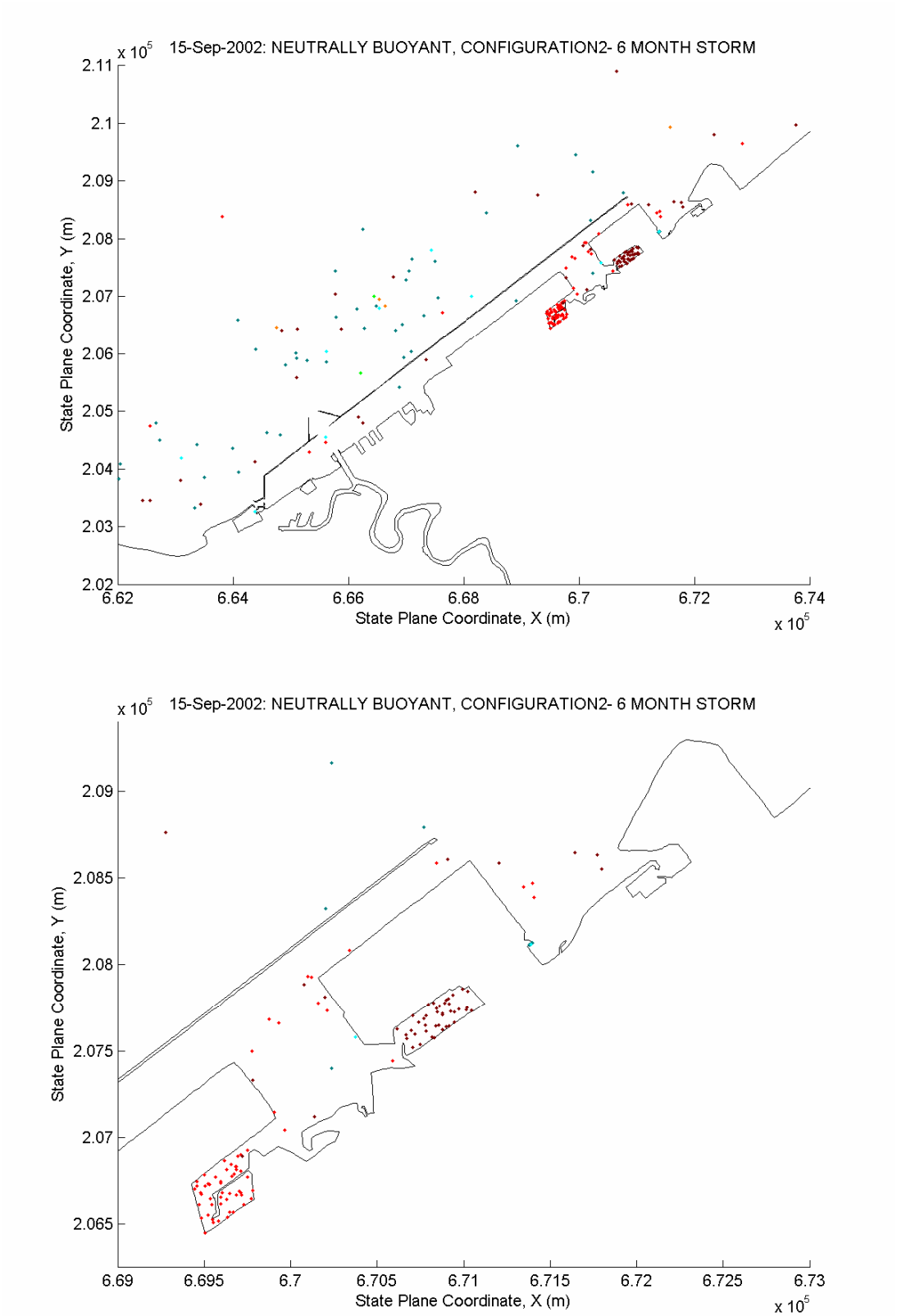

Figure 11 cont. (e and f).

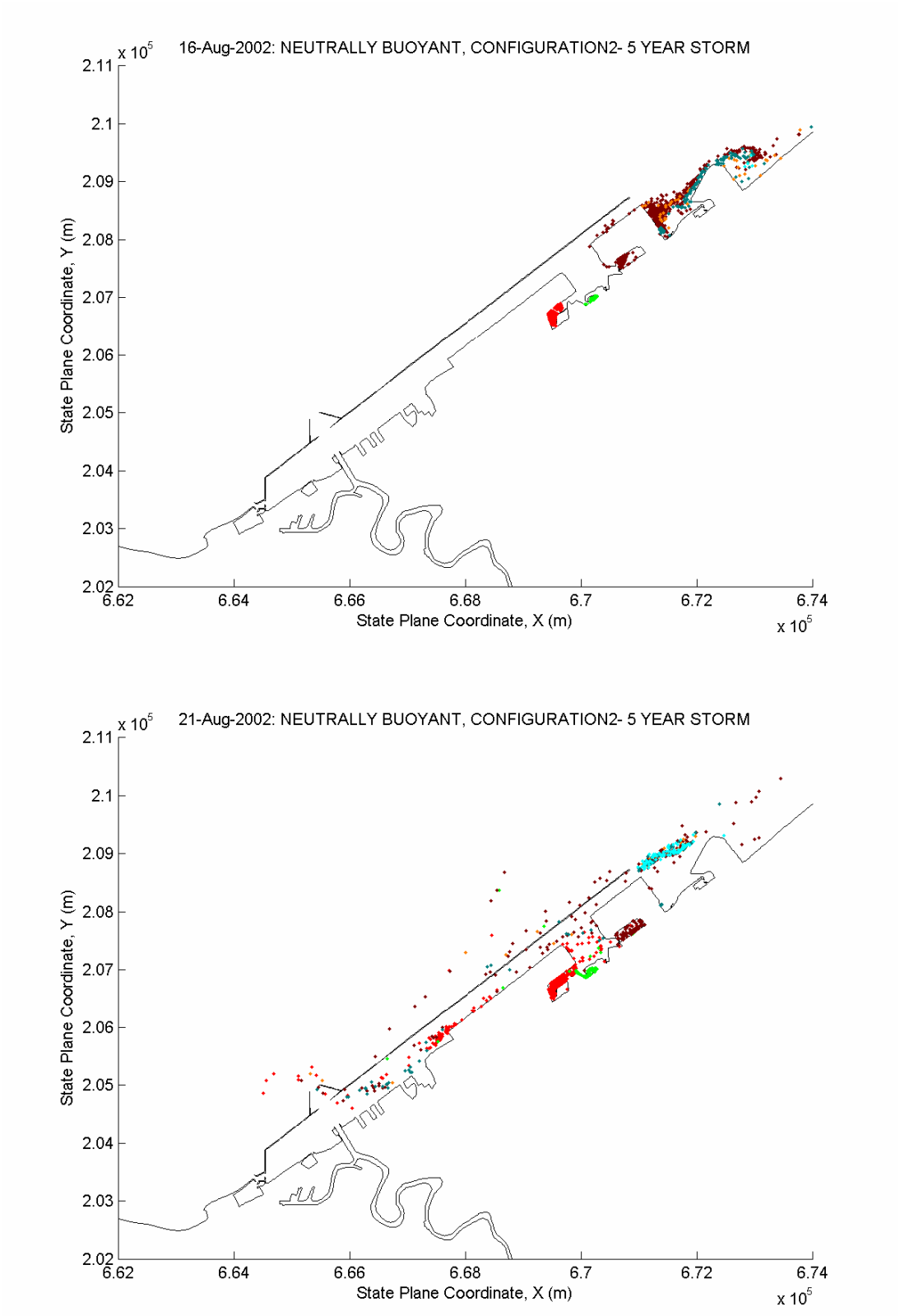

Figure 12. Particle position with time from 5-year storm (particles colored to differentiate CSO) – Configuration 2 (a and b)

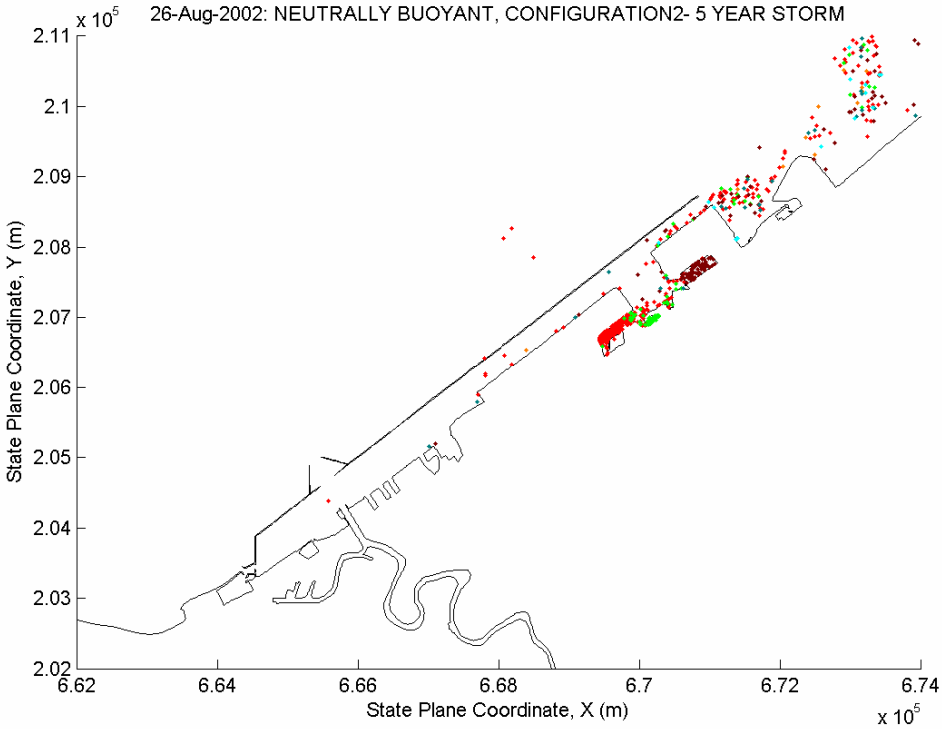

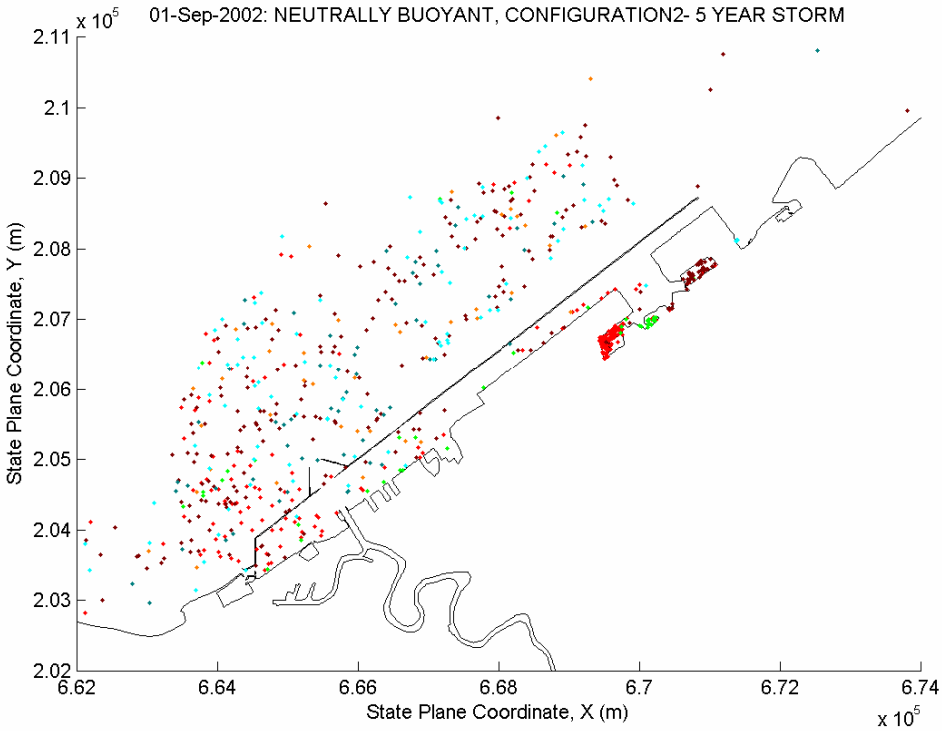

Figure 12. cont. (c and d).

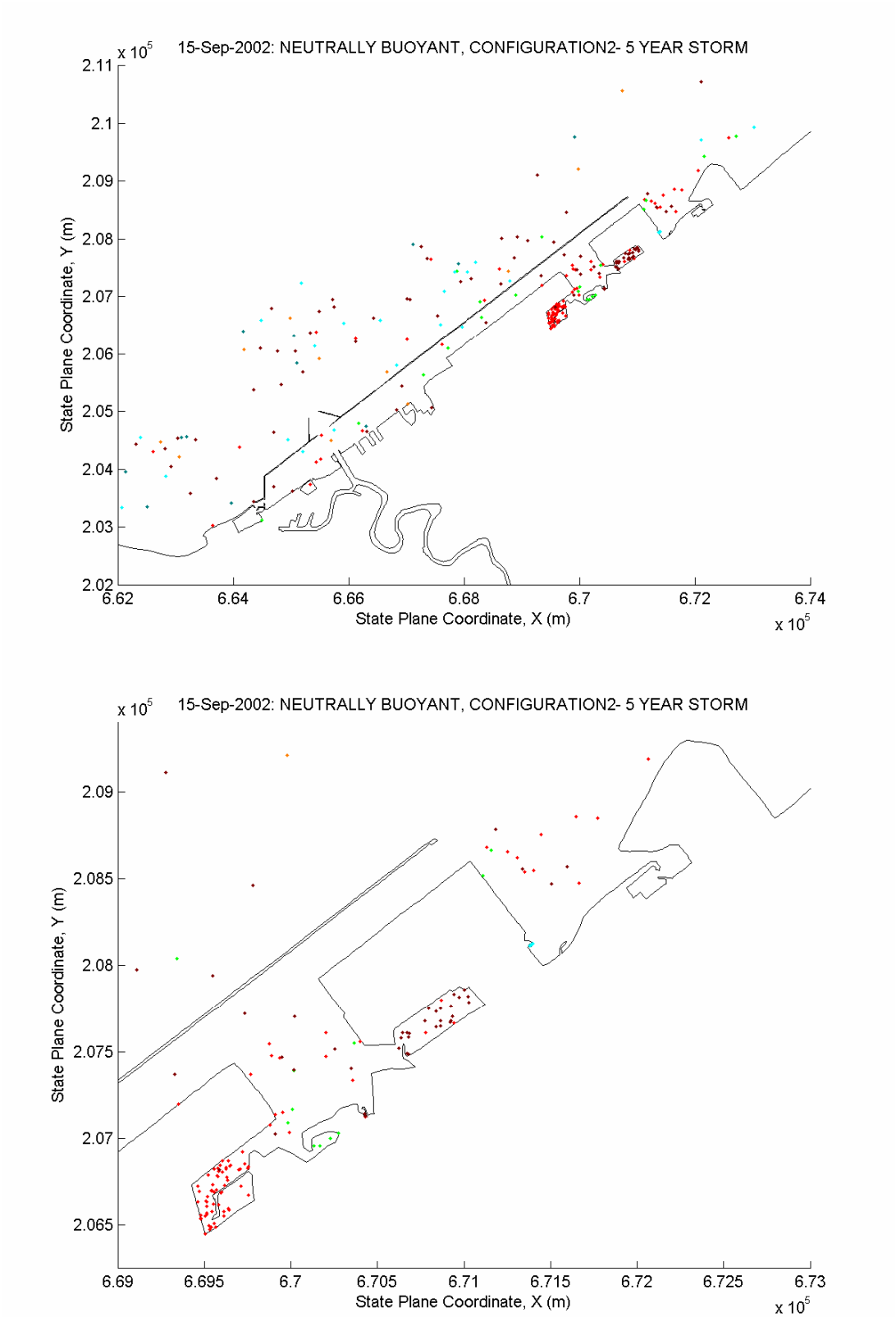

Figure 12. cont (e and f)

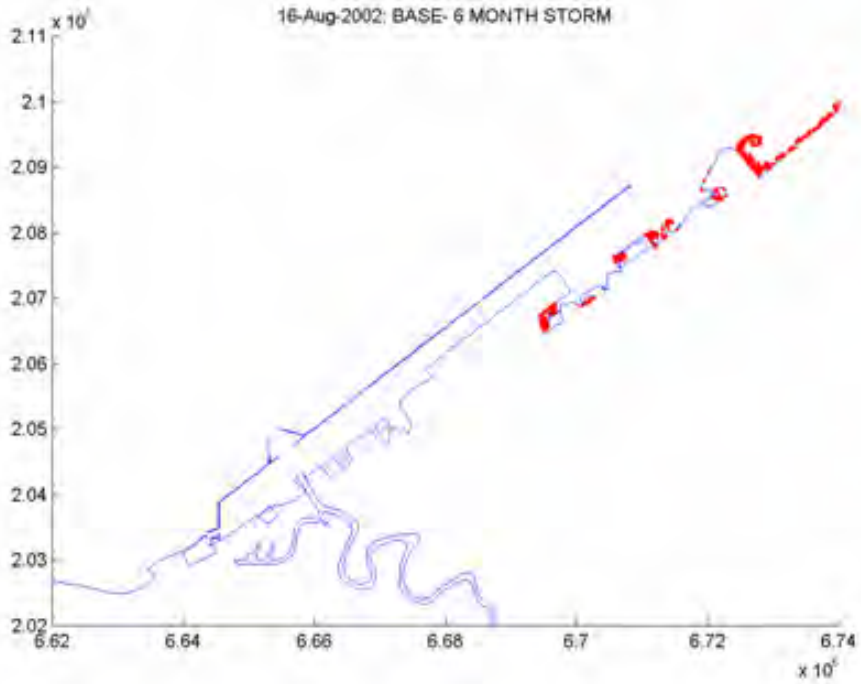

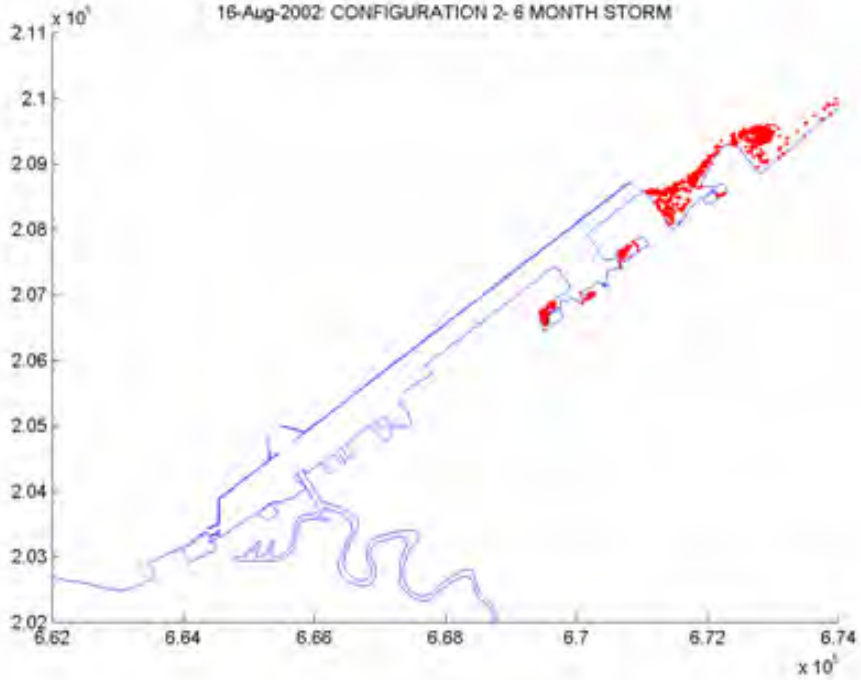

Figure 13. Particles around Cleveland Harbor 1 day after event from 6-month storm (a and b)

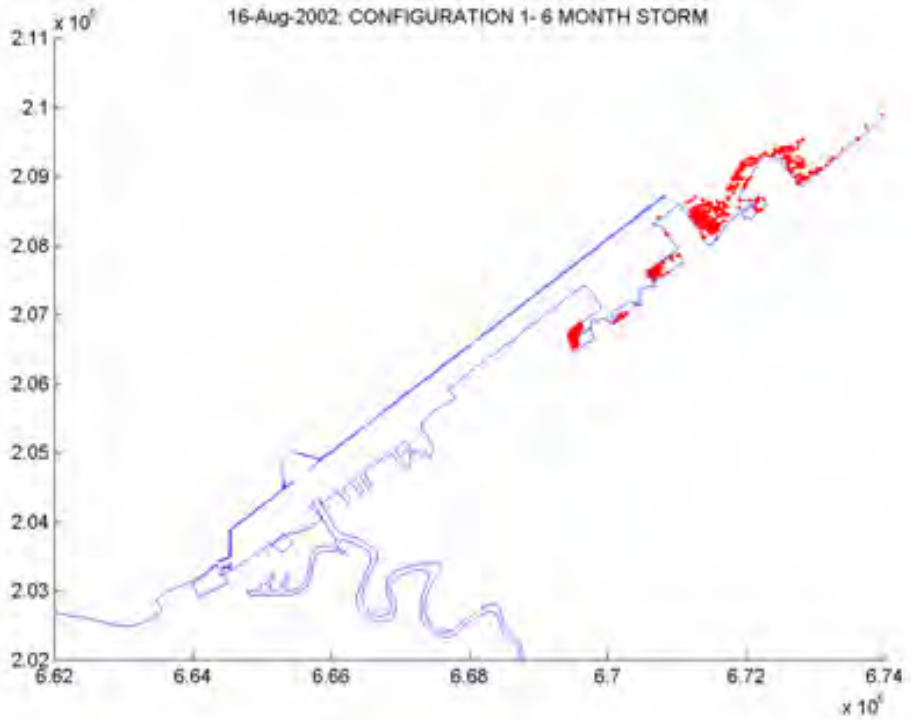

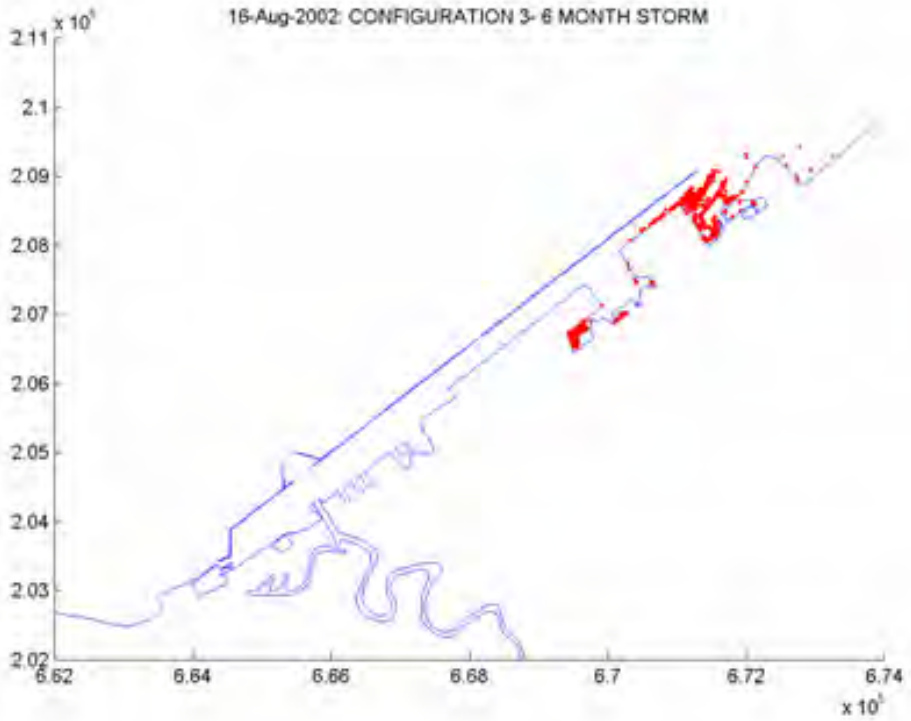

Figure 13. cont. (c and d)

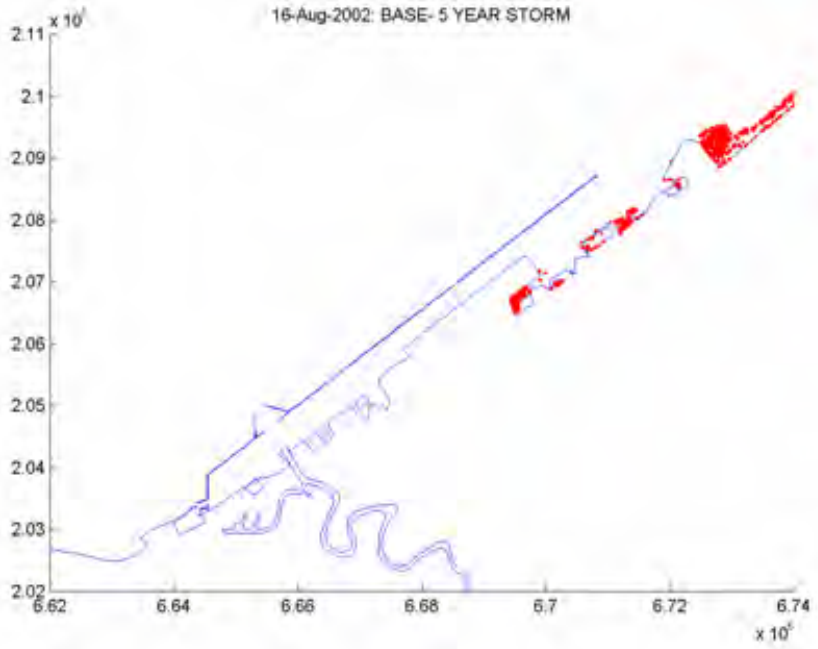

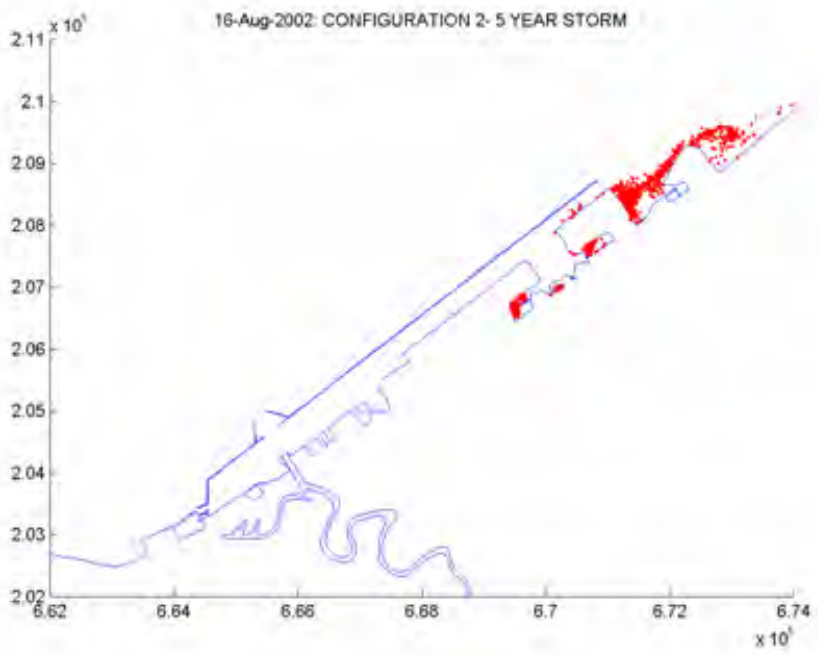

Figure14. Particles around Cleveland Harbor 1 day after event from 5-year storm (a and b)

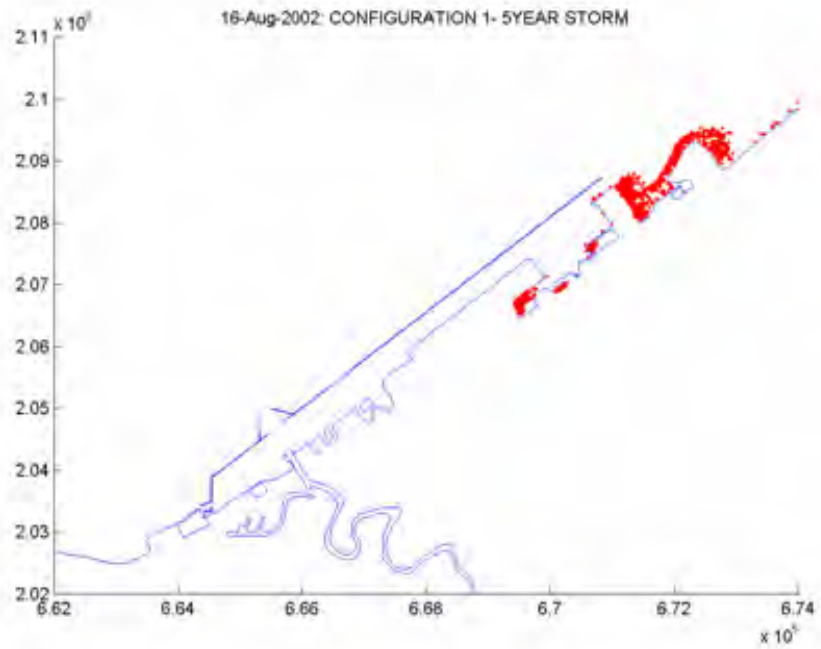

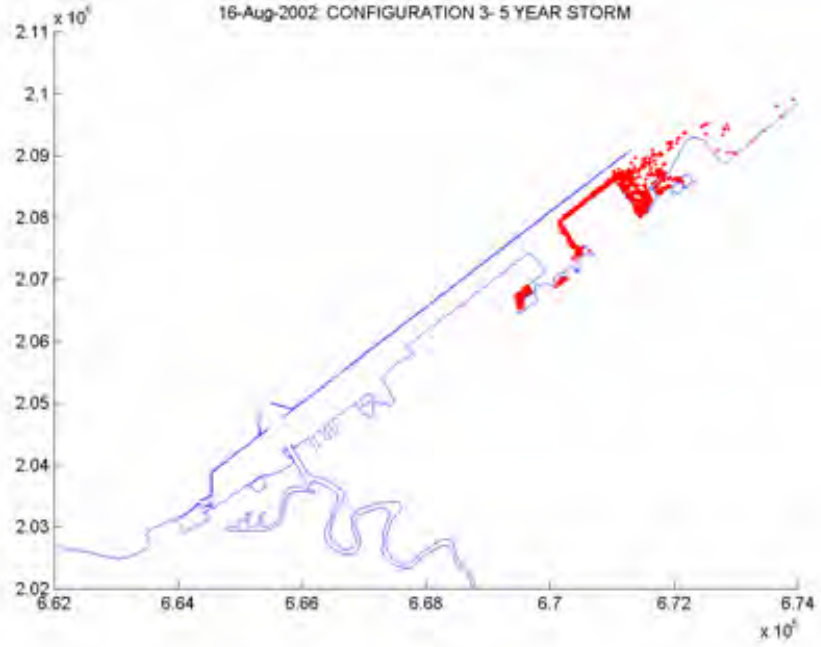

Figure14. cont. (c and d)

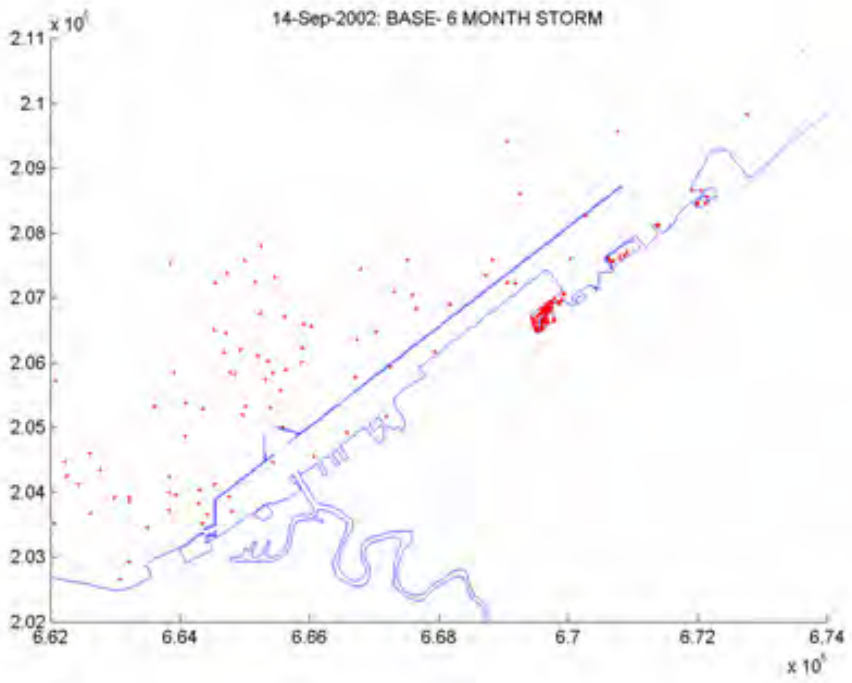

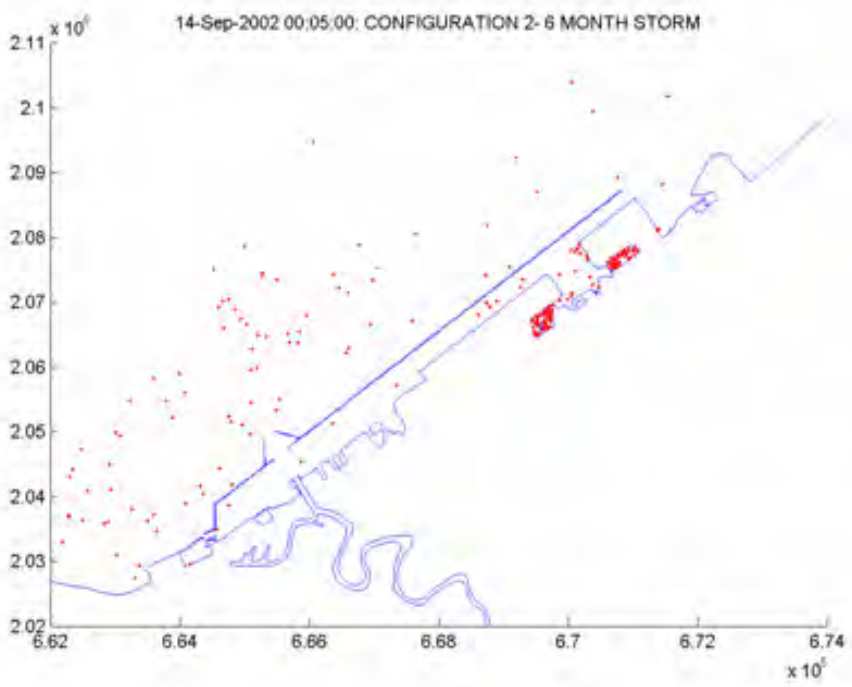

Figure 15. Particles around Cleveland Harbor 1 month after event from 6-month storm (a and b)

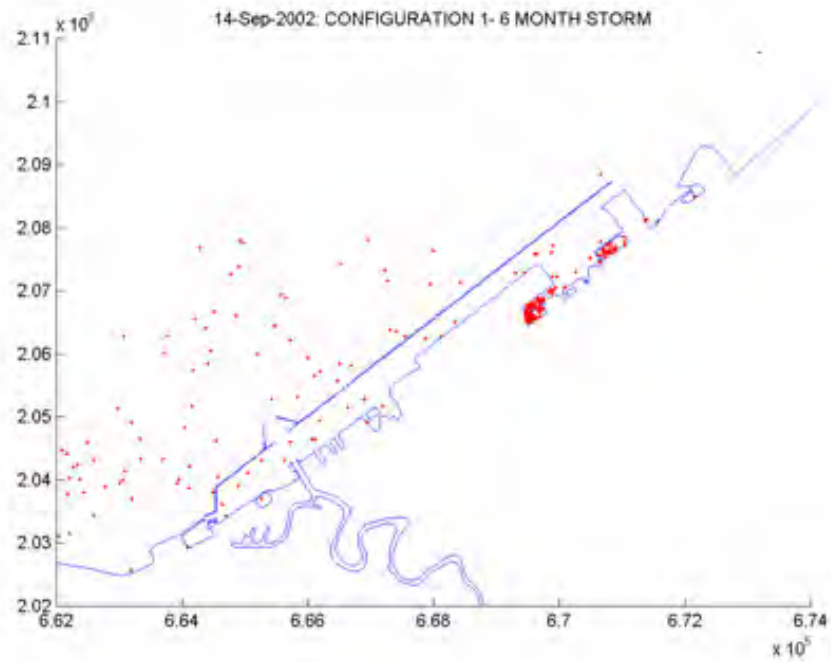

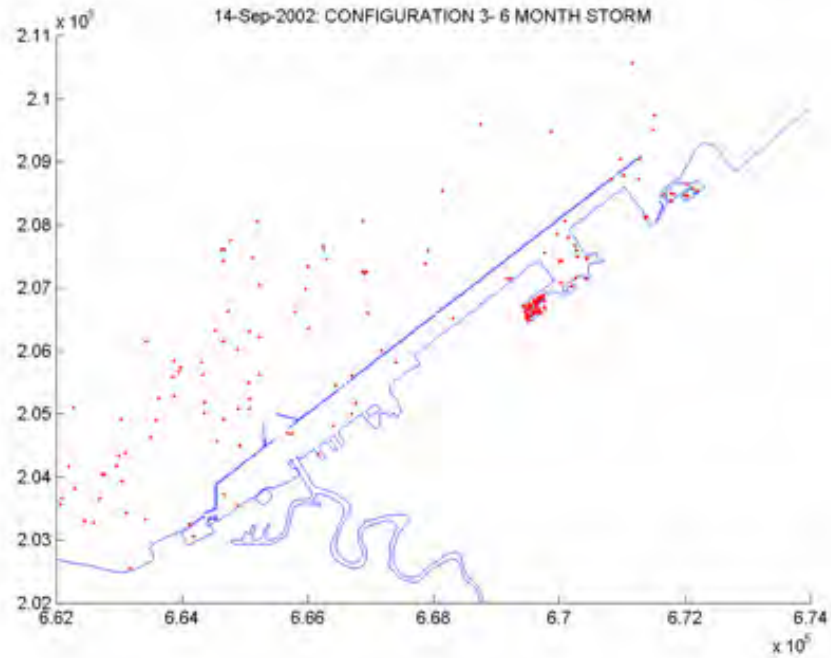

Figure 15. cont (c and d).

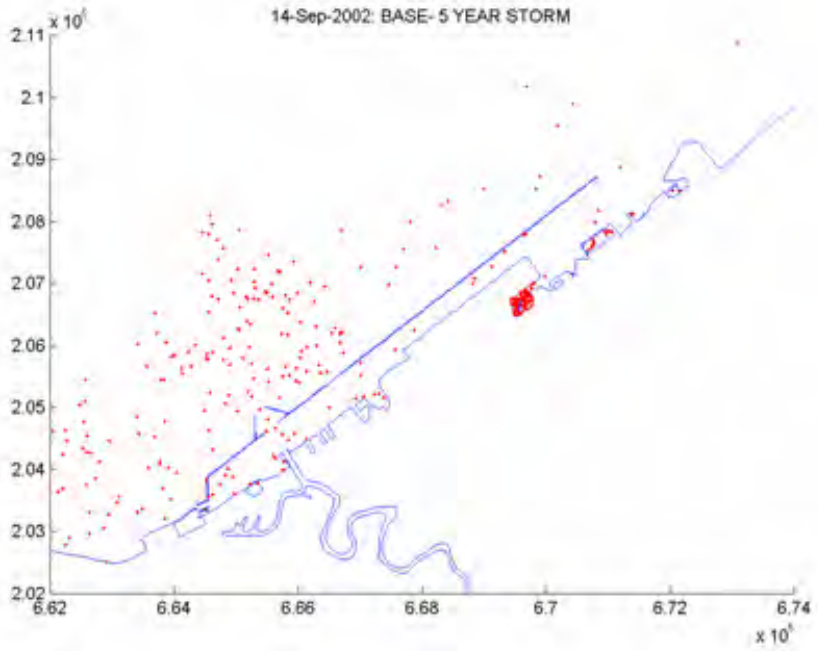

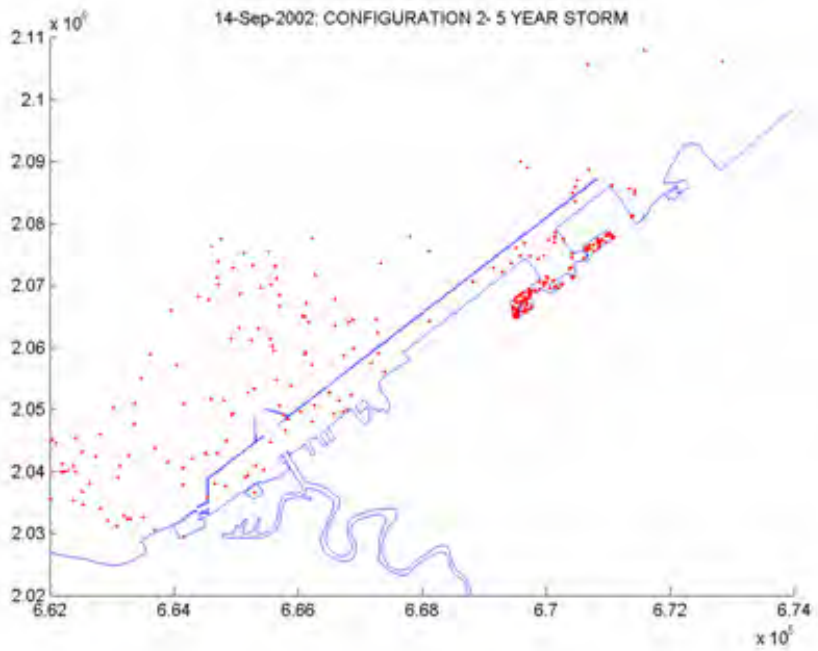

Figure16. Particles around Cleveland Harbor 1 month after event from 5-year storm (a and b).

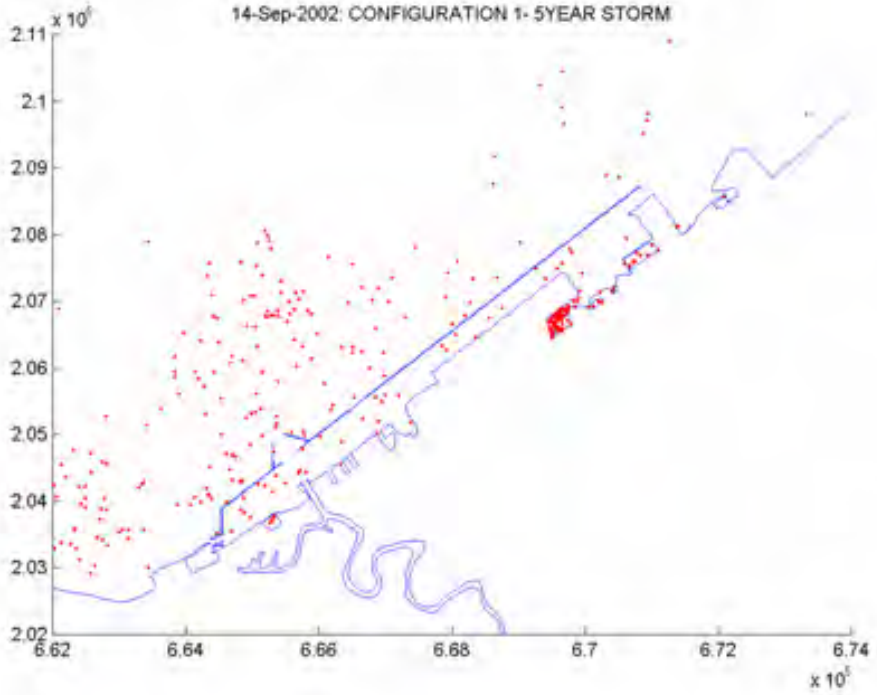

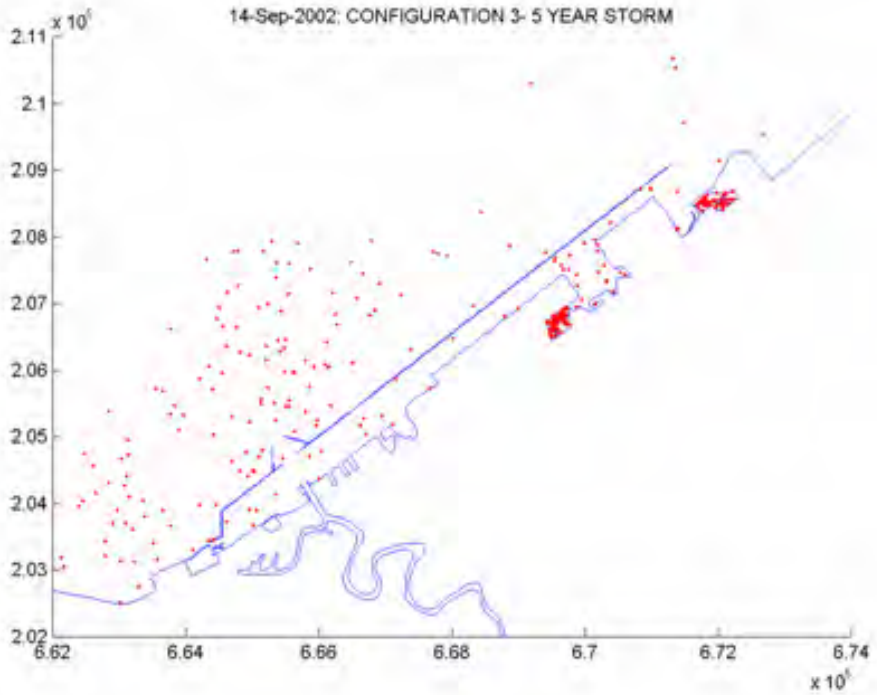

Figure16. cont. (c and d).

Debris Study (Floatable Particles)

Floatable particles are representative of floating debris in the harbor. In the case of floatables, wind effects became a key factor to particle transport. To add this attribute to PTM, particle velocities were treated in a slightly different method than the neutrally buoyant particles. Within PTM, the horizontal particle velocities are primarily determined by the summation of the advection velocity and diffusion velocity. For floatables, a wind velocity vector was added to the hydrodynamic velocity forcing.

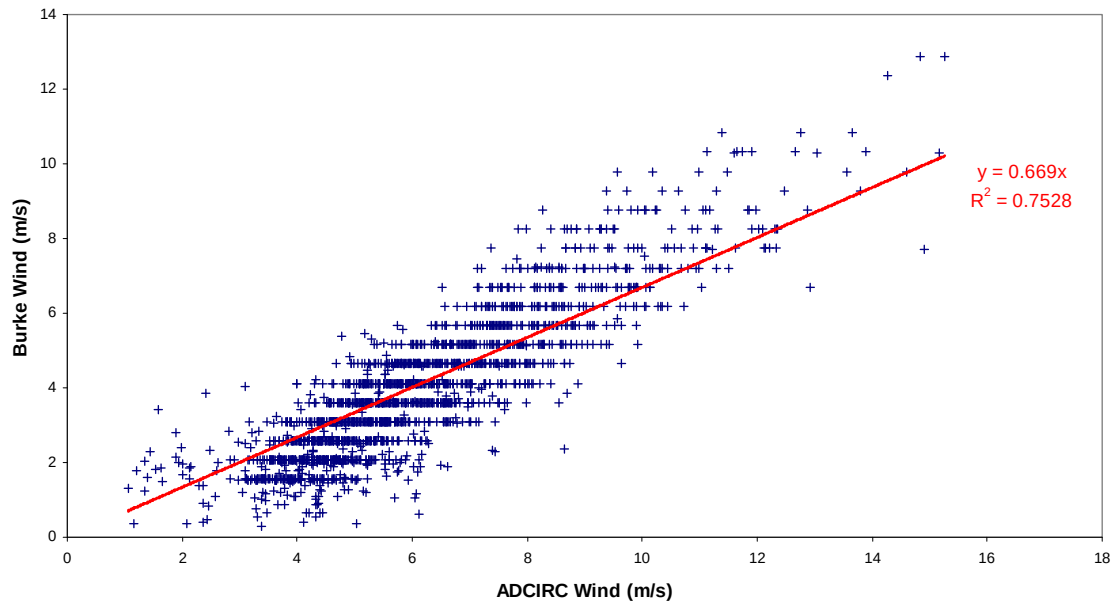

Figure 17. Comparison of observed wind at Burke Airport and ADCIRC model wind

$$\vec{v} = \vec{v} + K_w \vec{U} \tag{1}$$

Here, $\vec{U}$ is wind velocity vector measured at 10 m. The typical coefficient for K_w is 0.03. Observed winds at Burke Airport are about 70 percent of ADCIRC model winds (figure 17), which gives K_w = 0.02 when we use ADCIRC winds. The value of 0.3 for K_w is for open ocean wind. Cleveland Harbor is sheltered so that the K_w would be smaller than 3 percent. We use 1 percent in this study.

The results of the debris study were drastically different than the chemical transport study. Floatables exited the harbor rapidly. Figure 18 shows particles as they are being released during the storm event. Southwesterly winds took the particles eastward during this event. Most of the particles moved away from the Harbor 1 day after this period (figure 19). These results remain consistent for all configurations and for both storms.

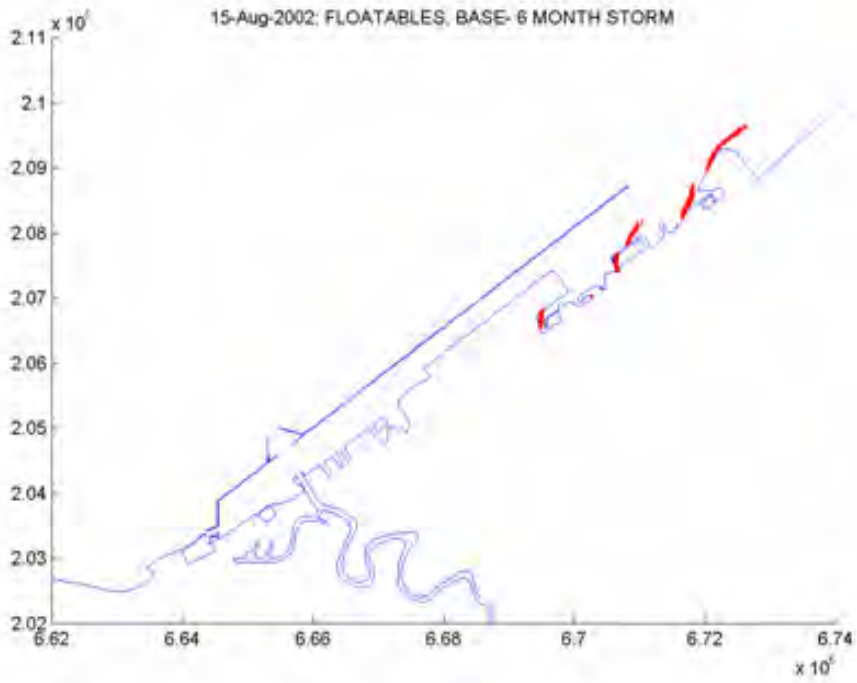

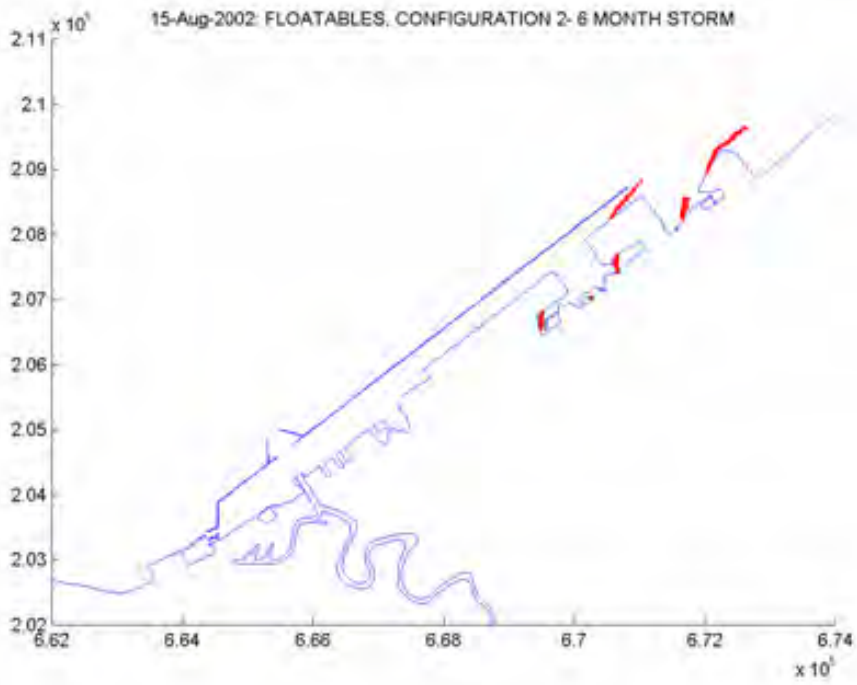

Figure18. Floatables around Cleveland Harbor during event from 6-month storm (a and b)

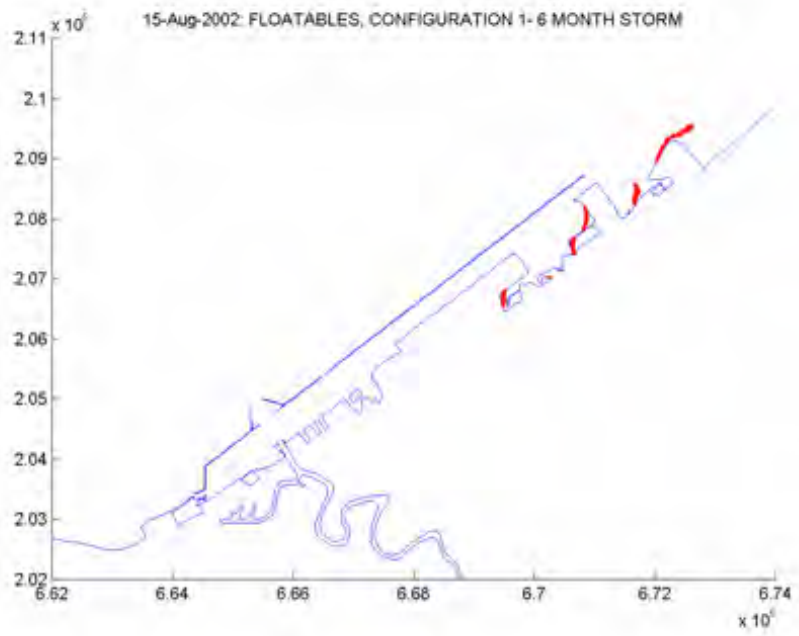

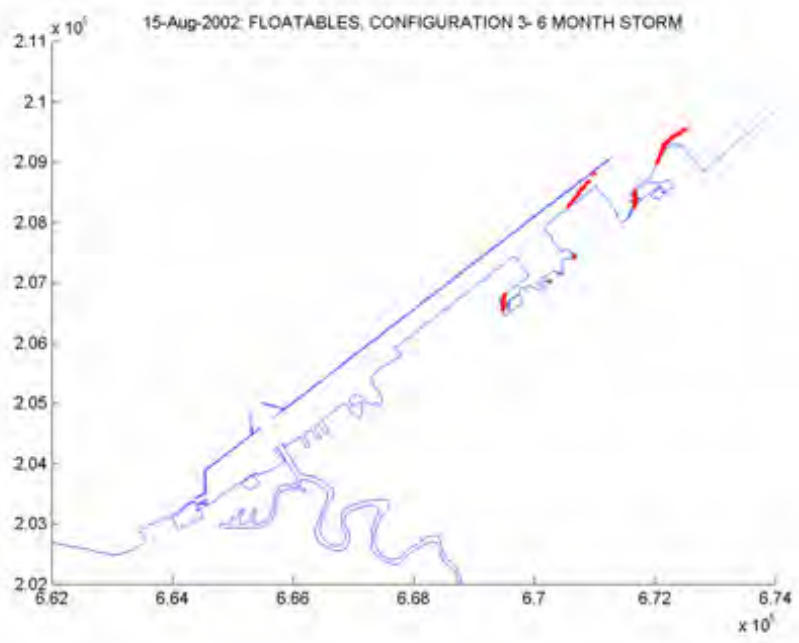

Figure18. cont. (c and d)

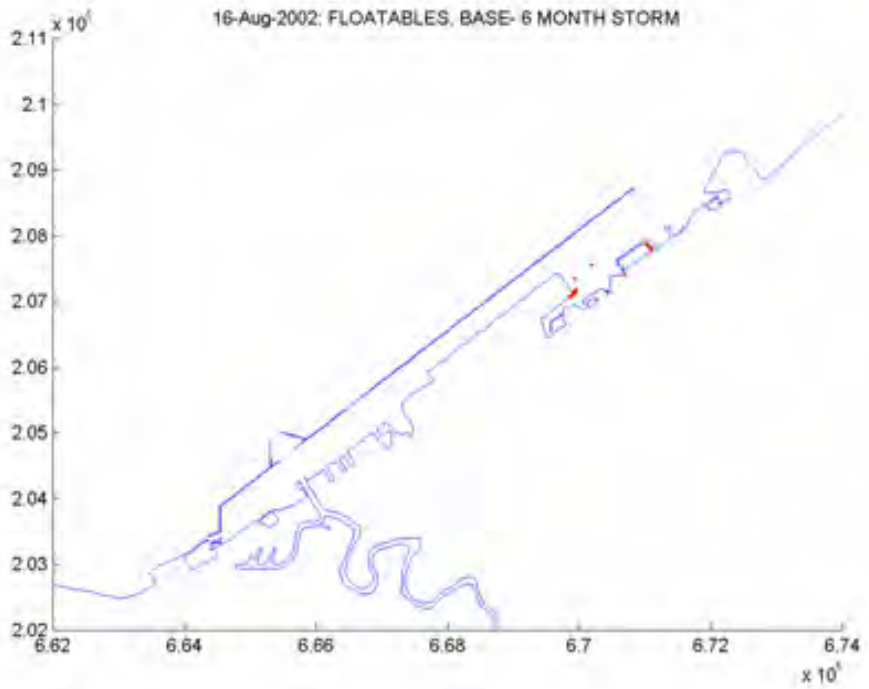

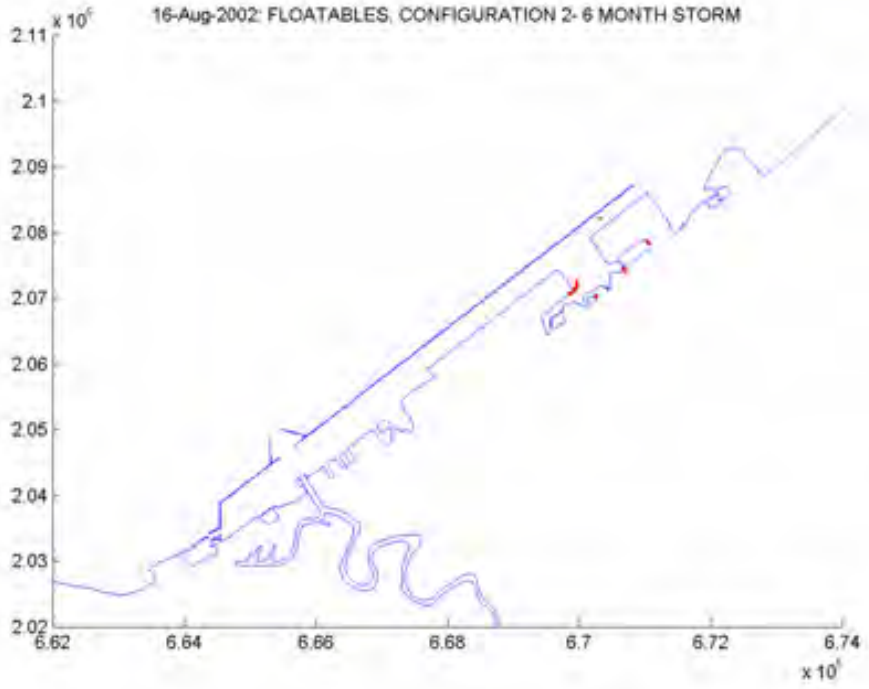

Figure19. Floatables around Cleveland Harbor 1 day after event from 6-month storm (a and b)

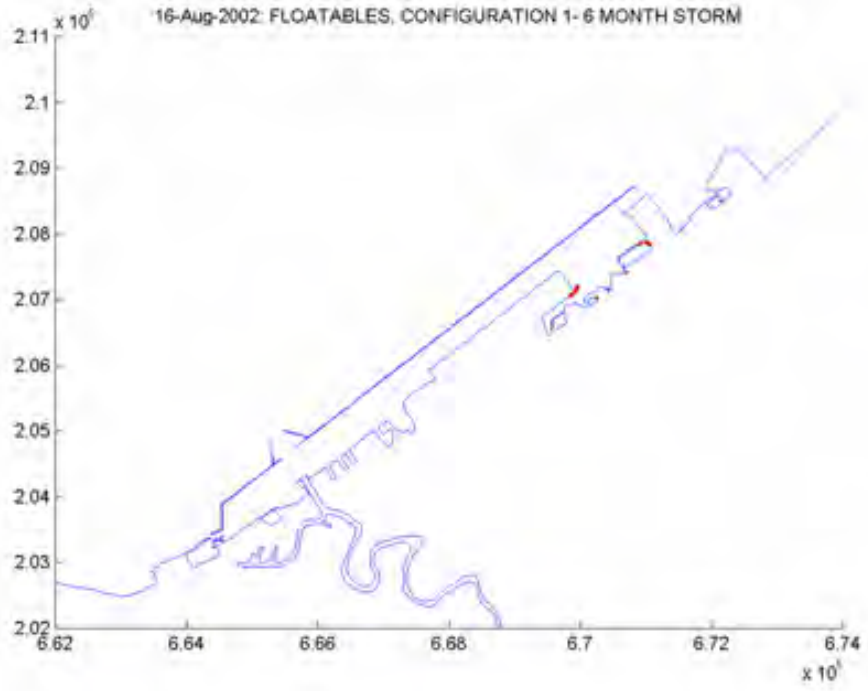

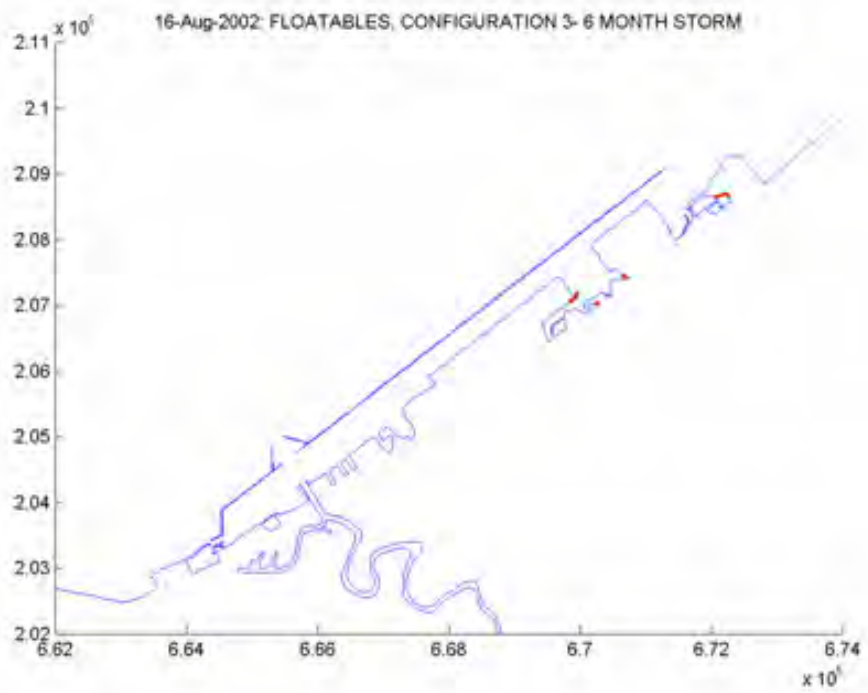

Figure19.cont (c and d)

Sediment Study

A brief study of sediment transport was performed using PTM. A more extensive near bed sediment study using GTRAN (SOW Task 6) has also been planned. In this PTM study, fine grain sediment (D50 = 100 microns) was discharged from the CSOs. Due to lack of data, the approach taken was a dimensionless sediment source. The mass rate of sediment entering at each CSO was taken as proportionate to the discharge rate of the CSO.

$$R = Qx10^{-1}$$

In this case R is the rate of sediment discharge and Q is the discharge rate of the CSO. If future data on the actual percentage of sediment to discharge is determined, then all values can be adjusted by the new factor.

A difference between the previous two cases of neutrally buoyant and floatable particles is that during sediment transport settling and resuspension processes become important. The distinction between this case and the previous cases is immediately visible. The transportation of sediment particles is not nearly as diffusive as in the neutrally buoyant particle case. Initially, a portion of the particles are transported away from the CSOs. These particles are then transported by the flow away from the harbor region. For the most part, even at this stage the particles that are transported are less spread out. But most important is that it is also evident that due to settling and recirculating patterns near many of the CSOs caused by the structures in the vicinity of outfalls, a large percentage of the suspended sediment is allowed to quickly settle in reasonably tight formations. Shown in figures 20a-20f are snapshots of sediment particle positions with time from the 5 year storm utilizing the base configuration. Initially (figure 20a) after one day the sediment that does not immediately settle is transported away from the CSOs. However, quickly (20b-c) it is obvious that a significant portion remains in a clustered tight formation. After a months time (20f) it can be seen that more sediment has been resuspended and transported outside of the immediate region of the CSO.

This trend is followed in the case of the configuration 2 (figure 21). However in this case because of the CDF, there are more areas of recirculating flow and therefore more areas of settled particles. Also noticeable in the figures are areas where particles do not seem to resuspend suggesting that enough time has passed that there is a great probability of burial by bed sediment.

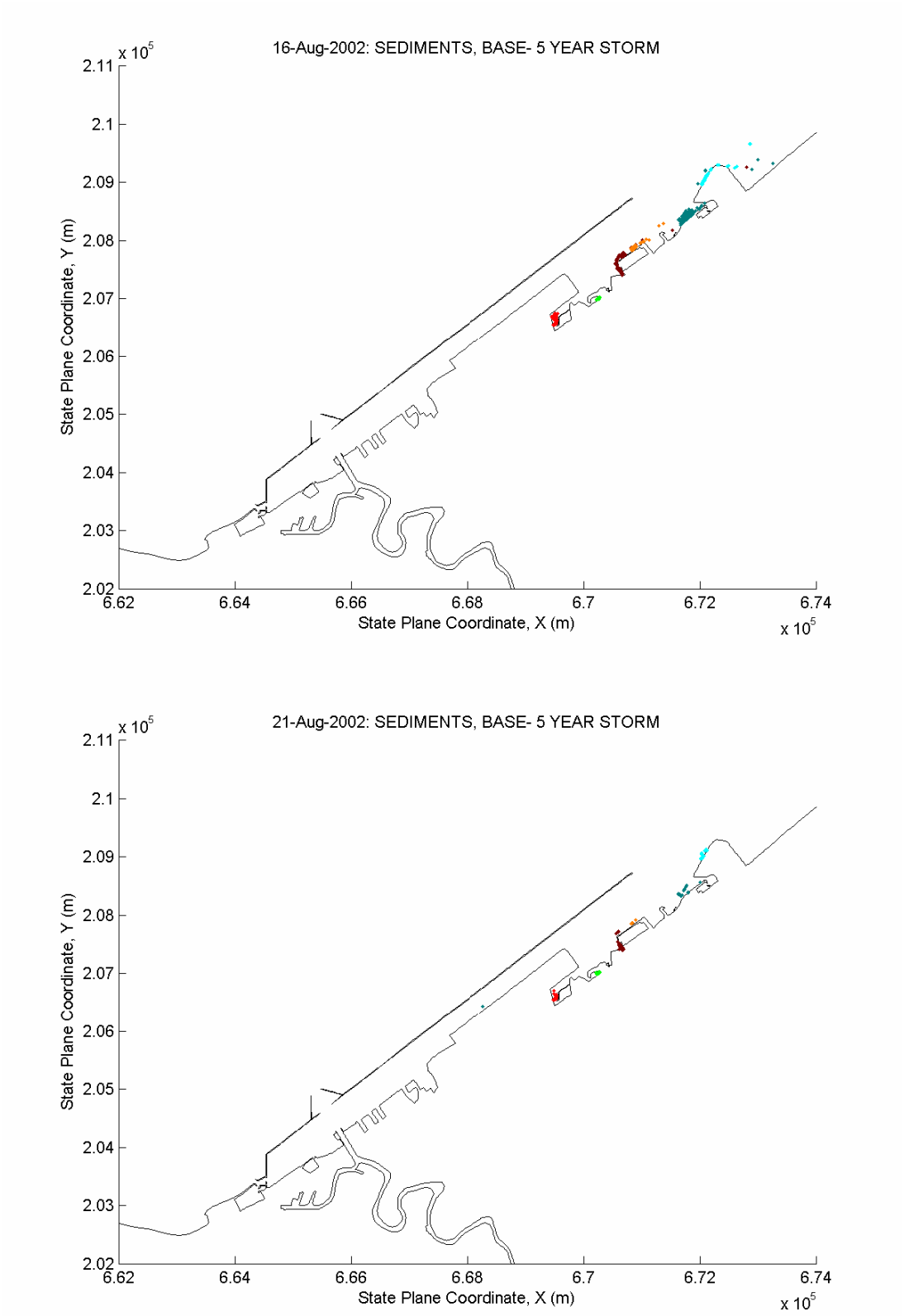

Figure 20. Sediment particle position with time from 5-year storm (particles colored to differentiate CSO) –Base (a and b)

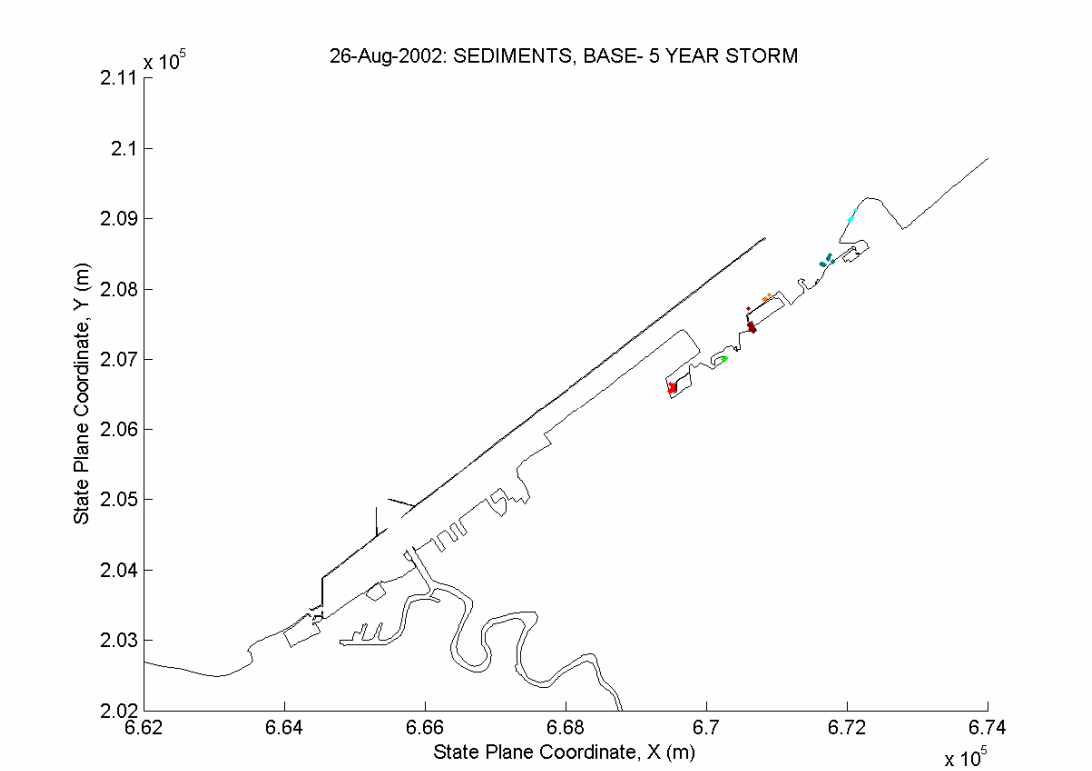

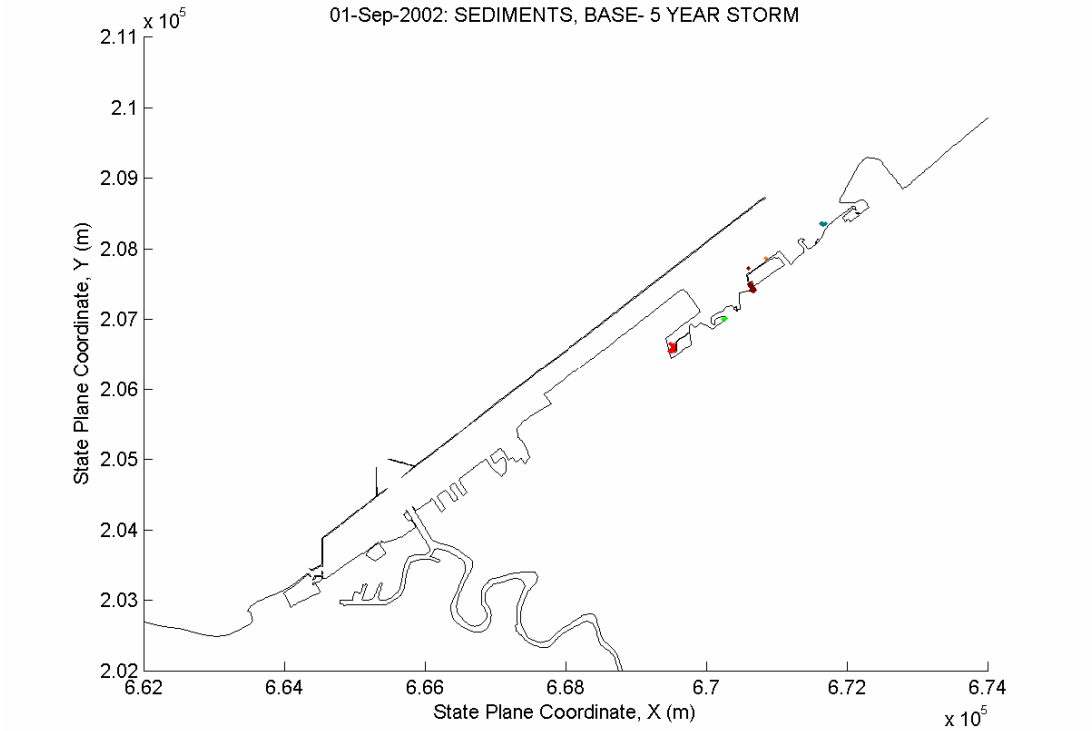

Figure 20 cont (c and d)

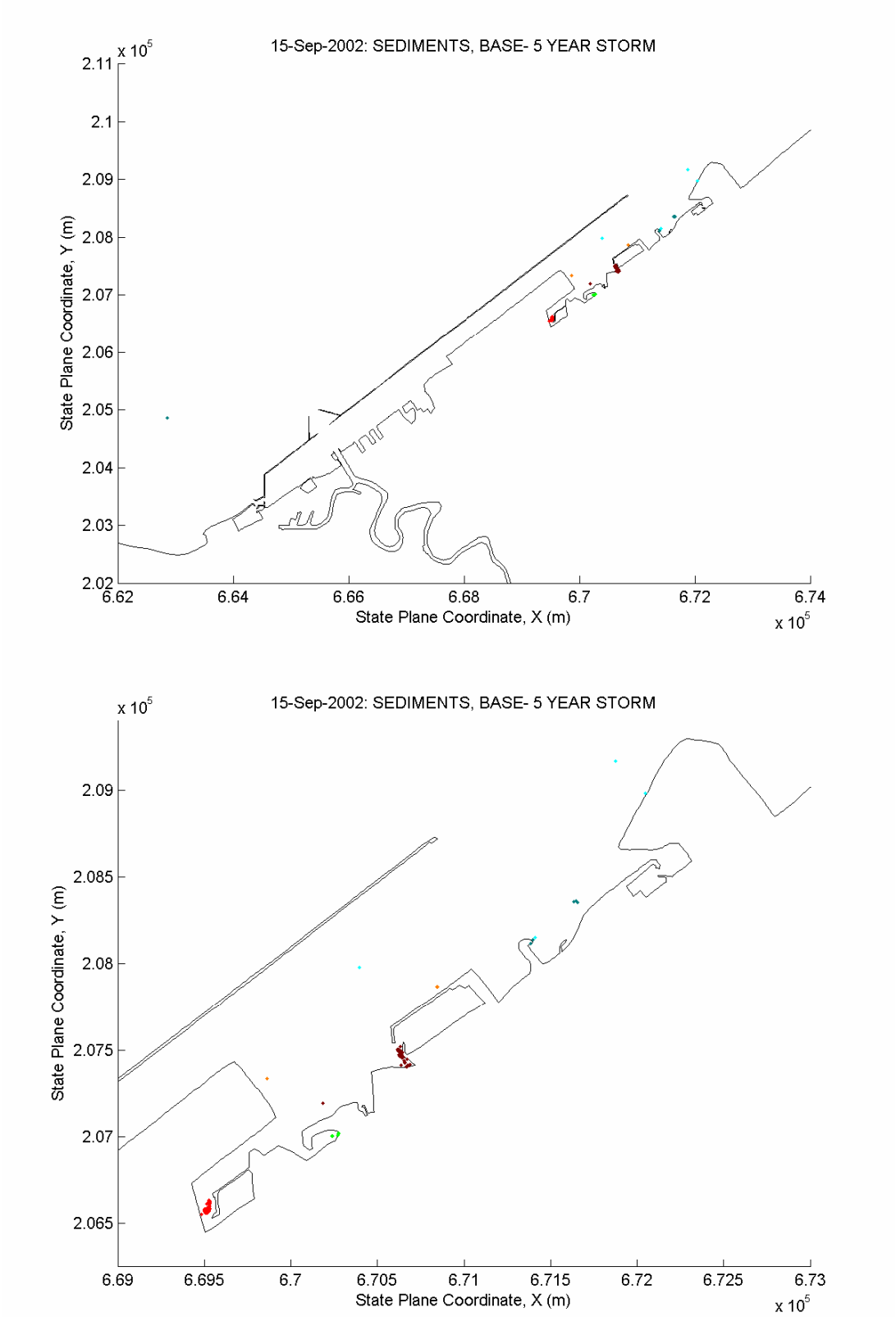

Figure 20. cont (e and f)

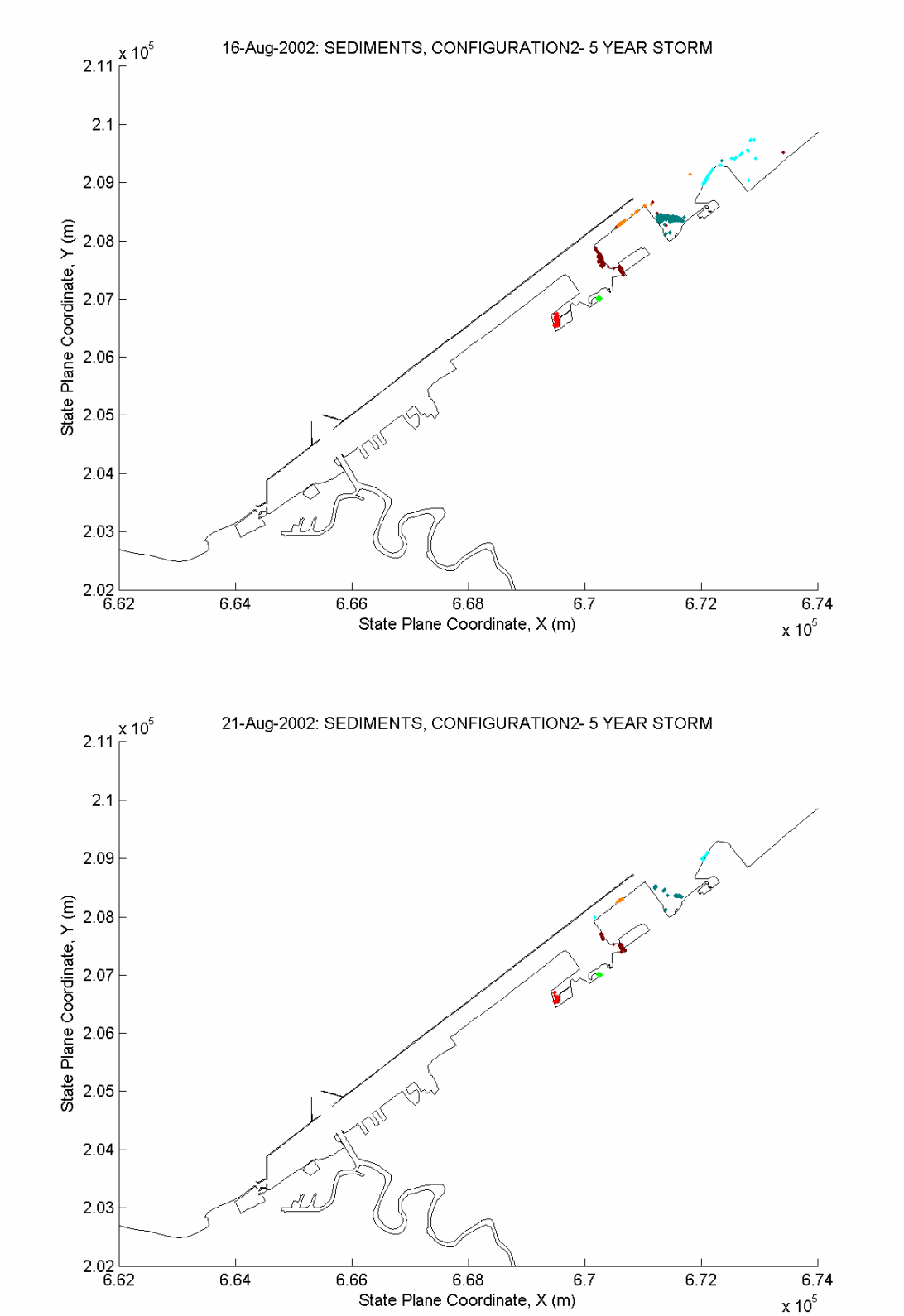

Figure 21. Sediment particle position with time from 5-year storm (particles colored to differentiate CSO) –Configuration 2 (a and b)

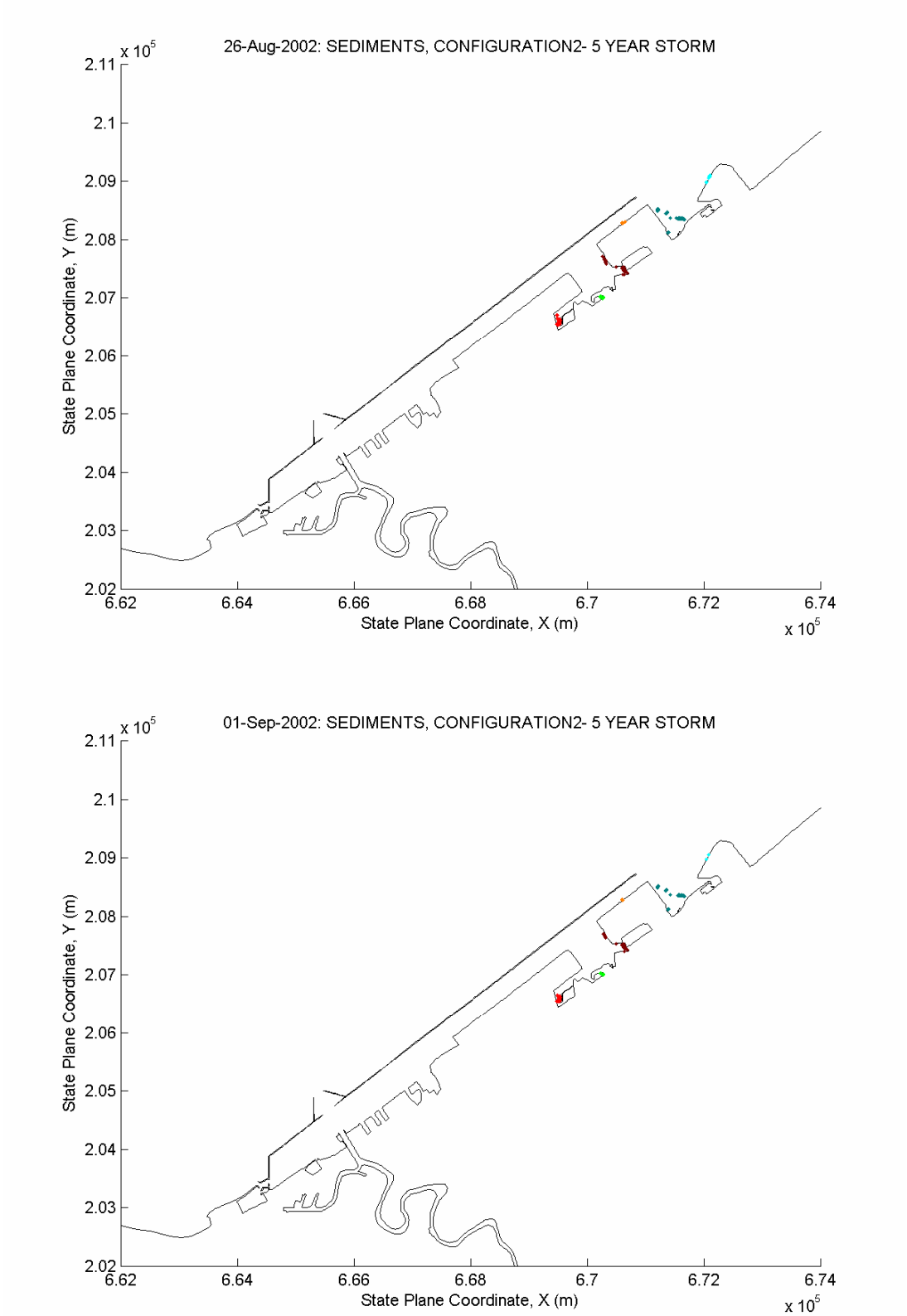

Figure 21. cont (c and d)

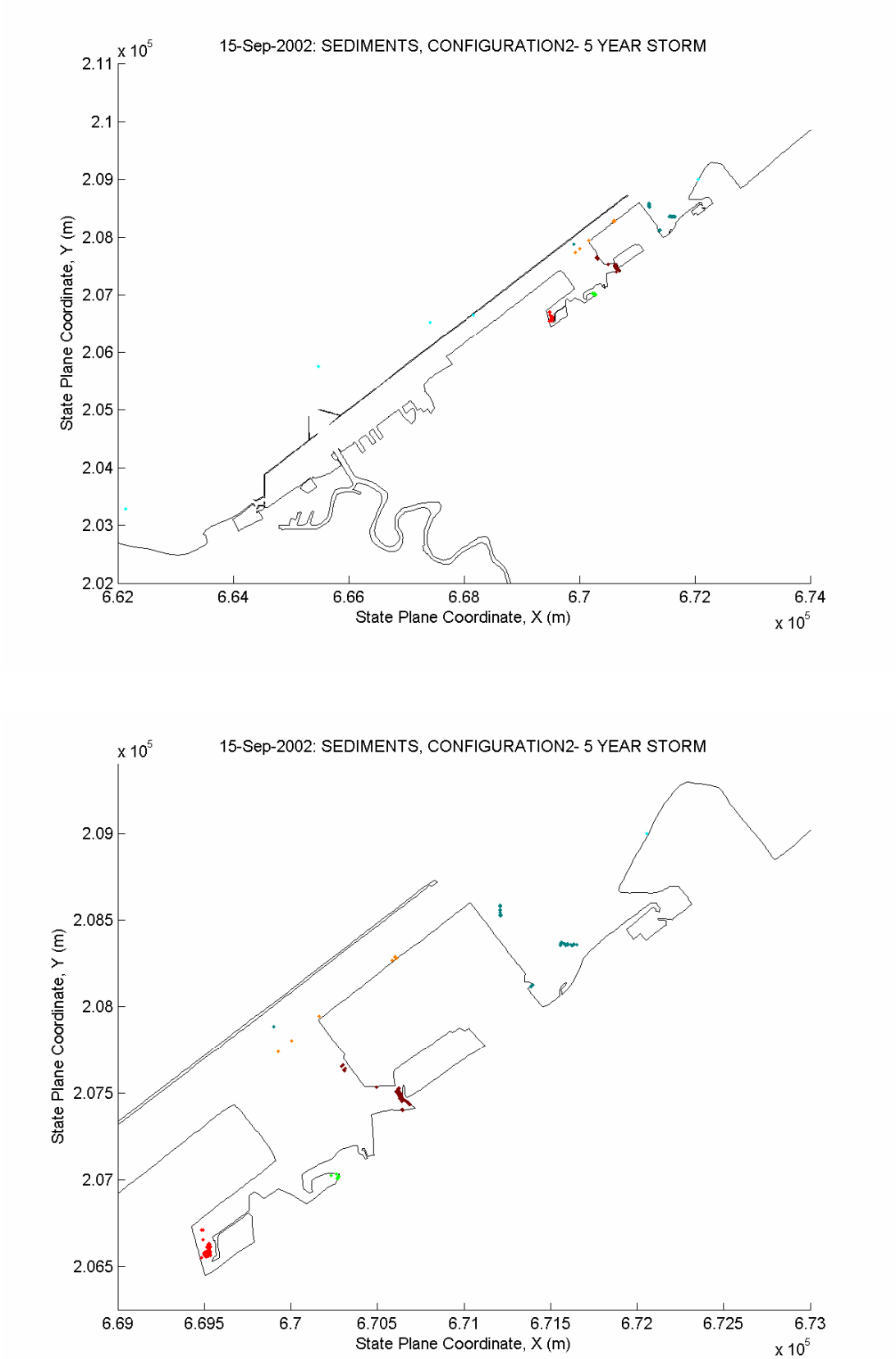

Figure 21. cont (e and f)

Concentration Analysis

Concentration analysis was performed using the calculated PTM simulation position results. Concentration values are reported in units of number of particles (FBC count) per volume of fluid. Figures 22 and 23 show the results of the base or existing configuration at several time steps for both the six month and five year month design storms respectively. As seen in the figures, initially there is a high concentration of particles close to the CSOs after all of the particles have been introduced into the flow for one day. Values above 5E7 particles per cubic meter were determined. The thin band of high concentration (red contours) quickly dissipates within a five day period. The band is broken into several smaller regions of highly concentrated particles as well as areas of smaller concentration due to advective mixing. Halfway through the simulation (September 1) most of the particles have dispersed, leaving primarily one region of high concentration near CSO 200. Particles (as mentioned previously) are trapped within this area. It should be noted, however, that for the purposes of these simulations, all calculations are conservative. Particles are not allowed to dissolve. It is probable that given time, the concentration in that region would decrease. Notable in these two simulations is the fact that the overall trend remains the same between the two design storms although the regions of higher concentration are slightly larger for the 5year storm.

Figures 24 and 25 show the concentration analysis results for configuration 2 for the sixth month and five year storms. The differences between these results and the previous results are obviously focused in the area of interest near the CDF. High levels of concentration develop near the east side of the proposed structure. However these areas quickly empty of particles and as can be seen in both figures, by 8/26 (10 days after all particles are introduced), the concentration is greatly reduced.

In Figures 26 and 27 concentration of sediment is shown for the base and configuration 2, 5 year design storm cases. These are primarily demonstrated as representative examples of sediment concentration in general. In this case concentration is a non-dimensional value. Because the original percentage of sediment to CSO discharge was unknown and therefore described as a proportion, the sediment concentration was non-dimensionalized. The real sediment concentration C_s is

$$C_s = N * 10 C_0 (kg / m^3)$$

where N is the dimensionless sediment concentration seen in the figure and C_0 is the sediment mass rate discharged from the CSO.

Similar to the previous figures in the sediment section of the particle transport it can be seen that the sediment concentrations appear to be much less diffused. Because of the process of settling and resuspension, much of the transport occurs through interaction with the bed and therefore isn't seen in the concentration values which only account for those particles that are in the water column. In addition, condensed regions of sediment remain trapped in areas of recirculating flow. Here sediment may be resuspended but then quickly deposit. There is no overall transport out of the trapped areas, so it appears as if sediment remains in the water column indefinitely.

Background levels of particulate concentration were not taken into account within these simulations. Therefore all concentration levels should be considered as additive values above the existing background level in the area.

Conclusions and Remaining Work

To address the issue of the CSO constituent fate in Cleveland Harbor and the effect of the construction of a CDF in the area, the Particle Tracking Model (PTM) was applied to four phases of construction. Neutrally buoyant particles as well as floatables were modeled to represent chemical transport and debris transport respectively. Particle path determination and concentration mapping were performed. It was established that generally most neutrally buoyant particles were transported out of the system within a thirty day period, except for two "hot spots" where particles were trapped by the contained flow areas. Concentration values quickly dissipated as a result of the particle transport, following the same trend. Floatable particles rapidly exited the system due to the additional factor of wind forcing.

Further work will be performed to determine the effect of nearbed sediment transport (particle density > water density) utilizing GTRAN which can better predict nearbed sediment pathways. Due to the lack of data regarding the sediment quantities, a method was devised to estimate sediment proportional values to discharge. Results were shown based on these proportional values. It is recommended that data be collected regarding the actual percentages of sediment within CSO discharges. In addition it is recommended that eventually the effect of the non-conservative aspects of chemical particle transports is considered.

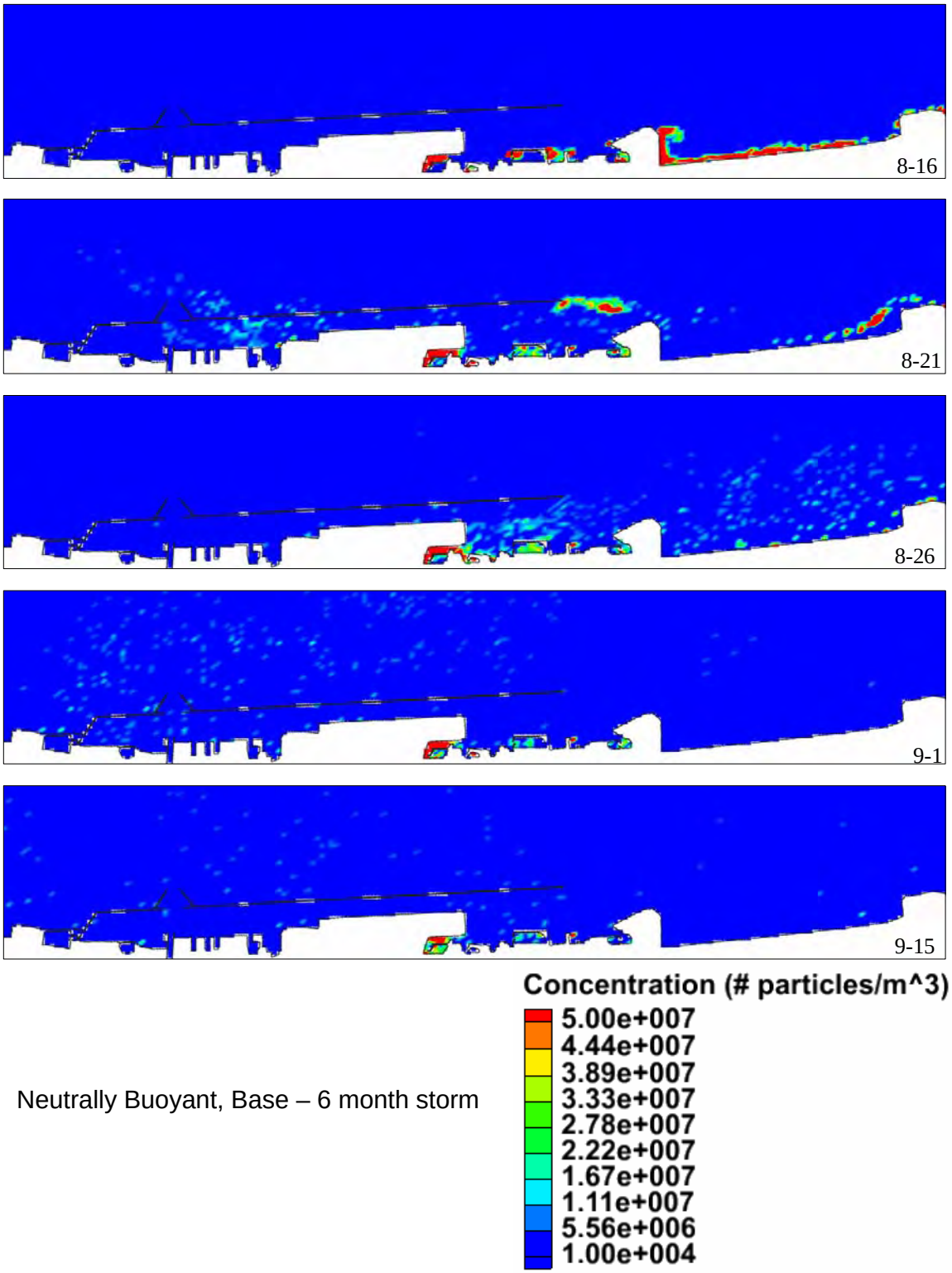

Figure 22. Concentration (particles per volume) values at 00:00 for 6month storm, base configuration.

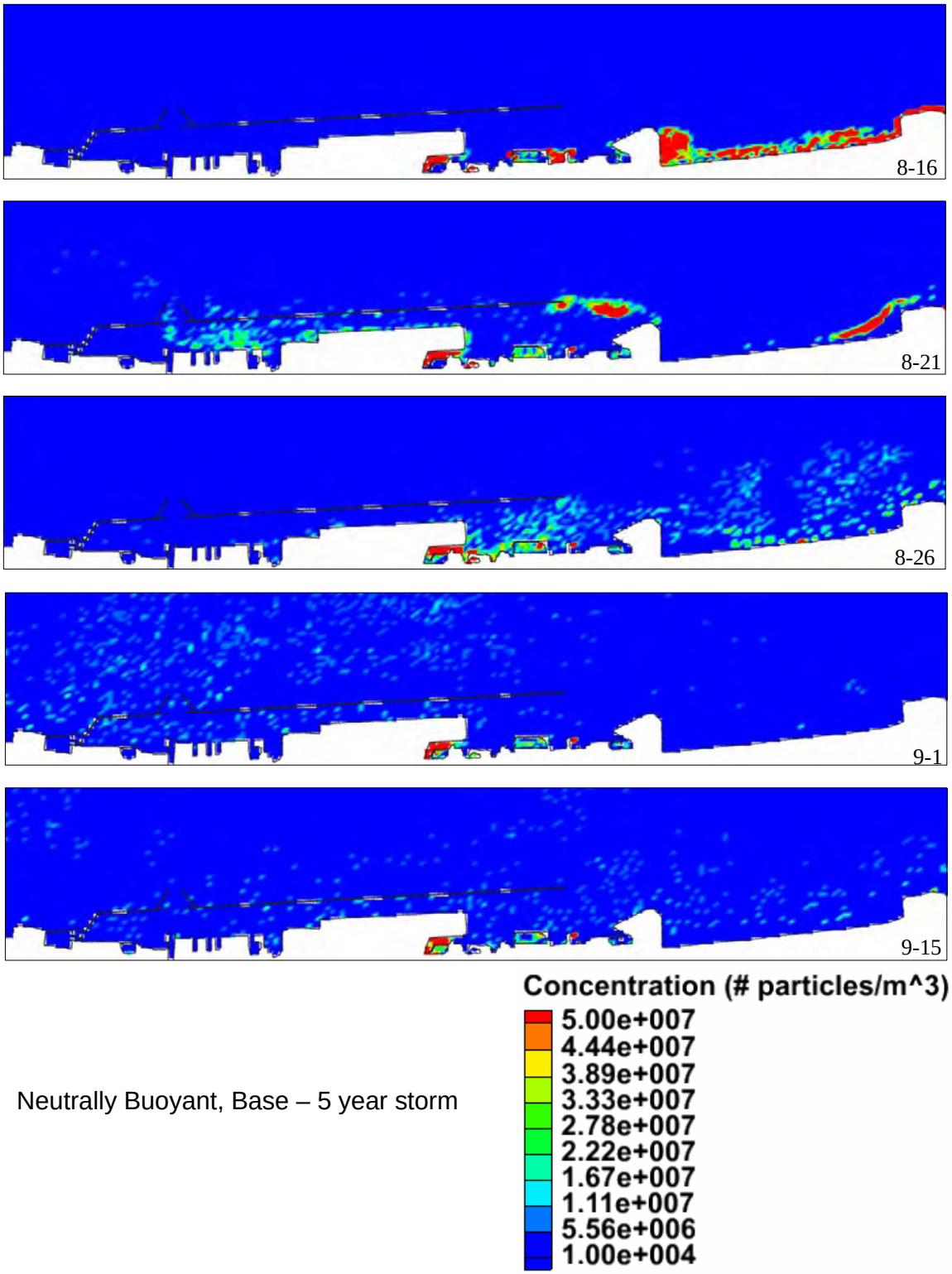

Figure23. Concentration (particles per volume) values at 00:00 for 5 year storm, base configuration.

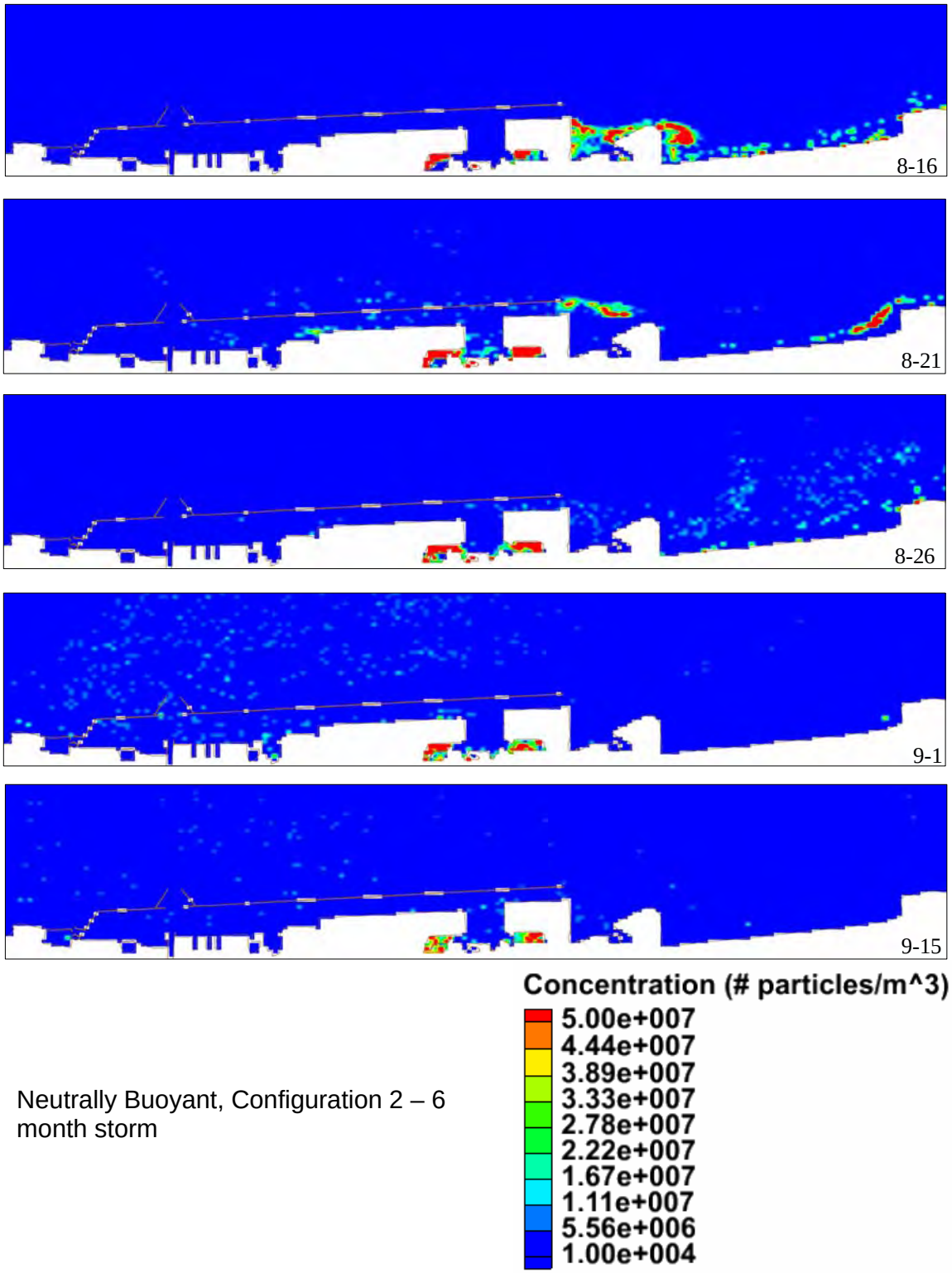

Neutrally Buoyant, Configuration 2 – 6 month storm

Figure24. Concentration (particles per volume) values at 00:00 for 6month storm, Configuration 2.

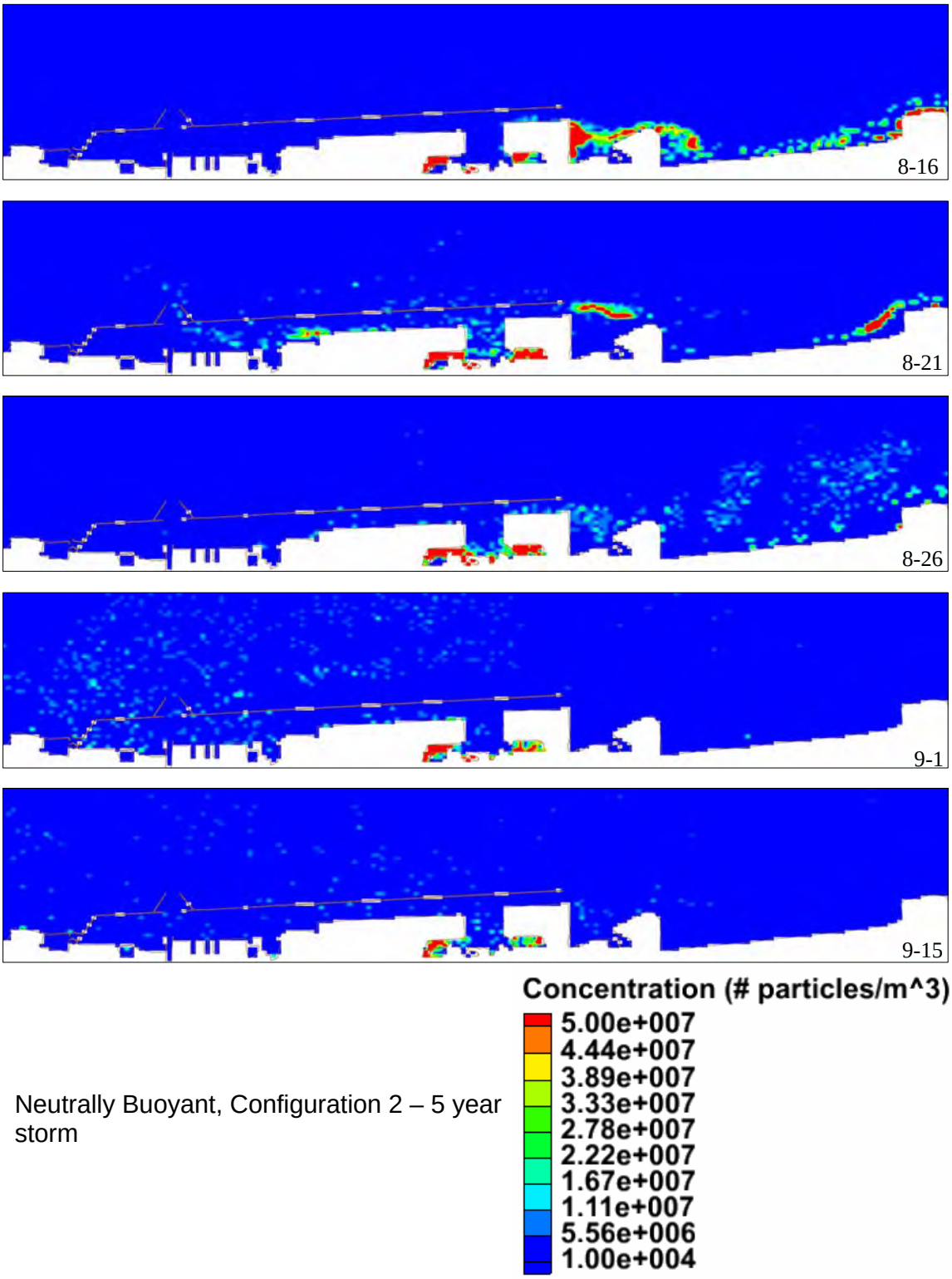

Neutrally Buoyant, Configuration 2 – 5 year storm

Figure25. Concentration (particles per volume) values at 00:00 for 5 year storm, Configuration 2.

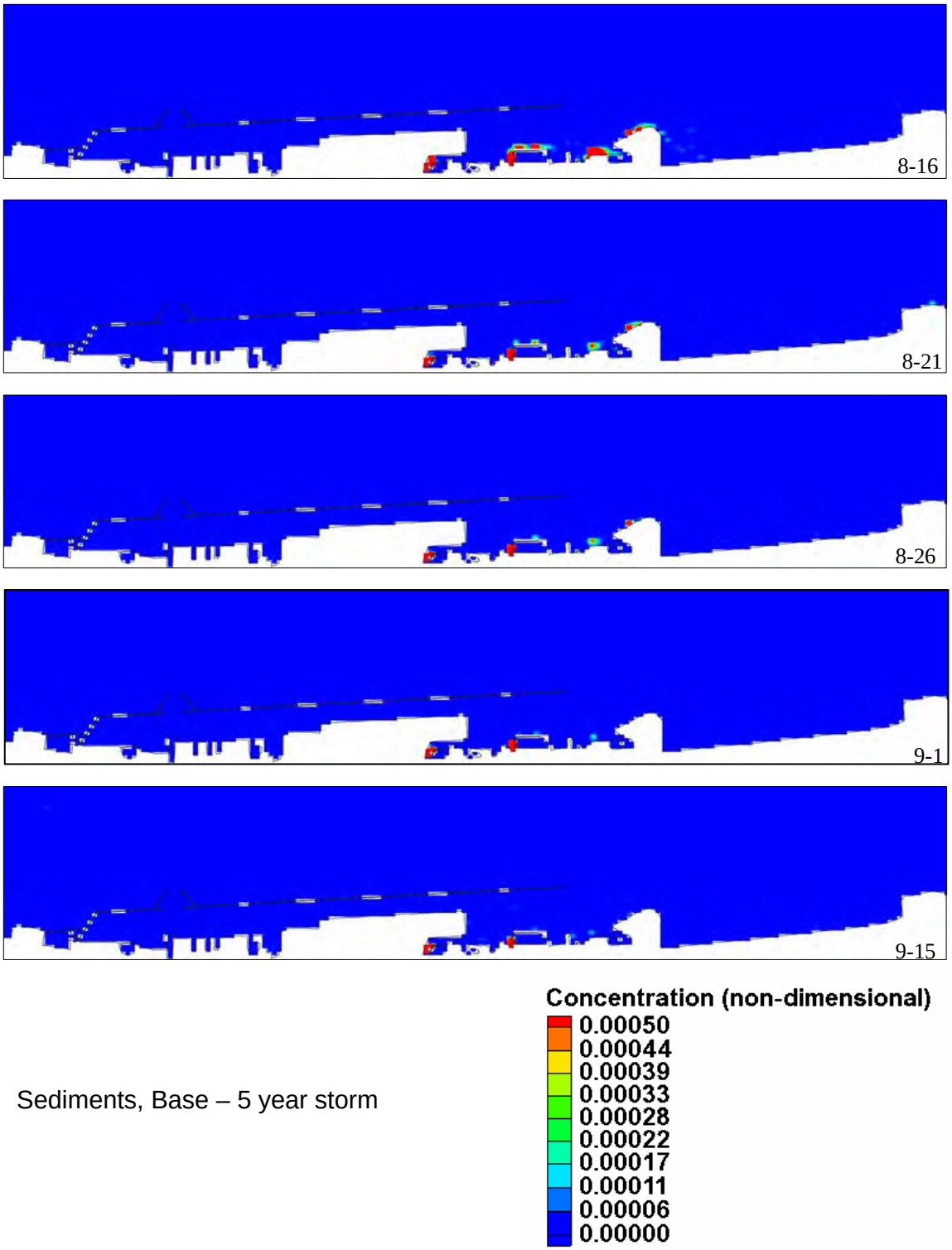

Figure26. Concentration (particles per volume) values at 00:00 for 5 year storm, Configuration 2.

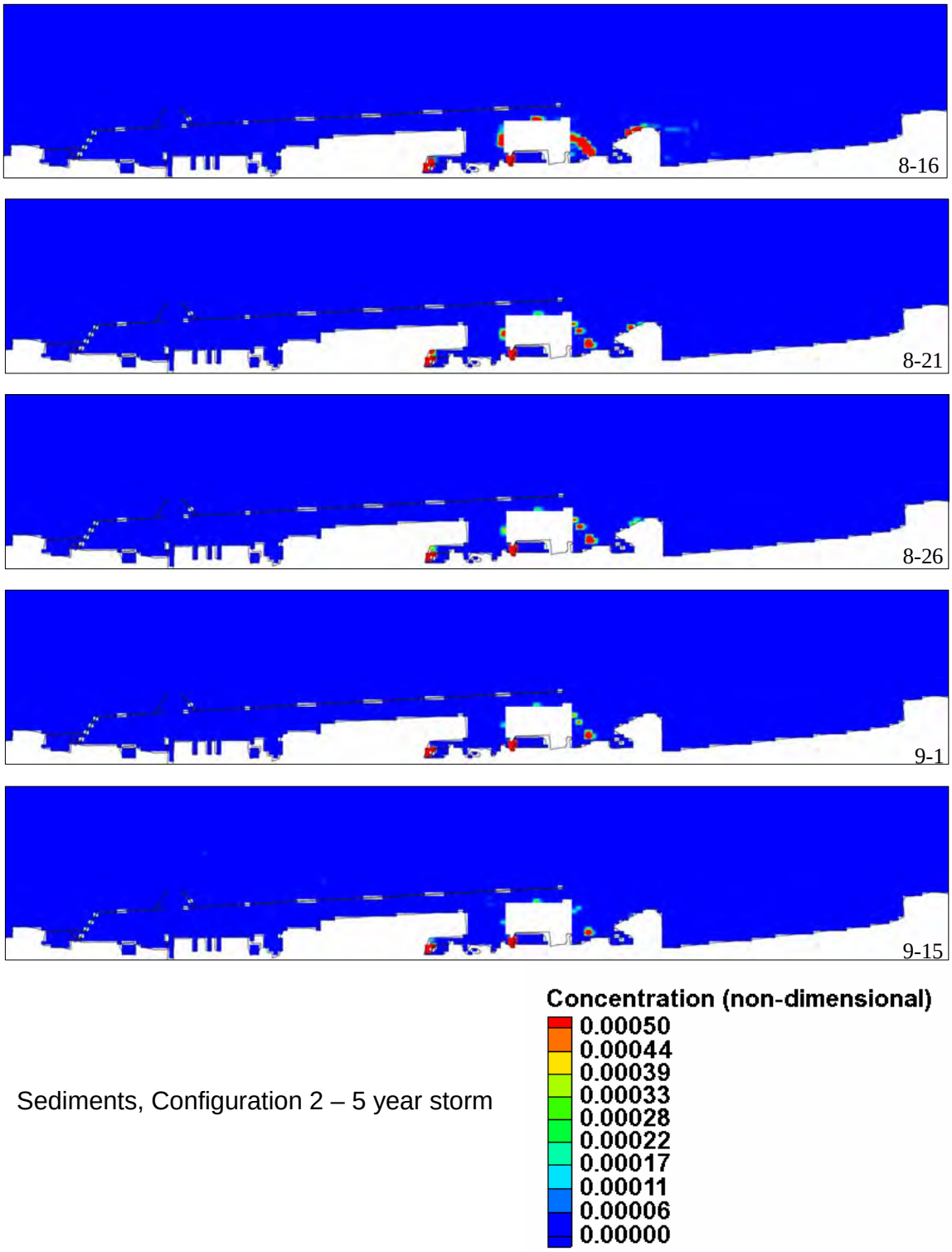

Figure27. Concentration (particles per volume) values at 00:00 for 5 year storm, Configuration 2.

References

Demirbilek, Z., Smith, J., Zundel, A., Jones, R., MacDonald, N., and Davies, M. (2004). "Particle Tracking Model (PTM) in the SMS: I. Graphical Interface," *Technical Report DOER-D4*, U.S. Army Engineer Research and Development Center, Vicksburg, Mississippi, USA.

Davies, M. H., MacDonald, N. J., Demirbilek, Z., Smith, S. J., Zundel, Z. K., and Jones, R. D. (2005). "Particle Tracking Model (PTM) II: Overview of features and capabilities," *Technical Report DOER-D5*, U.S. Army Engineer Research and Development Center, Vicksburg, Mississippi, USA.

Demirbilek, Z., Smith, S. J., Zundel, A. K., Jones, R. D., McDonald, N. J., and Davies, M.E. (2005). "Particle Tracking Model (PTM) in the SMS: III. Tutorial with examples," *Technical Report DOER-D6*, U.S. Army Engineer Research and Development Center, Vicksburg, Mississippi, USA.

Lackey, T.C. and MacDonald, N.J. (2007). "The Particle Tracking Model Description and Processes" *Proceedings XVIII World Dredging Congress 2007*, WEDA, Lake Buena Vista, Florida, USA.

Mark, David, Chapman, Raymond S., and Luong, Phu V. (2008), “Cleveland Harbor, Ohio Thermal Plume Transport Investigation” *Technical Report TR-08-x*, U.S. Army Corps of Engineers, Engineer Research and Development Center, Vicksburg, Mississippi, USA.

MacDonald, N.J., Davies, M.H., Zundel, A.K., Howlett, J.D., Demirbilek, Z., Gailani, J.Z., Lackey, T.C., and Smith, S.J. (2006). "PTM: Particle Tracking Model Report 1: Model Theory, Implementation, and Example Applications" *Technical Report TR-06-02*, U.S. Army Corps of Engineers, Engineer Research and Development Center, Vicksburg, Mississippi, USA.

Appendix A

6-month Design Storm													
Time	Rainfall	CSO 200		CSO 201		CSO 202		CSO 203		CSO 204		CSO 205	
Hours	Inches	Discharge CMS	Fecal Coliform #/sec	Discharge CMS	Fecal Coliform #/sec	Discharge CMS	Fecal Coliform #/sec	Discharge CMS	Fecal Coliform #/sec	Discharge CMS	Fecal Coliform #/sec	Discharge CMS	Fecal Coliform #/sec
0	0	0	0	0	0	0	0	0	0	0	0	0	0
0.25	0.0025	0	0	0	0	0	0	0	0	0	0	0	0
0.5	0.0025	0	0	0	0	0	0	0	0	0	0	0	0
0.75	0.0025	0	0	0	0	0	0	0	0	0	0	0	0
1	0.0025	0	0	0	0	0	0	0	0	0	0	0	0
1.25	0.015	0	0	0	0	0	0	0	0	0	0	0	0
1.5	0.015	0	0	0	0	0	0	0	0	0	0	0	0
1.75	0.015	0	0	0	0	0	0	0	0	0	0	0	0
2	0.015	0	0	0	0	0	0	0	0	0	0	0	0
2.25	0.005	0	0	0	0	0	0	0	0	0	0	0	0
2.5	0.005	0	0	0	0	0	0	0	0	0	0	0	0
2.75	0.005	0.02	5.74E+07	0	0	0	0	0	0	0	0	0	0
3	0.005	0.03	8.01E+07	0	0	0	0	0	0	0	0	0	0
3.25	0.1825	0.03	8.35E+07	0	0	0	0	0	0	0	0	0	0
3.5	0.1825	0.29	7.53E+08	0.10	2.60E+08	0.09	2.27E+08	0	0	0.13	3.43E+08	0.15	3.81E+08
3.75	0.1825	2.22	5.80E+09	0.85	2.22E+09	3.51	9.15E+09	0.41	1.08E+09	1.13	2.96E+09	1.45	3.79E+09
4	0.1825	4.10	1.07E+10	1.24	3.23E+09	6.95	1.81E+10	0.98	2.56E+09	3.72	9.71E+09	1.98	5.17E+09
4.25	0.065	4.87	1.27E+10	1.45	3.80E+09	8.24	2.15E+10	1.44	3.77E+09	7.67	2.00E+10	2.10	5.47E+09
4.5	0.065	4.43	1.16E+10	0.90	2.36E+09	7.38	1.93E+10	1.26	3.30E+09	8.07	2.11E+10	1.58	4.13E+09
4.75	0.065	3.12	8.14E+09	0.54	1.41E+09	4.91	1.28E+10	0.68	1.78E+09	6.98	1.82E+10	0.98	2.55E+09
5	0.065	2.44	6.36E+09	0.39	1.03E+09	3.63	9.46E+09	0.45	1.17E+09	5.30	1.38E+10	0.77	2.00E+09

5.25	0.005	2.19	5.70E+09	0.33	8.67E+08	3.07	8.03E+09	0.34	8.91E+08	4.02	1.05E+10	0.71	1.84E+09
5.5	0.005	1.84	4.79E+09	0.21	5.55E+08	2.41	6.30E+09	0.17	4.43E+08	3.07	8.01E+09	0.51	1.34E+09
5.75	0.005	1.19	3.11E+09	0.07	1.78E+08	1.30	3.39E+09	0	0	2.28	5.96E+09	0.25	6.50E+08
6	0.005	0.72	1.89E+09	0	0	0.42	1.11E+09	0	0	1.49	3.88E+09	0.09	2.44E+08
6.25	0	0.45	1.19E+09	0	0	0.02	4.96E+07	0	0	0.79	2.05E+09	0.02	4.96E+07
6.5	0	0.29	7.57E+08	0	0	0	0	0	0	0.29	7.59E+08	0	0
6.75	0	0.18	4.75E+08	0	0	0	0	0	0	0.03	8.30E+07	0	0
7	0	0.11	2.82E+08	0	0	0	0	0	0	0	0	0	0
7.25	0	0	0	0	0	0	0	0	0	0	0	0	0

5-Year Design Storm													
Time	Rainfall	CSO 200		CSO 201		CSO 202		CSO 203		CSO 204		CSO 205	
Hours	Inches	Discharge CMS	Fecal Coliform #/sec	Discharge CMS	Fecal Coliform #/sec	Discharge CMS	Fecal Coliform #/sec	Discharge CMS	Fecal Coliform #/sec	Discharge CMS	Fecal Coliform #/sec	Discharge CMS	Fecal Coliform #/sec
0	0	0	0	0	0	0	0	0	0	0	0	0	0
0.25	0.015	0	0	0	0	0	0	0	0	0	0	0	0
0.5	0.015	0	0	0	0	0	0	0	0	0	0	0	0
0.75	0.015	0	0	0	0	0	0	0	0	0	0	0	0
1	0.015	0	0	0	0	0	0	0	0	0	0	0	0
1.25	0.025	0	0	0	0	0	0	0	0	0	0	0	0
1.5	0.025	0	0	0	0	0	0	0	0	0	0	0	0
1.75	0.025	0	0	0	0	0	0	0	0	0	0	0	0
2	0.025	0	0	0	0	0	0	0	0	0	0	0	0
2.25	0.0575	0	0	0	0	0	0	0	0	0	0	0	0
2.5	0.0575	0	0	0	0	0	0	0	0	0	0	0	0
2.75	0.0575	0.04	1.12E+08	0	0	0	0	0	0	0	0	0	0
3	0.0575	0.06	1.56E+08	0	0	0	0	0	0	0	0	0	0
3.25	0.3575	0.06	1.62E+08	0	0	0	0	0	0	0	0	0	0
3.5	0.3575	0.56	1.47E+09	0.19	5.05E+08	0.17	4.41E+08	0	0	0.26	6.67E+08	0.28	7.41E+08
3.75	0.3575	4.32	1.13E+10	1.66	4.32E+09	6.82	1.78E+10	0.81	2.11E+09	2.21	5.76E+09	2.82	7.37E+09
4	0.3575	7.98	2.08E+10	2.41	6.28E+09	13.52	3.53E+10	1.91	4.99E+09	7.24	1.89E+10	3.86	1.01E+10
4.25	0.05	9.47	2.47E+10	2.83	7.39E+09	16.03	4.18E+10	2.81	7.33E+09	14.92	3.89E+10	4.08	1.06E+10
4.5	0.05	8.63	2.25E+10	1.76	4.58E+09	14.35	3.75E+10	2.46	6.42E+09	15.71	4.10E+10	3.08	8.03E+09
4.75	0.05	6.07	1.58E+10	1.05	2.73E+09	9.55	2.49E+10	1.33	3.47E+09	13.58	3.54E+10	1.90	4.97E+09
5	0.05	4.74	1.24E+10	0.77	2.00E+09	7.05	1.84E+10	0.87	2.28E+09	10.32	2.69E+10	1.49	3.89E+09

5.25	0.03	4.25	1.11E+10	0.65	1.69E+09	5.98	1.56E+10	0.66	1.73E+09	7.82	2.04E+10	1.37	3.58E+09
5.5	0.03	3.57	9.32E+09	0.41	1.08E+09	4.69	1.22E+10	0.33	8.63E+08	5.97	1.56E+10	1.00	2.61E+09
5.75	0.03	2.32	6.05E+09	0.13	3.47E+08	2.53	6.59E+09	0	0	4.44	1.16E+10	0.48	1.26E+09
6	0.03	1.41	3.67E+09	0	0	0.83	2.16E+09	0	0	2.90	7.56E+09	0.18	4.74E+08
6.25	0	0.88	2.31E+09	0	0	0.04	9.65E+07	0	0	1.53	3.99E+09	0.04	9.65E+07
6.5	0	0.56	1.47E+09	0	0	0	0	0	0	0.57	1.48E+09	0	0
6.75	0	0.35	9.24E+08	0	0	0	0	0	0	0.06	1.61E+08	0	0
7	0	0.21	5.48E+08	0	0	0	0	0	0	0	0	0	0
7.25	0	0	0	0	0	0	0	0	0	0	0	0	0

Appendix B: Particle Positions

- Particle Type
  - Neutrally Buoyant
  - Floatables
  - Sediment

- Geometry
  - Base
  - Configuration 1
  - Configuration 2
  - Configuration 3

- Hydrodynamics
  - 6 month storms
  - 5 year storms

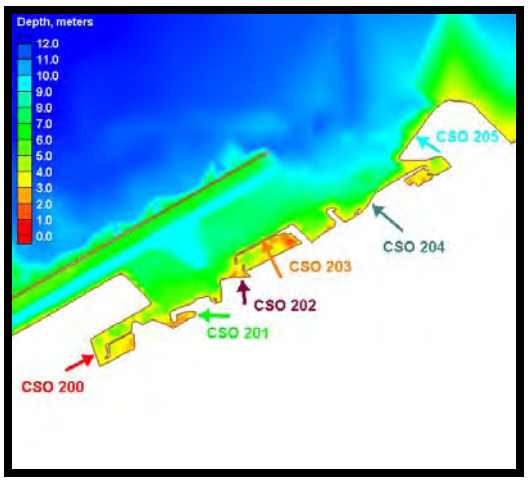

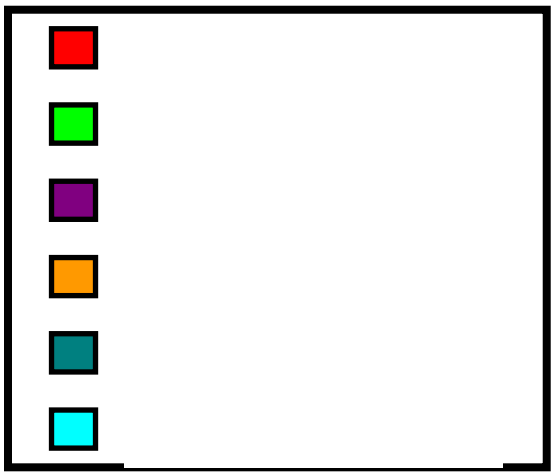

The figures are arranged by particle type, geometry and hydrodynamics. There are three particle types used, neutrally buoyant, floatables, and sediment. There are four different geometry types that are used and they are the base condition, configuration 1, configuration 2, and configuration 3. The hydrodynamics was used for 6 month and 5 years storms. Each particle type has a geometry and hydrodynamics representation.

Figure	Page Numbers
Neutrally Buoyant - Base – 6 Month	63-65
Neutrally Buoyant - Configuration 1 – 6 Month	66-68
Neutrally Buoyant - Configuration 2 – 6 Month	69-71
Neutrally Buoyant - Configuration 3 – 6 Month	72-74
Neutrally Buoyant - Base – 5 Year	75-77
Neutrally Buoyant - Configuration 1 – 5 Year	78-80
Neutrally Buoyant - Configuration 2 – 5 Year	81-83
Neutrally Buoyant - Configuration 3 – 5 Year	84-86
Floatables – Base – 6 Month	87-89
Floatables - Configuration 1 – 6 Month	90-92
Floatables - Configuration 2 – 6 Month	93-95
Floatables - Configuration 3 – 6 Month	96-98
Floatables - Base – 5 Year	99-101
Floatables - Configuration 1 – 5 Year	102-104
Floatables - Configuration 2 – 5 Year	105-107
Floatables - Configuration 3 – 5 Year	108-110
Sediments – Base – 6 Month	111-113
Sediments - Configuration 1 – 6 Month	114-116
Sediments - Configuration 2 – 6 Month	117-119
Sediments - Configuration 3 – 6 Month	120-122
Sediments - Base – 5 Year	123-125
Sediments - Configuration 1 – 5 Year	126-128
Sediments - Configuration 2 – 5 Year	129-131
Sediments - Configuration 3 – 5 Year	132-134

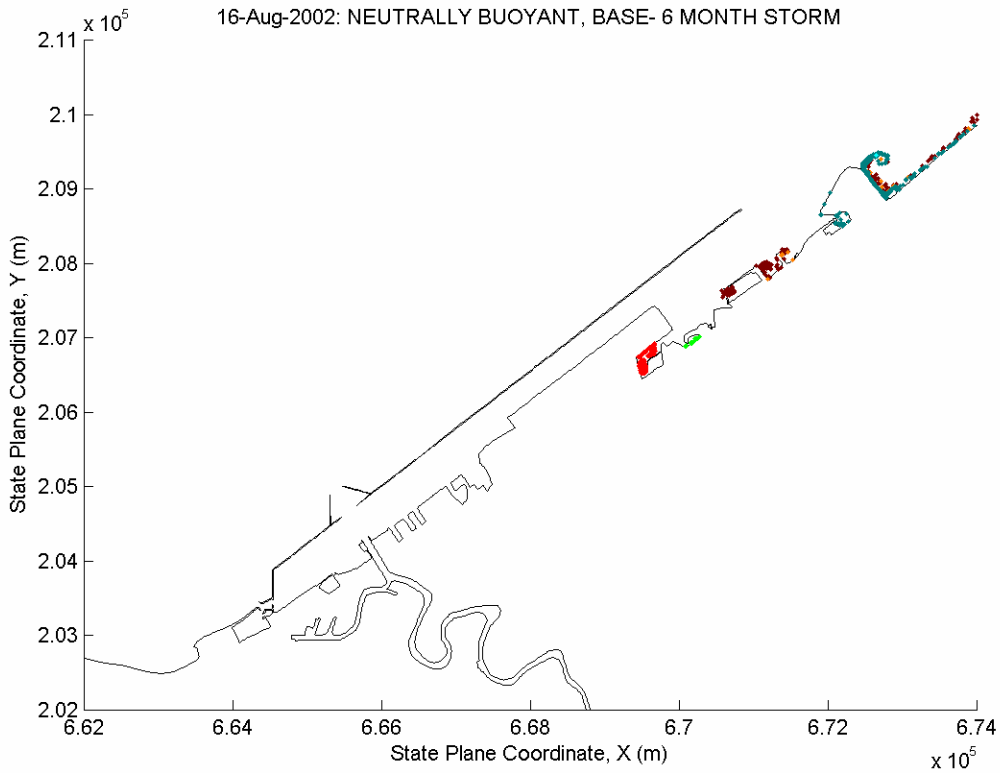
16-Aug-2002: NEUTRALLY BUOYANT, BASE- 6 MONTH STORM
x 10^5
2.11
2.1
2.09
2.08
2.07
2.06
2.05
2.04
2.03
2.02
State Plane Coordinate, Y (m)
6.62
6.64
6.66
6.68
6.7
6.72
6.74
State Plane Coordinate, X (m)
x 10^5

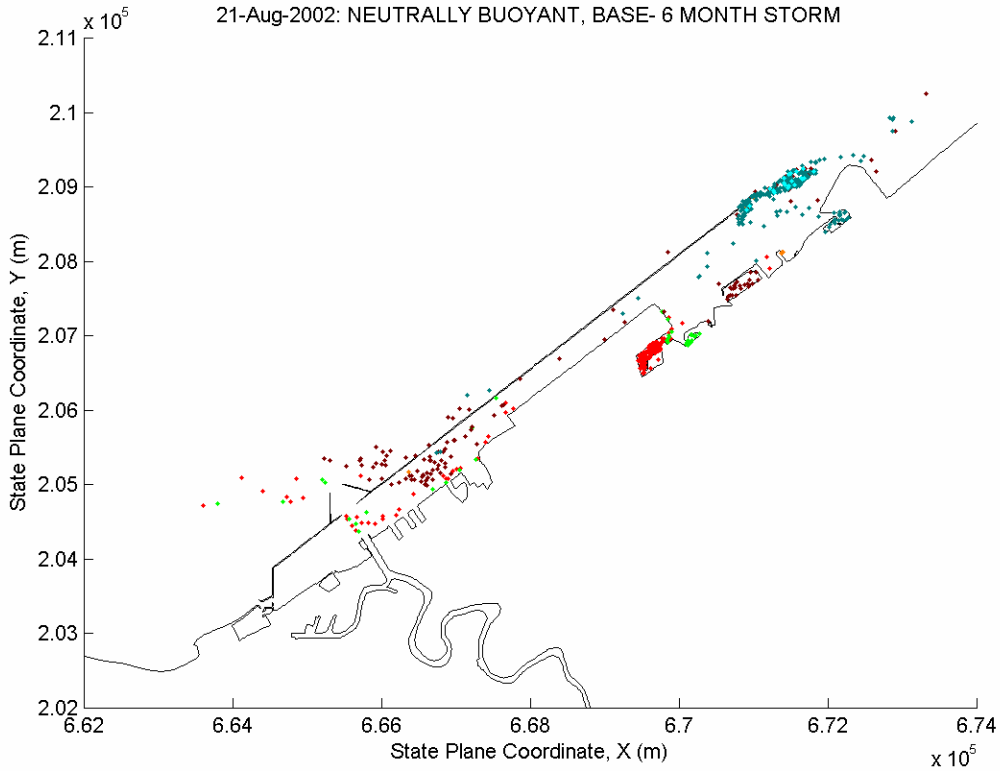
21-Aug-2002: NEUTRALLY BUOYANT, BASE- 6 MONTH STORM
x 10^5
2.11
2.1
2.09
2.08
2.07
2.06
2.05
2.04
2.03
2.02
State Plane Coordinate, Y (m)
6.62
6.64
6.66
6.68
6.7
6.72
6.74
State Plane Coordinate, X (m)
x 10^5

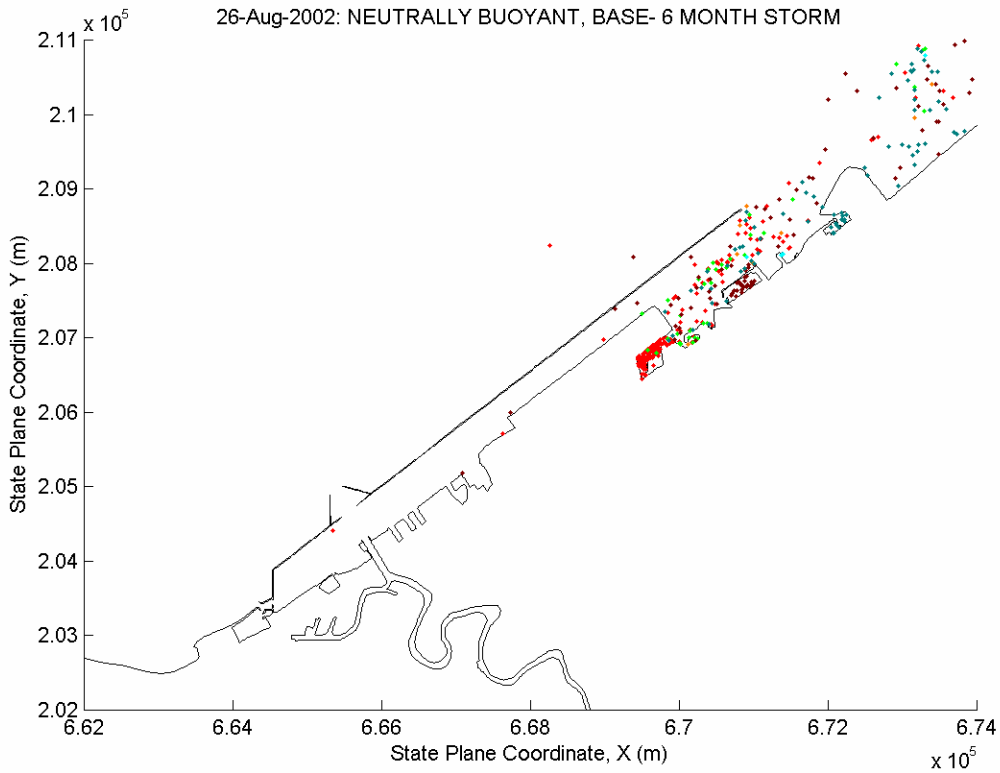
26-Aug-2002: NEUTRALLY BUOYANT, BASE- 6 MONTH STORM
x 10^5
2.11
2.1
2.09
2.08
2.07
2.06
2.05
2.04
2.03
2.02
State Plane Coordinate, Y (m)
6.62
6.64
6.66
6.68
6.7
6.72
6.74
State Plane Coordinate, X (m)
x 10^5

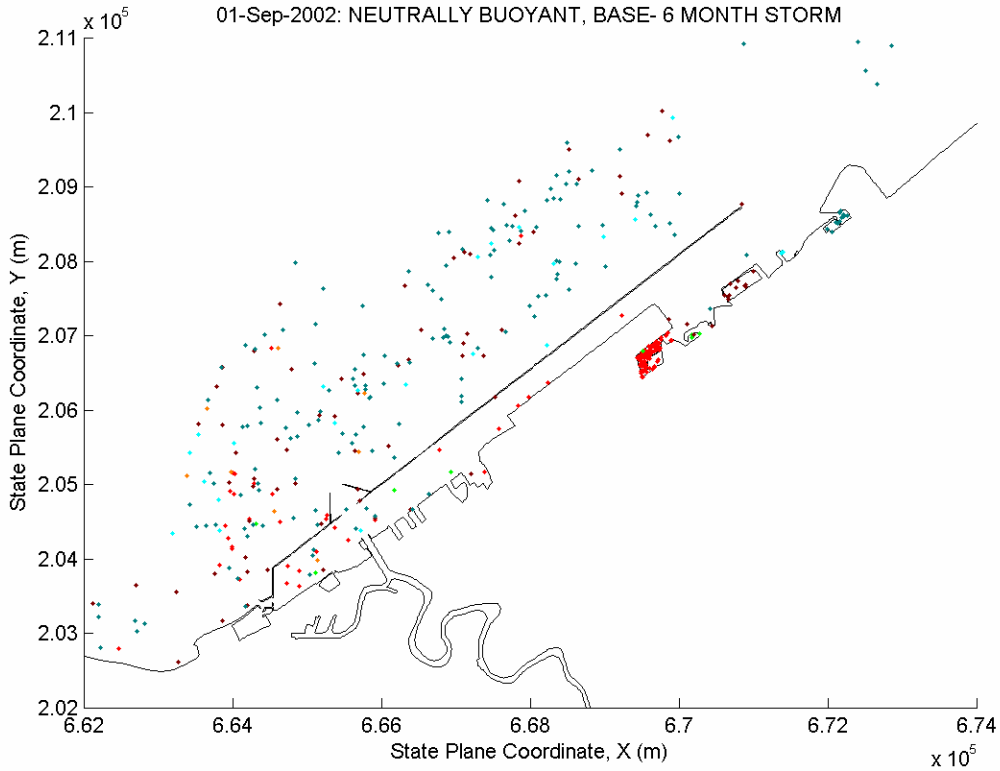
01-Sep-2002: NEUTRALLY BUOYANT, BASE- 6 MONTH STORM
x 10^5
2.11
2.1
2.09
2.08
2.07
2.06
2.05
2.04
2.03
2.02
State Plane Coordinate, Y (m)
6.62
6.64
6.66
6.68
6.7
6.72
6.74
State Plane Coordinate, X (m)
x 10^5

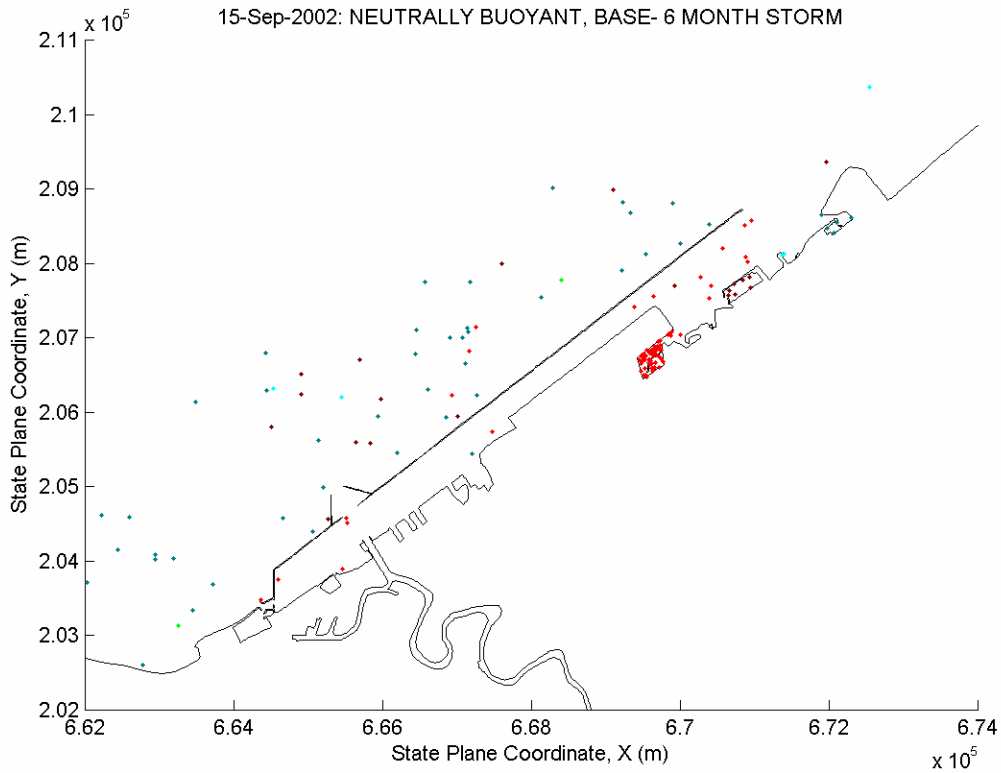
15-Sep-2002: NEUTRALLY BUOYANT, BASE- 6 MONTH STORM
x 10^5
2.11
2.1
2.09
2.08
2.07
2.06
2.05
2.04
2.03
2.02
State Plane Coordinate, Y (m)
6.62
6.64
6.66
6.68
6.7
6.72
6.74
State Plane Coordinate, X (m)
x 10^5

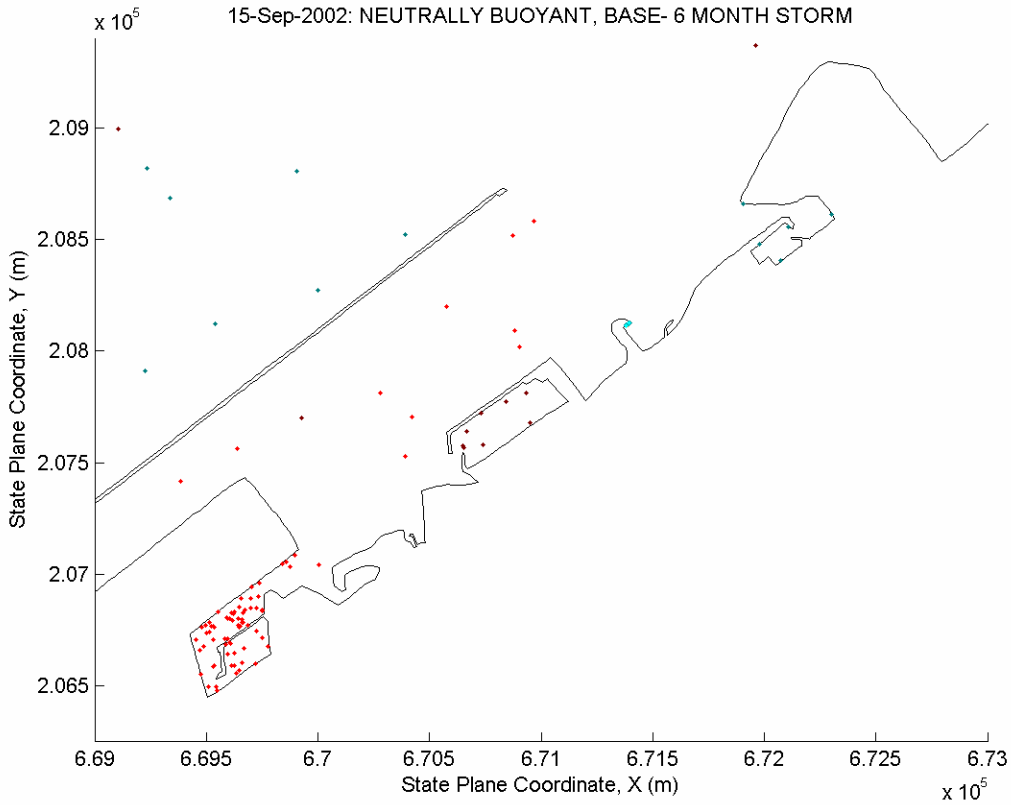
15-Sep-2002: NEUTRALLY BUOYANT, BASE- 6 MONTH STORM
x 10^5
2.09
2.085
2.08
2.075
2.07
2.065
State Plane Coordinate, Y (m)
6.69
6.695
6.7
6.705
6.71
6.715
6.72
6.725
6.73
State Plane Coordinate, X (m)
x 10^5

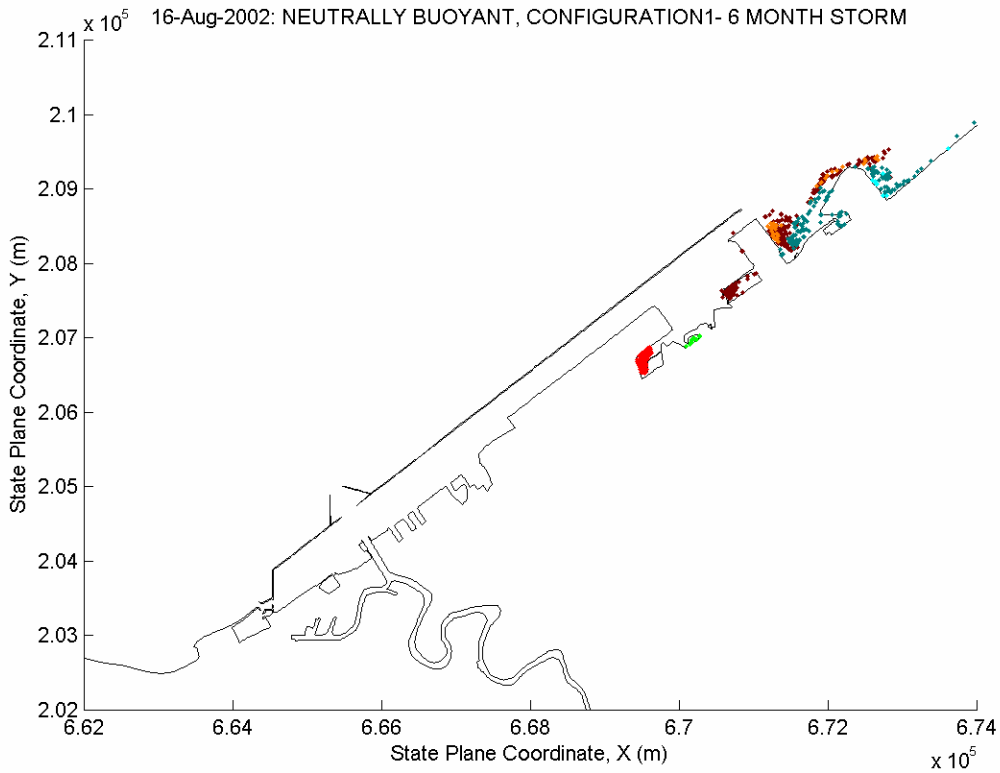
16-Aug-2002: NEUTRALLY BUOYANT, CONFIGURATION1- 6 MONTH STORM
x 10^5
2.11
2.1
2.09
2.08
2.07
2.06
2.05
2.04
2.03
2.02
State Plane Coordinate, Y (m)
6.62
6.64
6.66
6.68
6.7
6.72
6.74
State Plane Coordinate, X (m)
x 10^5

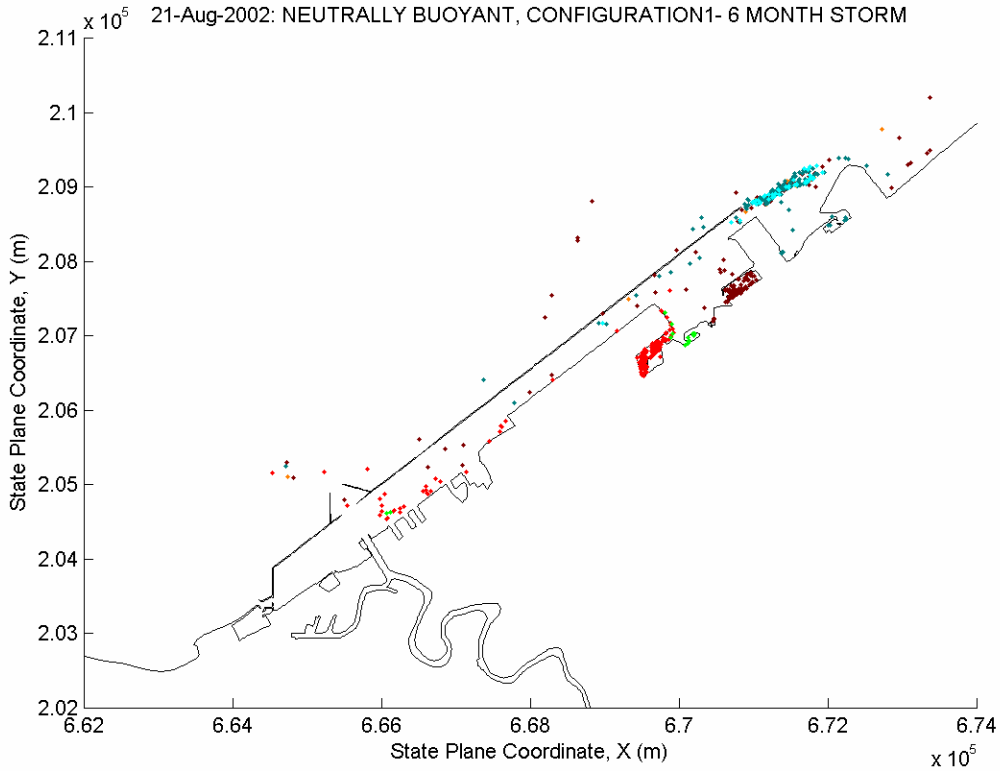
21-Aug-2002: NEUTRALLY BUOYANT, CONFIGURATION1- 6 MONTH STORM
x 10^5
2.11
2.1
2.09
2.08
2.07
2.06
2.05
2.04
2.03
2.02
State Plane Coordinate, Y (m)
6.62
6.64
6.66
6.68
6.7
6.72
6.74
State Plane Coordinate, X (m)
x 10^5

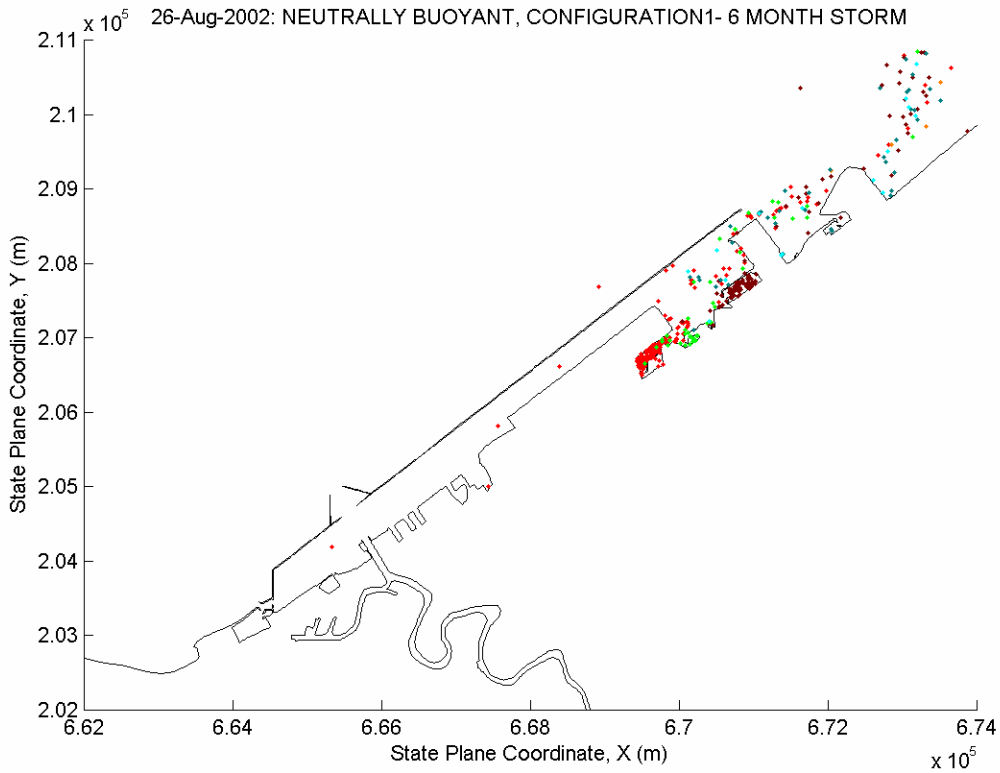
26-Aug-2002: NEUTRALLY BUOYANT, CONFIGURATION1- 6 MONTH STORM
x 10^5
2.11
2.1
2.09
2.08
2.07
2.06
2.05
2.04
2.03
2.02
State Plane Coordinate, Y (m)
6.62
6.64
6.66
6.68
6.7
6.72
6.74
State Plane Coordinate, X (m)
x 10^5

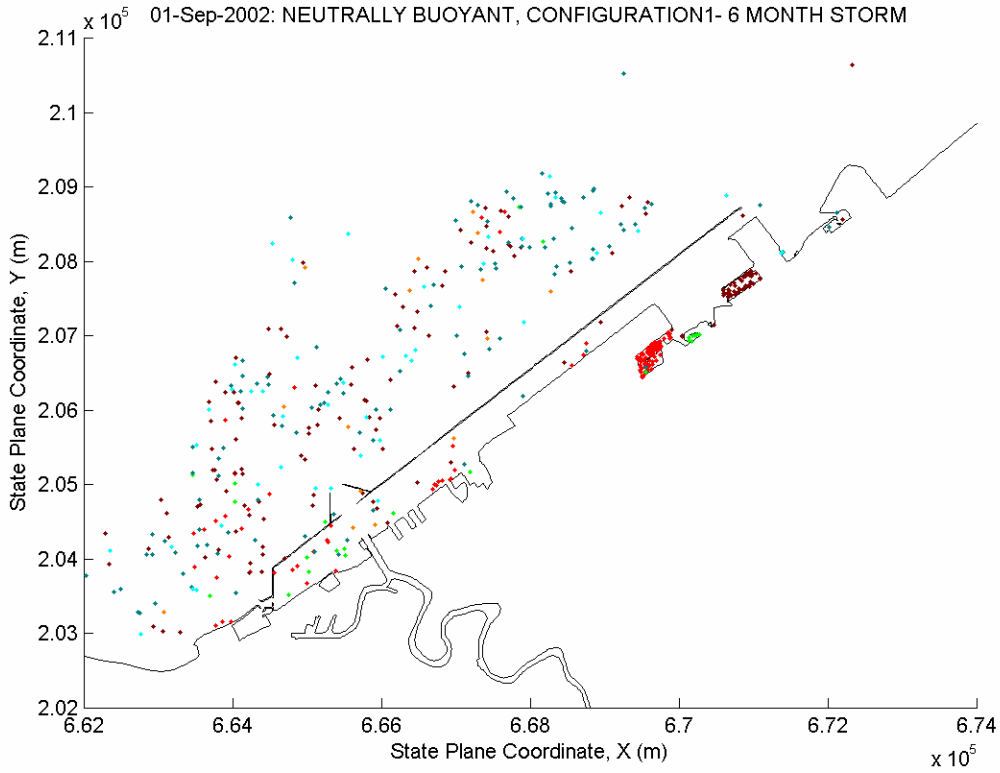
01-Sep-2002: NEUTRALLY BUOYANT, CONFIGURATION1- 6 MONTH STORM
x 10^5
2.11
2.1
2.09
2.08
2.07
2.06
2.05
2.04
2.03
2.02
State Plane Coordinate, Y (m)
6.62
6.64
6.66
6.68
6.7
6.72
6.74
State Plane Coordinate, X (m)
x 10^5

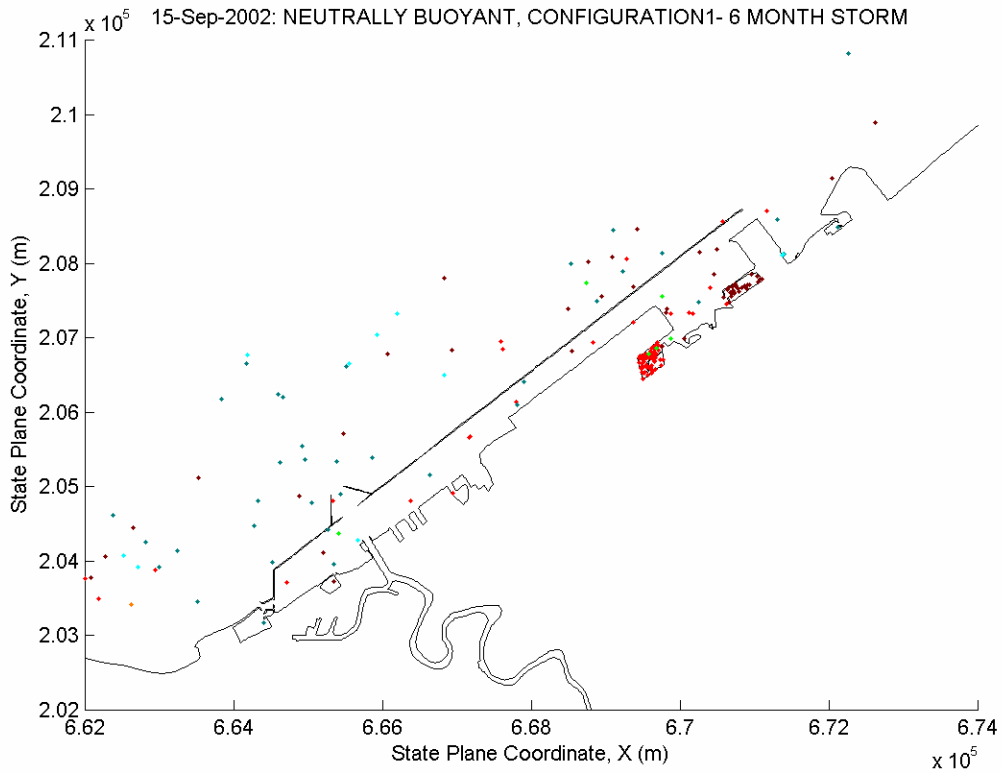
15-Sep-2002: NEUTRALLY BUOYANT, CONFIGURATION1- 6 MONTH STORM
x 10^5
2.11
2.1
2.09
2.08
2.07
2.06
2.05
2.04
2.03
2.02
State Plane Coordinate, Y (m)
6.62
6.64
6.66
6.68
6.7
6.72
6.74
State Plane Coordinate, X (m)
x 10^5

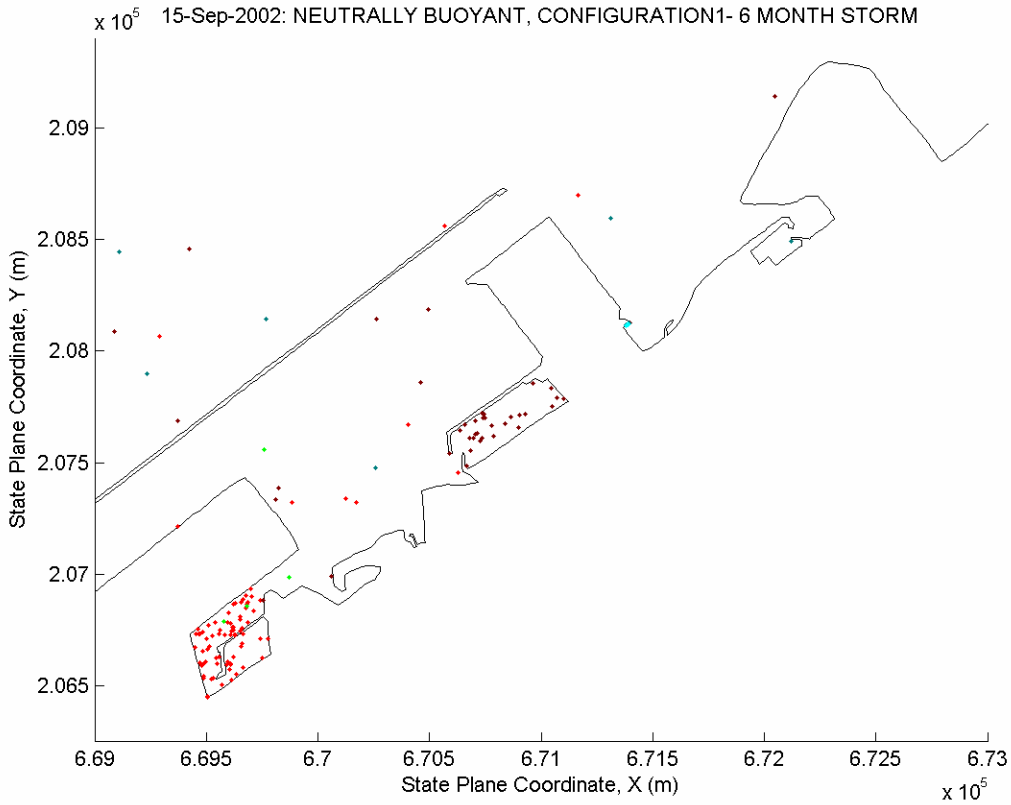
15-Sep-2002: NEUTRALLY BUOYANT, CONFIGURATION1- 6 MONTH STORM
x 10^5
2.09
2.085
2.08
2.075
2.07
2.065
State Plane Coordinate, Y (m)
6.69
6.695
6.7
6.705
6.71
6.715
6.72
6.725
6.73
State Plane Coordinate, X (m)
x 10^5

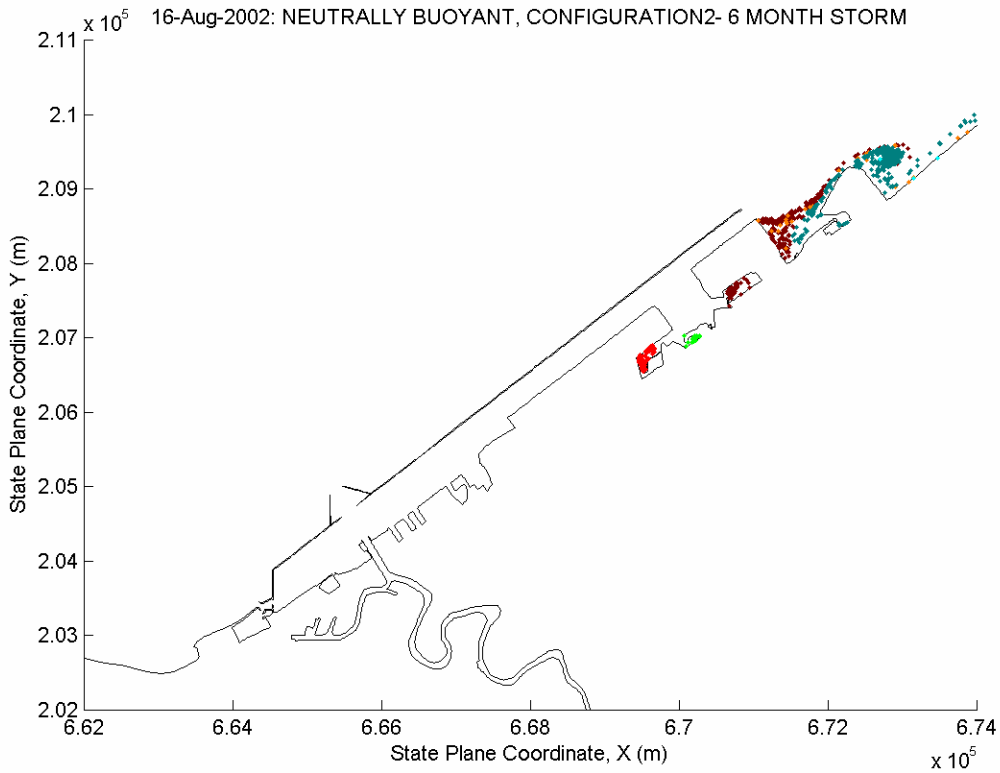
16-Aug-2002: NEUTRALLY BUOYANT, CONFIGURATION2- 6 MONTH STORM
x 10^5
2.11
2.1
2.09
2.08
2.07
2.06
2.05
2.04
2.03
2.02
State Plane Coordinate, Y (m)
6.62
6.64
6.66
6.68
6.7
6.72
6.74
State Plane Coordinate, X (m)
x 10^5

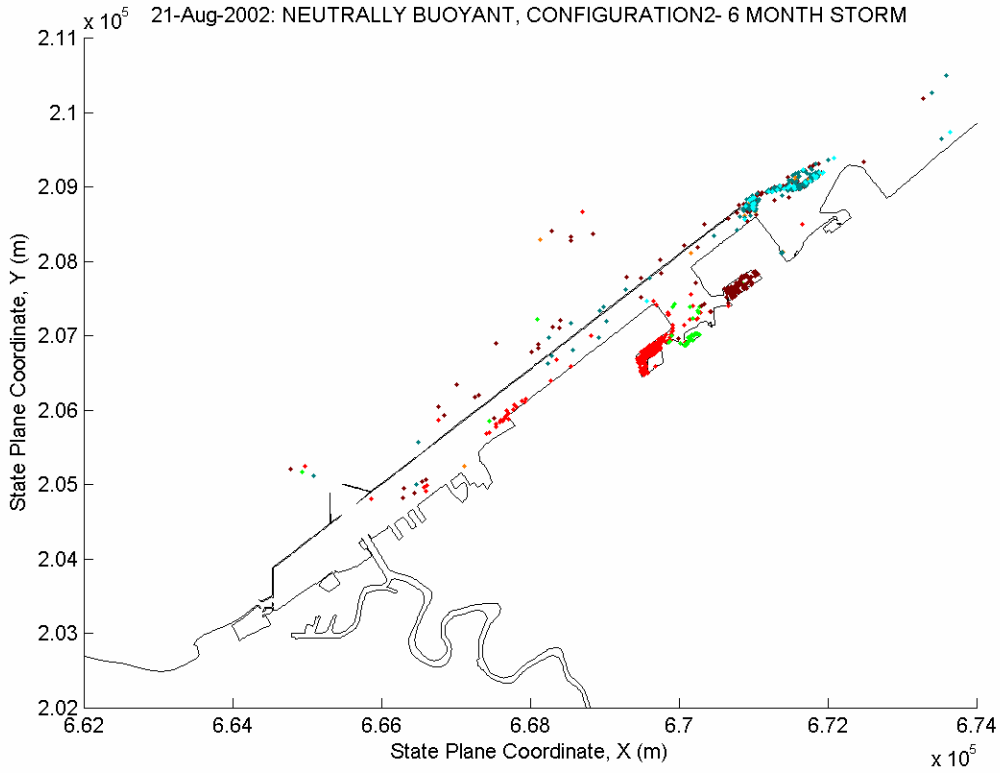
21-Aug-2002: NEUTRALLY BUOYANT, CONFIGURATION2- 6 MONTH STORM
x 10^5
2.11
2.1
2.09
2.08
2.07
2.06
2.05
2.04
2.03
2.02
State Plane Coordinate, Y (m)
6.62
6.64
6.66
6.68
6.7
6.72
6.74
State Plane Coordinate, X (m)
x 10^5

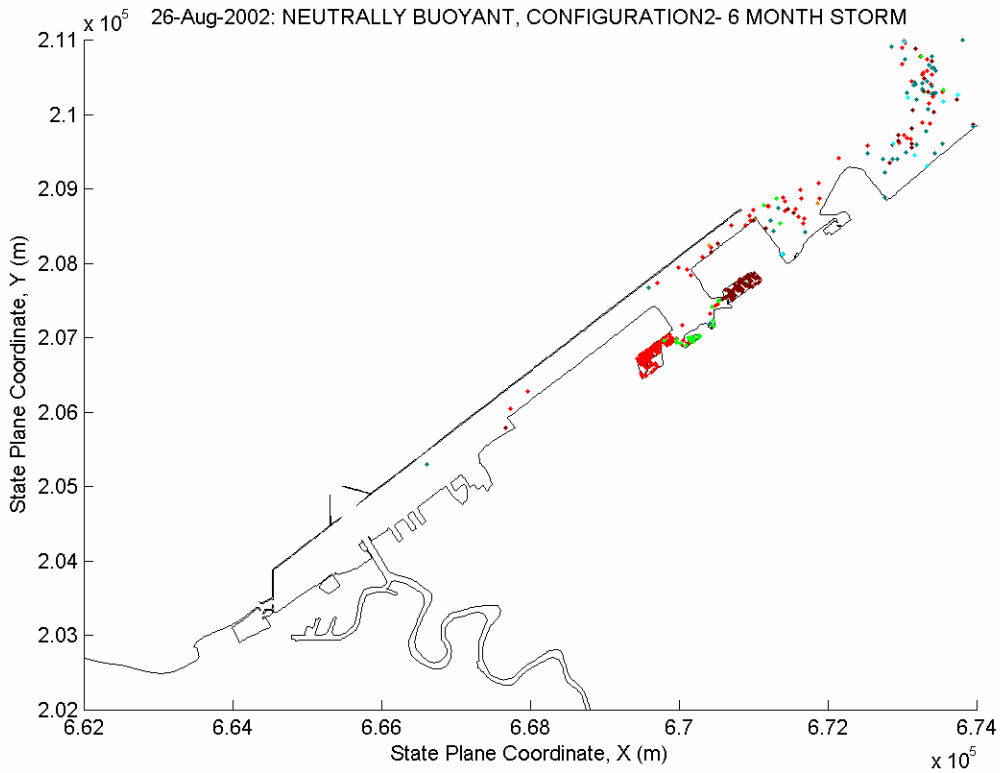
26-Aug-2002: NEUTRALLY BUOYANT, CONFIGURATION2- 6 MONTH STORM
x 10^5
2.11
2.1
2.09
2.08
2.07
2.06
2.05
2.04
2.03
2.02
State Plane Coordinate, Y (m)
6.62
6.64
6.66
6.68
6.7
6.72
6.74
State Plane Coordinate, X (m)
x 10^5

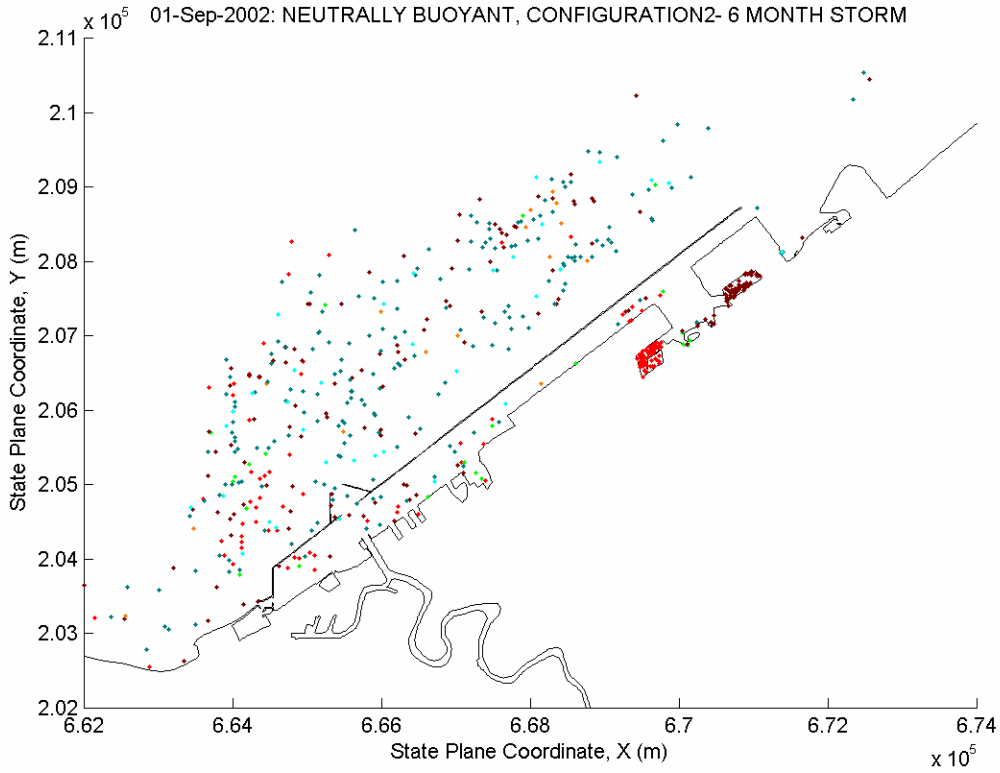
01-Sep-2002: NEUTRALLY BUOYANT, CONFIGURATION2- 6 MONTH STORM
x 10^5
2.11
2.1
2.09
2.08
2.07
2.06
2.05
2.04
2.03
2.02
State Plane Coordinate, Y (m)
6.62
6.64
6.66
6.68
6.7
6.72
6.74
State Plane Coordinate, X (m)
x 10^5

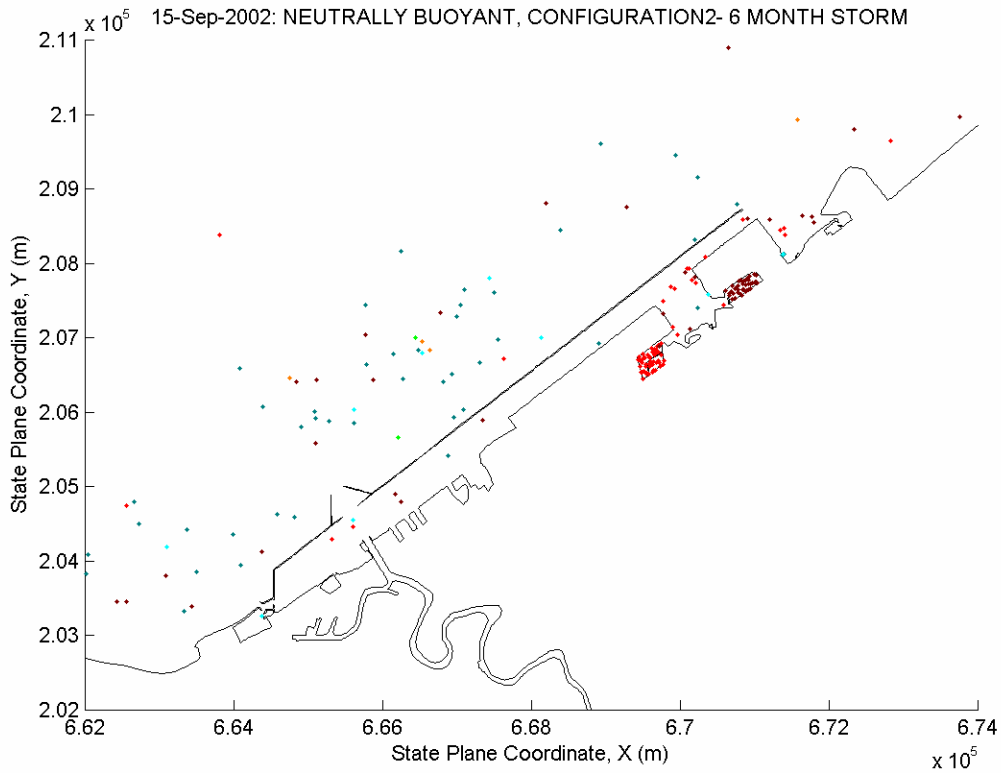
15-Sep-2002: NEUTRALLY BUOYANT, CONFIGURATION2- 6 MONTH STORM
x 10^5
2.11
2.1
2.09
2.08
2.07
2.06
2.05
2.04
2.03
2.02
State Plane Coordinate, Y (m)
6.62
6.64
6.66
6.68
6.7
6.72
6.74
State Plane Coordinate, X (m)
x 10^5

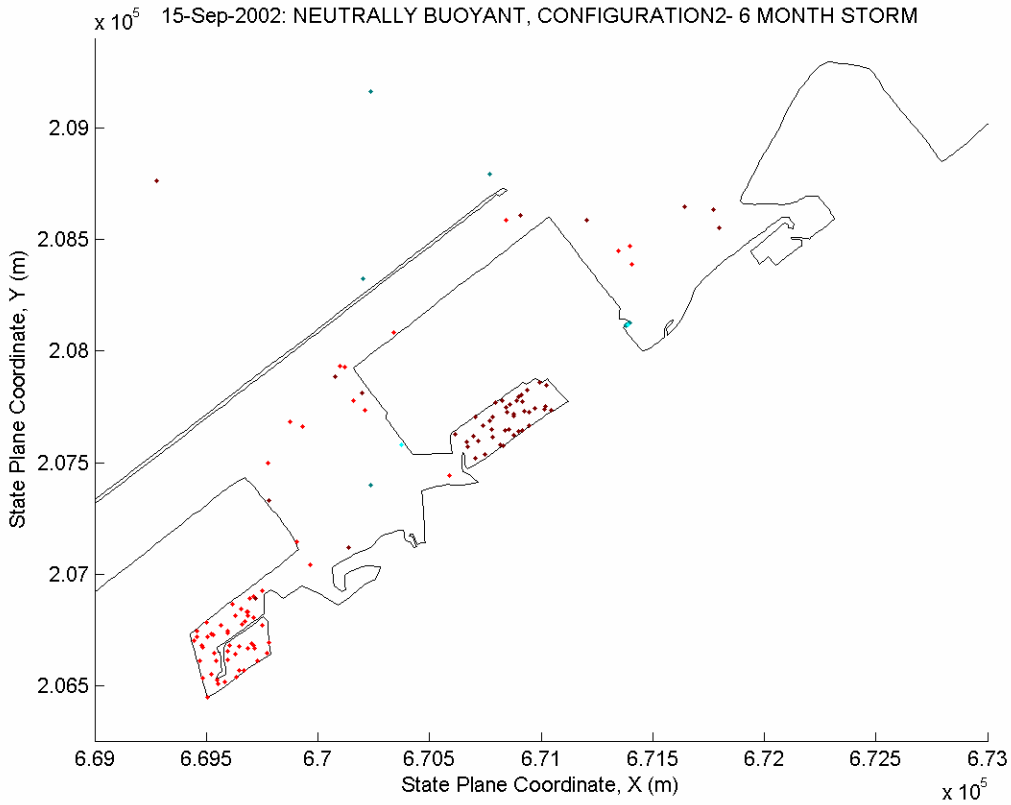
15-Sep-2002: NEUTRALLY BUOYANT, CONFIGURATION2- 6 MONTH STORM
x 10^5
2.09
2.085
2.08
2.075
2.07
2.065
State Plane Coordinate, Y (m)
6.69
6.695
6.7
6.705
6.71
6.715
6.72
6.725
6.73
State Plane Coordinate, X (m)
x 10^5

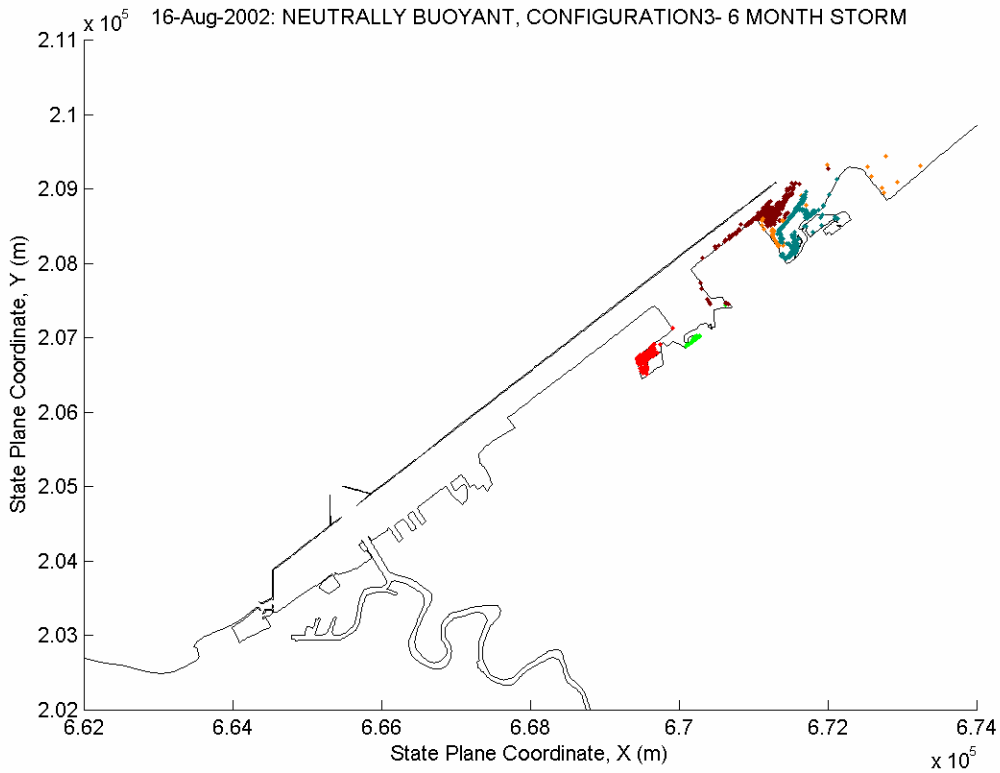
16-Aug-2002: NEUTRALLY BUOYANT, CONFIGURATION3- 6 MONTH STORM
x 10^5
2.11
2.1
2.09
2.08
2.07
2.06
2.05
2.04
2.03
2.02
State Plane Coordinate, Y (m)
6.62
6.64
6.66
6.68
6.7
6.72
6.74
State Plane Coordinate, X (m)
x 10^5

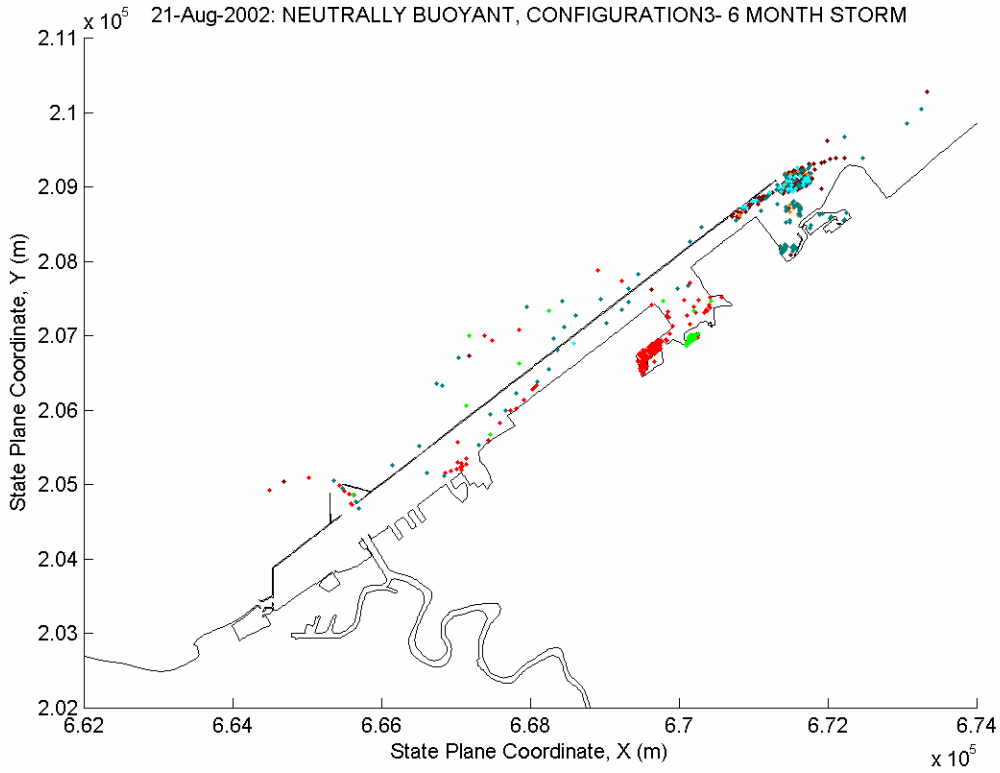
21-Aug-2002: NEUTRALLY BUOYANT, CONFIGURATION3- 6 MONTH STORM
x 10^5
2.11
2.1
2.09
2.08
2.07
2.06
2.05
2.04
2.03
2.02
State Plane Coordinate, Y (m)
6.62
6.64
6.66
6.68
6.7
6.72
6.74
State Plane Coordinate, X (m)
x 10^5

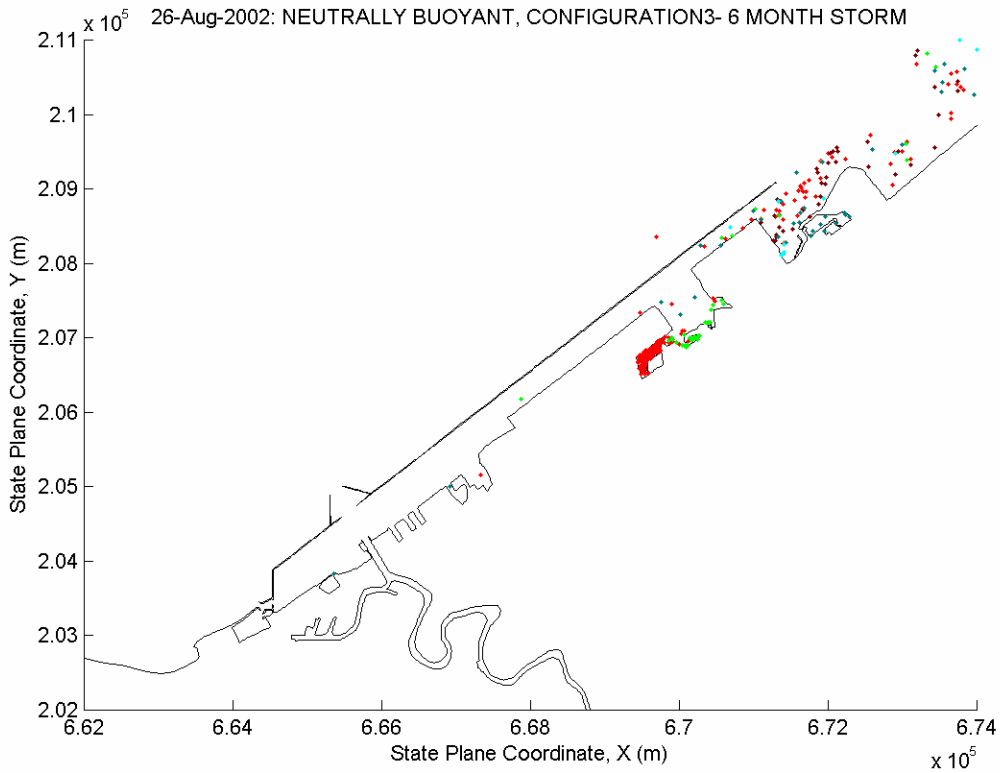
26-Aug-2002: NEUTRALLY BUOYANT, CONFIGURATION3- 6 MONTH STORM
x 10^5
2.11
2.1
2.09
2.08
2.07
2.06
2.05
2.04
2.03
2.02
State Plane Coordinate, Y (m)
6.62
6.64
6.66
6.68
6.7
6.72
6.74
State Plane Coordinate, X (m)
x 10^5

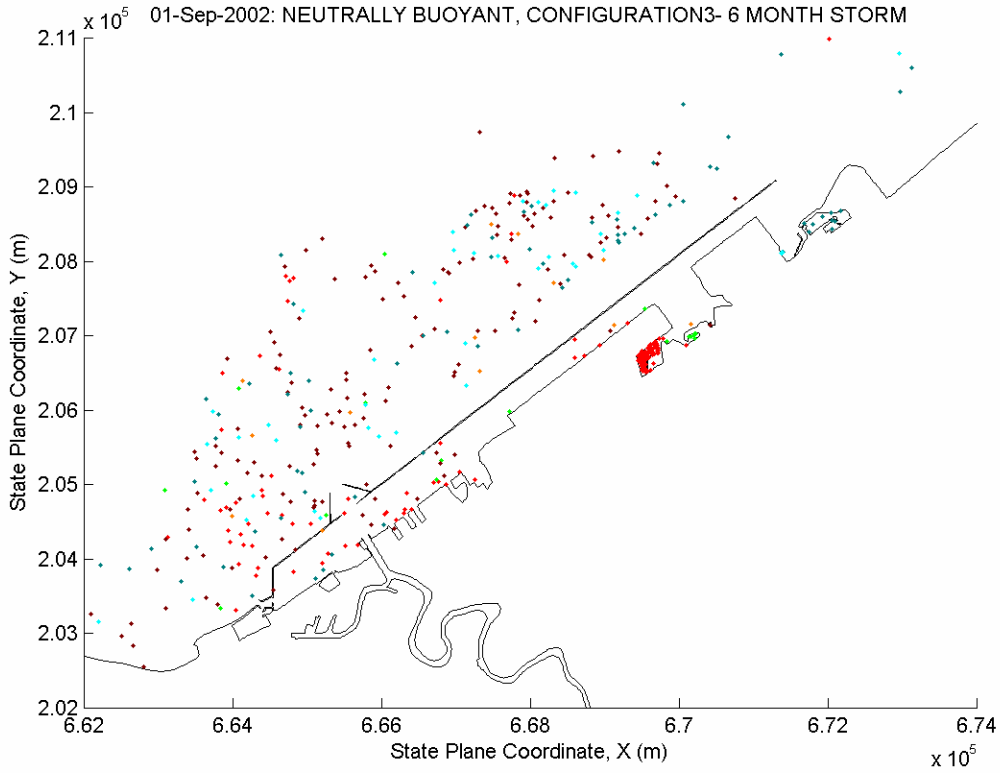
01-Sep-2002: NEUTRALLY BUOYANT, CONFIGURATION3- 6 MONTH STORM
x 10^5
2.11
2.1
2.09
2.08
2.07
2.06
2.05
2.04
2.03
2.02
State Plane Coordinate, Y (m)
6.62
6.64
6.66
6.68
6.7
6.72
6.74
State Plane Coordinate, X (m)
x 10^5

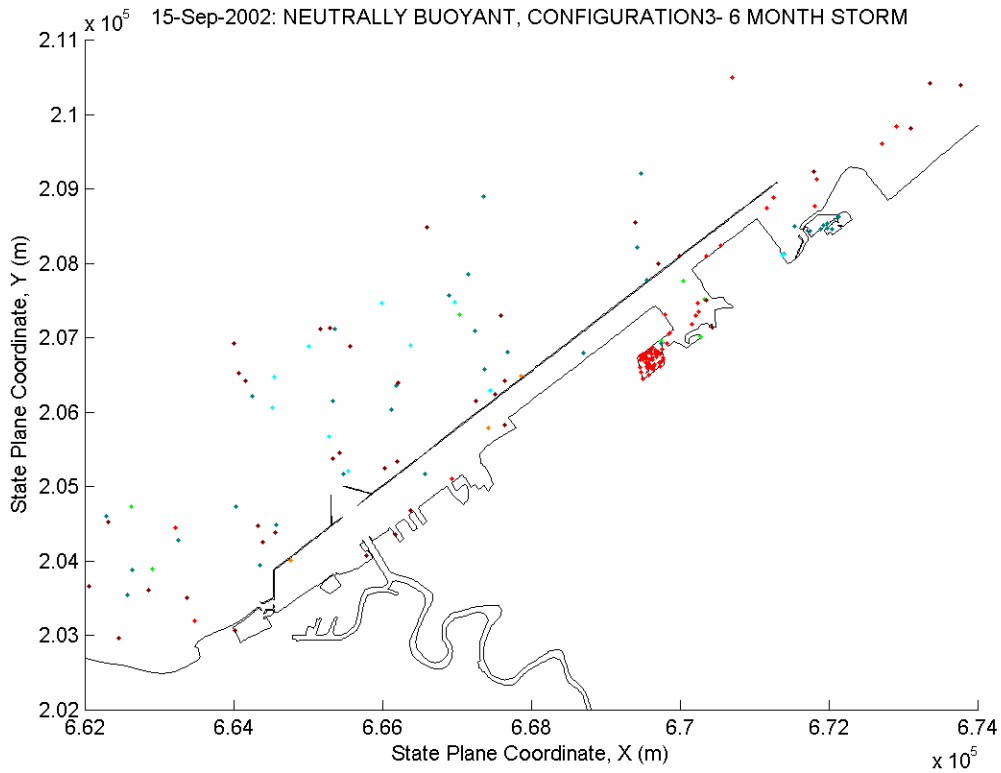
15-Sep-2002: NEUTRALLY BUOYANT, CONFIGURATION3- 6 MONTH STORM
x 10^5
2.11
2.1
2.09
2.08
2.07
2.06
2.05
2.04
2.03
2.02
State Plane Coordinate, Y (m)
6.62
6.64
6.66
6.68
6.7
6.72
6.74
State Plane Coordinate, X (m)
x 10^5

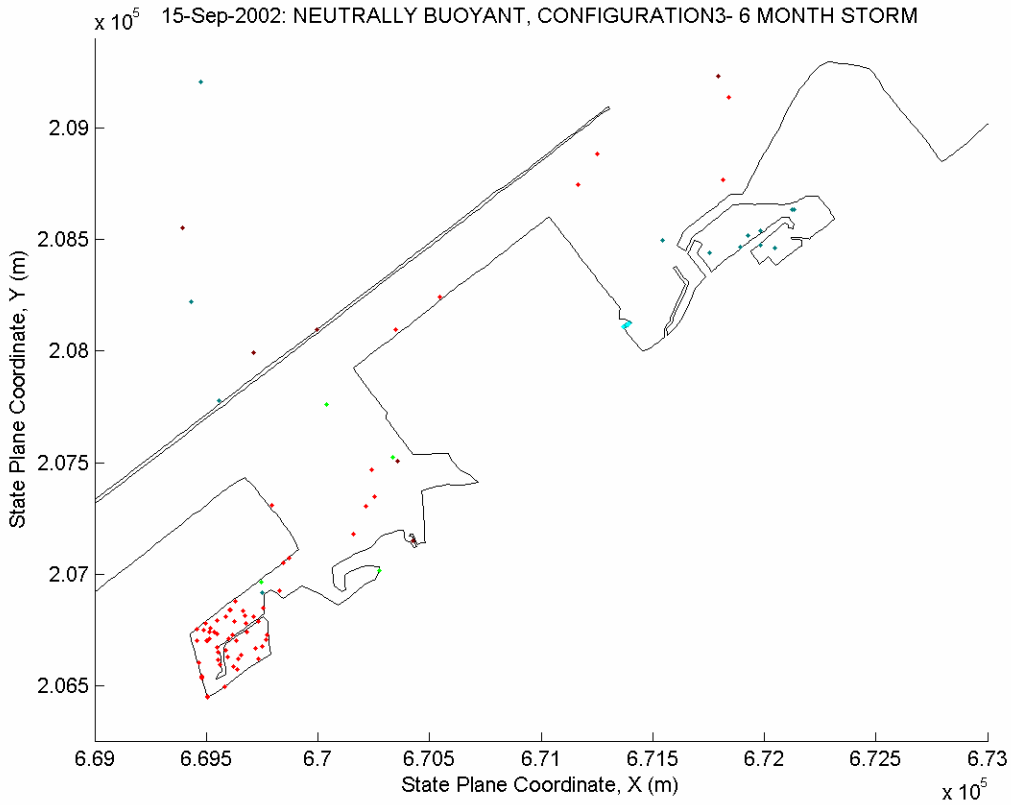
15-Sep-2002: NEUTRALLY BUOYANT, CONFIGURATION3- 6 MONTH STORM
x 10^5
2.09
2.085
2.08
2.075
2.07
2.065
State Plane Coordinate, Y (m)
6.69
6.695
6.7
6.705
6.71
6.715
6.72
6.725
6.73
State Plane Coordinate, X (m)
x 10^5

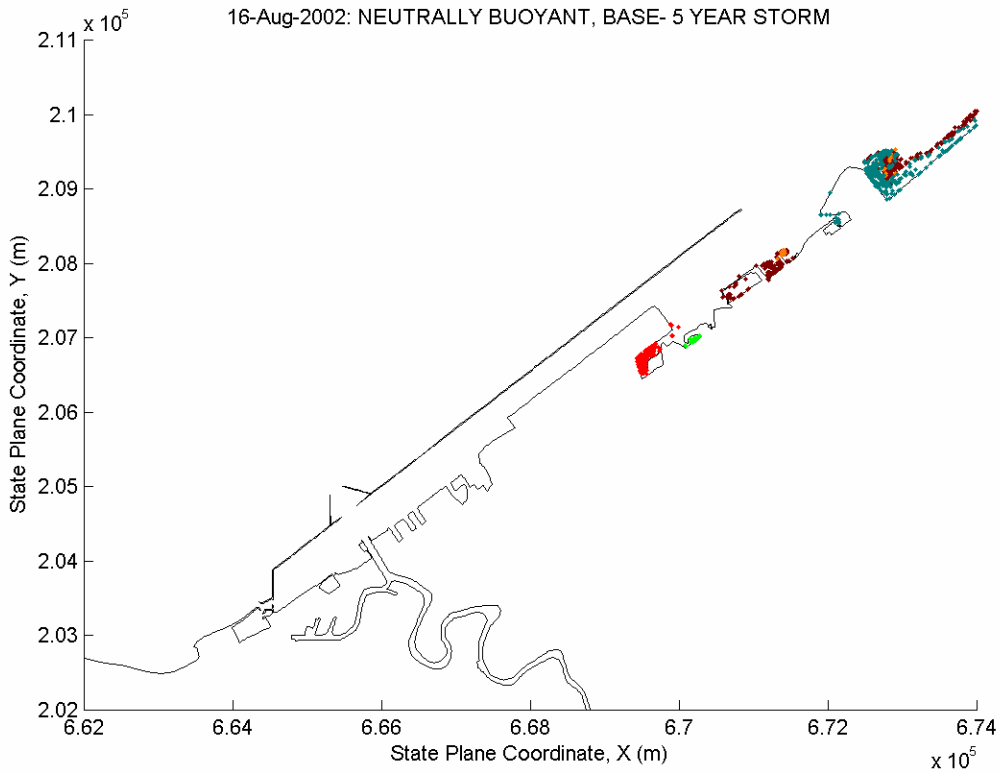
16-Aug-2002: NEUTRALLY BUOYANT, BASE- 5 YEAR STORM
x 10^5
2.11
2.1
2.09
2.08
2.07
2.06
2.05
2.04
2.03
2.02
State Plane Coordinate, Y (m)
6.62
6.64
6.66
6.68
6.7
6.72
6.74
State Plane Coordinate, X (m)
x 10^5

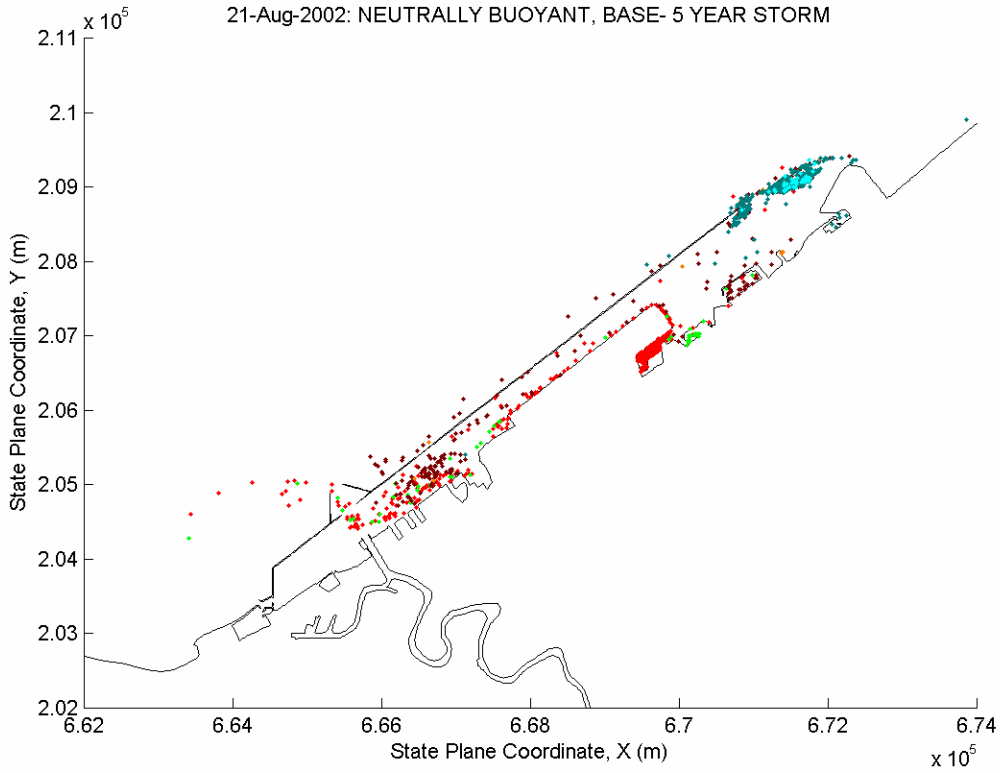
21-Aug-2002: NEUTRALLY BUOYANT, BASE- 5 YEAR STORM
x 10^5
2.11
2.1
2.09
2.08
2.07
2.06
2.05
2.04
2.03
2.02
State Plane Coordinate, Y (m)
6.62
6.64
6.66
6.68
6.7
6.72
6.74
State Plane Coordinate, X (m)
x 10^5

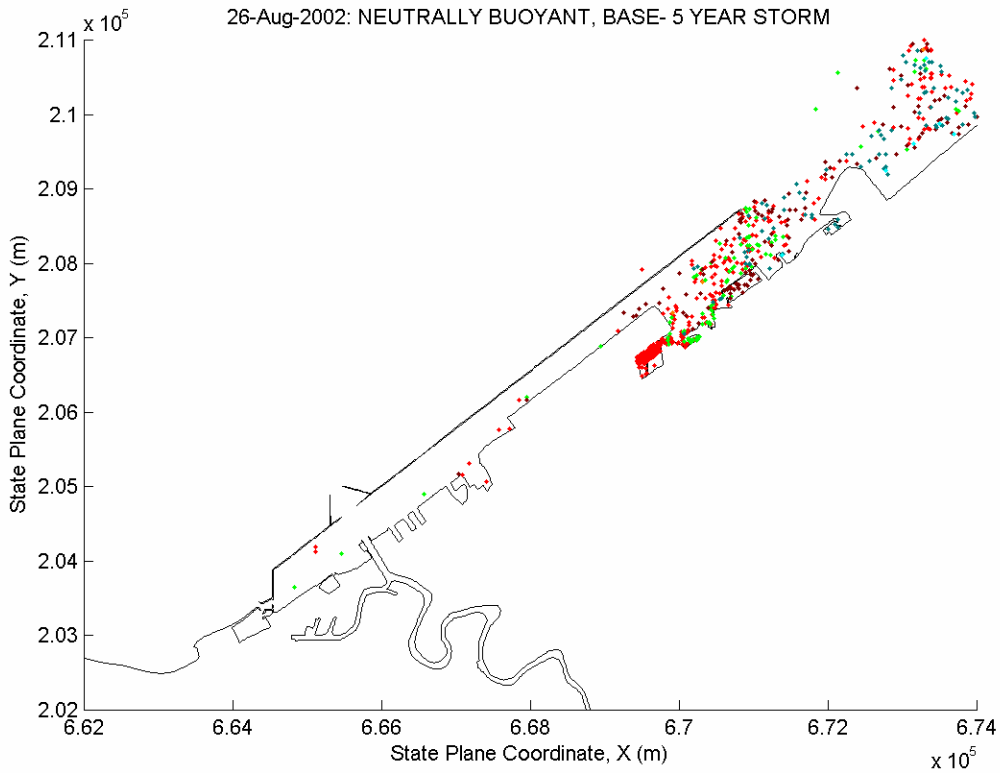
26-Aug-2002: NEUTRALLY BUOYANT, BASE- 5 YEAR STORM
x 10^5
2.11
2.1
2.09
2.08
2.07
2.06
2.05
2.04
2.03
2.02
State Plane Coordinate, Y (m)
6.62
6.64
6.66
6.68
6.7
6.72
6.74
State Plane Coordinate, X (m)
x 10^5

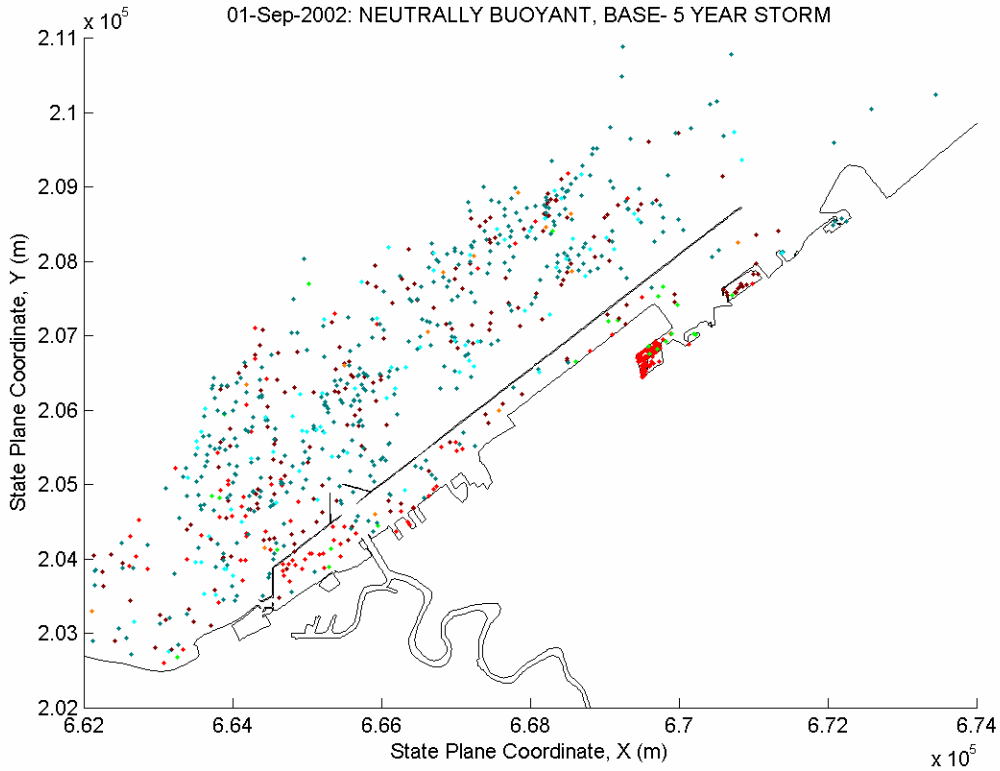
01-Sep-2002: NEUTRALLY BUOYANT, BASE- 5 YEAR STORM
x 10^5
2.11
2.1
2.09
2.08
2.07
2.06
2.05
2.04
2.03
2.02
State Plane Coordinate, Y (m)
6.62
6.64
6.66
6.68
6.7
6.72
6.74
State Plane Coordinate, X (m)
x 10^5

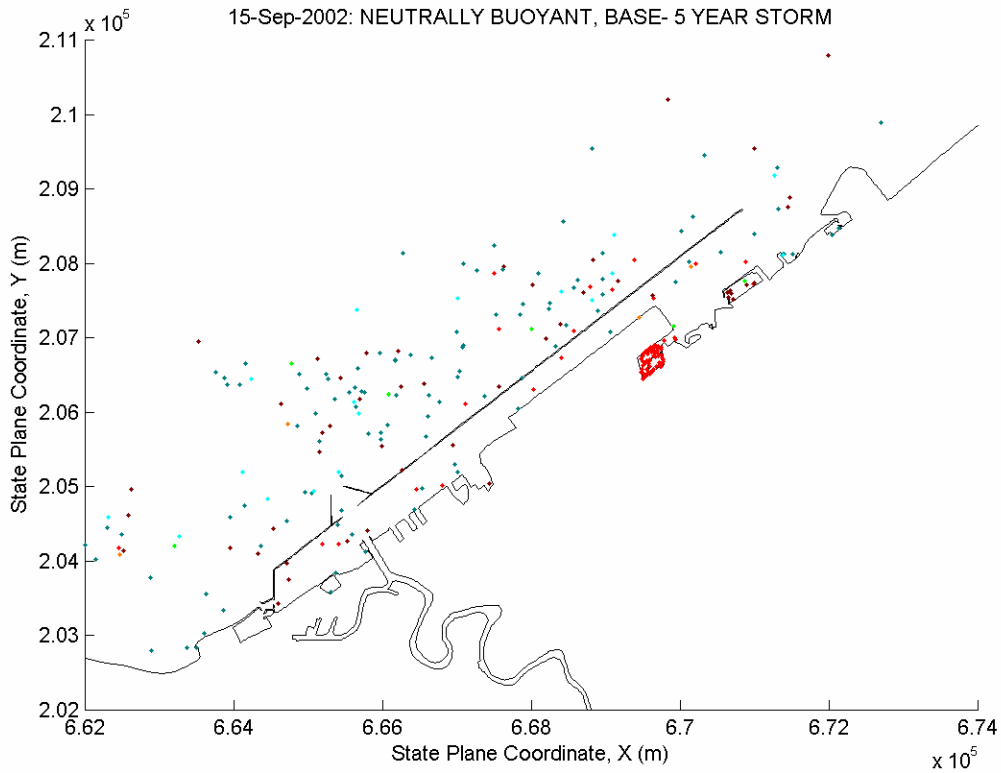
15-Sep-2002: NEUTRALLY BUOYANT, BASE- 5 YEAR STORM
x 10^5
2.11
2.1
2.09
2.08
2.07
2.06
2.05
2.04
2.03
2.02
State Plane Coordinate, Y (m)
6.62
6.64
6.66
6.68
6.7
6.72
6.74
State Plane Coordinate, X (m)
x 10^5

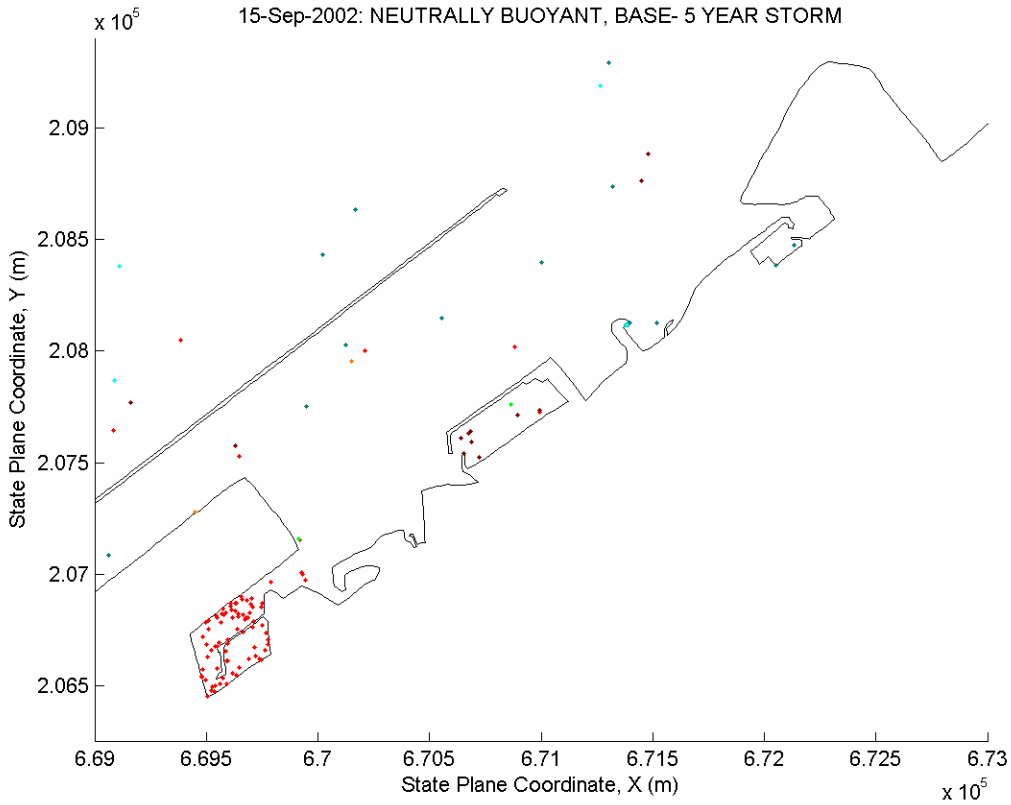
15-Sep-2002: NEUTRALLY BUOYANT, BASE- 5 YEAR STORM
x 10^5
2.09
2.085
2.08
2.075
2.07
2.065
State Plane Coordinate, Y (m)
6.69
6.695
6.7
6.705
6.71
6.715
6.72
6.725
6.73
State Plane Coordinate, X (m)
x 10^5

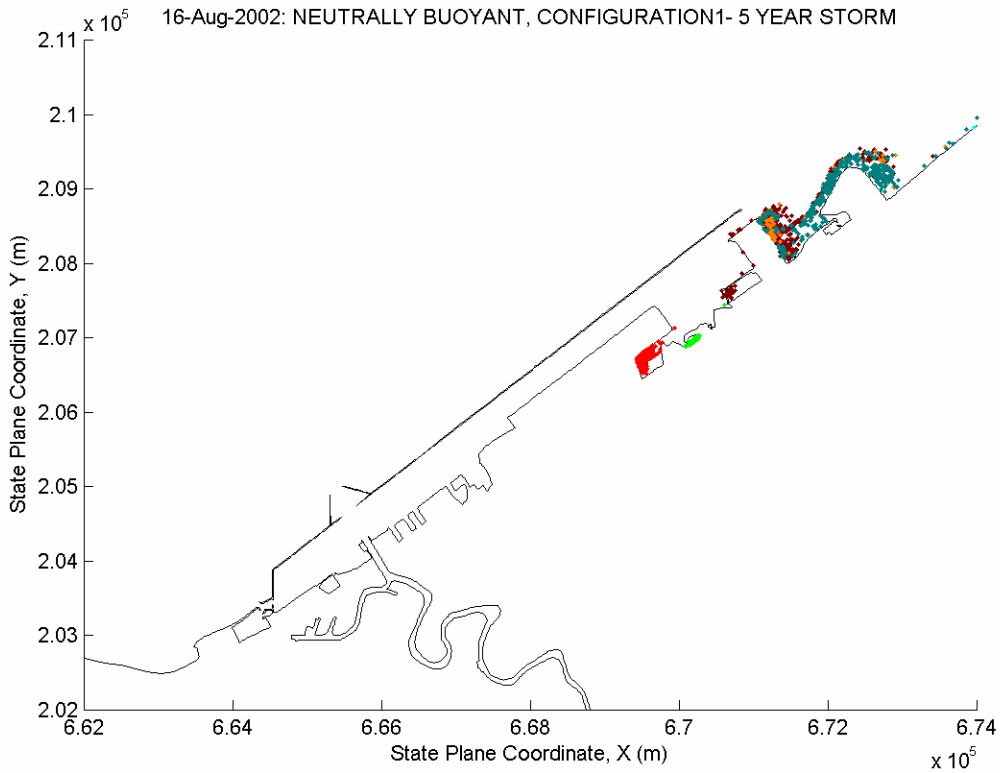
16-Aug-2002: NEUTRALLY BUOYANT, CONFIGURATION1- 5 YEAR STORM
x 10^5
2.11
2.1
2.09
2.08
2.07
2.06
2.05
2.04
2.03
2.02
State Plane Coordinate, Y (m)
6.62
6.64
6.66
6.68
6.7
6.72
6.74
State Plane Coordinate, X (m)
x 10^5

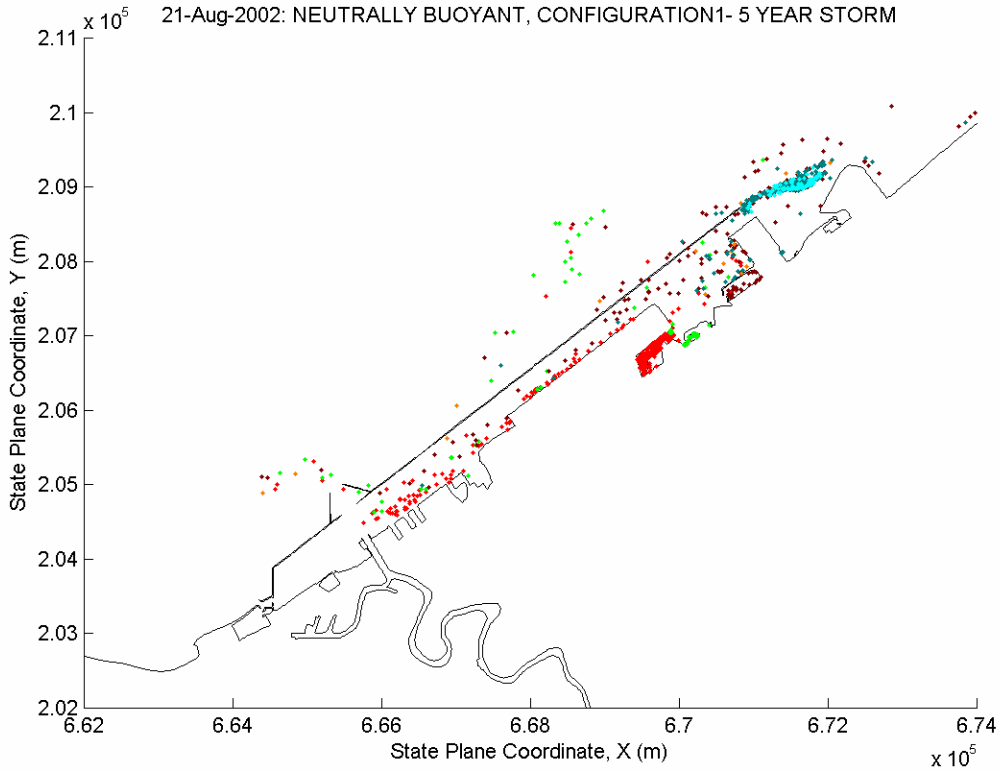
21-Aug-2002: NEUTRALLY BUOYANT, CONFIGURATION1- 5 YEAR STORM
x 10^5
2.11
2.1
2.09
2.08
2.07
2.06
2.05
2.04
2.03
2.02
State Plane Coordinate, Y (m)
6.62
6.64
6.66
6.68
6.7
6.72
6.74
State Plane Coordinate, X (m)
x 10^5

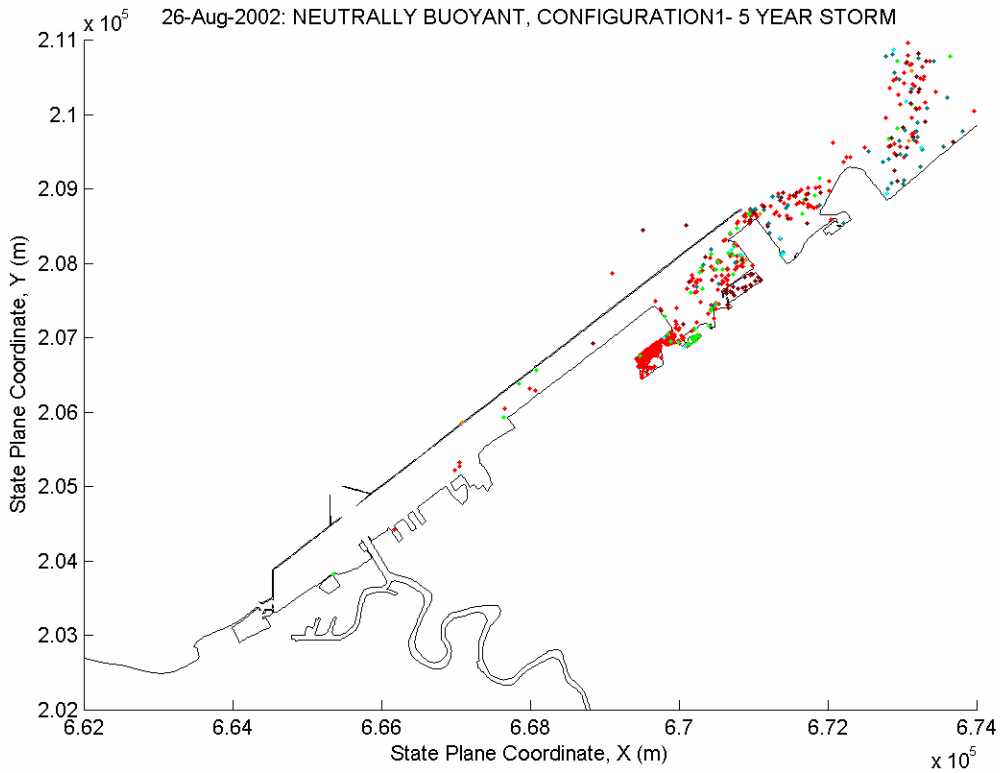
26-Aug-2002: NEUTRALLY BUOYANT, CONFIGURATION1- 5 YEAR STORM
x 10^5
2.11
2.1
2.09
2.08
2.07
2.06
2.05
2.04
2.03
2.02
State Plane Coordinate, Y (m)
6.62
6.64
6.66
6.68
6.7
6.72
6.74
State Plane Coordinate, X (m)
x 10^5

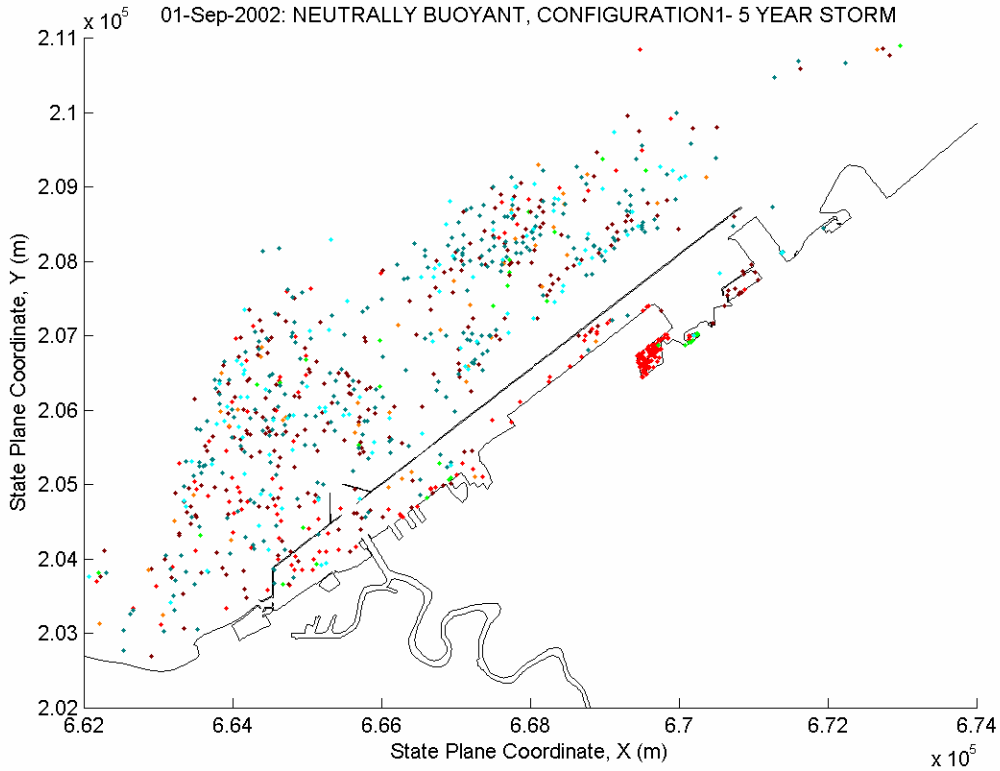
01-Sep-2002: NEUTRALLY BUOYANT, CONFIGURATION1- 5 YEAR STORM
x 10^5
2.11
2.1
2.09
2.08
2.07
2.06
2.05
2.04
2.03
2.02
State Plane Coordinate, Y (m)
6.62
6.64
6.66
6.68
6.7
6.72
6.74
State Plane Coordinate, X (m)
x 10^5

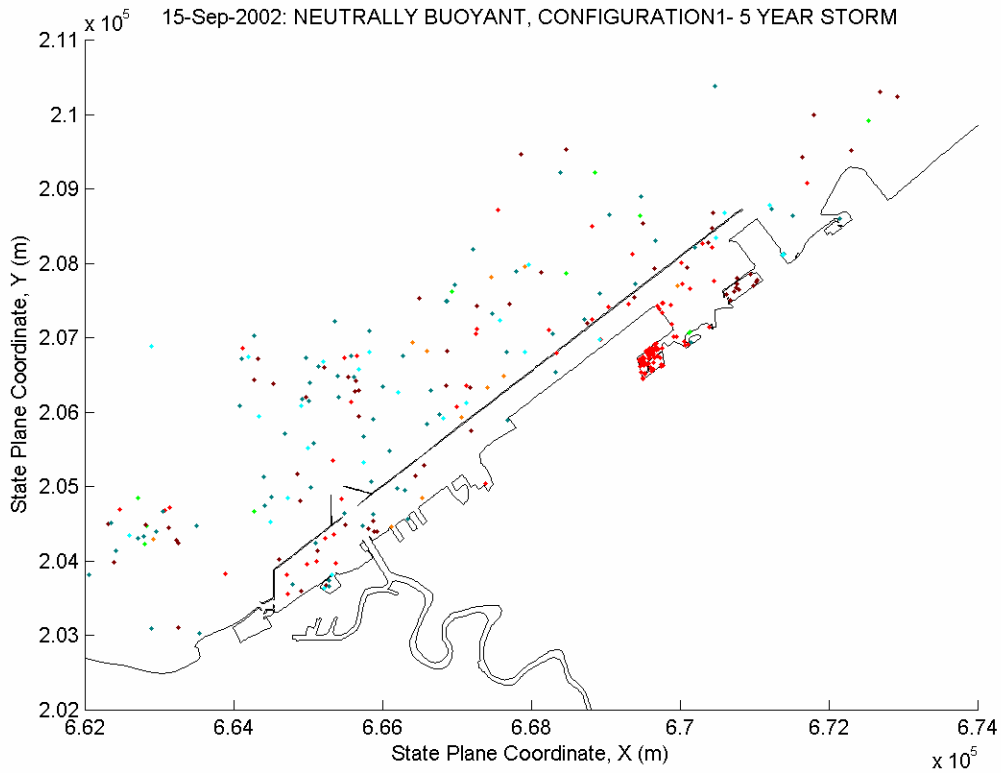
15-Sep-2002: NEUTRALLY BUOYANT, CONFIGURATION1- 5 YEAR STORM
x 10^5
2.11
2.1
2.09
2.08
2.07
2.06
2.05
2.04
2.03
2.02
State Plane Coordinate, Y (m)
6.62
6.64
6.66
6.68
6.7
6.72
6.74
State Plane Coordinate, X (m)
x 10^5

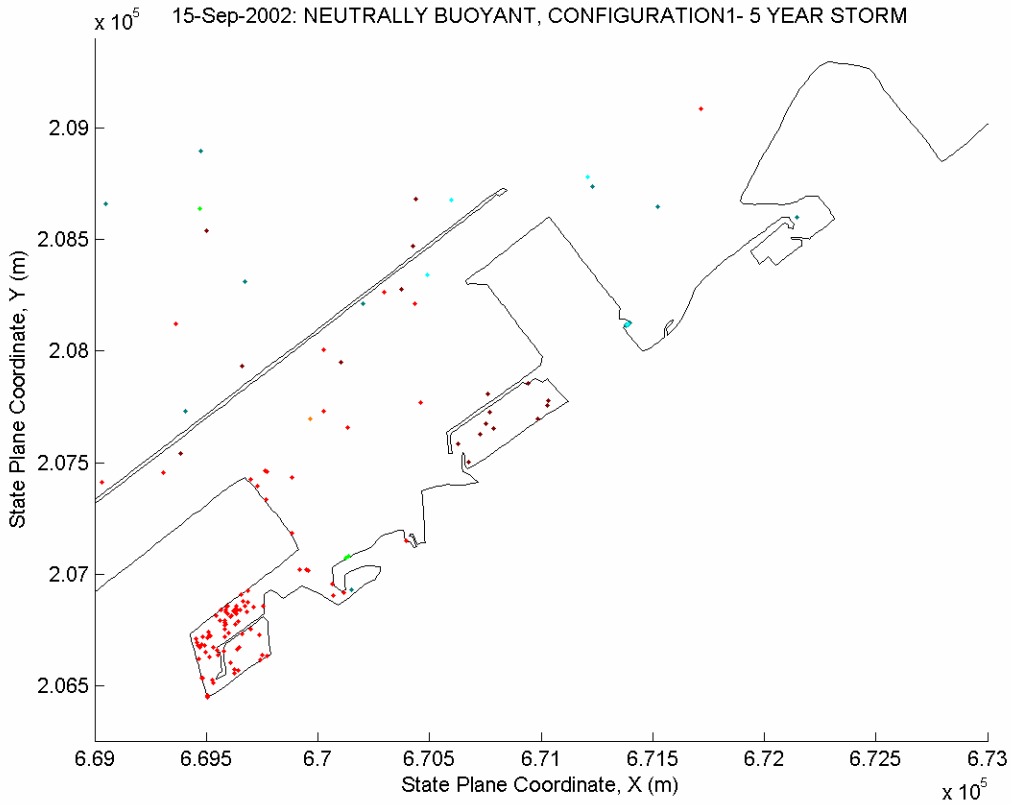
15-Sep-2002: NEUTRALLY BUOYANT, CONFIGURATION1- 5 YEAR STORM
x 10^5
2.09
2.085
2.08
2.075
2.07
2.065
State Plane Coordinate, Y (m)
6.69
6.695
6.7
6.705
6.71
6.715
6.72
6.725
6.73
State Plane Coordinate, X (m)
x 10^5

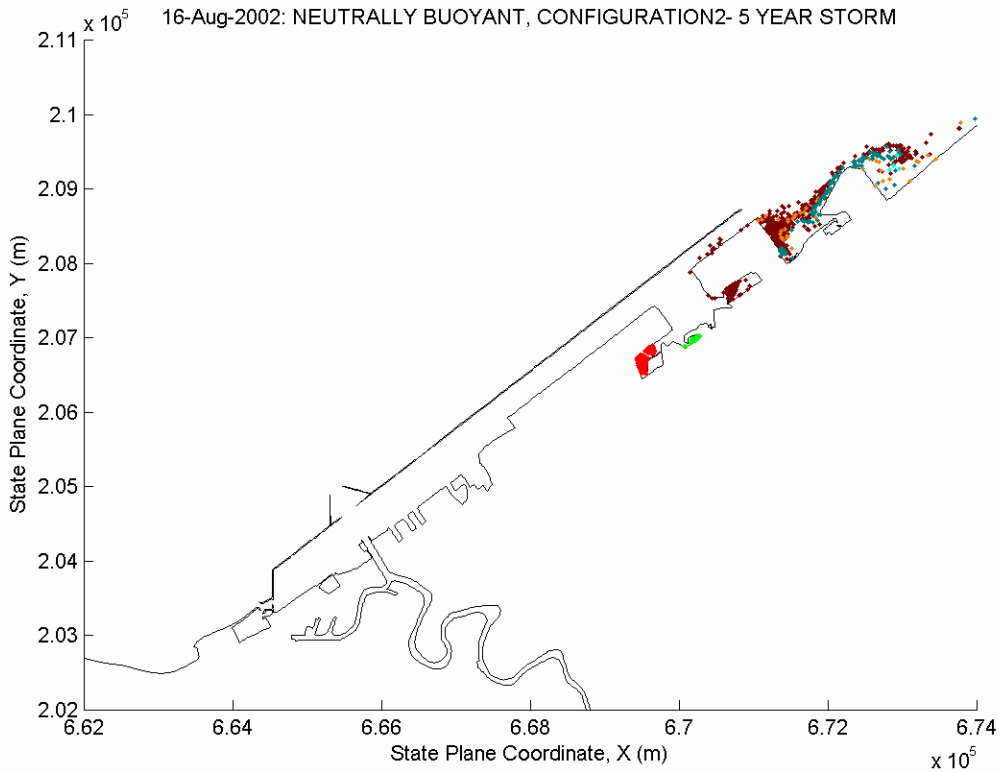
16-Aug-2002: NEUTRALLY BUOYANT, CONFIGURATION2- 5 YEAR STORM
x 10^5
2.11
2.1
2.09
2.08
2.07
2.06
2.05
2.04
2.03
2.02
State Plane Coordinate, Y (m)
6.62
6.64
6.66
6.68
6.7
6.72
6.74
State Plane Coordinate, X (m)
x 10^5

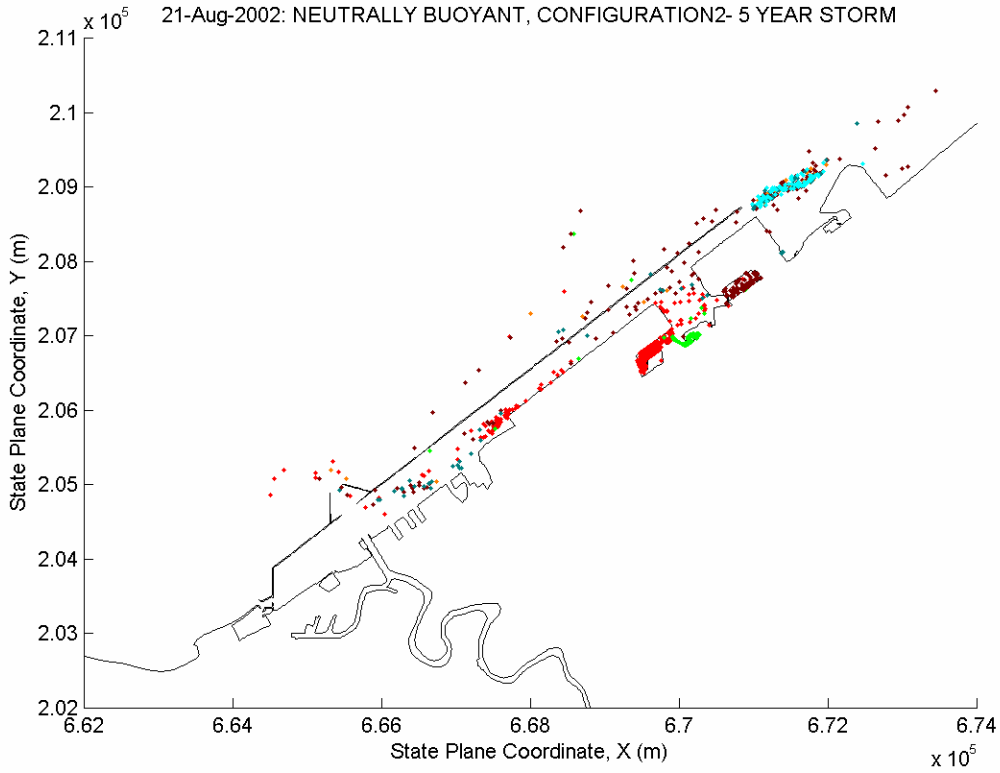
21-Aug-2002: NEUTRALLY BUOYANT, CONFIGURATION2- 5 YEAR STORM
x 10^5
2.11
2.1
2.09
2.08
2.07
2.06
2.05
2.04
2.03
2.02
State Plane Coordinate, Y (m)
6.62
6.64
6.66
6.68
6.7
6.72
6.74
State Plane Coordinate, X (m)
x 10^5

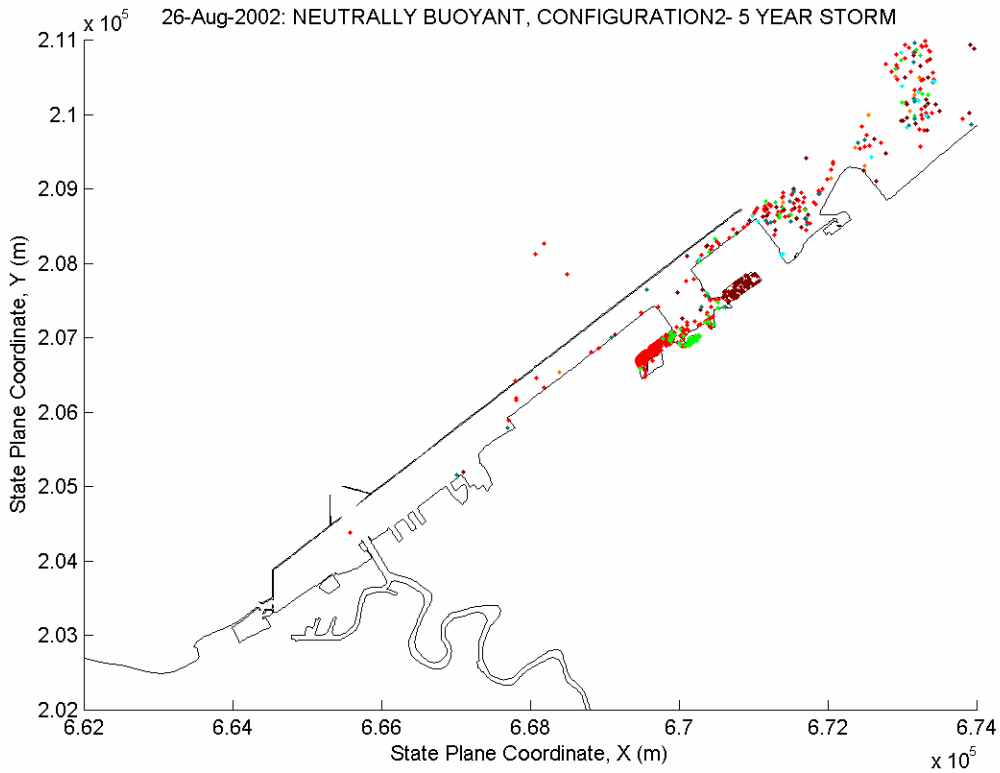
26-Aug-2002: NEUTRALLY BUOYANT, CONFIGURATION2- 5 YEAR STORM
x 10^5
2.11
2.1
2.09
2.08
2.07
2.06
2.05
2.04
2.03
2.02
State Plane Coordinate, Y (m)
6.62
6.64
6.66
6.68
6.7
6.72
6.74
State Plane Coordinate, X (m)
x 10^5

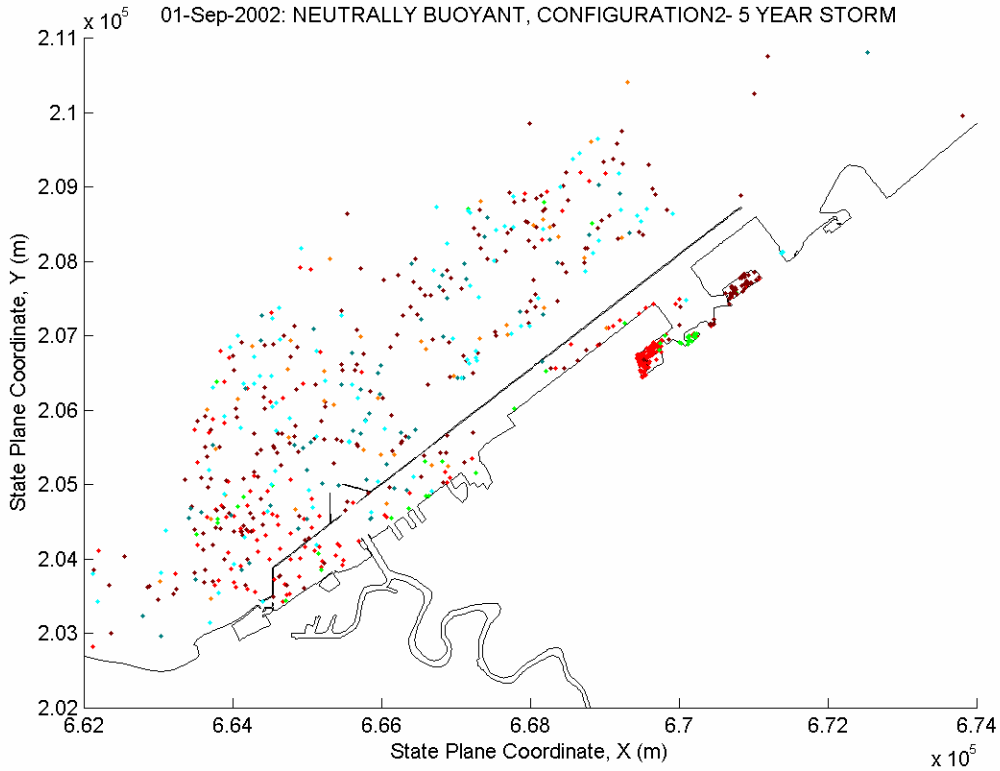
01-Sep-2002: NEUTRALLY BUOYANT, CONFIGURATION2- 5 YEAR STORM
x 10^5
2.11
2.1
2.09
2.08
2.07
2.06
2.05
2.04
2.03
2.02
State Plane Coordinate, Y (m)
6.62
6.64
6.66
6.68
6.7
6.72
6.74
State Plane Coordinate, X (m)
x 10^5

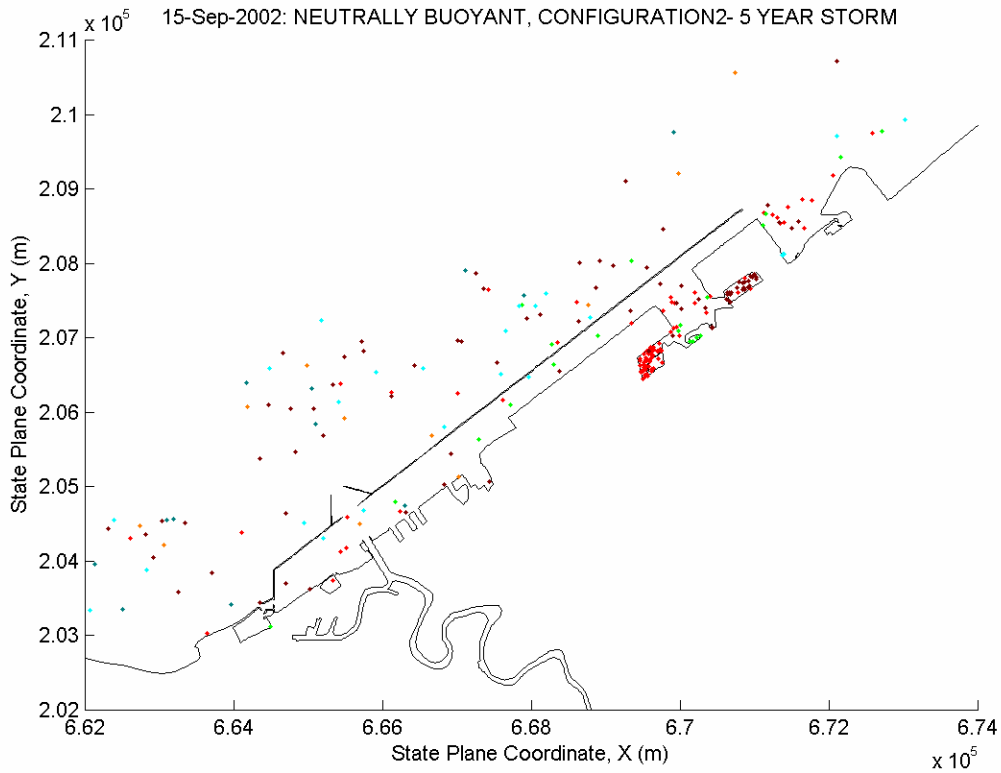
15-Sep-2002: NEUTRALLY BUOYANT, CONFIGURATION2- 5 YEAR STORM
x 10^5
2.11
2.1
2.09
2.08
2.07
2.06
2.05
2.04
2.03
2.02
State Plane Coordinate, Y (m)
6.62
6.64
6.66
6.68
6.7
6.72
6.74
State Plane Coordinate, X (m)
x 10^5

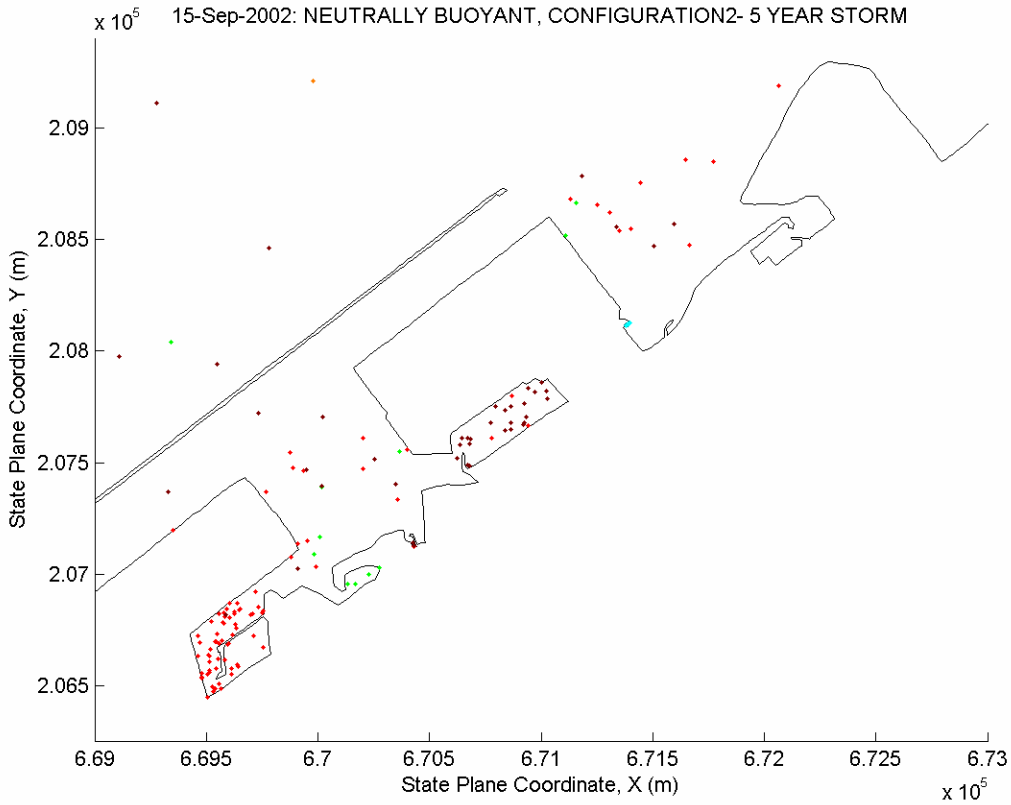
15-Sep-2002: NEUTRALLY BUOYANT, CONFIGURATION2- 5 YEAR STORM
x 10^5
2.09
2.085
2.08
2.075
2.07
2.065
State Plane Coordinate, Y (m)
6.69
6.695
6.7
6.705
6.71
6.715
6.72
6.725
6.73
State Plane Coordinate, X (m)
x 10^5

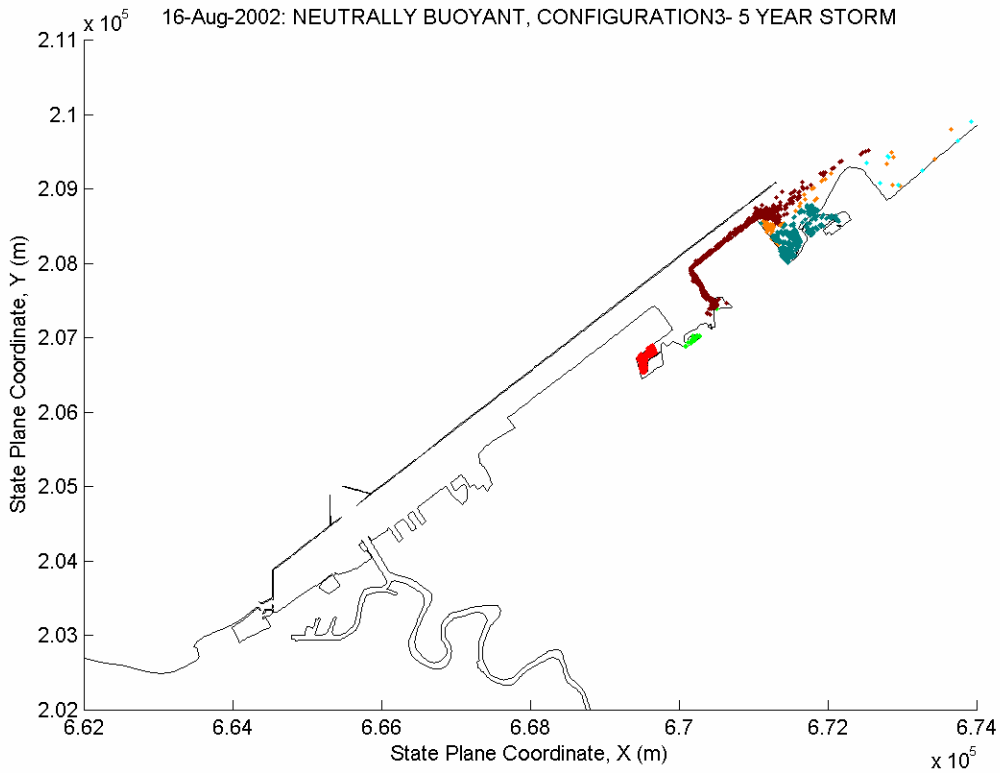
16-Aug-2002: NEUTRALLY BUOYANT, CONFIGURATION3- 5 YEAR STORM
x 10^5
2.11
2.1
2.09
2.08
2.07
2.06
2.05
2.04
2.03
2.02
State Plane Coordinate, Y (m)
6.62
6.64
6.66
6.68
6.7
6.72
6.74
State Plane Coordinate, X (m)
x 10^5

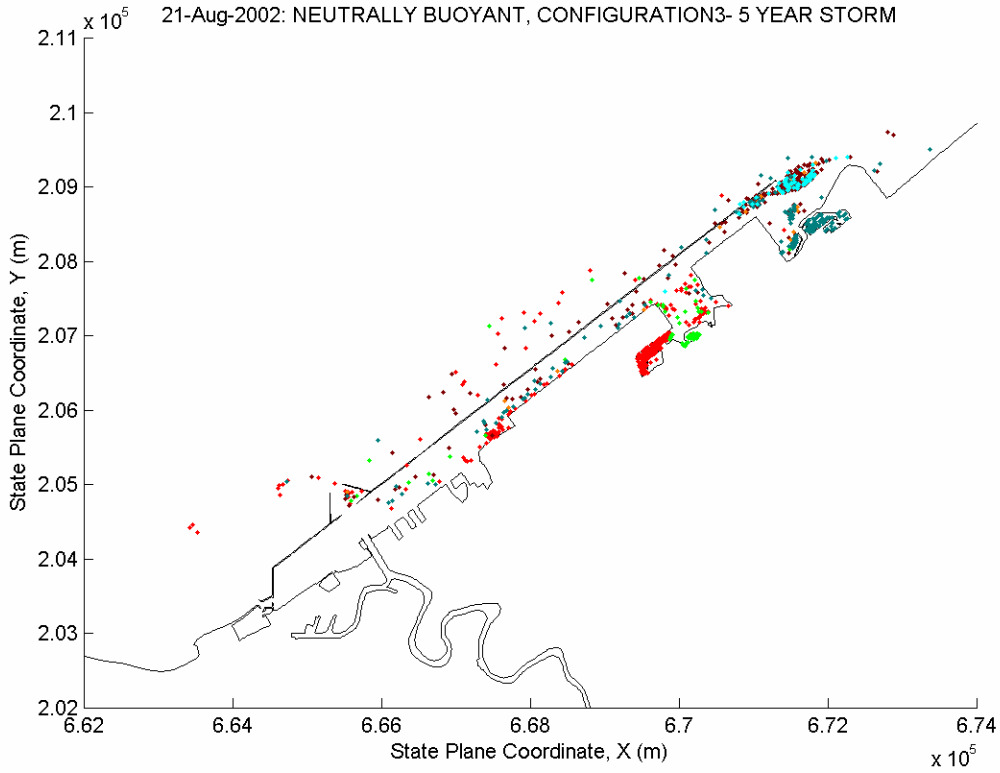
21-Aug-2002: NEUTRALLY BUOYANT, CONFIGURATION3- 5 YEAR STORM
x 10^5
2.11
2.1
2.09
2.08
2.07
2.06
2.05
2.04
2.03
2.02
State Plane Coordinate, Y (m)
6.62
6.64
6.66
6.68
6.7
6.72
6.74
State Plane Coordinate, X (m)
x 10^5

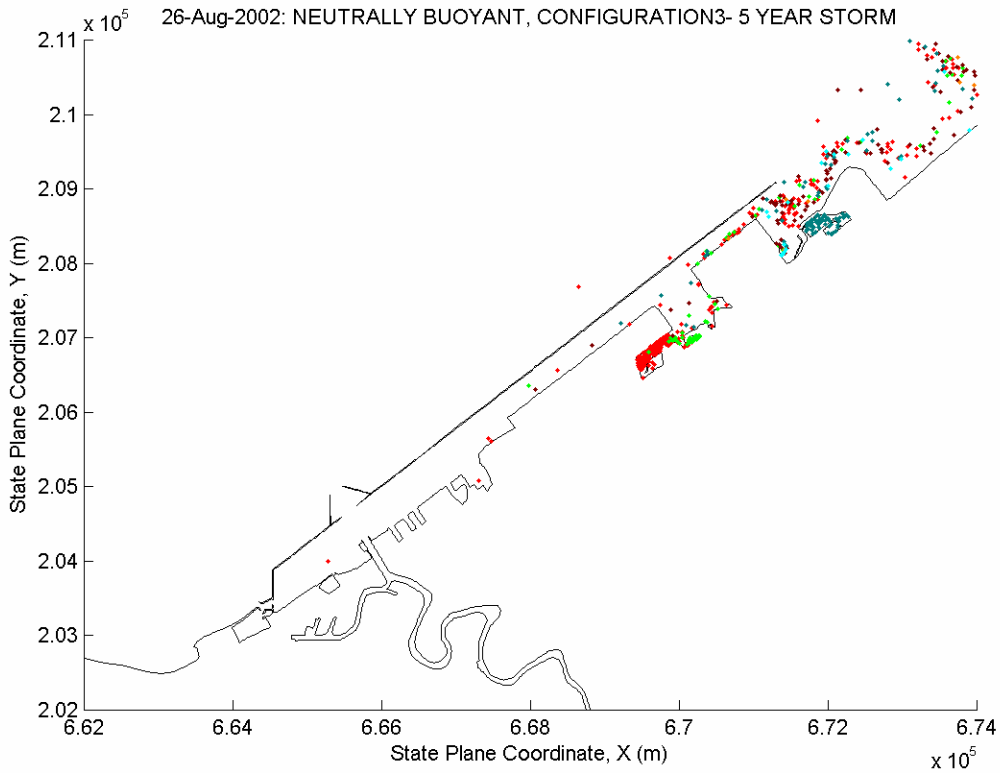
26-Aug-2002: NEUTRALLY BUOYANT, CONFIGURATION3- 5 YEAR STORM
x 10^5
2.11
2.1
2.09
2.08
2.07
2.06
2.05
2.04
2.03
2.02
State Plane Coordinate, Y (m)
6.62
6.64
6.66
6.68
6.7
6.72
6.74
State Plane Coordinate, X (m)
x 10^5

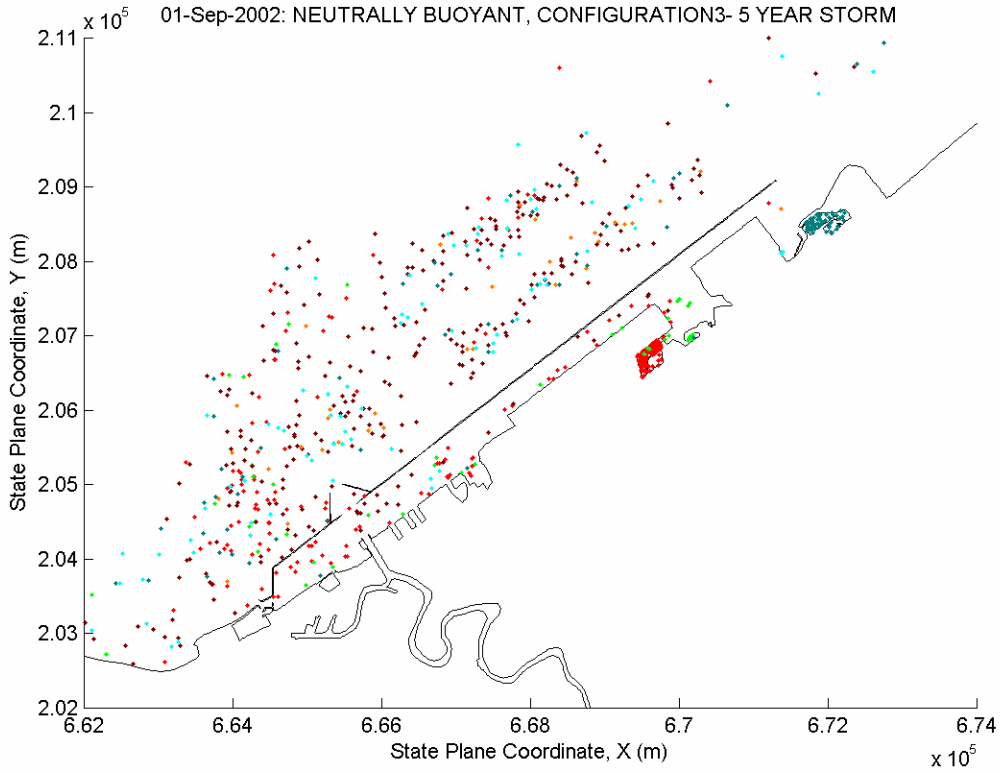
01-Sep-2002: NEUTRALLY BUOYANT, CONFIGURATION3- 5 YEAR STORM
x 10^5
2.11
2.1
2.09
2.08
2.07
2.06
2.05
2.04
2.03
2.02
State Plane Coordinate, Y (m)
6.62
6.64
6.66
6.68
6.7
6.72
6.74
State Plane Coordinate, X (m)
x 10^5

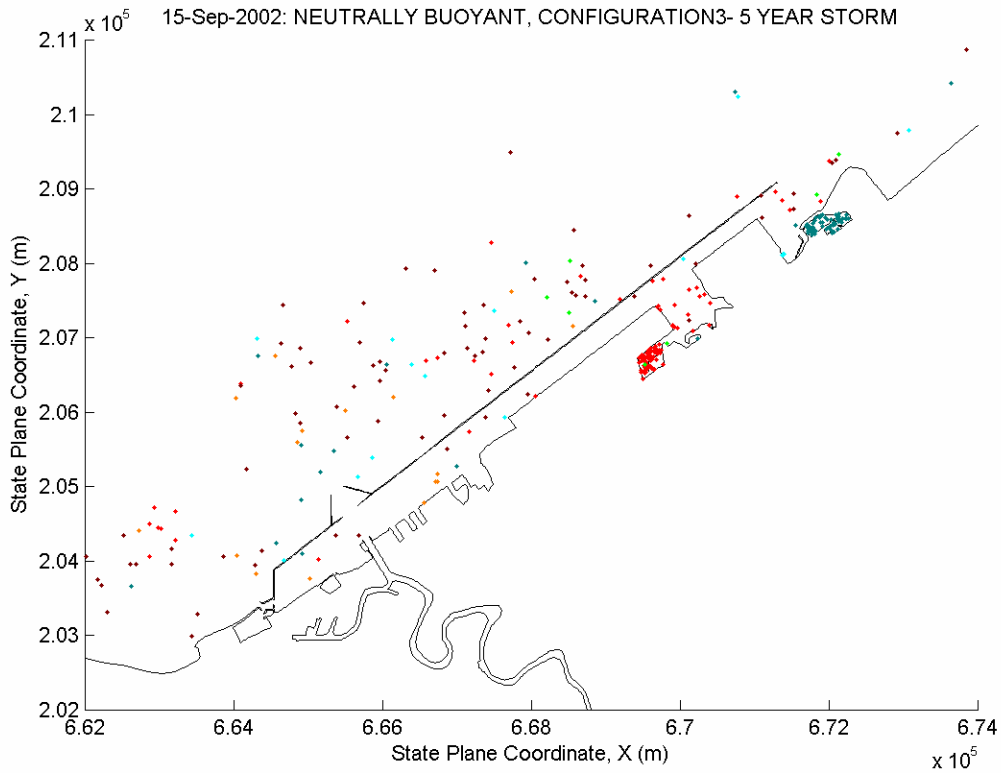
15-Sep-2002: NEUTRALLY BUOYANT, CONFIGURATION3- 5 YEAR STORM
x 10^5
2.11
2.1
2.09
2.08
2.07
2.06
2.05
2.04
2.03
2.02
State Plane Coordinate, Y (m)
6.62
6.64
6.66
6.68
6.7
6.72
6.74
State Plane Coordinate, X (m)
x 10^5

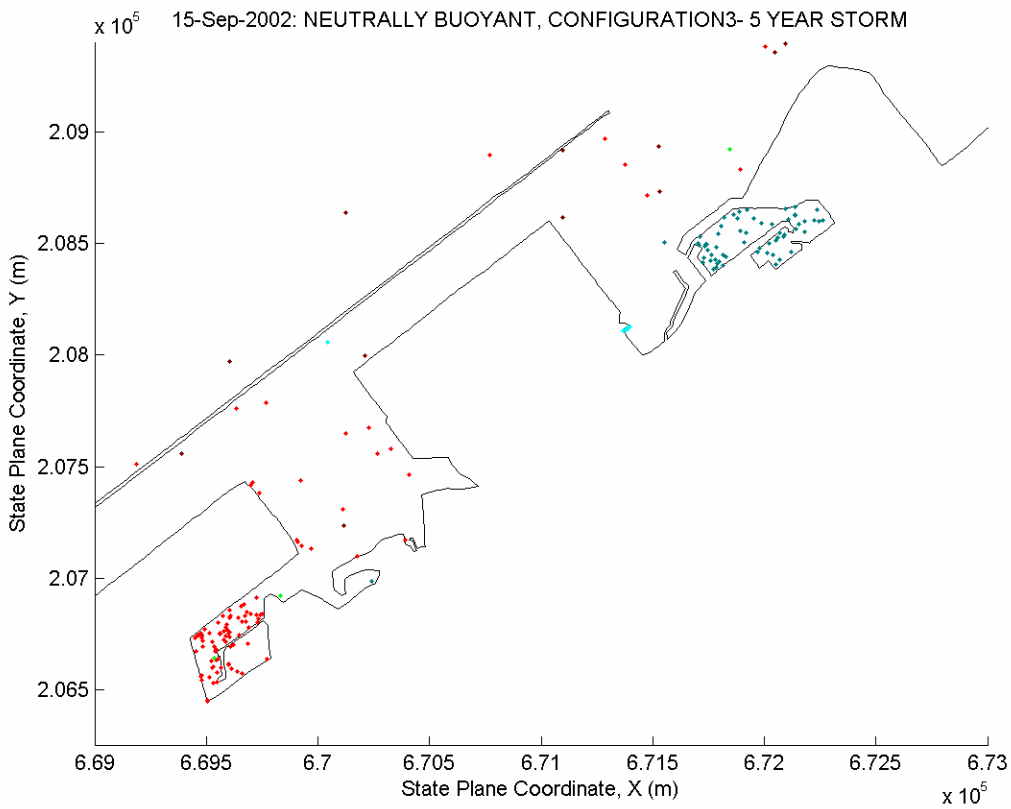
15-Sep-2002: NEUTRALLY BUOYANT, CONFIGURATION3- 5 YEAR STORM
x 10^5
2.09
2.085
2.08
2.075
2.07
2.065
State Plane Coordinate, Y (m)
6.69
6.695
6.7
6.705
6.71
6.715
6.72
6.725
6.73
State Plane Coordinate, X (m)
x 10^5

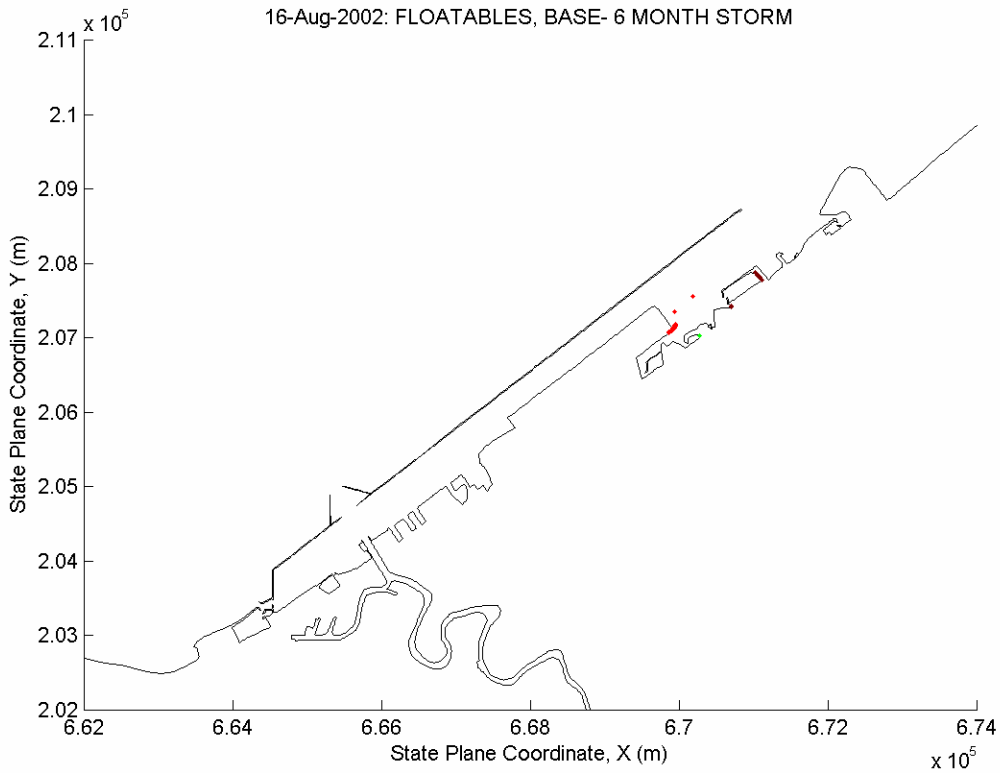
16-Aug-2002: FLOATABLES, BASE- 6 MONTH STORM
x 10^5
2.11
2.1
2.09
2.08
2.07
2.06
2.05
2.04
2.03
2.02
State Plane Coordinate, Y (m)
6.62
6.64
6.66
6.68
6.7
6.72
6.74
State Plane Coordinate, X (m)
x 10^5

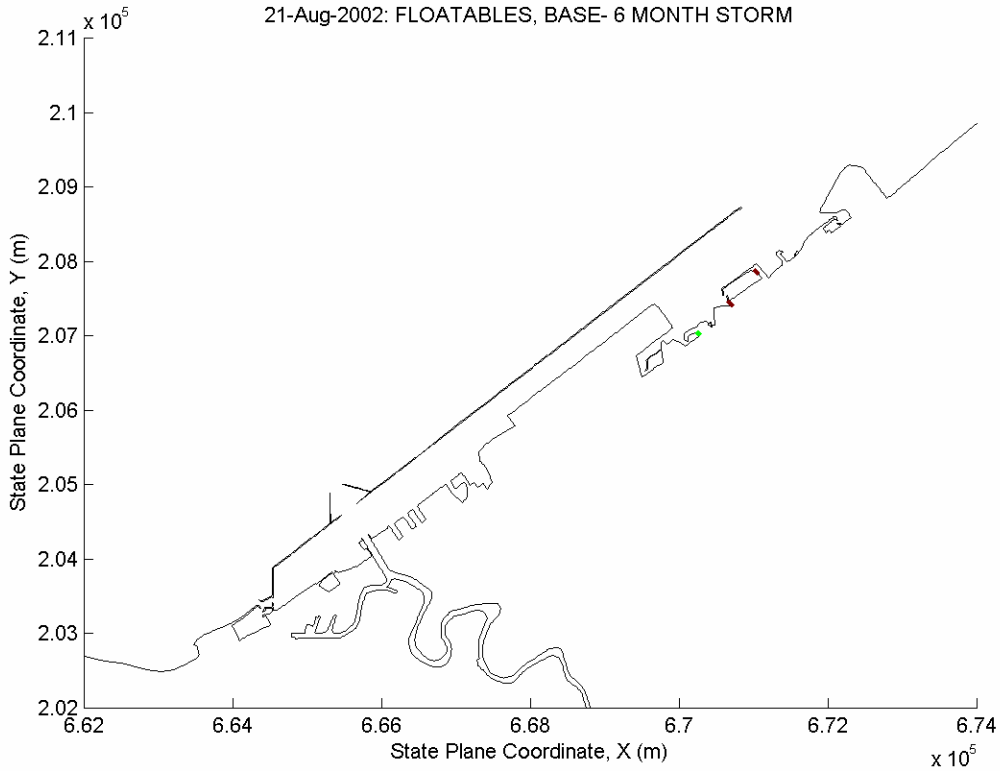
21-Aug-2002: FLOATABLES, BASE- 6 MONTH STORM
x 10^5
2.11
2.1
2.09
2.08
2.07
2.06
2.05
2.04
2.03
2.02
State Plane Coordinate, Y (m)
6.62
6.64
6.66
6.68
6.7
6.72
6.74
State Plane Coordinate, X (m)
x 10^5

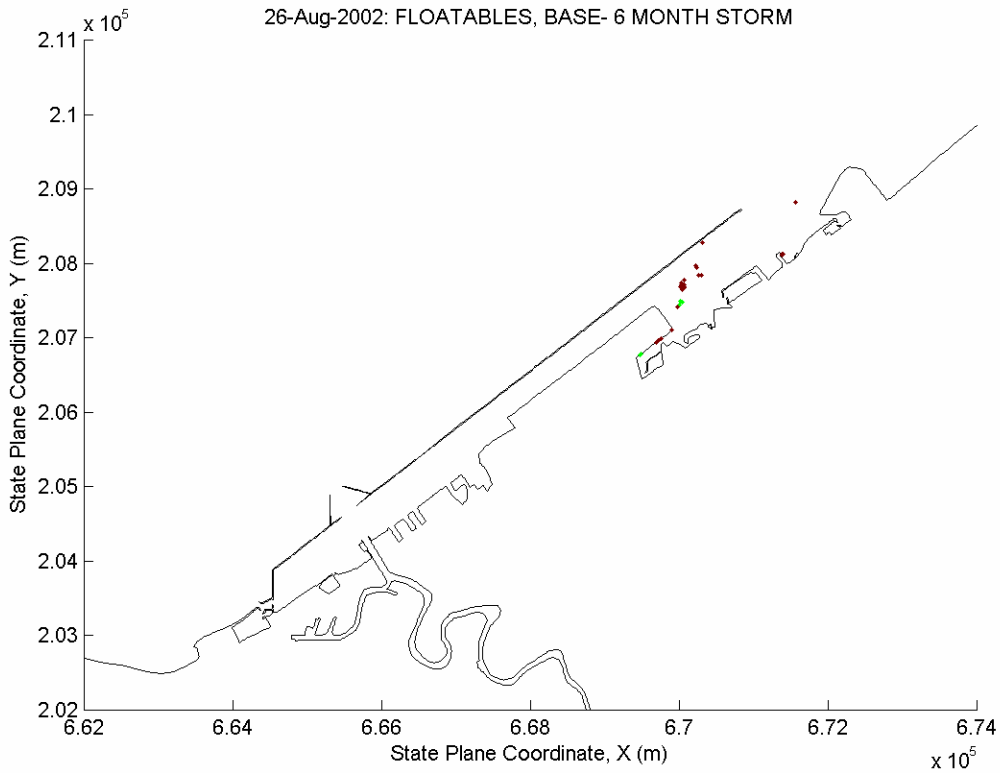
26-Aug-2002: FLOATABLES, BASE- 6 MONTH STORM
x 10^5
2.11
2.1
2.09
2.08
2.07
2.06
2.05
2.04
2.03
2.02
State Plane Coordinate, Y (m)
6.62
6.64
6.66
6.68
6.7
6.72
6.74
State Plane Coordinate, X (m)
x 10^5

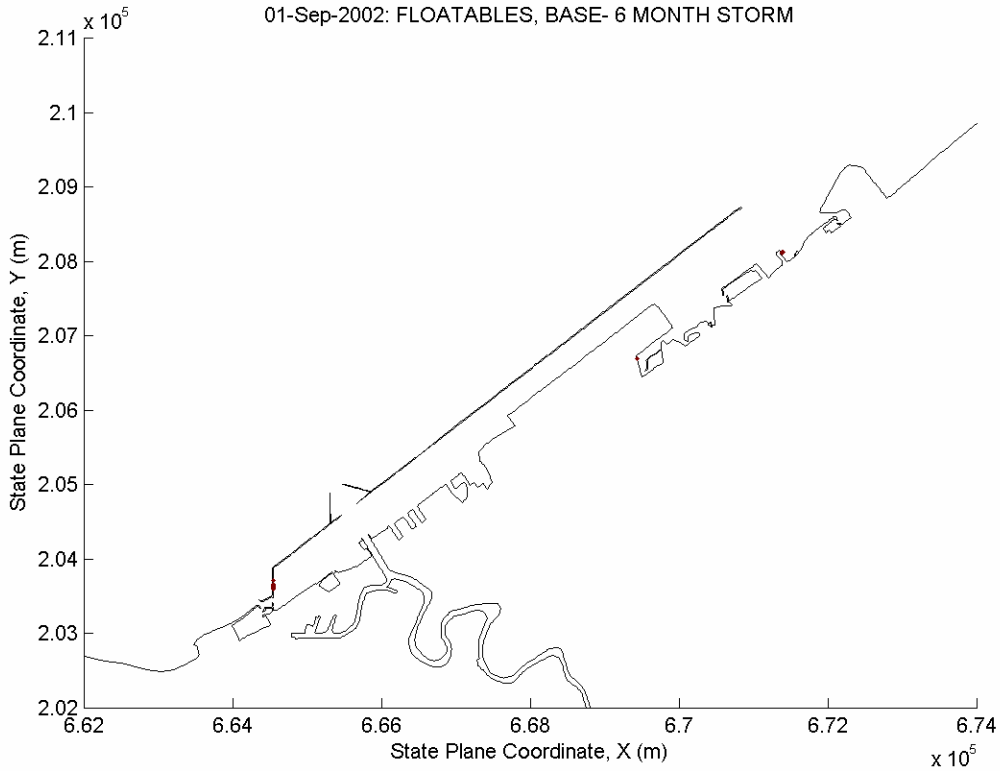
01-Sep-2002: FLOATABLES, BASE- 6 MONTH STORM
x 10^5
2.11
2.1
2.09
2.08
2.07
2.06
2.05
2.04
2.03
2.02
State Plane Coordinate, Y (m)
6.62
6.64
6.66
6.68
6.7
6.72
6.74
State Plane Coordinate, X (m)
x 10^5

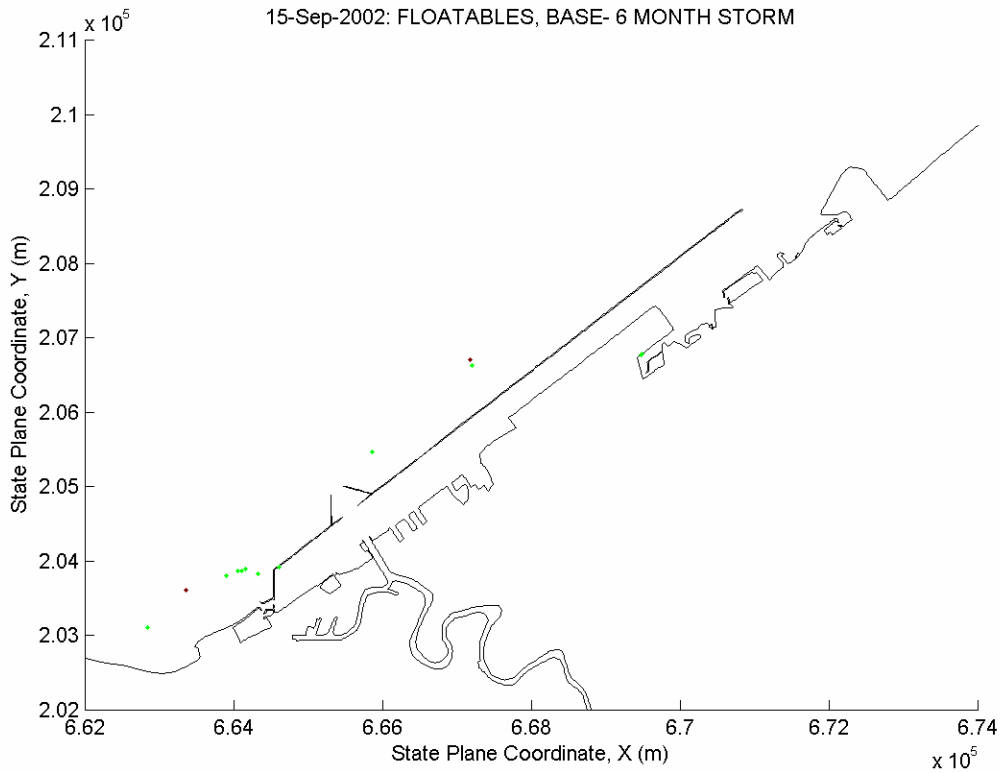
15-Sep-2002: FLOATABLES, BASE- 6 MONTH STORM
x 10^5
2.11
2.1
2.09
2.08
2.07
2.06
2.05
2.04
2.03
2.02
State Plane Coordinate, Y (m)
6.62
6.64
6.66
6.68
6.7
6.72
6.74
State Plane Coordinate, X (m)
x 10^5

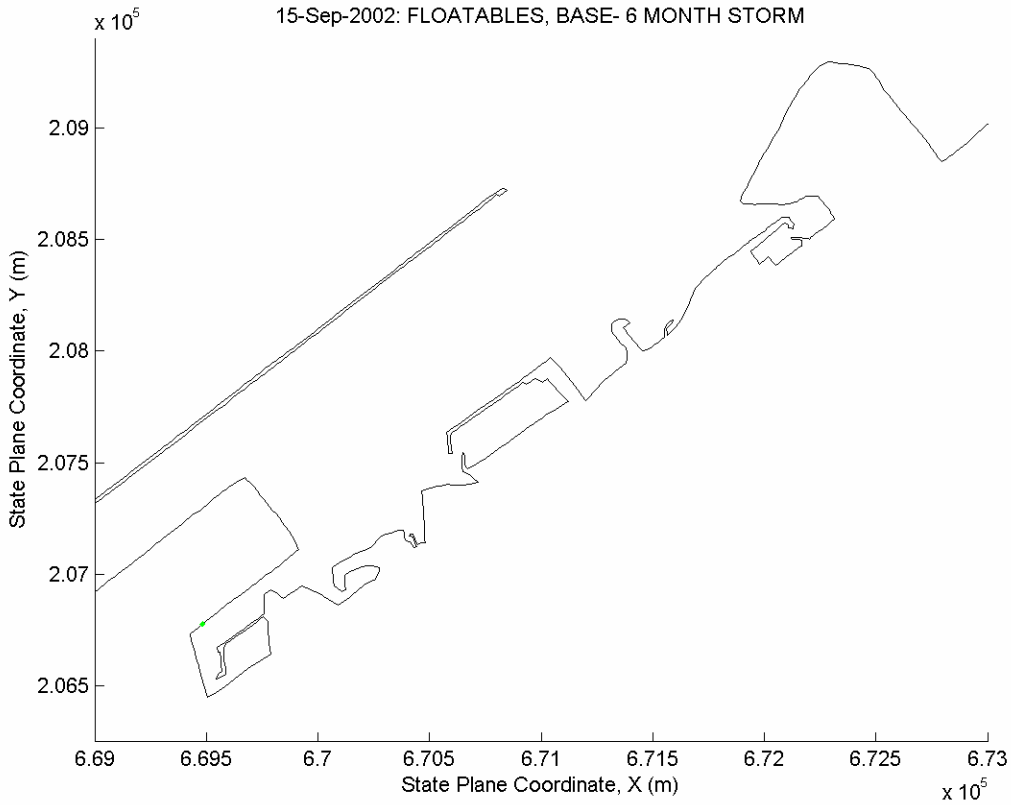
15-Sep-2002: FLOATABLES, BASE- 6 MONTH STORM
x 10^5
2.09
2.085
2.08
2.075
2.07
2.065
State Plane Coordinate, Y (m)
6.69
6.695
6.7
6.705
6.71
6.715
6.72
6.725
6.73
State Plane Coordinate, X (m)
x 10^5

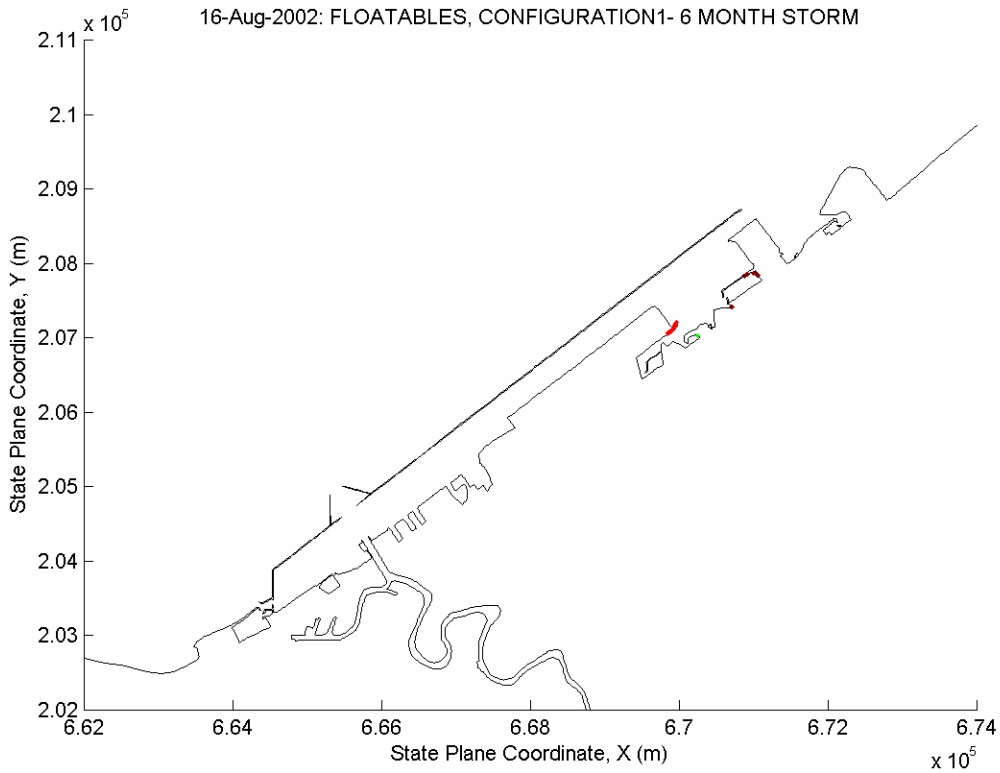
16-Aug-2002: FLOATABLES, CONFIGURATION1- 6 MONTH STORM
x 10^5
2.11
2.1
2.09
2.08
2.07
2.06
2.05
2.04
2.03
2.02
State Plane Coordinate, Y (m)
6.62
6.64
6.66
6.68
6.7
6.72
6.74
State Plane Coordinate, X (m)
x 10^5

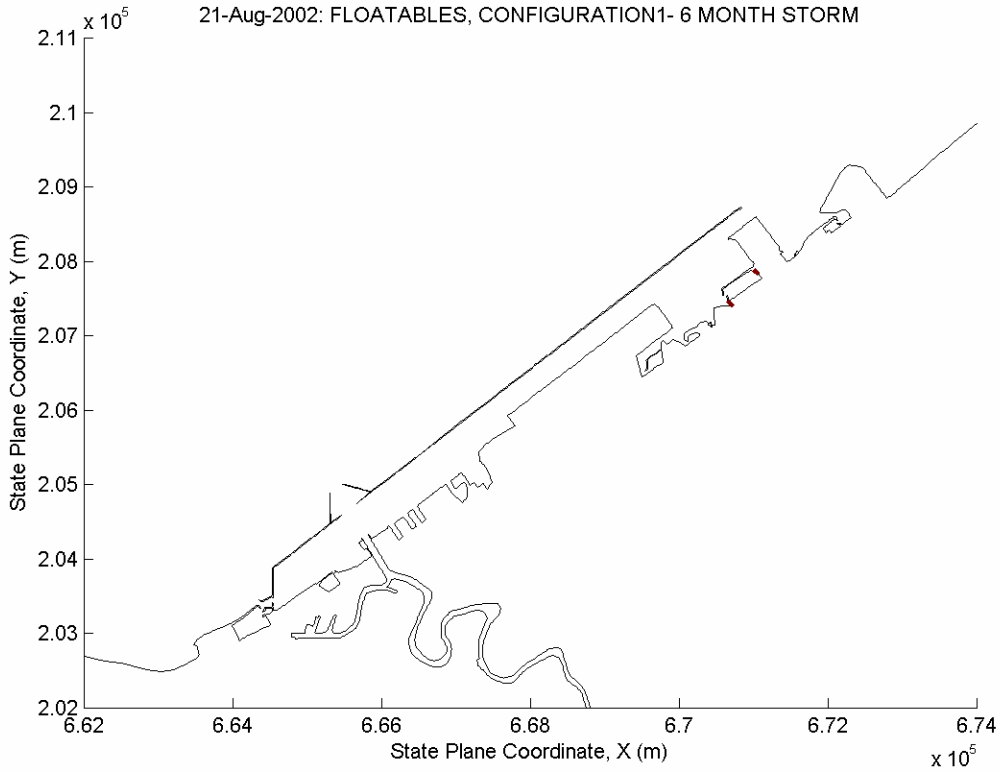
21-Aug-2002: FLOATABLES, CONFIGURATION1- 6 MONTH STORM
x 10^5
2.11
2.1
2.09
2.08
2.07
2.06
2.05
2.04
2.03
2.02
State Plane Coordinate, Y (m)
6.62
6.64
6.66
6.68
6.7
6.72
6.74
State Plane Coordinate, X (m)
x 10^5

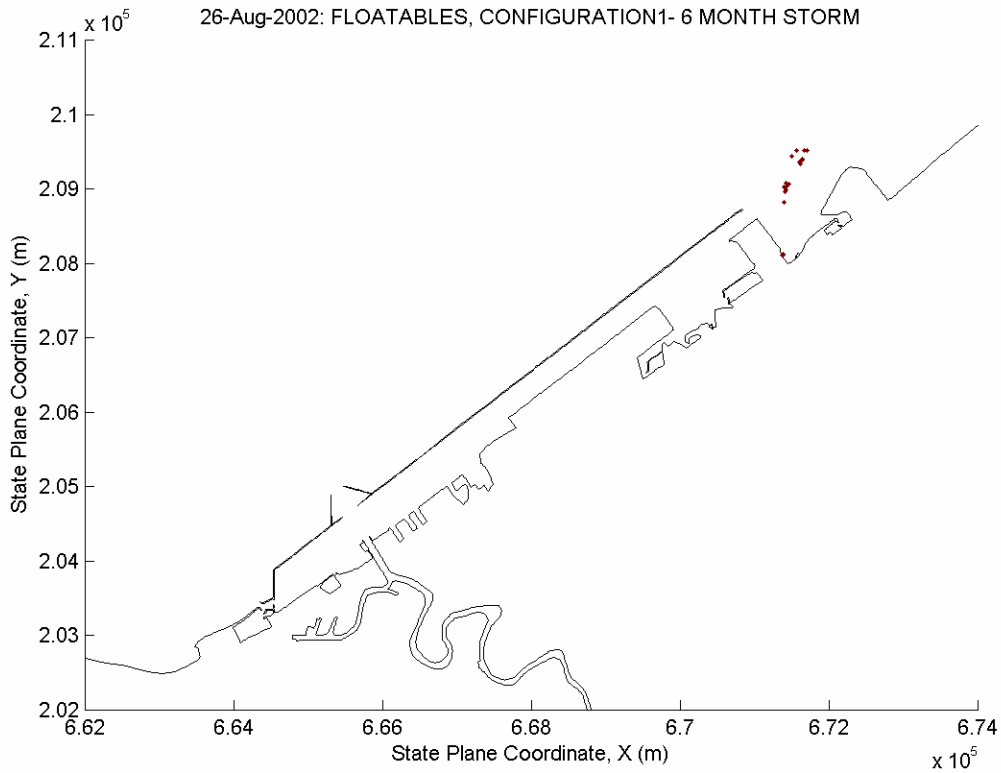
26-Aug-2002: FLOATABLES, CONFIGURATION1- 6 MONTH STORM
x 10^5
2.11
2.1
2.09
2.08
2.07
2.06
2.05
2.04
2.03
2.02
State Plane Coordinate, Y (m)
6.62
6.64
6.66
6.68
6.7
6.72
6.74
State Plane Coordinate, X (m)
x 10^5

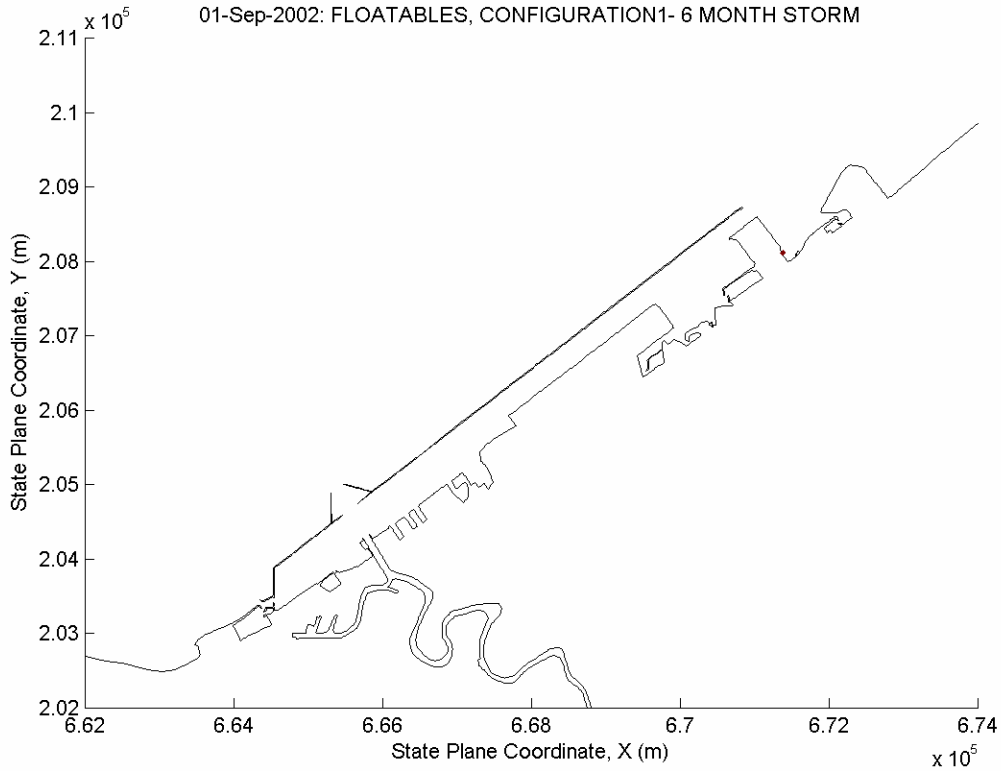
01-Sep-2002: FLOATABLES, CONFIGURATION1- 6 MONTH STORM
x 10^5
2.11
2.1
2.09
2.08
2.07
2.06
2.05
2.04
2.03
2.02
State Plane Coordinate, Y (m)
6.62
6.64
6.66
6.68
6.7
6.72
6.74
State Plane Coordinate, X (m)
x 10^5

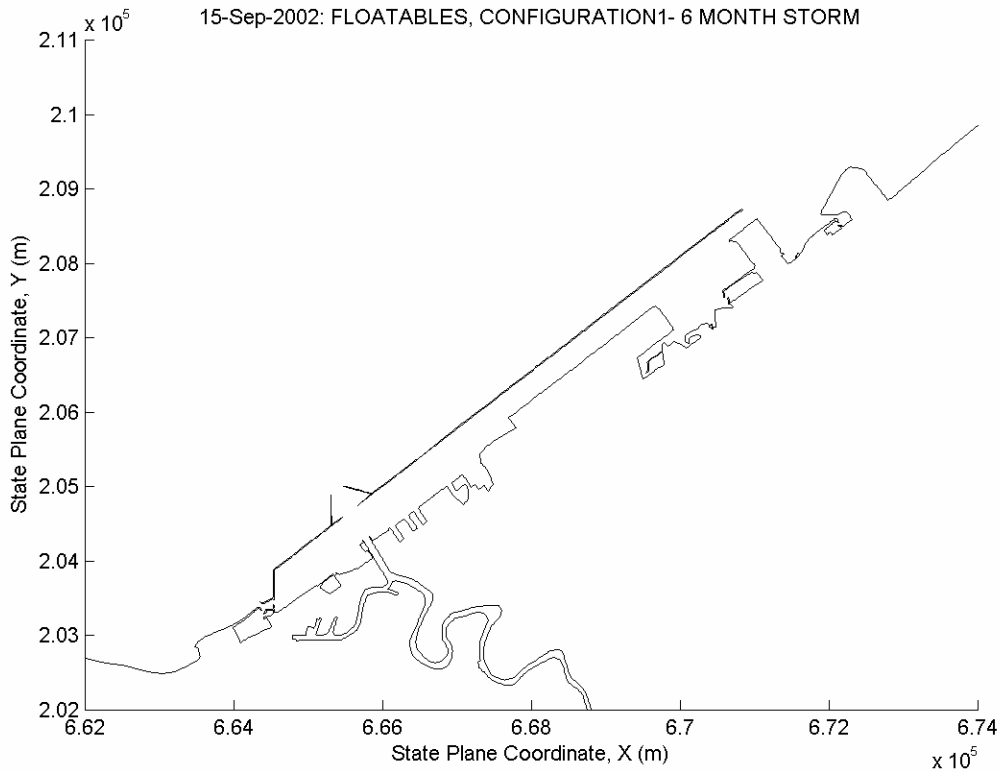
15-Sep-2002: FLOATABLES, CONFIGURATION1- 6 MONTH STORM
x 10^5
2.11
2.1
2.09
2.08
2.07
2.06
2.05
2.04
2.03
2.02
State Plane Coordinate, Y (m)
6.62
6.64
6.66
6.68
6.7
6.72
6.74
State Plane Coordinate, X (m)
x 10^5

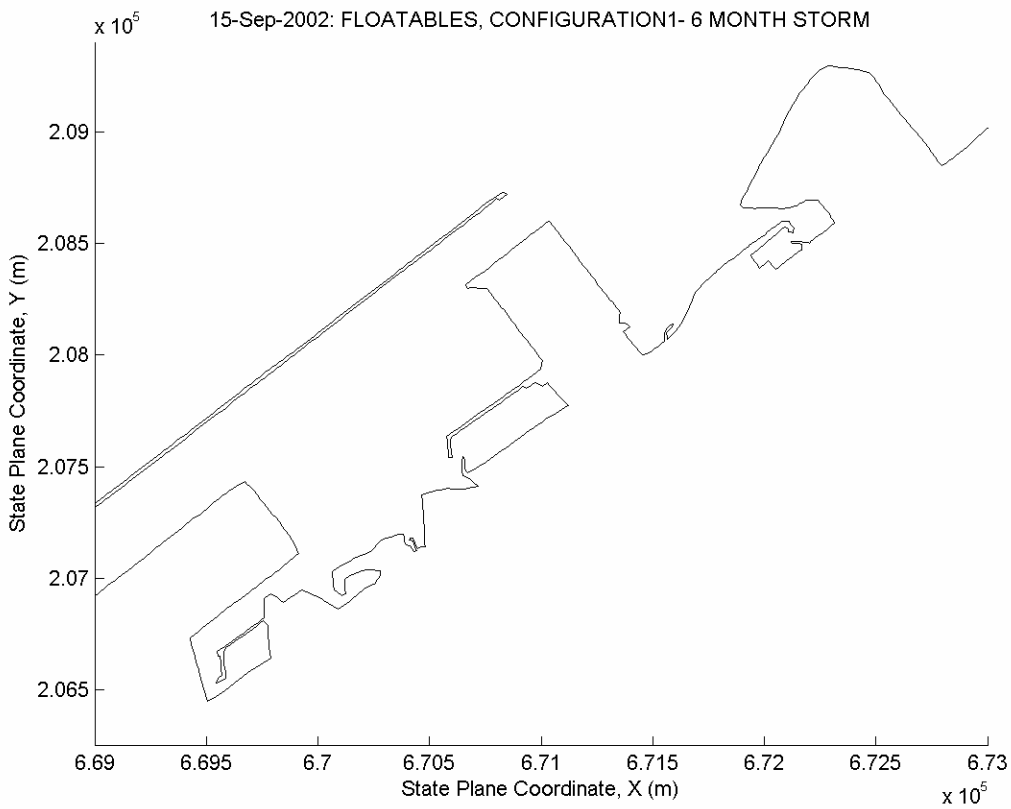
15-Sep-2002: FLOATABLES, CONFIGURATION1- 6 MONTH STORM
x 10^5
2.09
2.085
2.08
2.075
2.07
2.065
State Plane Coordinate, Y (m)
6.69
6.695
6.7
6.705
6.71
6.715
6.72
6.725
6.73
State Plane Coordinate, X (m)
x 10^5

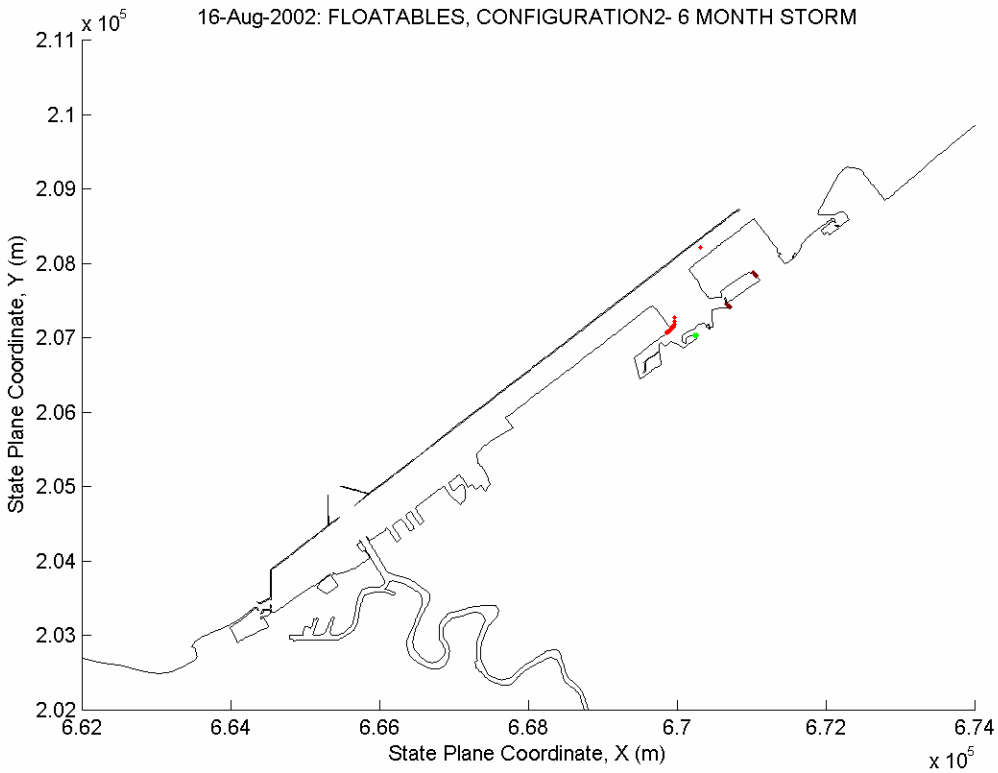
16-Aug-2002: FLOATABLES, CONFIGURATION2- 6 MONTH STORM
x 10^5
2.11
2.1
2.09
2.08
2.07
2.06
2.05
2.04
2.03
2.02
State Plane Coordinate, Y (m)
6.62
6.64
6.66
6.68
6.7
6.72
6.74
State Plane Coordinate, X (m)
x 10^5

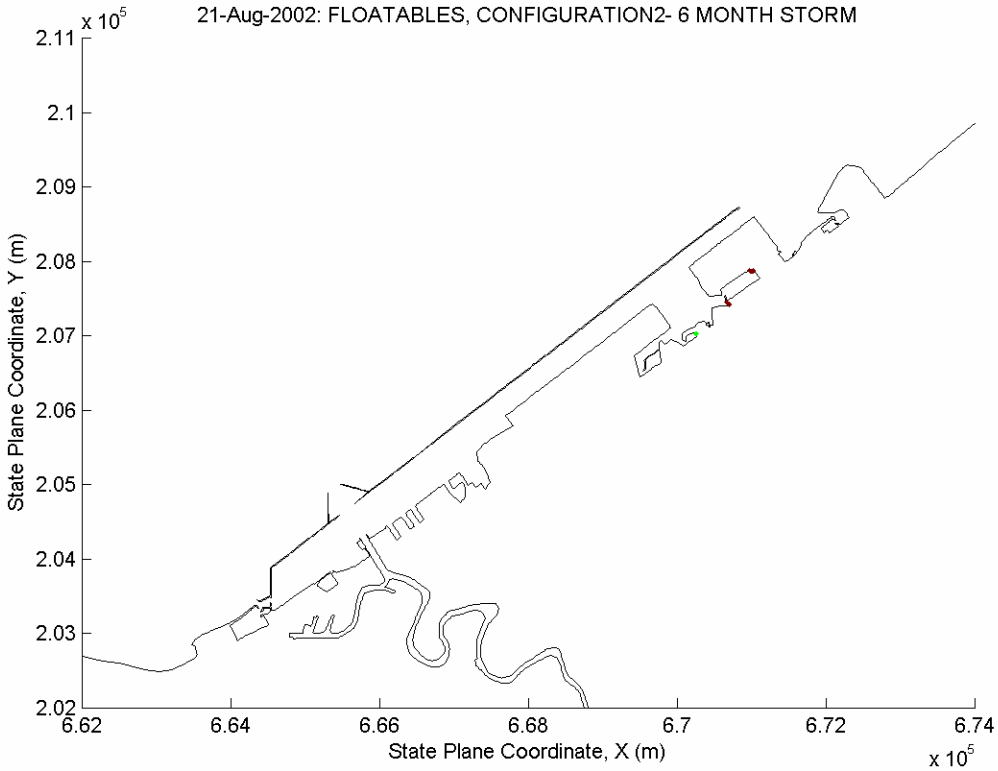
21-Aug-2002: FLOATABLES, CONFIGURATION2- 6 MONTH STORM
x 10^5
2.11
2.1
2.09
2.08
2.07
2.06
2.05
2.04
2.03
2.02
State Plane Coordinate, Y (m)
6.62
6.64
6.66
6.68
6.7
6.72
6.74
State Plane Coordinate, X (m)
x 10^5

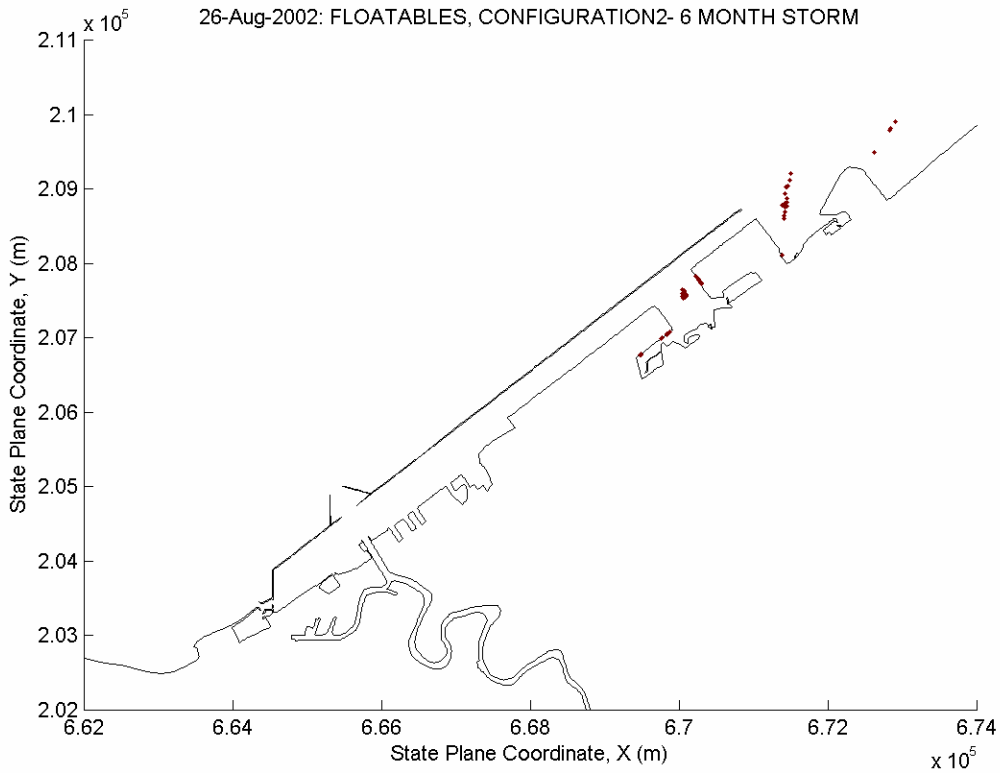
26-Aug-2002: FLOATABLES, CONFIGURATION2- 6 MONTH STORM
x 10^5
2.11
2.1
2.09
2.08
2.07
2.06
2.05
2.04
2.03
2.02
State Plane Coordinate, Y (m)
6.62
6.64
6.66
6.68
6.7
6.72
6.74
State Plane Coordinate, X (m)
x 10^5

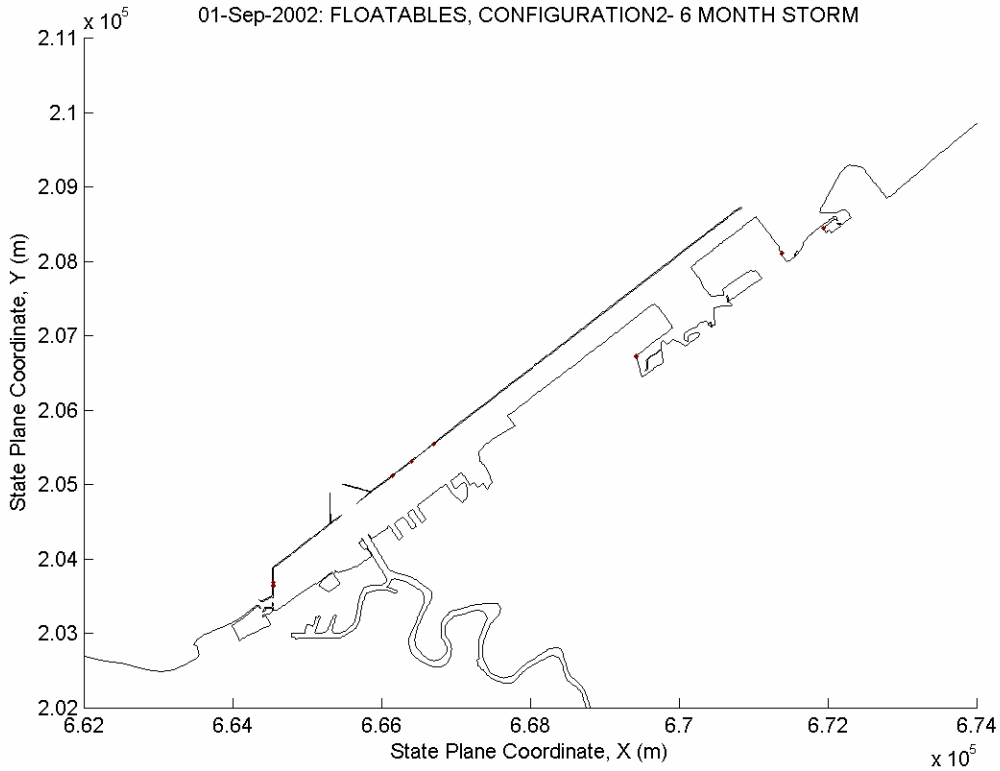
01-Sep-2002: FLOATABLES, CONFIGURATION2- 6 MONTH STORM
x 10^5
2.11
2.1
2.09
2.08
2.07
2.06
2.05
2.04
2.03
2.02
State Plane Coordinate, Y (m)
6.62
6.64
6.66
6.68
6.7
6.72
6.74
State Plane Coordinate, X (m)
x 10^5

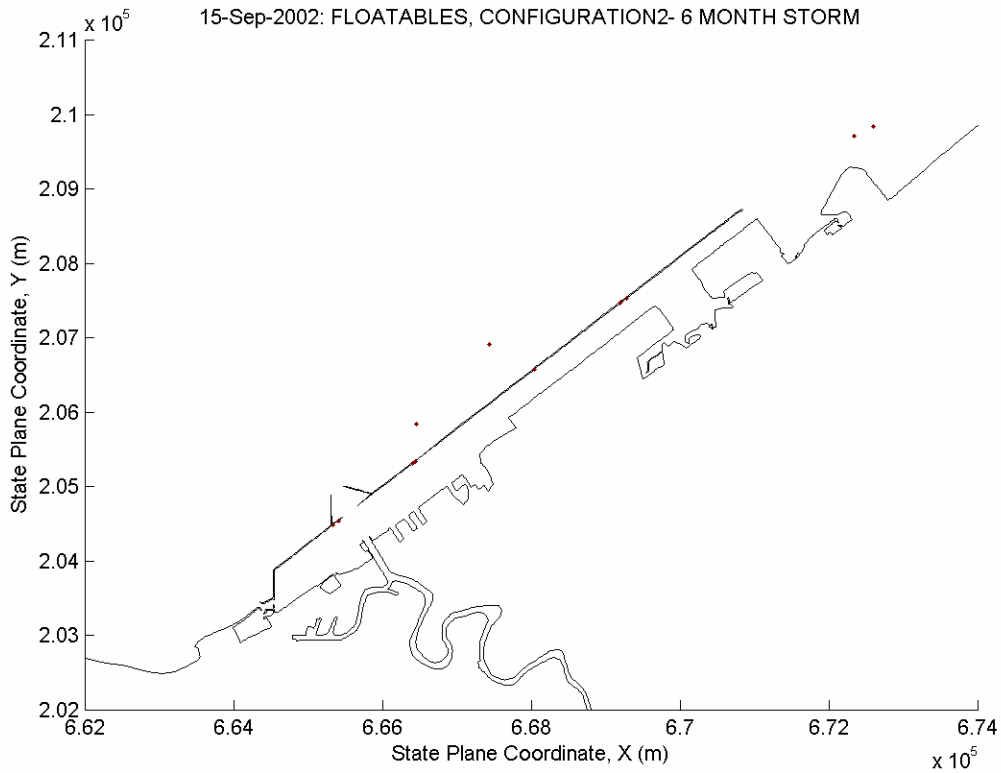
15-Sep-2002: FLOATABLES, CONFIGURATION2- 6 MONTH STORM
x 10^5
2.11
2.1
2.09
2.08
2.07
2.06
2.05
2.04
2.03
2.02
State Plane Coordinate, Y (m)
6.62
6.64
6.66
6.68
6.7
6.72
6.74
State Plane Coordinate, X (m)
x 10^5

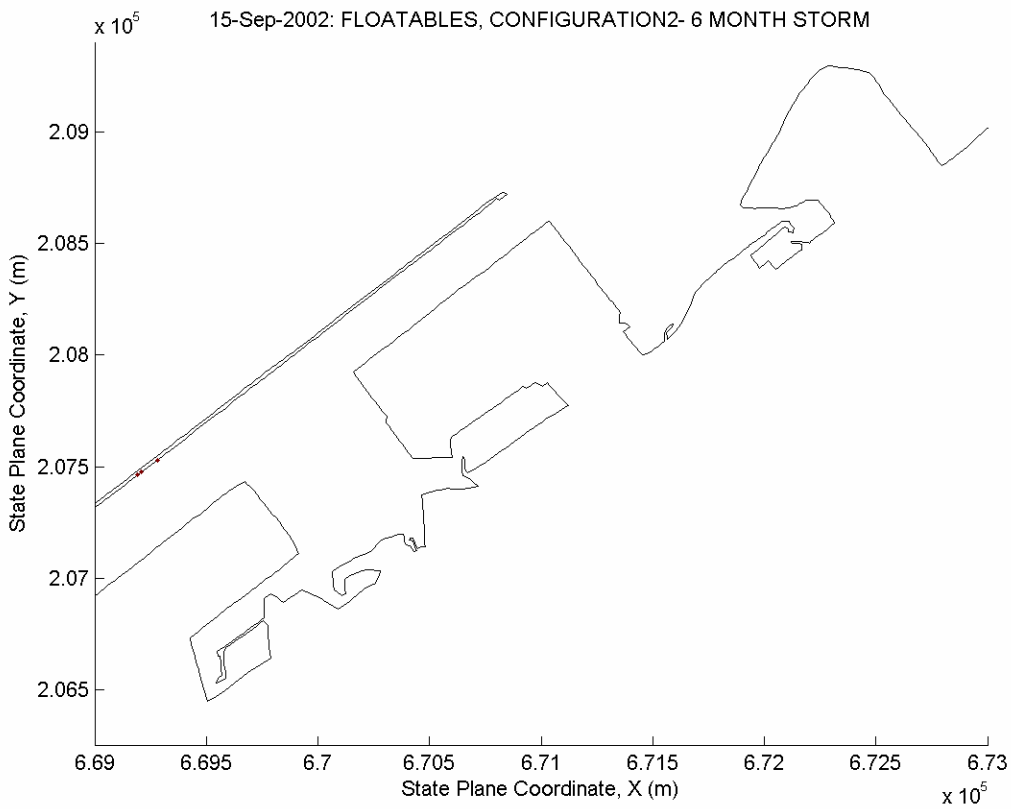
15-Sep-2002: FLOATABLES, CONFIGURATION2- 6 MONTH STORM
x 10^5
2.09
2.085
2.08
2.075
2.07
2.065
State Plane Coordinate, Y (m)
6.69
6.695
6.7
6.705
6.71
6.715
6.72
6.725
6.73
State Plane Coordinate, X (m)
x 10^5

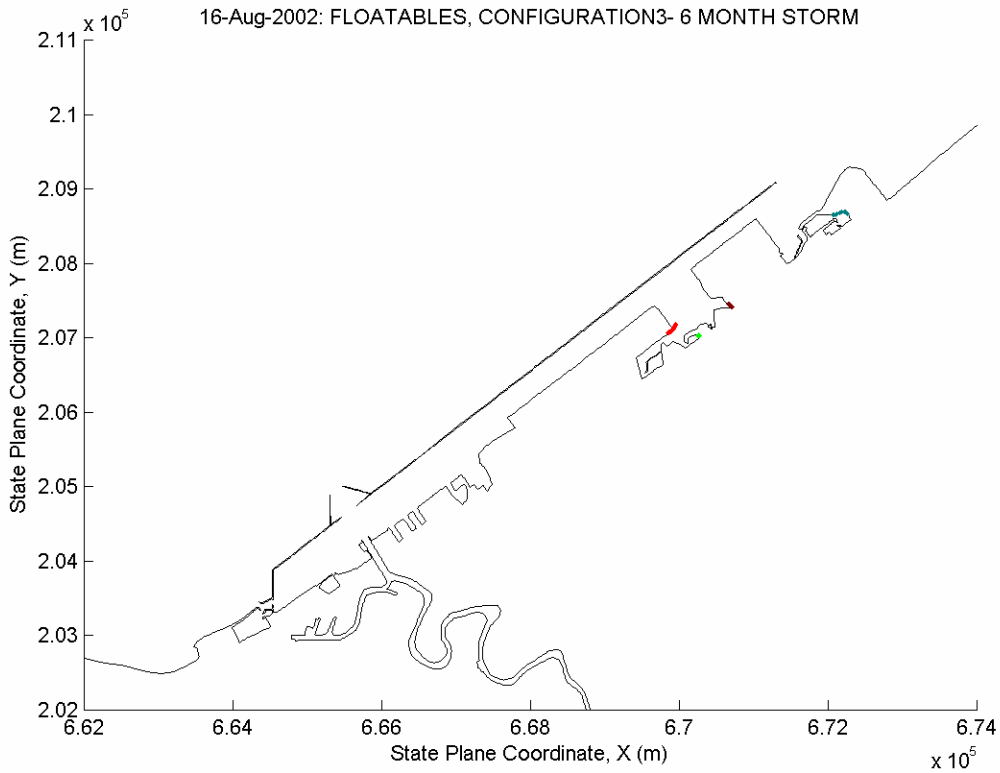
16-Aug-2002: FLOATABLES, CONFIGURATION3- 6 MONTH STORM
x 10^5
2.11
2.1
2.09
2.08
2.07
2.06
2.05
2.04
2.03
2.02
State Plane Coordinate, Y (m)
6.62
6.64
6.66
6.68
6.7
6.72
6.74
State Plane Coordinate, X (m)
x 10^5

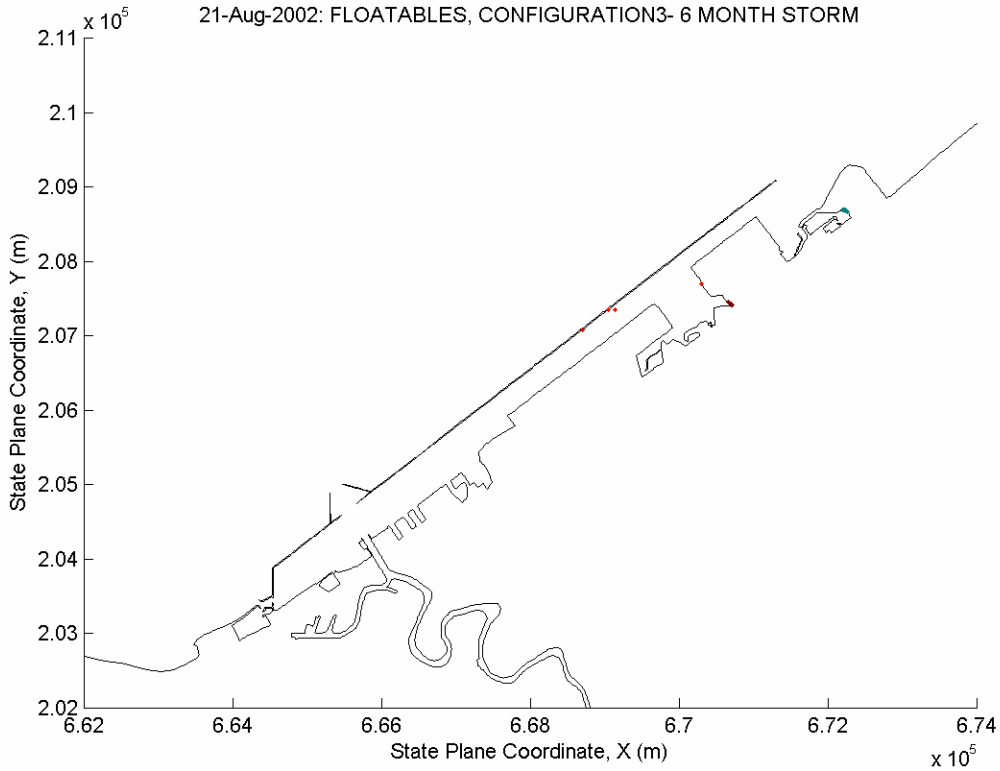
21-Aug-2002: FLOATABLES, CONFIGURATION3- 6 MONTH STORM
x 10^5
2.11
2.1
2.09
2.08
2.07
2.06
2.05
2.04
2.03
2.02
State Plane Coordinate, Y (m)
6.62
6.64
6.66
6.68
6.7
6.72
6.74
State Plane Coordinate, X (m)
x 10^5

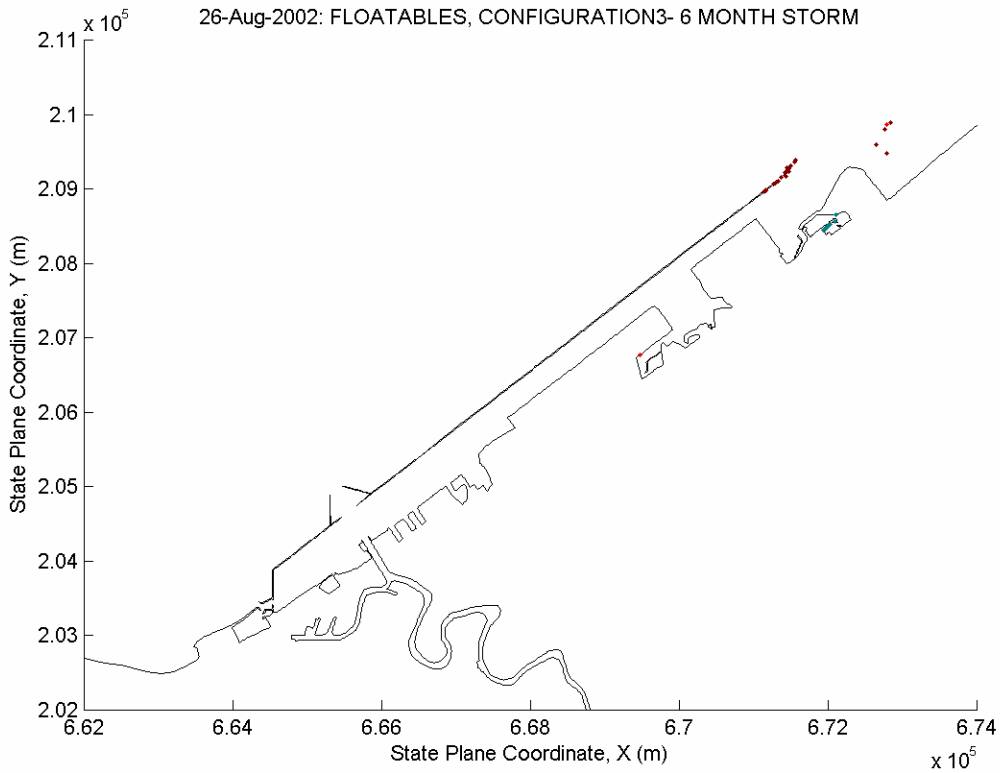
26-Aug-2002: FLOATABLES, CONFIGURATION3- 6 MONTH STORM
x 10^5
2.11
2.1
2.09
2.08
2.07
2.06
2.05
2.04
2.03
2.02
State Plane Coordinate, Y (m)
6.62
6.64
6.66
6.68
6.7
6.72
6.74
State Plane Coordinate, X (m)
x 10^5

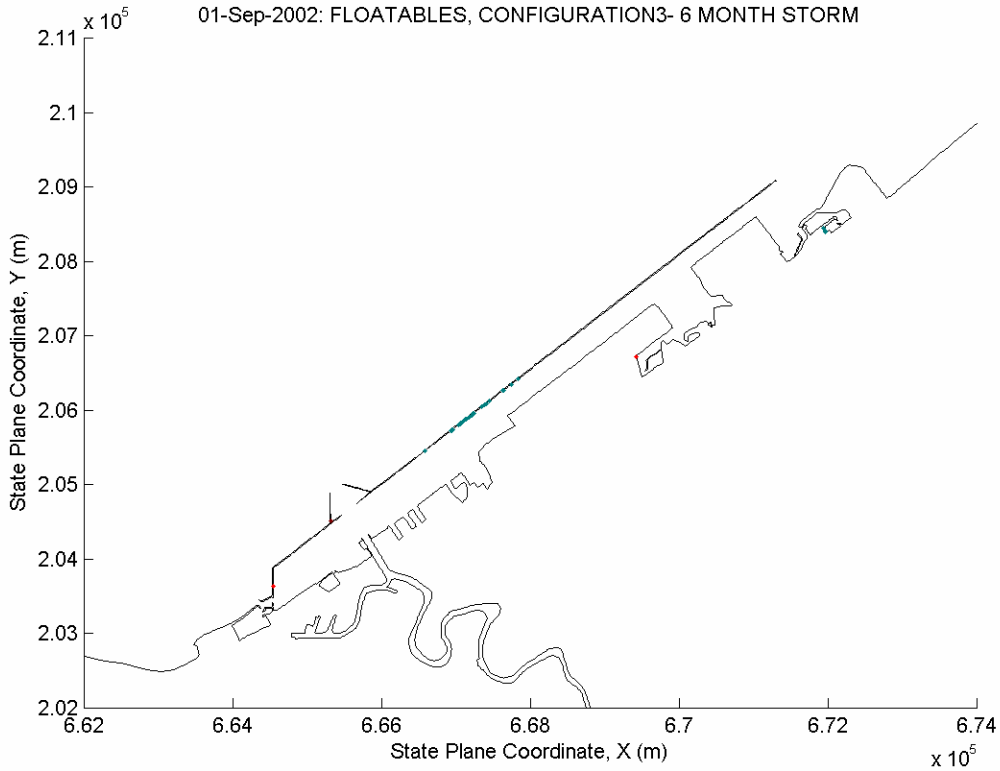
01-Sep-2002: FLOATABLES, CONFIGURATION3- 6 MONTH STORM
x 10^5
2.11
2.1
2.09
2.08
2.07
2.06
2.05
2.04
2.03
2.02
State Plane Coordinate, Y (m)
6.62
6.64
6.66
6.68
6.7
6.72
6.74
State Plane Coordinate, X (m)
x 10^5

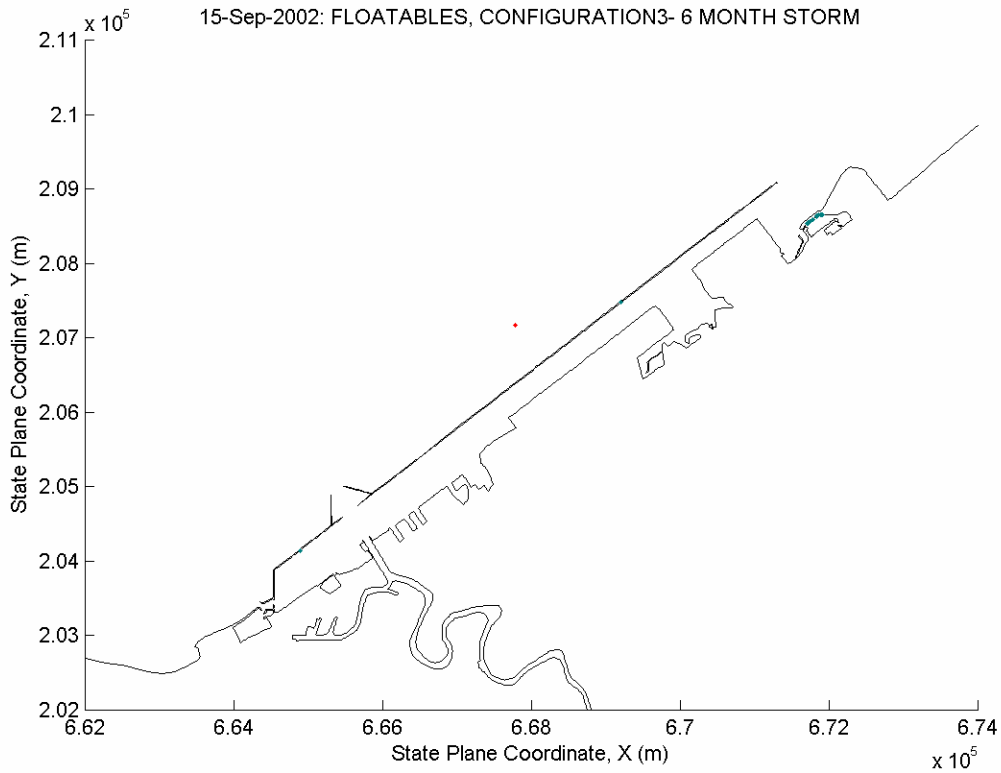
15-Sep-2002: FLOATABLES, CONFIGURATION3- 6 MONTH STORM
x 10^5
2.11
2.1
2.09
2.08
2.07
2.06
2.05
2.04
2.03
2.02
State Plane Coordinate, Y (m)
6.62
6.64
6.66
6.68
6.7
6.72
6.74
State Plane Coordinate, X (m)
x 10^5

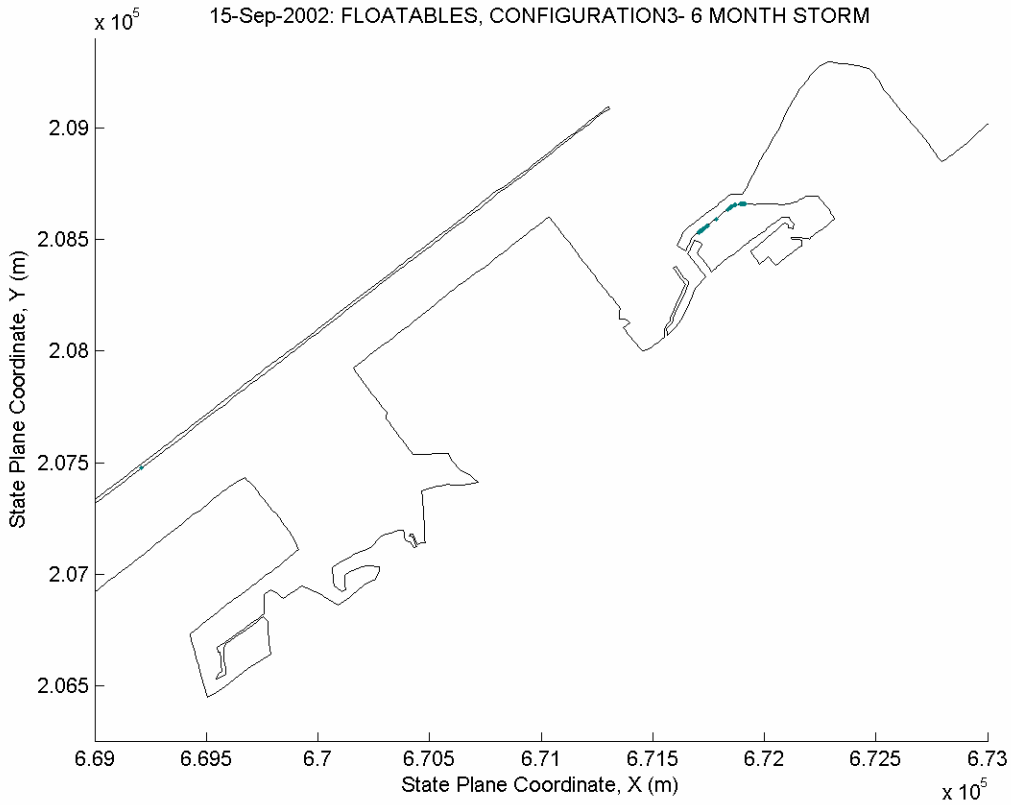
15-Sep-2002: FLOATABLES, CONFIGURATION3- 6 MONTH STORM
x 10^5
2.09
2.085
2.08
2.075
2.07
2.065
State Plane Coordinate, Y (m)
6.69
6.695
6.7
6.705
6.71
6.715
6.72
6.725
6.73
State Plane Coordinate, X (m)
x 10^5

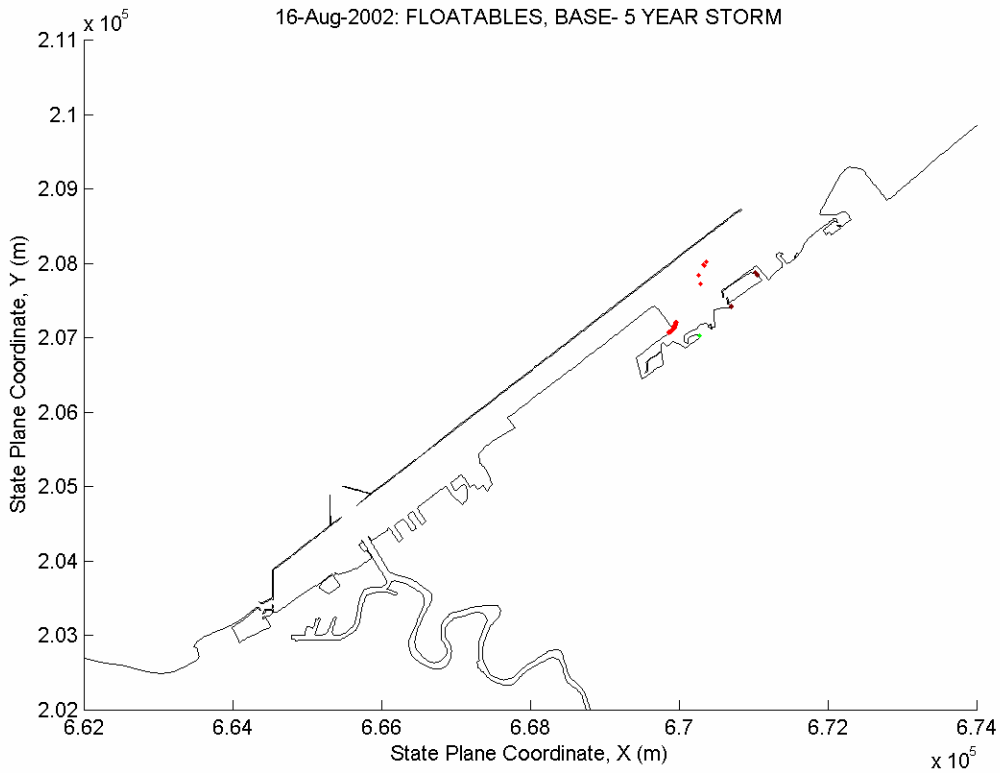
16-Aug-2002: FLOATABLES, BASE- 5 YEAR STORM
x 10^5
2.11
2.1
2.09
2.08
2.07
2.06
2.05
2.04
2.03
2.02
State Plane Coordinate, Y (m)
6.62
6.64
6.66
6.68
6.7
6.72
6.74
State Plane Coordinate, X (m)
x 10^5

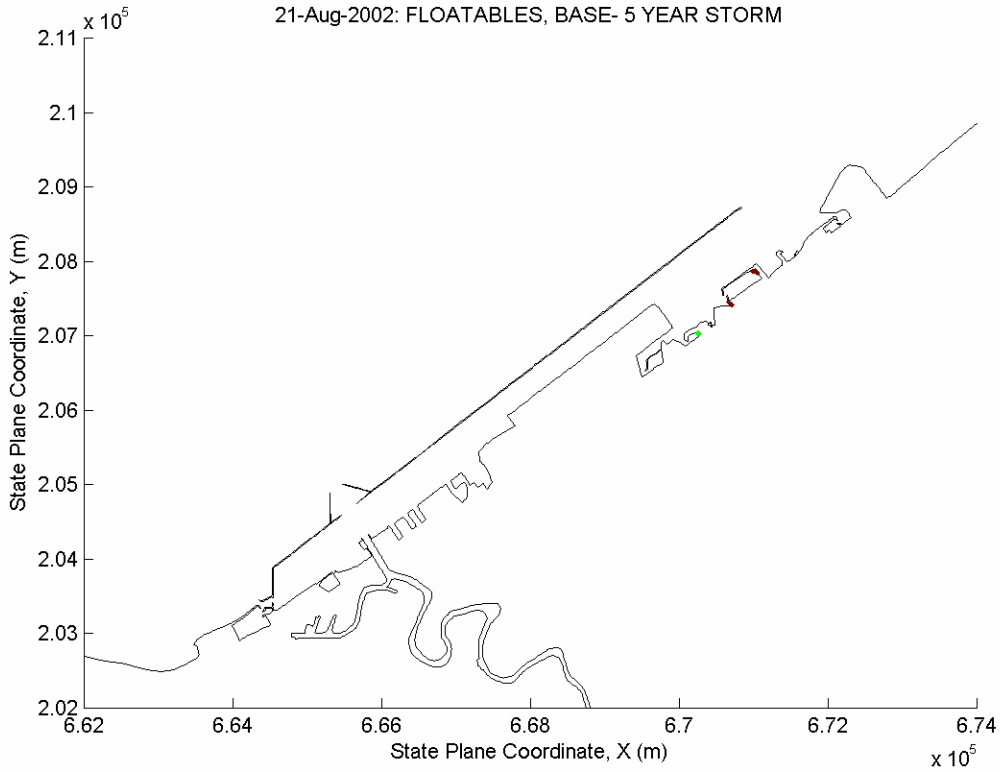
21-Aug-2002: FLOATABLES, BASE- 5 YEAR STORM
x 10^5
2.11
2.1
2.09
2.08
2.07
2.06
2.05
2.04
2.03
2.02
State Plane Coordinate, Y (m)
6.62
6.64
6.66
6.68
6.7
6.72
6.74
State Plane Coordinate, X (m)
x 10^5

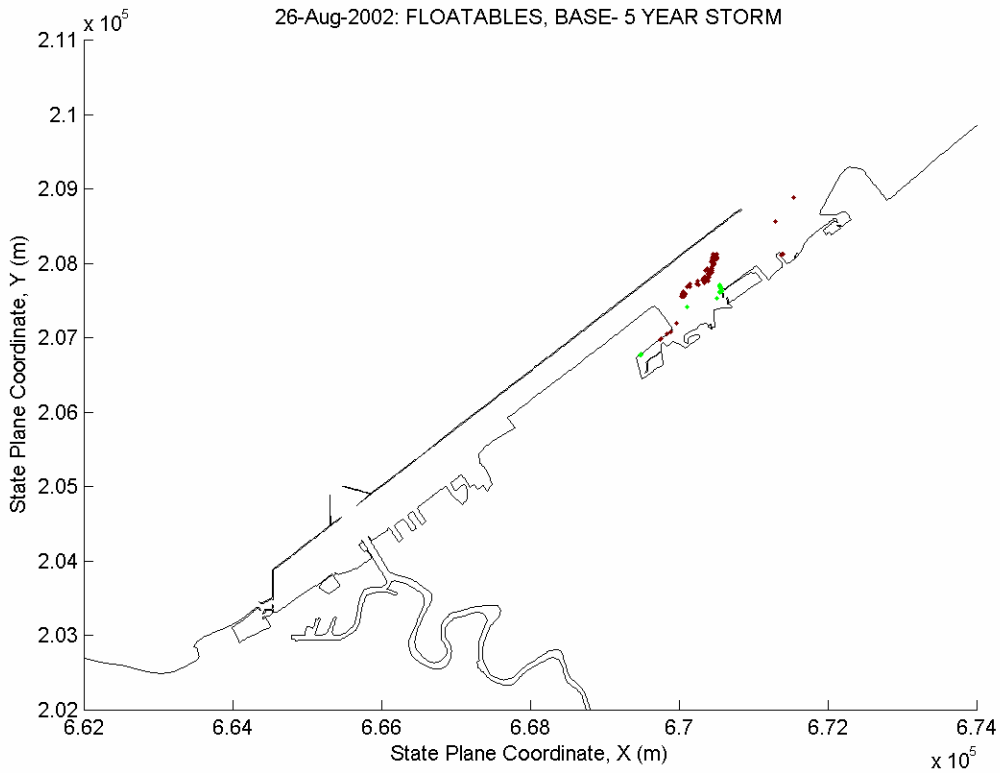
26-Aug-2002: FLOATABLES, BASE- 5 YEAR STORM
x 10^5
2.11
2.1
2.09
2.08
2.07
2.06
2.05
2.04
2.03
2.02
State Plane Coordinate, Y (m)
6.62
6.64
6.66
6.68
6.7
6.72
6.74
State Plane Coordinate, X (m)
x 10^5

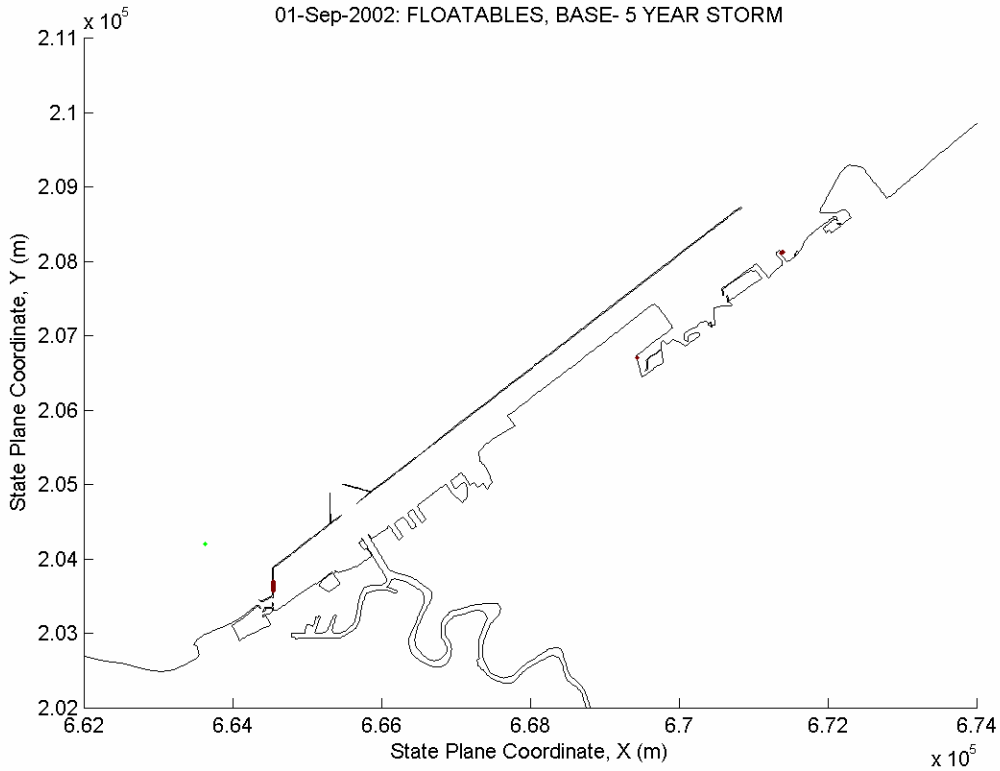
01-Sep-2002: FLOATABLES, BASE- 5 YEAR STORM
x 10^5
2.11
2.1
2.09
2.08
2.07
2.06
2.05
2.04
2.03
2.02
State Plane Coordinate, Y (m)
6.62
6.64
6.66
6.68
6.7
6.72
6.74
State Plane Coordinate, X (m)
x 10^5

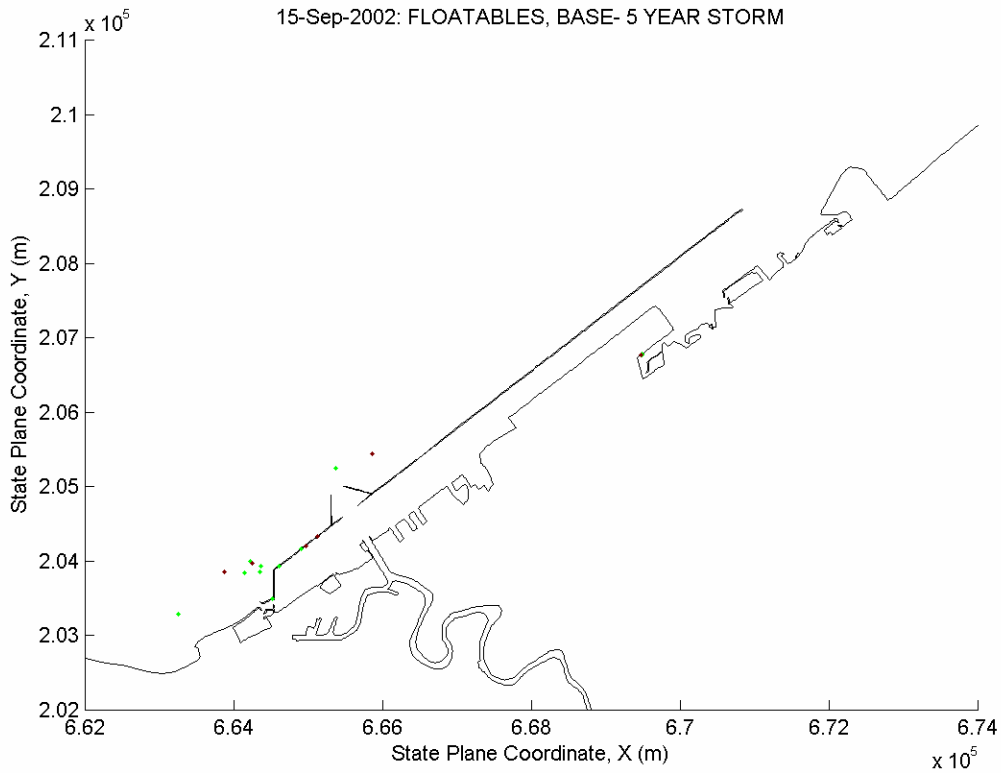
15-Sep-2002: FLOATABLES, BASE- 5 YEAR STORM
x 10^5
2.11
2.1
2.09
2.08
2.07
2.06
2.05
2.04
2.03
2.02
State Plane Coordinate, Y (m)
6.62
6.64
6.66
6.68
6.7
6.72
6.74
State Plane Coordinate, X (m)
x 10^5

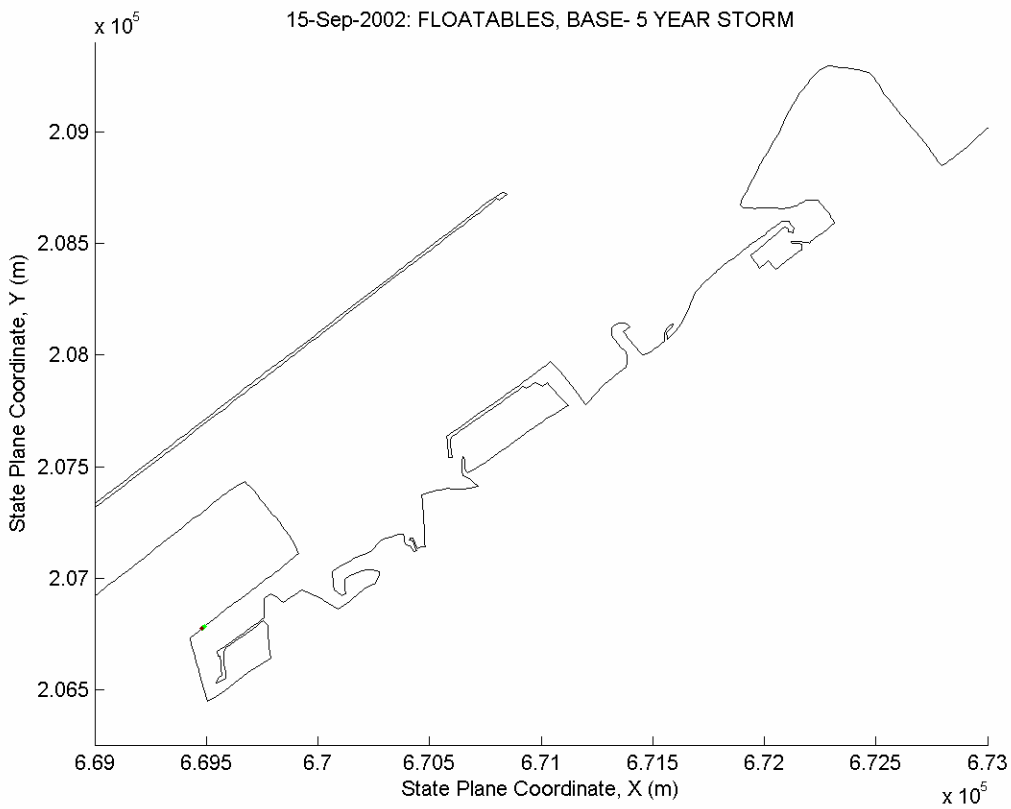
15-Sep-2002: FLOATABLES, BASE- 5 YEAR STORM
x 10^5
2.09
2.085
2.08
2.075
2.07
2.065
State Plane Coordinate, Y (m)
6.69
6.695
6.7
6.705
6.71
6.715
6.72
6.725
6.73
State Plane Coordinate, X (m)
x 10^5

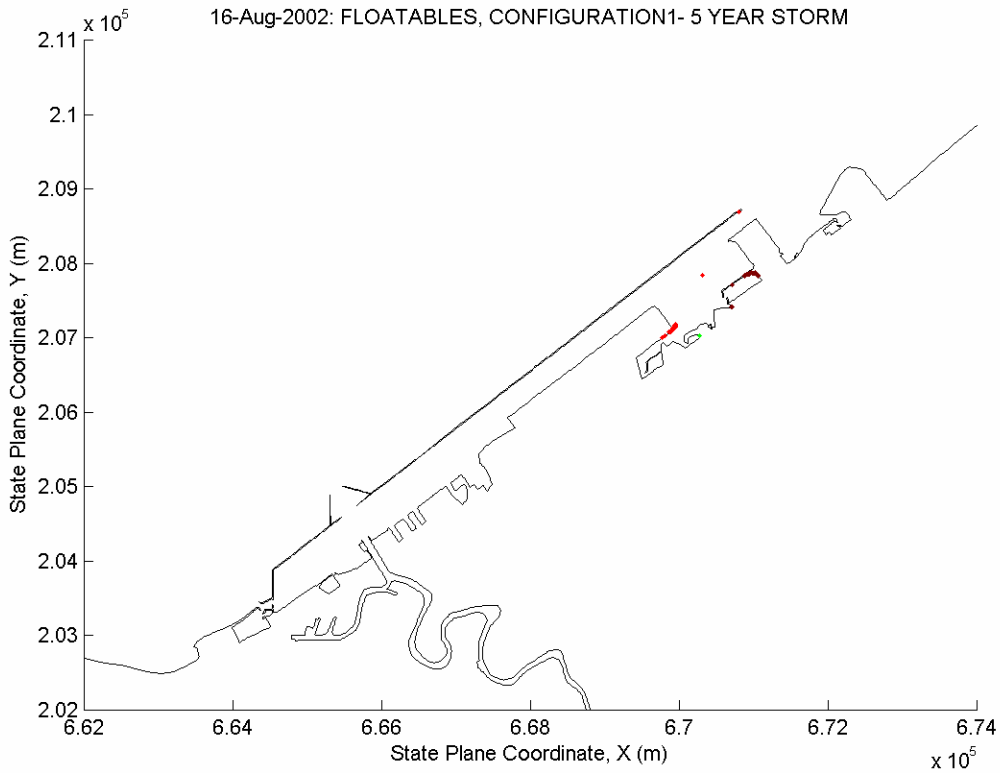
16-Aug-2002: FLOATABLES, CONFIGURATION1- 5 YEAR STORM
x 10^5
2.11
2.1
2.09
2.08
2.07
2.06
2.05
2.04
2.03
2.02
State Plane Coordinate, Y (m)
6.62
6.64
6.66
6.68
6.7
6.72
6.74
State Plane Coordinate, X (m)
x 10^5

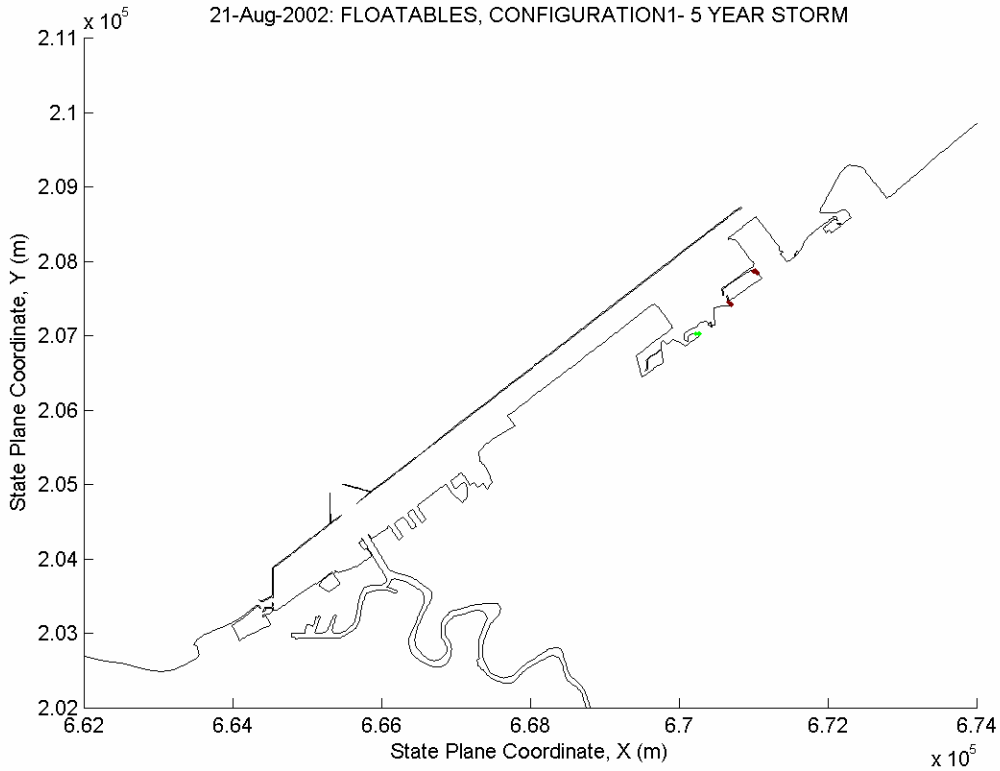
21-Aug-2002: FLOATABLES, CONFIGURATION1- 5 YEAR STORM
x 10^5
2.11
2.1
2.09
2.08
2.07
2.06
2.05
2.04
2.03
2.02
State Plane Coordinate, Y (m)
6.62
6.64
6.66
6.68
6.7
6.72
6.74
State Plane Coordinate, X (m)
x 10^5

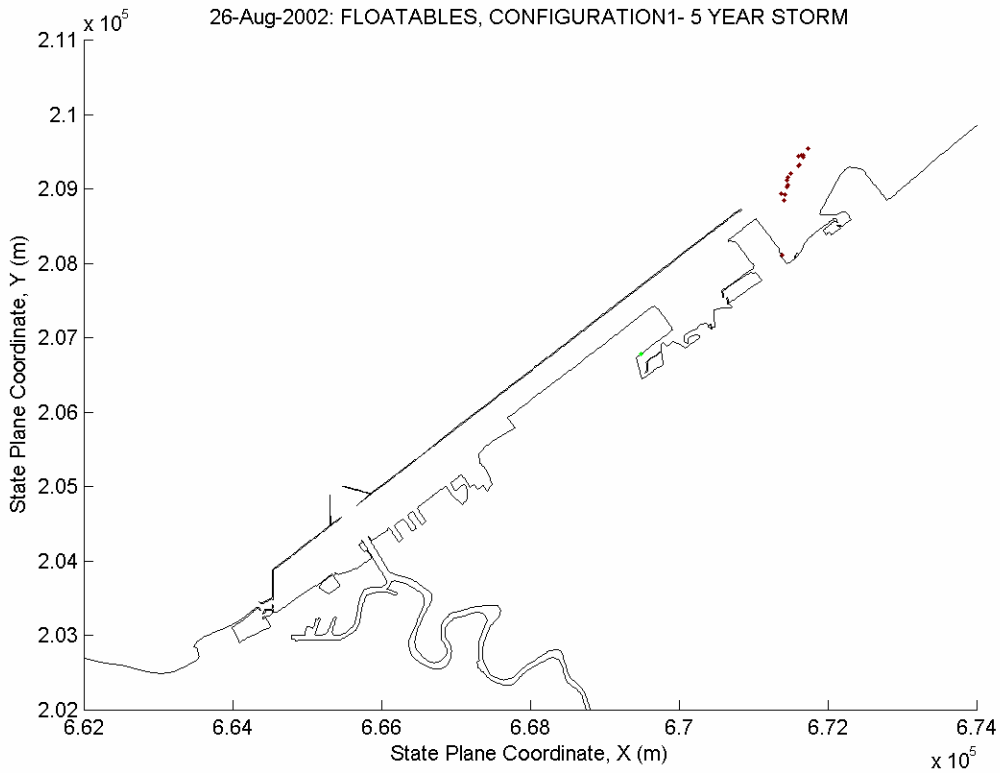
26-Aug-2002: FLOATABLES, CONFIGURATION1- 5 YEAR STORM
x 10^5
2.11
2.1
2.09
2.08
2.07
2.06
2.05
2.04
2.03
2.02
State Plane Coordinate, Y (m)
6.62
6.64
6.66
6.68
6.7
6.72
6.74
State Plane Coordinate, X (m)
x 10^5

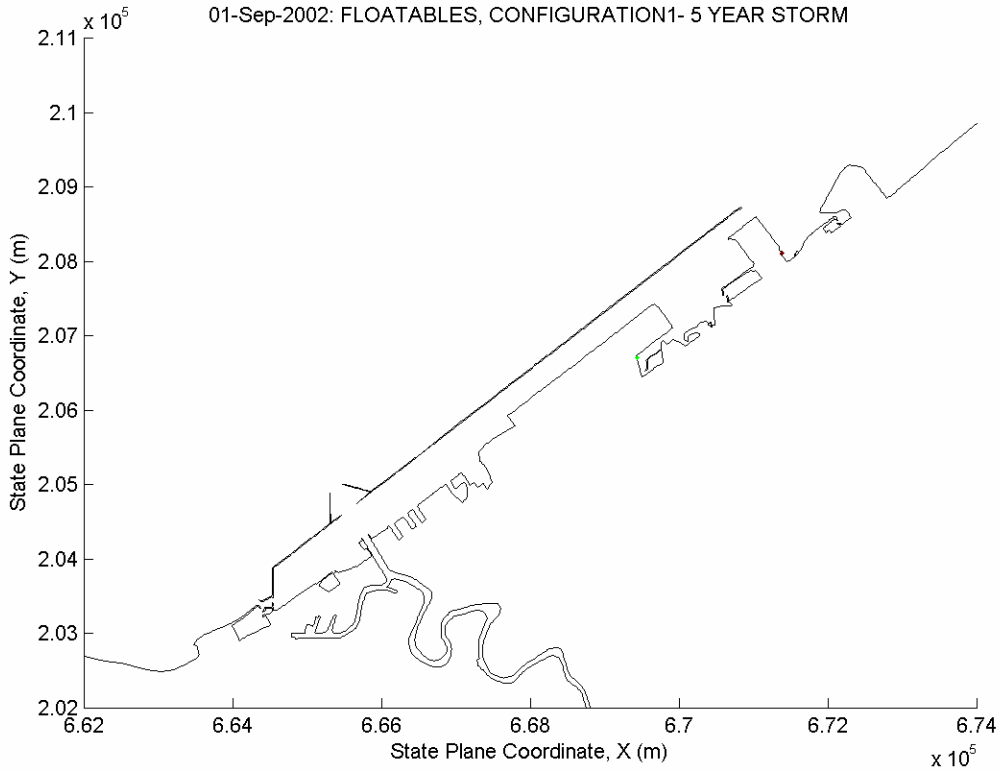
01-Sep-2002: FLOATABLES, CONFIGURATION1- 5 YEAR STORM
x 10^5
2.11
2.1
2.09
2.08
2.07
2.06
2.05
2.04
2.03
2.02
State Plane Coordinate, Y (m)
6.62
6.64
6.66
6.68
6.7
6.72
6.74
State Plane Coordinate, X (m)
x 10^5

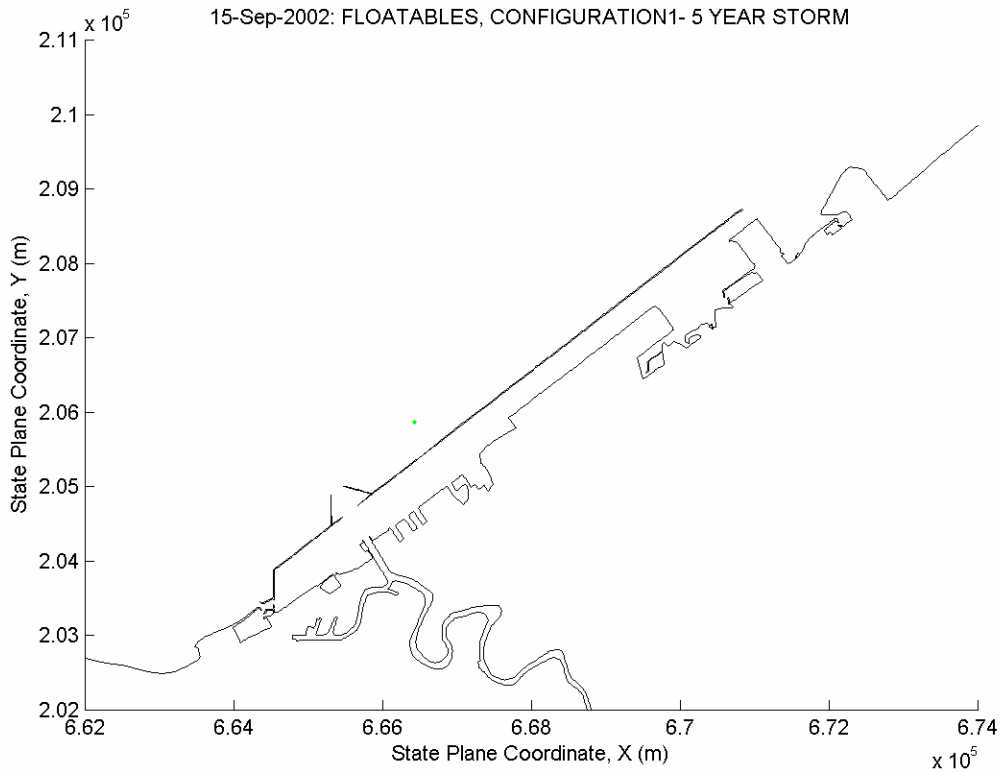
15-Sep-2002: FLOATABLES, CONFIGURATION1- 5 YEAR STORM
x 10^5
2.11
2.1
2.09
2.08
2.07
2.06
2.05
2.04
2.03
2.02
State Plane Coordinate, Y (m)
6.62
6.64
6.66
6.68
6.7
6.72
6.74
State Plane Coordinate, X (m)
x 10^5

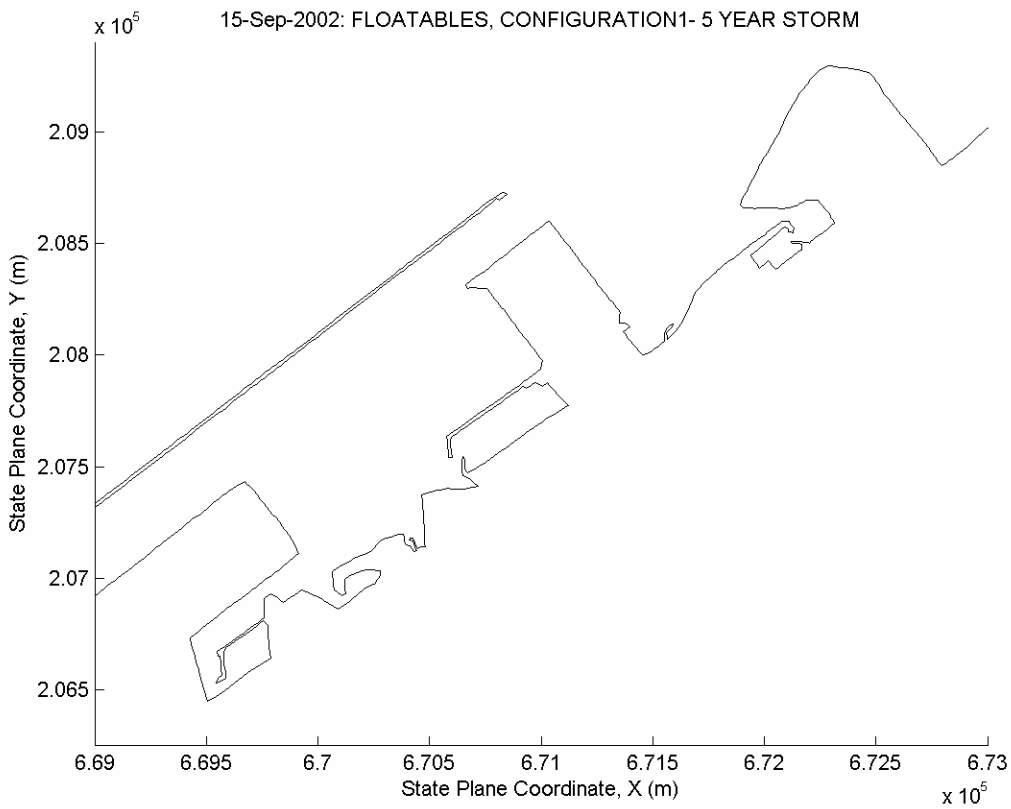
15-Sep-2002: FLOATABLES, CONFIGURATION1- 5 YEAR STORM
x 10^5
2.09
2.085
2.08
2.075
2.07
2.065
State Plane Coordinate, Y (m)
6.69
6.695
6.7
6.705
6.71
6.715
6.72
6.725
6.73
State Plane Coordinate, X (m)
x 10^5

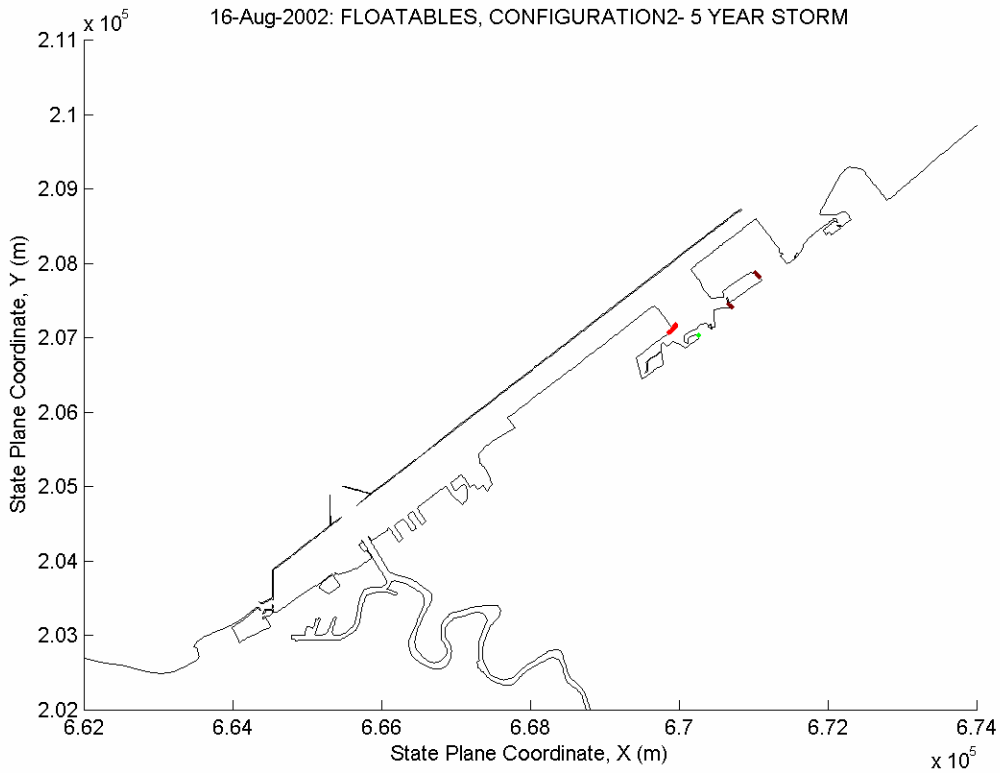
16-Aug-2002: FLOATABLES, CONFIGURATION2- 5 YEAR STORM
x 10^5
2.11
2.1
2.09
2.08
2.07
2.06
2.05
2.04
2.03
2.02
State Plane Coordinate, Y (m)
6.62
6.64
6.66
6.68
6.7
6.72
6.74
State Plane Coordinate, X (m)
x 10^5

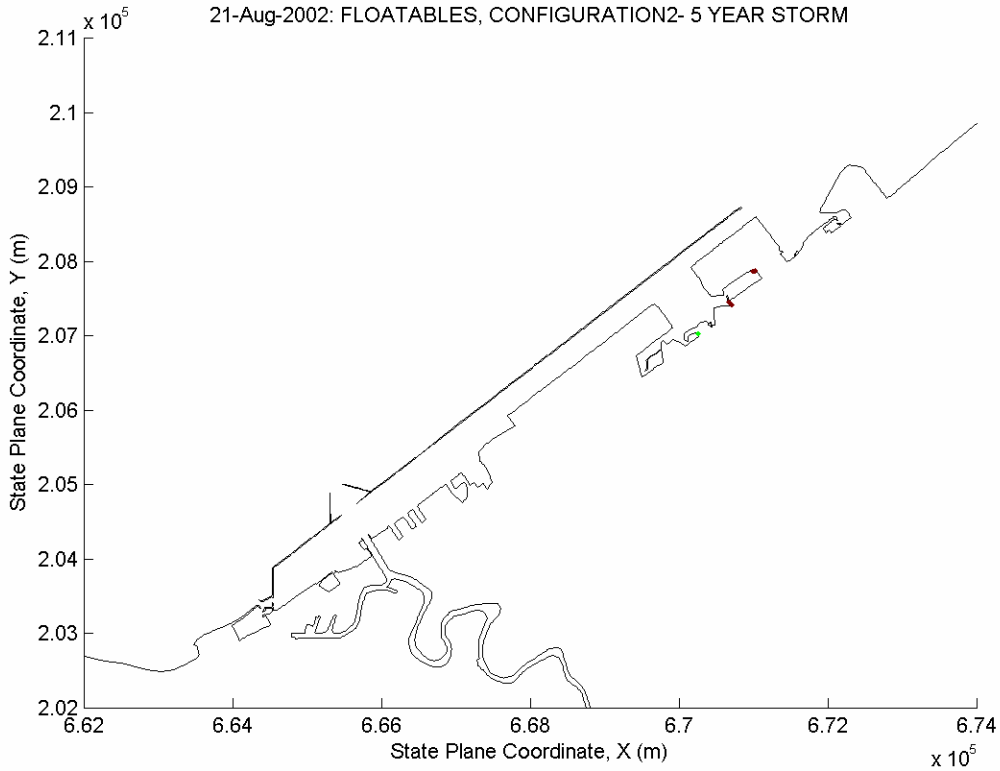
21-Aug-2002: FLOATABLES, CONFIGURATION2- 5 YEAR STORM
x 10^5
2.11
2.1
2.09
2.08
2.07
2.06
2.05
2.04
2.03
2.02
State Plane Coordinate, Y (m)
6.62
6.64
6.66
6.68
6.7
6.72
6.74
State Plane Coordinate, X (m)
x 10^5

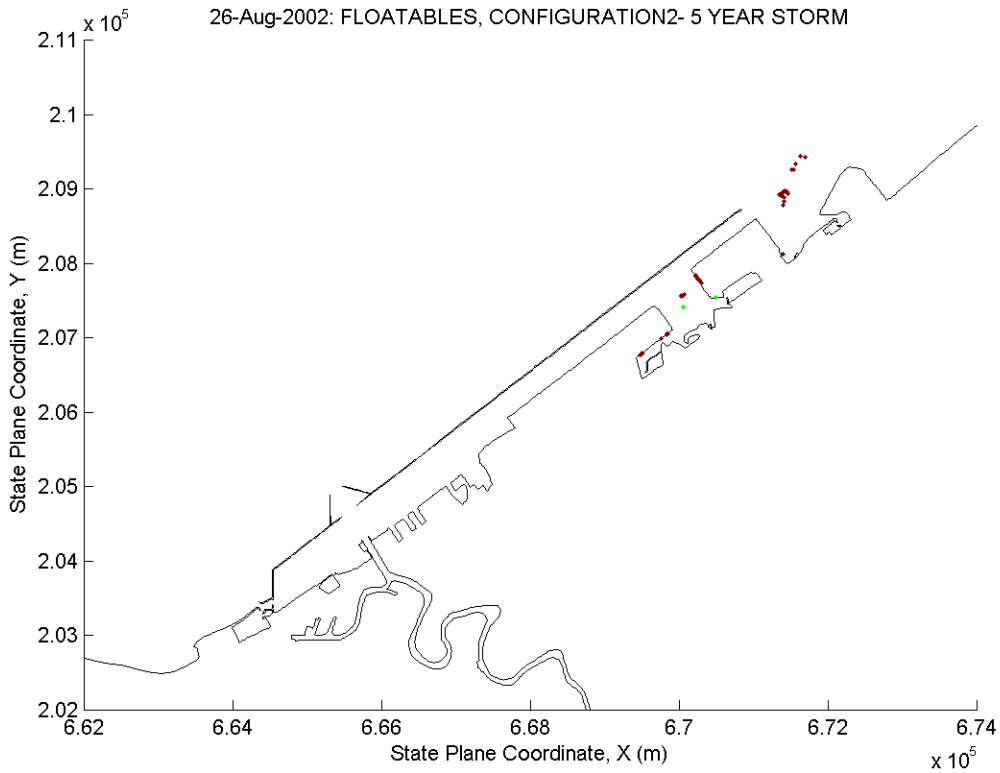
26-Aug-2002: FLOATABLES, CONFIGURATION2- 5 YEAR STORM
x 10^5
2.11
2.1
2.09
2.08
2.07
2.06
2.05
2.04
2.03
2.02
State Plane Coordinate, Y (m)
6.62
6.64
6.66
6.68
6.7
6.72
6.74
State Plane Coordinate, X (m)
x 10^5

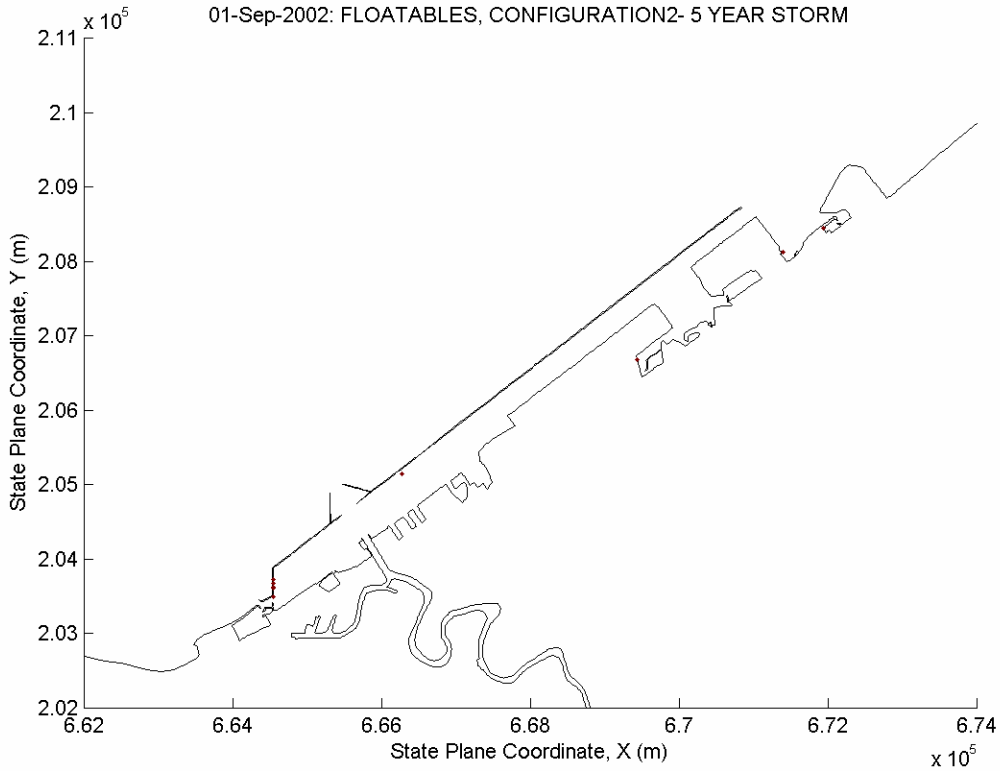
01-Sep-2002: FLOATABLES, CONFIGURATION2- 5 YEAR STORM
x 10^5
2.11
2.1
2.09
2.08
2.07
2.06
2.05
2.04
2.03
2.02
State Plane Coordinate, Y (m)
6.62
6.64
6.66
6.68
6.7
6.72
6.74
State Plane Coordinate, X (m)
x 10^5

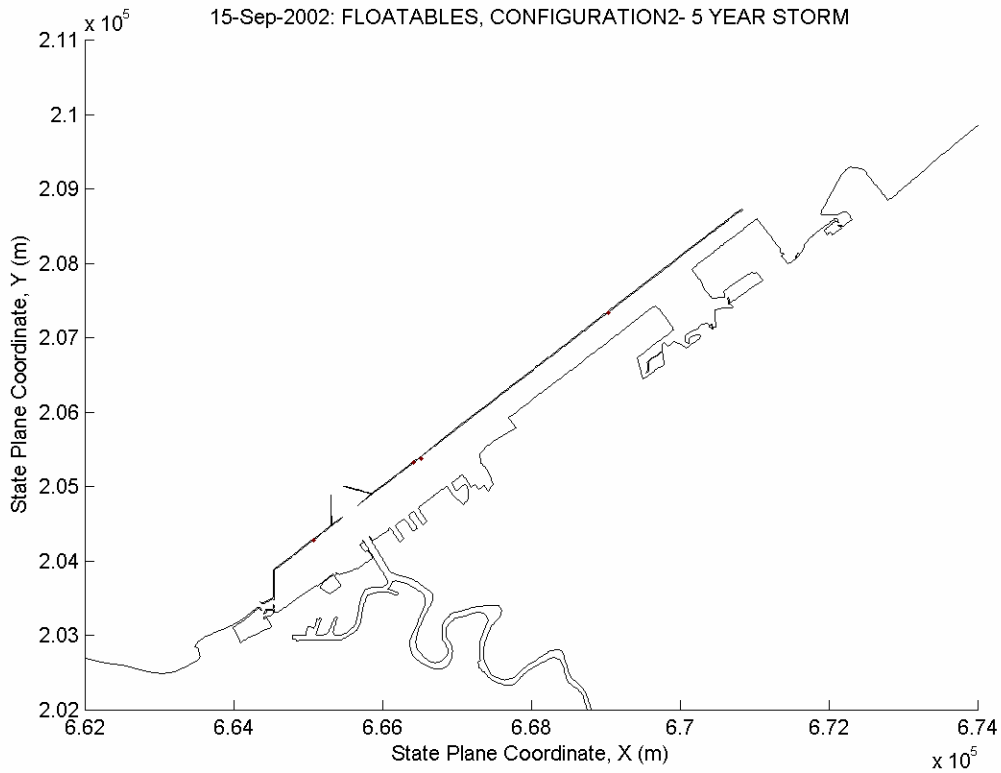
15-Sep-2002: FLOATABLES, CONFIGURATION2- 5 YEAR STORM
x 10^5
2.11
2.1
2.09
2.08
2.07
2.06
2.05
2.04
2.03
2.02
State Plane Coordinate, Y (m)
6.62
6.64
6.66
6.68
6.7
6.72
6.74
State Plane Coordinate, X (m)
x 10^5

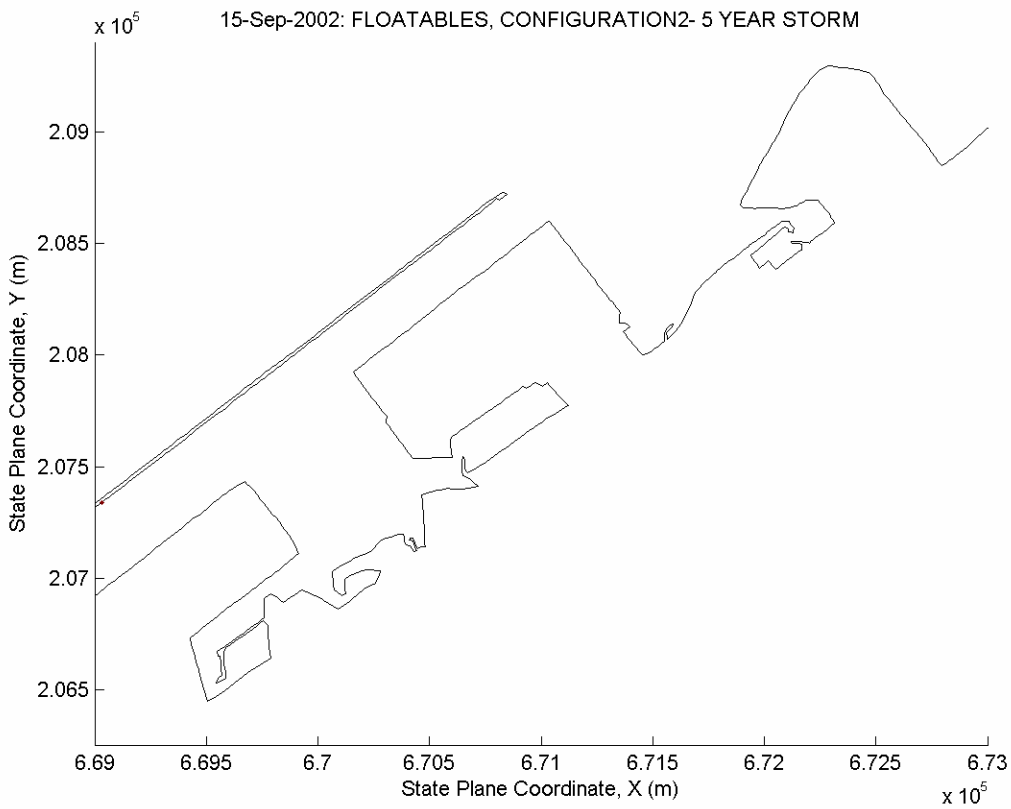
15-Sep-2002: FLOATABLES, CONFIGURATION2- 5 YEAR STORM
x 10^5
2.09
2.085
2.08
2.075
2.07
2.065
State Plane Coordinate, Y (m)
6.69
6.695
6.7
6.705
6.71
6.715
6.72
6.725
6.73
State Plane Coordinate, X (m)
x 10^5

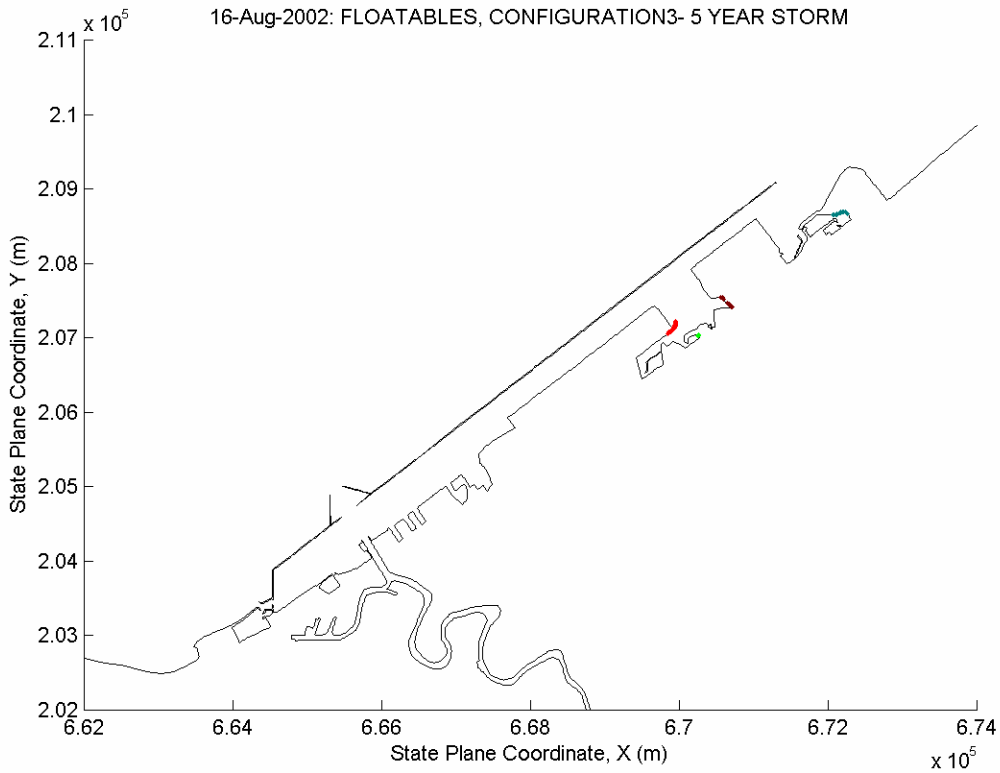
16-Aug-2002: FLOATABLES, CONFIGURATION3- 5 YEAR STORM
x 10^5
2.11
2.1
2.09
2.08
2.07
2.06
2.05
2.04
2.03
2.02
State Plane Coordinate, Y (m)
6.62
6.64
6.66
6.68
6.7
6.72
6.74
State Plane Coordinate, X (m)
x 10^5

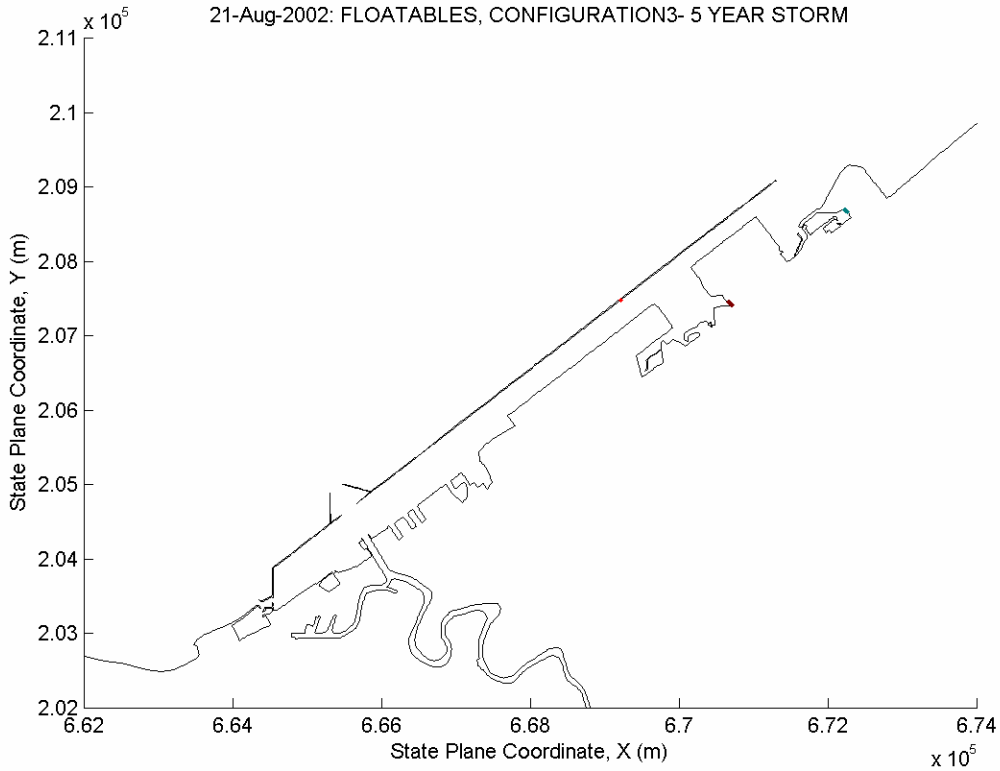
21-Aug-2002: FLOATABLES, CONFIGURATION3- 5 YEAR STORM
x 10^5
2.11
2.1
2.09
2.08
2.07
2.06
2.05
2.04
2.03
2.02
State Plane Coordinate, Y (m)
6.62
6.64
6.66
6.68
6.7
6.72
6.74
State Plane Coordinate, X (m)
x 10^5

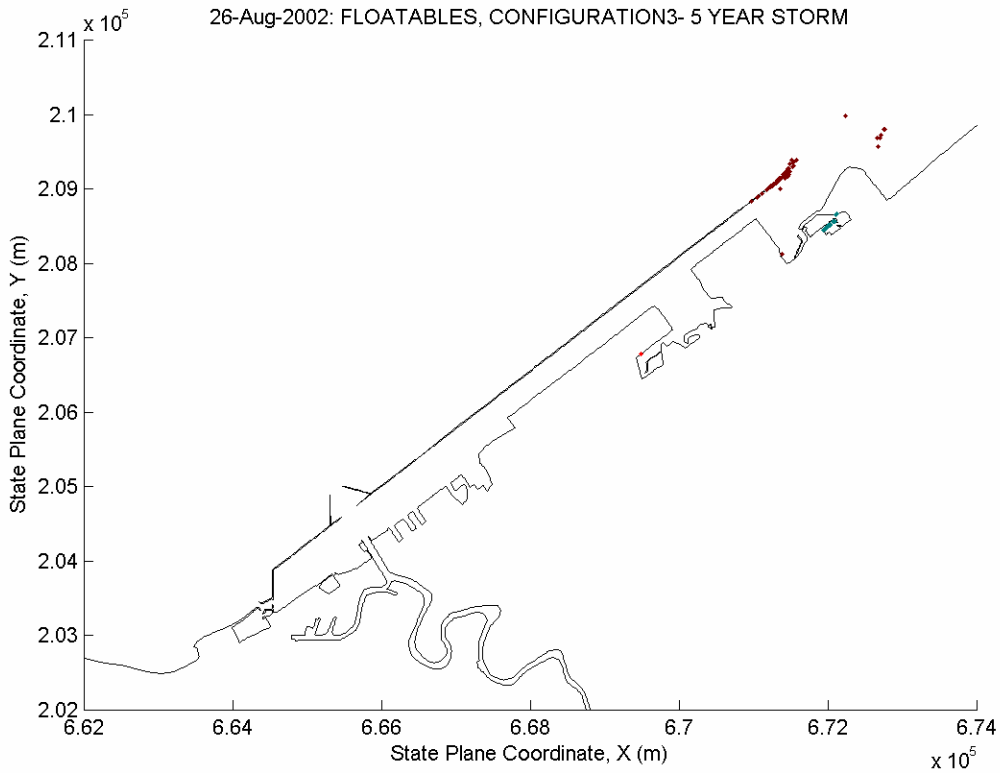
26-Aug-2002: FLOATABLES, CONFIGURATION3- 5 YEAR STORM
x 10^5
2.11
2.1
2.09
2.08
2.07
2.06
2.05
2.04
2.03
2.02
State Plane Coordinate, Y (m)
6.62
6.64
6.66
6.68
6.7
6.72
6.74
State Plane Coordinate, X (m)
x 10^5

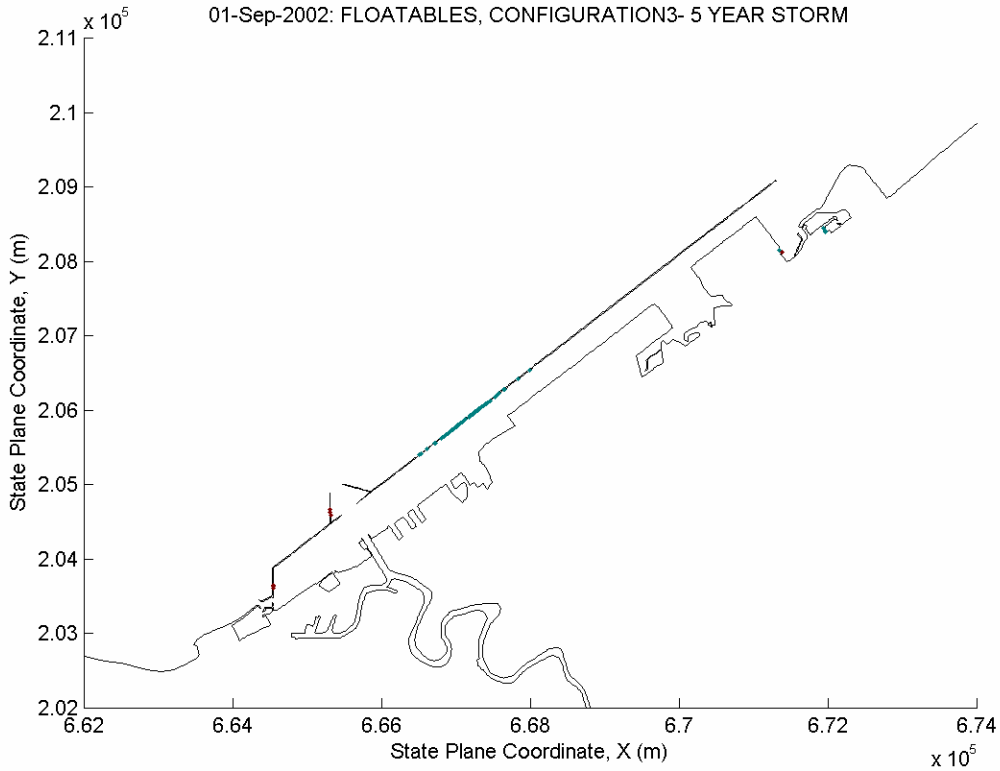
01-Sep-2002: FLOATABLES, CONFIGURATION3- 5 YEAR STORM
x 10^5
2.11
2.1
2.09
2.08
2.07
2.06
2.05
2.04
2.03
2.02
State Plane Coordinate, Y (m)
6.62
6.64
6.66
6.68
6.7
6.72
6.74
State Plane Coordinate, X (m)
x 10^5

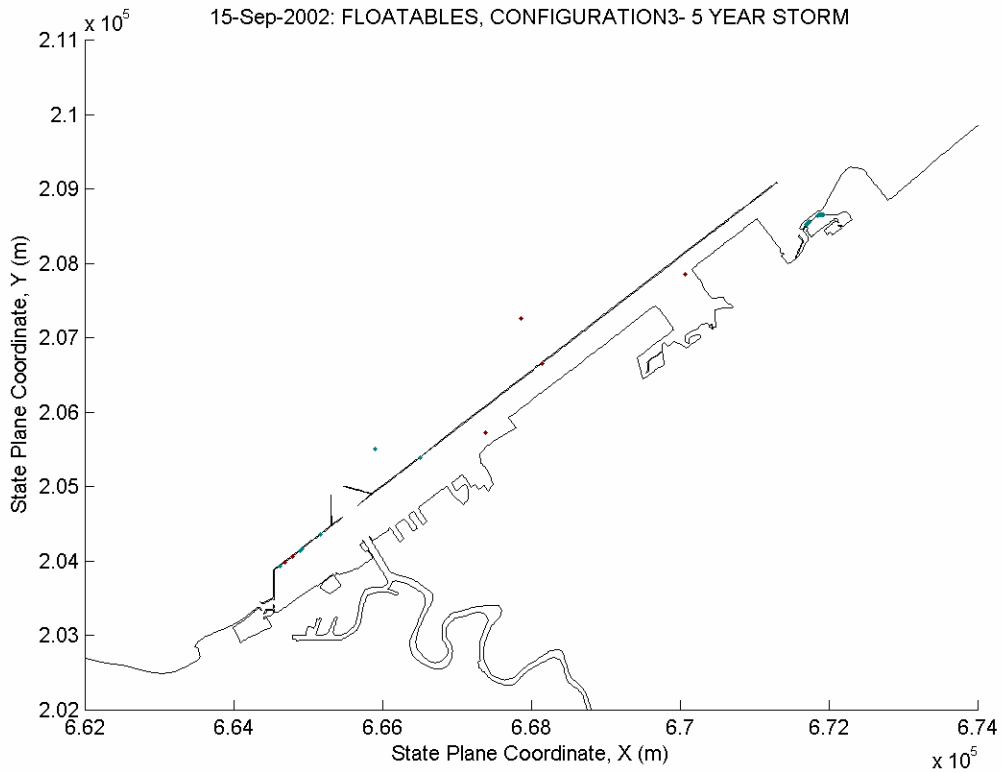
15-Sep-2002: FLOATABLES, CONFIGURATION3- 5 YEAR STORM
x 10^5
2.11
2.1
2.09
2.08
2.07
2.06
2.05
2.04
2.03
2.02
State Plane Coordinate, Y (m)
6.62
6.64
6.66
6.68
6.7
6.72
6.74
State Plane Coordinate, X (m)
x 10^5

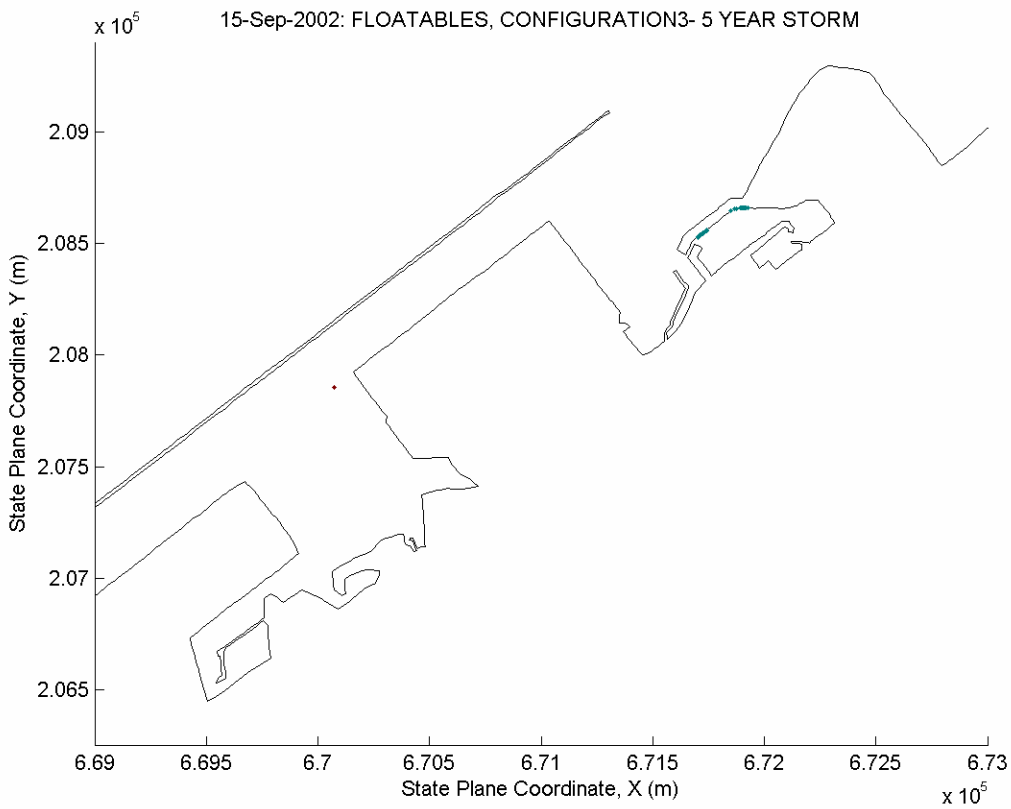
15-Sep-2002: FLOATABLES, CONFIGURATION3- 5 YEAR STORM
x 10^5
2.09
2.085
2.08
2.075
2.07
2.065
State Plane Coordinate, Y (m)
6.69
6.695
6.7
6.705
6.71
6.715
6.72
6.725
6.73
State Plane Coordinate, X (m)
x 10^5

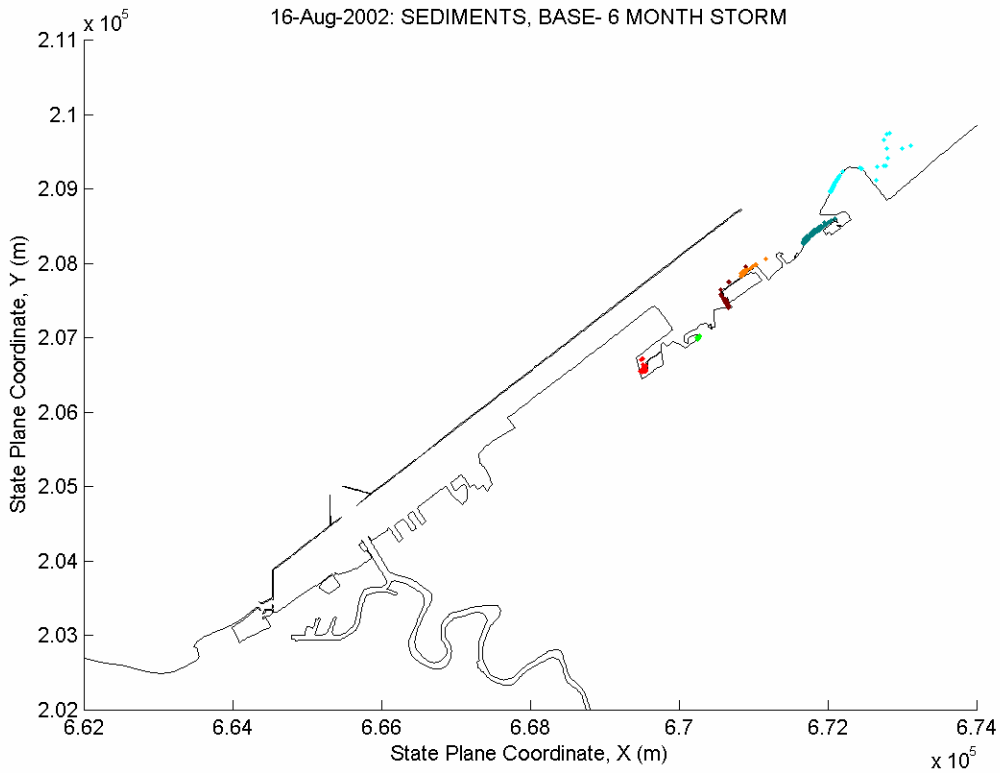
16-Aug-2002: SEDIMENTS, BASE- 6 MONTH STORM
x 10^5
2.11
2.1
2.09
2.08
2.07
2.06
2.05
2.04
2.03
2.02
State Plane Coordinate, Y (m)
6.62
6.64
6.66
6.68
6.7
6.72
6.74
State Plane Coordinate, X (m)
x 10^5

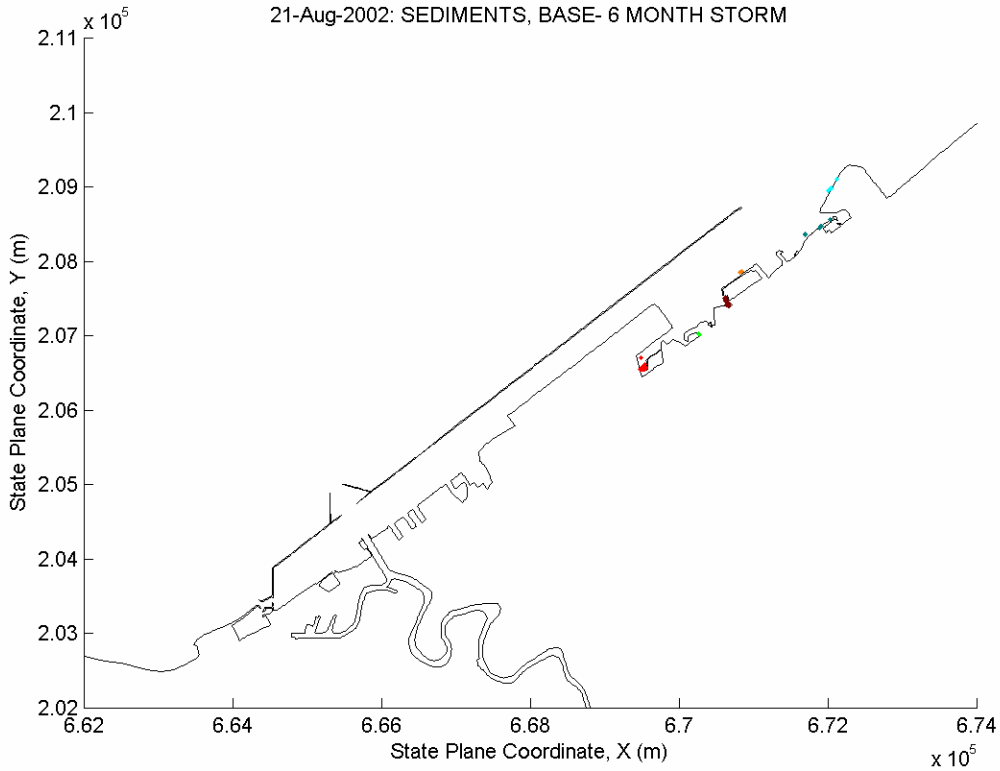
21-Aug-2002: SEDIMENTS, BASE- 6 MONTH STORM
x 10^5
2.11
2.1
2.09
2.08
2.07
2.06
2.05
2.04
2.03
2.02
State Plane Coordinate, Y (m)
6.62
6.64
6.66
6.68
6.7
6.72
6.74
State Plane Coordinate, X (m)
x 10^5

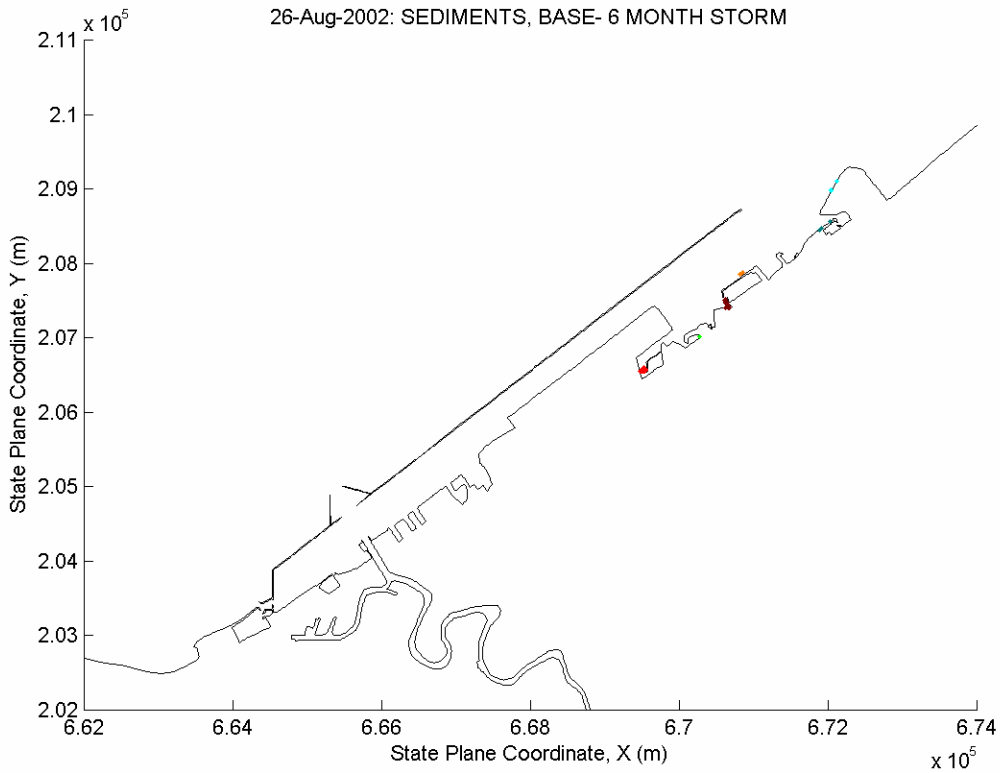
26-Aug-2002: SEDIMENTS, BASE- 6 MONTH STORM
x 10^5
2.11
2.1
2.09
2.08
2.07
2.06
2.05
2.04
2.03
2.02
State Plane Coordinate, Y (m)
6.62
6.64
6.66
6.68
6.7
6.72
6.74
State Plane Coordinate, X (m)
x 10^5

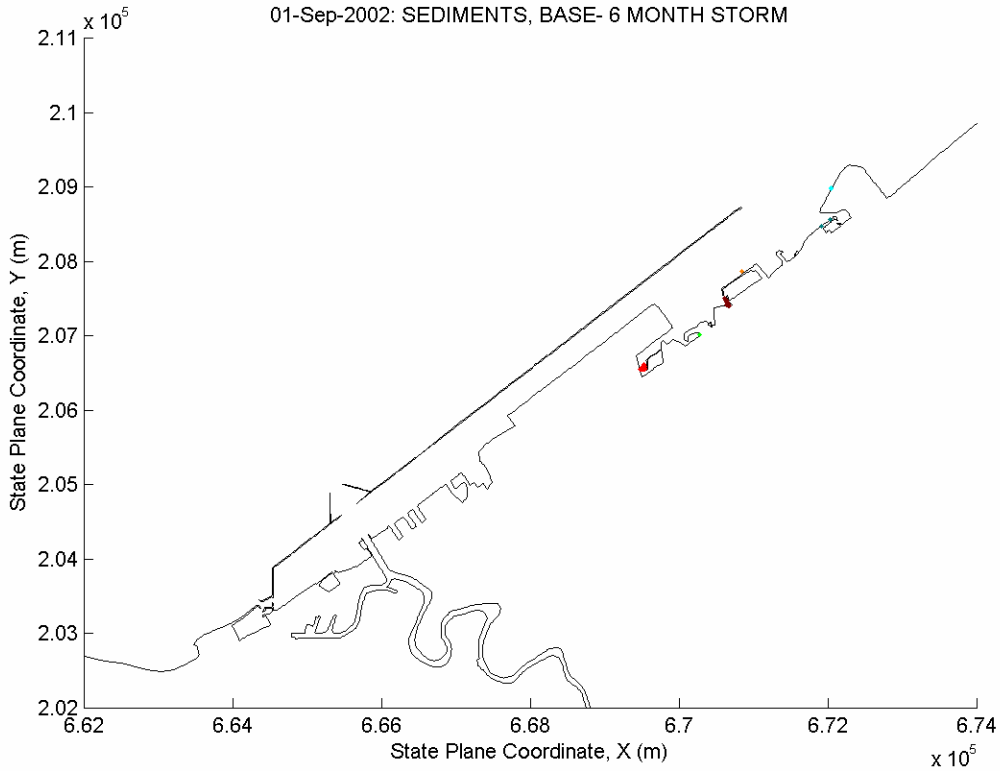
01-Sep-2002: SEDIMENTS, BASE- 6 MONTH STORM
x 10^5
2.11
2.1
2.09
2.08
2.07
2.06
2.05
2.04
2.03
2.02
State Plane Coordinate, Y (m)
6.62
6.64
6.66
6.68
6.7
6.72
6.74
State Plane Coordinate, X (m)
x 10^5

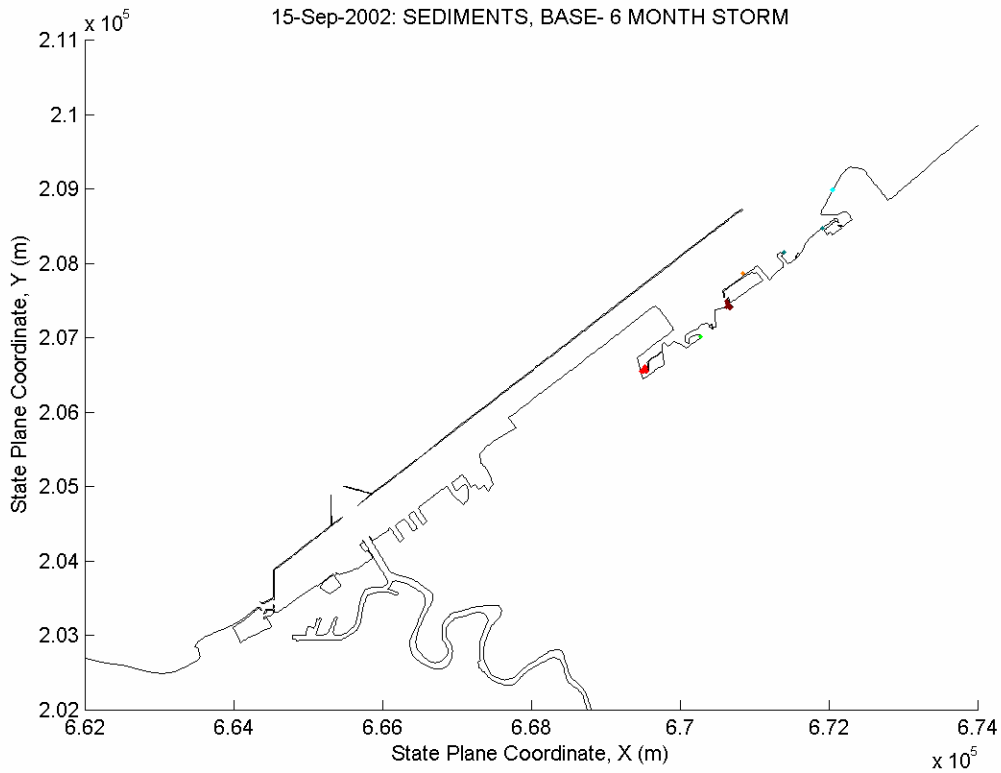
15-Sep-2002: SEDIMENTS, BASE- 6 MONTH STORM
x 10^5
2.11
2.1
2.09
2.08
2.07
2.06
2.05
2.04
2.03
2.02
State Plane Coordinate, Y (m)
6.62
6.64
6.66
6.68
6.7
6.72
6.74
State Plane Coordinate, X (m)
x 10^5

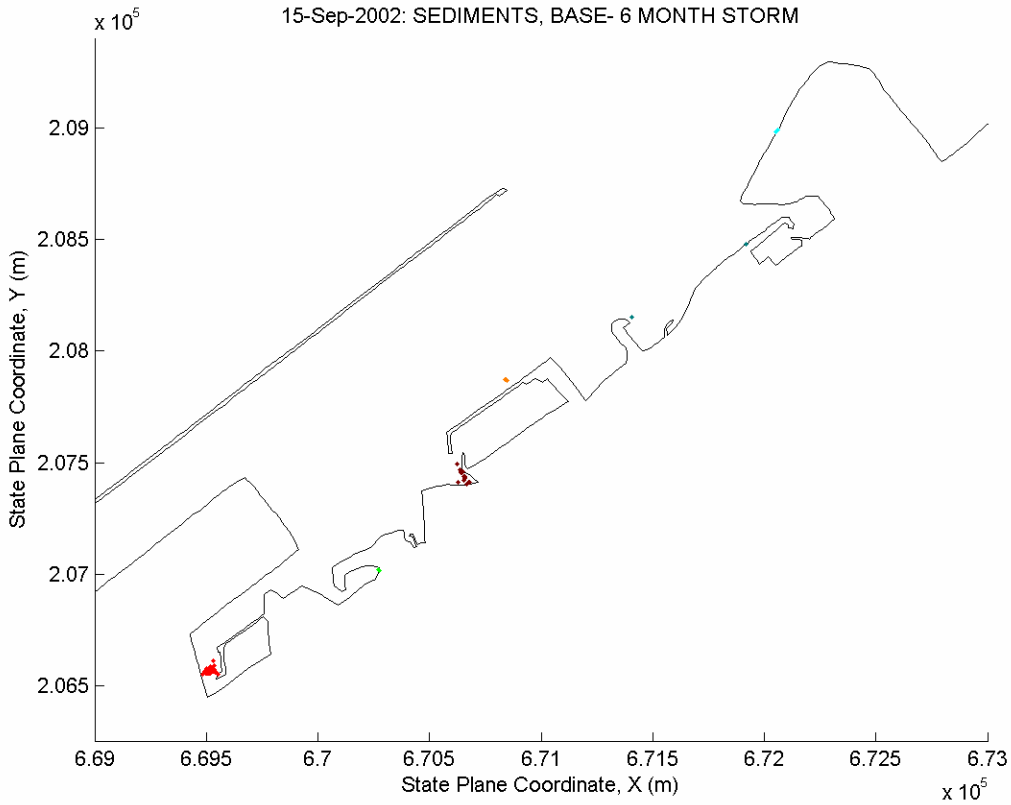
15-Sep-2002: SEDIMENTS, BASE- 6 MONTH STORM
x 10^5
2.09
2.085
2.08
2.075
2.07
2.065
State Plane Coordinate, Y (m)
6.69
6.695
6.7
6.705
6.71
6.715
6.72
6.725
6.73
State Plane Coordinate, X (m)
x 10^5

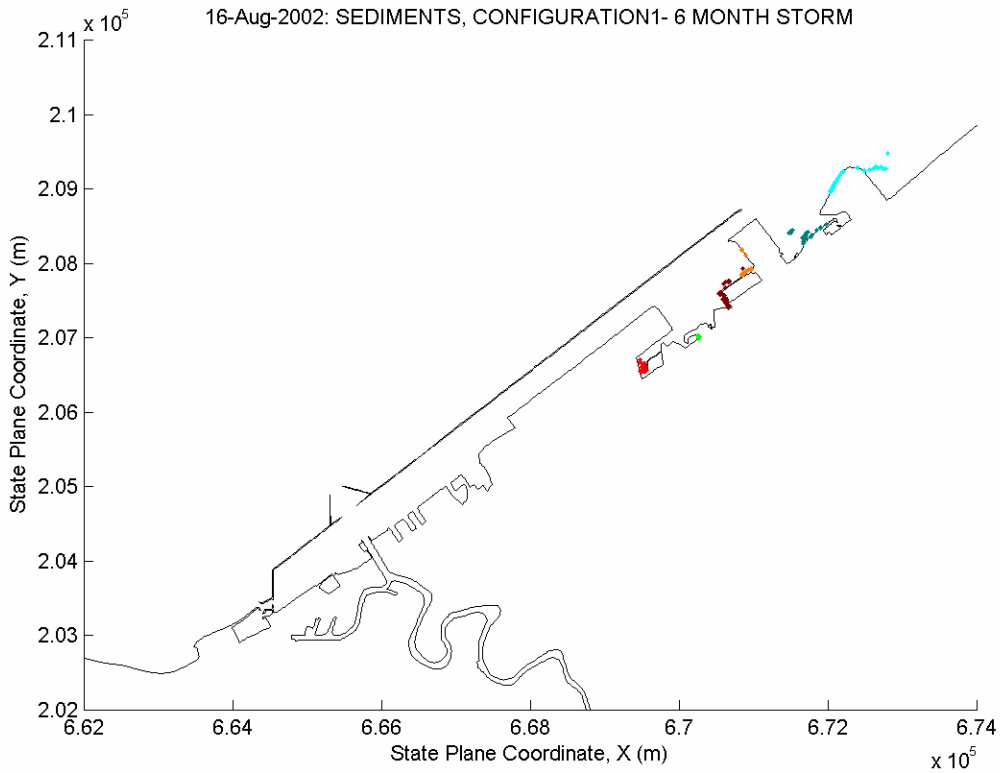
16-Aug-2002: SEDIMENTS, CONFIGURATION1- 6 MONTH STORM
x 10^5
2.11
2.1
2.09
2.08
2.07
2.06
2.05
2.04
2.03
2.02
State Plane Coordinate, Y (m)
6.62
6.64
6.66
6.68
6.7
6.72
6.74
State Plane Coordinate, X (m)
x 10^5

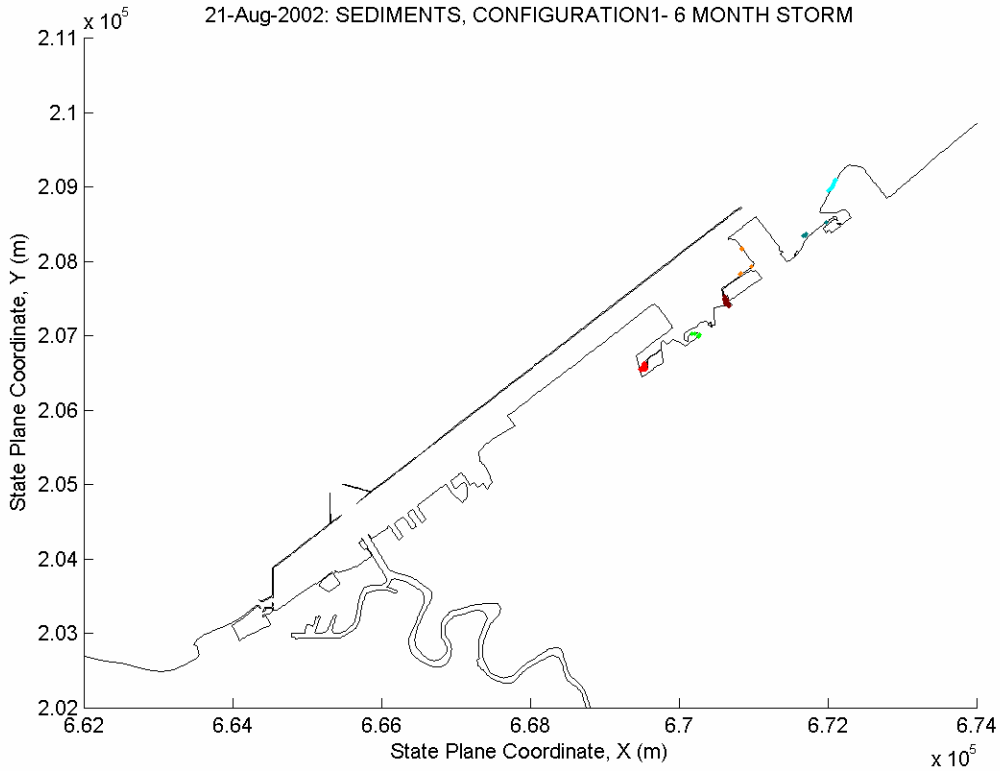
21-Aug-2002: SEDIMENTS, CONFIGURATION1- 6 MONTH STORM
x 10^5
2.11
2.1
2.09
2.08
2.07
2.06
2.05
2.04
2.03
2.02
State Plane Coordinate, Y (m)
6.62
6.64
6.66
6.68
6.7
6.72
6.74
State Plane Coordinate, X (m)
x 10^5

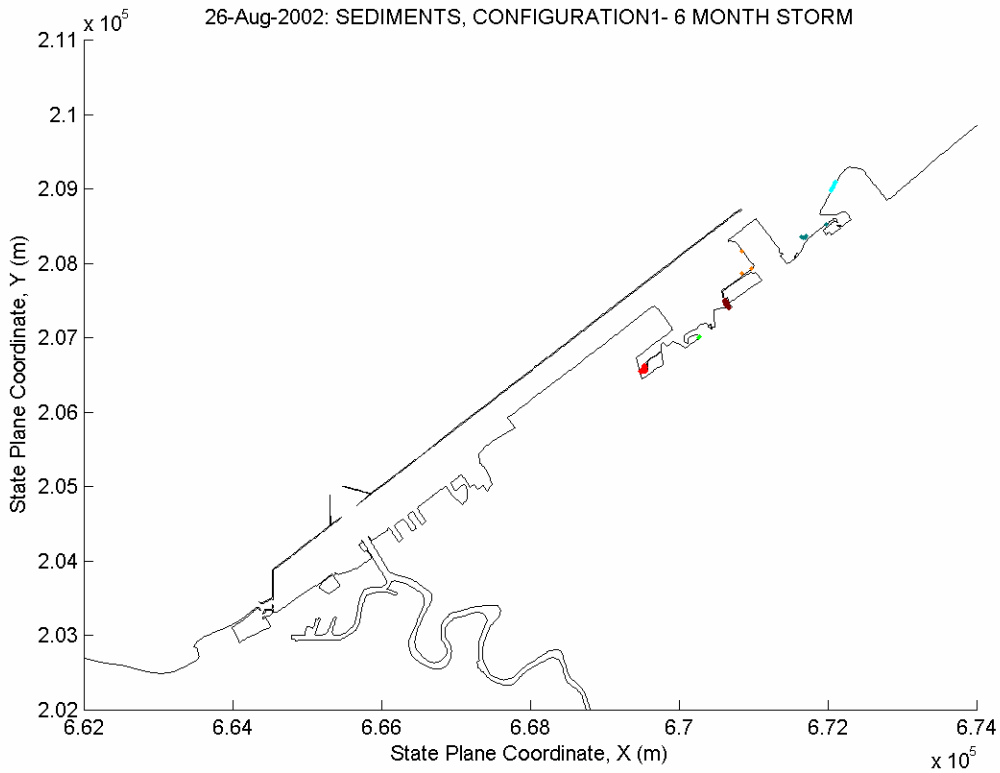
26-Aug-2002: SEDIMENTS, CONFIGURATION1- 6 MONTH STORM
x 10^5
2.11
2.1
2.09
2.08
2.07
2.06
2.05
2.04
2.03
2.02
State Plane Coordinate, Y (m)
6.62
6.64
6.66
6.68
6.7
6.72
6.74
State Plane Coordinate, X (m)
x 10^5

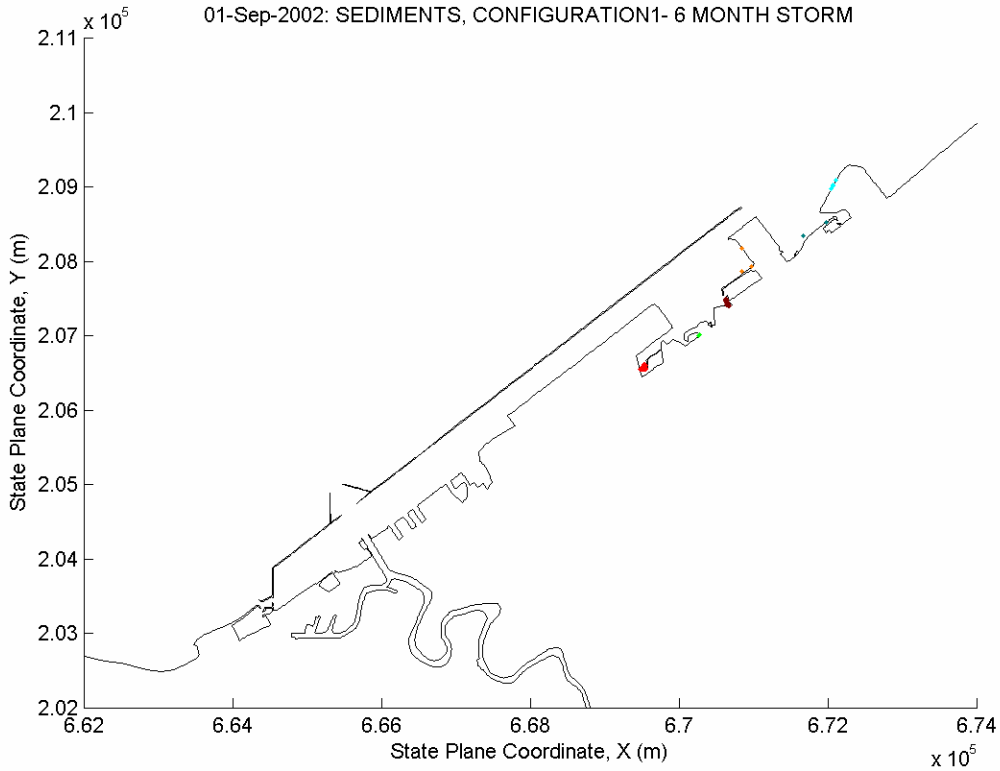
01-Sep-2002: SEDIMENTS, CONFIGURATION1- 6 MONTH STORM
x 10^5
2.11
2.1
2.09
2.08
2.07
2.06
2.05
2.04
2.03
2.02
State Plane Coordinate, Y (m)
6.62
6.64
6.66
6.68
6.7
6.72
6.74
State Plane Coordinate, X (m)
x 10^5

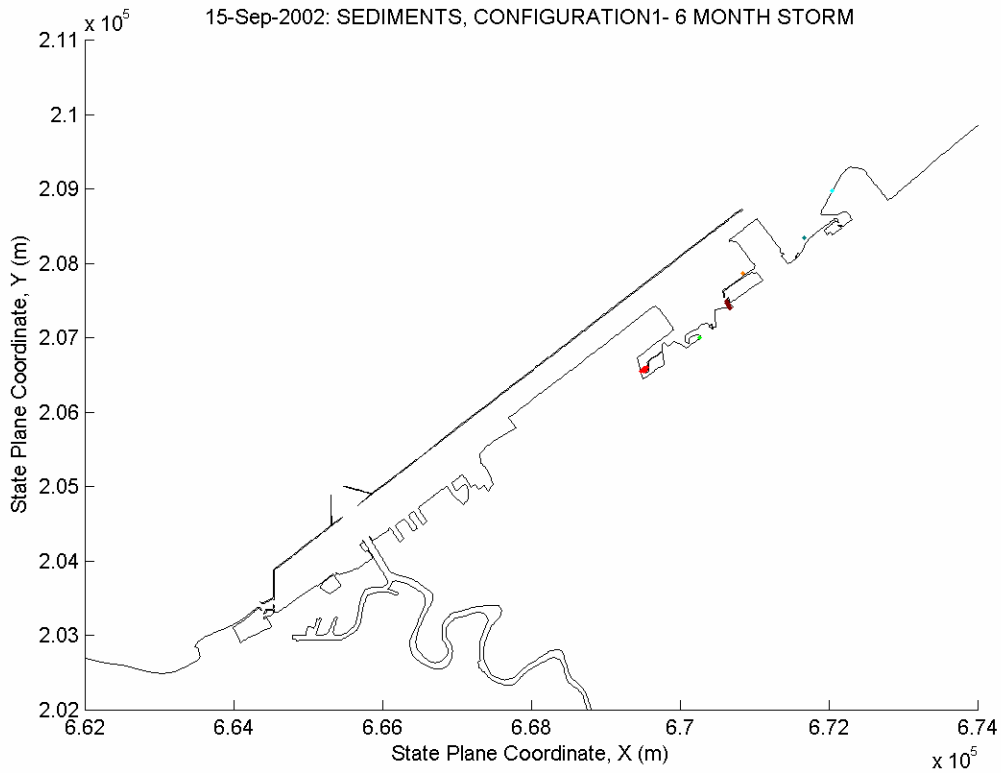
15-Sep-2002: SEDIMENTS, CONFIGURATION1- 6 MONTH STORM
x 10^5
2.11
2.1
2.09
2.08
2.07
2.06
2.05
2.04
2.03
2.02
State Plane Coordinate, Y (m)
6.62
6.64
6.66
6.68
6.7
6.72
6.74
State Plane Coordinate, X (m)
x 10^5

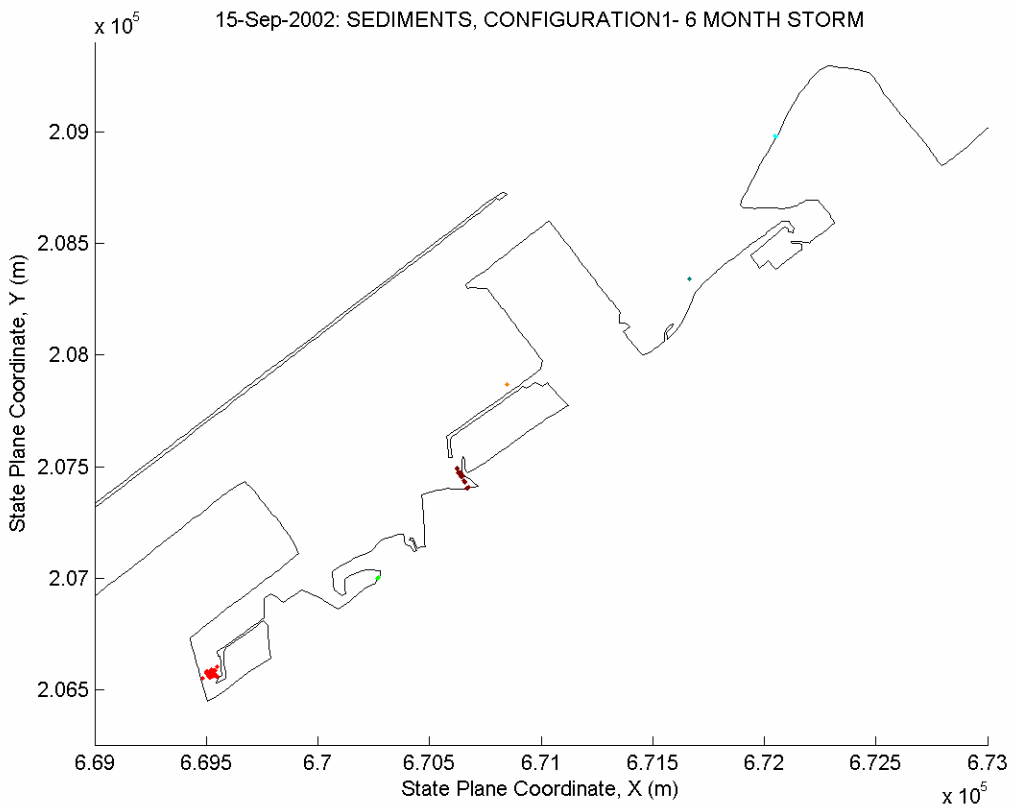
15-Sep-2002: SEDIMENTS, CONFIGURATION1- 6 MONTH STORM
x 10^5
2.09
2.085
2.08
2.075
2.07
2.065
State Plane Coordinate, Y (m)
6.69
6.695
6.7
6.705
6.71
6.715
6.72
6.725
6.73
State Plane Coordinate, X (m)
x 10^5

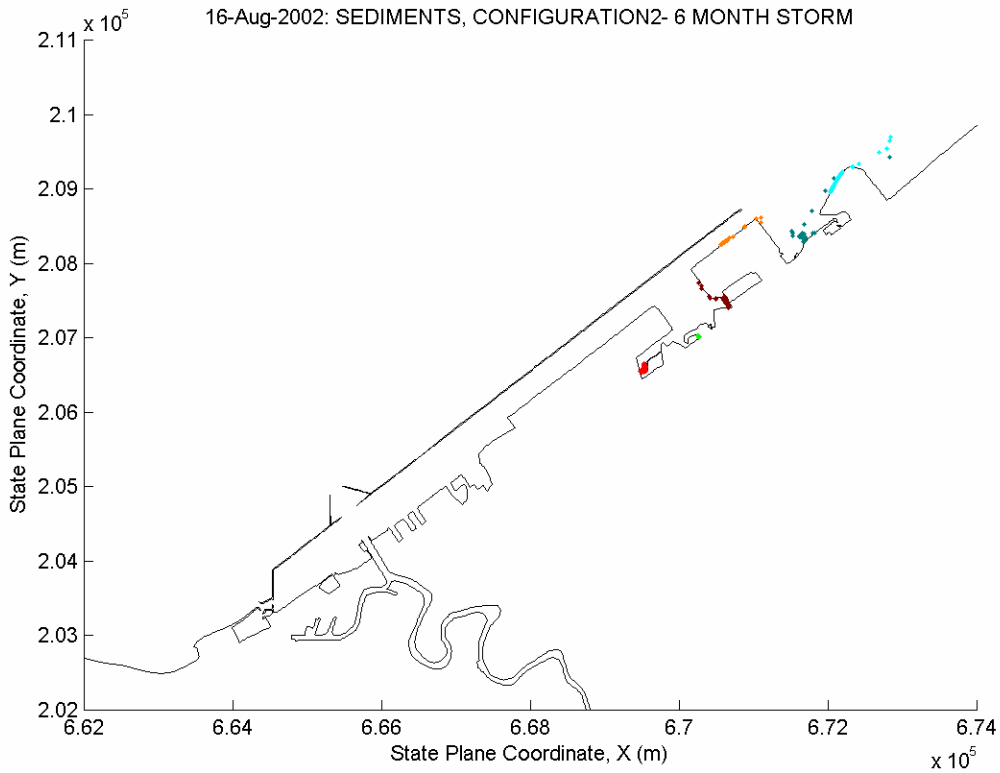
16-Aug-2002: SEDIMENTS, CONFIGURATION2- 6 MONTH STORM
x 10^5
2.11
2.1
2.09
2.08
2.07
2.06
2.05
2.04
2.03
2.02
State Plane Coordinate, Y (m)
6.62
6.64
6.66
6.68
6.7
6.72
6.74
State Plane Coordinate, X (m)
x 10^5

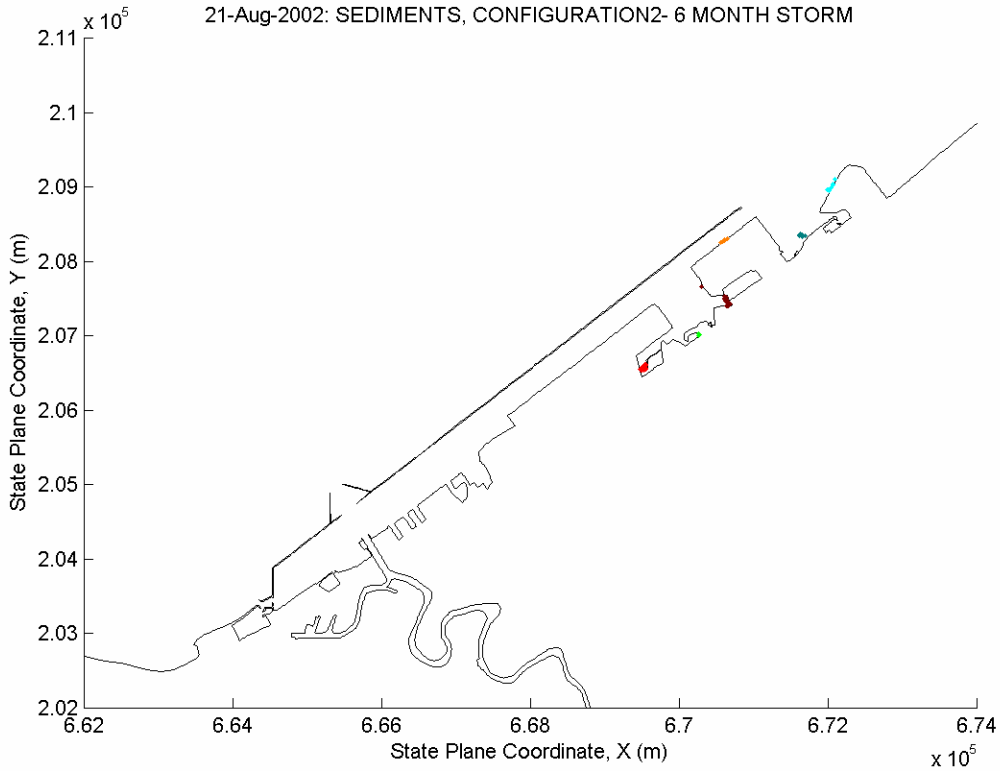
21-Aug-2002: SEDIMENTS, CONFIGURATION2- 6 MONTH STORM
x 10^5
2.11
2.1
2.09
2.08
2.07
2.06
2.05
2.04
2.03
2.02
State Plane Coordinate, Y (m)
6.62
6.64
6.66
6.68
6.7
6.72
6.74
State Plane Coordinate, X (m)
x 10^5

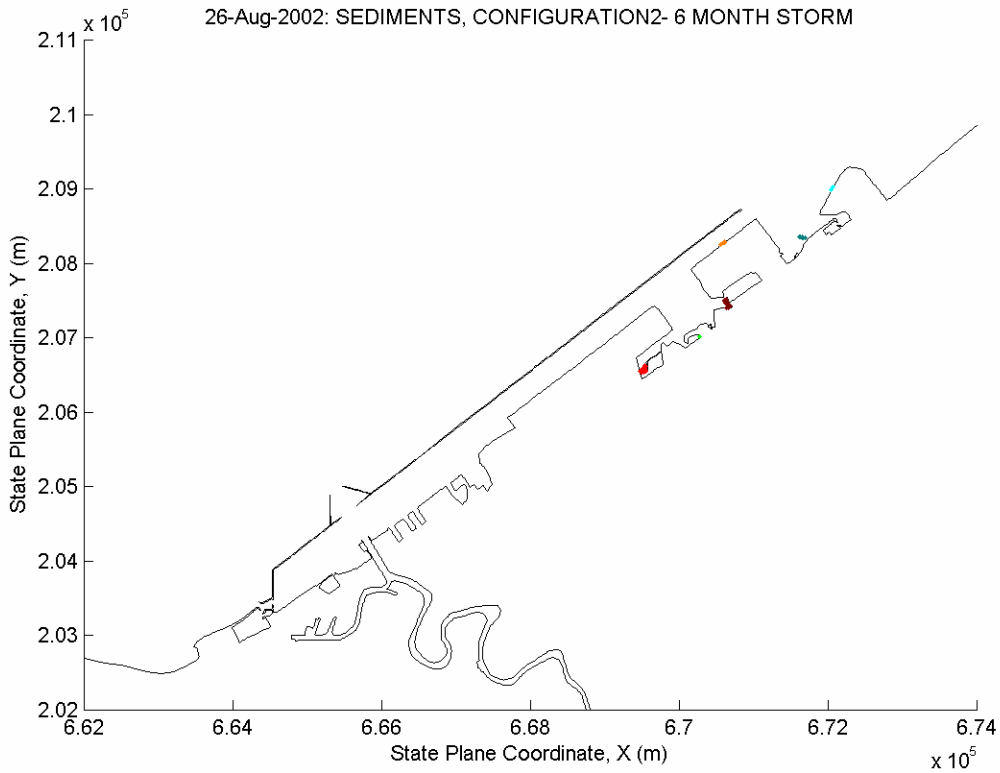
26-Aug-2002: SEDIMENTS, CONFIGURATION2- 6 MONTH STORM
x 10^5
2.11
2.1
2.09
2.08
2.07
2.06
2.05
2.04
2.03
2.02
State Plane Coordinate, Y (m)
6.62
6.64
6.66
6.68
6.7
6.72
6.74
State Plane Coordinate, X (m)
x 10^5

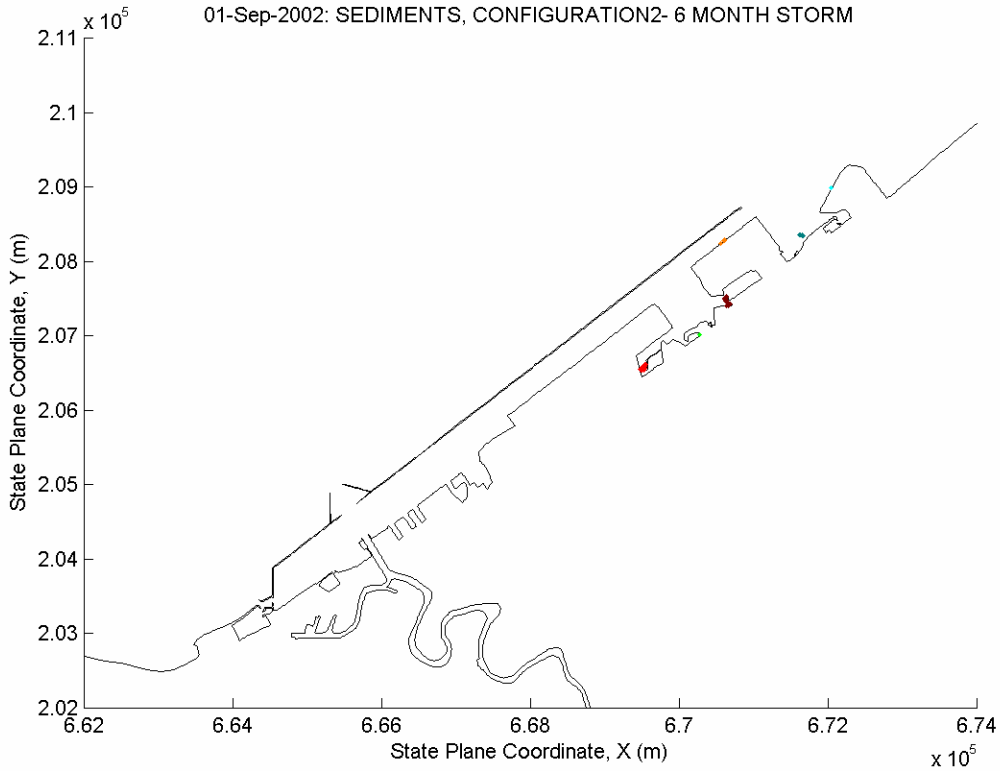
01-Sep-2002: SEDIMENTS, CONFIGURATION2- 6 MONTH STORM
x 10^5
2.11
2.1
2.09
2.08
2.07
2.06
2.05
2.04
2.03
2.02
State Plane Coordinate, Y (m)
6.62
6.64
6.66
6.68
6.7
6.72
6.74
State Plane Coordinate, X (m)
x 10^5

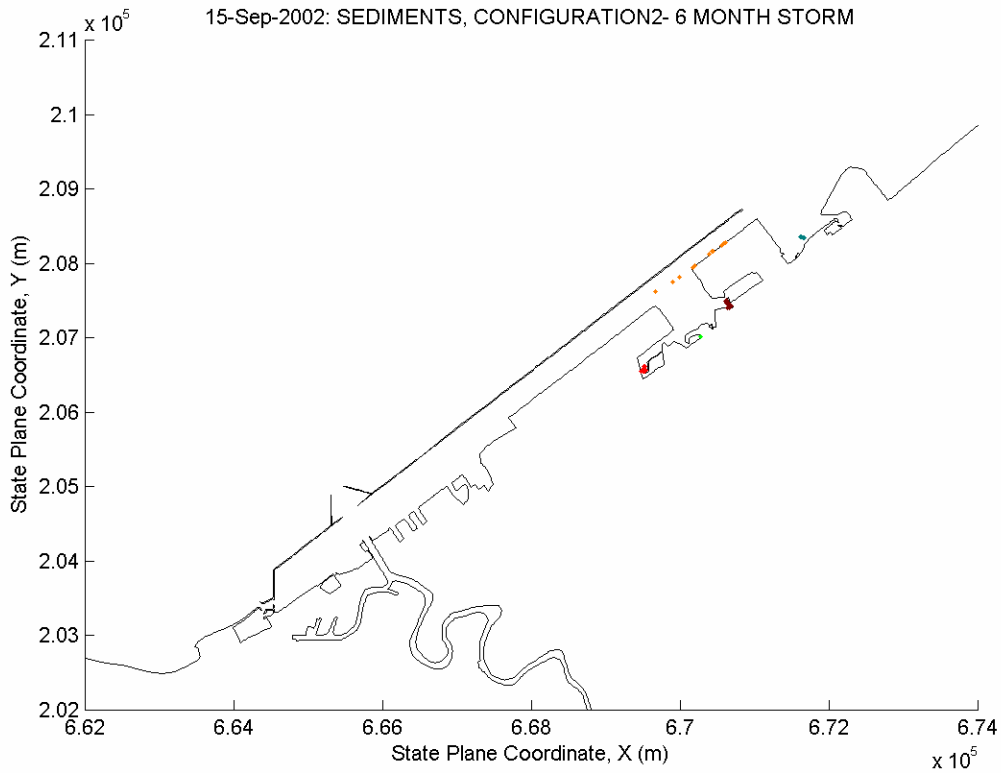
15-Sep-2002: SEDIMENTS, CONFIGURATION2- 6 MONTH STORM
x 10^5
2.11
2.1
2.09
2.08
2.07
2.06
2.05
2.04
2.03
2.02
State Plane Coordinate, Y (m)
6.62
6.64
6.66
6.68
6.7
6.72
6.74
State Plane Coordinate, X (m)
x 10^5

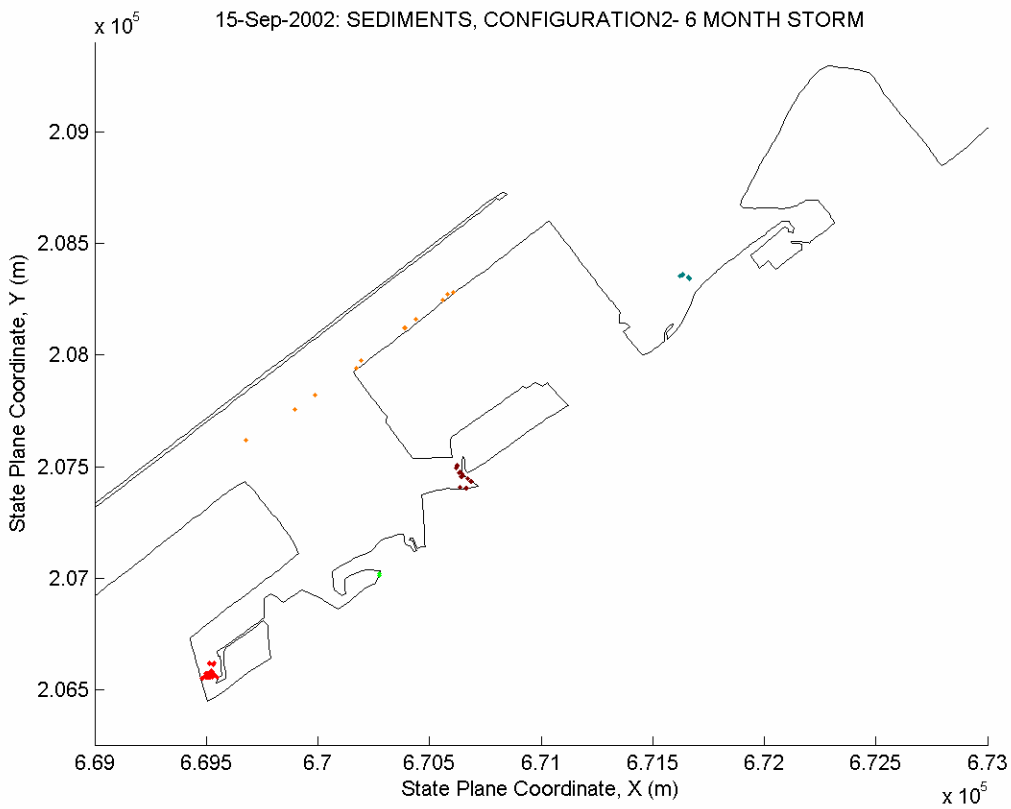
15-Sep-2002: SEDIMENTS, CONFIGURATION2- 6 MONTH STORM
x 10^5
2.09
2.085
2.08
2.075
2.07
2.065
State Plane Coordinate, Y (m)
6.69
6.695
6.7
6.705
6.71
6.715
6.72
6.725
6.73
State Plane Coordinate, X (m)
x 10^5

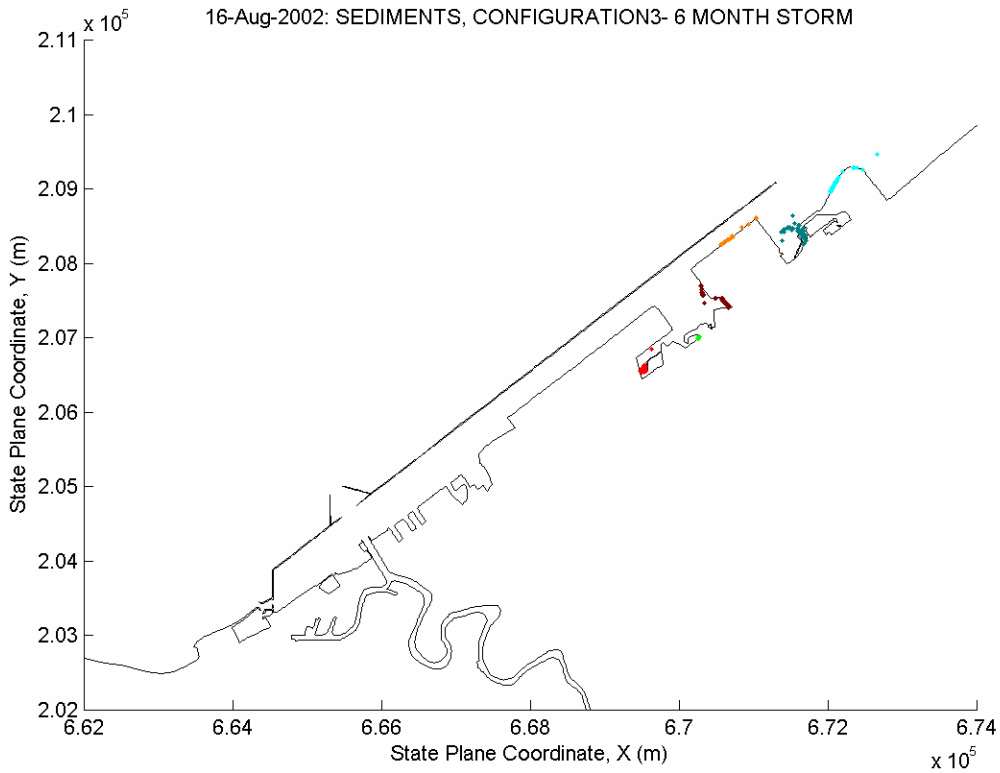
16-Aug-2002: SEDIMENTS, CONFIGURATION3- 6 MONTH STORM
x 10^5
2.11
2.1
2.09
2.08
2.07
2.06
2.05
2.04
2.03
2.02
State Plane Coordinate, Y (m)
6.62
6.64
6.66
6.68
6.7
6.72
6.74
State Plane Coordinate, X (m)
x 10^5

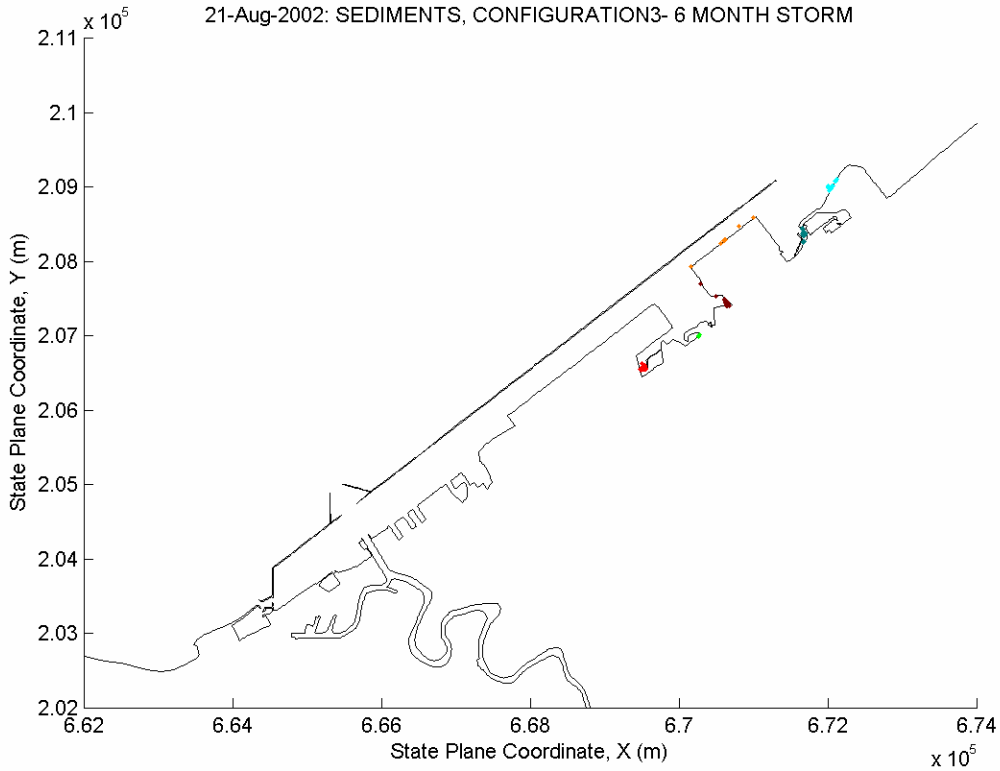
21-Aug-2002: SEDIMENTS, CONFIGURATION3- 6 MONTH STORM
x 10^5
2.11
2.1
2.09
2.08
2.07
2.06
2.05
2.04
2.03
2.02
State Plane Coordinate, Y (m)
6.62
6.64
6.66
6.68
6.7
6.72
6.74
State Plane Coordinate, X (m)
x 10^5

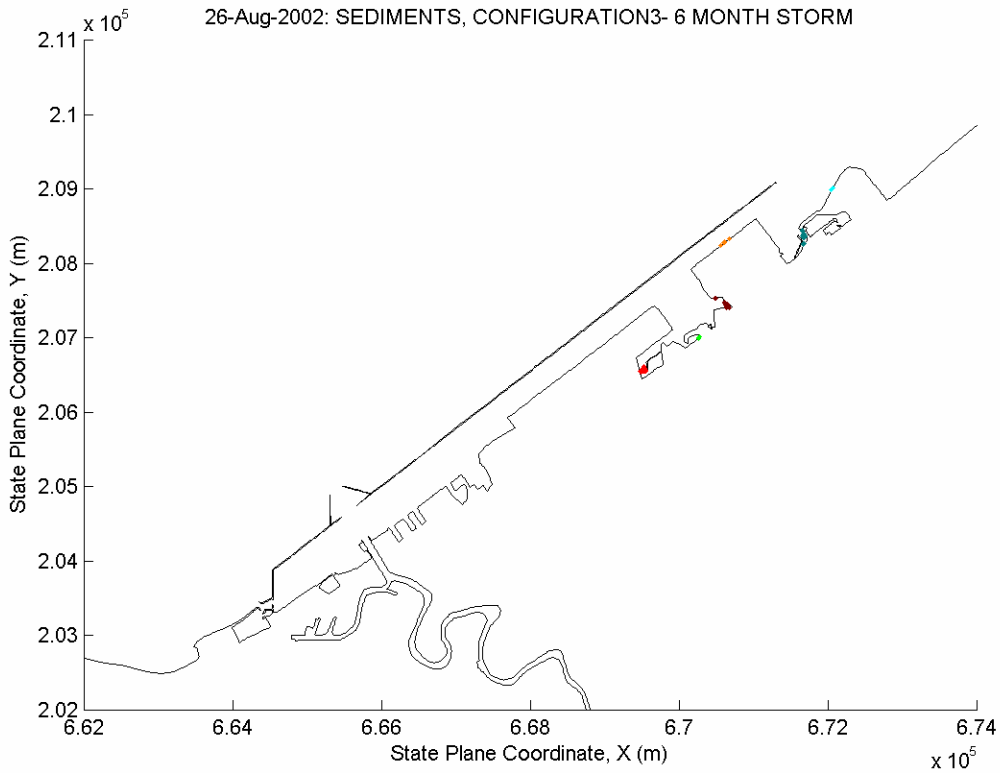
26-Aug-2002: SEDIMENTS, CONFIGURATION3- 6 MONTH STORM
x 10^5
2.11
2.1
2.09
2.08
2.07
2.06
2.05
2.04
2.03
2.02
State Plane Coordinate, Y (m)
6.62
6.64
6.66
6.68
6.7
6.72
6.74
State Plane Coordinate, X (m)
x 10^5

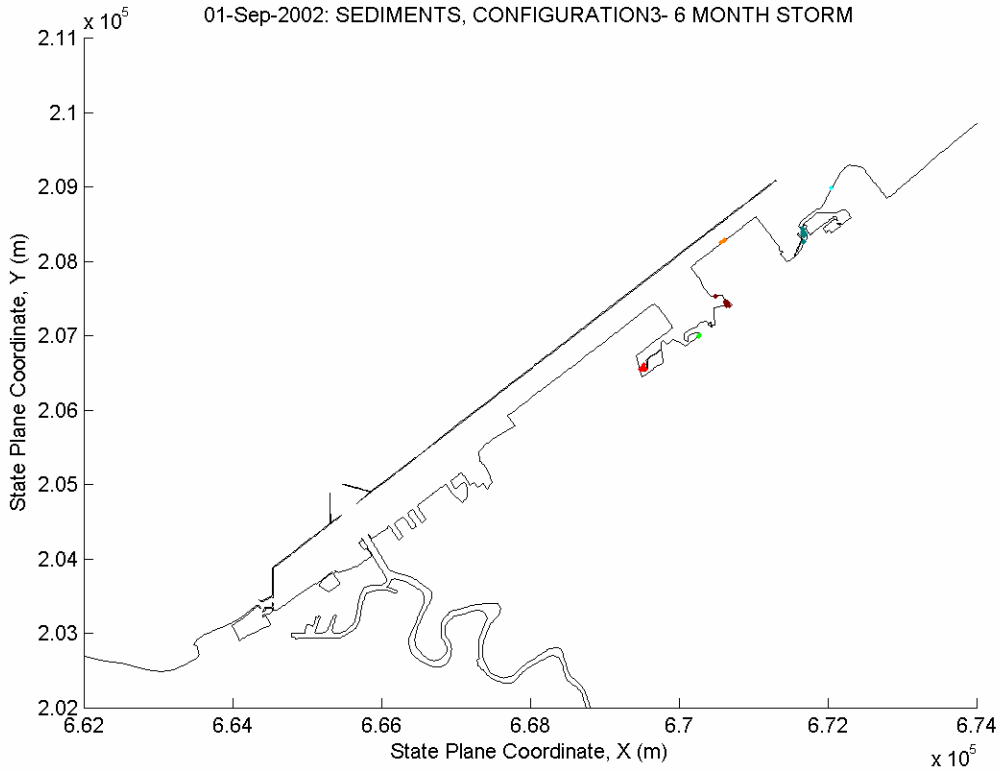
01-Sep-2002: SEDIMENTS, CONFIGURATION3- 6 MONTH STORM
x 10^5
2.11
2.1
2.09
2.08
2.07
2.06
2.05
2.04
2.03
2.02
State Plane Coordinate, Y (m)
6.62
6.64
6.66
6.68
6.7
6.72
6.74
State Plane Coordinate, X (m)
x 10^5

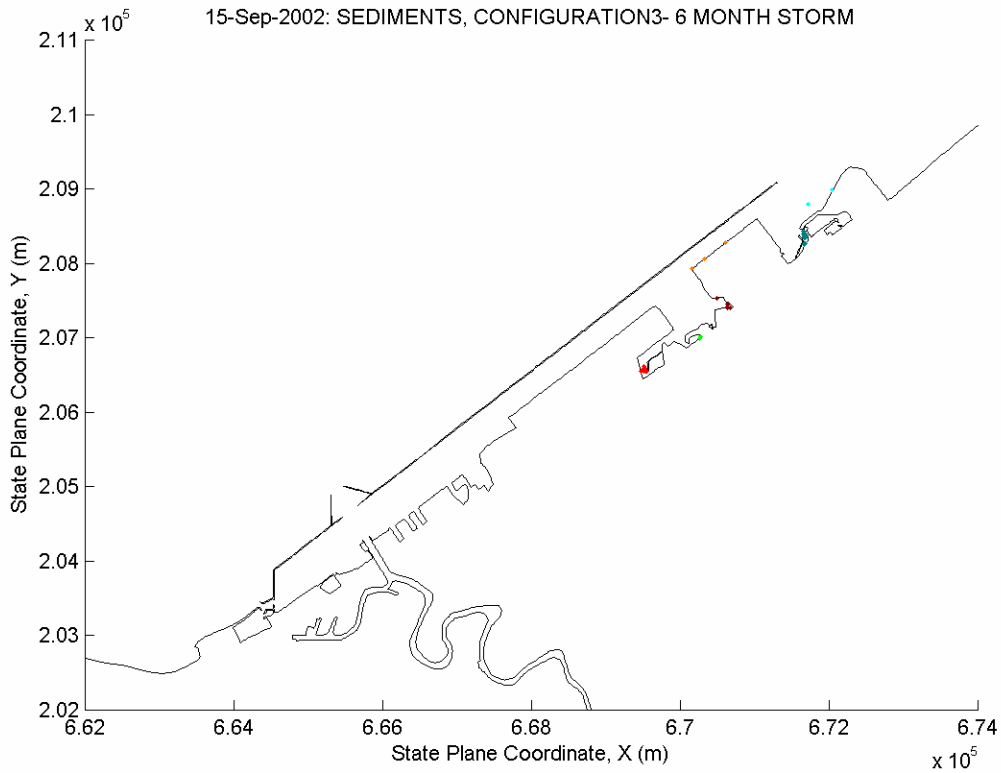
15-Sep-2002: SEDIMENTS, CONFIGURATION3- 6 MONTH STORM
x 10^5
2.11
2.1
2.09
2.08
2.07
2.06
2.05
2.04
2.03
2.02
State Plane Coordinate, Y (m)
6.62
6.64
6.66
6.68
6.7
6.72
6.74
State Plane Coordinate, X (m)
x 10^5

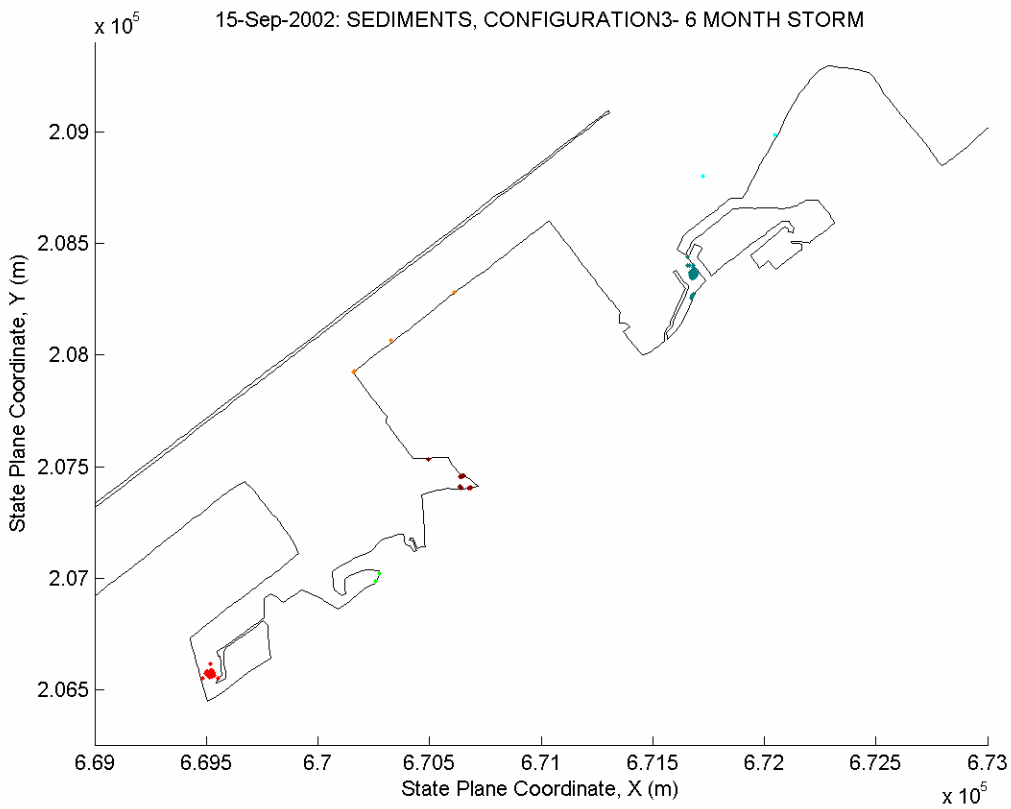
15-Sep-2002: SEDIMENTS, CONFIGURATION3- 6 MONTH STORM
x 10^5
2.09
2.085
2.08
2.075
2.07
2.065
State Plane Coordinate, Y (m)
6.69
6.695
6.7
6.705
6.71
6.715
6.72
6.725
6.73
State Plane Coordinate, X (m)
x 10^5

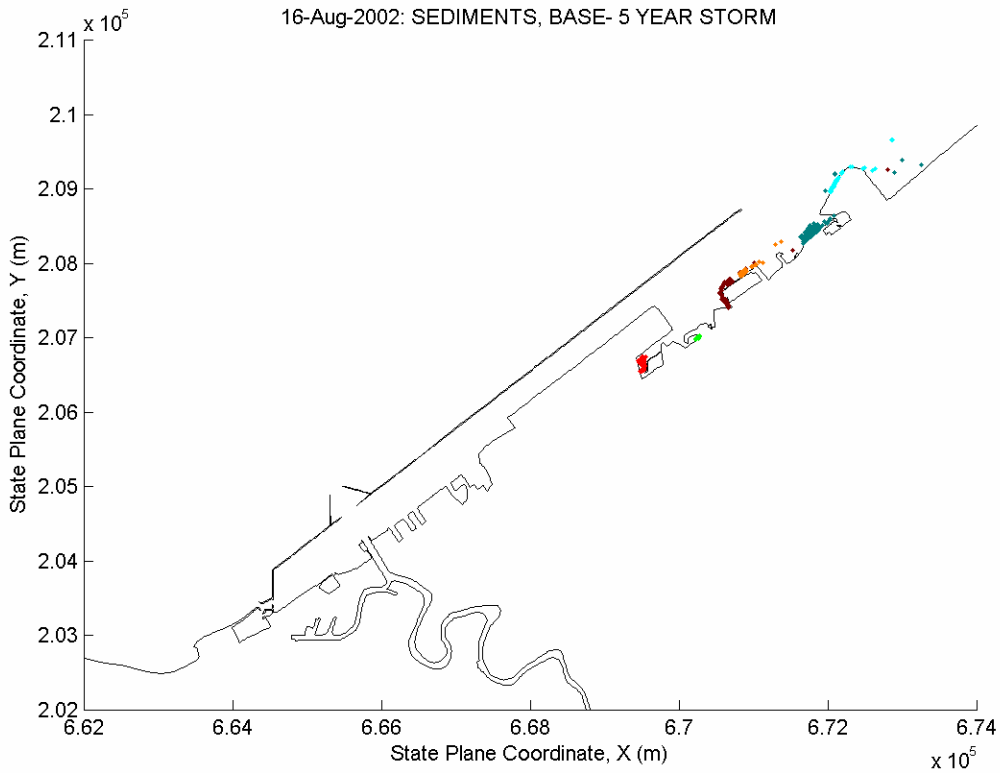
16-Aug-2002: SEDIMENTS, BASE- 5 YEAR STORM
x 10^5
2.11
2.1
2.09
2.08
2.07
2.06
2.05
2.04
2.03
2.02
State Plane Coordinate, Y (m)
6.62
6.64
6.66
6.68
6.7
6.72
6.74
State Plane Coordinate, X (m)
x 10^5

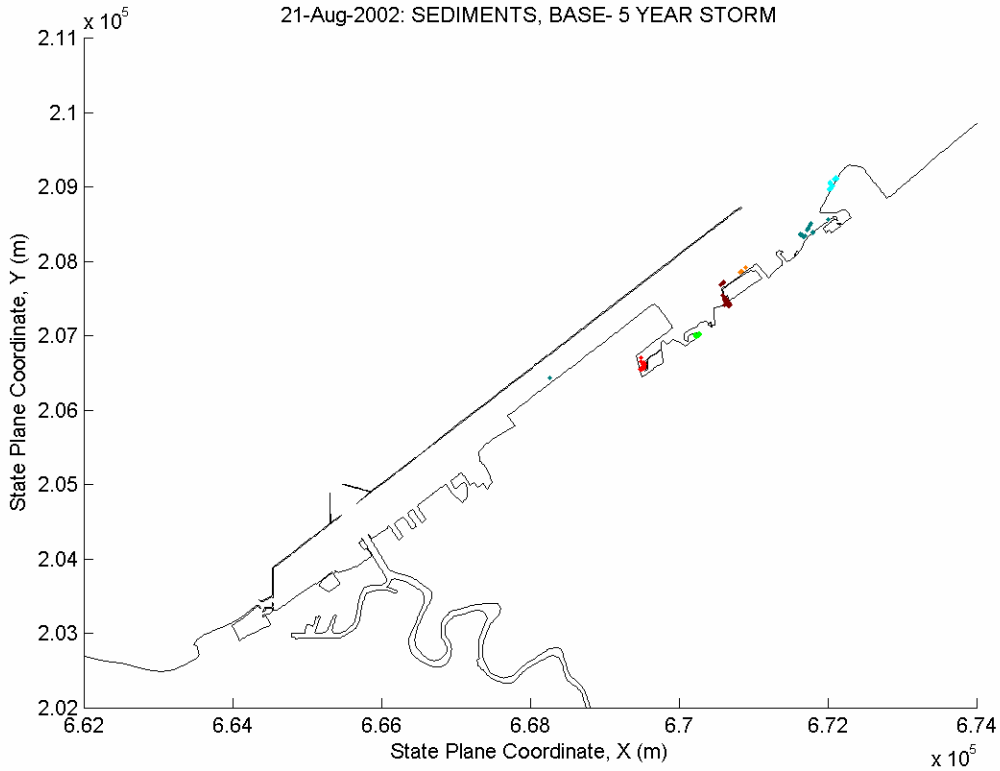
21-Aug-2002: SEDIMENTS, BASE- 5 YEAR STORM
x 10^5
2.11
2.1
2.09
2.08
2.07
2.06
2.05
2.04
2.03
2.02
State Plane Coordinate, Y (m)
6.62
6.64
6.66
6.68
6.7
6.72
6.74
State Plane Coordinate, X (m)
x 10^5

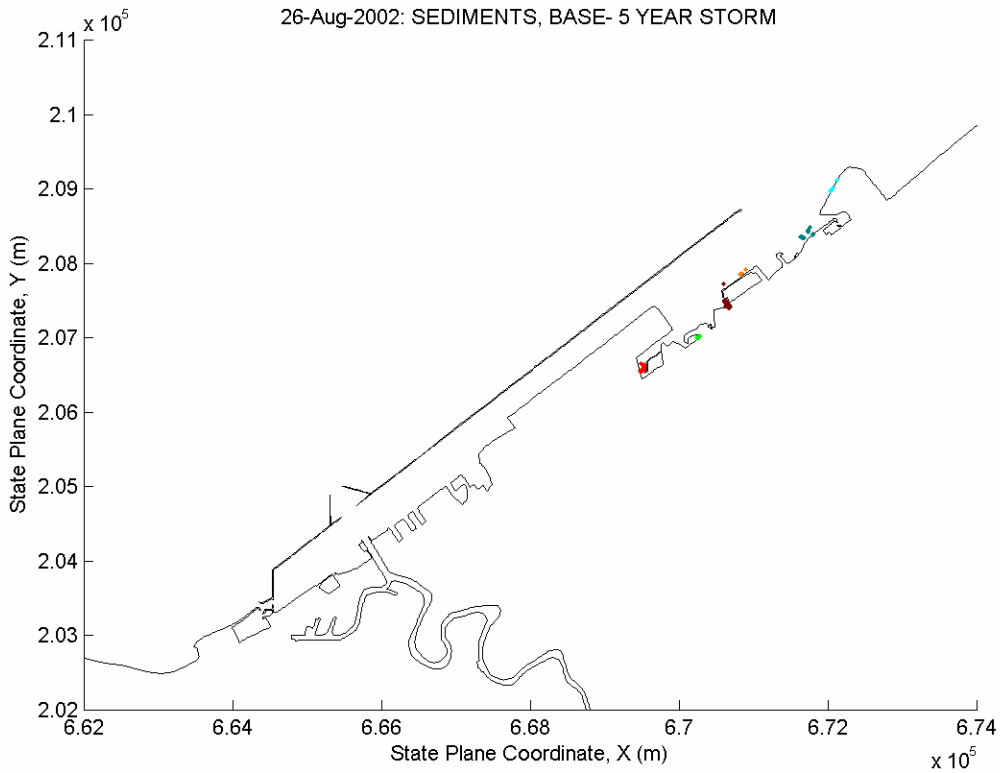
26-Aug-2002: SEDIMENTS, BASE- 5 YEAR STORM
x 10^5
2.11
2.1
2.09
2.08
2.07
2.06
2.05
2.04
2.03
2.02
State Plane Coordinate, Y (m)
6.62
6.64
6.66
6.68
6.7
6.72
6.74
State Plane Coordinate, X (m)
x 10^5

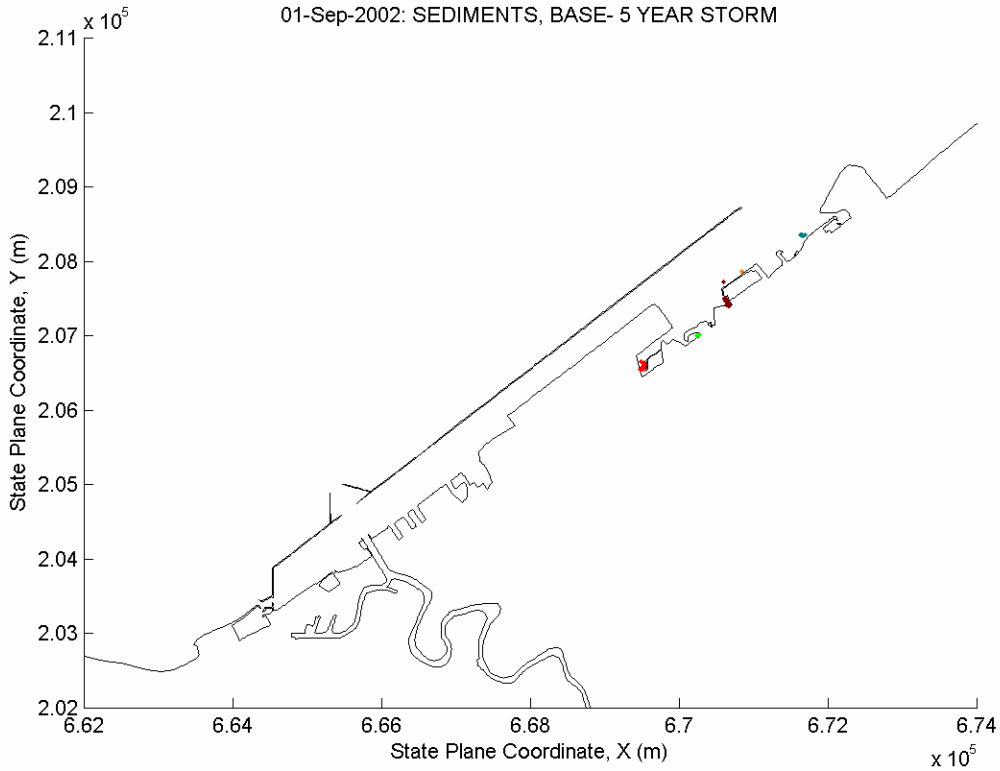
01-Sep-2002: SEDIMENTS, BASE- 5 YEAR STORM
x 10^5
2.11
2.1
2.09
2.08
2.07
2.06
2.05
2.04
2.03
2.02
State Plane Coordinate, Y (m)
6.62
6.64
6.66
6.68
6.7
6.72
6.74
State Plane Coordinate, X (m)
x 10^5

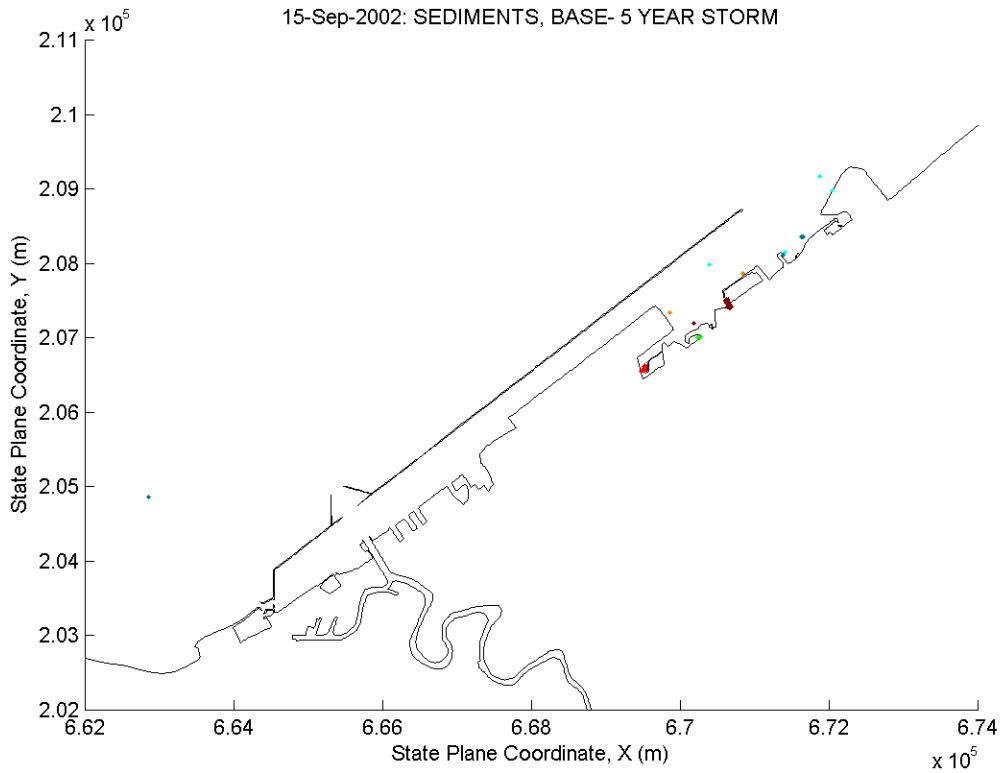
15-Sep-2002: SEDIMENTS, BASE- 5 YEAR STORM
x 10^5
2.11
2.1
2.09
2.08
2.07
2.06
2.05
2.04
2.03
2.02
State Plane Coordinate, Y (m)
6.62
6.64
6.66
6.68
6.7
6.72
6.74
State Plane Coordinate, X (m)
x 10^5

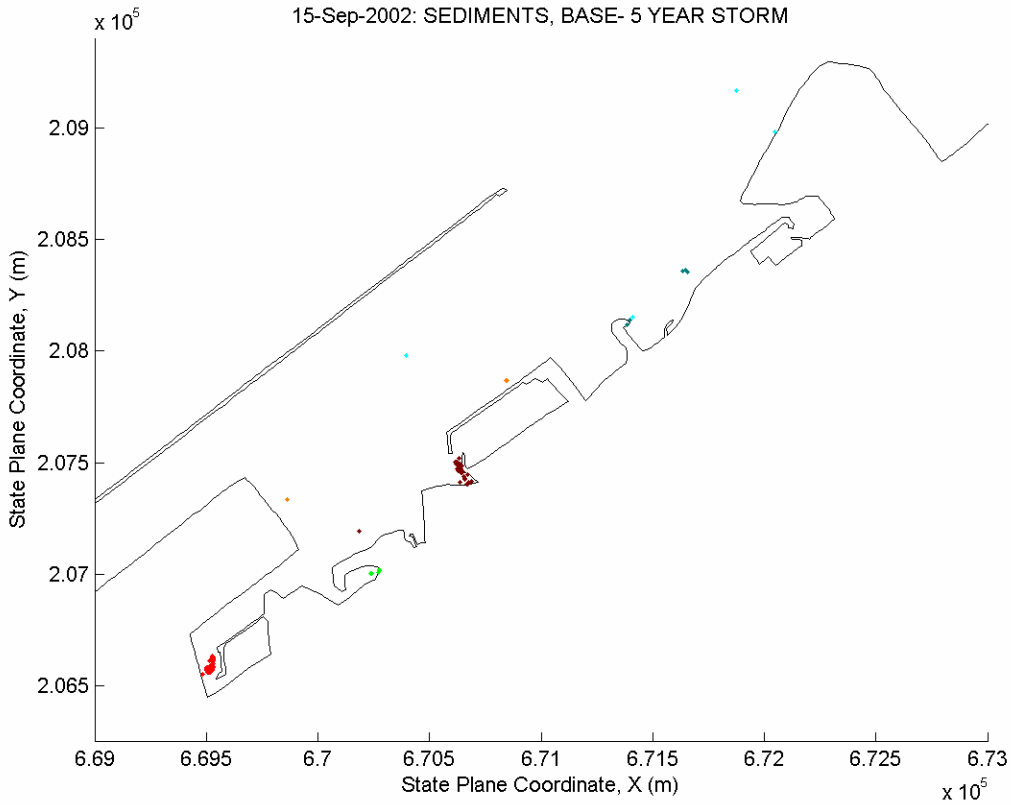
15-Sep-2002: SEDIMENTS, BASE- 5 YEAR STORM
x 10^5
2.09
2.085
2.08
2.075
2.07
2.065
State Plane Coordinate, Y (m)
6.69
6.695
6.7
6.705
6.71
6.715
6.72
6.725
6.73
State Plane Coordinate, X (m)
x 10^5

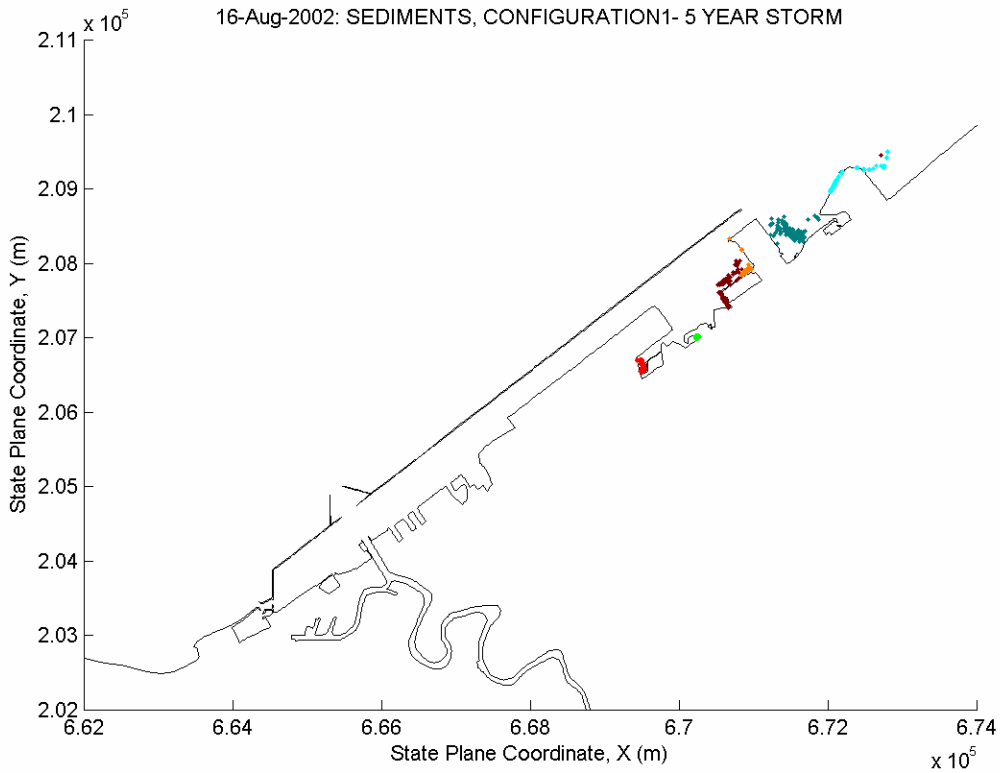
16-Aug-2002: SEDIMENTS, CONFIGURATION1- 5 YEAR STORM
x 10^5
2.11
2.1
2.09
2.08
2.07
2.06
2.05
2.04
2.03
2.02
State Plane Coordinate, Y (m)
6.62
6.64
6.66
6.68
6.7
6.72
6.74
State Plane Coordinate, X (m)
x 10^5

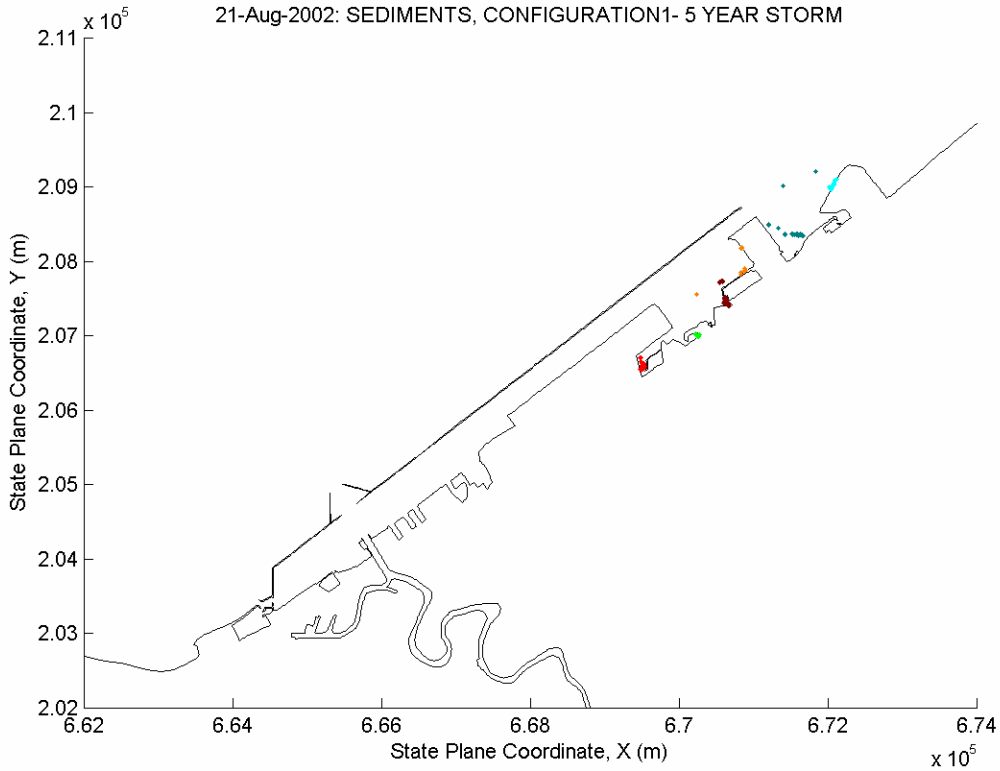
21-Aug-2002: SEDIMENTS, CONFIGURATION1- 5 YEAR STORM
x 10^5
2.11
2.1
2.09
2.08
2.07
2.06
2.05
2.04
2.03
2.02
State Plane Coordinate, Y (m)
6.62
6.64
6.66
6.68
6.7
6.72
6.74
State Plane Coordinate, X (m)
x 10^5

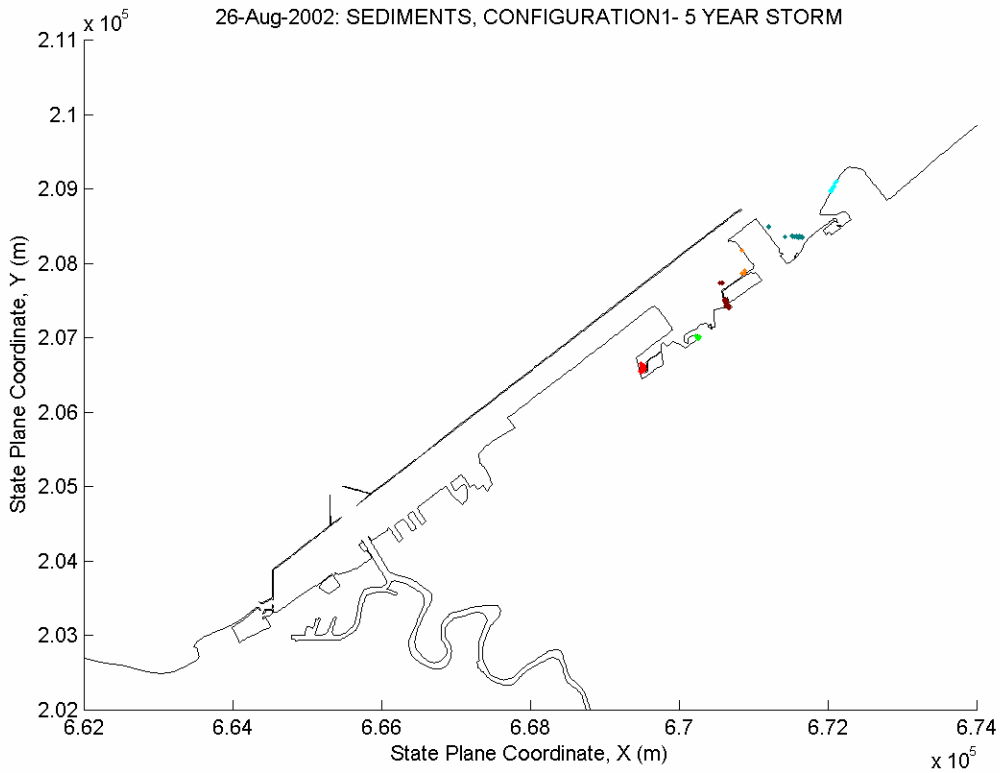
26-Aug-2002: SEDIMENTS, CONFIGURATION1- 5 YEAR STORM
x 10^5
2.11
2.1
2.09
2.08
2.07
2.06
2.05
2.04
2.03
2.02
State Plane Coordinate, Y (m)
6.62
6.64
6.66
6.68
6.7
6.72
6.74
State Plane Coordinate, X (m)
x 10^5

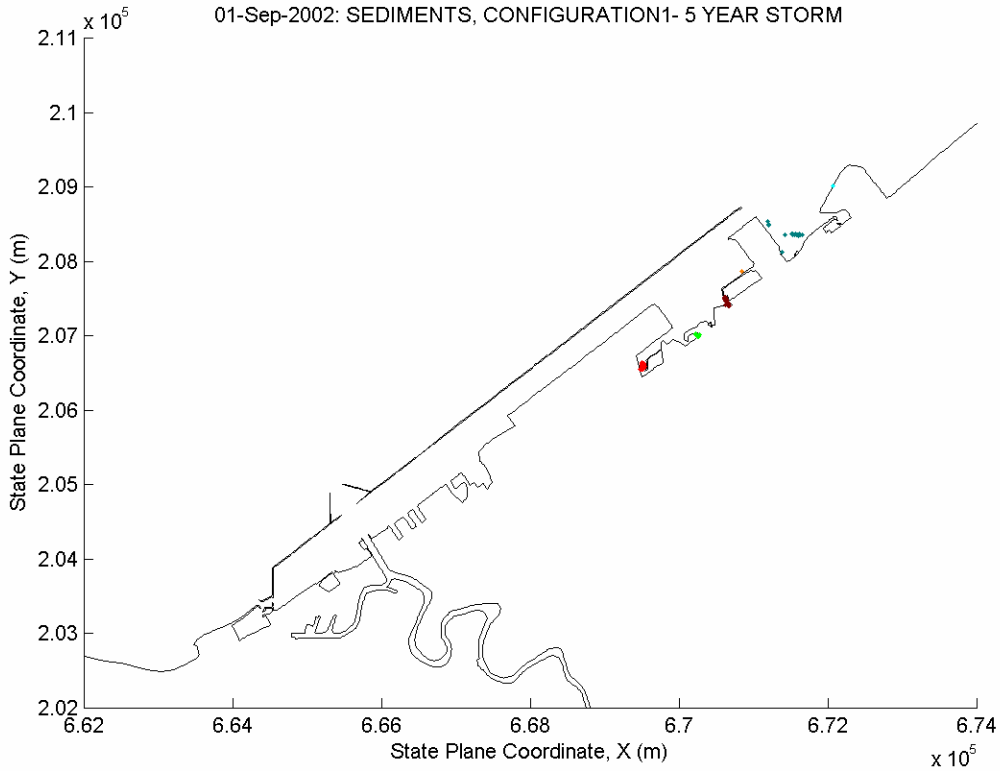
01-Sep-2002: SEDIMENTS, CONFIGURATION1- 5 YEAR STORM
x 10^5
2.11
2.1
2.09
2.08
2.07
2.06
2.05
2.04
2.03
2.02
State Plane Coordinate, Y (m)
6.62
6.64
6.66
6.68
6.7
6.72
6.74
State Plane Coordinate, X (m)
x 10^5

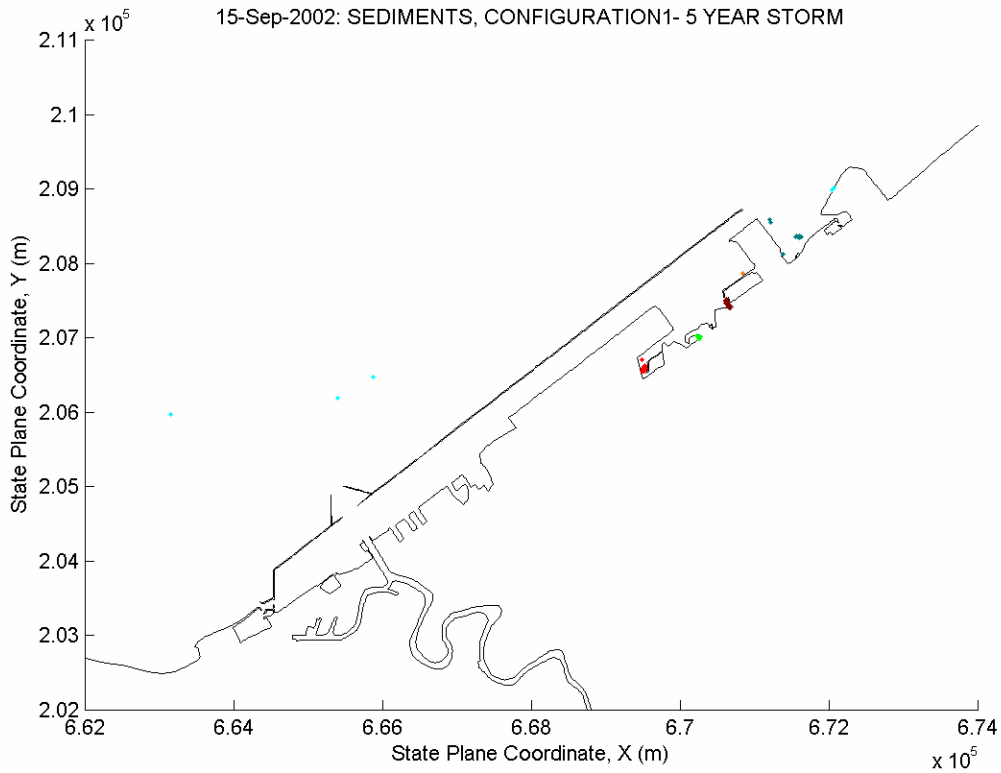
15-Sep-2002: SEDIMENTS, CONFIGURATION1- 5 YEAR STORM
x 10^5
2.11
2.1
2.09
2.08
2.07
2.06
2.05
2.04
2.03
2.02
State Plane Coordinate, Y (m)
6.62
6.64
6.66
6.68
6.7
6.72
6.74
State Plane Coordinate, X (m)
x 10^5

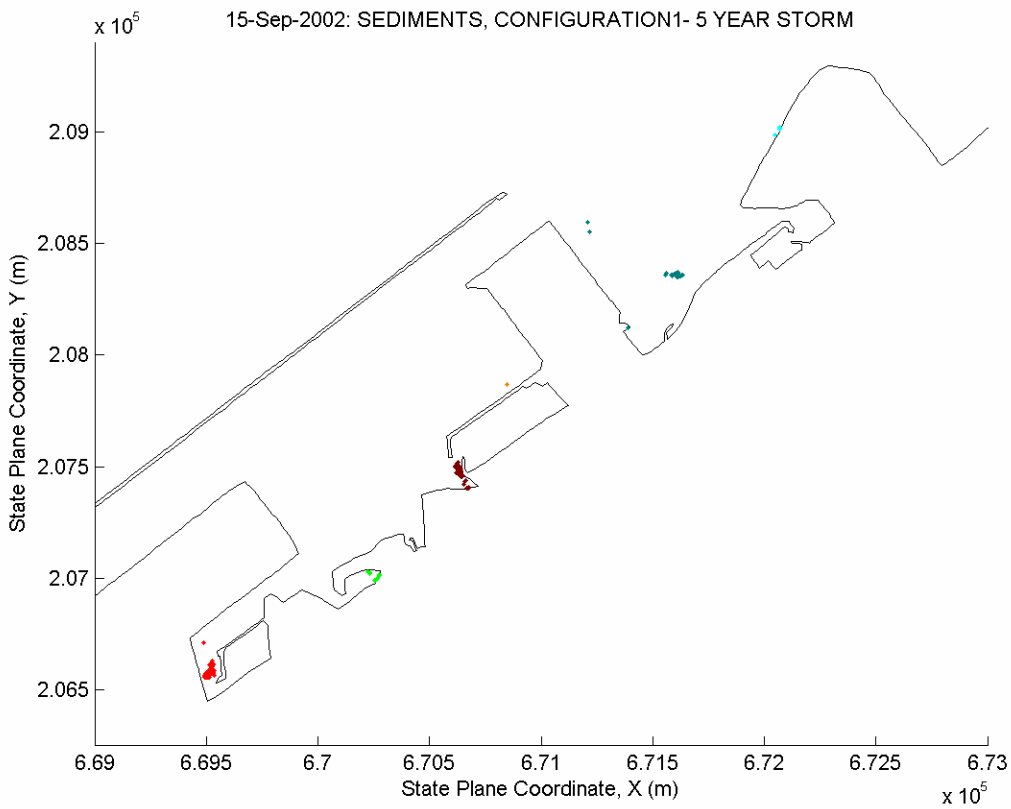
15-Sep-2002: SEDIMENTS, CONFIGURATION1- 5 YEAR STORM
x 10^5
2.09
2.085
2.08
2.075
2.07
2.065
State Plane Coordinate, Y (m)
6.69
6.695
6.7
6.705
6.71
6.715
6.72
6.725
6.73
State Plane Coordinate, X (m)
x 10^5

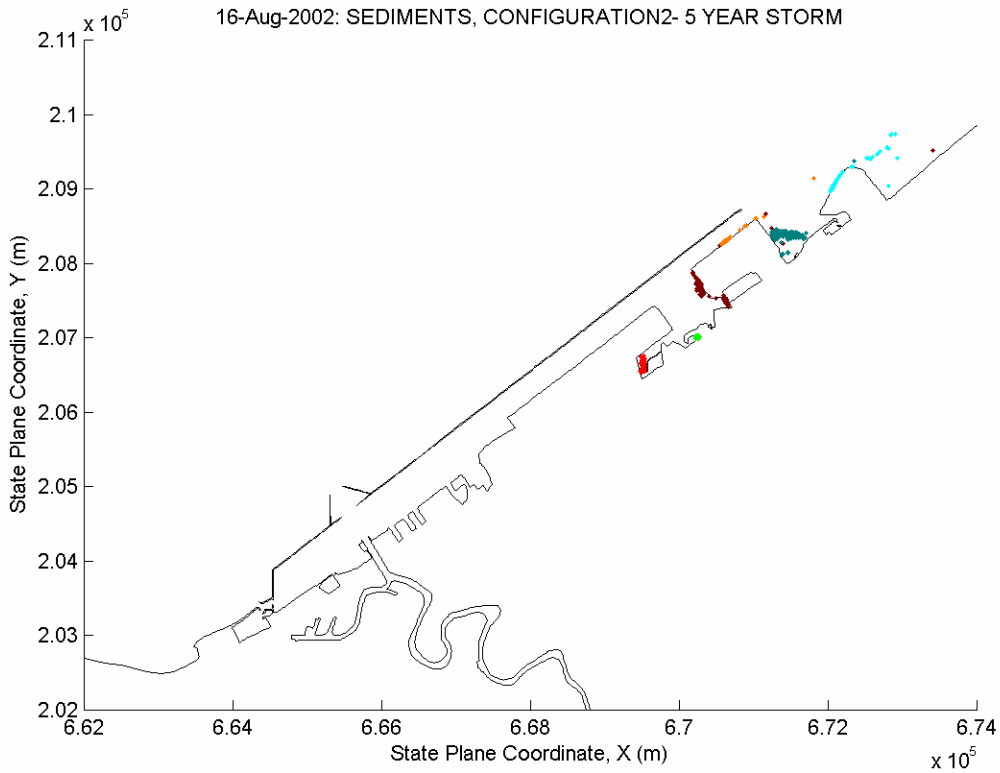
16-Aug-2002: SEDIMENTS, CONFIGURATION2- 5 YEAR STORM
x 10^5
2.11
2.1
2.09
2.08
2.07
2.06
2.05
2.04
2.03
2.02
State Plane Coordinate, Y (m)
6.62
6.64
6.66
6.68
6.7
6.72
6.74
State Plane Coordinate, X (m)
x 10^5

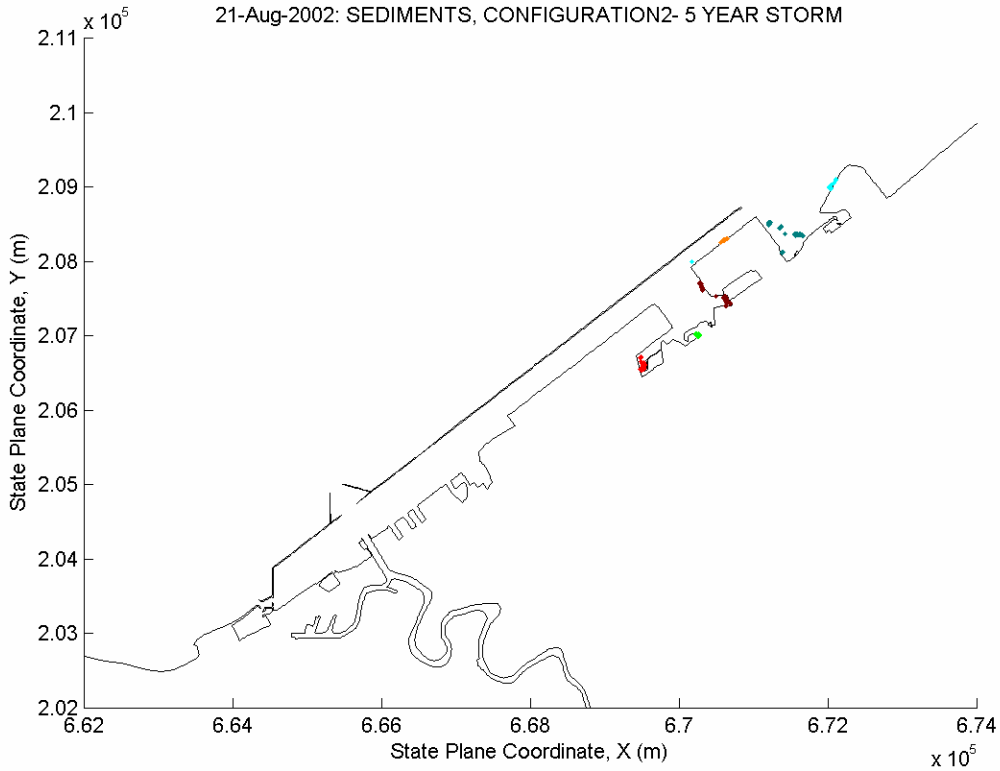
21-Aug-2002: SEDIMENTS, CONFIGURATION2- 5 YEAR STORM
x 10^5
2.11
2.1
2.09
2.08
2.07
2.06
2.05
2.04
2.03
2.02
State Plane Coordinate, Y (m)
6.62
6.64
6.66
6.68
6.7
6.72
6.74
State Plane Coordinate, X (m)
x 10^5

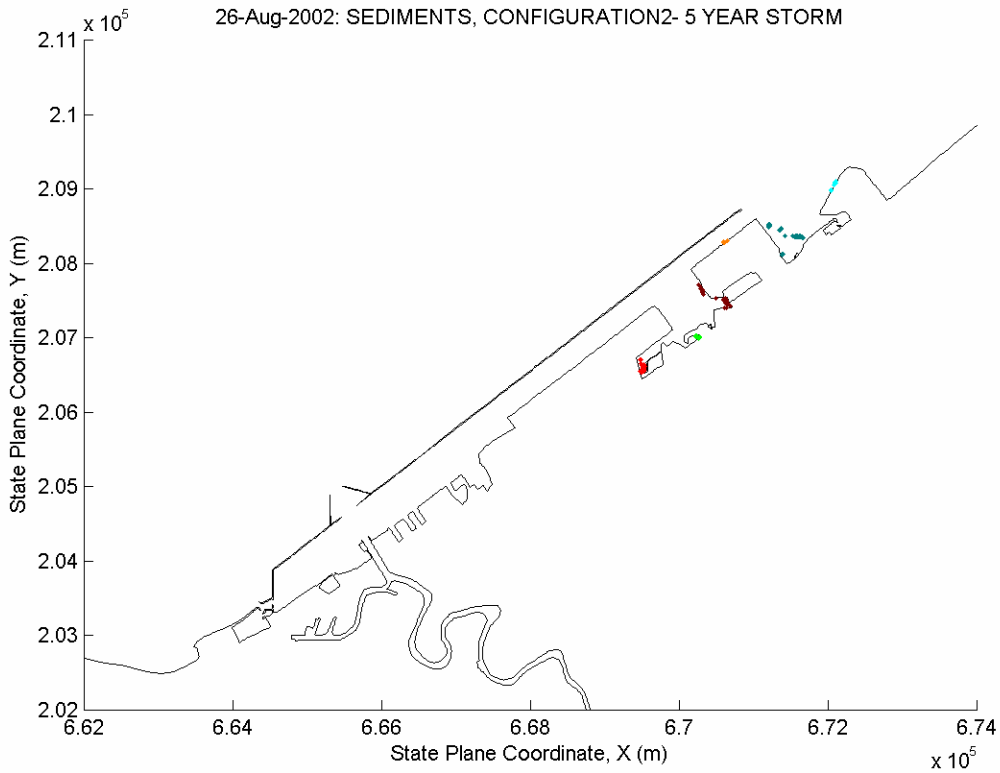
26-Aug-2002: SEDIMENTS, CONFIGURATION2- 5 YEAR STORM
x 10^5
2.11
2.1
2.09
2.08
2.07
2.06
2.05
2.04
2.03
2.02
State Plane Coordinate, Y (m)
6.62
6.64
6.66
6.68
6.7
6.72
6.74
State Plane Coordinate, X (m)
x 10^5

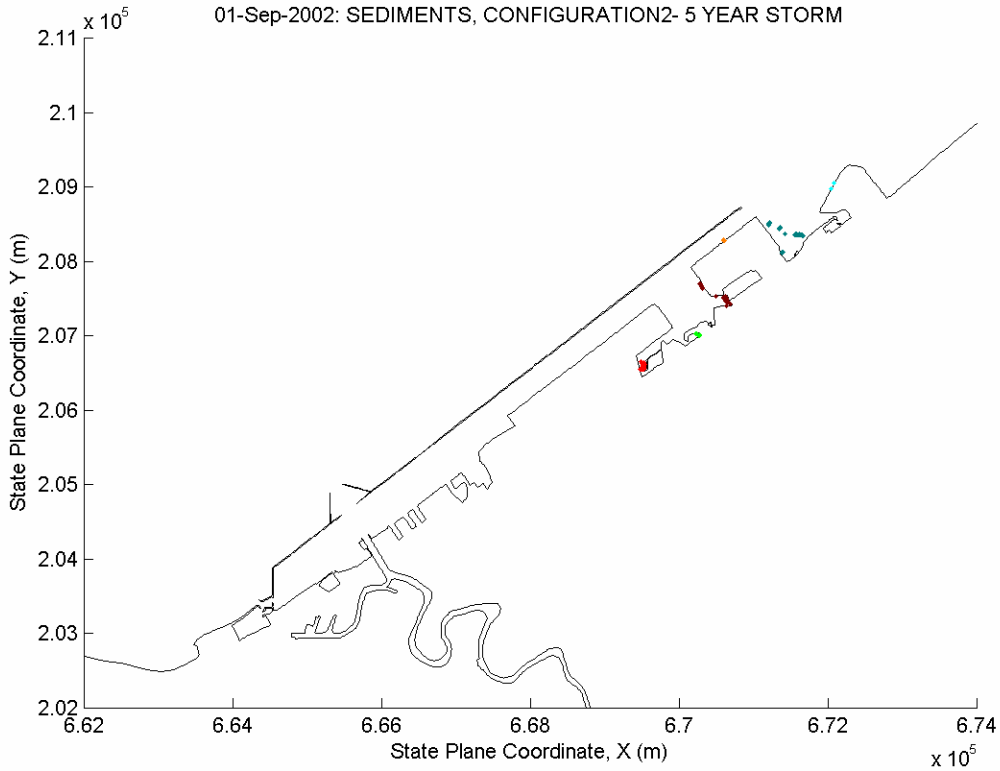
01-Sep-2002: SEDIMENTS, CONFIGURATION2- 5 YEAR STORM
x 10^5
2.11
2.1
2.09
2.08
2.07
2.06
2.05
2.04
2.03
2.02
State Plane Coordinate, Y (m)
6.62
6.64
6.66
6.68
6.7
6.72
6.74
State Plane Coordinate, X (m)
x 10^5

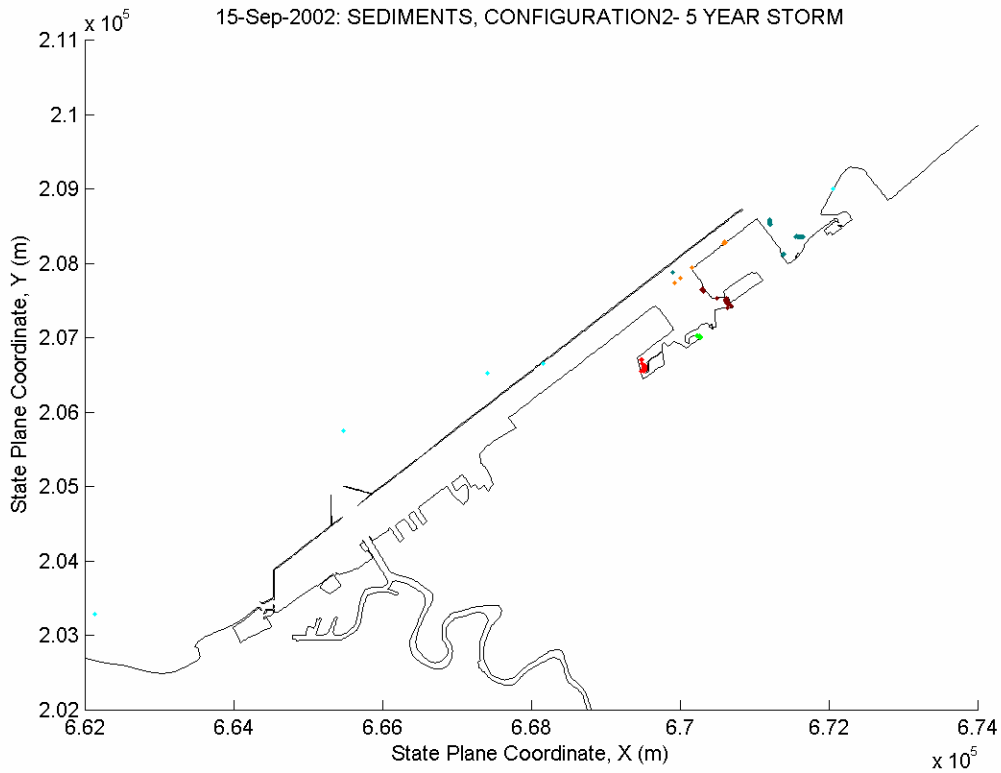
15-Sep-2002: SEDIMENTS, CONFIGURATION2- 5 YEAR STORM
x 10^5
2.11
2.1
2.09
2.08
2.07
2.06
2.05
2.04
2.03
2.02
State Plane Coordinate, Y (m)
6.62
6.64
6.66
6.68
6.7
6.72
6.74
State Plane Coordinate, X (m)
x 10^5

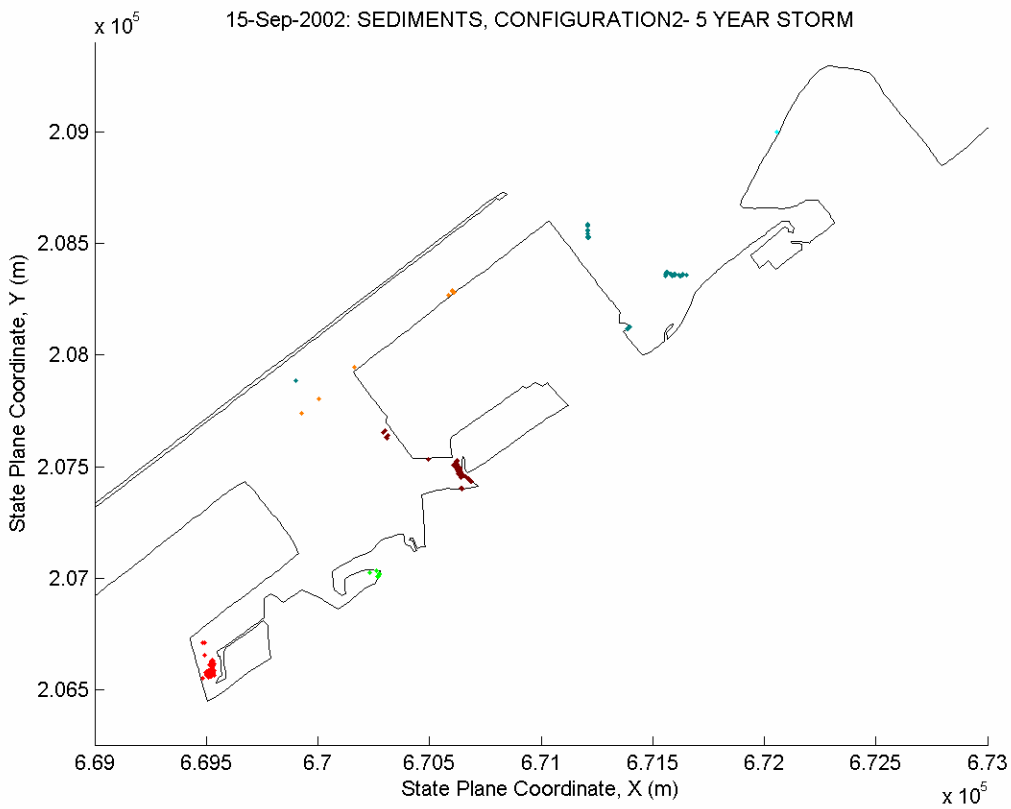
15-Sep-2002: SEDIMENTS, CONFIGURATION2- 5 YEAR STORM
x 10^5
2.09
2.085
2.08
2.075
2.07
2.065
State Plane Coordinate, Y (m)
6.69
6.695
6.7
6.705
6.71
6.715
6.72
6.725
6.73
State Plane Coordinate, X (m)
x 10^5

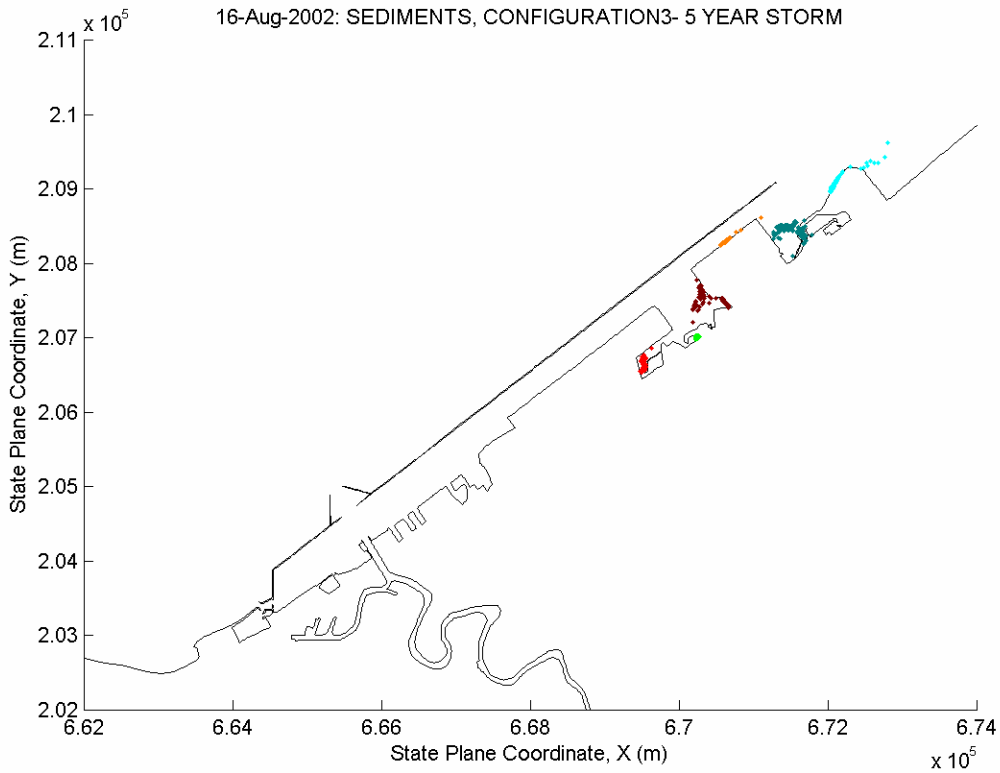
16-Aug-2002: SEDIMENTS, CONFIGURATION3- 5 YEAR STORM
x 10^5
2.11
2.1
2.09
2.08
2.07
2.06
2.05
2.04
2.03
2.02
State Plane Coordinate, Y (m)
6.62
6.64
6.66
6.68
6.7
6.72
6.74
State Plane Coordinate, X (m)
x 10^5

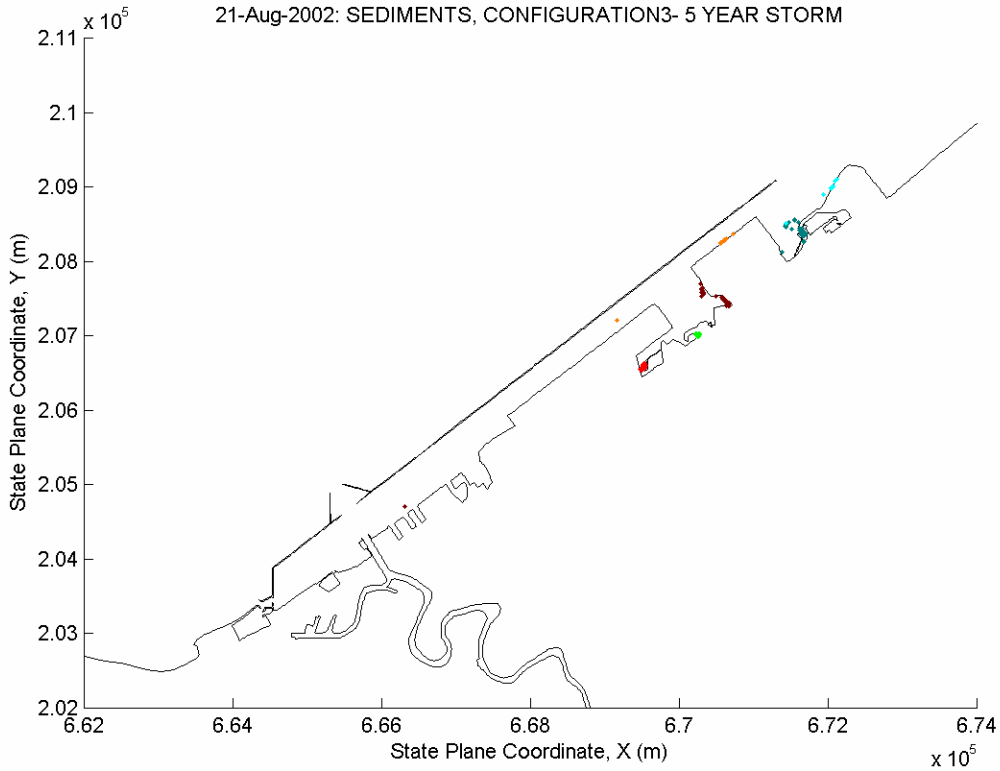
21-Aug-2002: SEDIMENTS, CONFIGURATION3- 5 YEAR STORM
x 10^5
2.11
2.1
2.09
2.08
2.07
2.06
2.05
2.04
2.03
2.02
State Plane Coordinate, Y (m)
6.62
6.64
6.66
6.68
6.7
6.72
6.74
State Plane Coordinate, X (m)
x 10^5

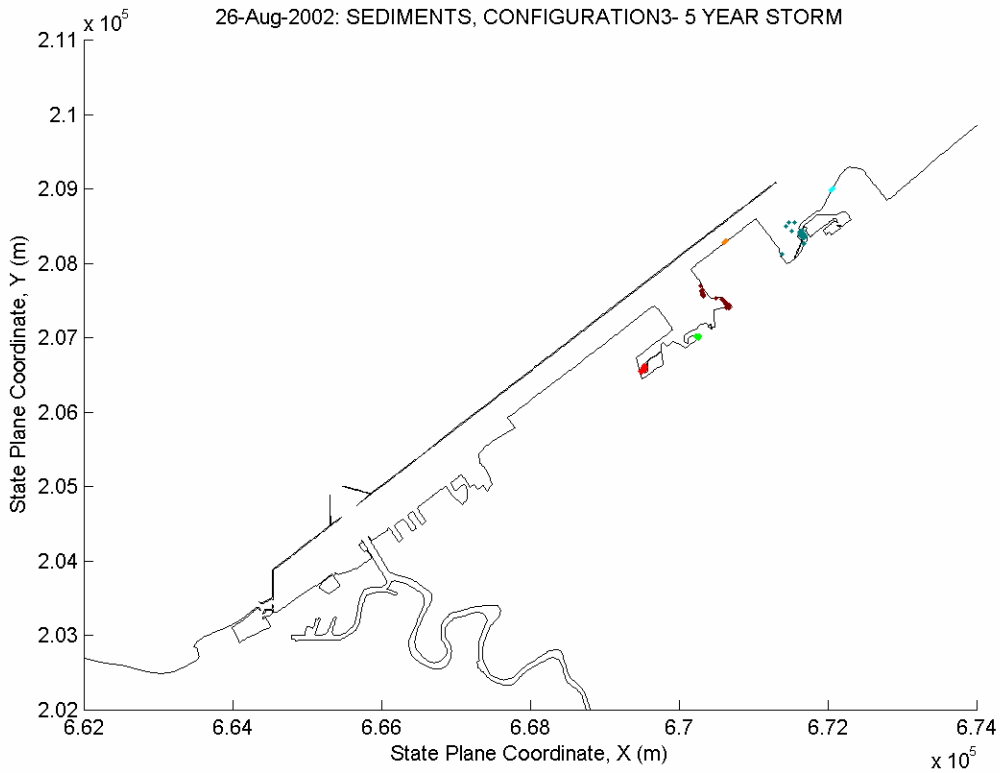
26-Aug-2002: SEDIMENTS, CONFIGURATION3- 5 YEAR STORM
x 10^5
2.11
2.1
2.09
2.08
2.07
2.06
2.05
2.04
2.03
2.02
State Plane Coordinate, Y (m)
6.62
6.64
6.66
6.68
6.7
6.72
6.74
State Plane Coordinate, X (m)
x 10^5

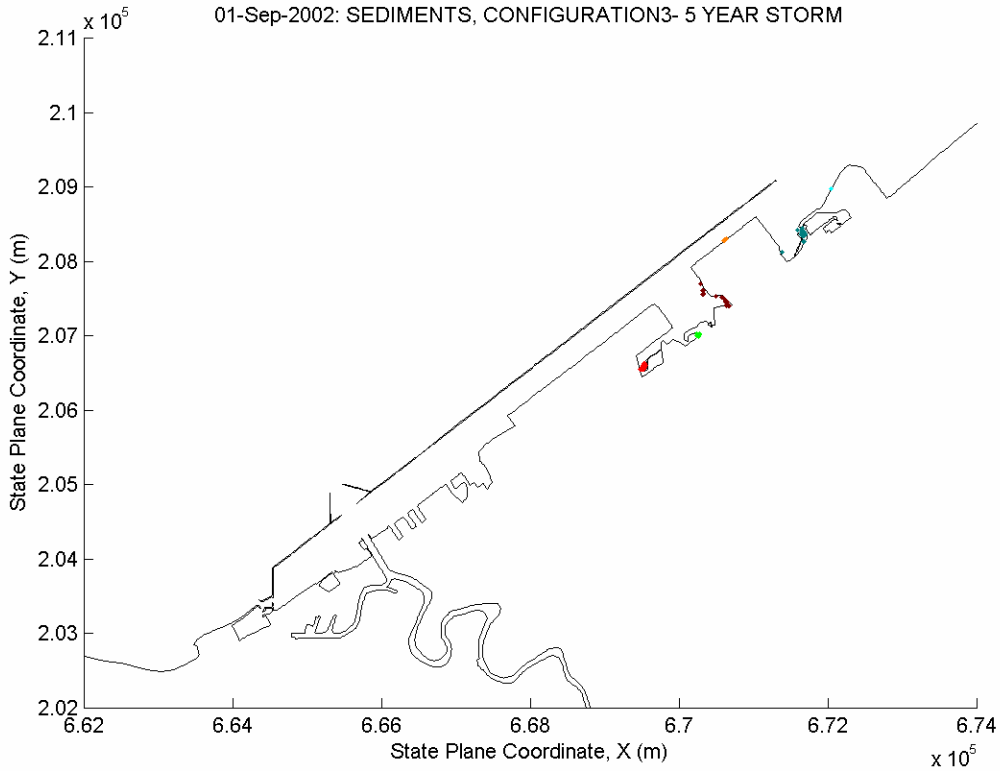
01-Sep-2002: SEDIMENTS, CONFIGURATION3- 5 YEAR STORM
x 10^5
2.11
2.1
2.09
2.08
2.07
2.06
2.05
2.04
2.03
2.02
State Plane Coordinate, Y (m)
6.62
6.64
6.66
6.68
6.7
6.72
6.74
State Plane Coordinate, X (m)
x 10^5

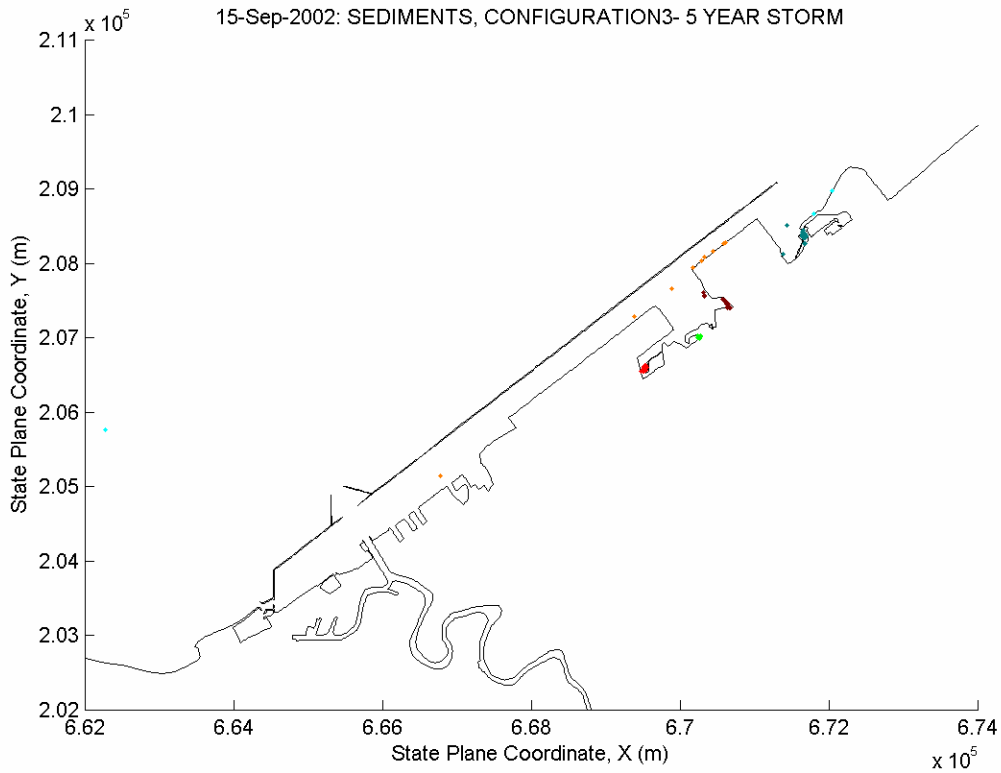
15-Sep-2002: SEDIMENTS, CONFIGURATION3- 5 YEAR STORM
x 10^5
2.11
2.1
2.09
2.08
2.07
2.06
2.05
2.04
2.03
2.02
State Plane Coordinate, Y (m)
6.62
6.64
6.66
6.68
6.7
6.72
6.74
State Plane Coordinate, X (m)
x 10^5

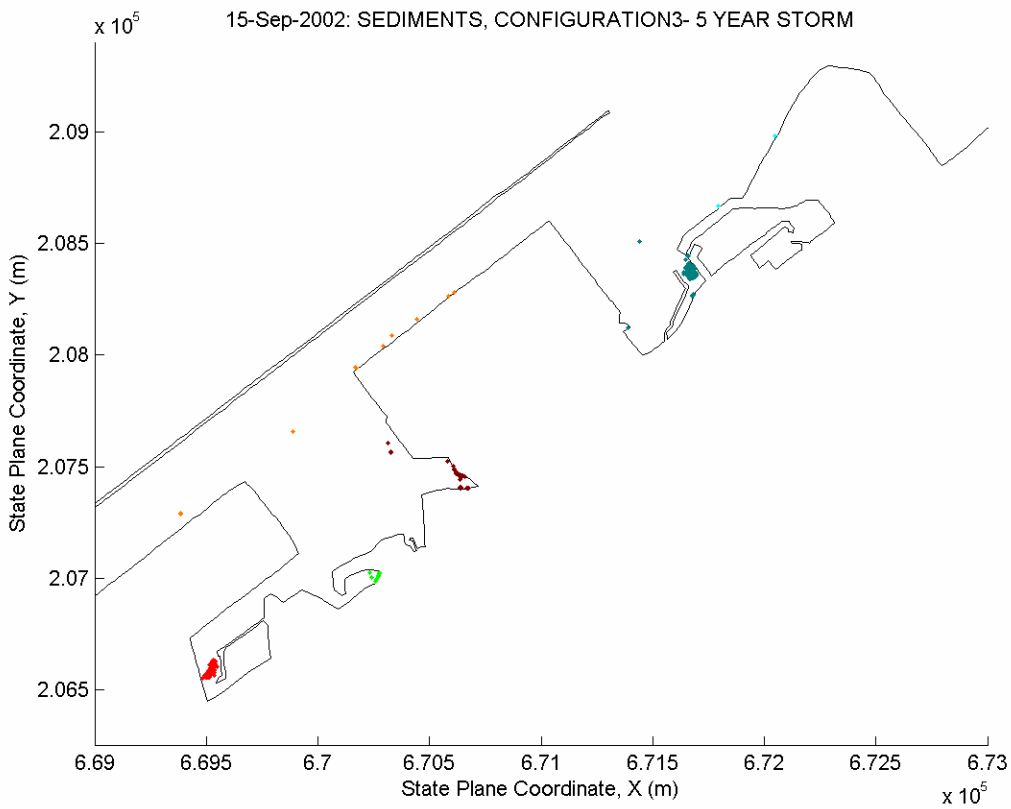
15-Sep-2002: SEDIMENTS, CONFIGURATION3- 5 YEAR STORM
x 10^5
2.09
2.085
2.08
2.075
2.07
2.065
State Plane Coordinate, Y (m)
6.69
6.695
6.7
6.705
6.71
6.715
6.72
6.725
6.73
State Plane Coordinate, X (m)
x 10^5

Appendix C: Concentration

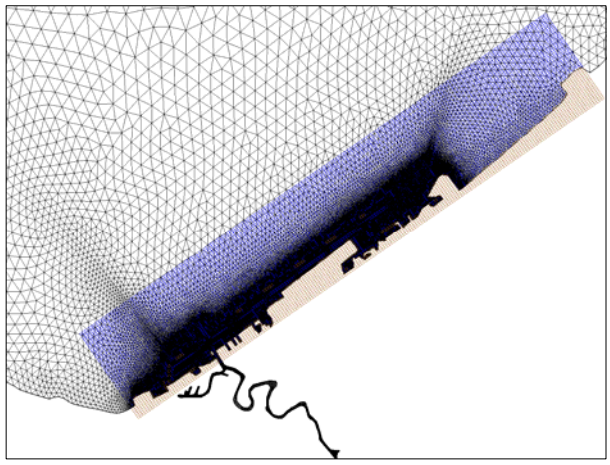

The representation above is the domain of the mesh with the grid used for subsequent concentration calculations.

The figures are arranged by particle type, geometry and hydrodynamics. There are two particle types used, neutrally buoyant, and sediments. There are four different geometry types that are used and they are the base condition, configuration 1, configuration 2, and configuration 3. The hydrodynamics was used for 6 month and 5 years storms. Each particle type has a geometry and hydrodynamics representation.

Figure	Page Number
Concentration – Neutrally Buoyant – Base – 6 Month	136
Concentration – Neutrally Buoyant – Base – 5 Year	137
Concentration – Neutrally Buoyant – Configuration 1 – 6 Month	138
Concentration – Neutrally Buoyant – Configuration 1 – 5 Year	139
Concentration – Neutrally Buoyant – Configuration 2 – 6 Month	140
Concentration – Neutrally Buoyant – Configuration 2 – 5 Year	141
Concentration – Neutrally Buoyant – Configuration 3 – 6 Month	142
Concentration – Neutrally Buoyant – Configuration 3 – 5 Year	143
Concentration – Sediments – Base – 6 Month	144
Concentration – Sediments – Base – 5 Year	145
Concentration – Sediments – Configuration 1 – 6 Month	146
Concentration – Sediments – Configuration 1 – 5 Year	147
Concentration – Sediments – Configuration 2 – 6 Month	148
Concentration – Sediments – Configuration 2 – 5 Year	149
Concentration – Sediments – Configuration 3 – 6 Month	150
Concentration – Sediments – Configuration 3 – 5 Year	151

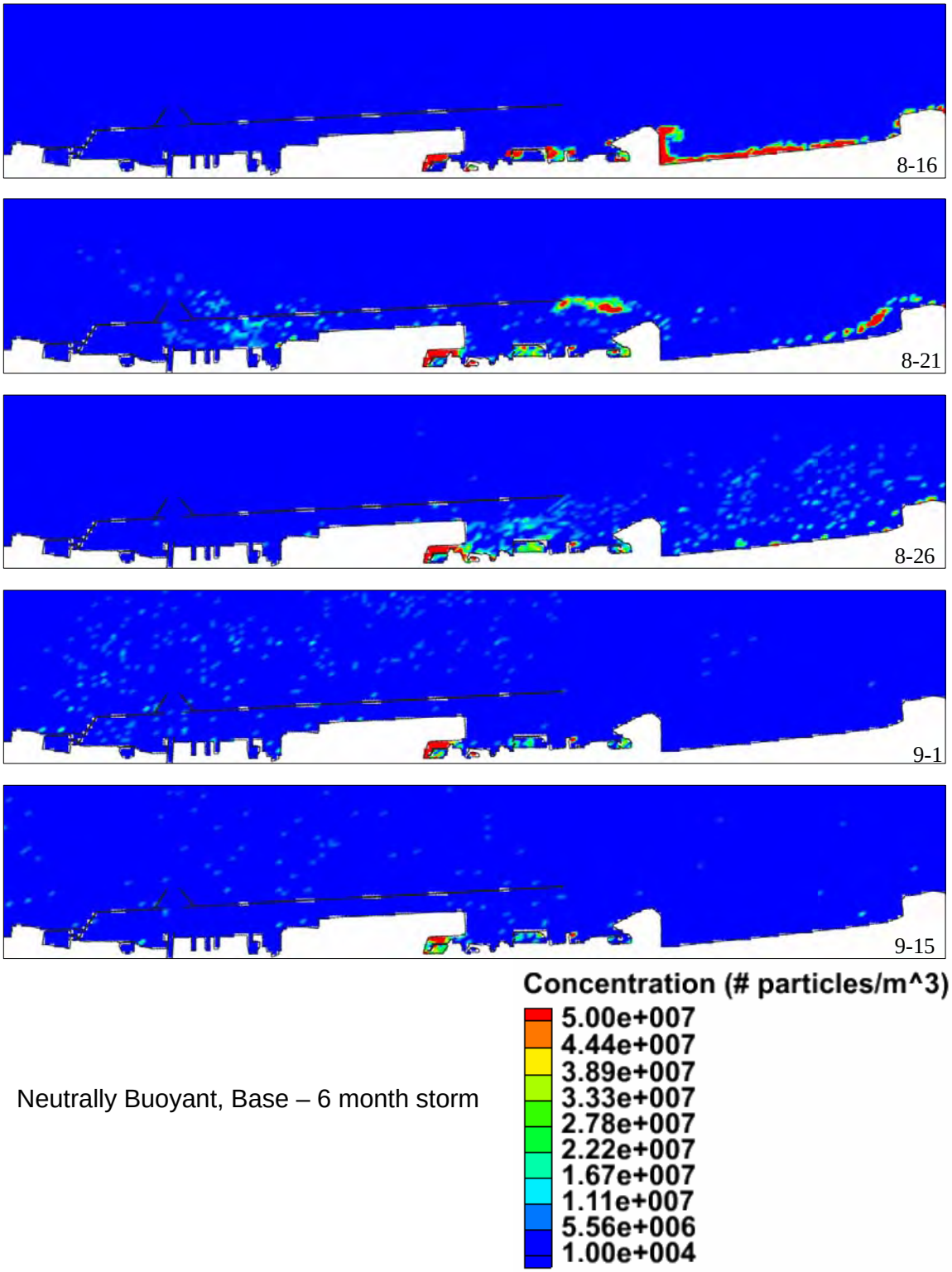

Neutrally Buoyant, Base – 6 month storm

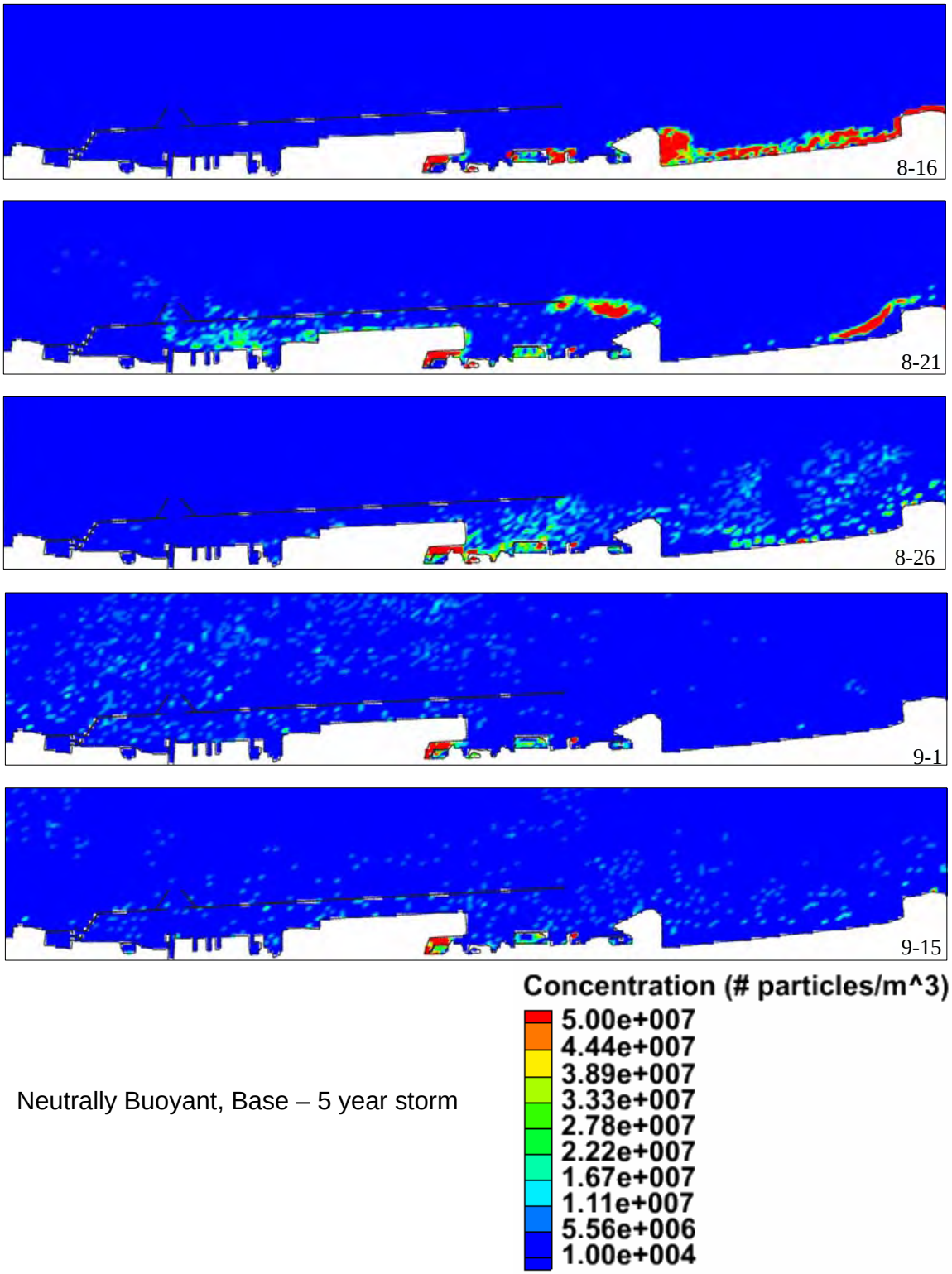

Neutrally Buoyant, Base – 5 year storm

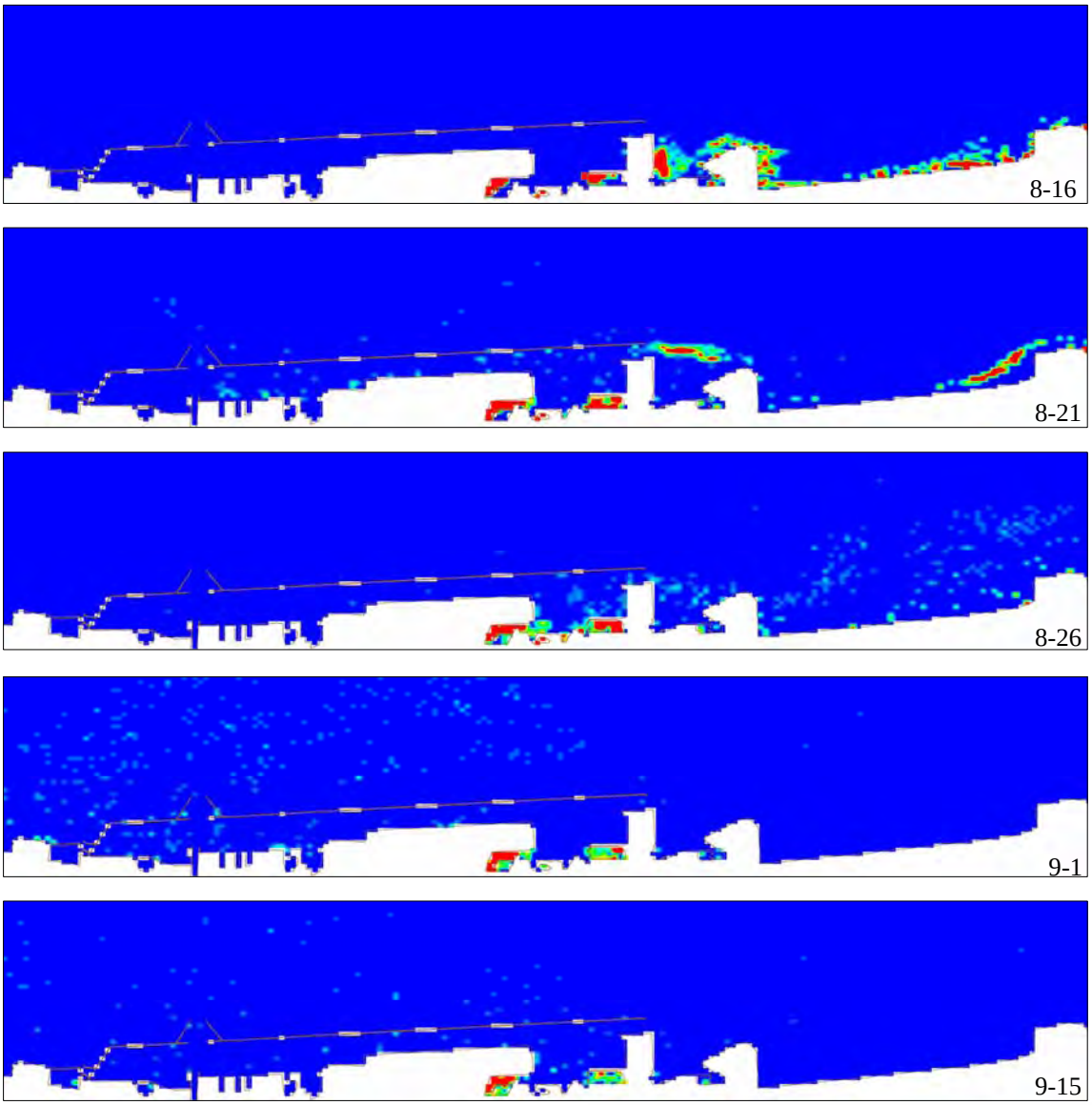

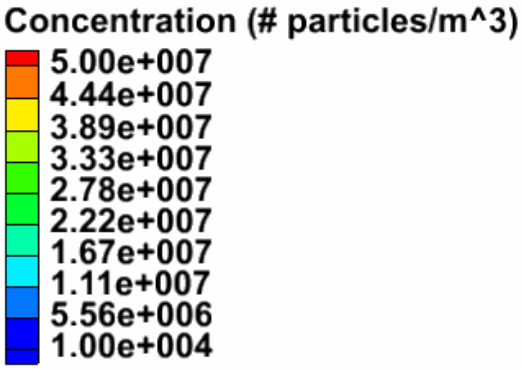

Neutrally Buoyant, Configuration 1 – 6 month storm

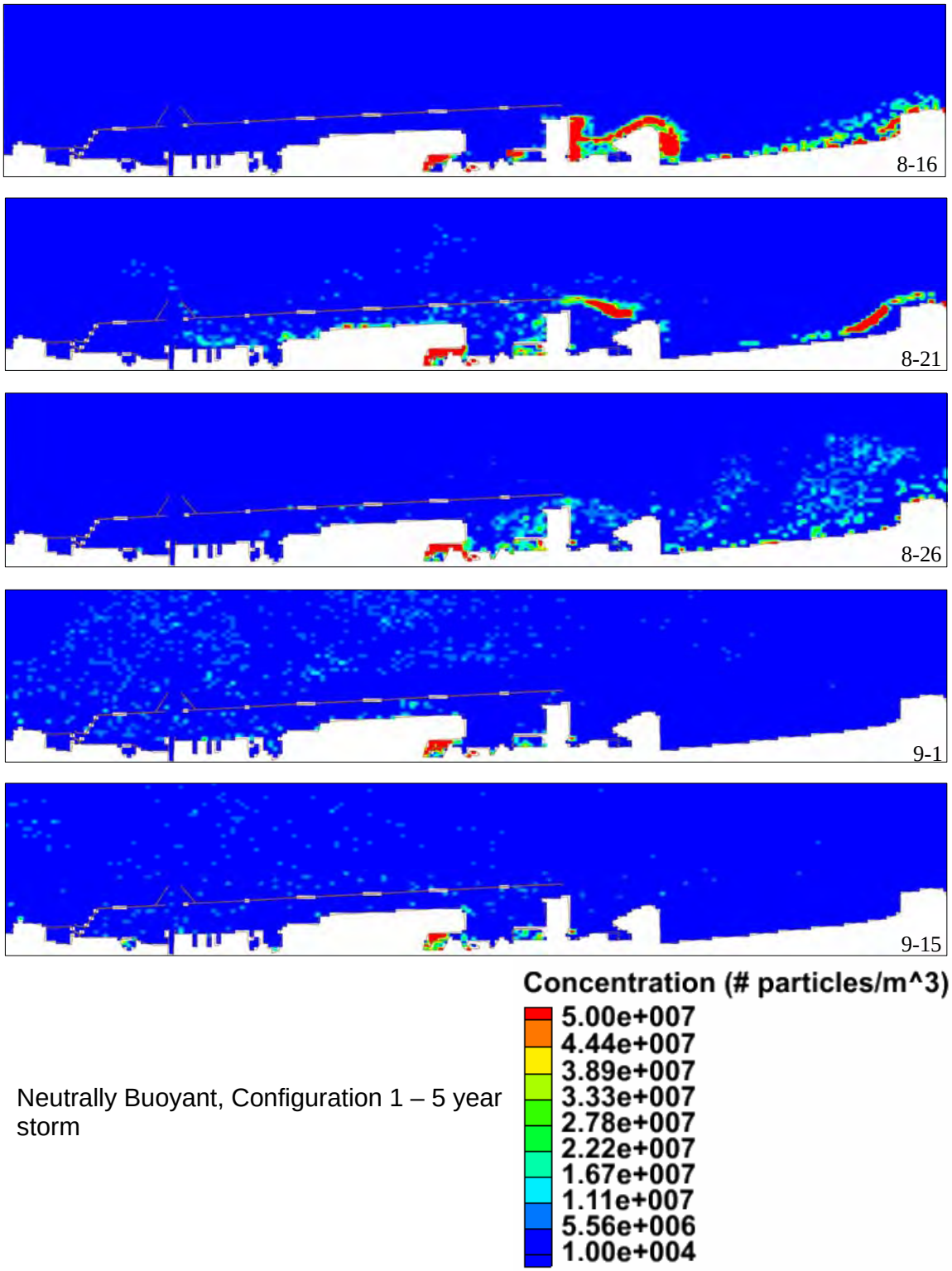

Neutrally Buoyant, Configuration 1 – 5 year storm

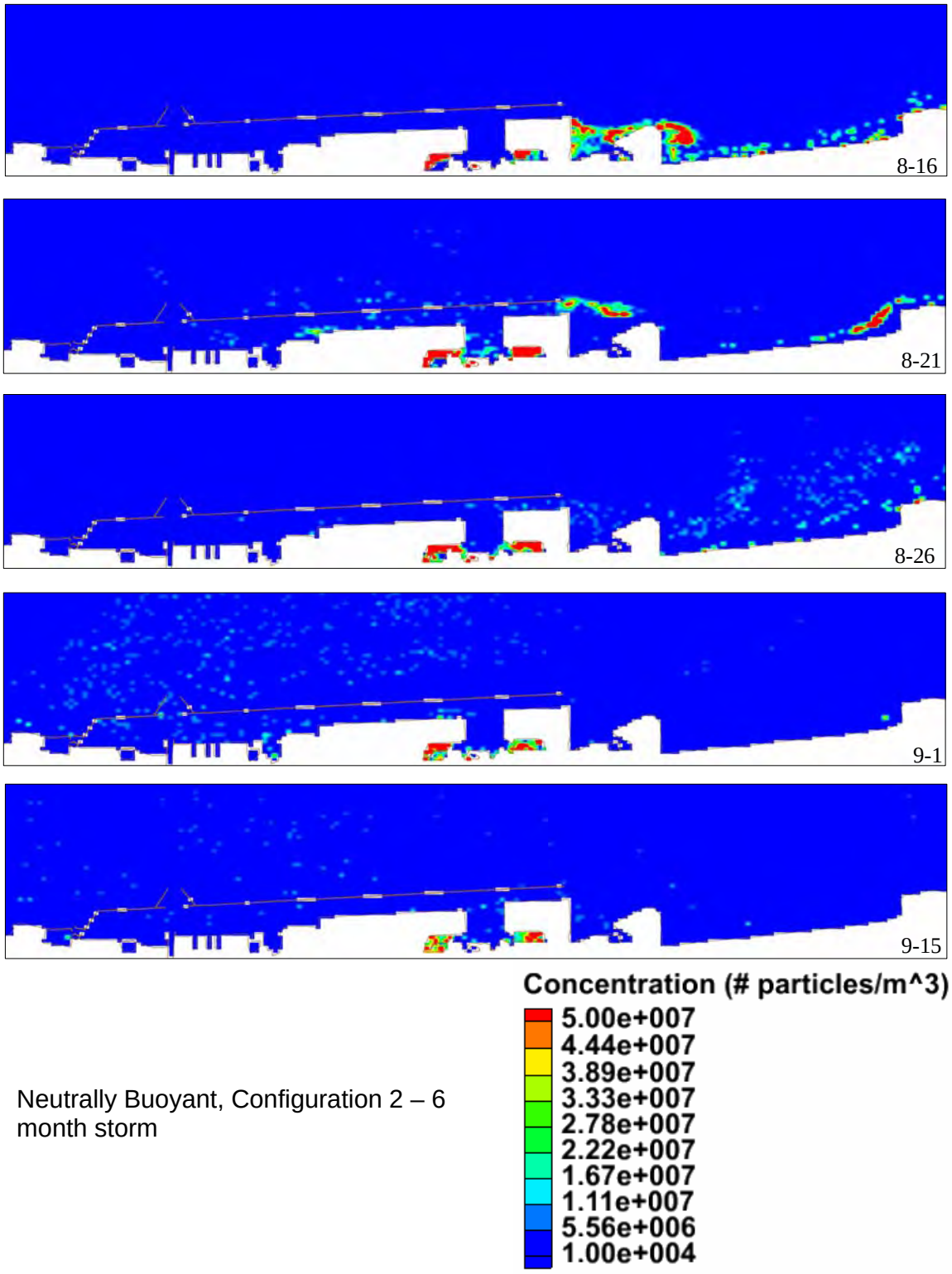

Neutrally Buoyant, Configuration 2 – 6 month storm

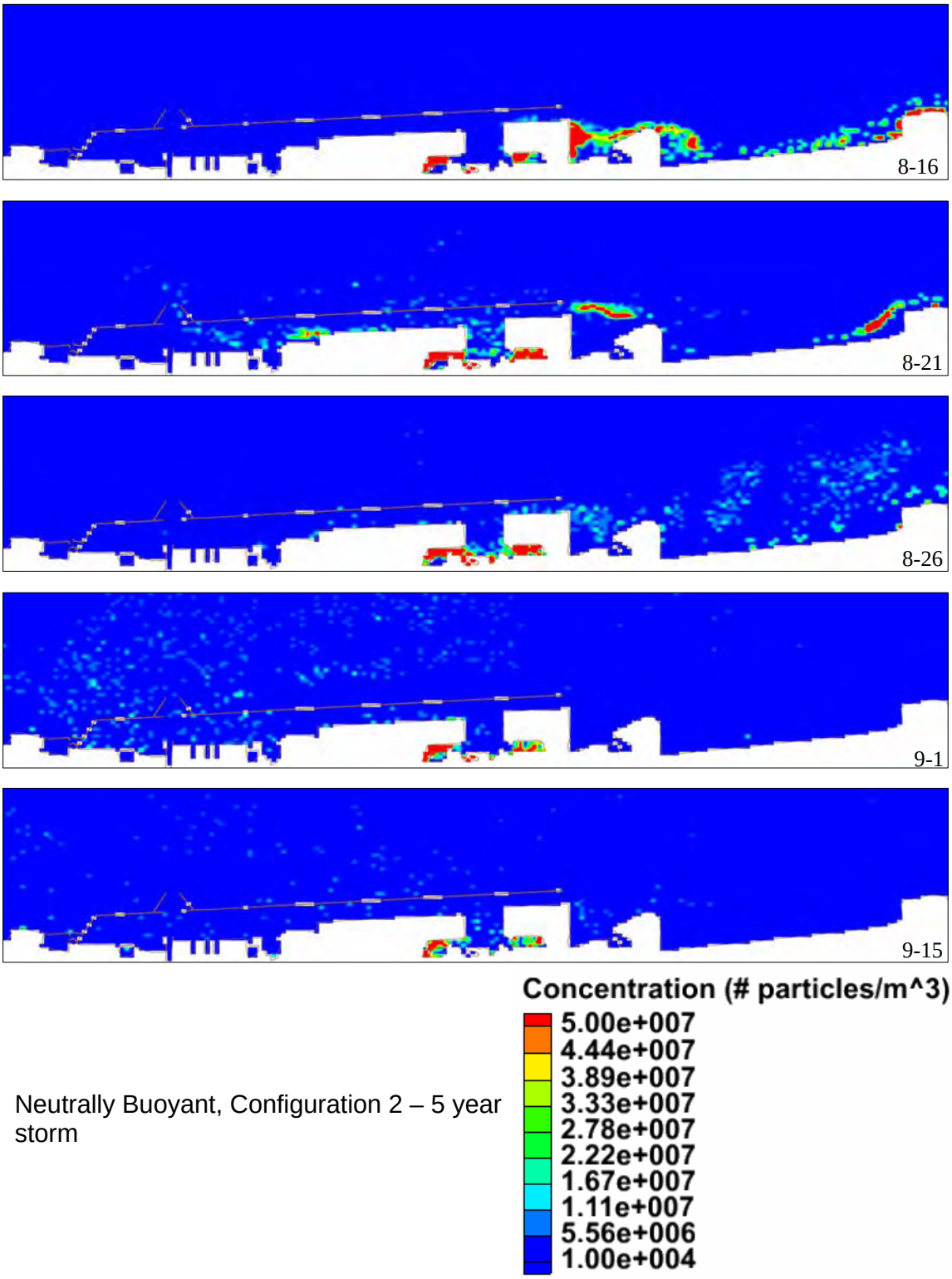

Neutrally Buoyant, Configuration 2 – 5 year storm

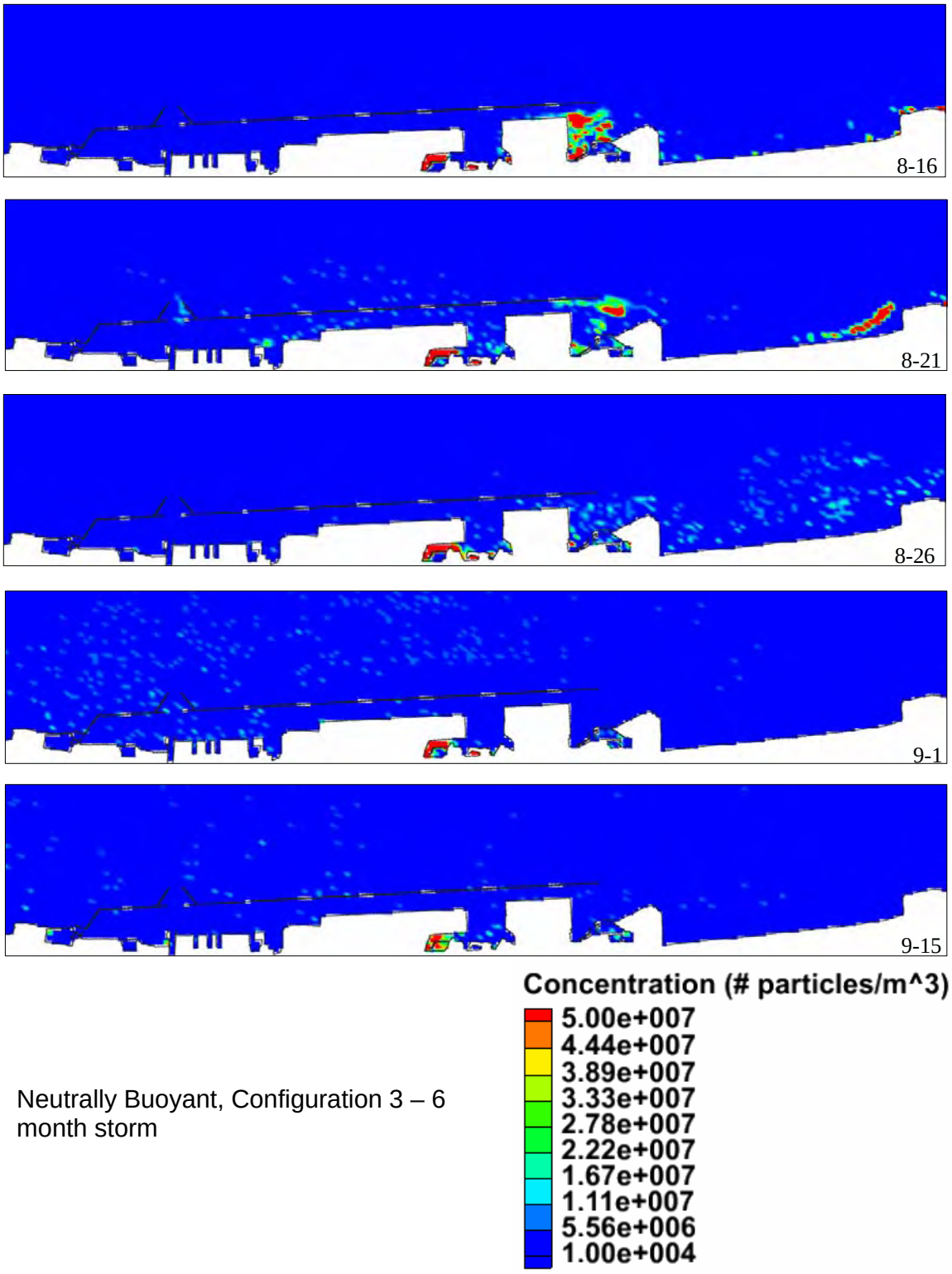

Neutrally Buoyant, Configuration 3 – 6 month storm

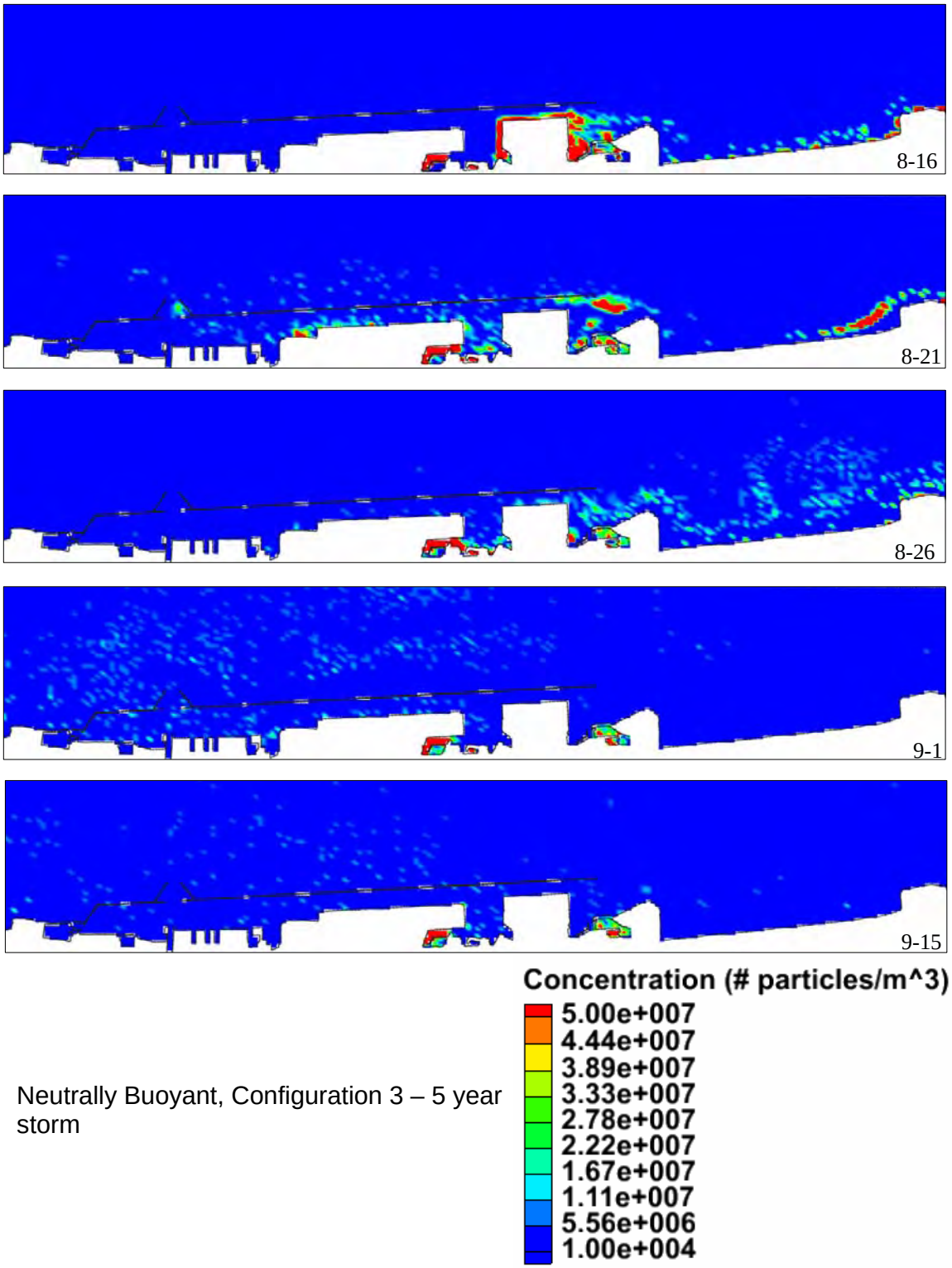

Neutrally Buoyant, Configuration 3 – 5 year storm

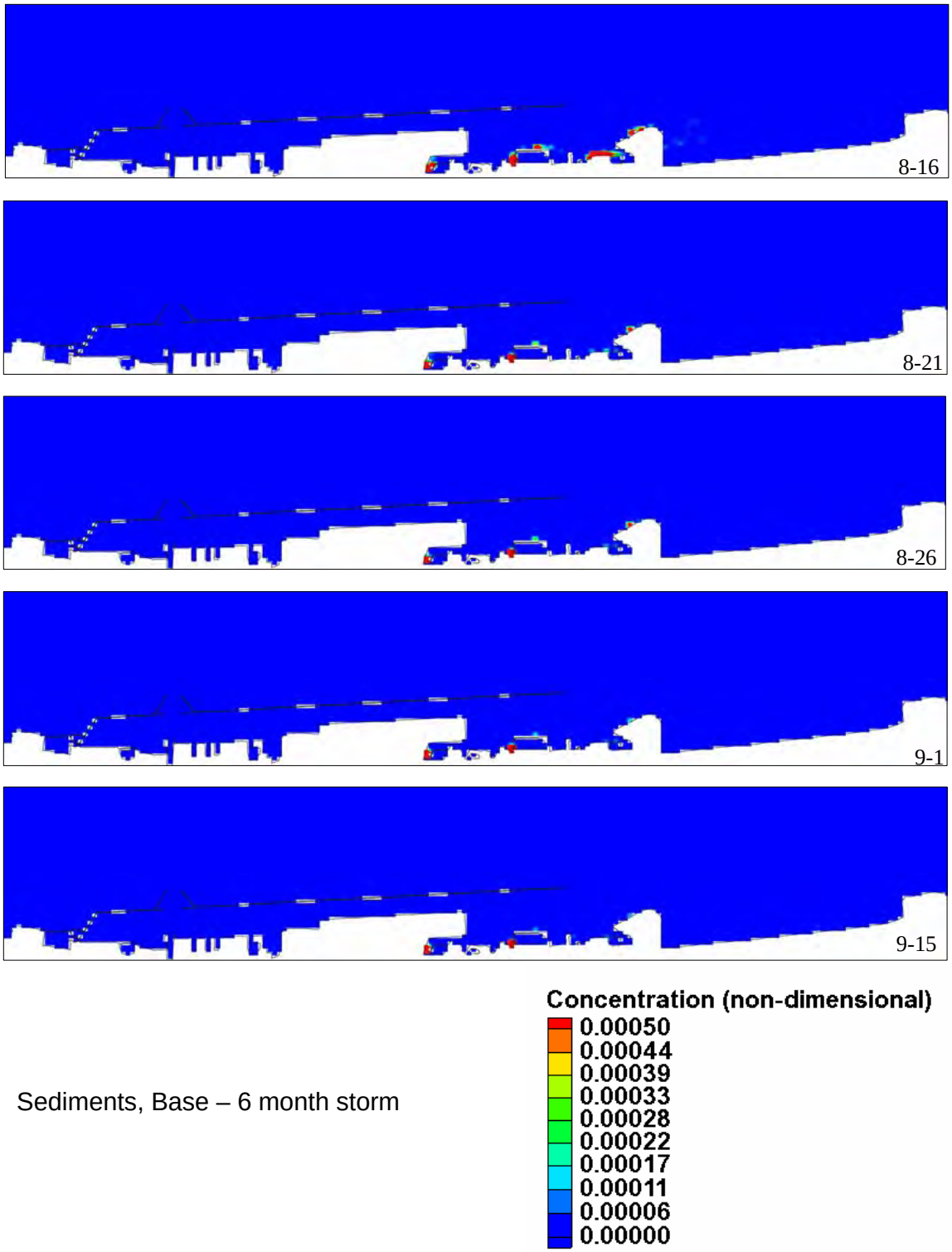

Sediments, Base – 6 month storm

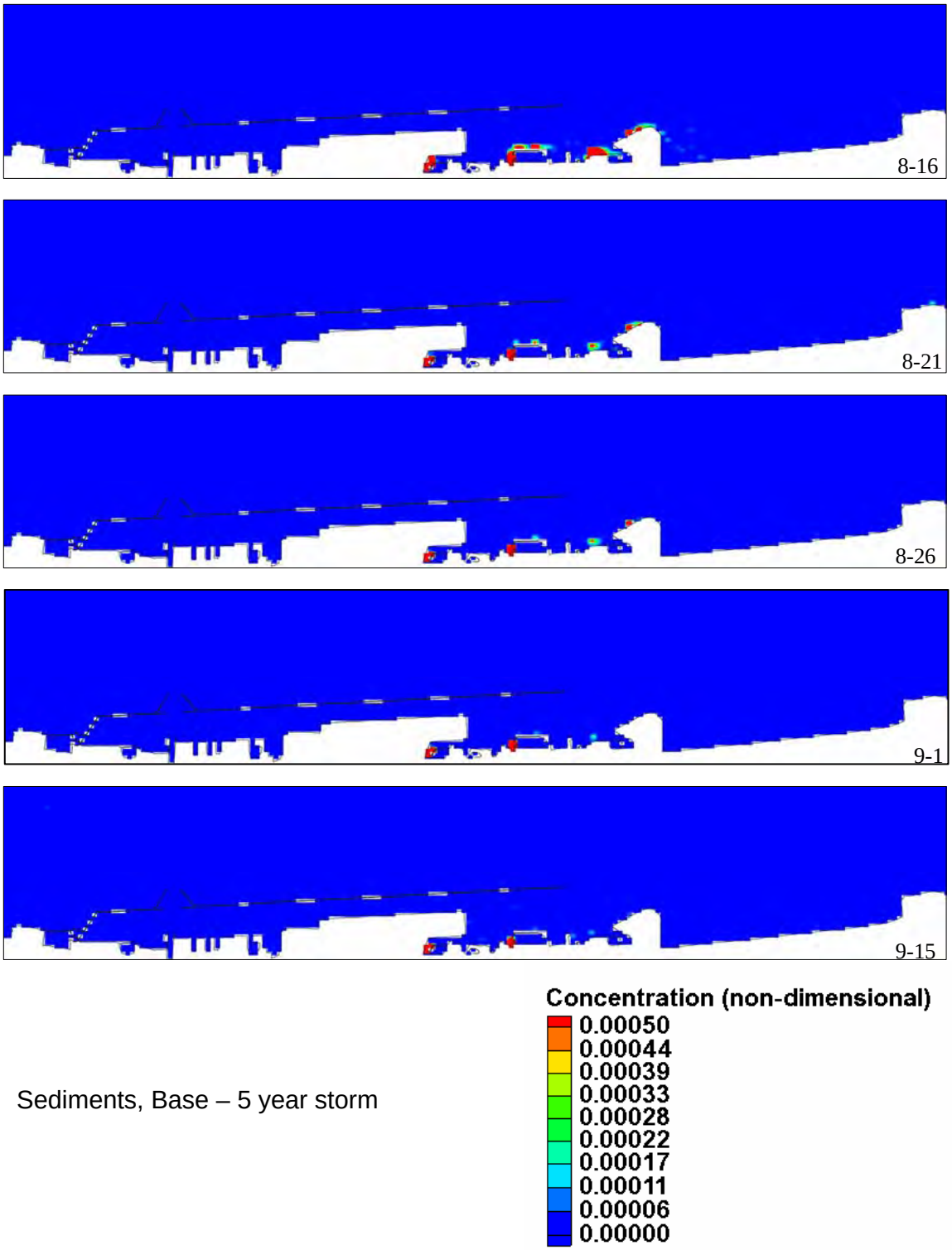

Sediments, Base – 5 year storm

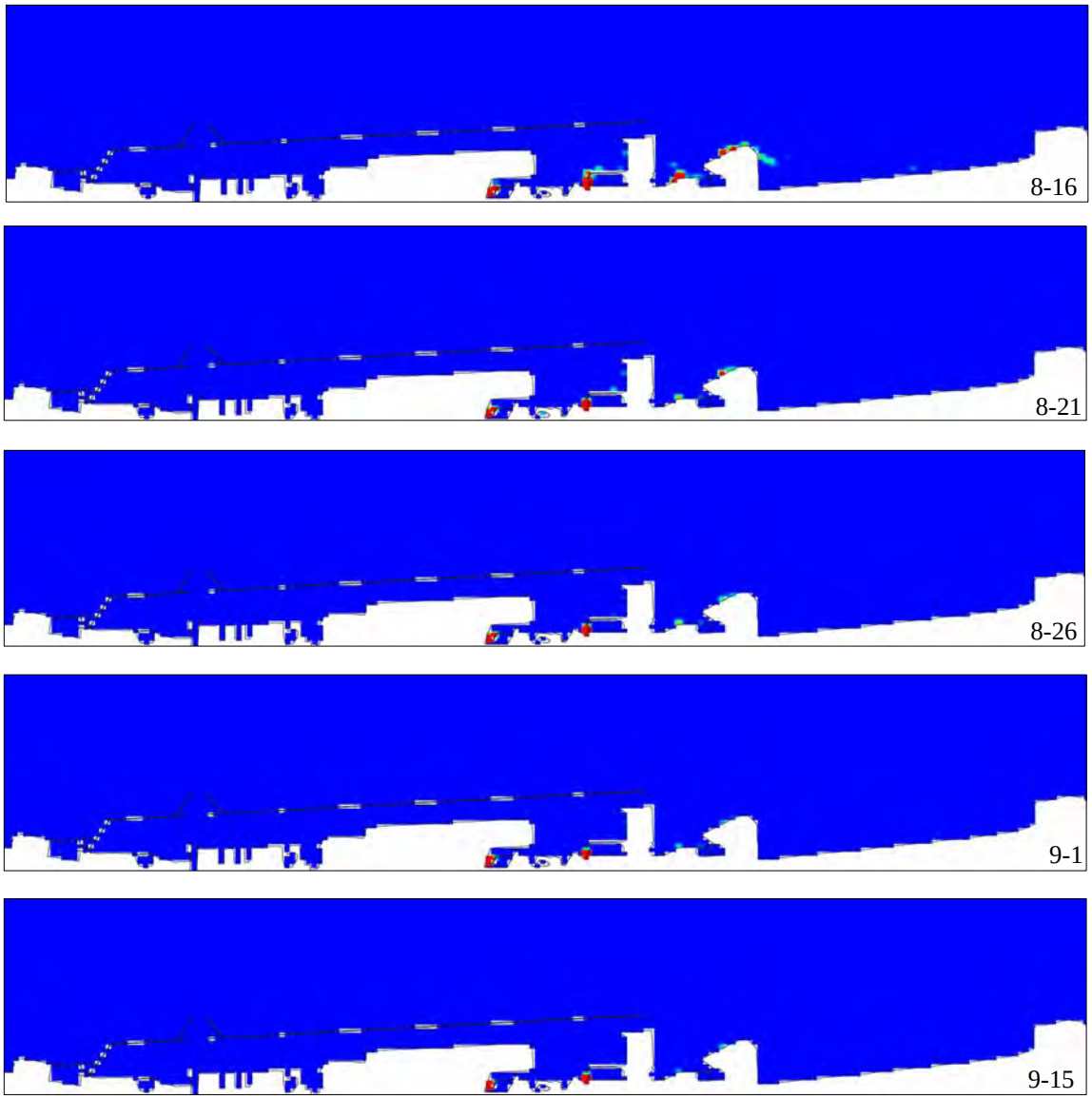

Sediments, Configuration 1 – 6 month storm

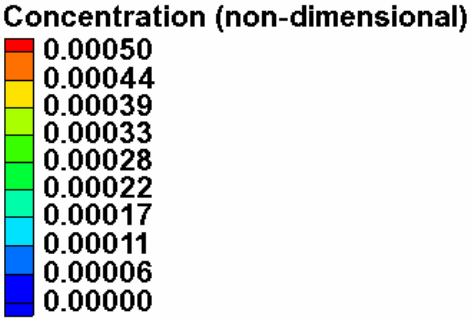

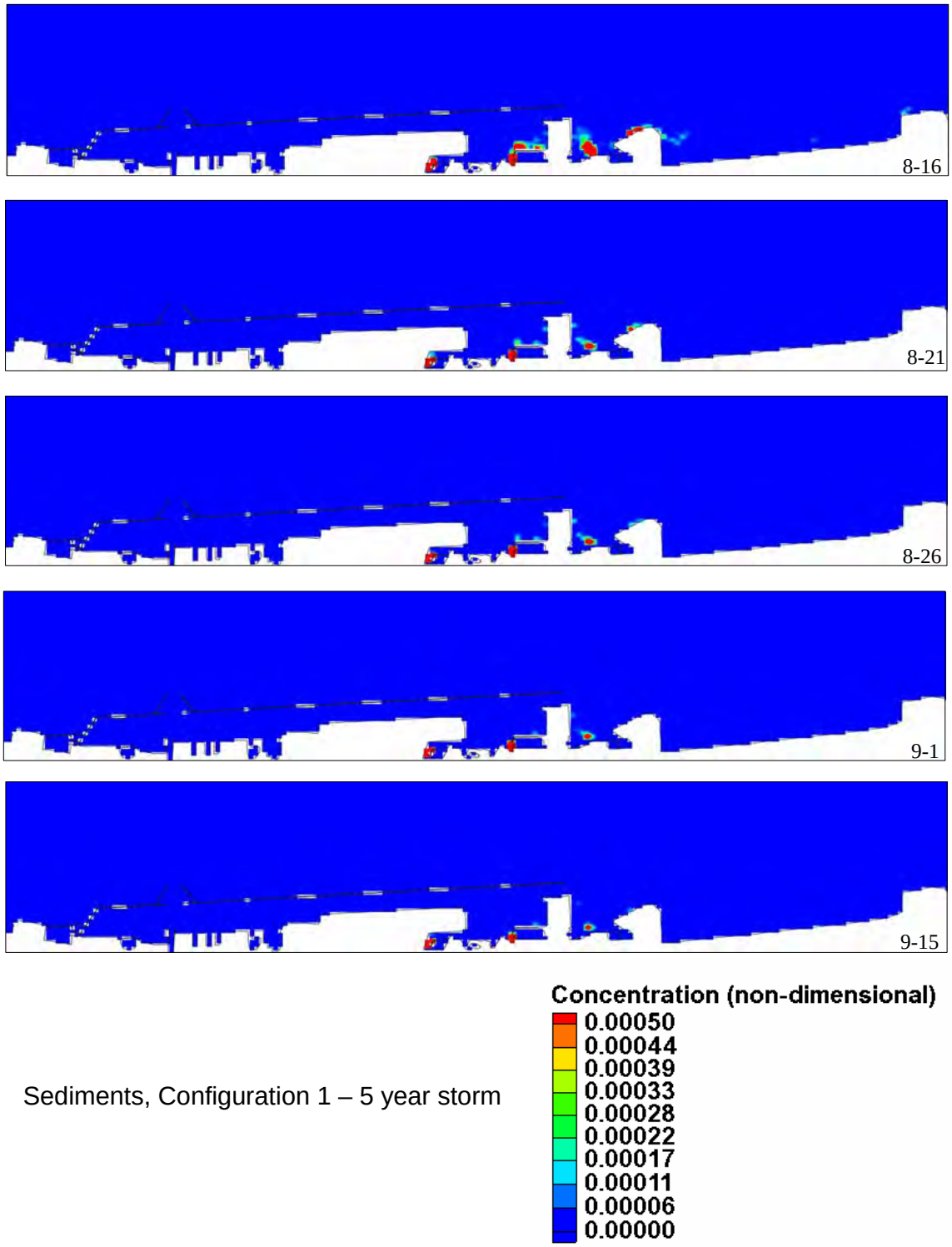

Sediments, Configuration 1 – 5 year storm

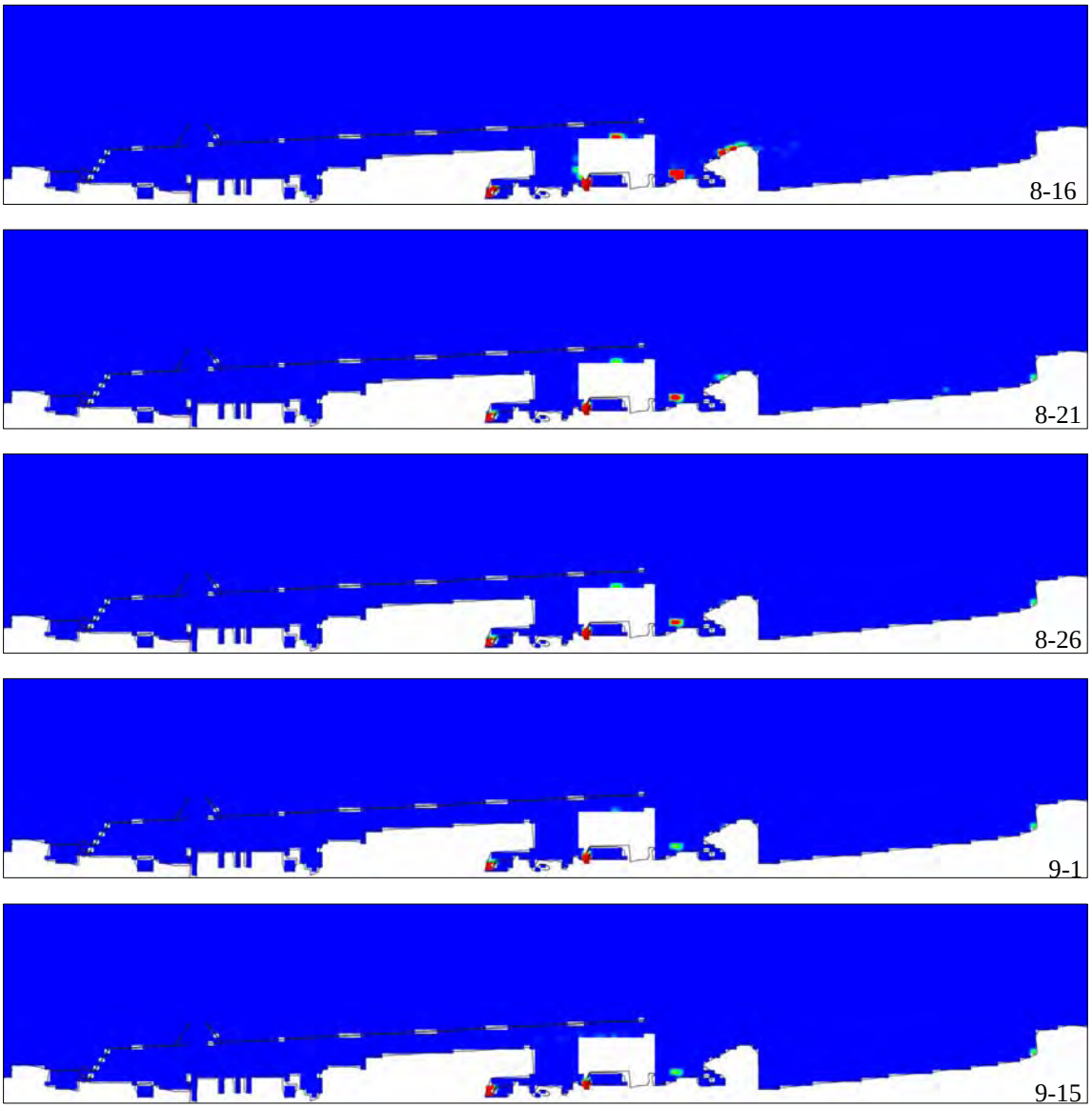

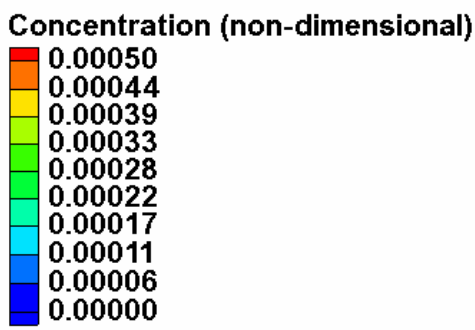

Sediments, Configuration 2 – 6 month storm

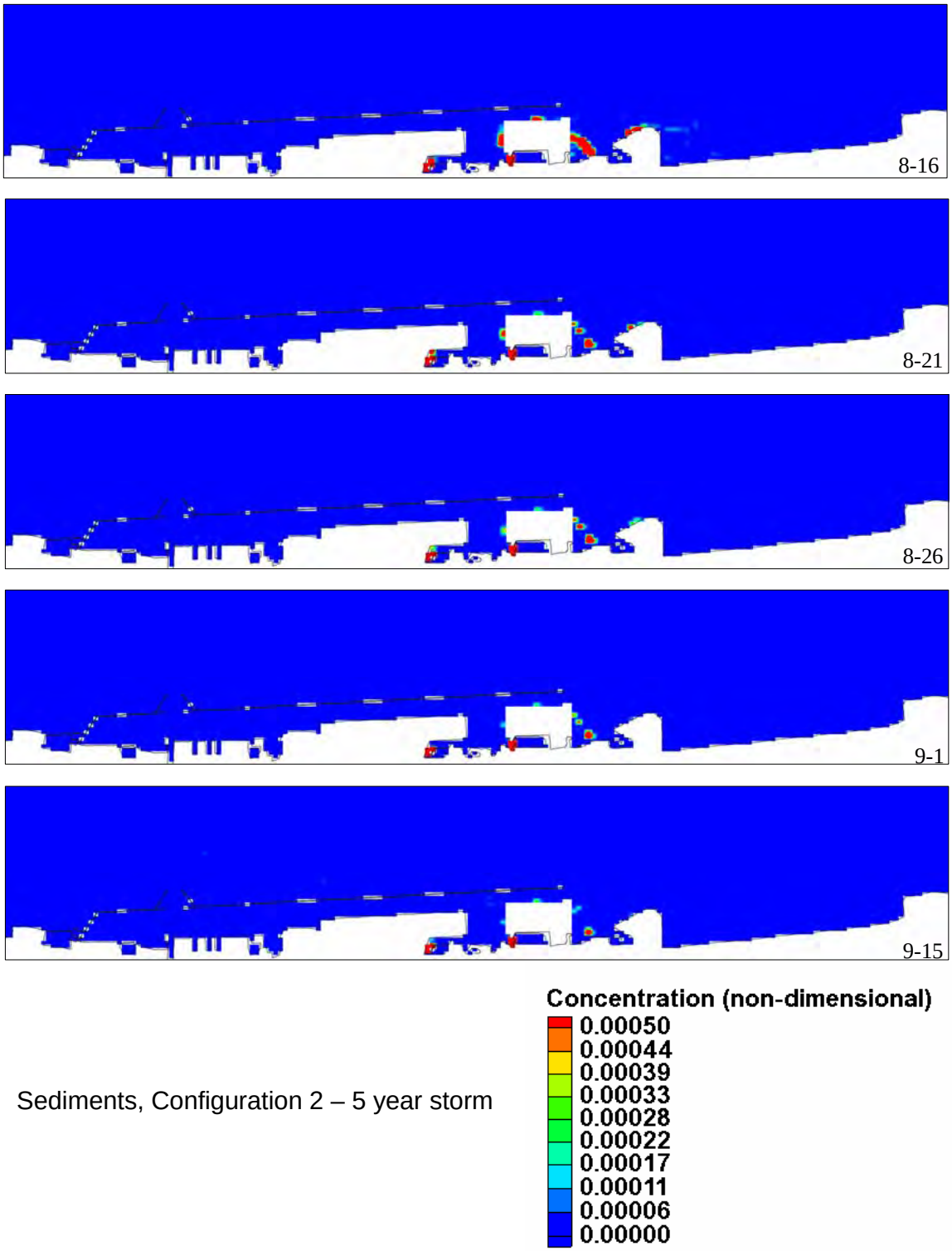

Sediments, Configuration 2 – 5 year storm

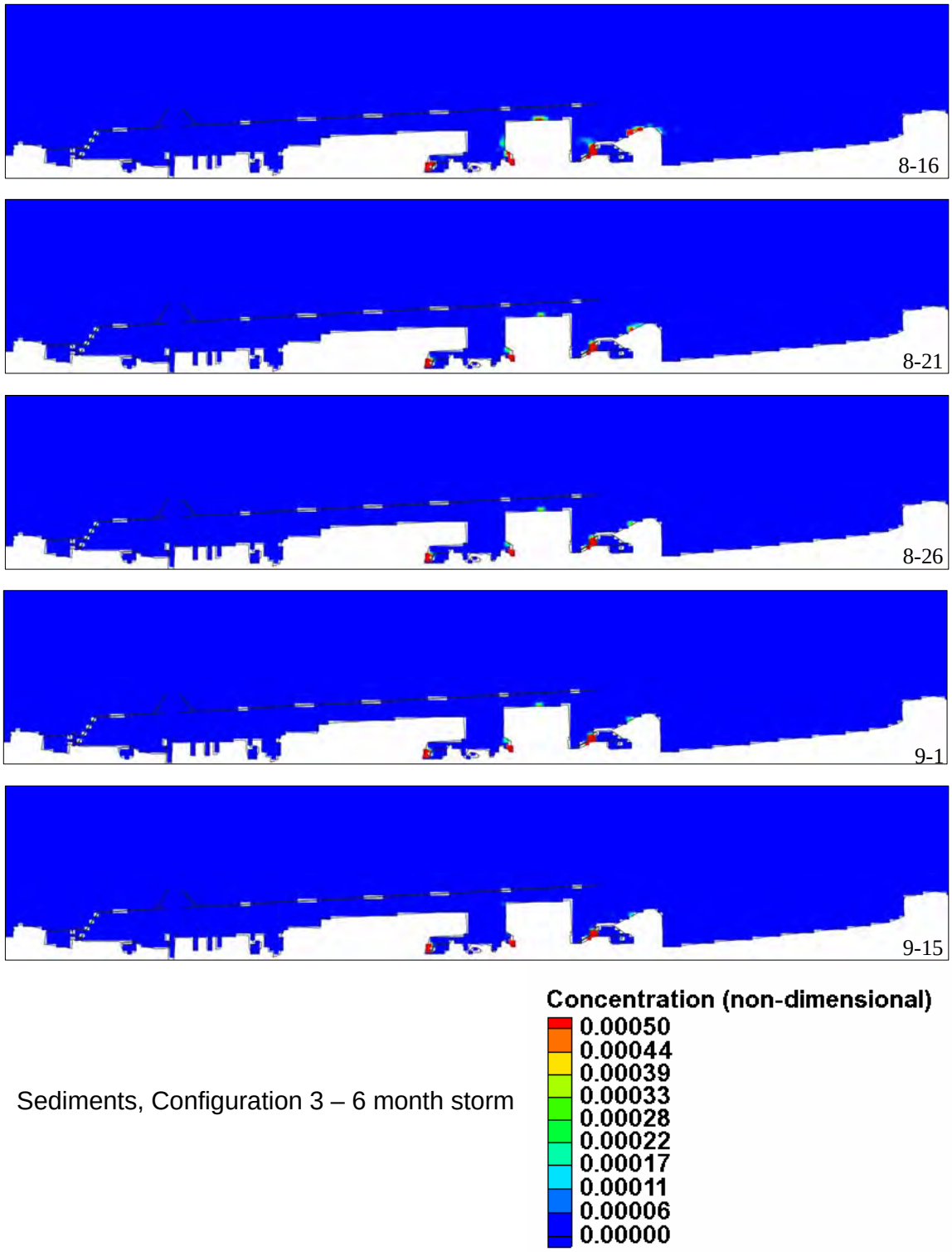

Sediments, Configuration 3 – 6 month storm

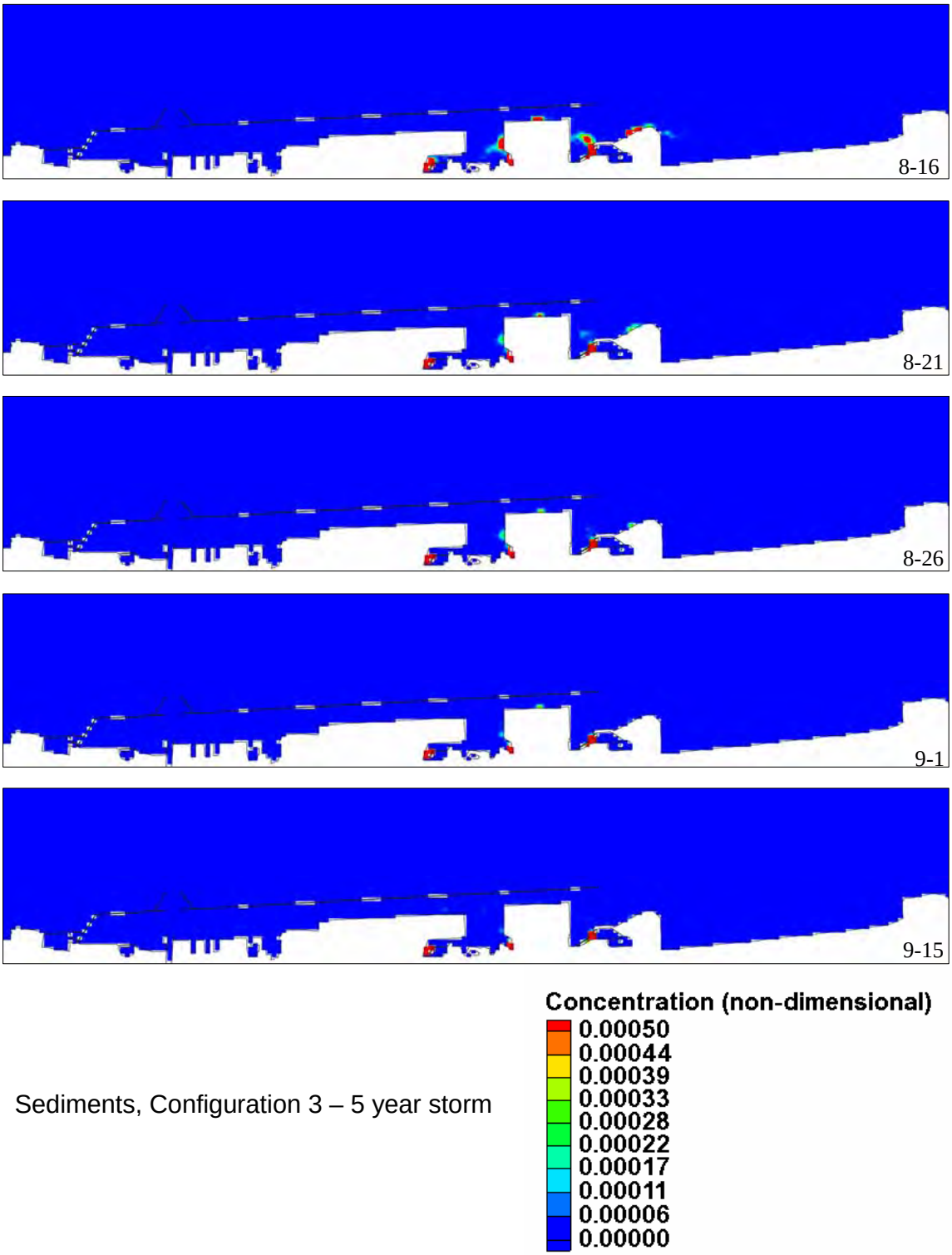

Sediments, Configuration 3 – 5 year storm

Sediment Transport Potential

A screening level approach has been applied to assess changes to sediment transport pathways for eroded bed sediments induced by proposed CDF configurations. In addition, changes to erosion/deposition patterns over the entire domain are also assessed. The sediment transport potential model GTRAN applied currents calculated by ADCIRC to predict transport magnitudes and pathways in the study area. GTRAN is a point model, which estimates potential transport and does not solve continuity of mass, i.e., it is a local transport model and it assumes unlimited sediment is available in the bed. GTRAN can include effects of waves as well as current on transport of non-cohesive sediment. However, since wave modeling was not part of the scope of work, only circulation parameters are provided to GTRAN through the external simulations with ADCIRC. GTRAN equations are applicable for coarse silt through all sand sizes. Although Cleveland Harbor is generally fine grained, transport pathways should still be well represented by GTRAN.

From input hydrodynamics and sediment bed conditions, GTRAN calculates sediment bed erosion rate as well as transport direction and magnitude through a collection of sediment transport methods. GTRAN automatically selects the appropriate transport method based on hydrodynamic conditions. Only one transport method was applied (van Rijn, 1984) for the Cleveland Harbor simulations because the harbor is current dominated and van Rijn is the appropriate method for these regimes. A description of the GTRAN sediment transport methods, including sediment transport equations, follows in the next section. GTRAN is a screening level model. Therefore, sediment transport potential calculations include simplifying assumptions and representations of the natural processes. Making such assumptions is standard practice in the field of numerical modeling and is not unique to sediment transport models. The following discussion of the approximations used for estimating transport rates using the van Rijn method is limited to general descriptions of the approximations applied.

It should be noted that all sediment transport methods, including van Rijn, applied in GTRAN are for non-cohesive sand and coarse silt (non-cohesive sediment). Cleveland Harbor sediments are finer than the range for which the van Rijn method is developed. However, the theory can be applied to assess relative magnitude of erosion potential for with and without project conditions. This is how GTRAN is applied in this study. Also, transport theories are available for non-cohesive sediment, but not for finer, cohesive sediment. Cohesive sediment erosion and transport is influenced my numerous, inter-dependent properties. Available transport algorithms require site-specific parameterization. This parameterization was outside this study scope.

Van Rijn current-dominated transport method

The van Rijn (1984) current-only total transport method was parameterized from van Rijn’s comprehensive theory of sediment transport in rivers. Although the method was

developed for sediment transport in the riverine environment, the method may also be appropriately applied in the marine environment under conditions for which waves contribute little to the bottom shear stress. The simpler, parameterized formulae approximate the full theory within ±25 percent and were developed for water depths less than 20 m, velocities between less than 5 m/s, and d_{50} between 0.1 and 2 mm. The resulting parameterized method estimates transport by the following simpler formulation:

$$q_t = q_b + q_s \tag{1}$$

$$q_b = 0.005\bar{U}h\left\{\frac{\bar{U}-\bar{U}_{cr}}{\left[(s-1)gd_{50}\right]^{1/2}}\right\}^{2.4}\left(\frac{d_{50}}{h}\right)^{1.2} \tag{2}$$

$$q_s = 0.012\bar{U}h\left\{\frac{\bar{U}-\bar{U}_{cr}}{\left[(s-1)gd_{50}\right]^{1/2}}\right\}^{2.4}\left(\frac{d_{50}}{h}\right)\left(D_*\right)^{-0.6} \tag{3}$$

where:

$$\begin{aligned} \bar{U}_{cr} &= 0.19\left(d_{50}\right)^{0.1}\log_{10}\left(\frac{4h}{d_{90}}\right) \text{ for } 0.1 \le d_{50} \le 0.5\,mm \\ \bar{U}_{cr} &= 8.50\left(d_{50}\right)^{0.6}\log_{10}\left(\frac{4h}{d_{90}}\right) \text{ for } 0.5 \le d_{50} \le 2.0\,mm \end{aligned} \tag{4}$$

$$D_* = \left|\frac{g(s-1)}{\upsilon^2}\right|^{1/3} d_{50} \tag{5}$$

q_t=total transport
q_b=bedload transport
q_s=suspended load transport
$\bar{U}$ = depth-averaged current
h = water depth
s = specific gravity of sediment
g = acceleration due to gravity
d_{50} = median grain diameter
d_{90} = sediment diameter for which 90 percent is finer by weight
ν = kinematic viscosity

Transport modeling

GTRAN is a point model, and it requires X, Y, and Z coordinates for each location where sediment transport magnitude and direction are calculated. The computational domain for GTRAN was defined by 2805 to 2842 discrete points spaced at 150 m. The number of points and spacing were selected so that there were sufficient points to define transport patterns in Cleveland Harbor, particularly near the proposed CDF. The GTRAN model was driven by currents obtained from ADCIRC circulation model results of 6-month and 5-year storms. Waves were not modeled as part of this scope of work; therefore, transport results were obtained by the van Rijn current-only method. GTRAN input includes bed grain size, bathymetry, and hydrodynamic/environmental conditions.

With the initial bed conditions specified, the model distributes environmental forcing conditions from ADCIRC large-domain circulation model to each of the computational points. The temporal resolution of the current information is 30 min. This resolution is adequate to define the temporal changes in current conditions for representing sediment transport. With local conditions determined, the model proceeds to estimate the current-related bottom shear stresses and to estimate the depth of the active sediment layer. The active sediment layer is defined as the depth of the sediment bed that is mobilized by sediment suspension and bed-load movement.

GTRAN calculates the total sediment transport magnitude and direction for each time step at each point. Direction (in degrees) is used to classify the transport into one of 20 directional bins. Each bin covers 18 degrees. Bins are centered on 0, 18, 36, 54, deg, etc. Transport rate is summed within each bin for the entire simulation length (six weeks) to calculate total transport rate for each defined bin over an event.

An example rose plot is given in Figure 1 with the corresponding values listed in Table 1. The figure shows transport with different magnitudes in bins 0 to 54 deg and 180 to 252 deg, with no transport reported in the remaining bins. This example shows transport in the northeast and southwest quadrants. It should be noted that the values shown in Figure 1 and Table 1 are given as an example and does not apply to the present study.

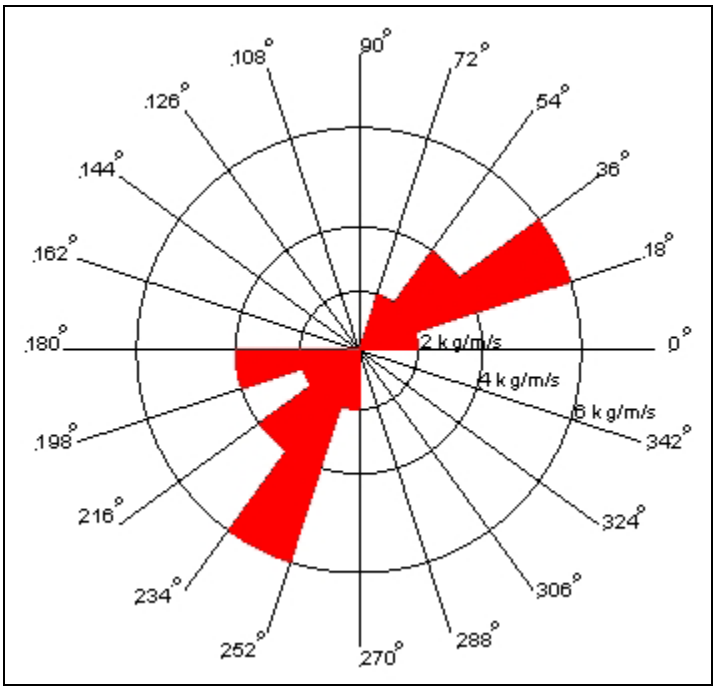

Figure 1. Example or rose plot direction and magnitude bins

Table 1: Rose Plot Angle and Magnitude Example

Angle (deg)	Magnitude (kg/m/s)
0 - 18	2
18 - 36	6
36 - 54	4
54 - 72	2
72 - 90	0
90 - 108	0
108 - 126	0
126 - 144	0
144 - 162	0
162 - 180	0
180 - 198	4
198 - 216	2
216 - 234	4
234 - 252	6
252 - 270	0
270 - 288	0
288 - 306	0
306 - 324	0
324 - 342	0
342 - 360	0

Transport results were calculated for three sediment diameters; d_{50} = 0.07, 0.10 and 0.20 mm for each event (six month and 5 year) and are presented as rose plots (directional distribution of transport) in Appendix C.

GTRAN Model Results

Results from GTRAN in the study area for the base condition with the 6-month storm and all three grain diameters are shown in the rose plots of Figures C1 through C3. Each red "wedge" in these figures represents transport for one of the 20 bin directions at each point. Area of the red colored wedge indicates relative transport potential. Therefore, the large wedges indicate high transport in a specific direction while small wedges indicate very small amounts of transport. GTRAN is generally used to look at relative transport and transport pathways and is not indicative of net transport because it does not account for deposition. Wedge areas are used to demonstrate relative magnitude of transport over a domain and transport pathways in a system. The model is successfully applied to identify transport trends in active regions. Unfortunately, Cleveland Harbor is a low energy environment with sand erosion occurring only in isolated areas, as shown in Figures C1-C3. Additional red wedges would be present nearshore and outside the breakwater if waves were included in the storm erosion/transport estimates. The only transport observed occurs off the north side of Dike 14 and transport is generally unidirectional. Similar results are shown for the 5-year storm in Figures C4 through C6. These figures show that current-generated stresses are insufficient to entrain and transport sediment within the harbor for any of the grain sizes simulated. As previously stated, wave-induced erosion is not included, so there is zero transport along much of the shoreline outside the harbor where waves would significantly contribute to transport. Transport offshore and to the west is exhibited around Dike 14. This is due to seiche-induced currents around this sharp bend.

It should be noted how wave action, not included in this scope, may influence results shown here, especially in the nearshore. Surface waves produce oscillatory flow on the sediment bed. The magnitude of this flow is a function of wave height, wave period, and water depth. The oscillation is symmetric in deep water and asymmetric in shallow water as the wave shoals and moves toward breaking. The orbital velocity is therefore strongest in shallower water. The lack of transport in some nearshore areas outside the breakwater in Figures C1-C6 is due to lack of wave influences in the model application. During storms, waves become larger and can produce transport in deeper water. Net transport under a wave would be zero because of the sinusoidal motion of the particles if currents were not present. In wave/current transport, waves act as a suspension mechanism and currents as the transport mechanism in deeper water. For example, the 5-year storm probably included some significant waves that would have moved sediment outside the breakwater. In the present study, the breakwater shelters the project area so effects of waves are minimal; especially from westerly waves, the predominant wave direction. The potential deposition patterns, discussed in the next section, should be representative of actual conditions in the harbor. Outside the breakwater, storm wave orbital velocity has a significant influence on erosion and transport and more sediment would be kept in suspension.

Identical simulations (6 month and five year event) were performed with project conditions. Results for with and without project conditions were similar in the vicinity of Dike 14. Results for Configuration 1 CDF are shown in Figures C7 through C12.

Although hardly visible in the figures (because of the large transport rates near Dike 14), slight transport is predicted between the proposed CDF and breakwater at one GTRAN point for all grain sizes and both storms (Figures C7 through C12). This demonstrates that the new channel will experience increase energy compared to the without project conditions channel.

Configurations 2 and 3 also showed similar transport in the vicinity of Dike 14 as the base case and Configuration 1 for both storms (Figures C13 through C24). However, no transport was observed between the CDF and the breakwater for these configurations. Configuration 1 estimated minimal transport; currents were slightly reduced in the channel for Configurations 2 and 3, thus eliminating any transport.

Sediment transport results from GTRAN indicated very little erosion and transport of bottom sediments of size 0.07 to 0.20 mm as a result of the proposed CDF plans. Another way to present the results is to observe the transport difference between a proposed configuration and the present (base) condition. Figures C25 through C60 show the increased difference and decreased difference in transport between each configuration and the base condition for each storm and grain size. Wedge size is re-calibrated for these difference plots so that the reader can visualize the differences. Difference plots cannot use the same scale as total transport plots (Figures C1-C24) because transport differences would not be visible in the figures. The figures show increase in transport between the Configuration 1 CDF and breakwater in Figures C25, C27, C29, C31, C33, and C35. It is interesting that transport north of Dike 14 decreases with the 6-month storm and increases with the 5-year storm with Configurations 1 and 2. Transport near Dike 14 decreases for both storms with Configuration 3 (Figures C49 to C60). However, this is only indicative of erosion and transport for coarser sediments. This does not include fine sediments or sediments already in suspension

Potential Suspension and Deposition

GTRAN showed areas where erosion and transport can occur for the different configurations (current only). However, the GTRAN results did not adequately address transport issues within the harbor where most of the sediment is fine-grained and much of it is already in suspension when it enters the harbor. Therefore, in addition to GTRAN results, the hydrodynamics from ADCIRC were examined to determine areas of high shear stress and potential suspension and deposition of fine-grained sediment. This section presents results which show potential areas of fine-grained sediment suspension as well as areas of potential deposition. This section also presents results of change in erosional and depositional areas generated by project conditions.

Fine Grained Suspension

Sediment is suspended if the shear stress of the fluid exceeds the critical shear stress for inception of sediment movement. Shear stress was calculated at each GTRAN grid point

by the Soulsby (1997) method with currents obtained from the 6-month and 5-year ADCIRC simulations. The maximum shear stress over the time series is shown in Figures C61-C64 for the six month return period event and Figures C65-C68 for the 5-year return period event. Low shear stresses are shown in blue and shear stresses as high as 0.5 Pa is indicated by red. Generally, shear stresses are low in the study area. The highest shear stresses occur off the north side of Dike 14 for both storms and all configurations. However, installation of the proposed CDF restricts flow between the CDF and the breakwater and results in higher shear stresses (0.15-0.2 Pa) in this area for all three configurations for both events.

The locations and frequency of potential fine-grained sediment suspension events were computed for each time step of the 6-month and 5-year ADCIRC results at each GTRAN grid point. A representative critical shear stress for fine-grained suspension of 0.12 Pa was applied. Although a reasonable approximation for the low density fine-grained surface layer, this critical shear stress is just used to represent potential change in scour areas. Actual crtical shear stress is site specific. Critical shear stress measurements for Cleveland Harbor were not part of this scope of work. The number of suspension occurrences (shear stress greater than 0.12 Pa), expressed as a percentage of the total number of time steps in the simulation, is shown in Figure C69-C72 (six month event) and C73-C76 (five-year event). The areas in white indicate that critical shear stress was not exceeded at any time at these locations, and for the assumed conditions, no fine-grained sediment would be suspended. All of the figures show that sediment is suspended ~3% of the time north of Dike 49 for the simulation period (six weeks). The base condition shows sediment suspended at the tip of the breakwater in the area of interest for both the 6-month and 5-year storms (Figures C69 and C73). Inclusion of the CDF indicates that sediment will be suspended and transported between the CDF and the breakwater less than 0.5 percent of the time during the six-week simulation. The areas of suspension are similar for the 6-month and 5-year storms; however, results with the 5-year storm show that suspension occurs farther west of the CDF for Configuration 1 and farther lakeward near the breakwater tip for Configurations 1 and 2.

The suspension frequency between the CDF configurations and base condition was compared for the 6-month (Figures C77 through C79) and 5-year (Figures C80 through C82) storms. Increases in potential suspension duration due to a configuration are shown as positive values and decreases are shown as negative values. It should be noted that negative values don’t necessarily indicate areas of increased deposition, only less suspension. Configurations 1 and 2 show an increase up to 0.15 percent in suspension events between the CDF and the breakwater, and a decrease up to 0.15 percent at the breakwater tip for the 6-month storm (Figures C77 and C78). Suspension duration also increases between the CDF and breakwater with Configuration 3; however,

the increase is less (~0.05 percent) (Figure C79). Similar differences are observed with the 5-year storm, but there is no difference in shear stress at the breakwater tip for Configurations 1 and 2 (Figures C80 and C81). Configuration 3 includes the extension of the breakwater and, as a result, shear stress decreases at the location of existing breakwater tip (Figure C82). However, no change in shear stress occurs at the proposed new tip from base conditions. Additionally, shear stress decreases north of Dike 14 with Configuration 3 with both the 6-month and 5-year storms.

The figures indicate that the hydrodynamics of the 6-month and 5-year storms will not significantly suspend additional sediment from the bottom. The areas where sediment suspension time periods increase will be between the CDF and breakwater, but these increases are 0.15 percent or less.

Deposition

The above analysis indicates areas where fine-grained sediment erosion changes may occur. However, changes in deposition patterns must also be assessed for each design scenario. A parameter was computed based on sediment size and flow magnitude to determine locations of potential sedimentation. Settling of suspended sediments can occur if the shear velocity, u_*, of the flow approaches the fall speed of the suspended sediment, w_s assuming the particles do not flocculate. Therefore, if the ratio of u_* to w_s is less than unity, settling of suspended sediment should occur. The shear velocity is defined as:

$$u_* = \sqrt{\frac{\tau}{\rho}} \tag{6}$$

in which τ is shear stress of the flow and ρ is density of the fluid. Fall velocity was calculated by the optimization of Soulsby (1997):

$$w_s = \frac{\nu}{d_{50}} \sqrt{10.36^2 + 1.049 D_*^3} - 10.36 \tag{7}$$

where υ is kinematic viscosity, d_{50} is the sediment diameter, and D_* is the dimensionless particle size parameter (Equation 5).

Suspended solids concentrations are spatially and temporally varying over the domain. Since there is no sediment transport model available for Cleveland Harbor, concentrations and settling rates cannot be quantified. However, the detailed hydrodynamic model permits us to quantify times were deposition will likely occur at each grid cell in the domain. For this assessment, it is assumed that fine-grained sediment

is always available in the water column for deposition. The percentage of deposition occurrences (as estimated using equations 6 and 7) was computed for each time step in the 6-month and 5-year storms over the GTRAN grid (Figures C83 through C90). The present (base) condition shows a high percentage of time for potential deposition midway between the East 55th State Marina and the breakwater. For all three configurations, deposition decreased between the CDF and breakwater due to higher shear stress magnitudes. The presence of the CDF increases potential deposition near the shoreline within and east of the breakwater. Additionally, the figures indicate deposition occurs 20-40 percent of the time outside the breakwater. It should be noted again that outside the breakwater, waves would have an impact on deposition potential. Inclusion of waves would keep sediment in suspension and show less deposition, especially outside of the breakwater.

Figures C91 through C96 show the percent change in time periods of potential deposition between the configuration plans and the base condition. In all configurations and with both storms less deposition occurred between the CDF and the breakwater by approximately 40 percent. Deposition increased along the sides of the CDF; predominately on the northeast side. Increased duration of deposition for Configuration 1 was approximately 30 to 35 percent along the northeast side and 25 to 30 percent along the southwest side for the 6-month and 5-year storms. Deposition time duration increased approximately 35 percent northeast of the Configuration 2 CDF and 15 to 20 percent on the southwest side for both storms. Deposition increase along the Configuration 3 CDF was typically 40 percent, northeast side, and 15 percent, southwest side.

Conclusions

The GTRAN model and shear stress analysis were applied to assess changes in erosion and deposition induced by CDF construction. Two major events were simulated. Analysis indicates that the area around the proposed CDF remains predominately non-erosional. Sediment suspension is not altered significantly by the CDF. However, time periods of potential deposition were altered significantly with the proposed CDF. Areas between the CDF and breakwater will experience less depositional conditions while areas to the east and west of the proposed CDF would experience more time periods where deposition can occur.

References

Soulsby, R.L., 1997. Dynamics of Marine Sands. Thomas Telford Publications, London, UK.

van Rijn, L. C. 1984. Sediment transport: Part I: Bed load transport; Part II: Suspended load transport; Part III: Bed forms and alluvial roughness. Journal of Hydraulic Engineering 110(10):1431–1456; 110(11):1613–1641; 110(12):1733–1754.

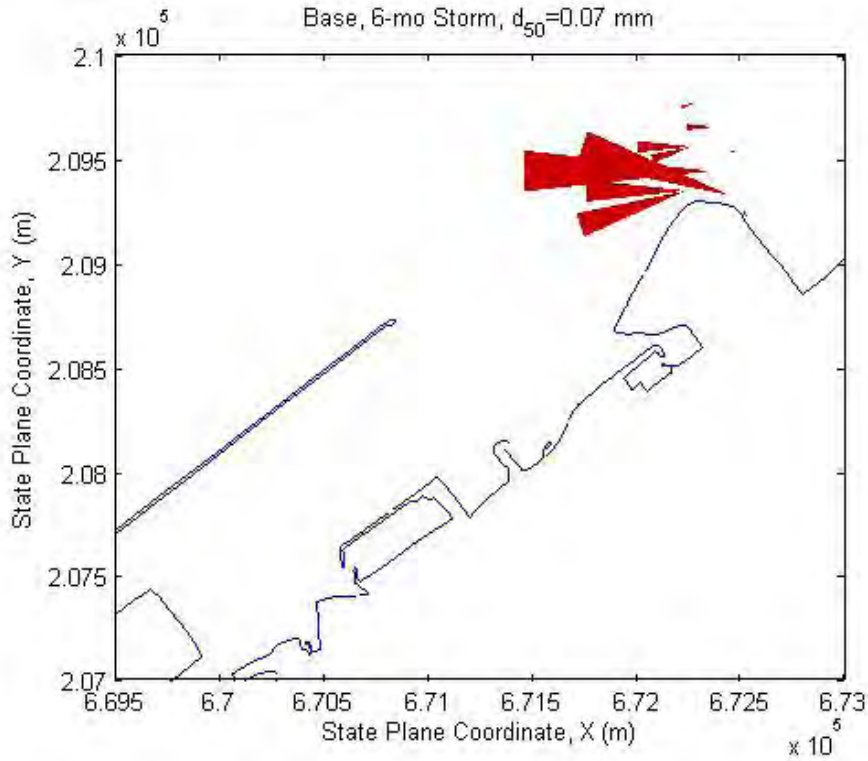

Figure C1. Sediment transport rose plots for Base conditions, 6-mo storm, d_{50}=0.07 mm

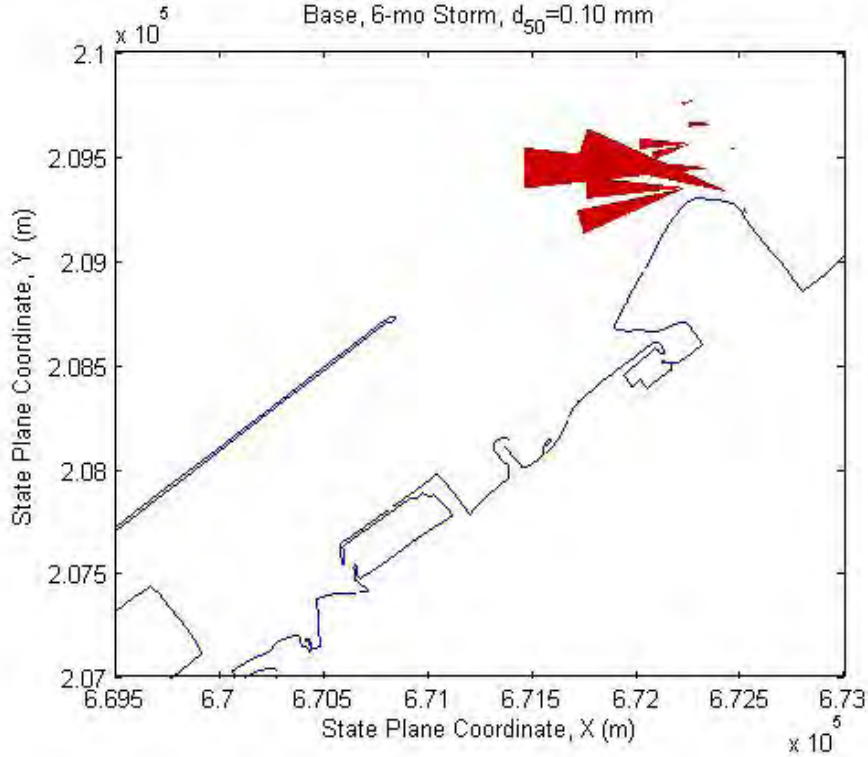

Figure C2. Sediment transport rose plots for Base conditions, 6-mo storm, d_{50}=0.10 mm

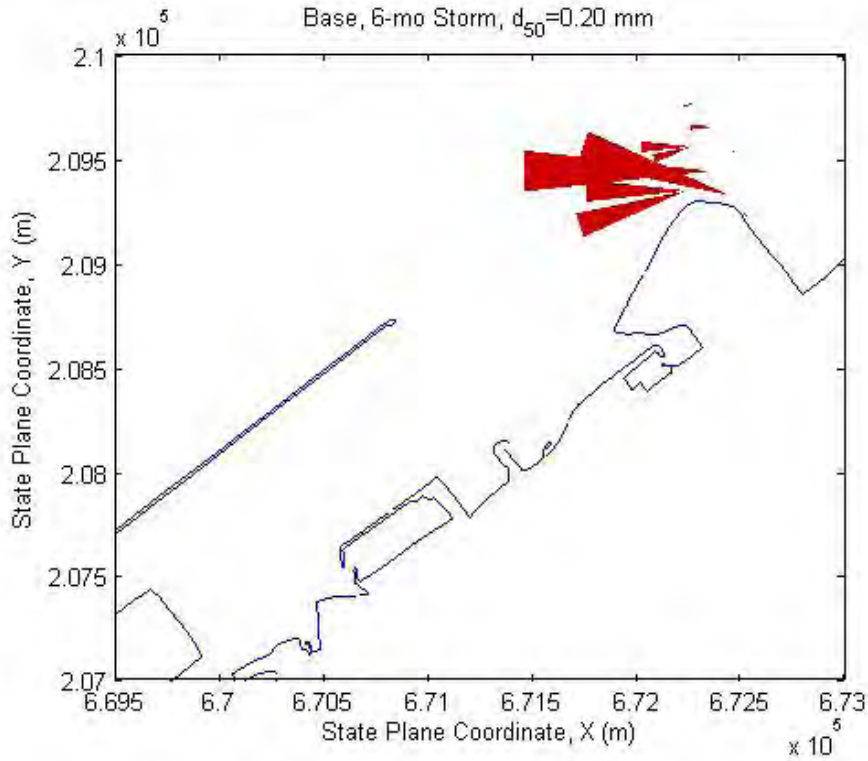

Figure C3. Sediment transport rose plots for Base conditions, 6-mo storm, d_{50}=0.20 mm

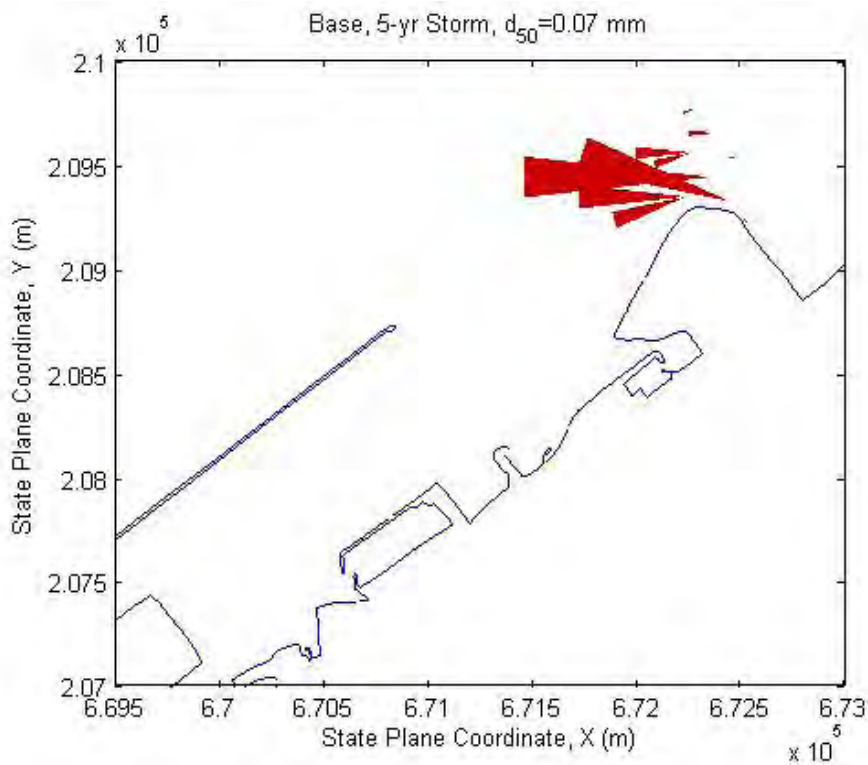

Figure C4. Sediment transport rose plots for Base conditions, 5-year storm, d_{50}=0.07 mm

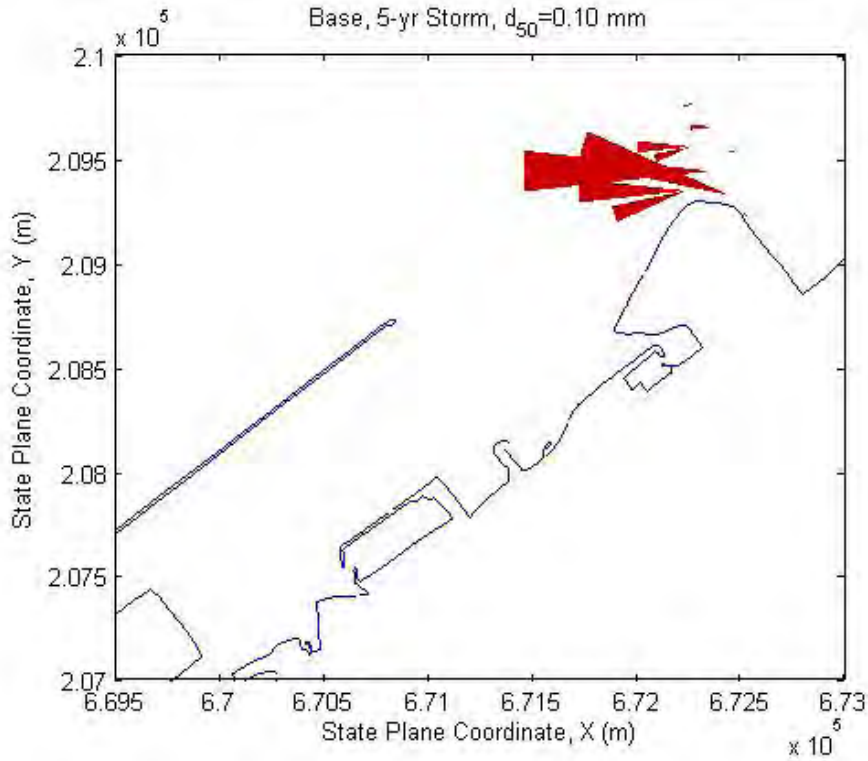

Figure C5. Sediment transport rose plots for Base conditions, 5-year storm, d_{50}=0.10 mm

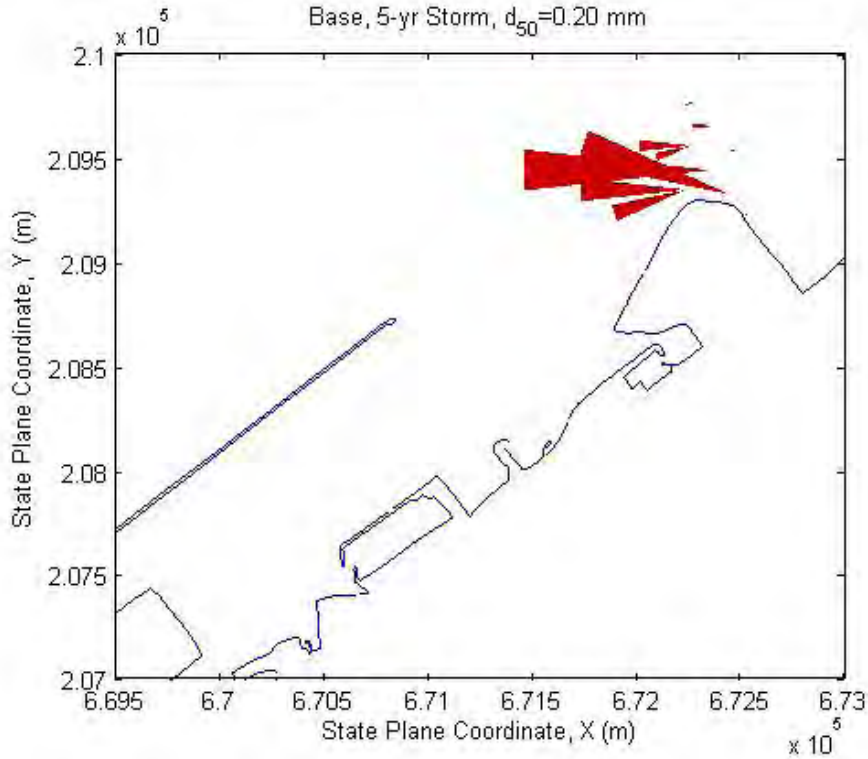

Figure C6. Sediment transport rose plots for Base conditions, 5-year storm, d_{50}=0.20 mm

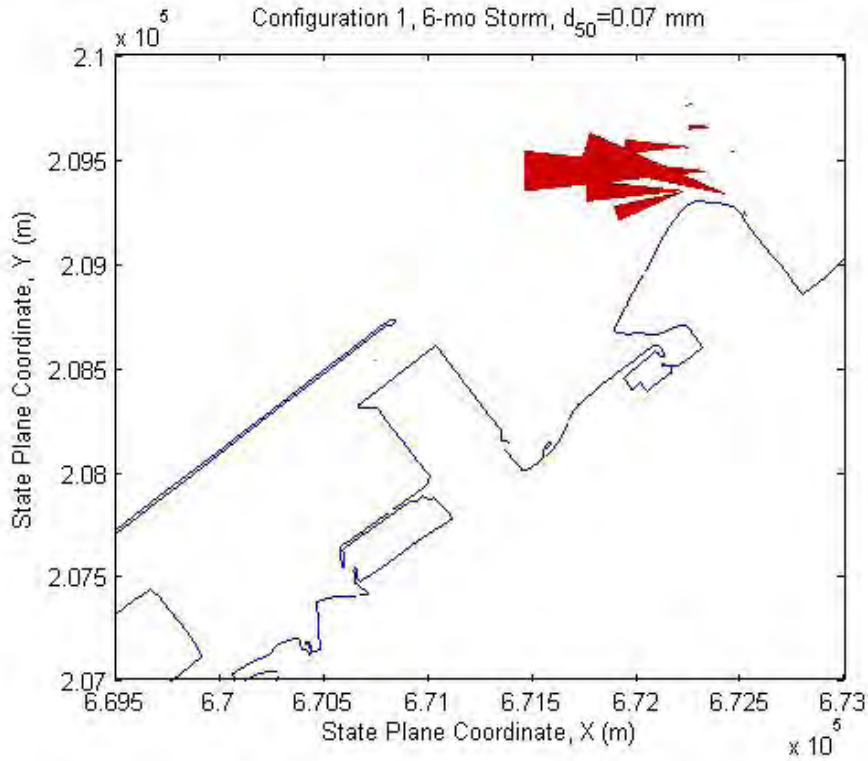

Figure C7. Sediment transport rose plots for Configuration 1, 6-mo storm, d_{50}=0.07 mm

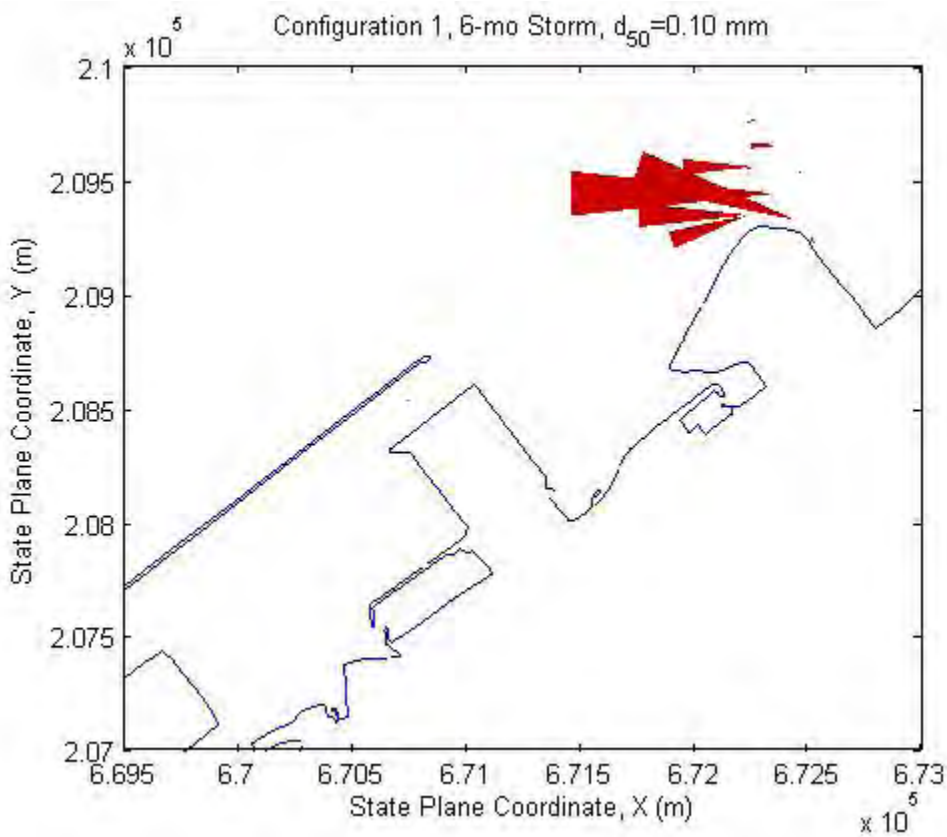

Figure C8. Sediment transport rose plots for Configuration 1, 6-mo storm, d_{50}=0.10 mm

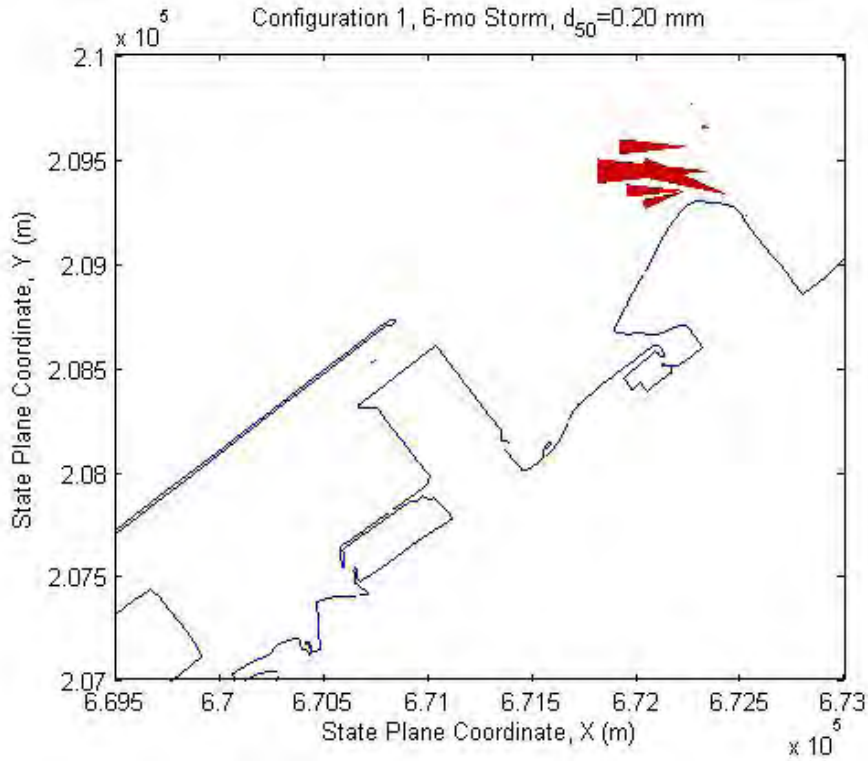

Figure C9. Sediment transport rose plots for Configuration 1, 6-mo storm, d_{50}=0.20 mm

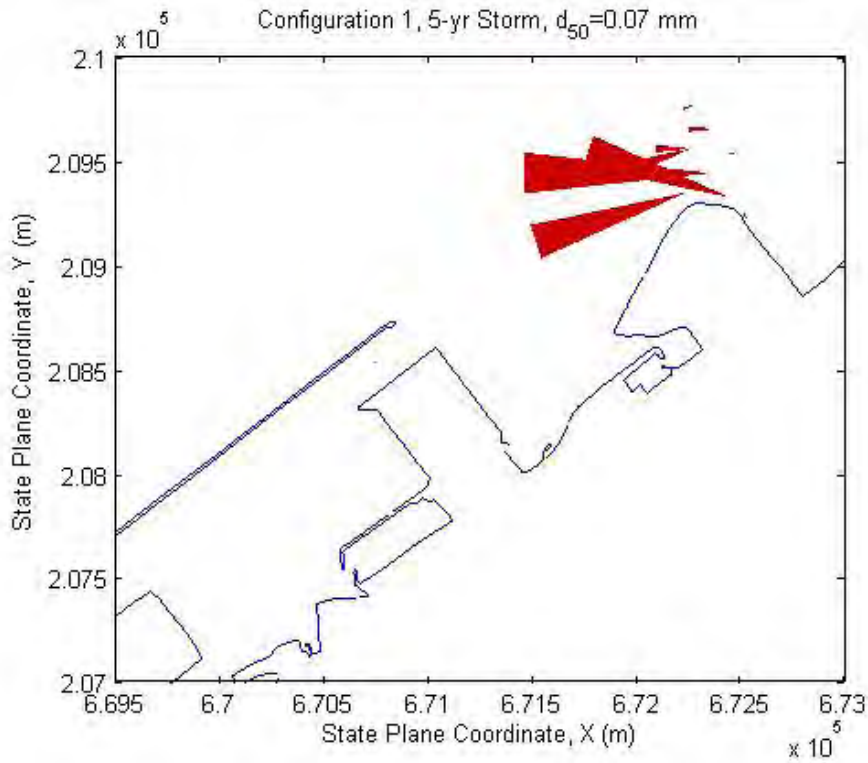

Figure C10. Sediment transport rose plots for Configuration 1, 5-year storm, d_{50}=0.07 mm

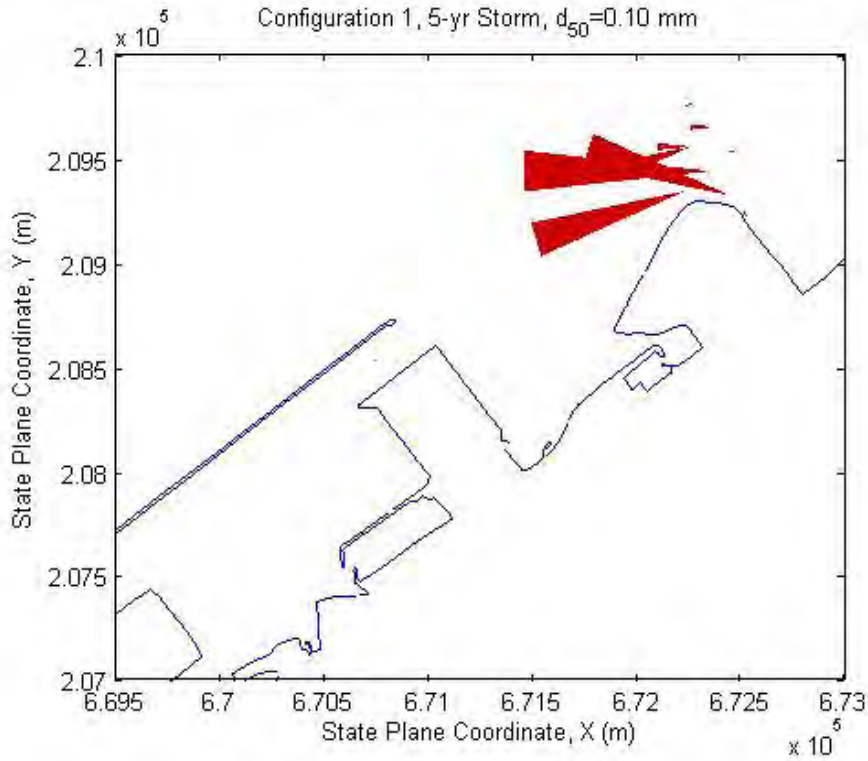

Figure C11. Sediment transport rose plots for Configuration 1, 5-year storm, d_{50}=0.10 mm

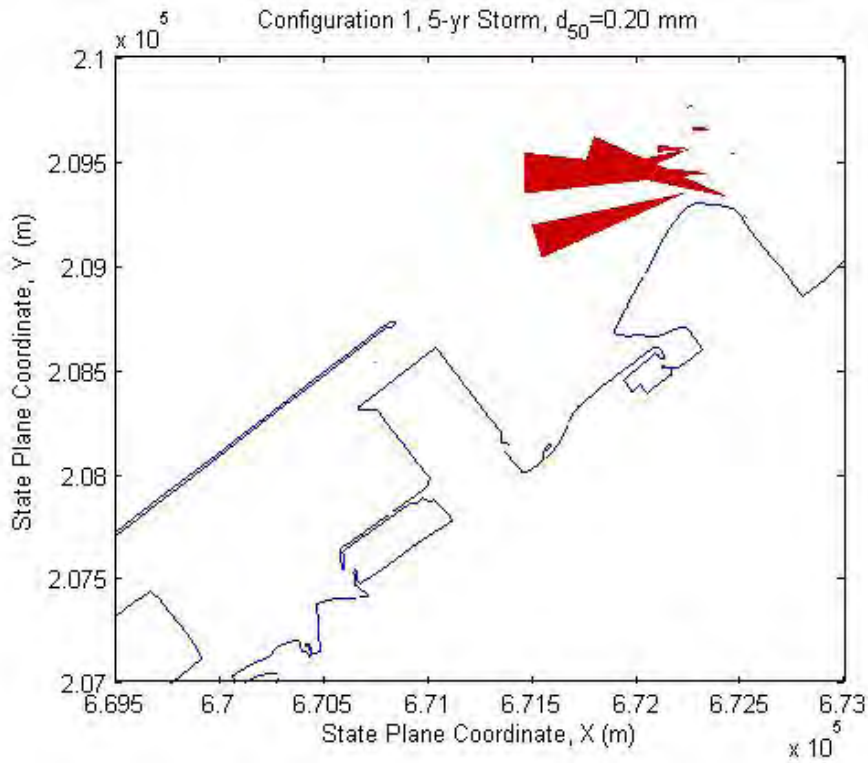

Figure C12. Sediment transport rose plots for Configuration 1, 5-year storm, d_{50}=0.20 mm

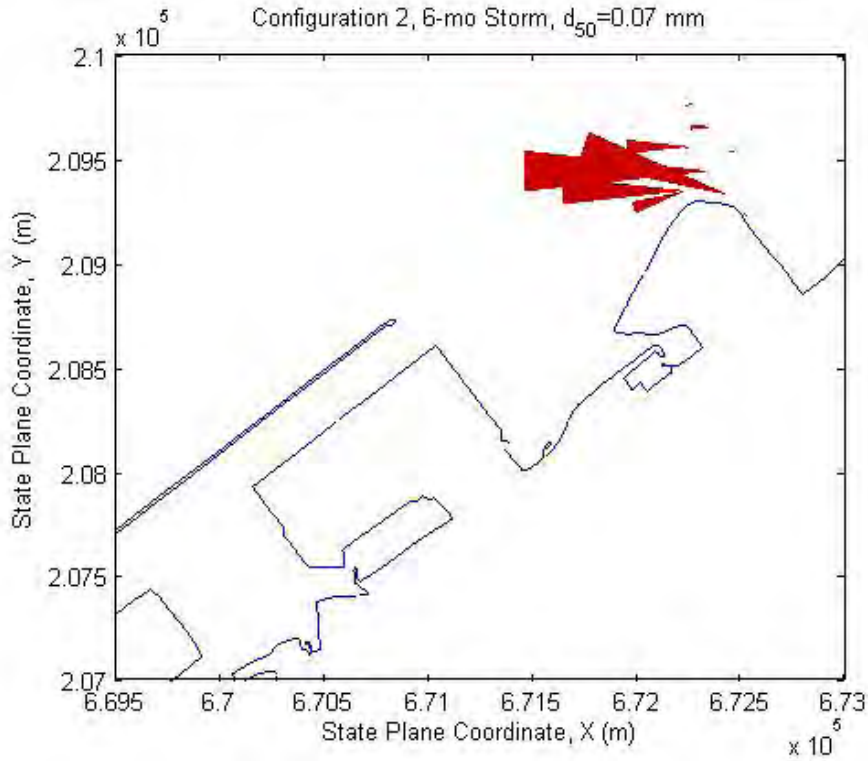

Figure C13. Sediment transport rose plots for Configuration 2, 6-mo storm, d_{50}=0.07 mm

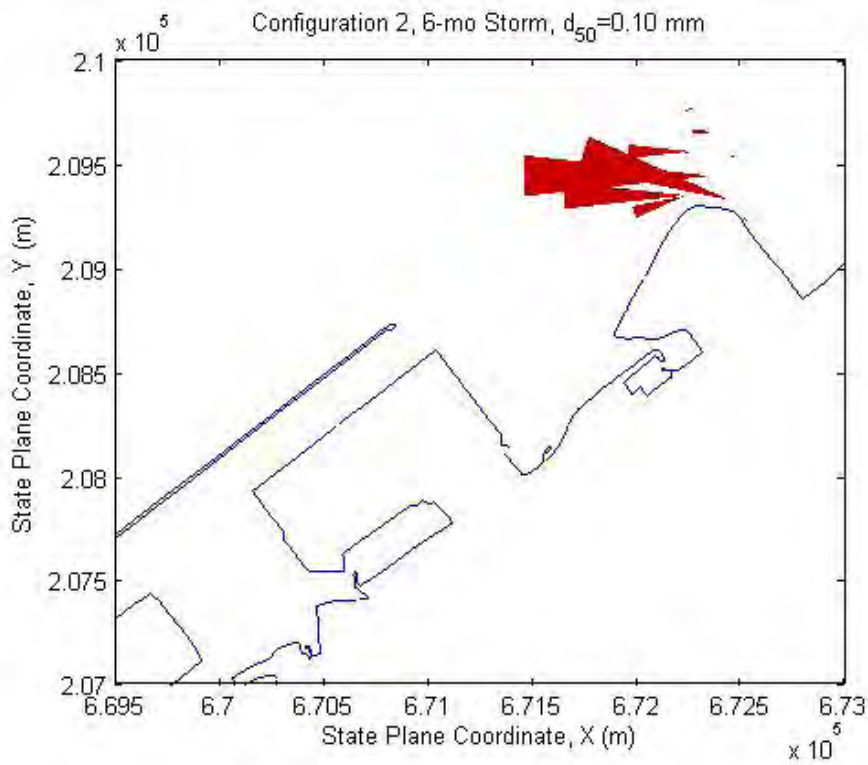

Figure C14. Sediment transport rose plots for Configuration 2, 6-mo storm, d_{50}=0.10 mm

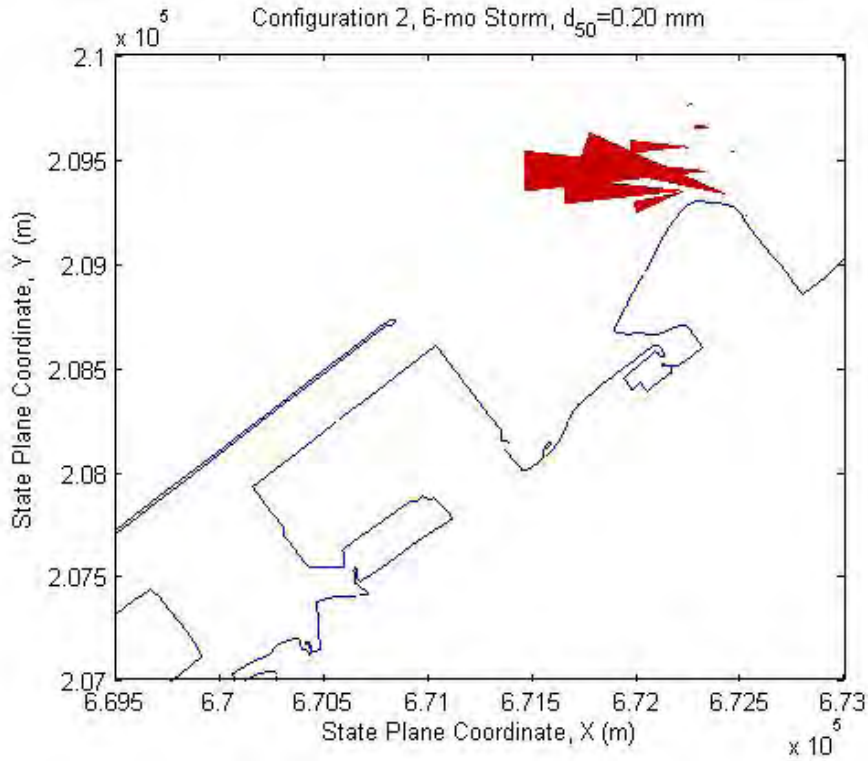

Figure C15. Sediment transport rose plots for Configuration 2, 6-mo storm, d_{50}=0.20 mm

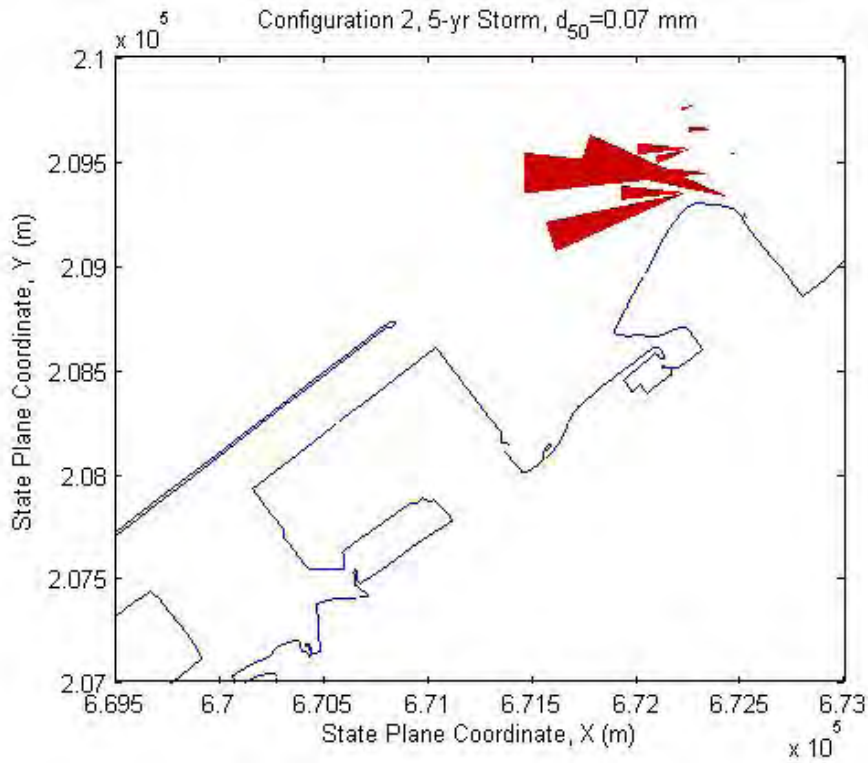

Figure C16. Sediment transport rose plots for Configuration 2, 5-year storm, d_{50}=0.07 mm

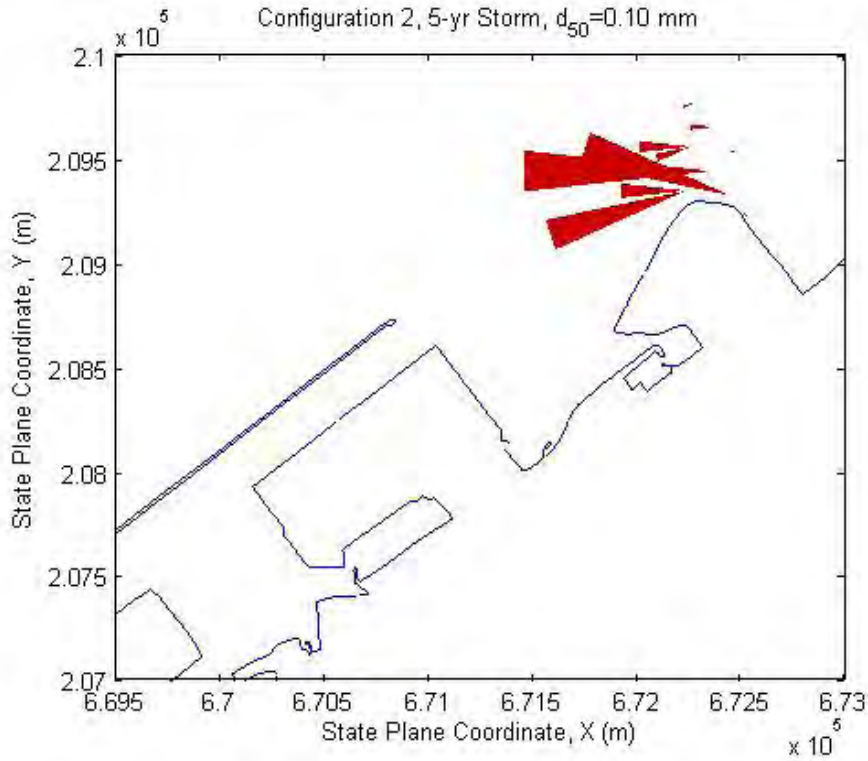

Figure C17. Sediment transport rose plots for Configuration 2, 5-year storm, d_{50}=0.10 mm

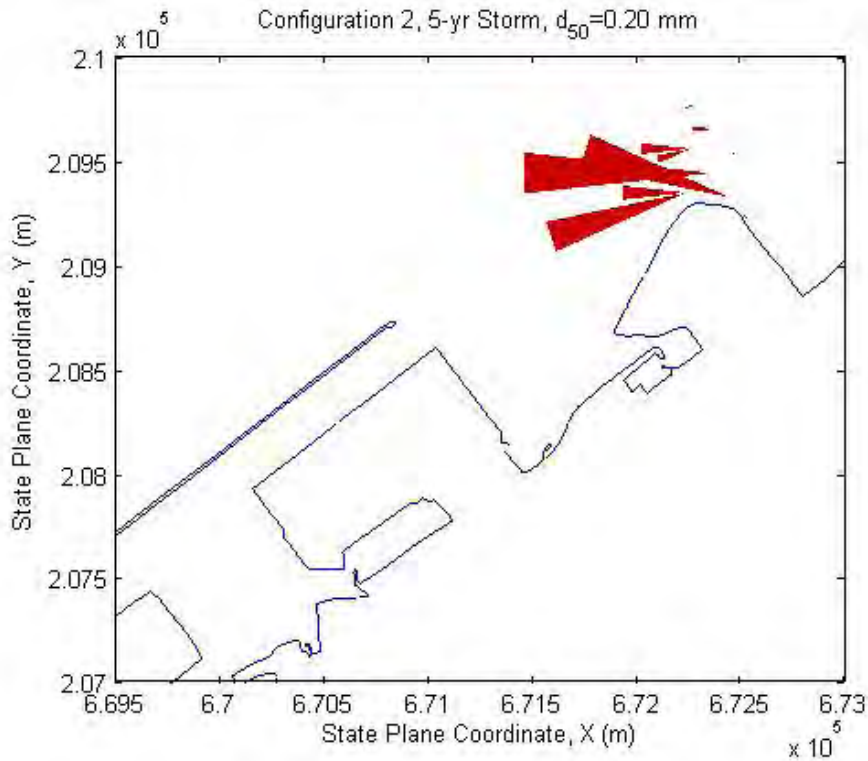

Figure C18. Sediment transport rose plots for Configuration 2, 5-year storm, d_{50}=0.20 mm

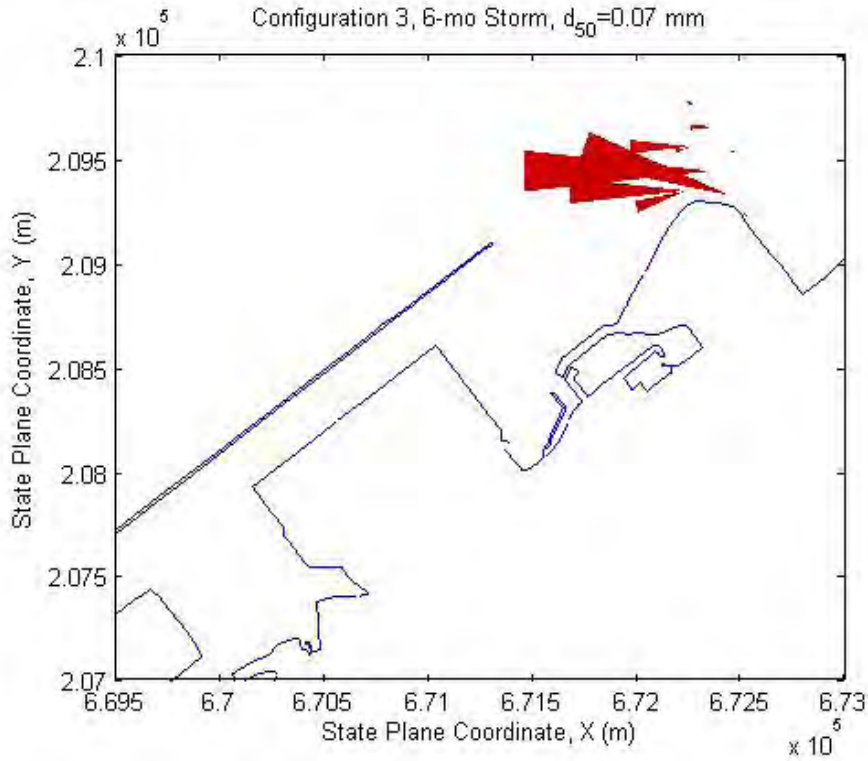

Figure C19. Sediment transport rose plots for Configuration 3, 6-mo storm, d_{50}=0.07 mm

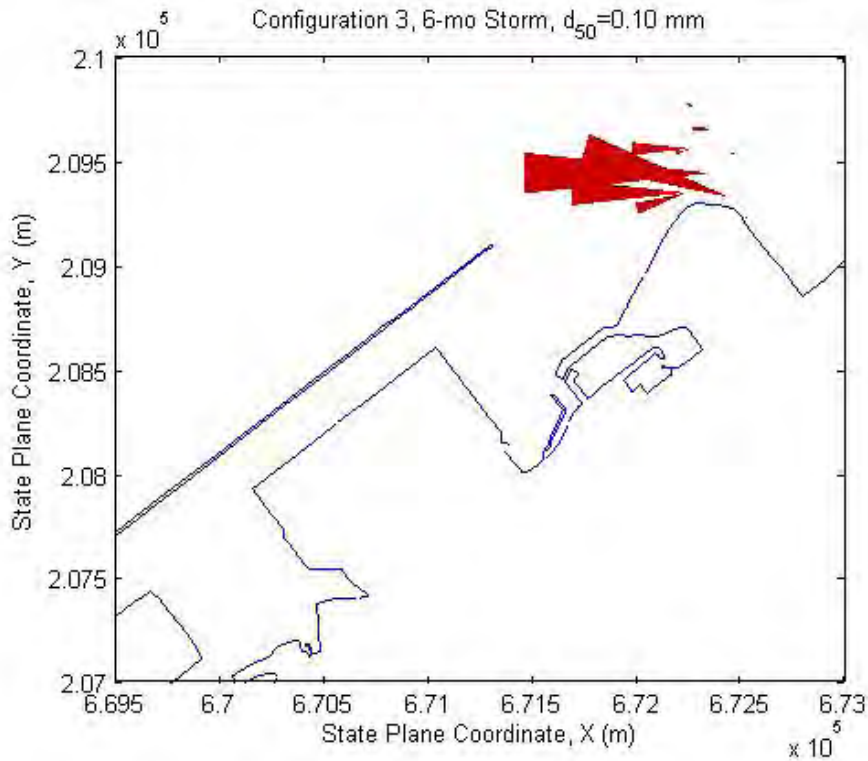

Figure C20. Sediment transport rose plots for Configuration 3, 6-mo storm, d_{50}=0.10 mm

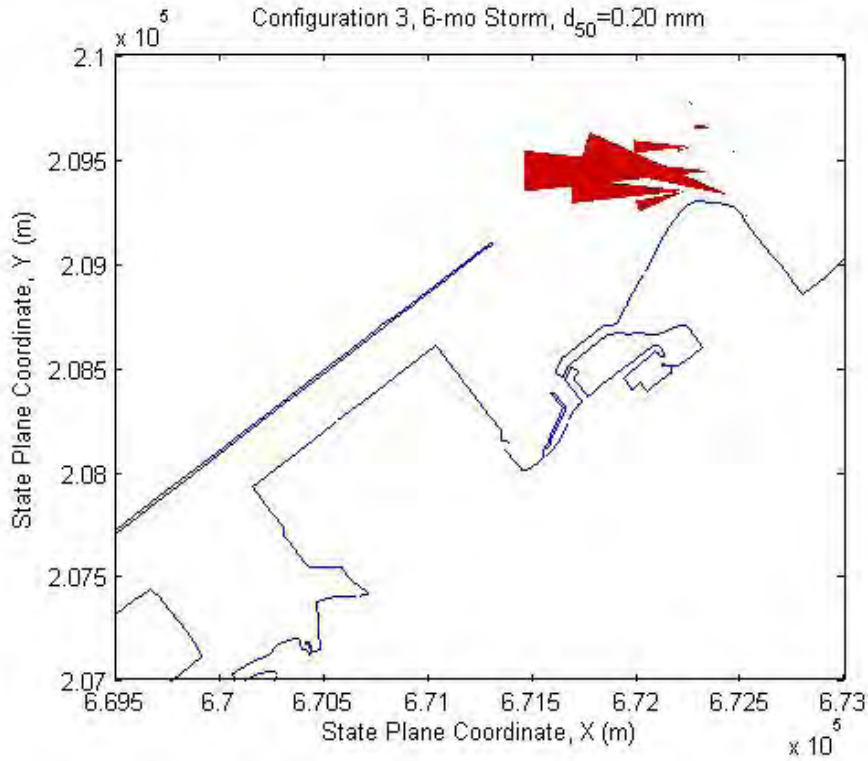

Figure C21. Sediment transport rose plots for Configuration 3, 6-mo storm, d_{50}=0.20 mm

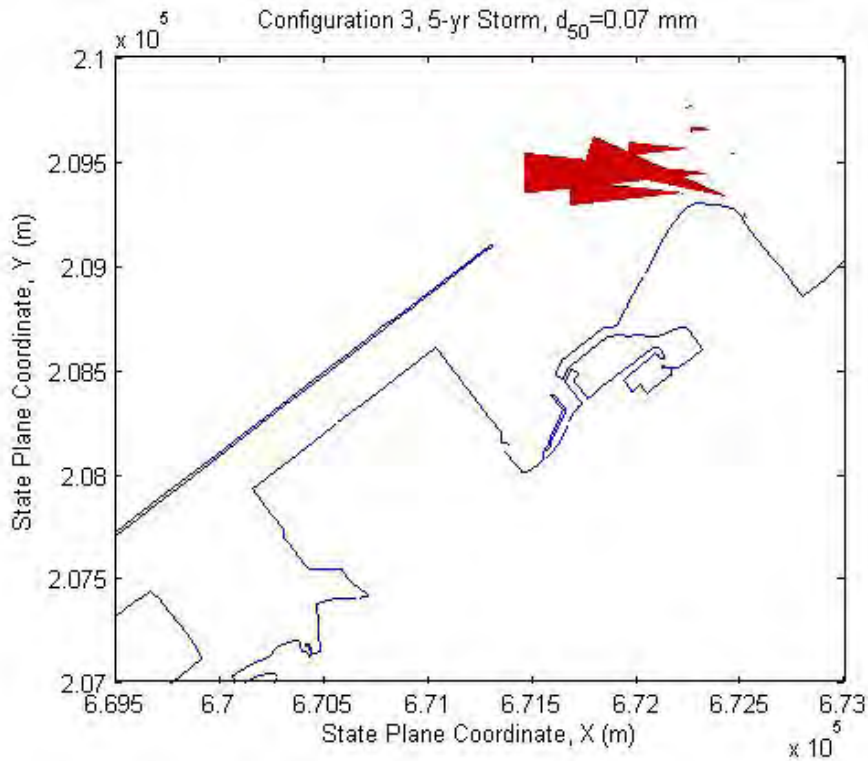

Figure C22. Sediment transport rose plots for Configuration 3, 5-year storm, d_{50}=0.07 mm

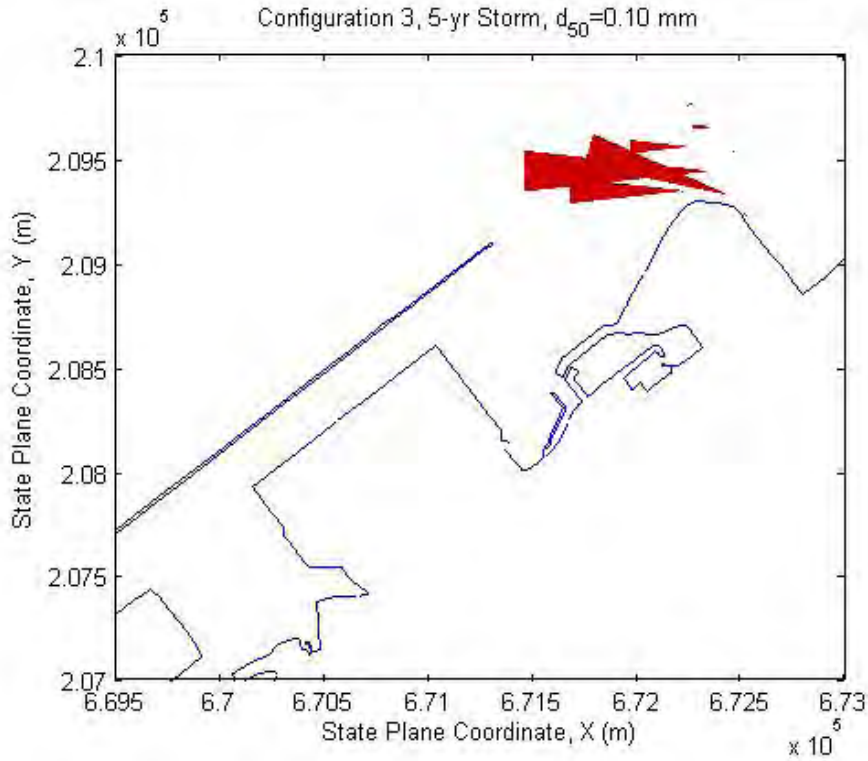

Figure C23. Sediment transport rose plots for Configuration 3, 5-year storm, d_{50}=0.10 mm

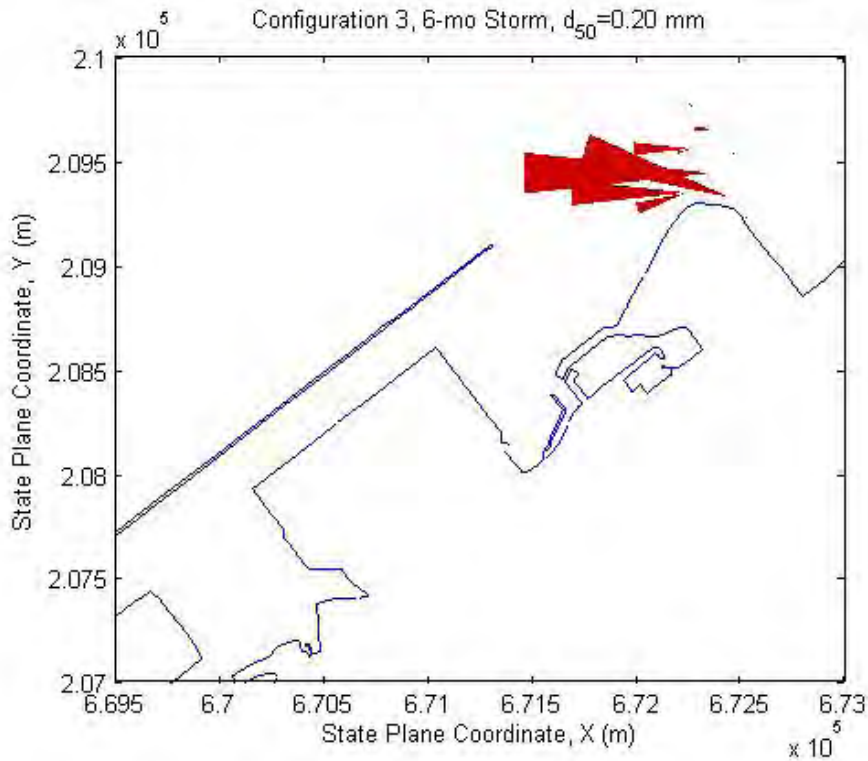

Figure C24. Sediment transport rose plots for Configuration 3, 5-year storm, d_{50}=0.20 mm

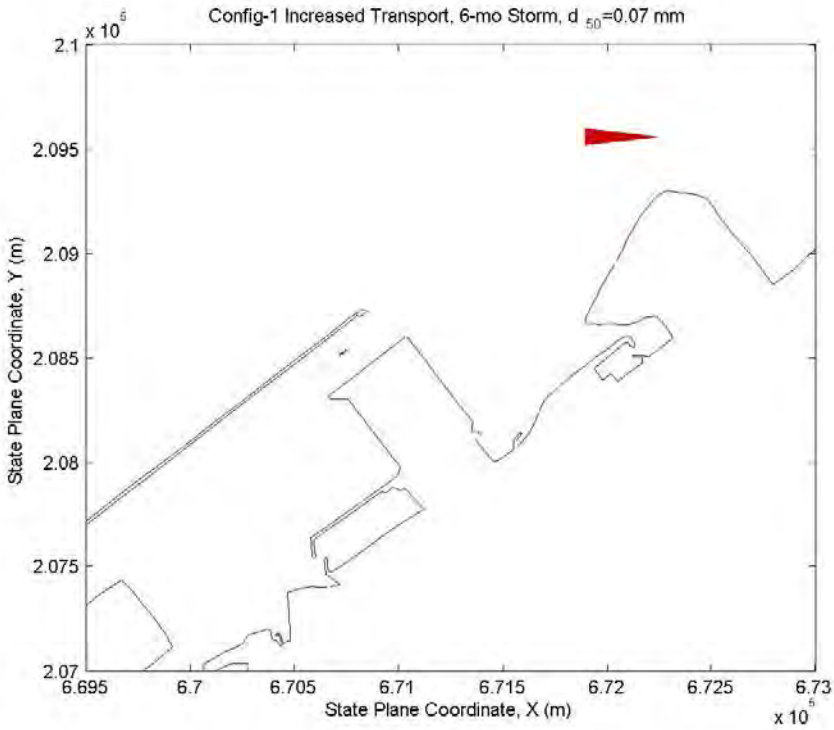

Figure C25. Configuration 1 increased transport, 6-mo storm, d_{50}=0.07 mm

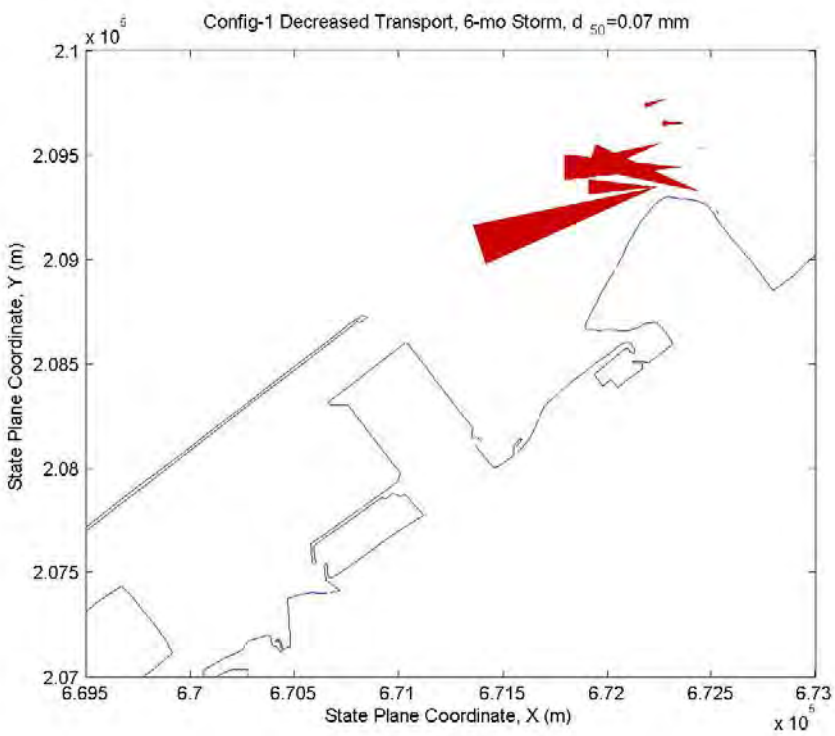

Figure C26. Configuration 1 decreased transport, 6-mo storm, d_{50}=0.07 mm

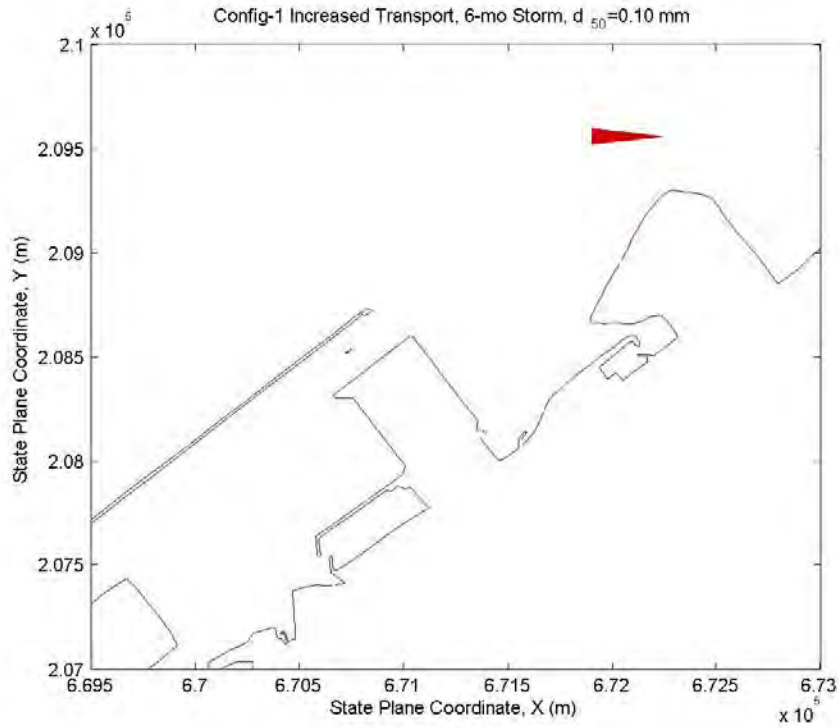

Figure C27. Configuration 1 increased transport, 6-mo storm, d_{50}=0.10 mm

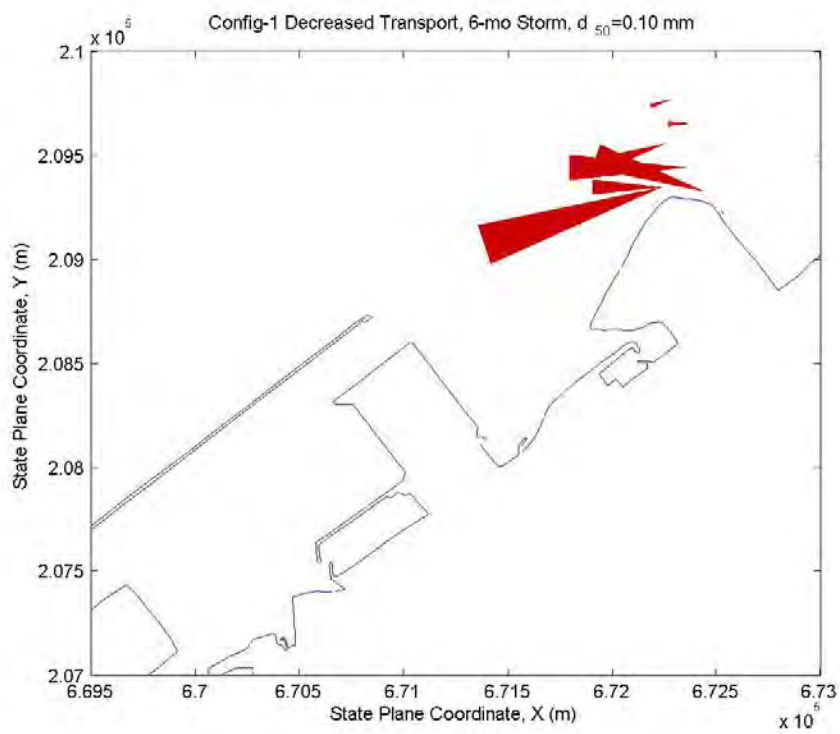

Figure C28. Configuration 1 decreased transport, 6-mo storm, d_{50}=0.10 mm

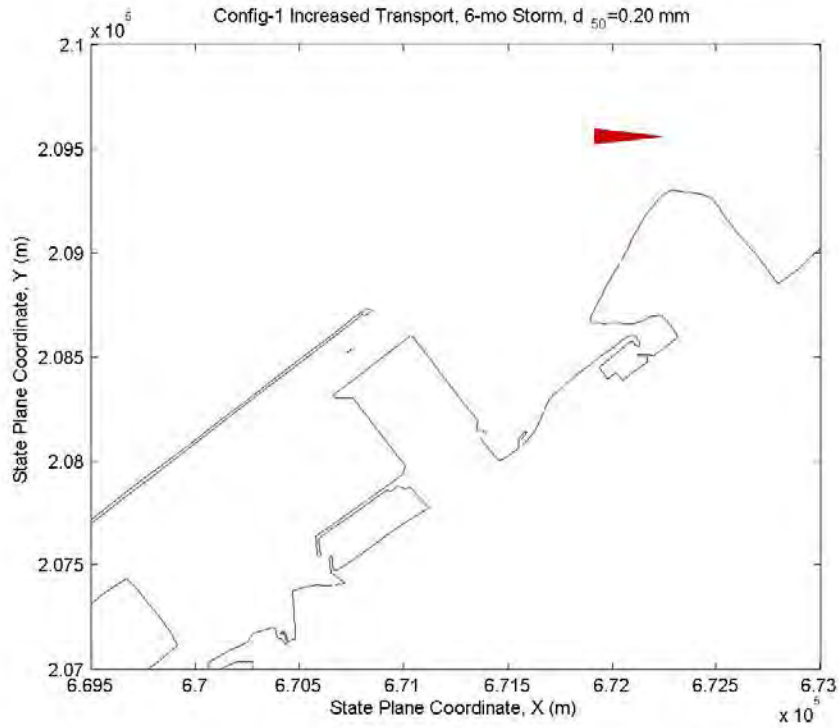

Figure C29. Configuration 1 increased transport, 6-mo storm, d_{50}=0.20 mm

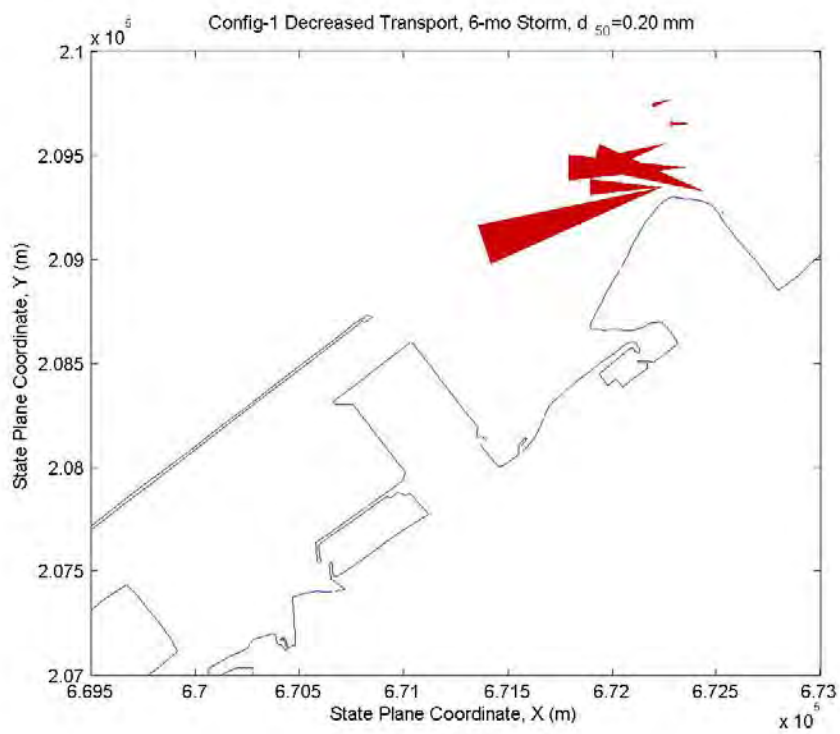

Figure C30. Configuration 1 decreased transport, 6-mo storm, d_{50}=0.20 mm

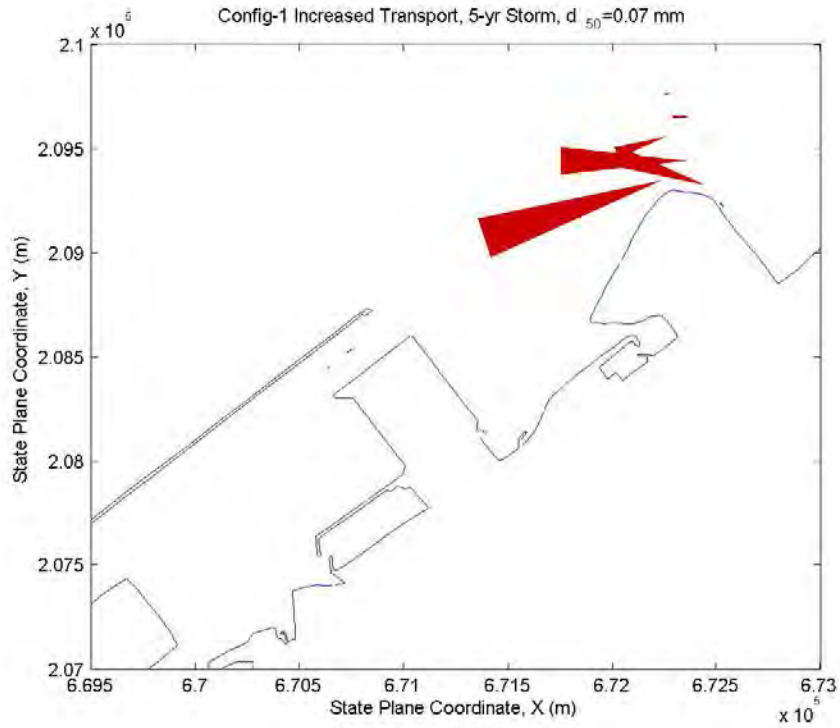

Figure C31. Configuration 1 increased transport, 5-year storm, d_{50}=0.07 mm

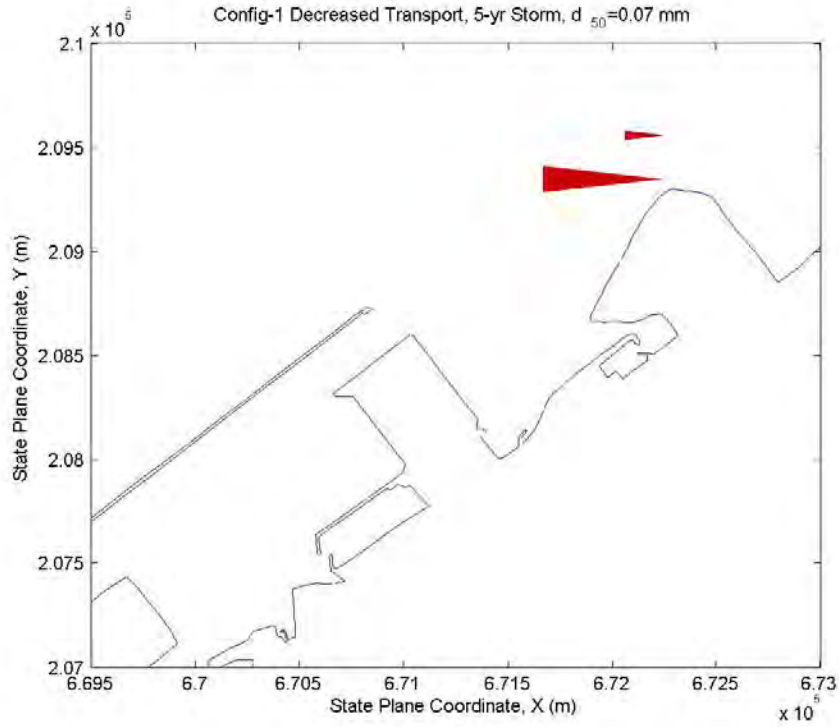

Figure C32. Configuration 1 decreased transport, 5-year storm, d_{50}=0.07 mm

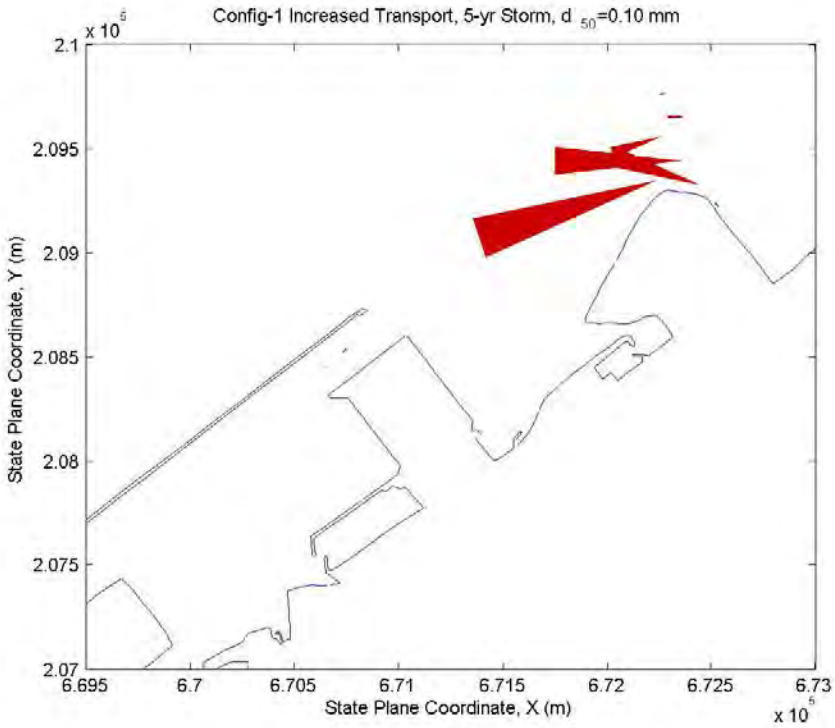

Figure C33. Configuration 1 increased transport, 5-year storm, d_{50}=0.10 mm

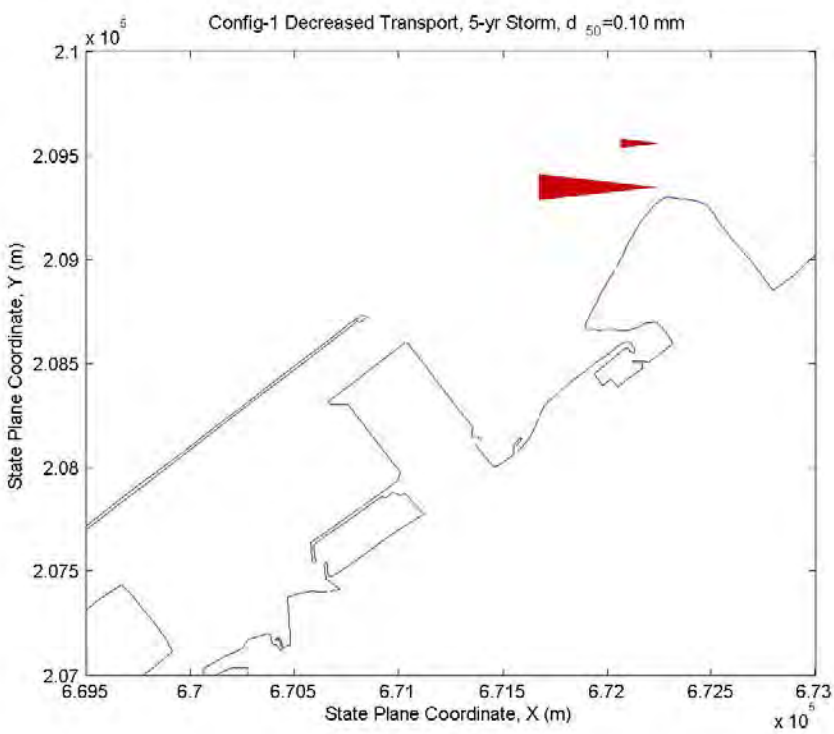

Figure C34. Configuration 1 decreased transport, 5-year storm, d_{50}=0.10 mm

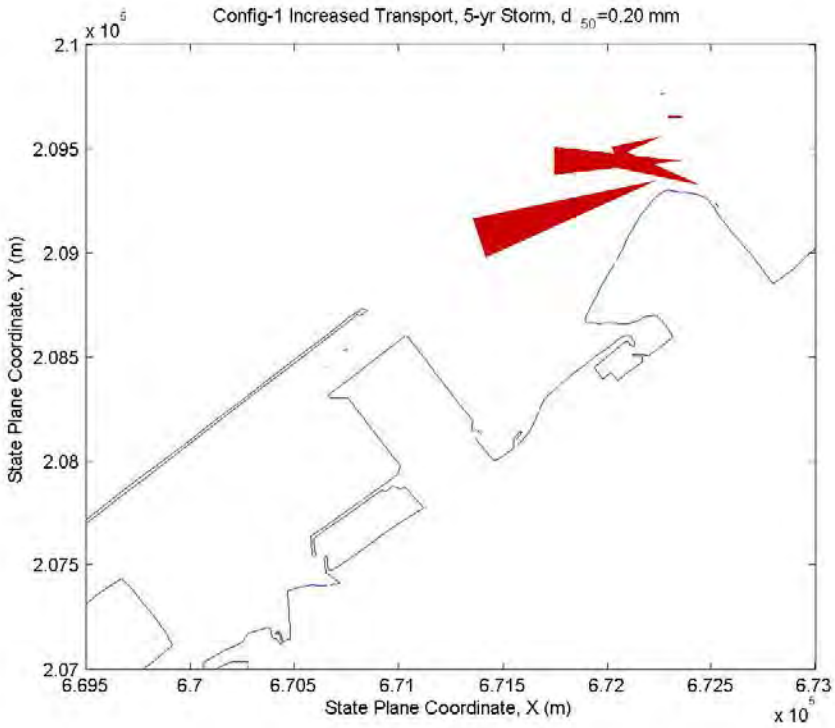

Figure C35. Configuration 1 increased transport, 5-year storm, d_{50}=0.20 mm

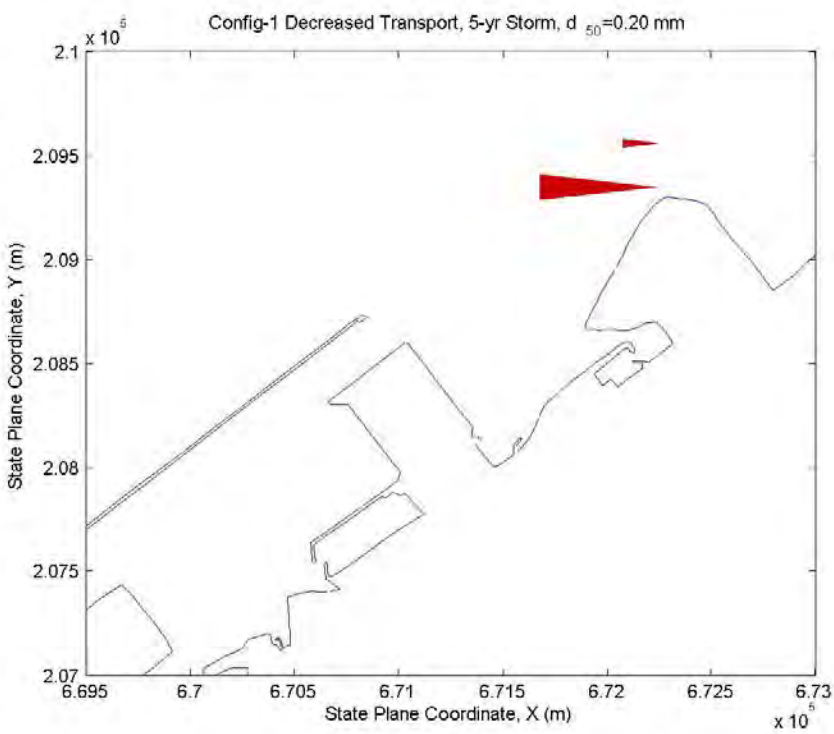

Figure C36. Configuration 1 decreased transport, 5-year storm, d_{50}=0.20 mm

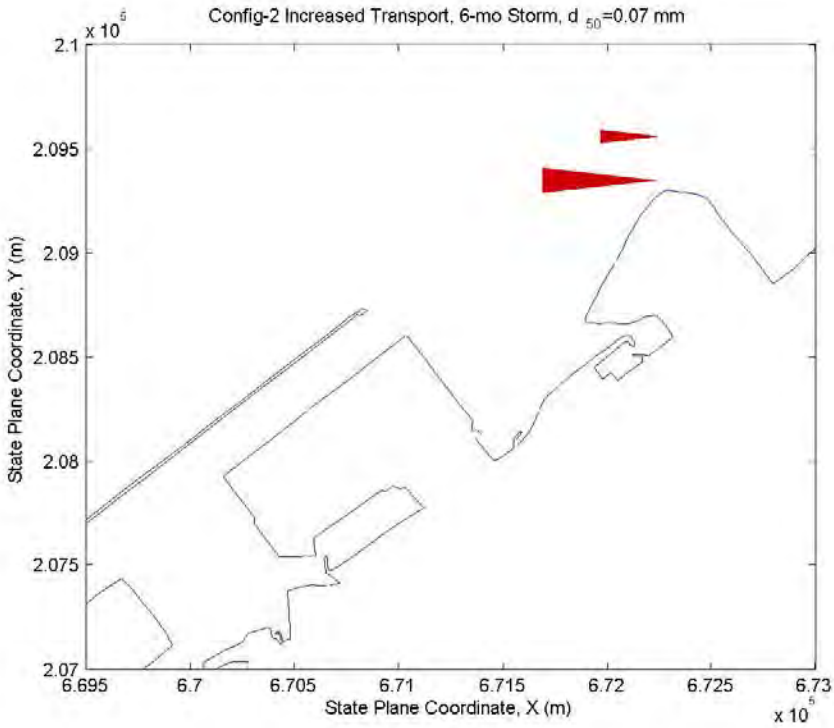

Figure C37. Configuration 2 increased transport, 6-mo storm, d_{50}=0.07 mm

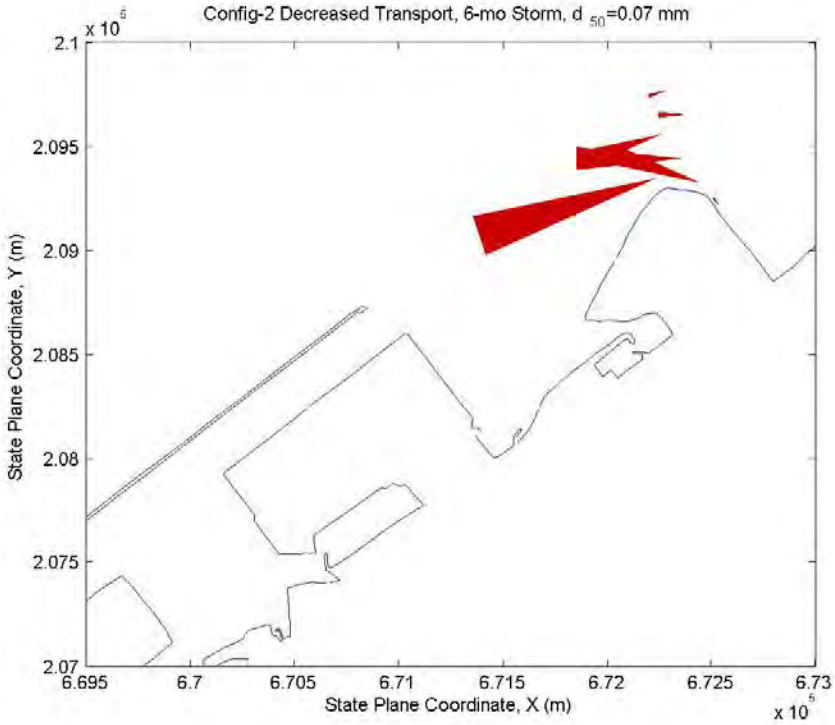

Figure C38. Configuration 2 decreased transport, 6-mo storm, d_{50}=0.07 mm

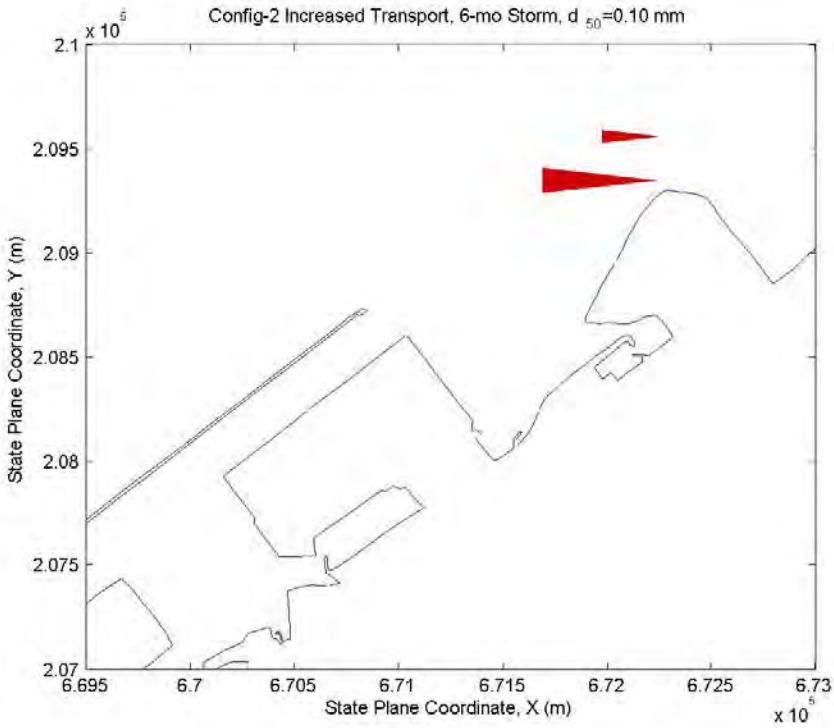

Figure C39. Configuration 2 increased transport, 6-mo storm, d_{50}=0.10 mm

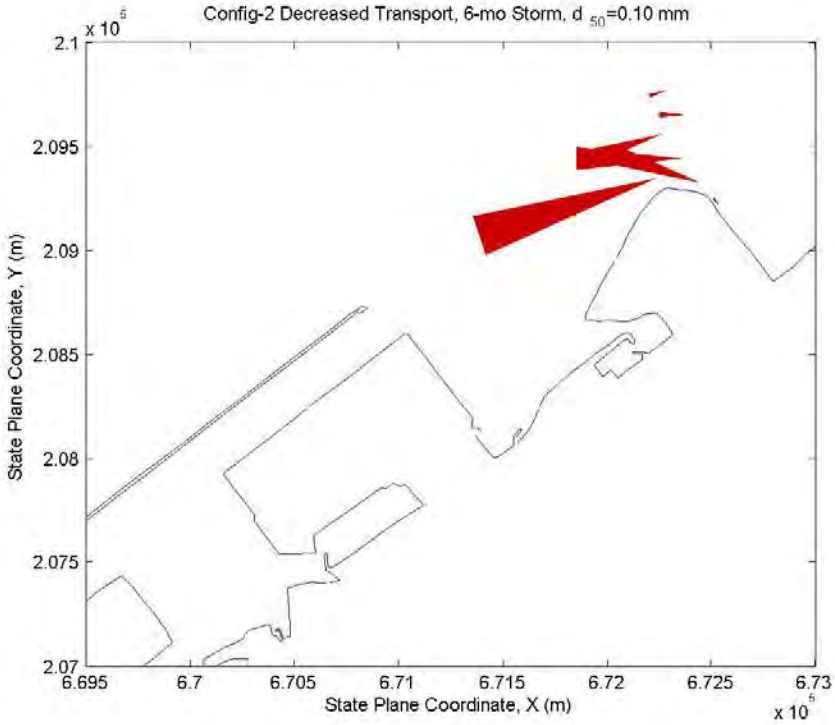

Figure C40. Configuration 2 decreased transport, 6-mo storm, d_{50}=0.10 mm

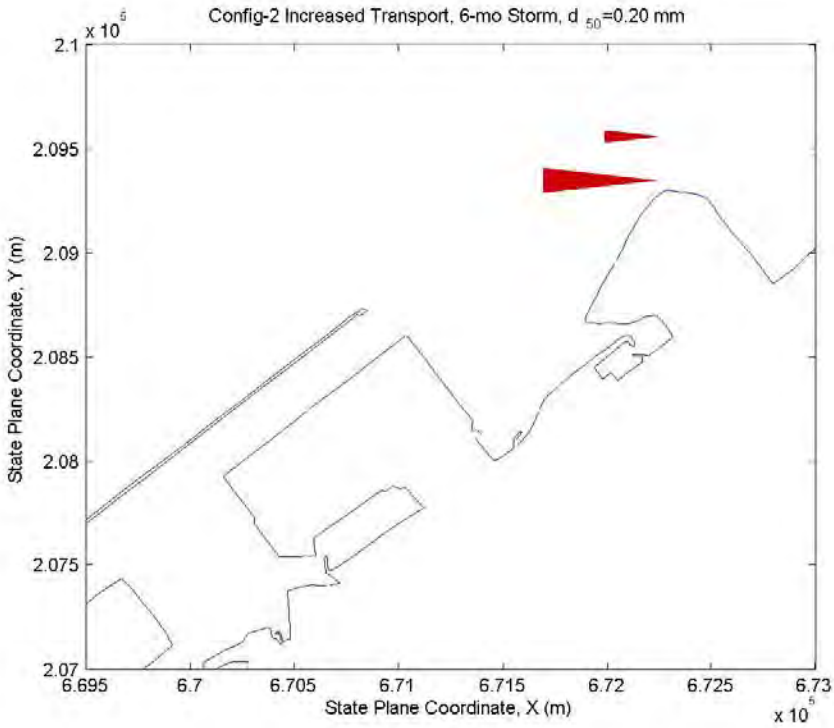

Figure C41. Configuration 2 increased transport, 6-mo storm, d_{50}=0.20 mm

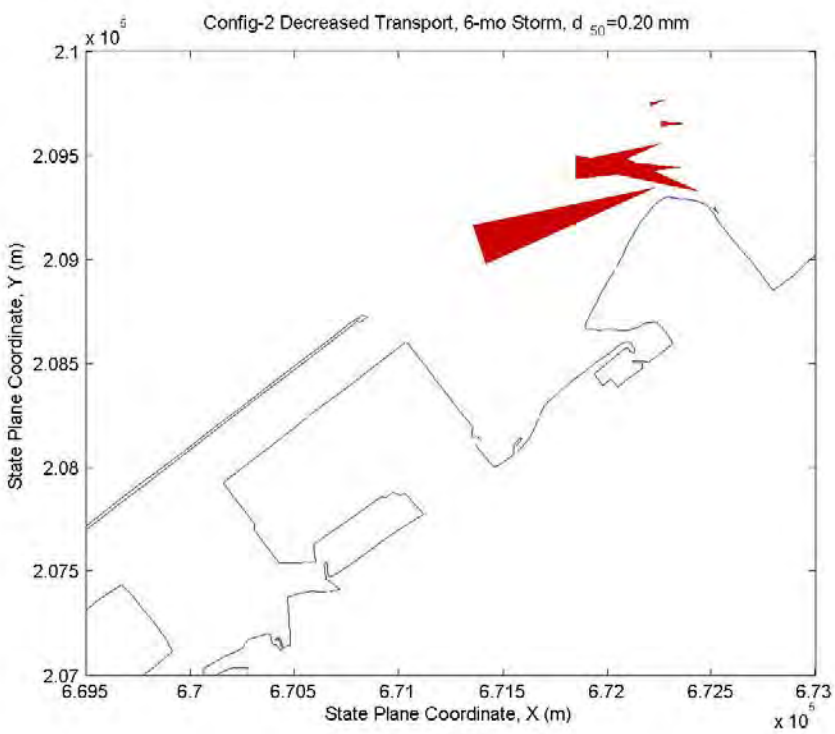

Figure C42. Configuration 2 decreased transport, 6-mo storm, d_{50}=0.20 mm

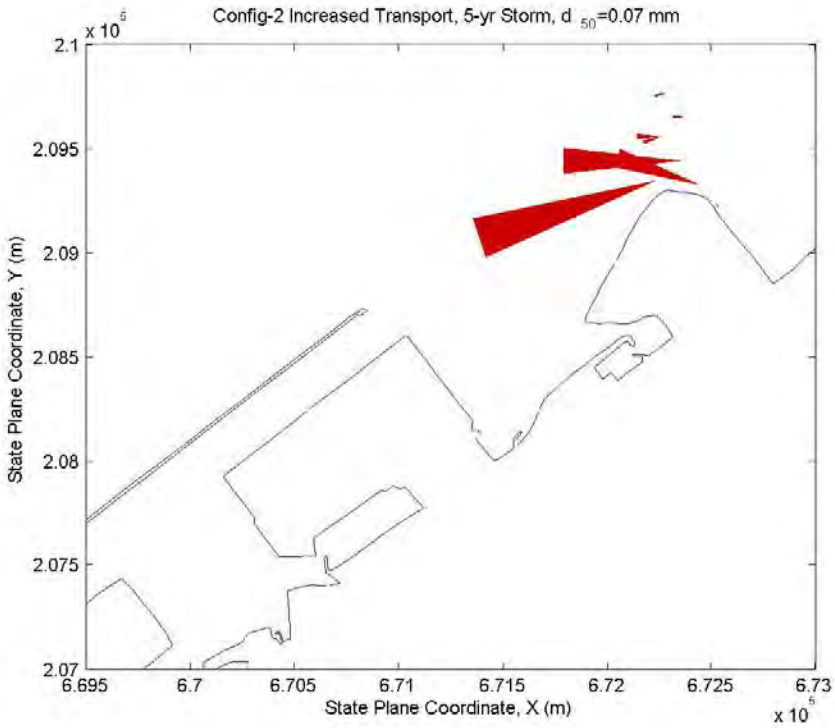

Figure C43. Configuration 2 increased transport, 5-year storm, d_{50}=0.07 mm

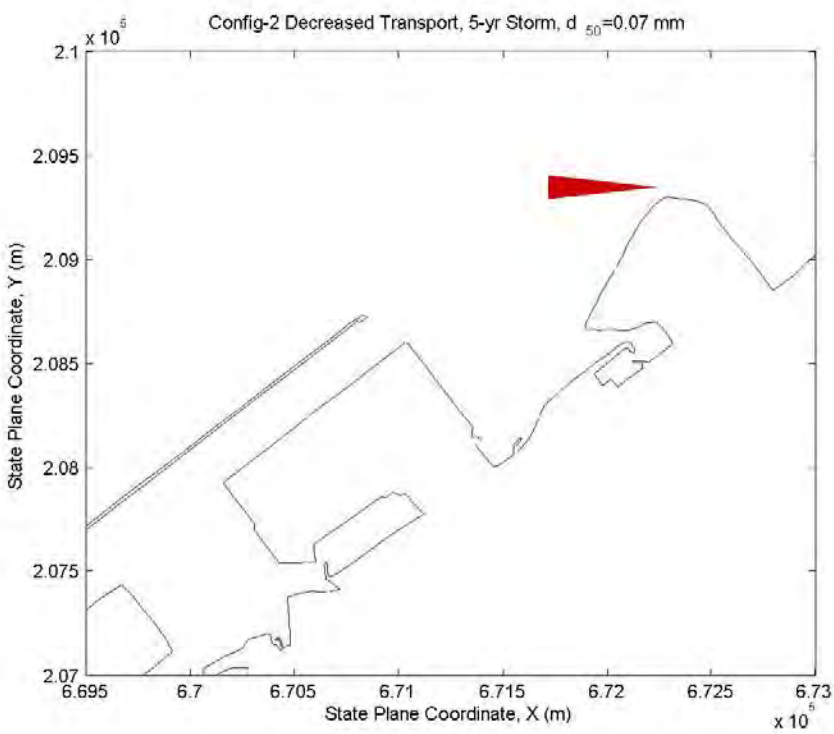

Figure C44. Configuration 2 decreased transport, 5-year storm, d_{50}=0.07 mm

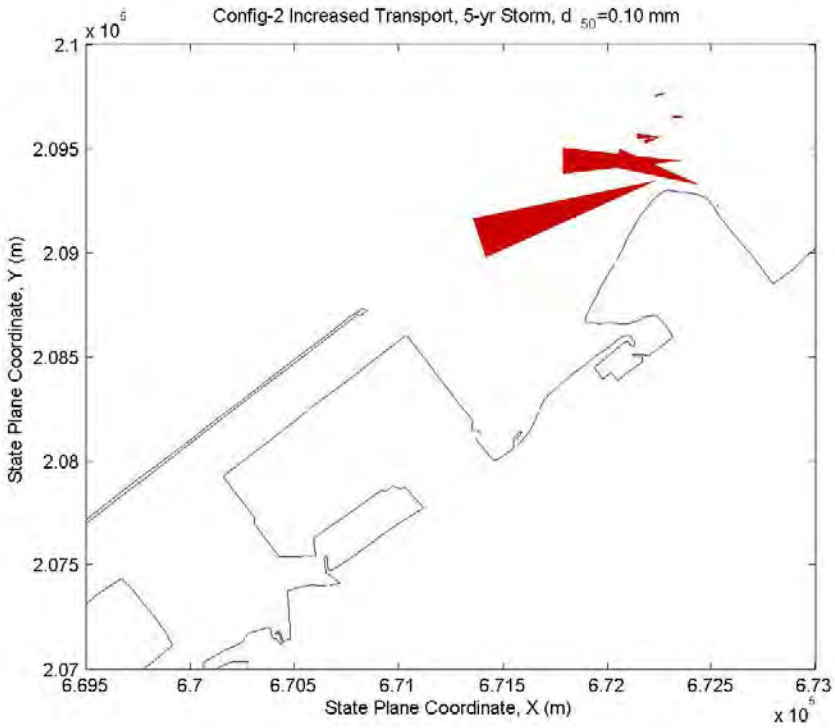

Figure C45. Configuration 2 increased transport, 5-year storm, d_{50}=0.10 mm

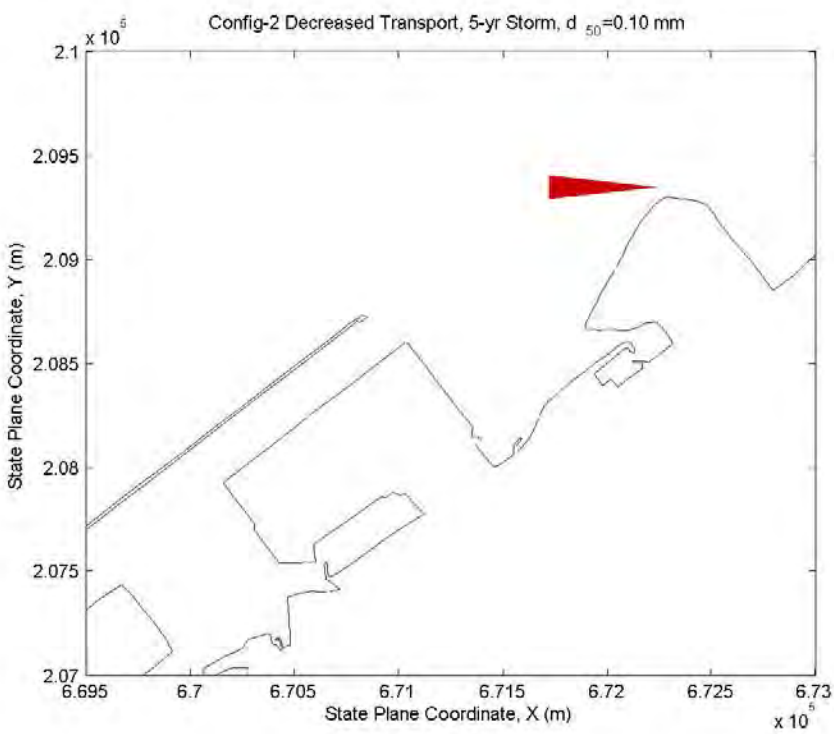

Figure C45. Configuration 2 decreased transport, 5-year storm, d_{50}=0.10 mm

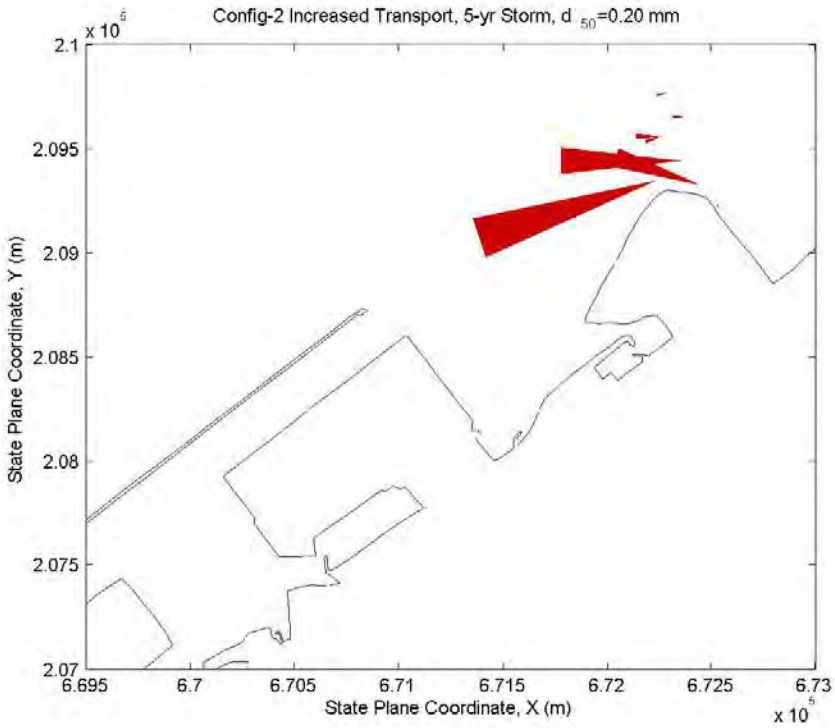

Figure C47. Configuration 2 increased transport, 5-year storm, d_{50}=0.20 mm

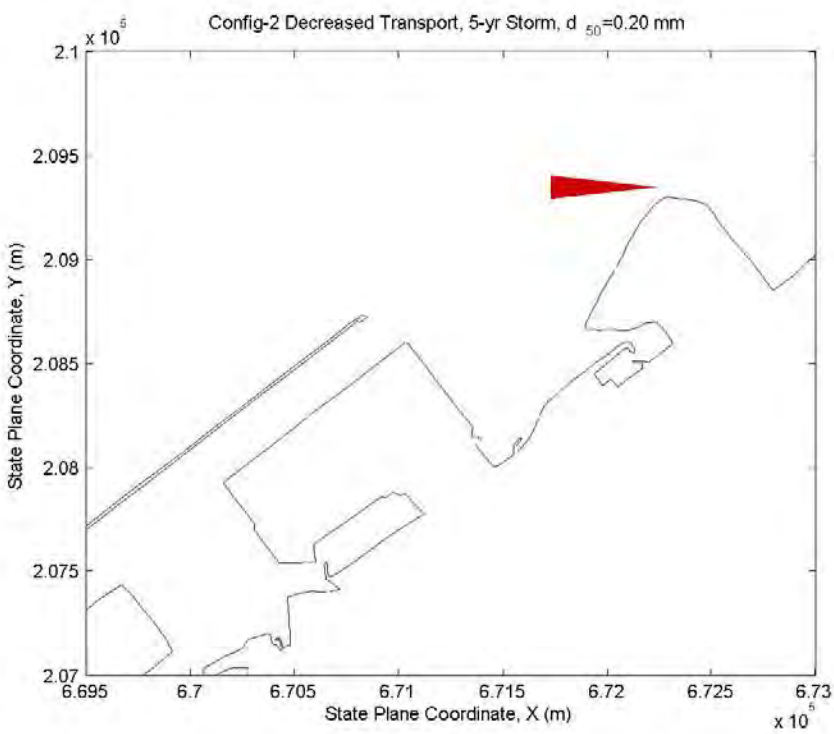

Figure C48. Configuration 2 decreased transport, 5-year storm, d_{50}=0.20 mm

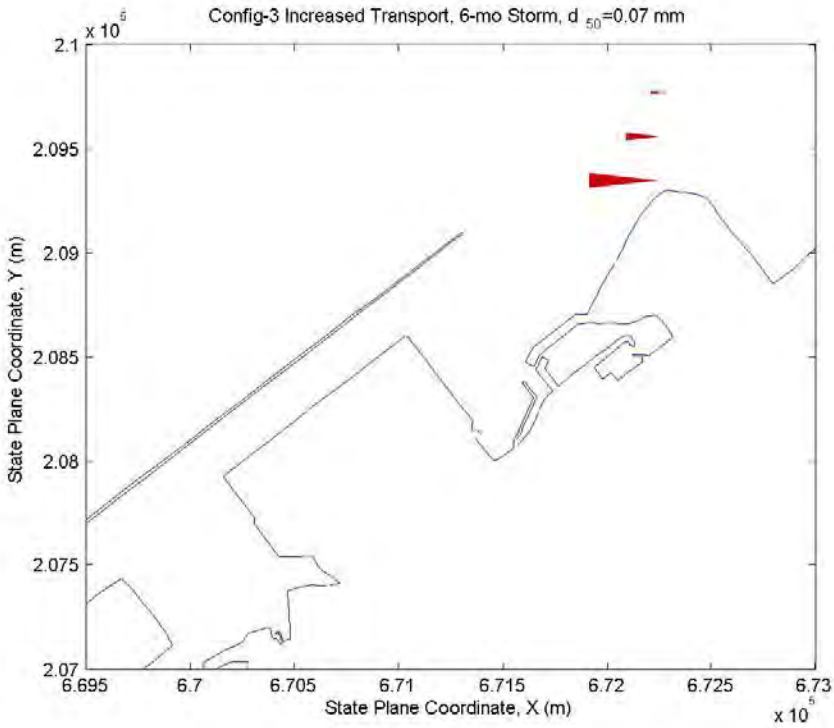

Figure C49. Configuration 3 increased transport, 6-mo storm, d_{50}=0.07 mm

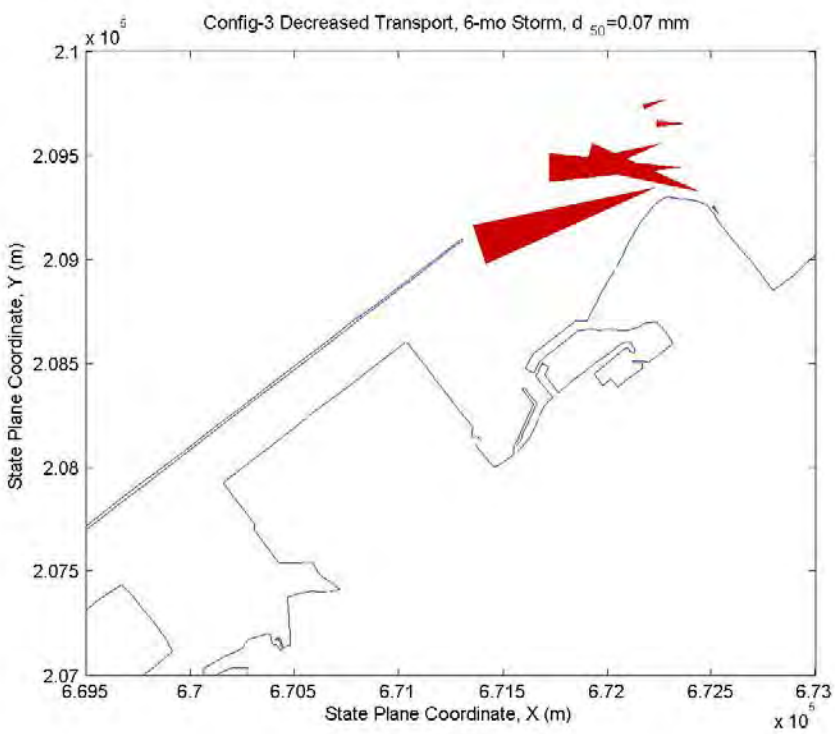

Figure C50. Configuration 3 decreased transport, 6-mo storm, d_{50}=0.07 mm

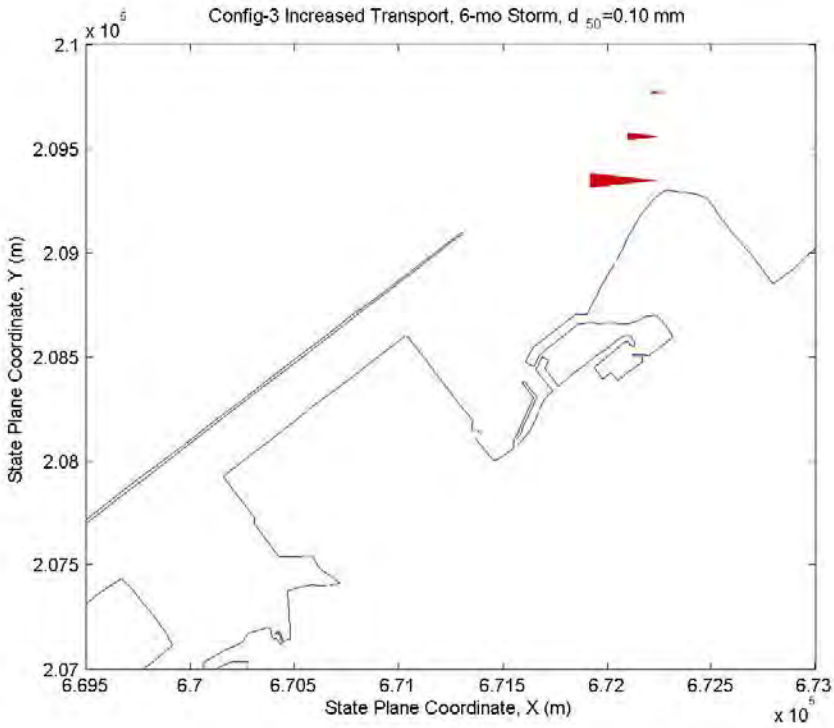

Figure C51. Configuration 3 increased transport, 6-mo storm, d_{50}=0.10 mm

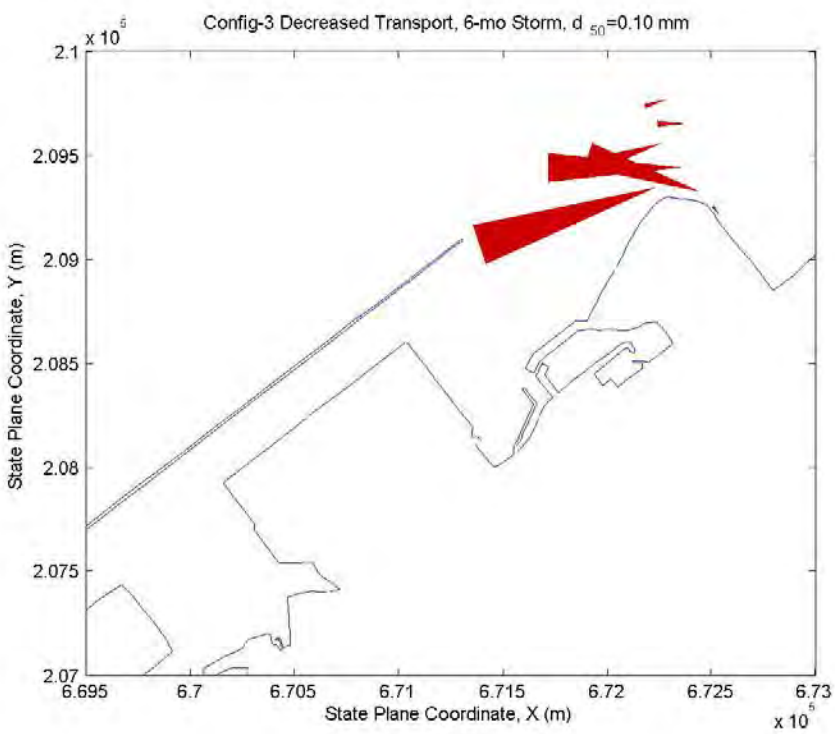

Figure C52. Configuration 3 decreased transport, 6-mo storm, d_{50}=0.10 mm

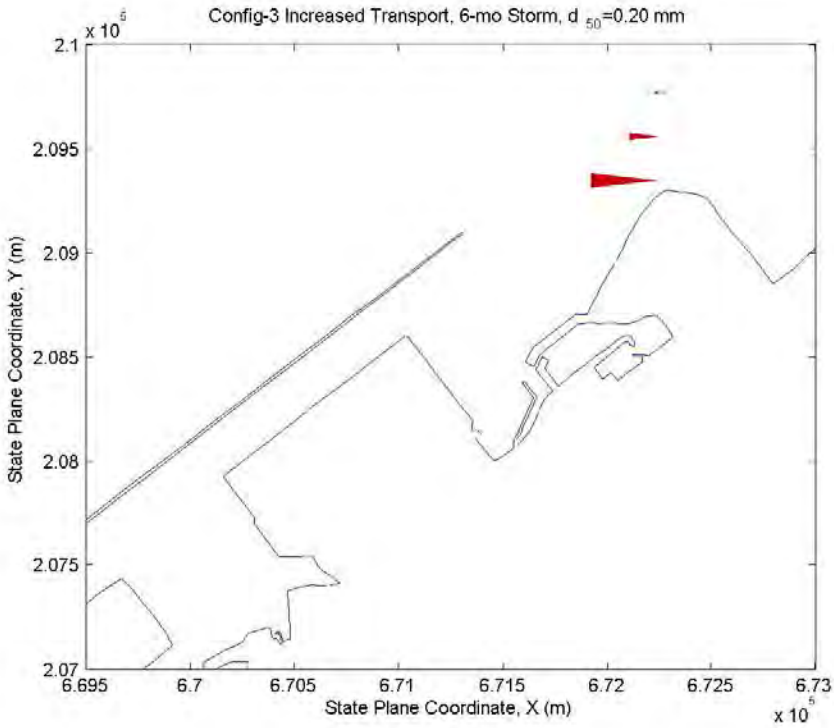

Figure C53. Configuration 3 increased transport, 6-mo storm, d_{50}=0.20 mm

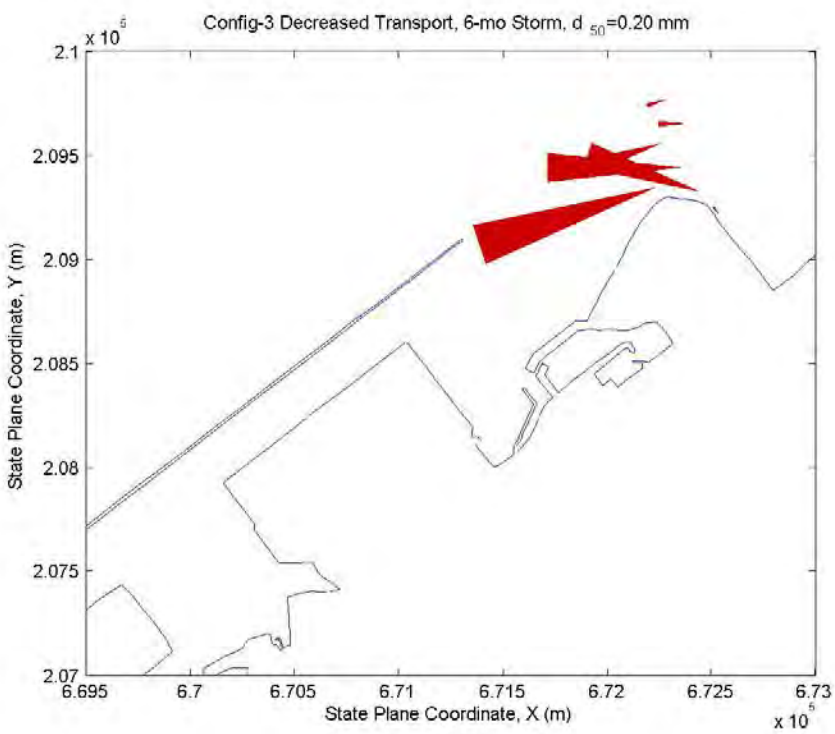

Figure C54. Configuration 3 decreased transport, 6-mo storm, d_{50}=0.20 mm

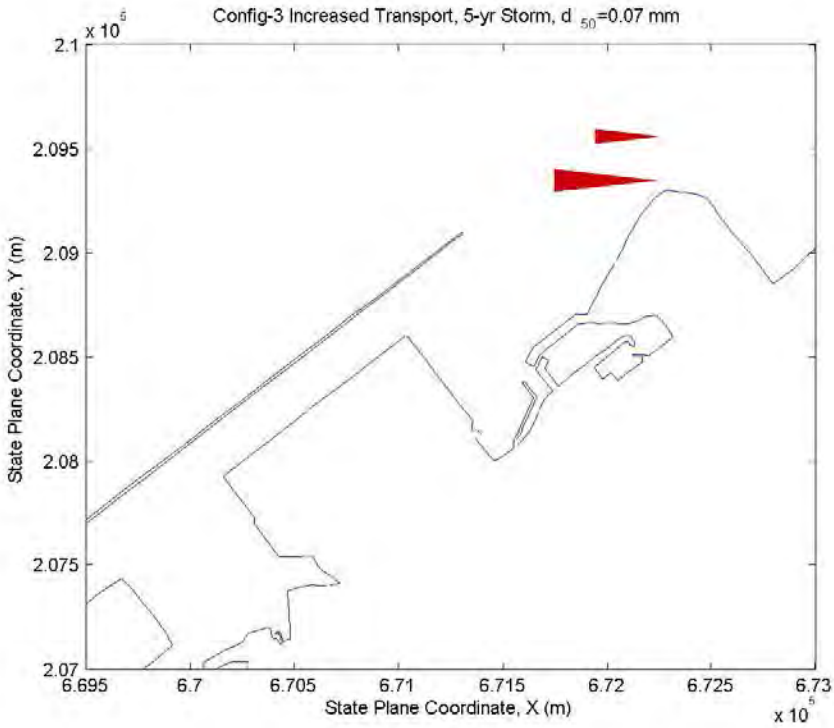

Figure C55. Configuration 3 increased transport, 5-year storm, d_{50}=0.07 mm

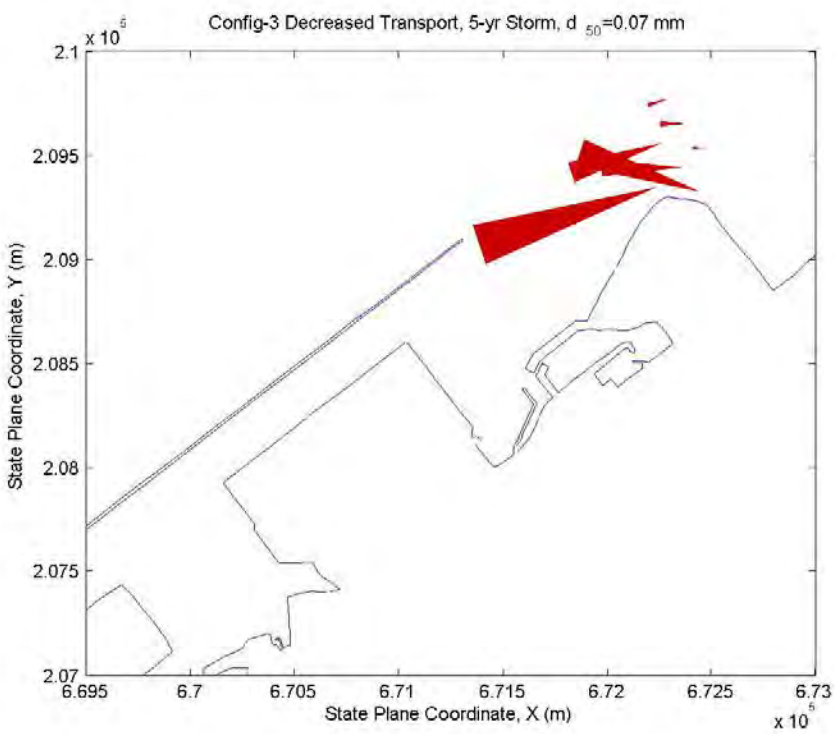

Figure C55. Configuration 3 decreased transport, 5-year storm, d_{50}=0.07 mm

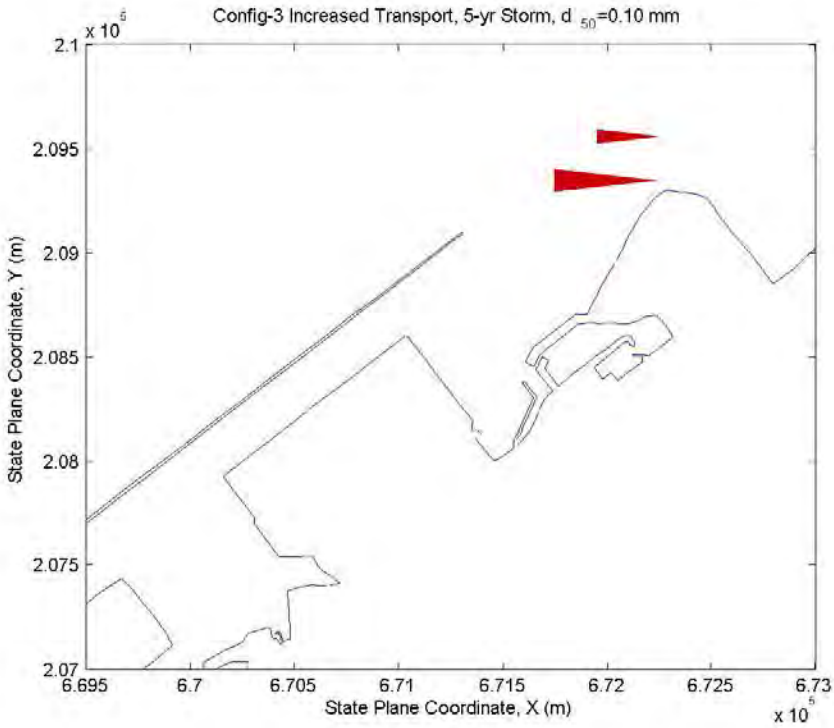

Figure C57. Configuration 3 increased transport, 5-year storm, d_{50}=0.10 mm

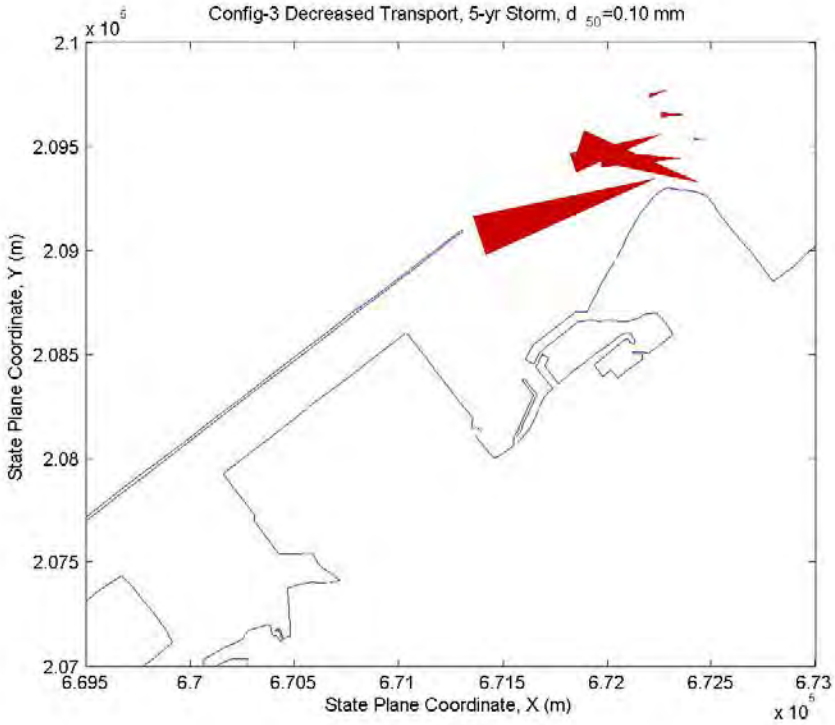

Figure C58. Configuration 3 decreased transport, 5-year storm, d_{50}=0.10 mm

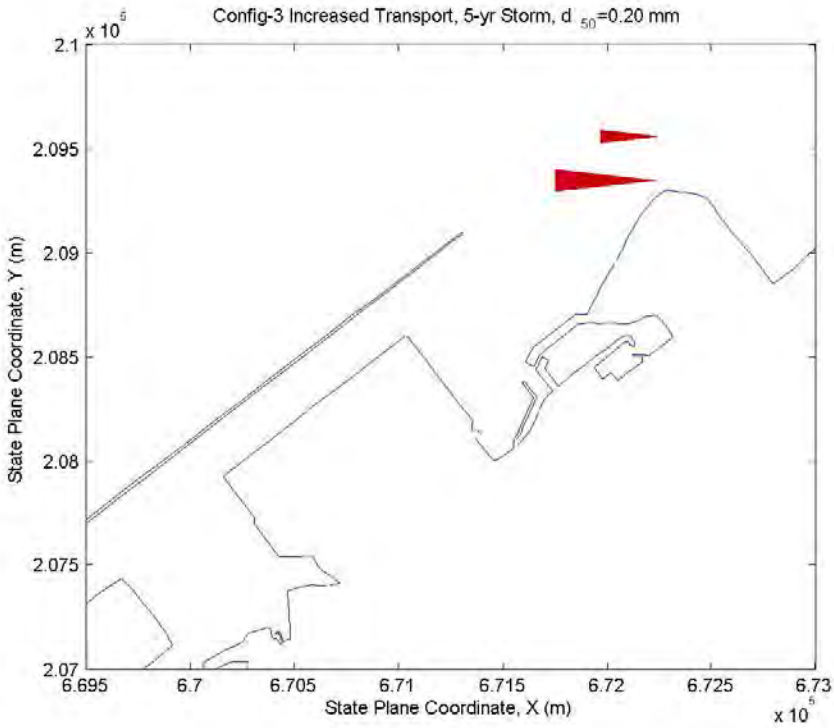

Figure C59. Configuration 3 increased transport, 5-year storm, d_{50}=0.20 mm

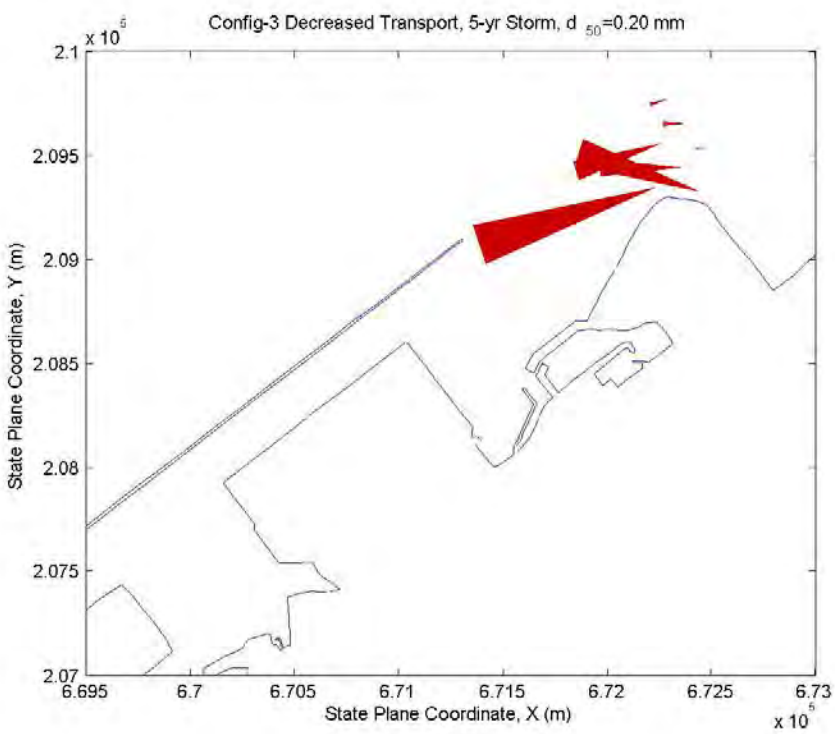

Figure C60. Configuration 3 decreased transport, 5-year storm, d_{50}=0.20 mm

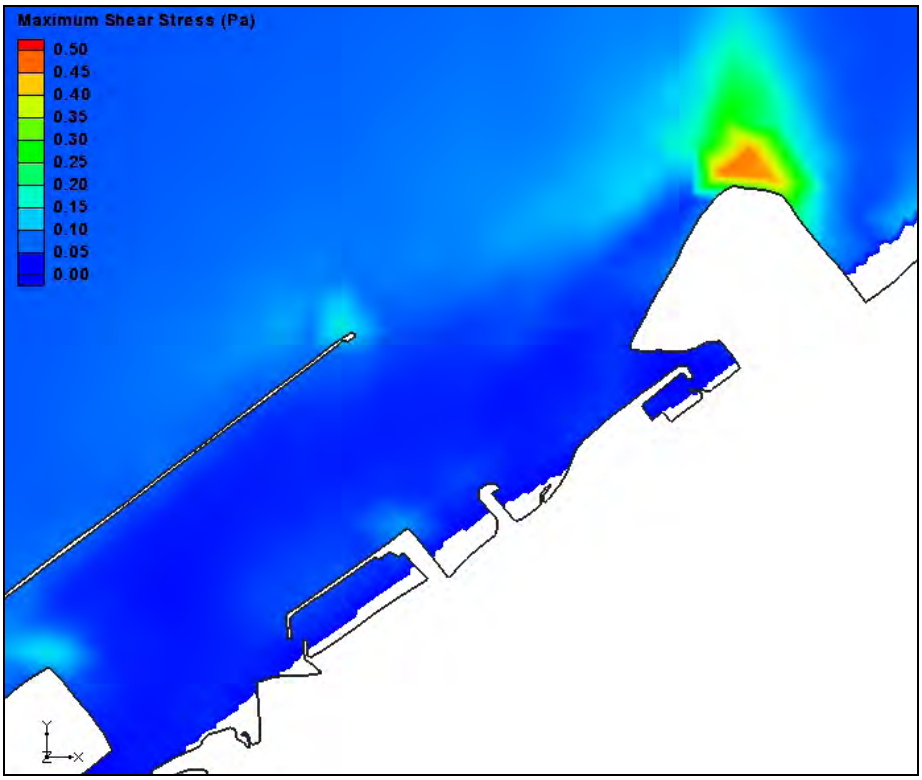

Figure C61. Maximum shear stress, Base condition, 6-month storm

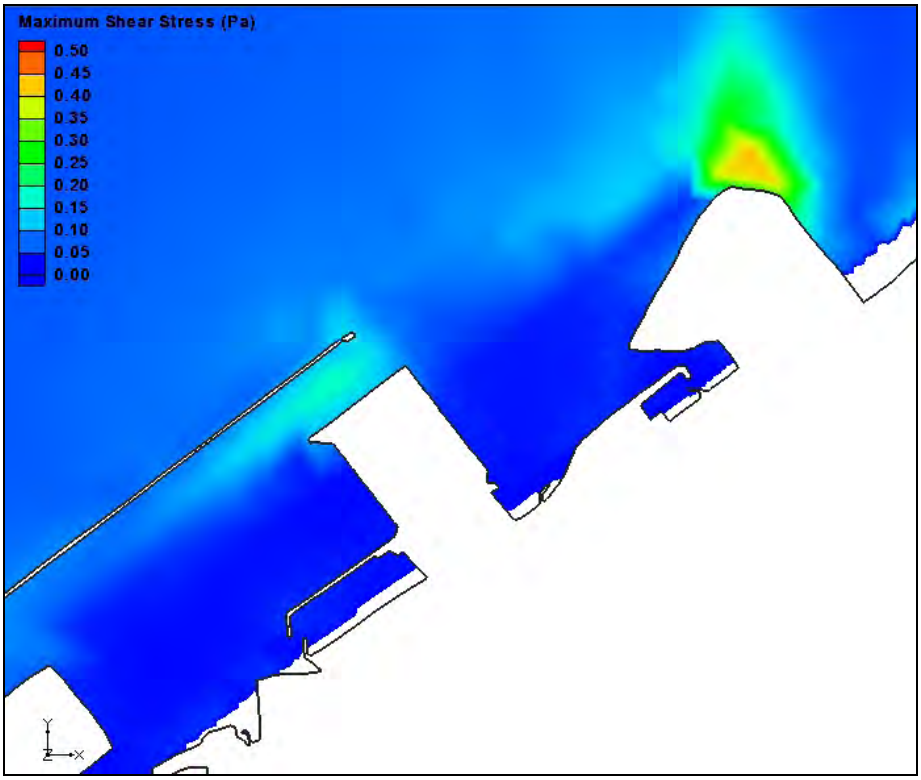

Figure C62. Maximum shear stress, Configuration 1, 6-month storm

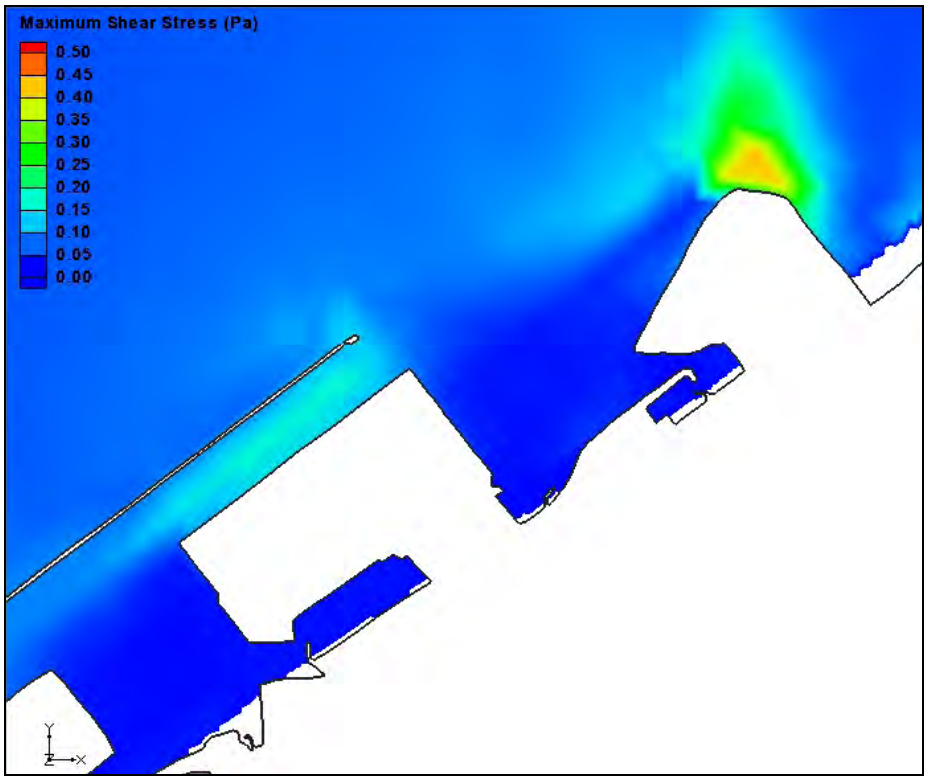

Figure C63. Maximum shear stress, Configuration 2, 6-month storm

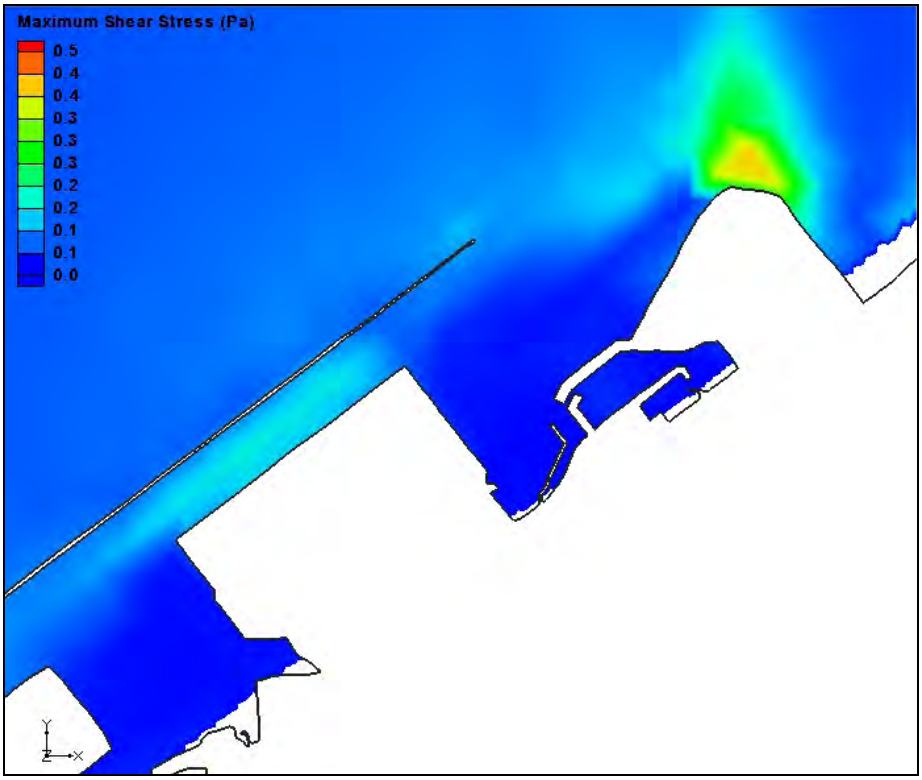

Figure C64. Maximum shear stress, Configuration 3, 6-month storm

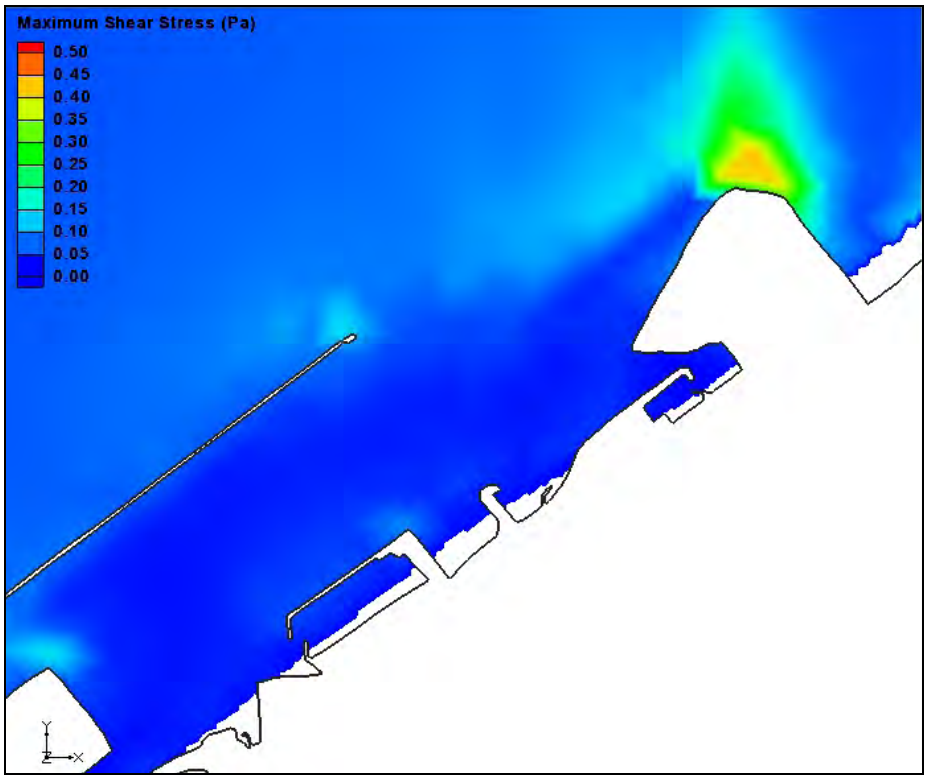

Figure C65. Maximum shear stress, Base condition, 5-year storm

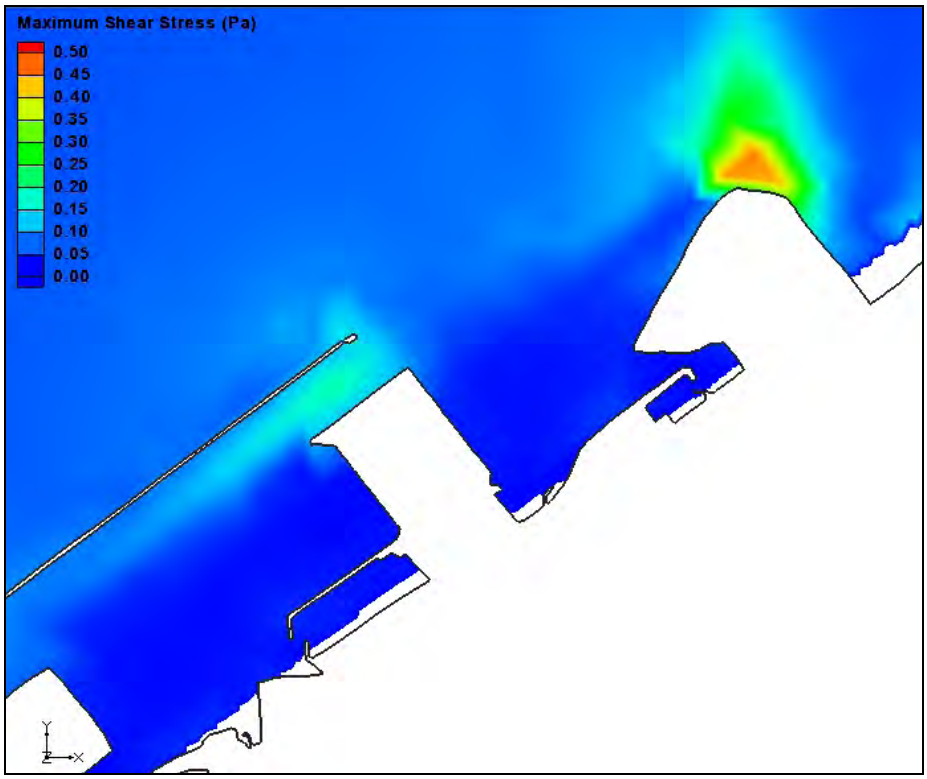

Figure C66. Maximum shear stress, Configuration 1, 5-year storm

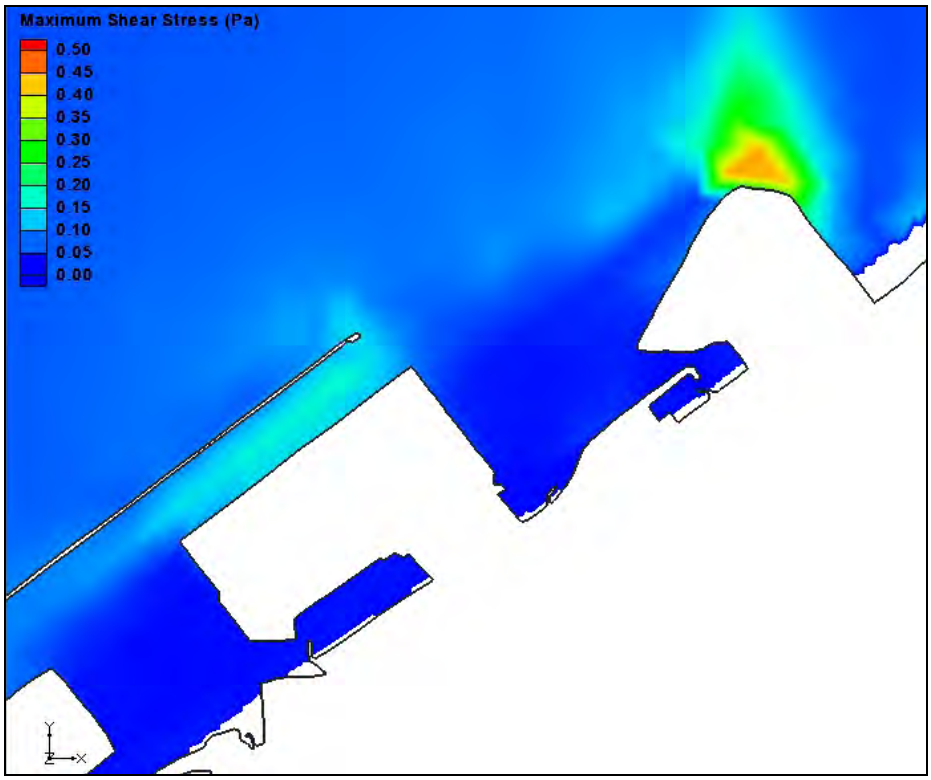

Figure C67. Maximum shear stress, Configuration 2, 5-year storm

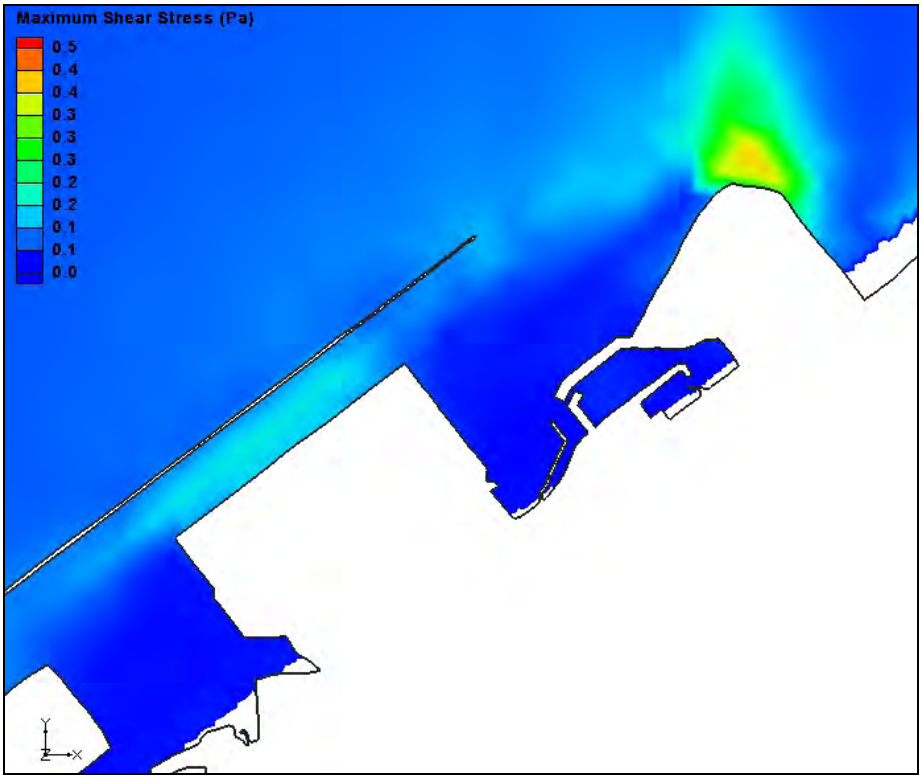

Figure C68. Maximum shear stress, Configuration 3, 5-year storm

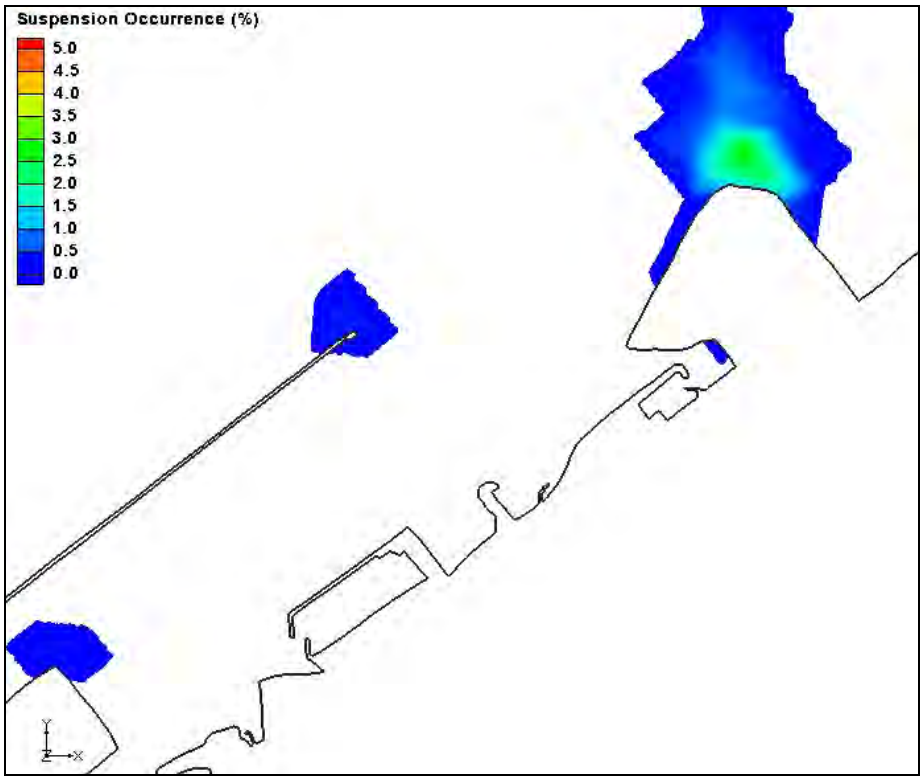

Figure C69. Percent of suspension occurrences, Base condition, 6-month storm

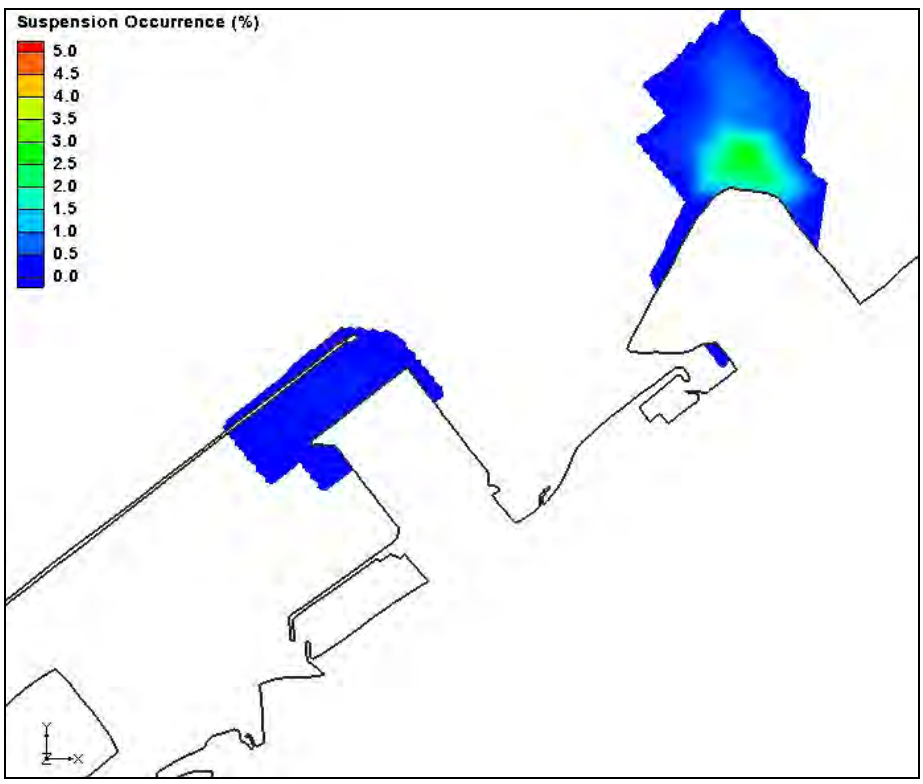

Figure C70. Percent of suspension occurrences, Configuration 1, 6-month storm

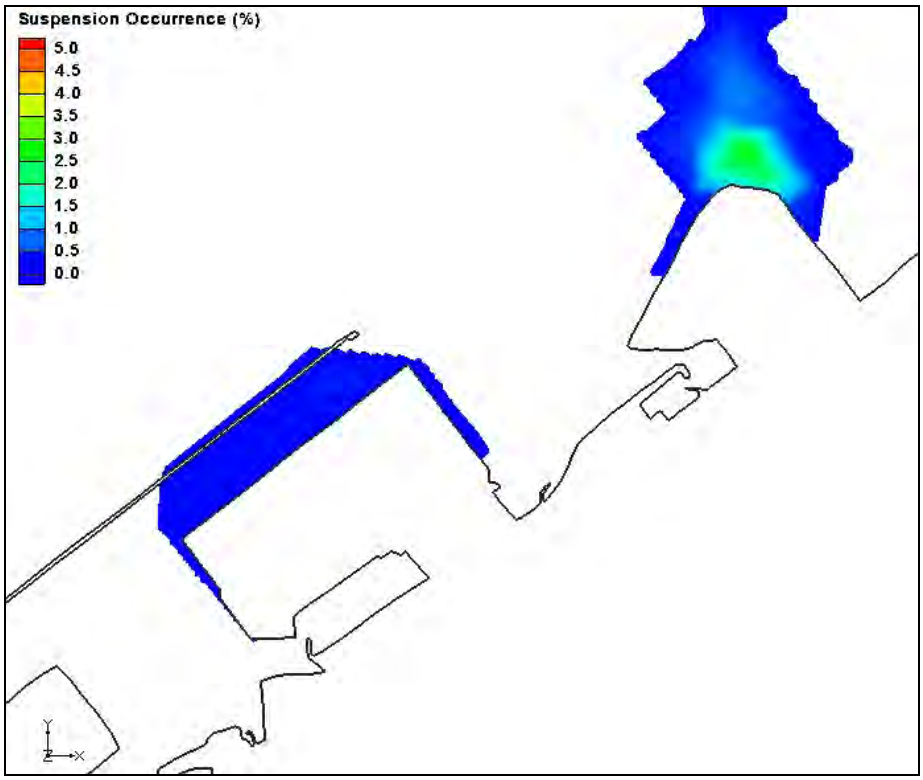

Figure C71. Percent of suspension occurrences, Configuration 2, 6-month storm

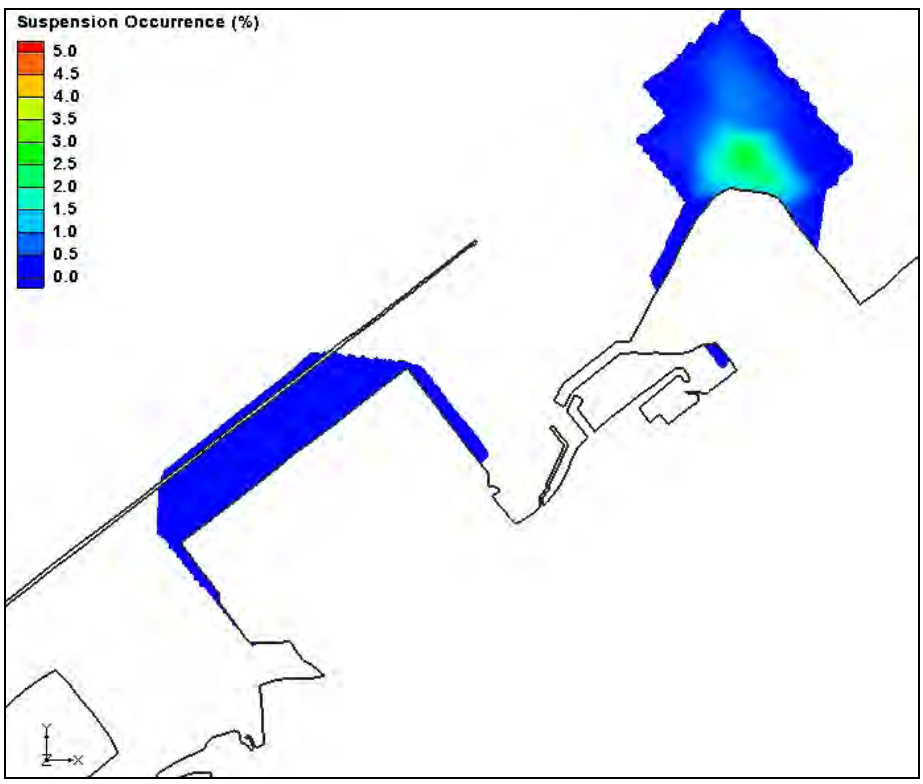

Figure C72. Percent of suspension occurrences, Configuration 3, 6-month storm

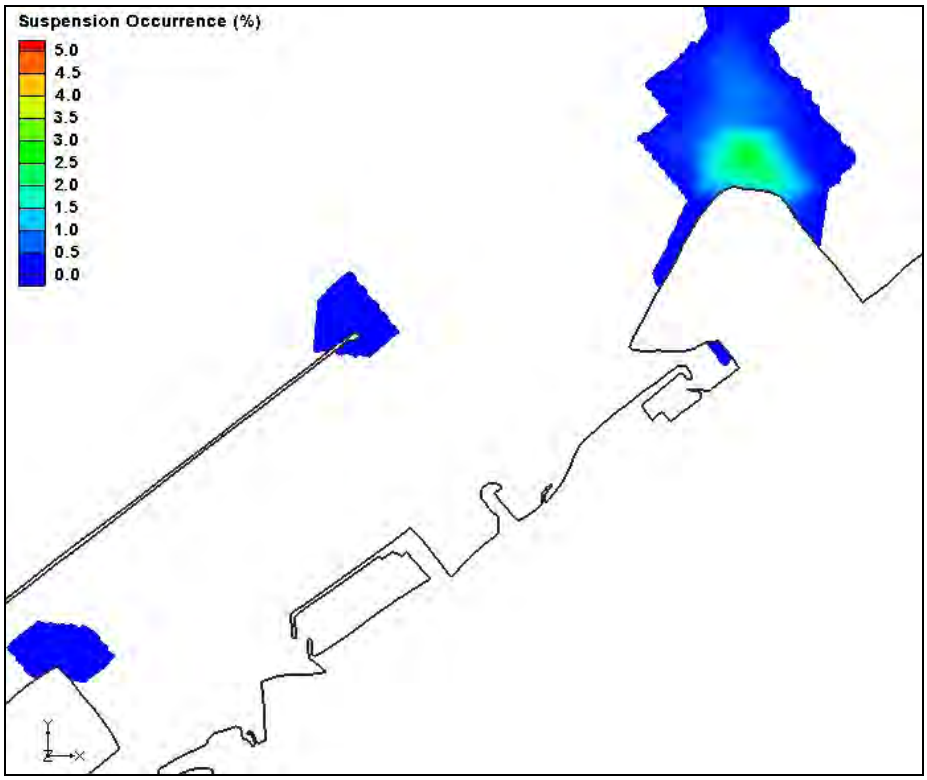

Figure C73. Percent of suspension occurrences, Base condition, 5-year storm

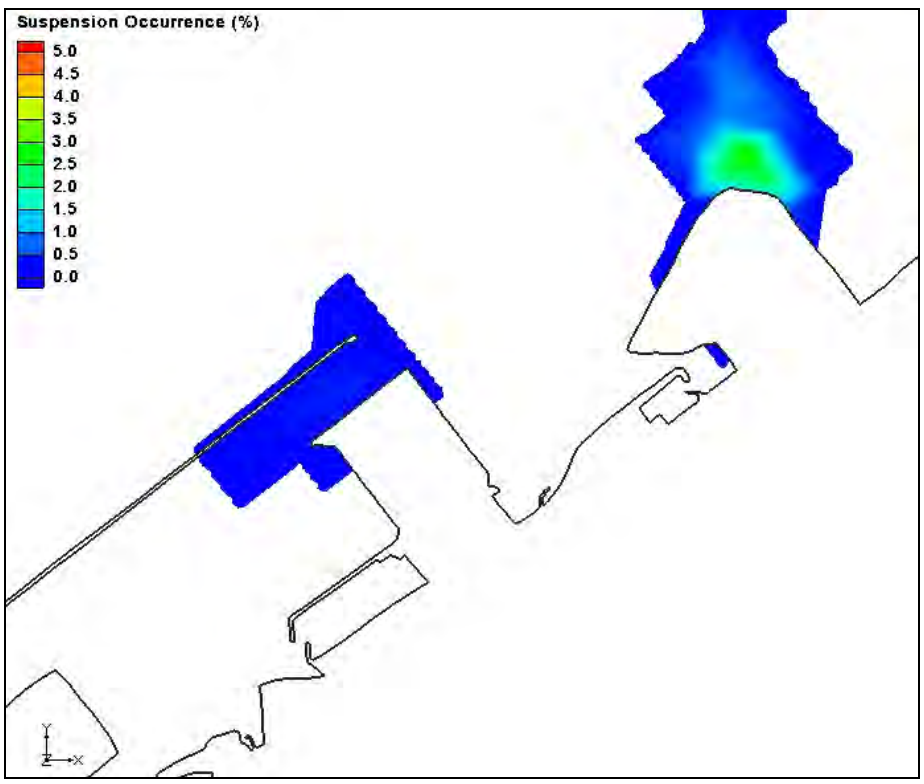

Figure C74. Percent of suspension occurrences, Configuration 1, 5-year storm

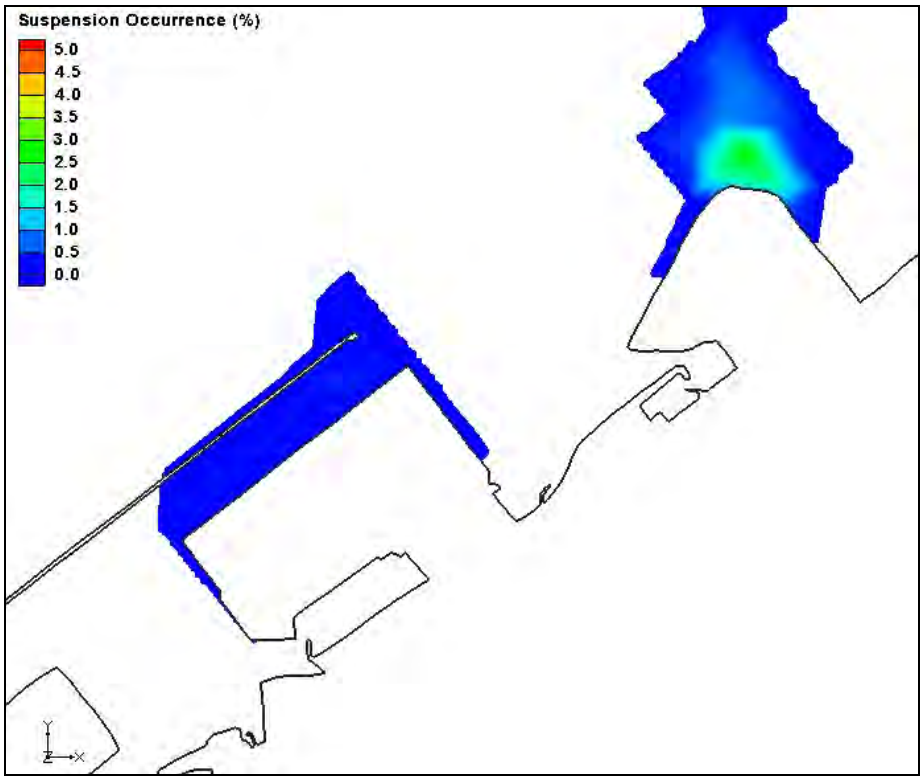

Figure C75. Percent of suspension occurrences, Configuration 2, 5-year storm

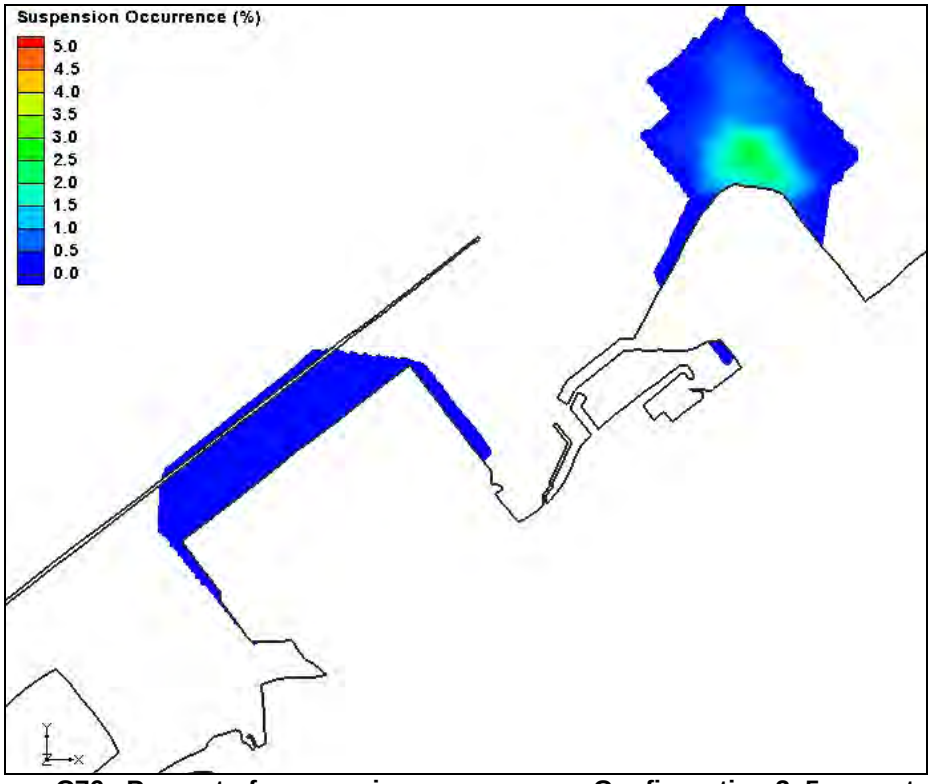

Figure C76. Percent of suspension occurrences, Configuration 3, 5-year storm

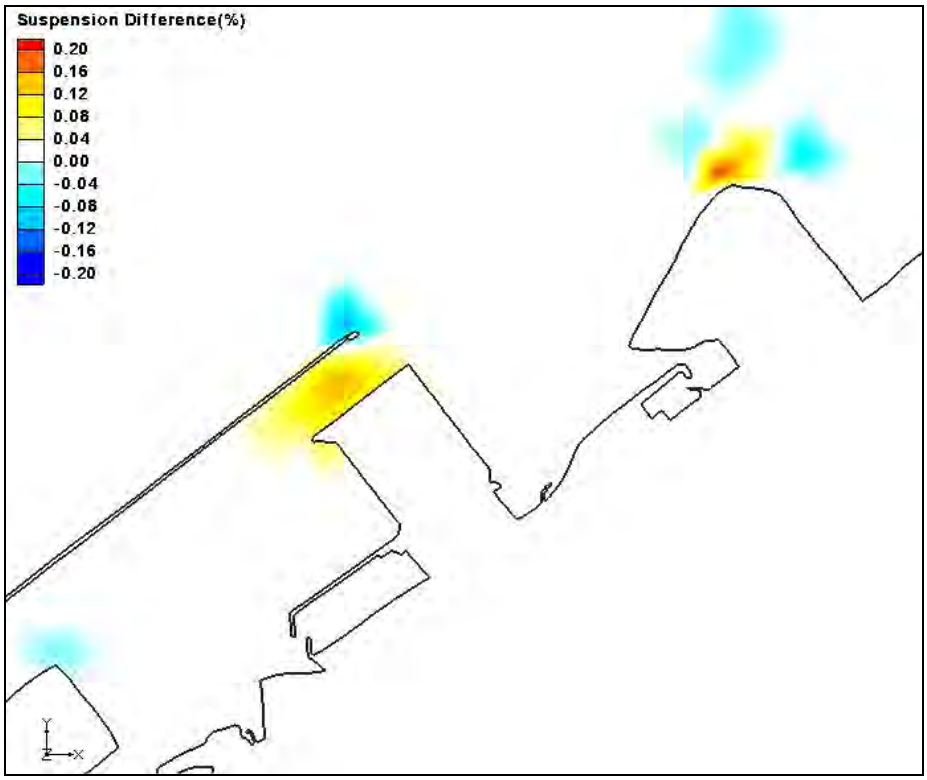

Figure C77. Difference in percent suspension, Configuration 1, 6-month storm

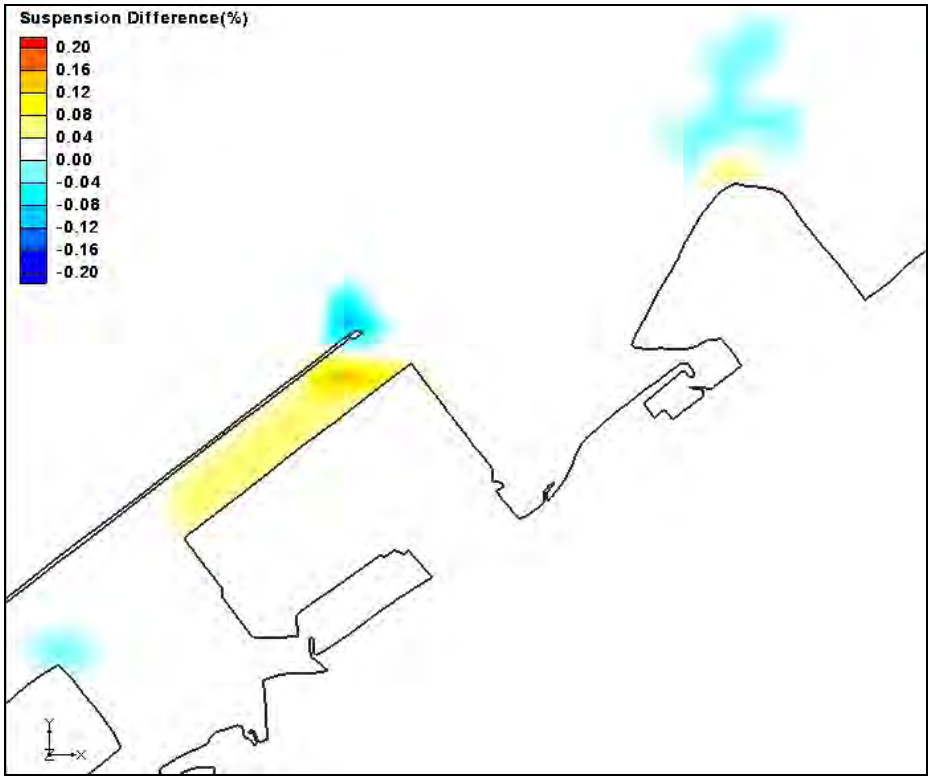

Figure C78. Difference in percent suspension, Configuration 2, 6-month storm

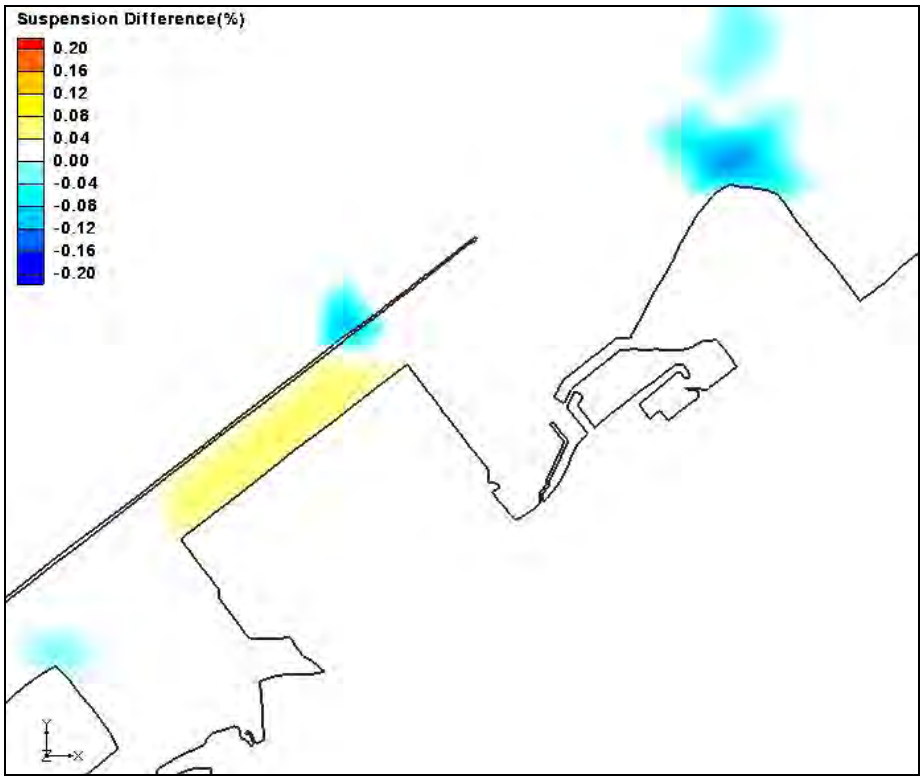

Figure C79. Difference in percent suspension, Configuration 3, 6-month storm

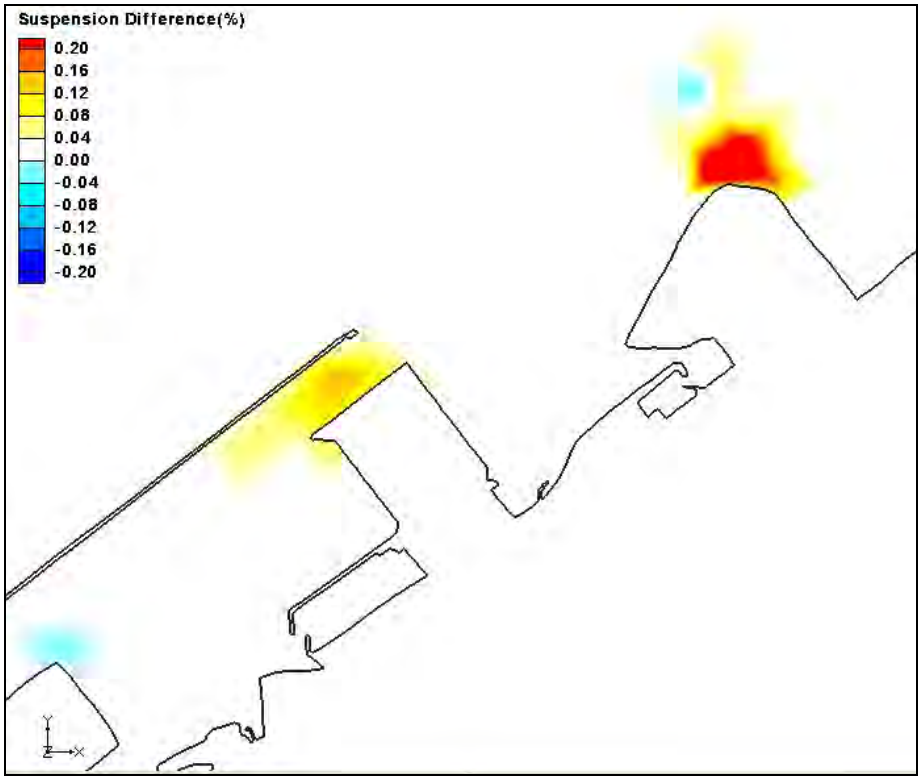

Figure C80. Difference in percent suspension, Configuration 1, 5-year storm

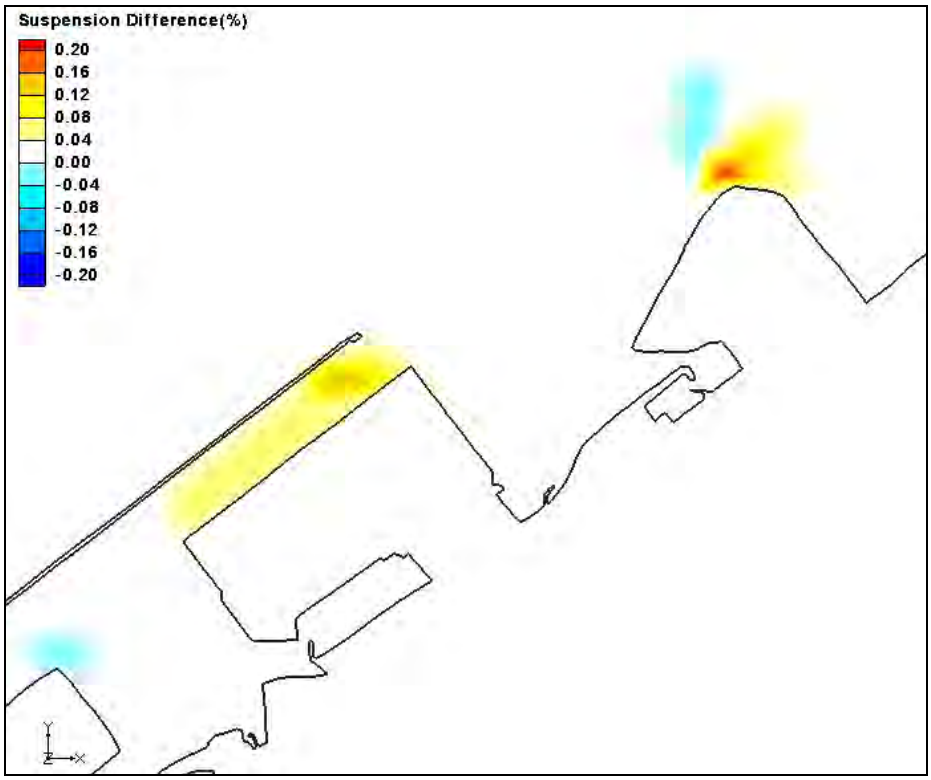

Figure C81. Difference in percent suspension, Configuration 2, 5-year storm

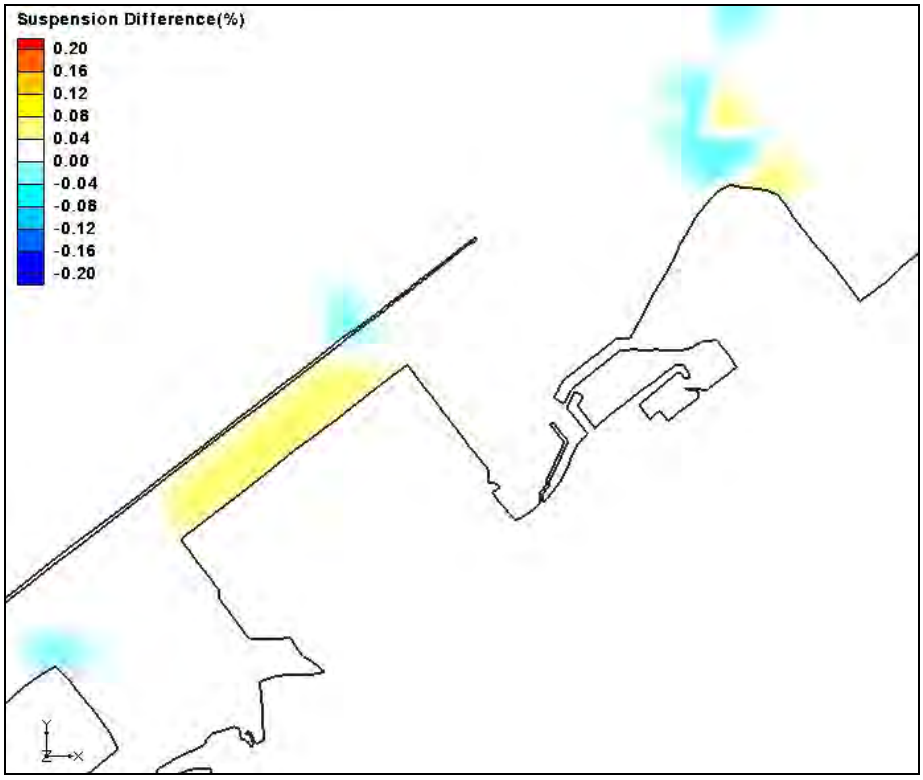

Figure C82. Difference in percent suspension, Configuration 3, 5-year storm

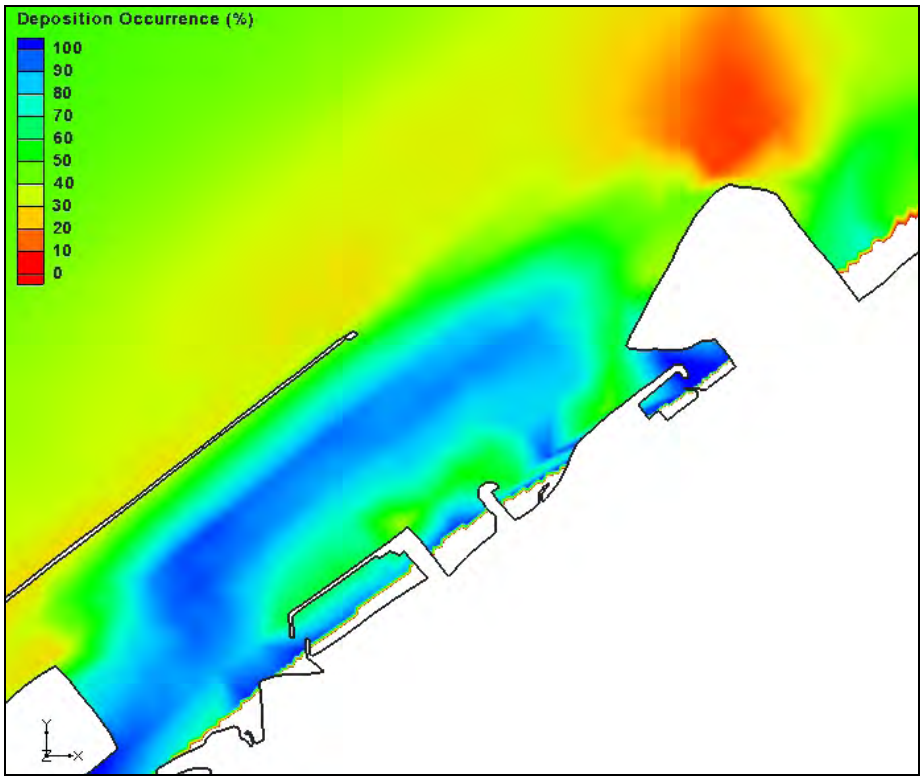

Figure C83. Percent of deposition occurrences, Base condition, 6-month storm

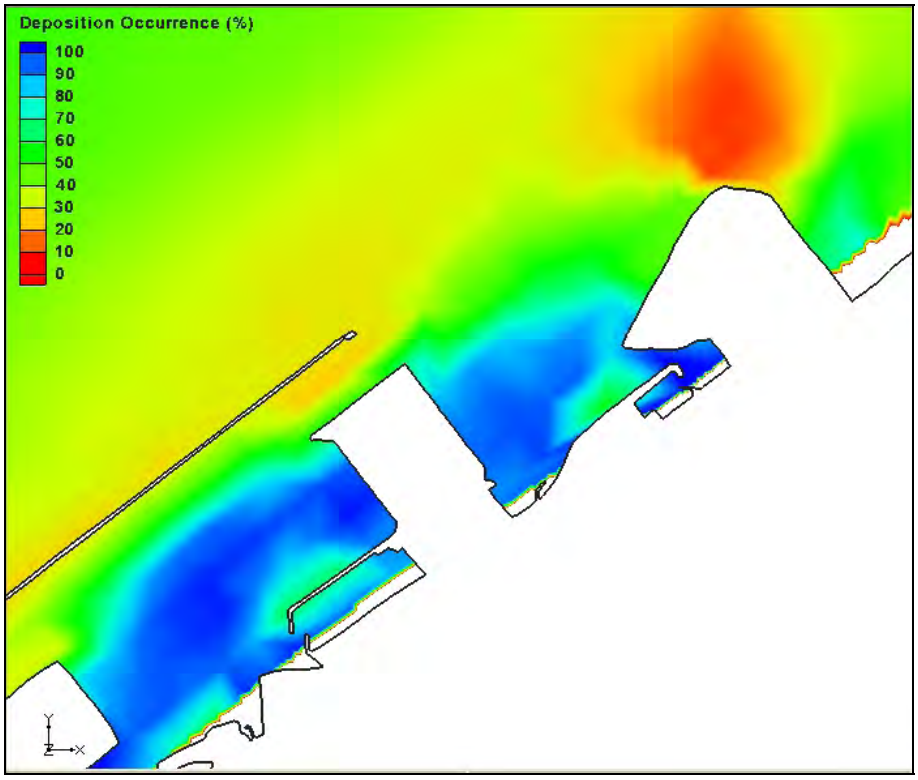

Figure C84. Percent of deposition occurrences, Configuration 1, 6-month storm

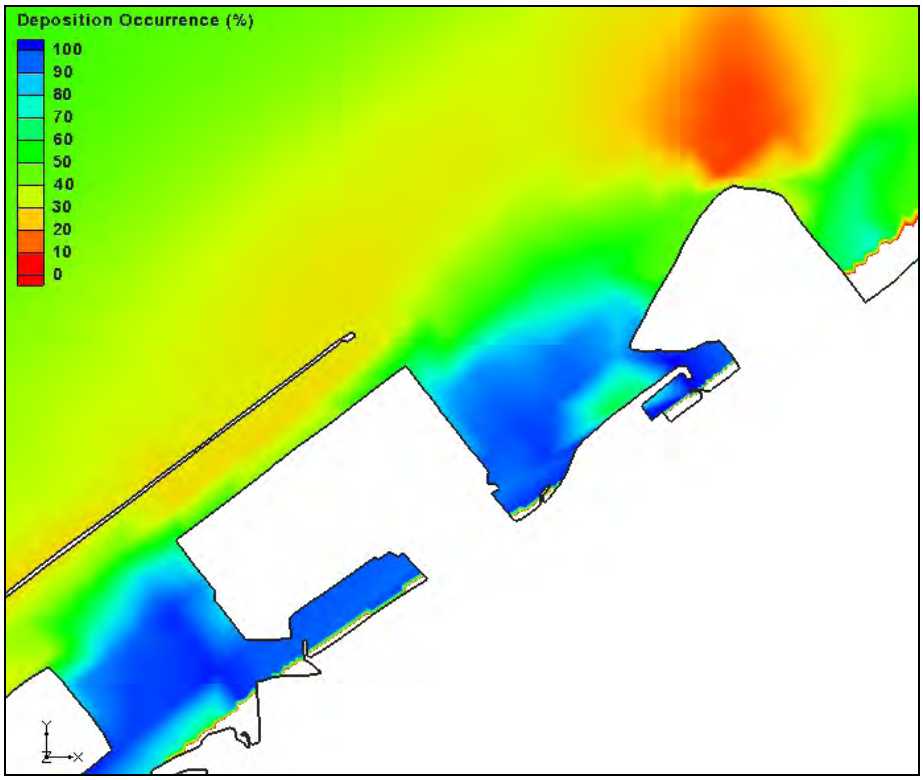

Figure C85. Percent of deposition occurrences, Configuration 2, 6-month storm

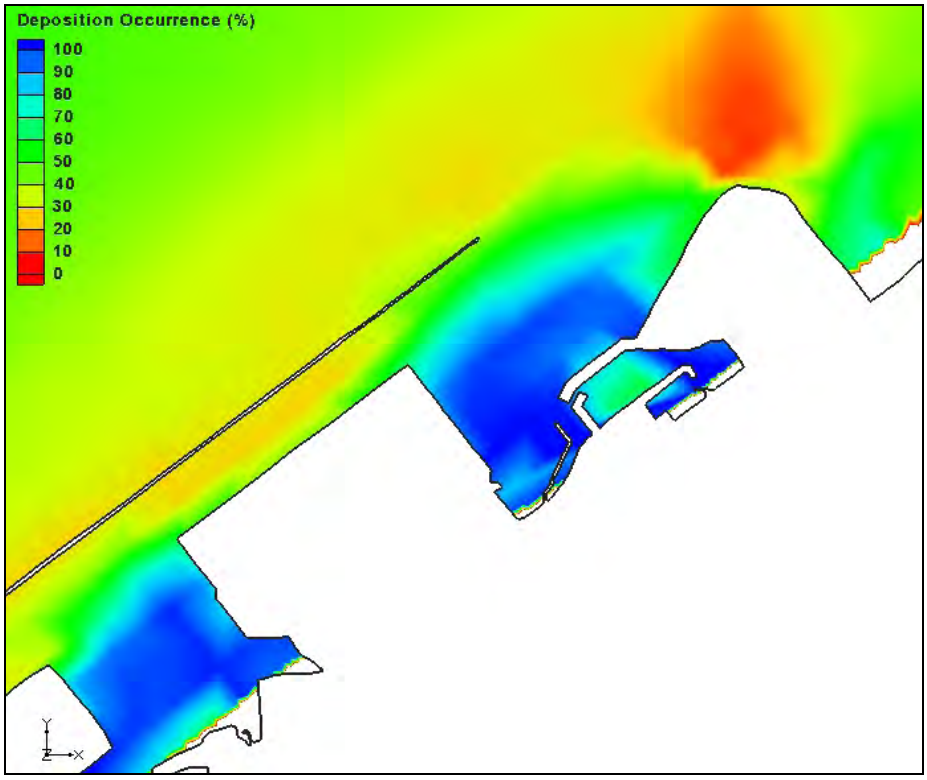

Figure C86. Percent of deposition occurrences, Configuration 3, 6-month storm

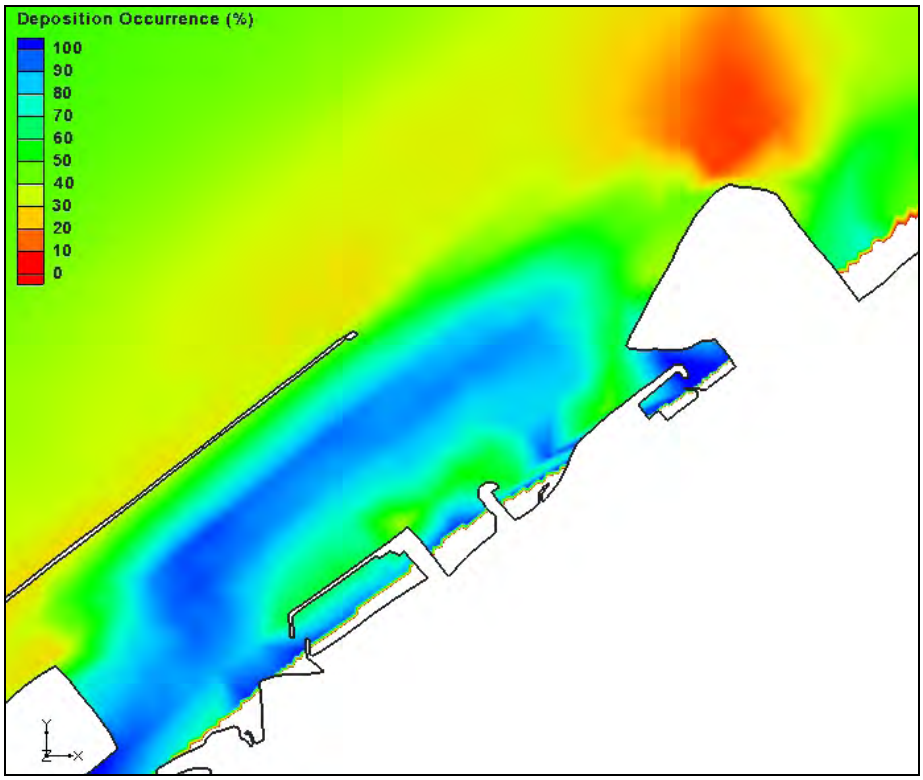

Figure C87. Percent of deposition occurrences, Base condition, 5-year storm

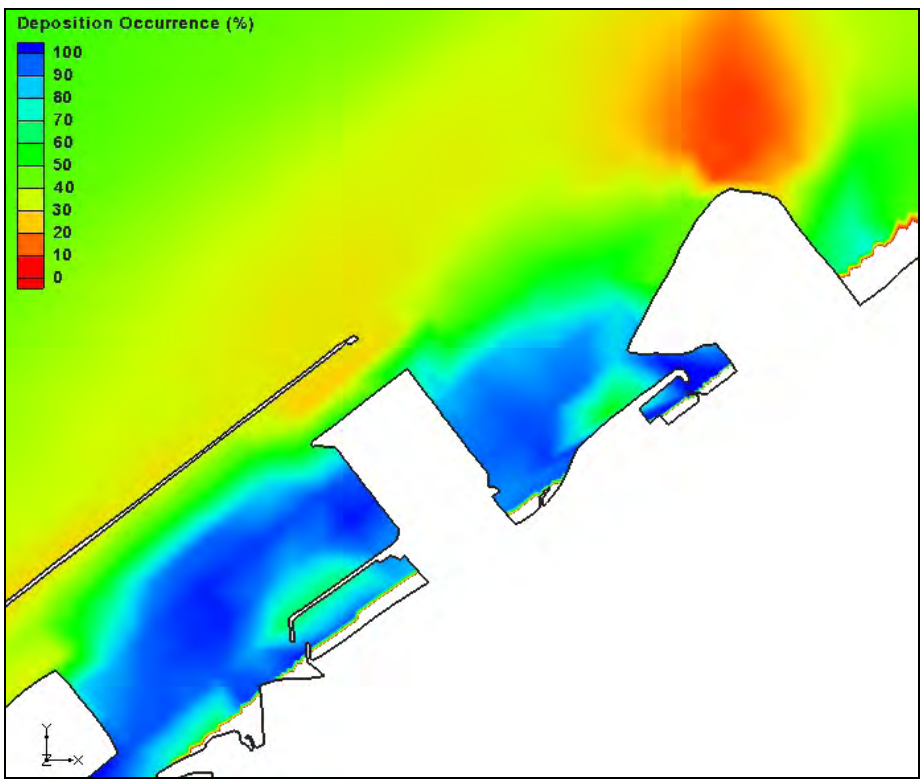

Figure C88. Percent of deposition occurrences, Configuration 1, 5-year storm

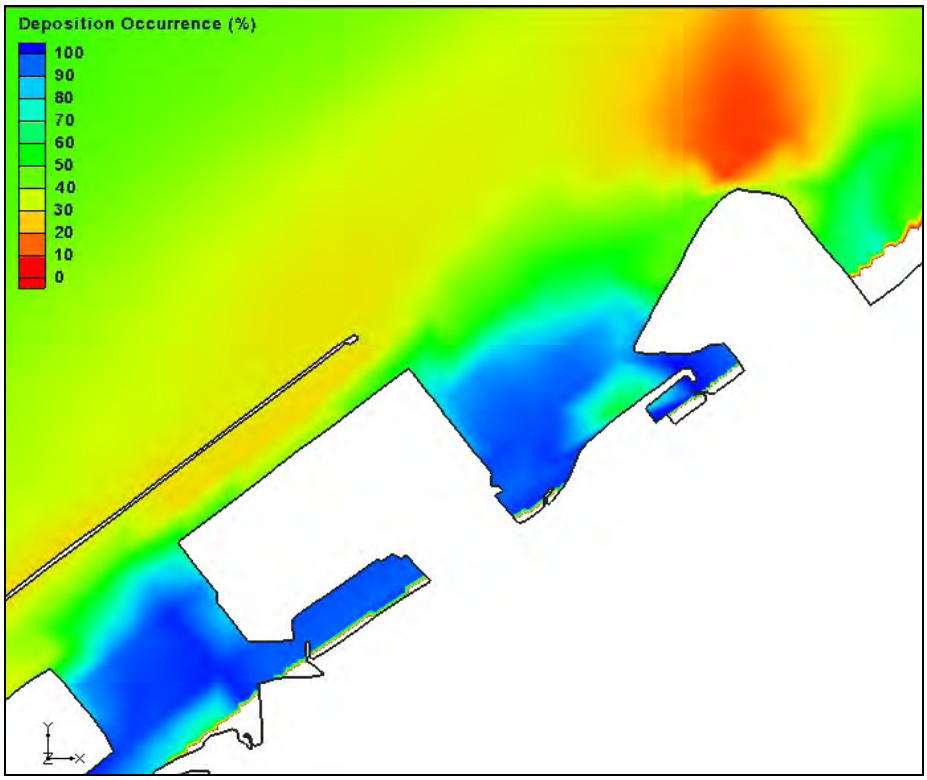

Figure C89. Percent of deposition occurrences, Configuration 2, 5-year storm

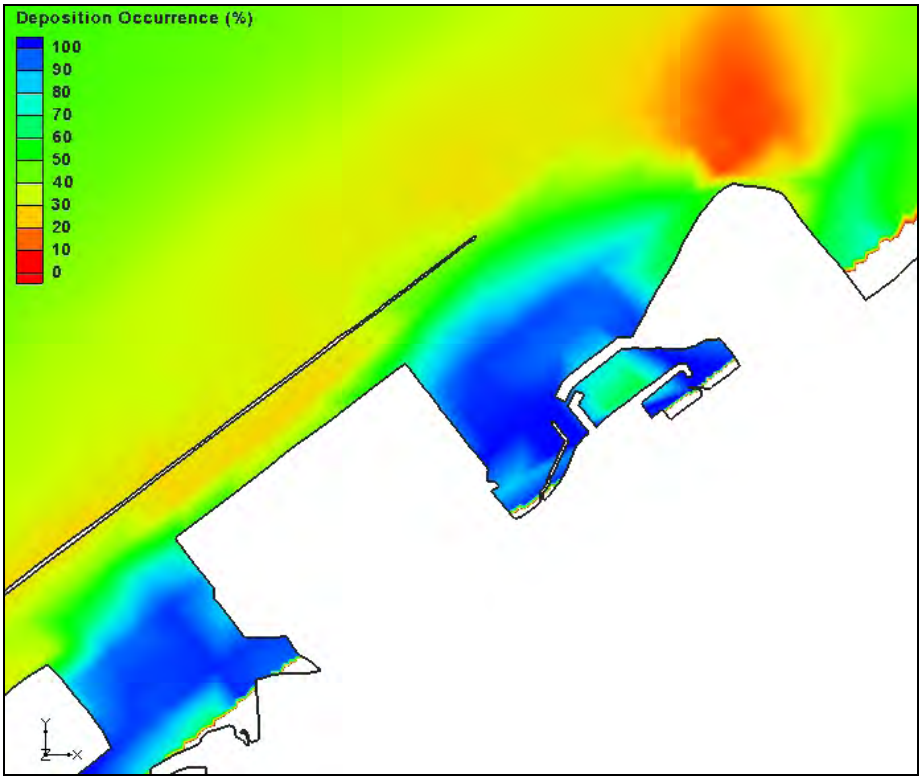

Figure C90. Percent of deposition occurrences, Configuration 3, 5-year storm

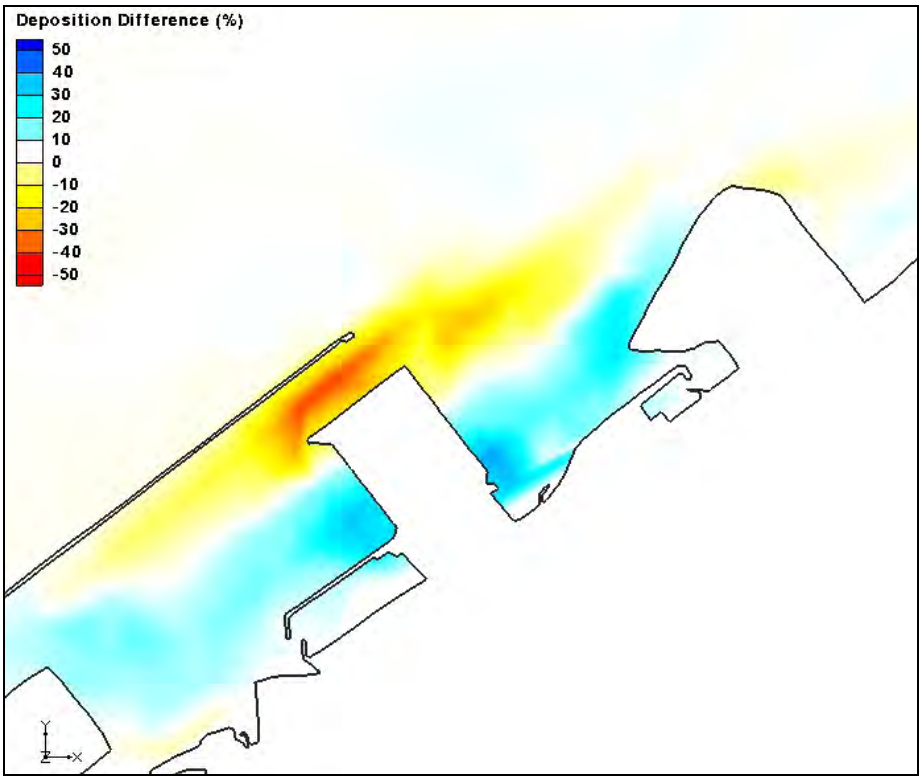

Figure C91. Difference in percent deposition, Configuration 1, 6-month storm

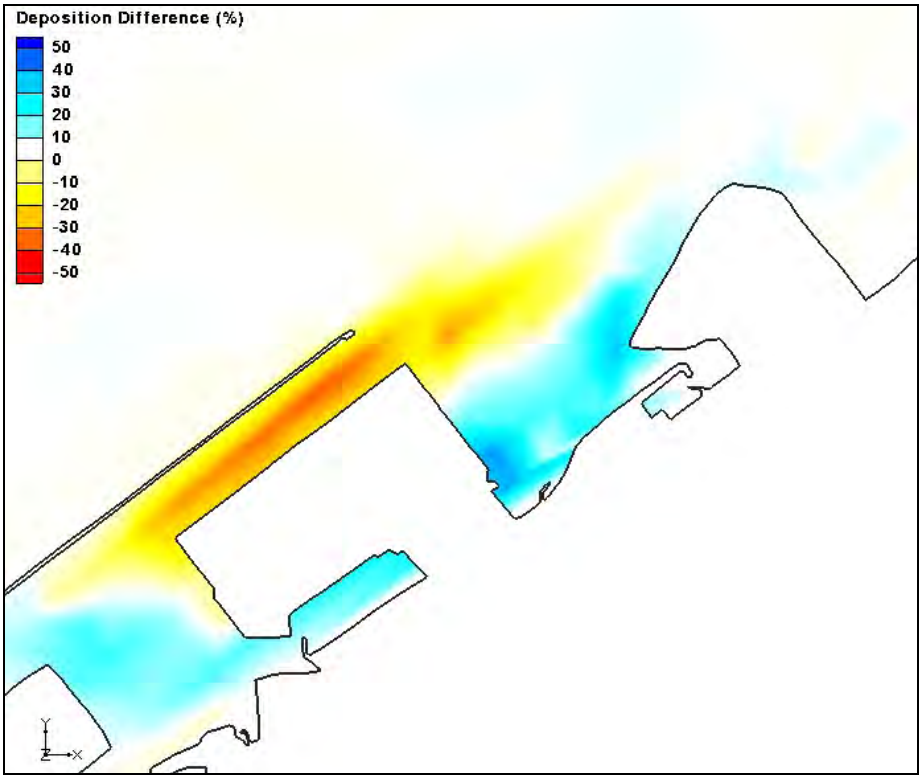

Figure C92. Difference in percent deposition, Configuration 2, 6-month storm

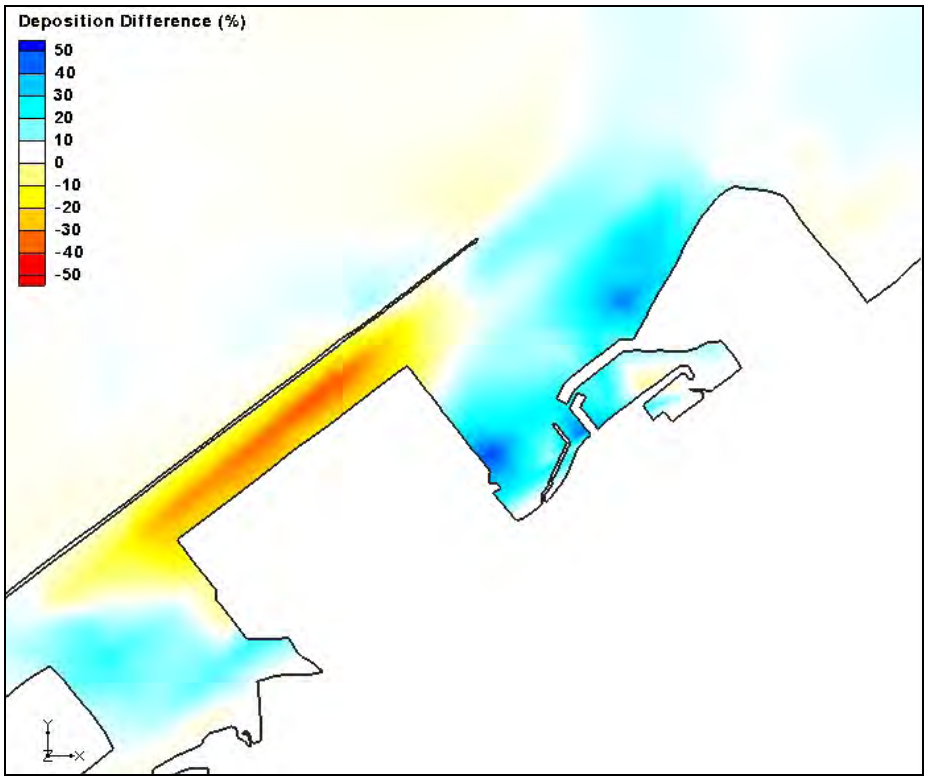

Figure C93. Difference in percent deposition, Configuration 3, 6-month storm

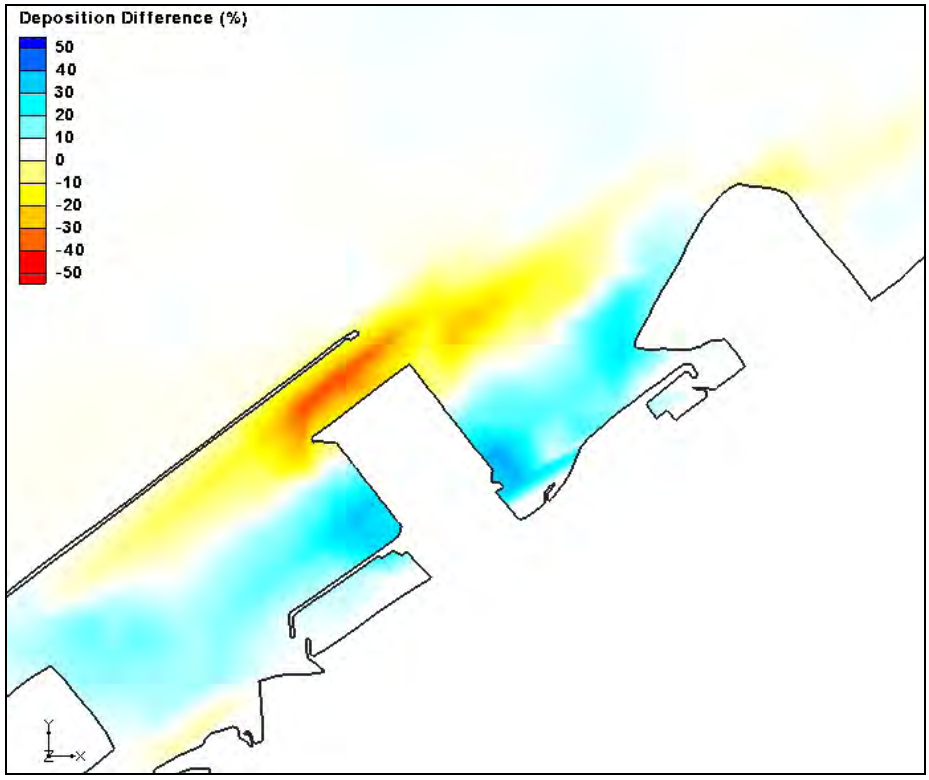

Figure C94. Difference in percent deposition, Configuration 1, 5-year storm

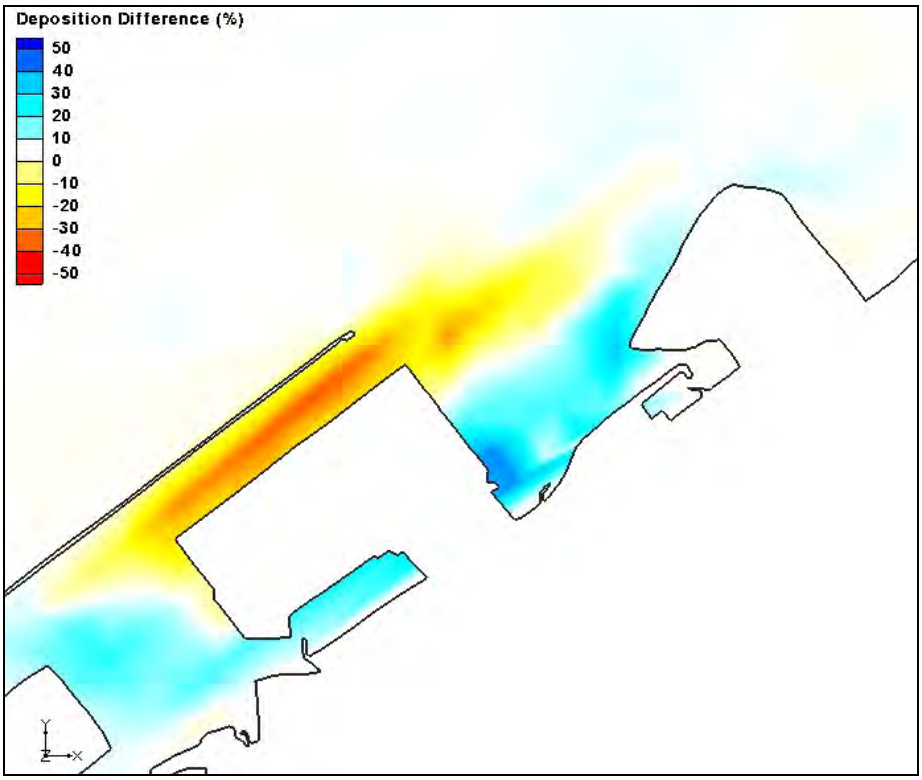

Figure C95. Difference in percent deposition, Configuration 2, 5-year storm

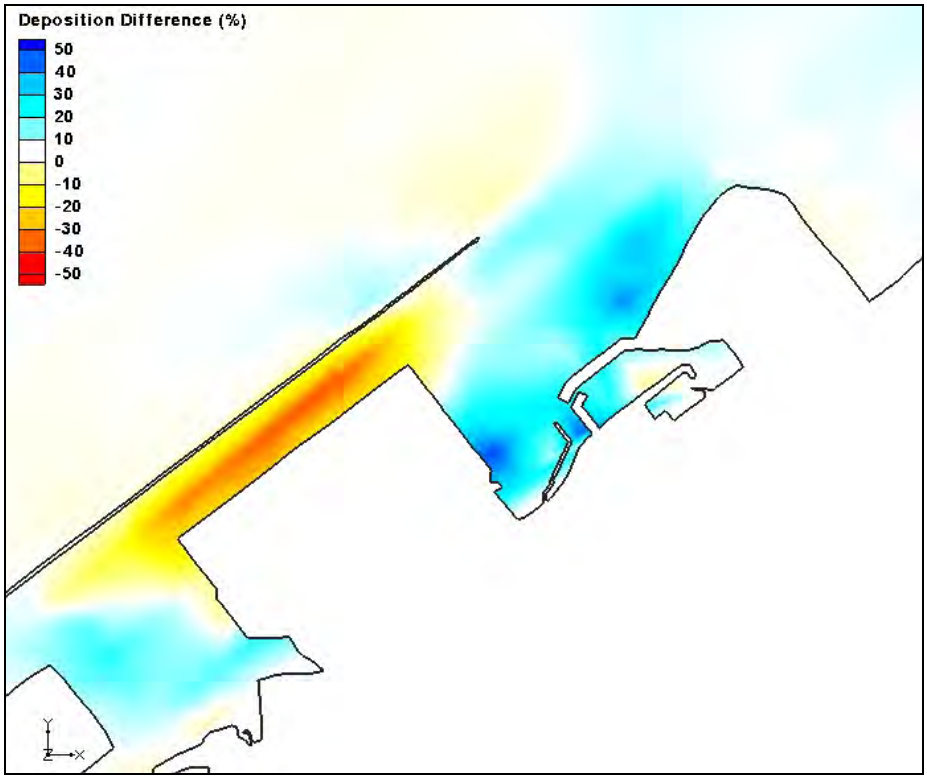

Figure C96. Difference in percent deposition, Configuration 3, 5-year storm